The Institute for Solid State Physics
The University of Tokyo

Activity Report 2019

ISSP

Activity Report 2019

Contents

	Pages
Preface	1
Research Highlights	2 - 39
Joint Research Highlights	40 - 51
Progress of Facilities	52 - 59
Conferences and Workshops	60 - 65
Subjects of Joint Research	66 - 163
Publications	164 - 200

Preface

We would like to offer the readers the scientific activity report of the Institute for Solid State Physics (ISSP) for the Japanese FY 2019.

ISSP was established in 1957 as a joint-use/research institute attached to the University of Tokyo. In every era, we aim to lead the frontier of “condensed matter physics and materials science” and contribute to science and technology from the view of basic research. We have promoted activities focused on research, education, and joint-use/joint-research.

The first part of the reports Research Highlights /Joint Research Highlights exhibits experimental and theoretical achievements in condensed matter physics and materials science. In 2019, the number of granted joint-research proposals is 1,421 and the total number of participants is 6,951.

The second part includes the reports on progress of facilities in 2019 as follows. (1) In International MegaGauss Science Laboratory, the pulse magnets can generate up to 87 Tesla (T) by non-destructive manner, and from 100 T up to 1200 T, the world strongest as an in-door record, by destructive methods to promote materials science under high magnetic field. (2) In the Supercomputer Center (SCC), the replacement of the System B is scheduled in Autumn 2020, which will be much more powerful than the current System. In Center of Computational Materials Science, the website "MateriApps" for information on application software in computational science has been constructed to support community members. The activity on deploying the MateriApps is awarded as the commendation for Science and Technology by the Minister of Education, Culture, Sports, Science and Technology (MEXT) in 2019. (3) In Neutron Science Laboratory, the technical progress of High Resolution Chopper (HRC) spectrometer has been proceeded under high pressure and low temperature environment in cooperation with KEK. (4) The Laser and Synchrotron Research (LASOR) center has 10 groups in 2019, where ISSP has integrated the two streams, namely the extreme lasers and synchrotron radiations, into the common platform. In Synchrotron Radiation Laboratory, operand spectroscopy is available by using lasers at Harima branch.

In the following parts, nine reports of international and domestic conferences and workshops, subjects of joint research, and list of publications have been presented.

In order to develop the international scientific network as scientific hub, new programs including the short time (up to 3 months) international collaboration, international visiting researchers, and graduate students study abroad, as well as foreign visiting professor and international workshop programs, have been conducted since 2017.

All these facts confirm that ISSP continues to develop successfully and dynamically as the global center of excellence of condensed matter physics and materials science. We appreciate continuous support and cooperation of communities for our activities.

July, 2020

Hatsumi MORI
Director
Institute for Solid State Physics,
The University of Tokyo

Field-Induced Switching of Ferro-Quadrupole Order Parameter in $PrTi_2Al_{20}$

Takigawa, Sakakibara, and Nakatsuji Groups

The series of Pr-based cubic compounds PrT_2X_{20} (T = Ir, Rh, X = Zn; T = V, Ti, X = Al) has been actively studied recently to explore novel phenomena caused by multipoles of 4*f* electrons because the non-Kramers Γ_3 doublet ground states in the crystalline electric field (CEF) has active quadrupole ($O_Z = 3z^2\text{-}r^2$ and $O_X = \sqrt{3}\,(x^2\text{-}y^2)$) and an octupole ($T_{XYZ} = xyz$) moments but no magnetic dipole moment [1]. Among this series, $PrTi_2Al_{20}$ shows the highest transition temperature of 2 K into a simple ferro-ordered state of O_Z quadrupole moment.

We have performed ^{27}Al-NMR and magnetization measurements on high quality single crystals of $PrTi_2Al_{20}$ and unexpectedly observed discontinuous switching of quadrupole order parameter by applying small magnetic fields $\boldsymbol{B}$ of a few tesla along [001] and [110] but not along [111] directions [2]. The symmetry of order parameters for different field directions were determined as shown in Fig. 1. For $\boldsymbol{B}$ along [111], there is a single ordered phase of O_Z type below T_Q = 2.2 K, which is independent of B. Here we expect coexistence of three domains, where the symmetry axis $\boldsymbol{Z}$ of the quadrupole moment points along three equivalent <001> directions. The quadrupole order parameter can be conveniently represented as a two-dimensional vector with O_Z and O_X chosen to be the basis (rightmost panel of Fig. 1) [3]. For example, order parameters of the three domains for $\boldsymbol{B} /\!/ [111]$ is given by $O_Z = 3x^2 - r^2 = -O_Z/2 + \sqrt{3}\,O_X/2$ and $3y^2 - r^2 = -O_Z/2 + \sqrt{3}\,O_X/2$, corresponding to the polar angle of 0 and $\pm 2\pi/\sqrt{3}$.

For $\boldsymbol{B}$ along [001], however, discontinuous jump of the NMR frequency occurs near 2 tesla with a finite range of field where two lines coexist, indicating a first order phase transition (Fig. 2a). From the analysis of NMR spectra and

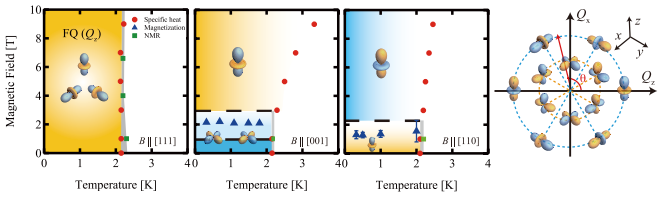

Fig. 1. The temperature vs. magnetic field phase diagram of the ferro-quadrupole order in $PrTi_2Al_{20}$ for B // [111], [001], and [110]. The order parameters are indicated by graphical symbols corresponding to specific values of θ in the order parameter space shown in the rightmost panel. The phase boundaries are determined by the peak of $d(C/T)/dt$, C being the specific heat, splitting of the NMR lines, or kink in the Knight shift. The dashed lines for $\boldsymbol{B} /\!/$ [001] and [110] indicate the region of coexistence of high- and low-field phases. For $\boldsymbol{B} /\!/$ [001] and [110], there is no phase transition but only a crossover as a function of temperature in high fields.

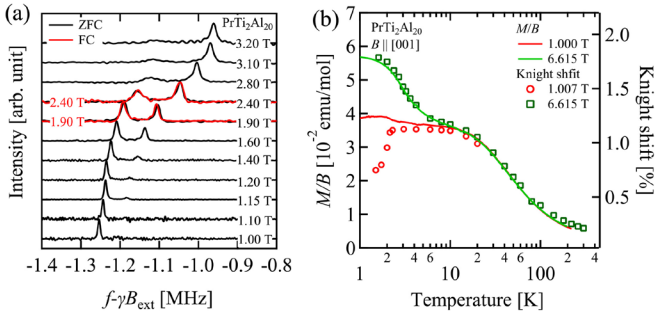

Fig. 2. (a) Magnetic-field dependence of the NMR spectrum (plotted as a function of shift from the nuclear Zeeman frequency) for B // [001] at 1.5 K. (b) The temperature dependences of the Knight shift at low (1T) and high (6.6T) magnetic field along [001] are compared with those of the magnetic susceptibility.

magnetic susceptibility, we conclude that while the high field phase has ferro-order of O_Z with $\boldsymbol{Z} /\!/ \boldsymbol{B}$, the order parameter of the low field phase is closer to O_X type ($\theta \sim \pm\pi/2$). For $\boldsymbol{B}$ along [110], the order parameter changes from O_Z with $\boldsymbol{Z} /\!/ \boldsymbol{B}$ in low fields to $\boldsymbol{Z} \sim -\boldsymbol{B}$ in high fields. The field-induced transition was also confirmed by measurements of heat capacity and magnetocaloric effect [4].

We have developed a Landau theory to identify symmetry allowed interactions between quadrupole and magnetic field, which can account for the experimentally observed switching of the order parameter [2]. Frist, the magnetic field induces mixing between Γ_3 ground doublet and excited CEF levels, leading to the van-Vleck paramagnetism. This anisotropic Zeeman interaction, which is quadratic in $\boldsymbol{B}$, turns out to stabilize the order parameters observed in the high field phases both for $\boldsymbol{B} /\!/ [001]$ and $\boldsymbol{B} /\!/ [110]$, leaving only a crossover as a function of temperature. On the other hand, we found that symmetry allows interaction between quadrupoles on neighboring Pr sites, which is responsible for the ferro-quadrupole order, to depend also quadratically on $\boldsymbol{B}$ for small $\boldsymbol{B}$. This anisotropic interaction competes against the Zeeman interaction and can stabilize the order parameter of the low field phases. Therefore, the observed switching of the order parameter can be explained if the anisotropy of the quadrupole-quadrupole interaction wins the Zeeman interaction at low fields but becomes suppressed at high fields compared with the Zeeman interaction. We have indeed succeeded in reproducing the experimental phase diagram by assuming a non-monotonic field dependence of the anisotropic quadrupole interaction.

Although the mechanism for such a non-trivial field dependence of the quadrupole interaction is not understood yet, anomalous behavior of the NMR Knight shift in the quadrupole ordered states provides an important insight. As shown in Fig. 2(b), the Knight shift at Al sites, which probes the polarization of conduction electron spin, shows the identical temperature dependence to the magnetic susceptibility at a high field (6.6T). At a low field (1T), however, they show remarkable separation below the ordering

temperature, indicating that the hybridization between 4*f* and conduction electrons (*c*-*f* hybridization) is strongly influenced by the quadrupole order. Since the quadrupole-quadrupole interaction is mediated by the *c*-*f* hybridization, this means that the quadrupole order modifies the quadrupole-quadrupole interaction via redistribution of 4*f* charge density, which in turn should affect the order itself. We suspect that such a feedback mechanism may be the key to understand the field-induced discontinuous transition.

References
[1] T. Onimaru and H. Kusunose, J. Phys. Soc. Jpn. **85**, 082002 (2016).
[2] T. Taniguchi *et al.*, J. Phys. Soc. Jpn. **88**, 084707 (2019).
[3] K. Hattori and H. Tsunetsugu, J. Phys. Soc. Jpn. **83**, 034709 (2014).
[4] S. Kittaka *et al.*, J. Phys. Soc. Jpn. **89**, 043701 (2020).

Authors
T. Taniguchi, K. Hattori[a], M. Yoshida, H. Takeda, S. Nakamura, T. Sakakibara, M. Tsujimoto, A. Sakai, Y. Matsumoto, S. Nakatsuji, and M. Takigawa
[a]Tokyo Metropolitan University

Fluctuation-Induced First-Order Transition and Tricritical Point in a Cubic Chiral Magnet EuPtSi

Sakakibara Group

The cubic chiral compound EuPtSi (space group $P2_13$) helimagneitcally orders at T_N=4.0 K with the propagation vector $\boldsymbol{q}_1^*$=(0.2,0.3,0.04). There has been growing interest in this compound because a skyrmion lattice phase with a triple-*q* structure emerges in a magnetic field applied along the [111] direction [1,2]. One of the intriguing features of this compound is that the transition at T_N is of first order [1-3]. We studied the helimagnetic transition on a single crystal of EuPtSi by means of high-precision magnetization measurements, and found that the transition, which is of first order at low fields, becomes of second order at high fields, and there exists a tricritical point (TCP) in the phase diagram [4].

Figure 1 shows the temperature derivative of the magnetization, *dM*/*dT*, in magnetic fields *H* applied along the [110] direction. At *H* = 1.8 kOe, the first-order transition (FOT) is characterized by a sharp peak in *dM*/*dT* at *T* = 4.0 K. By increasing *H*, $T_N(H)$ defined by the peak position in *dM*/*dT* moves to the lower temperature side with a decrease in the peak amplitude. Above *H* = 8.8 kOe, the shape of *dM*/*dT* dramatically changes and excibits a step function like jump at $T_N(H)$, implying that the transition becomes of second order above 8.8 kOe.

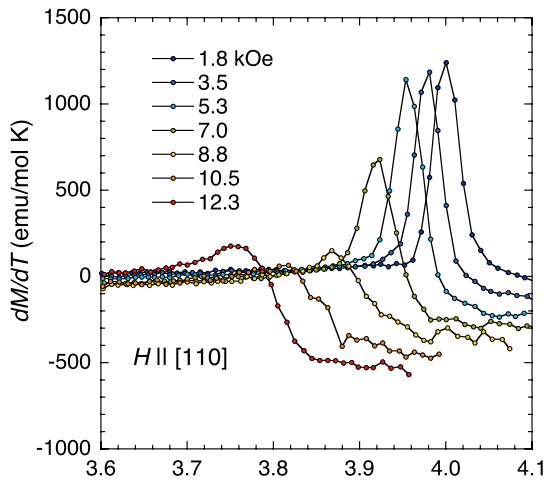

Fig. 1. Temperature derivative of the magnetization *dM*/*dT* of EuPtSi in fields applied along the [110] direction.

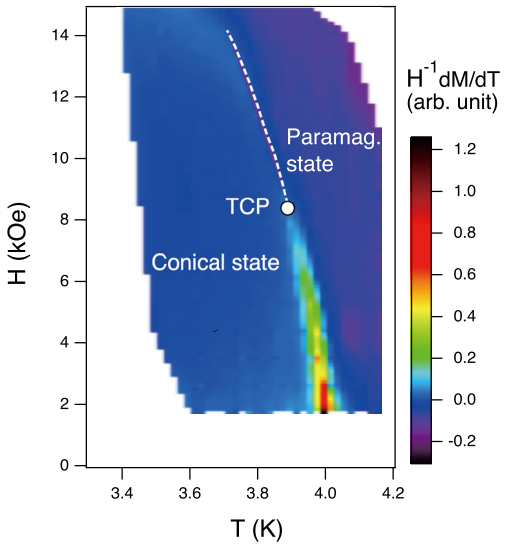

Fig. 2. Phase boundary between the paramagnetic and the single-*q* helical (conical) states of EuPtSi, constructed by colour contour mapping of the *dM*/*dT* data with *H*||[110]. The bright line in low fields indicates the first-order boundary, whereas the dashed line shows the second-order one. TCP denotes the position of the tricritical point.

In order to construct the phase boundary between the paramagnetic and the ordered states, we show in Fig. 2 the color contour mapping of the *dM*/*dT* data for *H*||[110]. The bright line in the low-field region indicates the FOT boundary, and the dashed line in the high-field region denotes the second-order one. In between there is a TCP as indicated in the figure. A similar crossover of the transition has also been observed for [111] and [100] directions [4].

In systems described by order parameters with *n*>4 components, a usual second-order phase transition is avoided due to interactions among critical fluctuations of the order parameters [5]. FOT then takes place when the correlation length exceeds a certain limit, where a discontinuous phase transition occurs to a state energetically favorable. This fluctuation-induced FOT takes place even for systems in which the mean-field theory predicts second-order phase transitions, and the actual transition temperature is suppressed much below the mean-field transition temperature. In EuPtSi, the lattice-symmetry operations on $\boldsymbol{q}_1^*$ yields 12 distinct propagation vectors, which is large enough in number to drive the transition to be first order. Applying a magnetic field reduces the symmetry of the system, and the number of components of the order parameter is effectively decreased, leading to a second-order phase transition. The presence of TCP in the phase diagram in Fig. 2 supports this scenario of a fluctuation-induced FOT in EuPtSi. This situation is favorable for the occurrence of multi-*q* orders such as the skyrmion lattice phase, since they need to be stabilized against a single-*q* helical (or a conical) phase.

References
[1] M. Kakihana *et al.*, J. Phys. Soc. Jpn. **87**, 023701 (2018).
[2] K. Kaneko *et al.*, J. Phys. Soc. Jpn. **88**, 013702 (2019).
[3] D.G. Franco *et al.*, Phys. Rev. B **96**, 014401, (2017).
[4] T. Sakakibara *et al.*, J. Phys. Soc. Jpn. **88**, 093701 (2019).
[5] P. Bak, S. Krinsky and D. Mukamel, Phys. Rev. Lett. **36**, 52 (1976).

Authors
T. Sakakibara, S. Nakamura, S. Kittaka
M. Kakihana[a], M. Hedo[a], T. Nakama[a], and Y. Onuki[a]
[a]University of Ryukyus

Effects of Molecular Dynamics on the Anhydrous Proton Conductivity of Imidazolium Hydrogen Dicarboxylates

Mori Group

Hydrogen (H) is a ubiquitous element, which plays important role in a wide range of fields from the deep underground to the interstellar space, and from inorganic oxides to biosystems. Proton (H^+) migration in solids is one of such extensively studied research topics. Recently, anhydrous organic proton conductors, which can show proton conductivity at above 100 °C without humidification, have attracted scientific interests owing not only to their wide applicability as solid-state electrolytes for fuel cells, but also to their peculiar proton conduction mechanism mediated not by water molecules. However, there have been only a few reports about anhydrous organic proton conductors.

Previously, we investigated the "intrinsic" proton conductivities of imidazolium succinate (= Im-Suc; Fig. 1a) and glutarate (= Im-Glu; Fig. 1b), by single-crystal measurements, and successfully disclosed two key factors for realization of anhydrous proton conductivity: (1) the hydrogen-bond (H-bond) network structures, and (2) difference of the proton donating/accepting abilities between acid and base molecules, i.e., ΔpK_a [1]. In this study, we newly prepared high-quality single crystals of another salt, imidazolium fumarate (Im-Fum; Fig. 1c), in addition to Im-Suc and Im-Glu, and investigated the effect of molecular "dynamics" on the anhydrous proton conductivities of these three salts [2].

Im-Fum has similar 2D H-bond network structure as Im-Suc and Im-Glu (Fig. 1), and showed the anisotropic proton conductivity consistent with the previously disclosed "static" key factors (1) and (2). Interestingly, Im-Fum exhibits linear dependence on the reciprocal temperature in contrast to non-linear dependence in Im-Suc and Im-Glu. We speculated that it is contributed by the imidazolium cation in the 2D H-bond network because the E_a showed quite high values in Im-Suc and Im-Glu similar to the other imidazolium-based salts, and that the molecular orientation of imidazolium cation is different between Im-Fum and the other two. Thus, we investigated the dynamic property of imidazolium cations in these salts by high-temperature X-ray structure analyses and solid-state ^{2}H NMR.

In Im-Suc, a structural transition was observed in X-ray structural analysis at ca. 80 °C, accompanied with the in-plane orientational disorder of imidazolium molecules in one out of two layers. Consistently, the proton conductivity showed abrupt increase at ca. 80 °C, which indicates that the imidazolium libration motion promotes proton conduction in Im-Suc (Fig. 2 upper). On the other hand, no significant

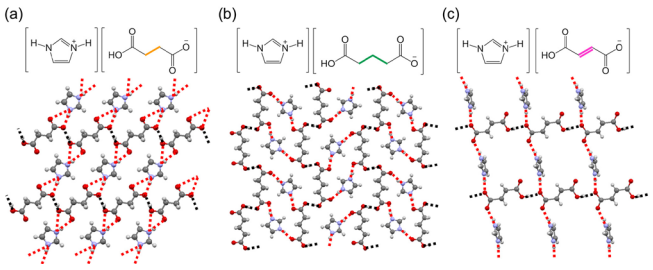

Fig. 1. (upper) Chemical structures and (lower) H-bond network structures of (a) Im-Suc, (b) Im-Glu, and (c) Im-Fum. Red and black dashed lines denote N–H…O and O–H…O H-bonds, respectively.

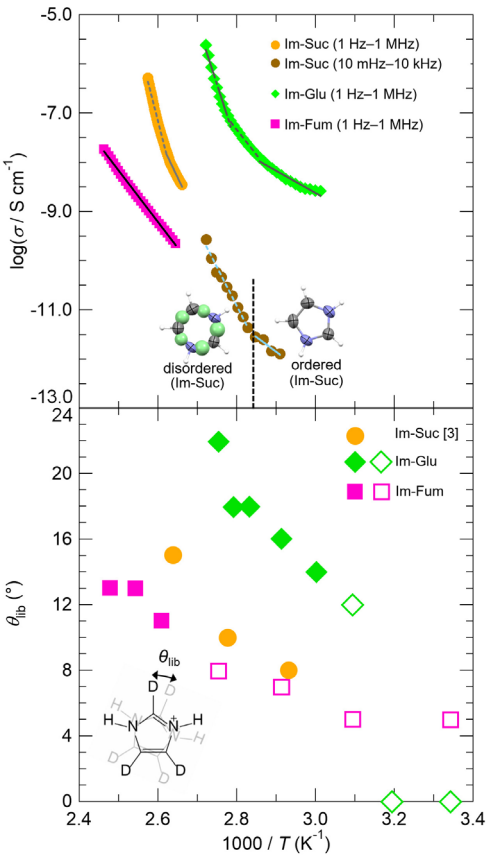

Fig. 2. (upper) The single-crystal proton conductivity (σ) and (lower) libration angle θ_{lib} *vs.* 1000/*T* plots for Im-Suc (orange and dark orange circles), Im-Glu (green diamonds), and Im-Fum (pink squares). In upper graph, the lines denote the Arrhenius fitting, and the inset figures show ordered/disordered imidazolium cation in Im-Suc below/above the transition temperature, ca. 80 °C. In bottom graph, filled circles, diamonds, and squares denote libration angles of Im-Suc (orange)[3], Im-Glu (green), and Im-Fum (pink) in the proton-conducting temperatures, and open markers denote those below proton-conducting temperatures. Inset shows the model for the libration motion of imidazolium cations.

changes were observed for Im-Glu and Im-Fum in X-ray analyses.

Then, in order to investigate the local dynamics of imidazolium cations, we performed the solid-state ^{2}H NMR experiments for Im-Glu and Im-Fum using imidazole-d_3 molecules (Fig. 2 lower inset). By spectral simulations assuming the two-site jump model describing the libration motion of imidazolium molecules, we estimated the librational rates k_{lib} and angles θ_{lib}. Comparing the libration angles θ_{lib} and proton conductivities σ of Im-Glu and Im-Fum together with the reported values of Im-Suc [3], magnitude of θ_{lib} is Im-Glu > Im-Suc > Im-Fum, in consistent with the same relationship of σ. This result clearly indicates that the libration motion of the imidazolium cations promotes proton conduction in these salts.

We consider that this "dynamic" factor synergistically contributes to anhydrous proton conductivity with the already mentioned the "static" factors. Imidazolium molecules lie within the 2D H-bond network in Im-Suc and Im-Glu whereas imidazolium sticks out from the network in Im-Fum (Fig. 1). In former case, directions of libration and proton conduction matches, and the libration can make additional H-bonds or short contacts to promote the proton transfer in the H-bond network, leading to the nonlinear dependence of σ in the Arrhenius plot, whereas it is not for the latter case.

In conclusion, in addition to previously disclosed "static" key factors, (1) H-bond network structures and (2) ΔpK_a between acid and base molecules, we revealed that (3) the molecular "dynamics" is another key factor for realization of anhydrous proton conductivity. These "static" and "dynamic" factors synergistically play important roles, which is thought as peculiar nature of Grotthuss-type conduction in anhydrous solids.

References

[1] Y. Sunairi, A. Ueda, J. Yoshida, K. Suzuki, and H. Mori, J. Phys. Chem. C **122**, 11623 (2018).
[2] Y. Sunairi, S. Dekura, A. Ueda, T. Ida, M. Mizuno, and H. Mori, J. Phys. Soc. Jpn. **89**, 051008 (2020).
[3] T. Umiyama, R. Ohashi, T. Ida, and M. Mizuno, Chem. Lett. **42**, 1323 (2013).

Authors

Y. Sunairi, S. Dekura, A. Ueda[a], T. Ida[b], M. Mizuno[b], and H. Mori
[a]Kumamoto University
[b]Kanazawa University

Topological Properties of τ-Type Organic Conductors

Osada Group

It is desirable that topological phases can be realized in organic molecular crystals with high designability. However, the search for topological states in organic crystals has met with some challenges. Generally, organic molecular crystals have too poor symmetry to protect topological states. The width of their tight-binding band is too narrow to cause the band inversion. Moreover, organic molecules consist of light elements with correspondingly small spin–orbit coupling (SOC). So far, only a few molecular crystals, such as a two-dimensional (2D) Dirac semimetal α-(BEDT-TTF)$_2$I$_3$ and a 3D nodal-line Dirac semimetal Pd(dddt)$_2$, have been studied as topological materials in the field of organic conductors.

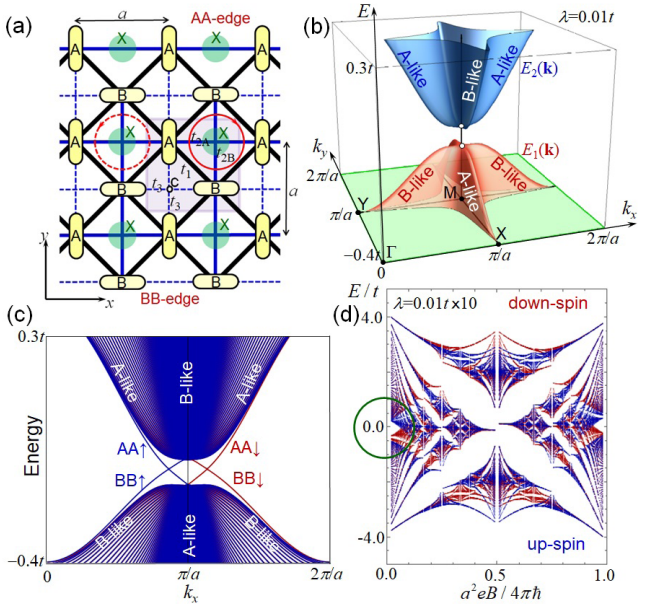

Fig. 1. (a) Schematics of a conducting layer of τ-type organic conductors. A and B indicate donor molecule sites, and X indicates anion sites. (b) Bulk band dispersion of τ-type conductors with finite spin-orbit coupling (SOC). A gap opens at the quadratic band contact point at M. (c) Energy dispersion of the system with finite width. Helical edge states along AA and BB edges appear in the gap. (d) Hofstadter butterfly (energy spectra as a function of magnetic field) of τ-type conductors. Blue and Red patterns correspond to up-spin and down-spin, respectively. The value of SOC is enlarged to see its effect easily.

Here, we demonstrate that the conducting layer of τ-type organic layered conductor, τ-(EDO-S,S-DMEDT-TTF)$_2$X$_{1+y}$ and τ-(P-S,S-DMEDT-TTF)$_2$X$_{1+y}$ (X=AuBr$_2$, I$_3$, IBr$_2$), is a 2D electron system with unique topological properties [1]. On each layer, donor molecules (EDO-S,S-DMEDT-TTF or P-S,S-DMEDT-TTF) form a square lattice, and anion molecules (X) are arranged on it with a checkerboard pattern as shown in Fig. 1(a). This lattice structure is a modification of Mielke's lattice, which is a typical flat band system, so that topological natures of Mielke's lattice are inherited. In addition, rather strong spin-orbit coupling (SOC) can be expected in τ-type conductors, although SOC is generally weak in organic materials. It results from the strong in-plane potential modulation generated by the inorganic anion X. Using a Kane-Mele type model, we discuss possible topological properties of the τ-type organic conductors.

In the absence of SOC, the conduction and valence bands with four-fold rotational symmetry show quadratic band touching. Since the Fermi level is located in the conduction band, the actual τ-type organic conductors (y = 0.75~0.875) have is a star-shaped electron Fermi surface. Under the in-plane uniaxial strain breaking the four-fold symmetry, the band contact point splits into a pair of Dirac cones. This is a kind of Lifshitz transition from a 2D Luttinger semimetal to a 2D Dirac semimetal.

Once the SOC becomes finite, a small gap opens at the band contact point as seen in Fig. 1(b). The product of the valence band parity values at symmetric point (time-reversal invariant momentums) is -1. This fact indicates that the gapped state is a topologically nontrivial insulator with band inversion. In fact, there exists a helical edge state characteristic to the quantum spin Hall insulator (Z_2-topological insulator) along each edge as shown in Fig. 1(c). Therefore, the actual τ-type conductors could be regarded as heavily-doped topological insulators. Since they have finite spin-dependent Berry curvature at the Fermi level, finite spin Hall effect could appear although its experimental detection needs microfabrication of samples.

Because of finite spin-dependent orbital magnetic moment due to SOC, the Landau levels (LLs) have additional spin splitting to the Zeeman effect. Figure 1(d) shows the Hofstadter butterfly of the LLs for each spin subband. Since the Zeeman effect is not included in this figure, the difference of both spin levels indicates the orbital contribution to the spin splitting due to SOC. At the zero-field limit, we can see the Chern number below the SOC gap takes finite values of -1 or +1 depending on the spin. As actual τ-type conductors are doped up to 10% of the conduction band, the orbital contribution to the spin splitting is about several % of the Zeeman splitting, which is possible to detect experimentally in the Shubnikov-de Haas oscillations at low temperature and high magnetic fields.

Reference

[1] T. Osada, J. Phys. Soc. Jpn. **88**, 114707 (2019).

Authors

T. Osada, T. Taen, K. Uchida, M. Sato, and A. Kiswandhi

Nonequilibrium Dynamics in Strongly Correlated Electrons in One Dimension and Clogged Charge Current

Tsunetsugu Group

Understanding nonequilibrium dynamics in strongly correlated systems is an important issue and a big challenge for both theorists and experimentalists. Recently proposed generalized hydrodynamic (GHD) theory [1] succeeds in describing nonequilibrium dynamics in one-dimensional models that are exactly solvable through the Bethe ansatz (BA) equations. Its fundamental degrees of freedom are local distribution function of multiple types of "quasiparticles" corresponding to real roots and complex roots (strings) in the BA equations. These distribution functions evolve in space and time following continuity equations, and these equations include effective velocities that need to be determined self-consistently from the local distribution functions.

We have applied the GHD theory to the one-dimensional Hubbard model and studied quench dynamics with a partitioning protocol [2]. The system is initially divided at the origin $x = 0$ to two semi-infinite parts. The left part is equilibrated at a fixed temperature with half-filling electron density, while the right part is set empty and has no electrons. At time $t = 0$, the two parts are connected and start to evolve. In this case, local physical quantities depend only on the ray $\xi = x/t$, and vary continuously in the transient region $V_L < \xi < V_R$. We have calculated charge and energy densities, $n(\xi)$, $e(\xi)$, and their currents, $j_n(\xi)$, $j_e(\xi)$, and examined the proportionality relation between $j_n(\xi)$ and $j_e(\xi)$. An interesting finding is a phenomenon we named *clogging*. Inside the transition region, there appears at high temperatures a region that has *zero charge current* although nonzero energy current flows. This clogged region locates next to the left part with half-filling electron density. A similar behavior was found for spin current in quantum spin systems [3]. We proved its presence in the infinite temperature limit, and also confirmed by numerical calculations a finite region size, which shrinks with decreasing temperature. In the clogged region, one type of quasiparticles have the same charge as electron and they flow towards the empty side as one expects. This charge current is cancelled by the counterflow carried by other types of quasiparticles that are bound states of multiple electrons. All the types of quasiparticles carry negative energy towards the empty part, thus leading to a nonzero energy current in the clogged region.

The clogging of charge current is an interesting unexpected behavior in nonequilibrium dynamics of strongly correlated electrons in one dimension, and it is worth trying to observe it in experiments.

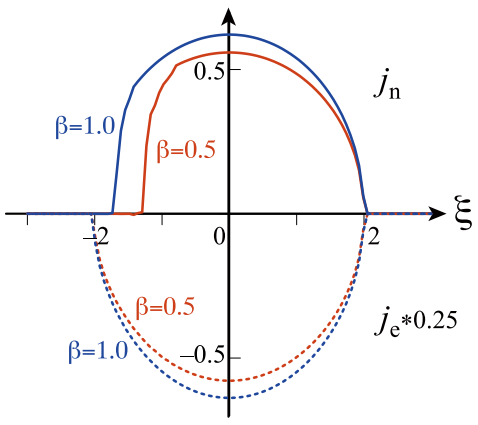

Fig. 1. Profile of charge and energy currents at reciprocal temperature $\beta = 0.5$ and 1.0. Coulomb repulsion is $U = 8$, and energy units are the electron transfer energy. Charge current j_n is normalized by the electron charge –|e|.

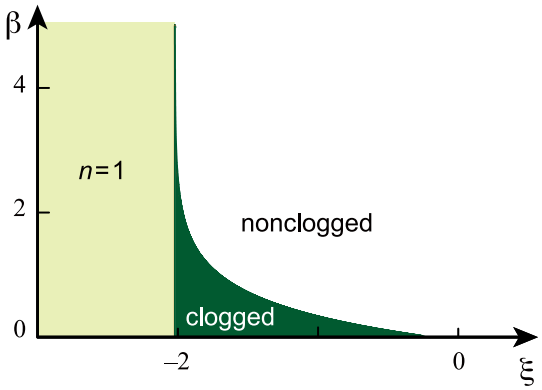

Fig. 2. Change of clogged region with reciprocal temperature β at U=8.

References

[1] O.A. Castro-Alvaredo, *et al.*, Phys. Rev. X **6**, 041065 (2016); B. Bertini *et al.*, Phys. Rev. Lett. **117**, 207201 (2016).
[2] Y. Nozawa and H. Tsunetsugu, Phys. Rev. B **101**, 035121 (2020).
[3] L. Piroli *et al.*, Phys. Rev. B **96**, 115124 (2017).

Authors

H. Tsunetsugu and Y. Nozawa

High-Harmonic Generation in Solids

Kato Group

Recently, high-harmonic generation (HHG) in solids has been experimentally observed. In contrast to that of the gaseous media, solids have the vastly diverse nature such as in their band structures, energy gaps, crystalline anisotropy, magnetism, and so on. Thus, HHG shows various properties depending on the materials, and clarifying the universal properties of HHG in solids should be needed to progress the high-intensity optical technology.

Based on this motivation, we have theoretically investigated HHG mechanism in solids. In Ref. [1] and [2], we have shown that the HHG mechanism can be classified into three regimes depending on the field intensity: (i) the multiphoton absorption regime, (ii) ac Zener regime, and (iii) semimetal regime. This consideration enables us to predict that HHG in graphene would show unique properties in its ellipticity dependence, and this was identified in the experiment [3]. In this consideration, a concept of the field-induced dynamic band structure is essential to gaining a full understanding of extreme nonlinear optics in solids. Although fundamental mechanisms of HHG in solids have already been revealed [3], the connection between HHG and other high-field phenomena, such as the dynamical Franz-Keldysh effect, above-threshold ionization, and dynamical localization has

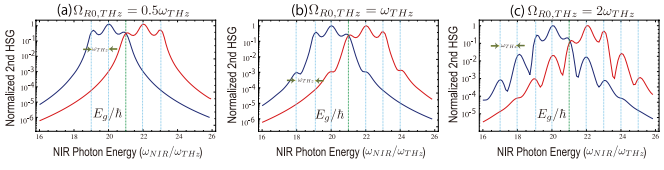

Fig. 1. NIR frequency dependence of 2nd HSG for $E_g = 21\omega_{THz}$ in the case of (a) $\Omega_{THz} = 0.5\omega_{THz}$, (b) $\Omega_{THz} = \omega_{THz}$, and (c) $\Omega_{THz} = 2\omega_{THz}$. The blue and red lines indicate positive and negative 2nd HSG, respectively.

not been clarified yet. It appears that HHG and these optical phenomena are different aspects of the same electron interaction with the strong light field. We tried to clarify the relation between HHG and these phenomena, by supposing the pump-probe spectroscopy where weak near infrared (NIR) and strong terahertz (THz) light are simultaneously imposed.

The weak NIR and strong THz lights induce the high-order sideband generation (HSG), which changes depending on the THz intensity and NIR frequency. These changes are considered as a probe of the modified states of solids under strong THz light irradiation. Figures 1 (a)-(c) show the intensities of 2nd positive and negative HSG as a function of NIR frequency (ω_{NIR}) for different THz intensities (Ω_{THz}). These figures indicate that with increasing the THz intensities, more peaks at different frequencies of ω_{THz} become visible, which reflects the modified state of the system has new energy levels around the band-gap energy. By an analytical consideration, we have shown that these energy levels (subbands) are derived from a concept of the field-induced dynamic band structure, as shown in Fig. 2(a). We have also shown that kth Bessel function, $\Omega_{\mathrm{THz}}J_k(\Omega_{\mathrm{THz}}/\omega_{\mathrm{THz}})$, effectively describes mixing matrix elements between the kth subband and the valence band, which can be used for a rough estimate of the transition amplitude. This presumption could be identified by numerical calculation, as shown in Fig. 2(b), where the positive 2nd HSG resonates to subbands with their energy levels $E_g = 20\omega_{\mathrm{THz}}$, $E_g = 19\omega_{\mathrm{THz}}$, and $E_g = 18\omega_{\mathrm{THz}}$, respectively (see Fig. 2(a)). These non-monotonic properties are generally confirmed in other high-field phenomena such as the dynamical Franz-Keldysh effect and dynamical localization. Thus, we could clarify the relationship between HHG and other high-field phenomena and suggest a new experiment for identifying oscillatory behavior that would be observed in field-intensity dependence of HHG in solids [5].

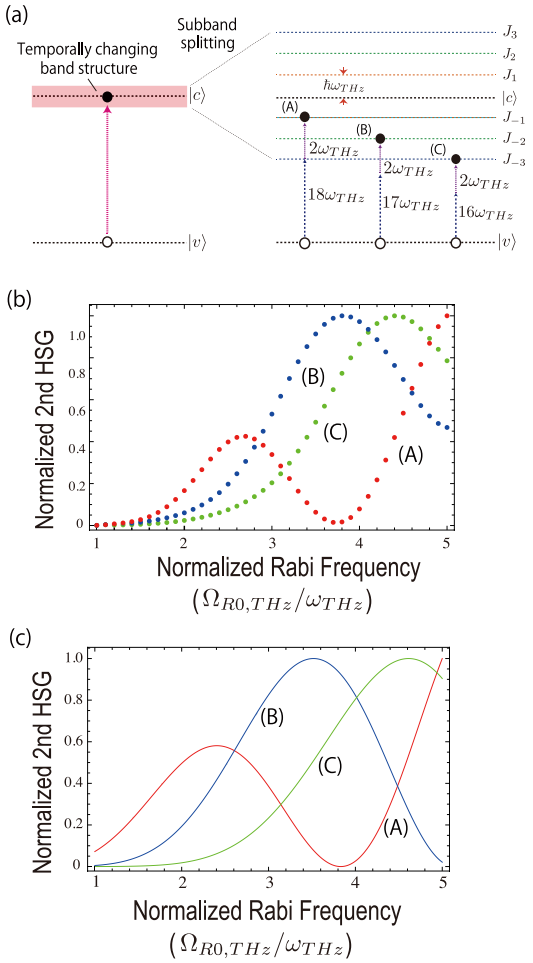

Fig. 2. (a) Schematic diagram of the subband picture originating from temporally changing band structure. (b) Numerical results of positive 2nd HSG as a function of $\Omega_{\mathrm{THz}}/\omega_{\mathrm{THz}}$. Here, the red, blue, and green dots indicate (A) $\omega_{\mathrm{NIR}} = 18\omega_{\mathrm{THz}}$, (B) $\omega_{\mathrm{NIR}} = 17\omega_{\mathrm{THz}}$, and (C) $\omega_{\mathrm{NIR}} = 16\omega_{\mathrm{THz}}$, respectively, whose processes are illustrated in (a). Inset figure: Analytic results of 2nd HSG as a function of $\Omega_{\mathrm{THz}}/\omega_{\mathrm{THz}}$. The red, blue, and green lines show $|xJ_{-1}(x)|^2$, $|xJ_{-2}(x)|^2$, and $|xJ_{-3}(x)|^2$, respectively, where $x = \Omega_{\mathrm{THz}}/\omega_{\mathrm{THz}}$.

References

[1] T. Tamaya *et al*., Phys. Rev. Lett. **116**, 016601 (2016).
[2] T. Tamaya *et al*., Phys. Rev. B **94**, 241107(R) (2016).
[3] N. Yoshikawa, T. Tamaya, and K. Tanaka, Science **356**, 736 (2017).
[4] T. Tamaya and T. Kato, Phys. Rev. B **100**, 081203(R) (2019).
[5] P. Xia*, T. Tamaya*, C. Kim, F. Lu, T. Kanai, N. Ishii, J. Itatani, H. Akiyama, and T. Kato: arXiv:2004.04492. (*equally contributed)

Authors
T. Tamaya and T. Kato

Electric Control of Flying Qubit on Quantum Hall Edge Channels

Katsumoto Group

For composing a quantum circuit with electron spins, "flying qubits" (FQs) are used for transferring quantum information between qubit clusters. A simple realization of FQ is an electron wave packet, which brings 1 qubit information as its spin. In a flight process, quantum decoherence, *i.e.* loss of information should be avoided, and also a unitary operation on the FQ is desirable. In the quantum Hall effect one-dimensional channels are formed at the sample edges (quantum Hall edge channel, QHEC) and the quantum coherence of electronic states on them are robust against disturbances from the environment. Also when the magnetic

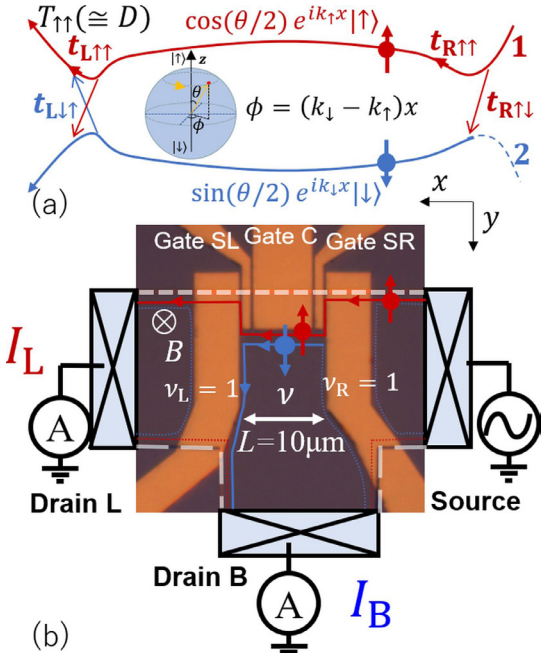

Fig. 1. (a) Schematic diagram of unitary operation on an electron spin flying qubit. An FQ is injected to channel-1 and some portion of the wave packet tunnels into channel-2 with down spin (gaining of zenith angle.) During the travel, the FQ gains azimuth angle via the difference in the kinetic phase. The spin state is detected as the overall transmission amplitude. (b) Optical micrograph of metallic gates (regions with orange color) configuration fabricated on a 2DES. Edge conduction channels and measurement circuits are illustrated and superposed.

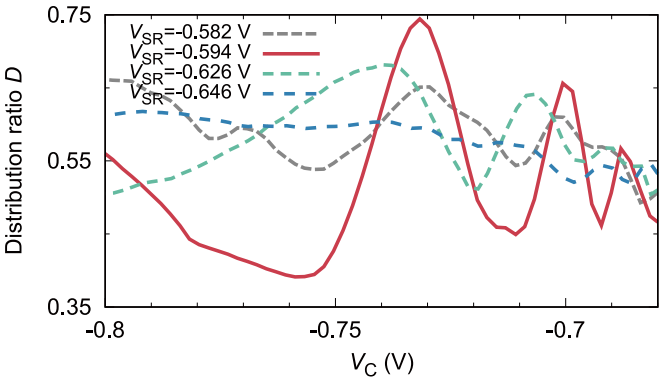

Fig. 2. Current distribution ratio to drain L, which is equal to the overall transmission coefficient of channel-1 in Fig.1(b) as a function of center gate voltage.

field is strong enough, the electronic states of QHECs are spin-polarized due to the Zeeman energy and the exchange effect (quantum Hall ferromagnet). Hence in a spin up and down pair of QHEC, the spin and orbital degrees of freedom are quantum mechanically entangled. If one can separate an electron wave packet into two QHECs in such a pair, operations on the orbitals readily change the spin states. For example, spin precession can be realized through the Aharonov-Bohm (AB) interference. Here we report unitary operation of FQs on QHECs by using non-adiabatic inter edge channel tunneling.

Figure 1(a) shows the scheme of the unitary operation. From the right end, an electron wave packet with up spin is injected into QHEC-1 and experiences partial inter-edge tunneling to QHEC-2, which corresponds to a gain of zenith angle in electron. During the travel to the left crossing, a phase difference is given, which corresponds to an azimuth angle rotation. The partition rate to QHEC-1 reflects both zenith and azimuth angles. We realized such quantum interference circuits on semiconductor (AlGaAs/GaAs) two-dimensional system (2DES) and micro-fabricated Schottky gates on it. In Fig.1(b), we illustrate the channels for FQs, the terminals and measurement circuits superposed on an optical micrograph of the sample gate configuration on a 2DES. The first crossing point is realized by Gate SR as a sharp corner, where inter edge tunneling is caused by spin-orbit interaction. The phase difference between QHEC-1 and 2 is developed during the travel along the down edges of Gate SR, C and SL. This process corresponds to the precession of the spin around the zenith axis (z-axis). At the left end of the device, the two QHEC are intermixed again and the total transmission rate to the electrode L reflects both zenith and azimuth angles.

In Fig. 2, we plot the current partition ratio (distribution ratio, D) to drain L as a function of the gate voltage applied to gate C (V_C). The parameter is the gate voltage applied to gate SR (V_{SR}). A large oscillation versus V_C is visible and the amplitude strongly depends on V_{SR}. The oscillation is a consequence of interference in kinetic phases of QHEC-1 and 2, or equivalently precession of electron spin (azimuth angle rotation) [1]. Here V_C is changing the distance between the two channels. The amplitude depends on the zenith angle of the spin, and should be largest making the visibility 100%, when the spin is in xy-plane. Hence from the amplitude we can deduce the zenith angle, *e.g.* 14 degree for V_{SR}= -0.549 V.

From the above, we conclude that unitary operation on electron spin FQ can be done electrically by using spin-polarized QHEC.

Reference
[1] T. Nakajima, K. T. Lin, and S. Komiyama, AIP Conf. Proc. **1566**, 301 (2013).

Authors
T. Shimizu, Y. Hashimoto, A. Endo, T. Nakamura, and S. Katsumoto

Spin Excitations Propagation Dynamics along Skyrmion Strings

Otani Group

Magnetic skyrmions, topological solitons characterized by a two-dimensional swirling spin texture, have recently attracted attention as stable particle-like objects. In three-dimensional systems, the skyrmion can form a string structure by extending in the third dimension, which consists of the uniform stacking of two-dimensional skyrmions along the string direction. Skyrmion strings can be considered as an analog of the vortex line in a superfluid, type-II superconductors, and trapped dilute-gas Bose-Einstein condensates or the cosmic string in the universe. They are all flexible, and some of these strings are proposed to host a resonant oscillation mode propagating through the string path. This implies the possible coherent signal transfer along skyrmion strings, whereas the propagation character of their excitations has rarely been investigated before.

Experimentally, such skyrmion strings appear in a series of bulk magnets with chiral cubic atomic lattice. The examples are metallic B20 or β-Mn-type Co-Zn-Mn alloys and insulating Cu_2OSeO_3, the latter of which is the target of this work. In these materials, the Dzyaloshinskii–Moriya (DM) interaction is the key to the skyrmion formation. For a limited temperature range, these compounds host a hexagonal lattice of skyrmion strings aligned along the static magnetic field (H) direction. This skyrmion crystal (SkX) phase is predicted to host three distinctive magnetic resonance modes (Fig. 1a–c), i.e., the counter-clockwise (CCW) and clockwise (CW) rotational modes both excited by an oscillating magnetic field $H^{\nu} \perp H$, as well as the breathing (B) mode excited by $H^{\nu} /\!/ H$, which have

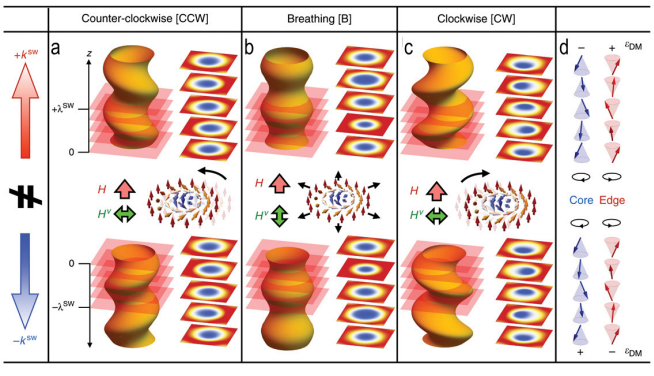

Fig. 1. **a-c** Schematic illustration of CCW, breathing, and CW excitation modes on skyrmion strings. The central part represents the local oscillation manner of skyrmion at the $z = 0$ plane. The upper and lower parts are the snapshot images describing how the spin excitation launched at $z = 0$ propagates on the skyrmion strings, along the $\pm z$ direction parallel and antiparallel to H, respectively. The cross-sectional images describing the size and position of skyrmion at selected z-planes (shown by red layers) are also indicated. **d** The direction of the local magnetic moment at the core and edge position of skyrmion in each z layer. Black rounded arrows denote the sense of local moment precession in the time domain, and ± symbols indicate the sign of local Dzyaloshinskii-Moriya interaction energy gain ϵDM.

recently been identified by magnetic resonance experiments. However, these previous works mostly focused on the character of non-propagating uniform excitations with wave number $k^{SW} = 0$. To understand their propagation character, the employment of a different experimental approach sensitive to the $k^{SW} \neq 0$ regime, as well as the theoretical identification of their dispersion relation, is essential.

In the present study, we experimentally demonstrate the coherent propagation of spin excitations along skyrmion strings for the chiral-lattice magnet Cu_2OSeO_3. We find that the counter-propagating spin excitations show different propagation behavior, and the degree of non-reciprocity, as well as the associated group velocity and decay length, are strongly dependent on the character of the excitation modes. Our theoretically calculated dispersion relations well reproduce these experimental features. The observed decay lengths exceed 50 μm, reflecting the excellent long-range order of the skyrmion-string structure. The present results revealed the peculiar propagation dynamics of skyrmion-string excitations and suggest that skyrmion string can be an excellent medium for magnon transport with unique functionalities. Our combined experimental and theoretical analyses offer a comprehensive account of the propagation dynamics of skyrmion-string excitations and suggest the possibility of unidirectional information transfer along such topologically protected strings.

Reference

[1] S. Seki, M. Garst, J. Waizner, R. Takagi, N. D. Khanh, Y. Okamura, K. Kondou, F. Kagawa, Y. Otani, and Y. Tokura, Nat. Commun. **11**, 256 (2020).

Authors

S. Seki[a,b,c], M. Garst[d], J. Waizner[e], R. Takagi[a,b], N. D. Khanh[b], Y. Okamura[a], K. Kondou[b], F. Kagawa[a,b], Y. Otani and Y. Tokura[a,b]

[a]The University of Tokyo

[b]RIKEN Center for Emergent Matter Science (CEMS)

[c]PRESTO, Japan Science and Technology Agency (JST)

[d]Institut für Theoretische Festkörperphysik, Karlsruher Institut für Technologie

[e]Institut für Theoretische Physik, Universität zu Köln

Creation of Magnetic Skyrmions by Surface Acoustic Waves

Otani Group

Non-collinear and non-coplanar spin textures, such as chiral domain walls and helical or triangular spin structures, bring about diverse functionalities. Among them, magnetic skyrmions, particle-like non-coplanar topological spin structures characterized by a non-zero integer topological charge called the skyrmion number (N_{sk}), have great potential for various spintronic applications, such as energy-saving, non-volatile memory, and non-von Neumann devices. Current pulses can nucleate skyrmion in thin-film samples but require relatively large current densities, which probably causes Joule heating. Moreover, skyrmion creation is localized at a specific position in the film, depending on the sample design. Here, we experimentally demonstrate an approach to skyrmion creation employing surface acoustic waves (SAWs); in asymmetric multilayers of Pt/Co/Ir, propagating SAWs induce skyrmions in a wide area of the magnetic film (Fig. 1a,b). We use multilayer films of Pt/Co/Ir in which the formation of thermodynamically stable skyrmions has already been well-studied in previous

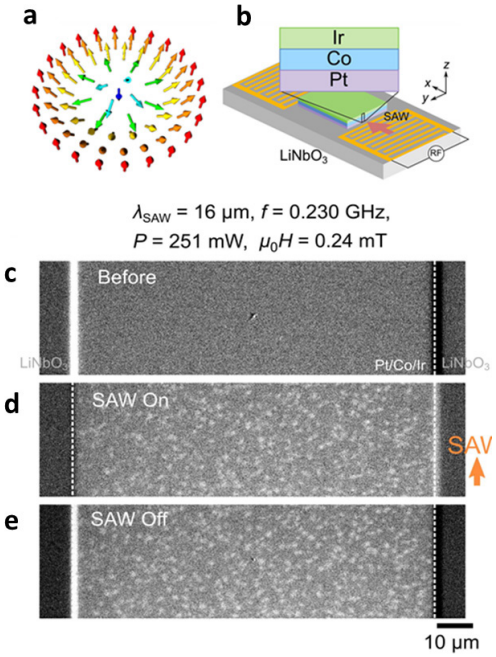

Fig. 1. **a**, Schematic spin configuration of Néel skyrmion. **b**, Schematic illustration of the device structure. Pt/Co/Ir films are deposited on LiNbO3 substrates, and interdigital transducers (IDTs) are fabricated on both sides of a rectangular-shaped Pt/Co/Ir film. Surface acoustic waves (SAWs) are excited by applying radio-frequency (RF) voltage to IDTs. **c-e**, Polar Kerr images before (a), during (b), and after (c) exciting a propagating surface acoustic wave (SAW) with the wavelength (λ_{SAW}) of 16 μm by applying radio-frequency (RF) voltage with the power (P) of 251 mW. The white dashed lines represent the boundaries between Pt/Co/Ir film and LiNbO3 substrate. The orange arrow represents the propagation direction of SAW.

research. All measurements were performed at room temperature, and the magnetic field (H) was applied perpendicular to the film plane. Firstly, we determined, from magnetic images taken before and after the application of SAWs at various H, the magnetic field H_{sk} at which skyrmions begin to appear in the ferromagnetic state without SAWs. The magnetic field evolution of polar Kerr images in a Pt/Co/Ir film with the nominal Co thickness of d_{Co} = 0.55 nm shows that maze domains firstly appear at $\mu_0 H$ = 0.01 mT and transforms to thermodynamically stable skyrmions 3 μm in diameter at 0.21 mT. A further increase in H makes the skyrmions annihilate and leads to the ferromagnetic state at $\mu_0 H$ = 0.31 mT. Here, we note that the size of the observed skyrmions is relatively large, indicating that the dipole-dipole interaction plays an essential role in their stabilization, in addition to the interfacial DMI, and these types of skyrmion are sometimes called a 'skyrmion bubble'.

Figures 1c–e represent the magnetic images before and during excitation by the propagating SAWs. Before exciting with SAWs, we observe no magnetic contrast (Fig. 1c), which indicates that the sample is in the single-domain ferromagnetic state. When the SAW is continuously excited, skyrmions appear (Fig. 1d); skyrmions are nucleated over almost the whole region of a rectangular-shaped Pt/Co/Ir film of width 100 μm and length 400 μm because of the long propagation length of the SAWs. Even after turning off the SAW, most of the skyrmions survive, indicating the emergence of metastable skyrmions (Fig. 1e). The density (n_{sk}) of the nucleated skyrmions in the ferromagnetic state gradually increases with RF power above the threshold of P = 100 mW (Fig. 2a). When H is close to H_{sk}, the number of skyrmions dramatically increases after exciting with SAWs. Besides, when the skyrmions coexist with the ferromagnetic state before exciting with SAWs, that is, $H < H_{sk}$, skyrmions

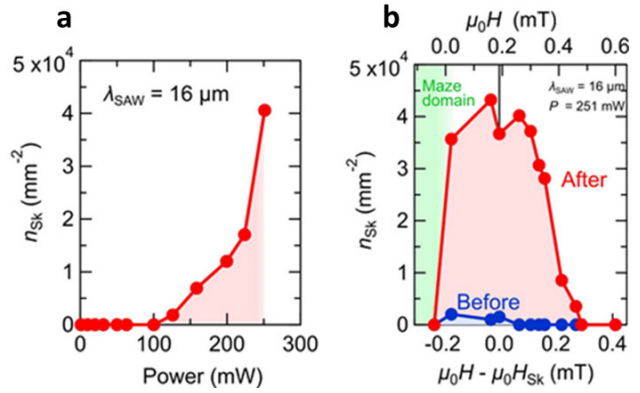

Fig. 2. **a**, Density of skyrmions (n_{sk}) as a function of the power of the RF signal that excites the SAWs. **b**, Magnetic field dependence of n_{sk} before and after exciting a SAW with λ_{SAW} = 16 μm and P = 251 mW.

are also created. The value of n_{sk} after exciting with SAWs is much larger than that before exciting with SAWs (Fig. 2b). In contrast, skyrmions cannot be created in the high field region. This is probably because, in the high field region, the energetically stable ferromagnetic state cannot accommodate skyrmions due to the gain in Zeeman energy, even when SAWs are excited.

Micromagnetic simulations reveal that inhomogeneous torque arising from both SAWs and thermal fluctuations creates magnetic textures, with pair structures consisting of a Néel skyrmion like and an antiskyrmion-like structure. Subsequently, such pairs transform into a Néel skyrmion due to the instability of the antiskyrmion-like structure in a system with interfacial Dzyaloshinskii–Moriya interaction. Our findings provide a tool for efficient manipulation of topological spin objects without heat dissipation and over large areas, given that the propagation length of SAWs is of the order of millimeters.

Reference

[1] T. Yokouchi, S. Sugimoto, B. Rana, S. Seki, N. Ogawa, S. Kasai, and Y. Otani, Nat. Nanotechnol. **15**, 361 (2020).

Authors
T. Yokouchi[a], S. Sugimoto[b], B. Rana[a], S. Seki[a,c,d], N. Ogawa[a,c], S. Kasaia[b,c] and Y. Otani
[a]RIKEN Center for Emergent Matter Science (CEMS)
[b]National Institute for Materials Science (NIMS)
[c]PRESTO, Japan Science and Technology Agency (JST)
[d]The University of Tokyo

Large Magnetic Anisotropy of $L1_0$ Ultrathin Film Grown by Nitrogen-surfactant Epitaxy

Komori Group

For the development of useful magnetic materials, important are uniaxial magnetic anisotropy with high magnetic moment, coercivity, and transition temperature. Moreover, for their wide use, rare-element free materials are strongly required. One of the excellent candidates of such magnetic materials is $L1_0$ FeNi with large uniaxial anisotropy energy, K_u, up to 1.3 MJm^{-3}. While its single crystal cannot be prepared by conventional macroscopic crystal growth, the single-crystal films have been fabricated by layer-by-layer epitaxial growth on Cu(001) and other substrates in a vacuum. The K_u values of the films are, however, lower than the above ideal one. Thus, the magnetic anisotropy perpendicular to the film has not been realized because the in-plane film shape anisotropy is larger than the magnetocrystalline anisotropy. The limitation in the epitaxial films has been attributed to the imperfect atomic layer-by-layer mode in the alternative deposition process of Fe and Ni atoms and the intermixing of the two elements at the interface.

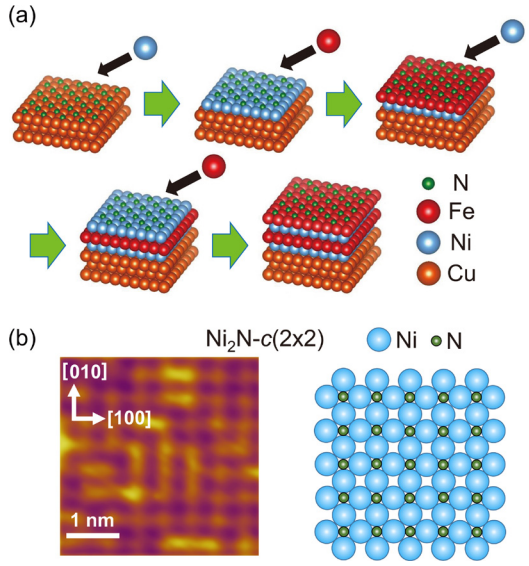

Fig. 1. (a) Schematic model of an FeN/Ni/Fe/Ni film formation process on Cu(001) by surfactant epitaxy using N atoms. First, monolayer c(2x2) Ni_2N is formed on Cu(001) surface as shown in (b) by N adsorption and Ni deposition. Then, 1-ML Fe is deposited below 150 K. After annealing above 300 K, N atoms segregate to the Fe surface and Fe_2N monolayer is formed. Next, on top of this surface, 1-ML Ni is deposited below 150 K. By repeating deposition and annealing, the $L1_0$ FeNi film is prepared. (b) STM image of a Ni_2N atomic layer on Cu(001) (left) and its ball model (right). The 0.5-ML N form c(2x2) structure with 1x1 Ni atoms [1].

We have demonstrated significant improvement of the uniaxial magnetic anisotropy of an $L1_0$ FeNi epitaxial film prepared by surfactant epitaxy of Fe and Ni atomic layers using nitrogen (N) atoms and the deposition on a cooled Cu(001) substrate [1]. The N-surfactant epitaxy, that is, successive and selected segregation of the N atoms to the surface during the alternate Fe and Ni monolayer

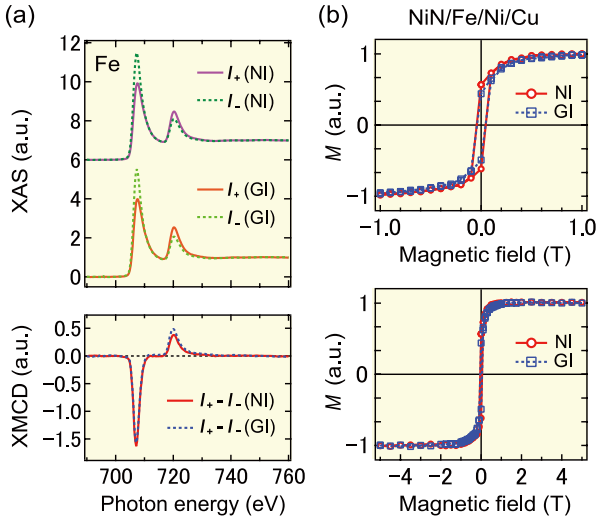

Fig. 2. (a) Fe L-edge XAS (upper) and XMCD (lower) spectra of the NiN/Fe/Ni trilayer for the NI and GI geometries. In the NI (GI) geometry, the magnetic field direction is 0° (55°) off from the surface normal to the [100] direction of the Cu(001) substrate. The XAS intensity was measured with the photon helicity parallel (I_+) and antiparallel (I_-) to the external magnetic field of 5 T at 8 K. (b) Narrow- (upper) and wide- (lower) range Fe magnetization (M) curves of the NiN/Fe/Ni trilayer [1].

(ML) deposition in the present case, suppresses the mixing between Fe and Ni atoms during the deposition and annealing. The schema is given in Fig. 1(a). It was previously shown on the N-adsorbed Cu(001) substrate that N atoms segregate to the surface during the Fe and Co deposition without mixing between the deposited metal and the substrate Cu atoms [2]. This is quite in contrast to the mixing during the deposition of magnetic transition metals on the same substrate [3]. Sharp interface between the atomic layers of Fe and Ni in the film is ensured by the present method. A monatomic layer is grown on the cooled substrate while bilayer islands are formed at room temperature. Satisfactory growth of the $L1_0$ FeNi films up to four monolayers was confirmed after post-annealing process at 430 K by *in-situ* X-ray photoelectron spectroscopy, scanning tunneling microscopy and low energy electron diffraction. Magnetic properties were studied using element-specific soft-X-ray magnetic circular dichroism (XMCD). The value of Fe $L_{2,3}$ XMCD is an order of magnitude larger than that of Ni $L_{2,3}$ XMCD, and thus the Fe monolayer dominates the magnetism of the film. The results of the NiN/Fe/Ni trilayer are shown in Fig. 2. The Fe hysteresis curve measured at 8 K indicates the out-of-plane magnetocrystalline anisotropy is large enough for overcoming the in-plane film shape anisotropy. According to the XMCD sum rule analyses, both Fe and Ni magnetic moments increase with increasing the thickness of the FeNi film.

References

[1] K. Kawaguchi *et al.*, Phys. Rev. Material **4**, 054403 (2020).
[2] D. Sekiba *et al.*, Surf. Sci. **590**, 138 (2005).
[3] H. L. Meyerheim *et al.*, Phys. Rev. B **71**, 035409 (2005).

Authors

K. Kawaguchi,T. Miyamachi, T. Iimori, Y. Takahashi, T. Hattori, T. Yokoyama[a], M. Kotsugi[b], and F. Komori
[a]Institute for Molecular Science
[b]Tokyo University of Science

Enhanced Critical Magnetic Field for Mono-Layer Superconductor by Step Confinement

Hasegawa Group

In a usual superconductor, electrons that have opposite momentum are bound to form a Cooper pair. Under magnetic fields, the pairs lose their stability as the field exerts forces that unbalance the electrons' momenta. Since breaking the pairs costs an energy, however, superconductivity survives up to a certain magnetic field. Enhancing the robustness against magnetic field is technically important, *e.g.* for generating high magnetic fields. In the case of thin films, superconductivity is naturally robust against the in-plane magnetic field because the above-mentioned orbital breaking mechanism is suppressed due to the geometrical limitation. It would therefore be an impact if one finds approaches that make them robust against magnetic fields in other directions. We report here that for a single atomic layer superconductor narrowing terraces by steps improves the tolerance against the out-of-plane magnetic field.

Here as a monolayer (ML) superconductor, we used a Pb-induced reconstructed structure, $\sqrt{3} \times \sqrt{43}$ Pb/Si(111), whose nominal Pb coverage is 1.23 ML. An STM image and a tunneling spectrum taken on the structure at 0.4 K

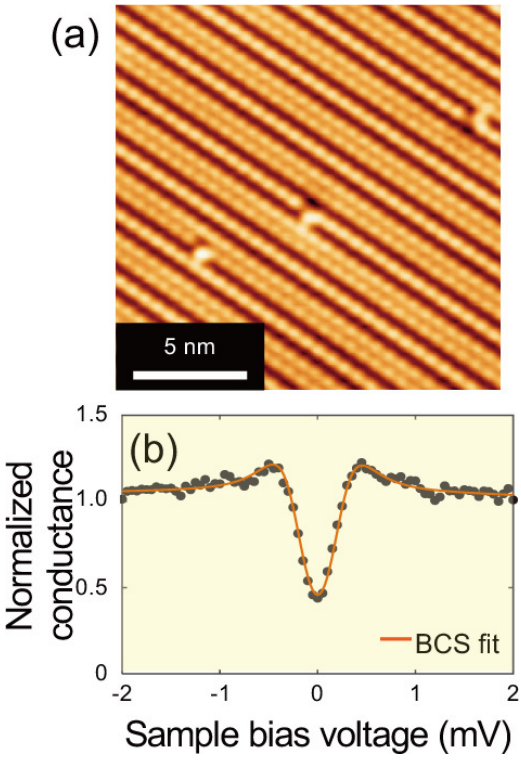

Fig. 1. (a) Atomically resolved image and (b) tunneling conductance spectrum taken on the $\sqrt{3} \times \sqrt{43}$ Pb/Si(111) structure at 0.4 K.

are presented in Fig. 1. From a fitting of the spectrum with the Dynes function, whose curve is drawn with a red line in Fig. 1(b), we found the gap is 0.28 meV. Figures 2(a) show an STM image taken in a wider area (1μm×1μm). The whole surface is covered with the $\sqrt{3} \times \sqrt{43}$ phase including the area close to the step edges. In the same area as Fig. 2(a), we have taken spatial mappings of tunneling conductance at zero bias voltage (ZBC: zero bias conductance), which corresponds to the minimum conductance in the superconducting gap, under various out-of-plane magnetic fields. The amount of the magnetic field ranges from 0 to 400 mT, as shown in Figs. 2(b-h). The ZBC mapping taken under zero field (Fig. 2(b)) demonstrates almost uniform distribution of the deep gaps (low ZBC value) over the entire surface, indicting uniform superconductivity including the area of steps. The steps do not locally break the superconductivity of the ML Pb structure.

When the out-of-plane magnetic fields of 30-100 mT (Figs. 2(c-f)) are applied, several round protrusions of high-ZBC (light green) area are observed. The size of the protrusion is mostly uniform and the diameter is ~100 nm.

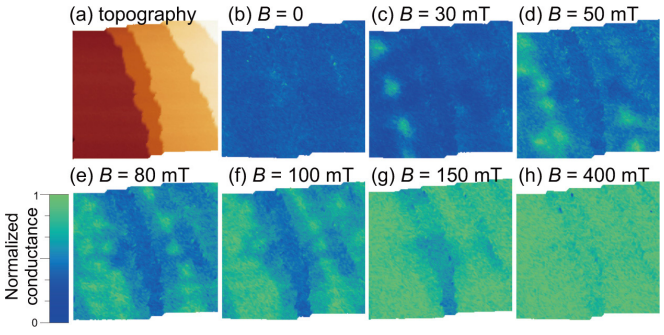

Fig. 2. (a) STM image of $\sqrt{3} \times \sqrt{43}$ Pb/Si(111). (b-h) zero bias conductance mappings in the same field of view with (a) taken under the out-of-plane magnetic field of 0, 30 mT, 50 mT, 80 mT, 100 mT, 150 mT, and 400 mT, respectively.

The number of the protrusions increases with the magnetic field, and the ZBC value at the center of the protrusions is almost same as the saturated ZBC measured at high magnetic fields (*e.g.* 400 mT of Fig. 2(h)). These features lead us to identify these protrusions as a vortex. We noticed in the mapping of 80 and 100 mT (Figs. 2(e, f)) that the vortices are formed only around the middle of wide terraces, apparently repelled from the step edges. In a narrow terrace that is observed vertically around the center of the images, no vortices are found. The apparent repelling of vortices by step edges can be explained with the presence of Josephson vortices at the step edges [1]. A Josephson vortex, formed at a Josephson junction, has an extended core along the junction with suppressed breaking of superconductivity, and therefore appeared dark (blue) along the junction, that is, along the step edges in our case. Since all the vortices including Josephson's exhibit repulsive interaction with each other, the conventional vortices seem repelled from the step edges.

In parallel with the vortex formation, the amount of ZBC behind the vortices gradually increases with the applied magnetic field. At 150 mT (Fig. 2(g)), the vortices almost lose their contrast with the background, which signals saturation of ZBC. Strikingly, in the narrow terrace, ZBC is still low, clearly demonstrating suppression of the superconductivity breaking there. In order to break the superconductivity of the narrow terrace, further increase in the magnetic field was required up to 400 mT (Fig. 2(h)), where all the area reached the saturated ZBC value. The spatially resolved ZBC evolution presented in Fig. 2 clearly demonstrates that the field that makes ZBC saturated, which corresponds to the critical magnetic field, is larger in the narrow terrace than the wide terraces.

From the ZBC evolutions we then investigated how the critical field (H_{c2}) depends on the terrace width w. For the quantitative analysis we first estimated H_{c2} at various sites by measuring the amount of the out-of-plane magnetic field that saturates ZBC, and then dependence of the estimated H_{c2} on terrace width w was investigated. Our analysis indicated a clear crossover around w = 200 nm; for w > 200 nm H_{c2} is constant whereas for w < 200 nm H_{c2} increases steeply with the reduction in w.

According to the Ginzburg-Landau (GL) equation, H_{c2} of low dimensional superconductors whose cross-section is narrower than $2\sqrt{2}\xi$ is given by a formula of $H_{c2} = 4\phi_0/\pi w^2$, where w is the width (the length of short side) of the cross-section and ϕ_0 is magnetic flux quantum. We thus expected our H_{c2} measured on narrow terraces (< 200 nm) are also explained with the formula. However, H_{c2} of our step-confined terraces was found markedly larger than the formula. In order to explain our results, we had to introduce a width-reduction factor w_0 in the formula as $H_{c2} = 4\phi_0/\pi(w\text{-}w_0)2$, and found good agreements with w_0 = 37 nm. The effective reduction in terrace width is probably due to the presence of Josephson vortices; their presence effectively reduces the terrace width through the modification of the boundary condition at the edges. Based on our experimental results we thus conclude that the step confinement makes the superconductor tolerant against the out-of-plane magnetic field more effectively than the geometrical confinement. It should be noted here that since the steps work as a Josephson junction, the superconductivity is not totally disconnected; coherent supercurrent flows across the steps, which is an important aspect for practical applications.

Reference

[1] S. Yoshizawa *et al.*, Phys. Rev. Lett. **113**, 247004 (2014).

Authors

F. Oguro, Y. Sato, K. Asakawa, M. Haze, and Y. Hasegawa

Carrier Transport in Gradient-Doped Photoelectrochemical Electrodes

Lippmaa Group

The interest in developing electrode materials for photoelectrochemical water splitting cells stems from a vision of a sustainable and pollution-free hydrogen-based energy cycle. In essence, the technique is reliant on the development of wide-gap semiconductor materials that are electrochemically and structurally stable over an extended time period, measured in years, in a hydrogen or oxygen evolution reaction under sunlight illumination. Perovskite titanates such as $SrTiO_3$ provide the prerequisite stability in water, but suffer from a variety of intrinsic factors that rate-limit the solar-to-chemical energy conversion process. The primary rate-limiting issues are the non-optimal band gap of 3.2 eV and a short, sub nanosecond photocarrier lifetime. The band gap can be brought down closer to the optimal value of around 2 eV by doping, but adding dopants to the crystal also tends to further shorten the carrier lifetime to picosecond range, negating any possibility of high-efficiency diffusive photocarrier transport from the bulk of the semiconductor to the water interface to drive the water splitting reaction.

We have recently attempted to determine the role of Ti-site dopants on the energy conversion efficiency under ultraviolet band-gap excitation using non-doped and Nb-doped $SrTiO_3$ single crystals (A-D) shown in Fig. 1.

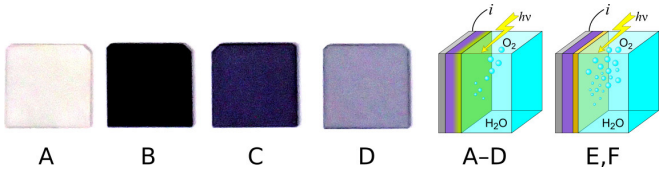

Fig. 1. (A to D) Nb:$SrTiO_3$ single-crystal electrode materials, with doping levels of A:0%, B:1%, C:0.1%, D:0.04%. (A-D) photoelectrochemical cell configuration. Electrode crystal shown in violet, surface depletion layer in yellow. (E,F) Cell configuration for thin film samples consisting of a $SrTiO_3$ film (yellow) on a metallic Nb:$SrTiO_3$ substrate (violet).

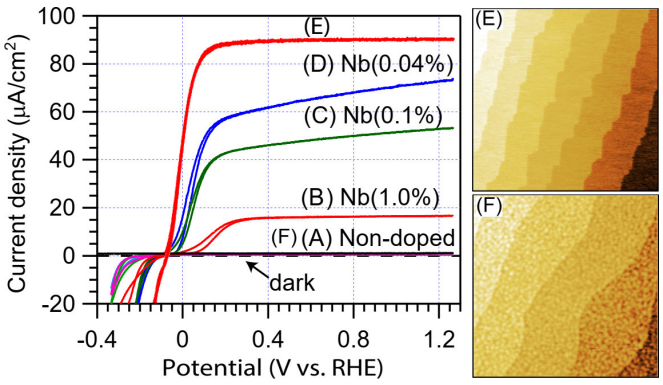

Fig. 2. Illustration of energy conversion efficiency, which is proportional to the cyclic voltammetry current for crystals A to F. The atomic force microscope images for films E and F illustrate the difference in surface morphology related to lower (E) and higher (F) point defect densities in the films.

The corresponding cyclic voltammetry curves are shown in Fig. 2, where the current density is directly proportional to the efficiency of the energy conversion process, i.e., the number of generated gas molecules. The photoresponse of a non-doped 0.5-mm-thick $SrTiO_3$ crystal (A) is zero due to the large resistance of the insulating crystal, which prevents current flow in an electrochemical cell (PEC) illustrated in Fig. 1(A-D). Photoinduced holes in the surface depletion layer of the substrate crystal, marked with a yellow gradient in the PEC diagram in Fig. 1, drive the oxygen evolution reaction but the short lifetime of photocarriers prevents diffusive photoelectron transport through the bulk part of the crystal, stopping the water splitting reaction.

Electron transport becomes possible when bulk conductivity is induced by slight Nb doping of $SrTiO_3$ at the Ti site. As shown in Fig. 2, the efficiency gradually increases as the doping level is reduced from 1% to 0.04% (B to D). Further doping reduction will lead to reduced efficiency due to increasing internal resistance of the substrate crystals.

Improvement of the PEC efficiency can be achieved with a bilayer heterostructure design that combines a non-doped defect-free $SrTiO_3$ crystal in the ~100 nm thick surface depletion region of the electrode with a slightly-doped Nb:$SrTiO_3$ substrate, illustrated in Fig. 1(E,F). Photocarrier recombination losses are minimized and extraction efficiency maximized in the depletion region where the high internal field associated with the surface band bending drives fast carrier transport, whereas bulk doping is used to promote electron transport in the bulk diffusive region of the electrode. Ideally, a continuously varying doping gradient could be used to match the bulk doping level to the width of the surface depletion layer by growing a crystal with a depth-direction gradient of the doping level.

As a simplified demonstration of this concept, we grew a high-crystallinity film with a minimal point defect density and an atomically flat surface morphology (Fig. 2, E) on a highly-doped Nb:$SrTiO_3$ substrate [1]. The importance of defect density control can be seen in a comparison electrode, which was grown at a low temperature and thus contained a high density of point defects (Fig. 2, F). The energy conversion performance of the defect-rich film was, as expected, nearly zero.

This work demonstrates the importance of point defect density control in PEC electrode materials and shows that depth-graded doping control can be a viable strategy for designing efficient hydrogen generation photoelectrochemical electrodes.

Reference
[1] S. Kawasaki, R. Takahashi, and M. Lippmaa, J. Phys. Chem. C, **123**, 15551 (2019).

Authors
S. Kawasaki[a], R. Takahashi, and M. Lippmaa
[a]NIMS

The Roles of Step-Site and Zinc in Surface Chemistry of Formic Acid on Clean and Zn-mModified Cu(111) and Cu(997) Surfaces

Yoshinobu Group

Methanol is of great interest as a source of future hydrogen energy systems, because it is a useful chemical that can produce hydrogen. On the other hand, the synthesis of methanol from CO_2 and H_2 ($CO_2 + 3H_2 \rightarrow CH_3OH + H_2O$) is one of the effective use of CO_2, where the Cu/ZnO catalyst has been used for this reaction. However, the details of reaction mechanism including intermediate species have not been fully elucidated yet. The chemistry of formic acid (HCOOH) on Cu surfaces is important, because the formate species (HCOO) is one of the stable intermediate species in methanol synthesis.

In this study, we systematically investigated the adsorption, desorption and decomposition of formic acid (HCOOH) on Cu(111), Cu(997), Zn-Cu(111) and Zn-Cu(997) using high-resolution X-ray photoelectron spectroscopy (HR-XPS), temperature programmed desorption (TPD) and infrared reflection absorption spectroscopy (IRAS) [1]. On the clean Cu(111) surface, 13% of formic acid molecules adsorbed at 83 K were dissociated to form bidentate formate species by heating at 300 K (Fig. 1a); however, on the Zn-Cu(111) surface, only 4% or less of adsorbed HCOOH were dissociated into the bidentate formate species (Fig. 1b). On the other hand, 13% of adsorbed HCOOH were already dissociated into monodentate formate species on Cu(997)

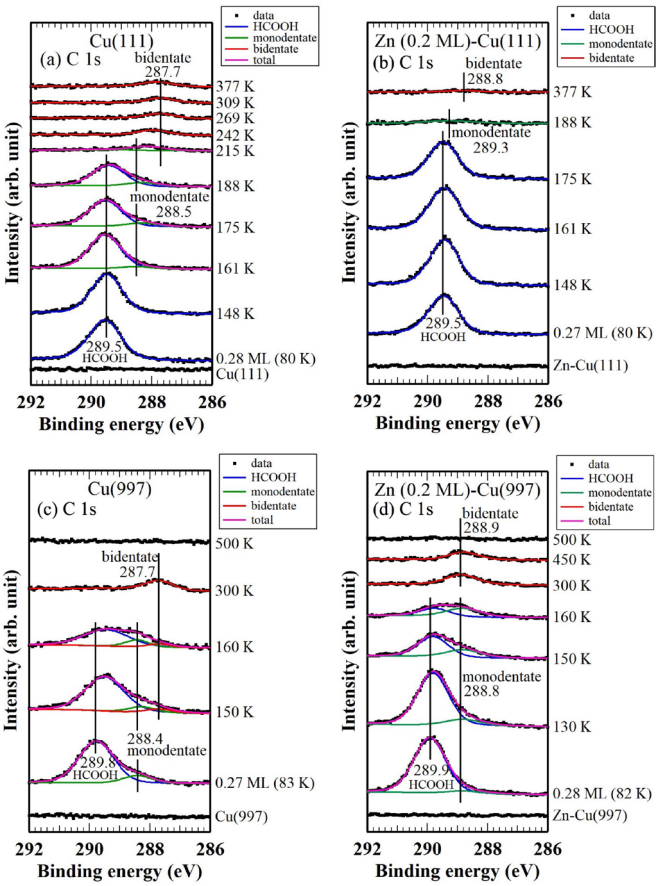

Fig. 1. C 1s XPS spectra of formic acid and formate species as a function of temperature on (a) Cu(111), (b) Zn-Cu(111), (c) Cu(997) and (d) Zn-Cu(997)

even at 83 K and 17% of adsorbed formic acid molecules were transformed to bidentate formate species by heating (Fig.1c). Thus, the stepped Cu surface has higher reactivity for HCOOH dissociation at low temperature. On the Zn-Cu(997) surface, 20% of formic acid became bidentate formate species in contrast to the case with Zn-Cu(111) (Fig. 1d); the Zn deposited Cu step surface shows special activity for adsorption and dissociation of formic acid.

The desorption peak maxima of the formate decomposition products (CO_2 and H_2) on Zn-Cu(997) were shifted to higher temperature than those on Cu(997) in TPD results. Thus, the Zn on Cu surfaces plays an important role in the stabilization of formate species, which probably leads to the decrease in the activation barrier for hydrogenation on the Zn-Cu surface. The bidentate formate species at the Zn-Cu sites can remain after heating at 472 K on Zn-Cu(997); we found that the formate species at Zn-Cu step sites are further stabilized. Therefore, in the real Zn-Cu catalysts that have many step sites, we think that the synergy by the Zn and Cu step site can play a vital role in methanol synthesis.

Reference

[1] Y. Shiozawa, T. Koitaya, K. Mukai, S. Yoshimoto, and J. Yoshinobu, J. Chem. Phys. 152, 044703 (2020).

Author
J. Yoshinobu

The Structural Study on Microbial Rhodopsins and the Characterization of New Microbial Rhodopsin Families

Inoue Group

Rhodopsin is photo-receptive heptahelical transmembrane protein in which a retinal chromophore is covalently bound to a conserved lysine residue in the seventh transmembrane helix (TM7), and animal and microbial rhodopsin families are known so far. Animal rhodopsins are present in animal retina to transfer visual signal to brain and are also related to non-visual light sensing in various tissues. Microbial rhodopsins show diverse functions: light-driven ion pump, light-gated ion channel, phototactic sensor, light-dependent regulation of gene expression and enzyme, and so on. Both types of rhodopsins are being widely used in optogenetics to control various cellular events, such as neural activity, gene expression, dynamic protein localization, and so on, by light.

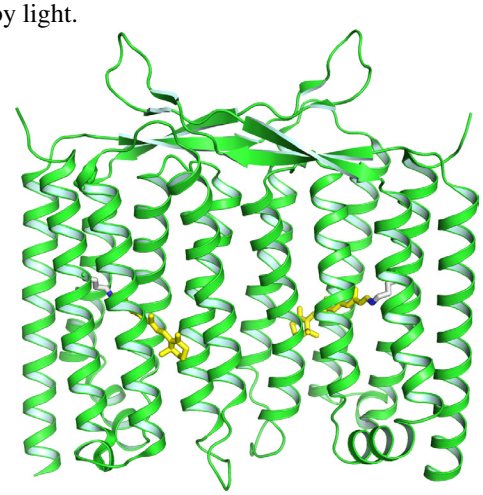

Fig. 1. The x-ray crystallographic structure of HeR

Recently, we discovered the third class of rhodopsin, heliorhodopsin (HeR), which is evolutionally distinct from both of microbial and animal rhodopsins. In 2019, we reported the three-dimensional structure of HeR at atomic level by the x-ray crystallographic analysis (Fig. 1) [1]. It revealed that HeR forms dimers and a fenestration is present near the β-ionone ring of the retinal chromophore. The biochemical experiment suggested that this fenestration is used for the uptake of the retinal chromophore from the environment. This molecular character unique for HeR is considered to be physiologically important for microorganisms having HeR without retinal synthetic genes. Also, the bioinformatic analysis suggested that, while HeR is widely distributed in many gram-positive bacteria, no gram-negative bacteria do not have HeR in their genomes. Because many typical microbial rhodopsins are used by many gram-negative bacteria, the absence of HeR in them is a highly unexpected fact suggesting that the physiological function of HeR would be related to the structure of the cellular membrane of gram-positive bacteria without outer membranes. The study on the ultrafast photoisomerization process of the retinal chromophore in HeR revealed that its isomerization process is similar to those of typical microbial rhodopsins despite of considerably different amino acid residues surrounding the chromophore. A convergent evolution may have occurred in typical microbial rhodopsins and HeR to achieve efficient retinal isomerization with high quantum yields.

The three-dimensional atomic structure of *Gloeobacter* rhodopsin (GR) was solved by the x-ray crystallographic analysis. The electron microscopic observation revealed that GR exists as a pentamer, and the structural detail obtained in our study will provide new insights to understand the mechanism of oligomerization of membrane protein.

A new type of rhodopsin showing unique isomerization process and microbial rhodopsin without retinal binding lysine (Rh-noK) were also identified from bacteria [2]. The former has a new type of amino acid residues in the TM3 consisting of threonine, alanine and threonine called the "TAT motif" at the position where typical proton pumping rhodopsin has the DTD (aspartic acid-threonine-aspartic acid) or DTE (aspartic acid-threonine-glutamic acid) motifs. In the study of Rh-noK, we revealed that ca. 10% of 5,558

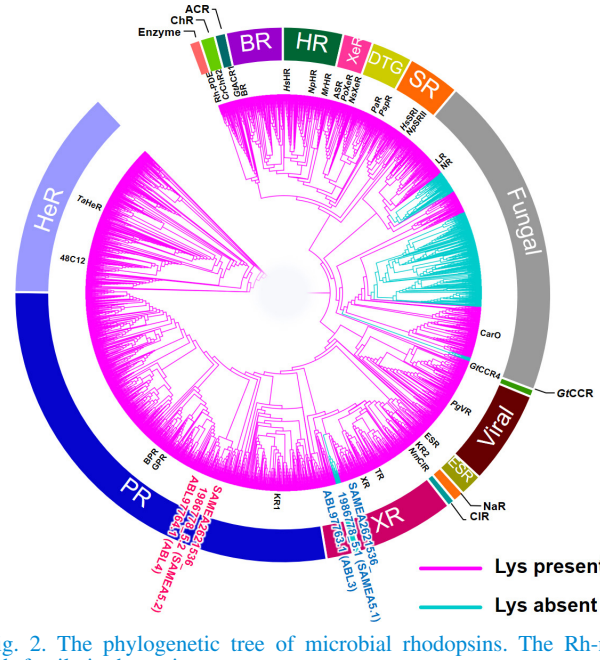

Fig. 2. The phylogenetic tree of microbial rhodopsins. The Rh-noK sub-family is shown in cyan.

microbial rhodopsins do not have the lysine residue in TM7 which typically is used to bind the retinal chromophore by making a covalent Schiff base linkage (Fig. 2). A colored protein was formed by introducing a lysine residue at this position, and, interestingly, additional introduction of an aspartate functioning as a counterion to the protonated retinal Schiff-base recovered the light-driven outward proton pumping function. This suggests that the Rh-noK protein was recently evolved from natural outward proton pumping rhodopsin, and most of structural elements important for the pump function has been retained even after the lack of the retinal binding lysine and counterion aspartate. The physiological roles of TAT rhodopsin and Rh-noK have not been revealed yet, and they will be investigated in the near future.

References
[1] W. Shihoya, K. Inoue *et al*., Nature **574**, 132 (2019).
[2] C. Kataoka, K. Inoue *et al*., J. Phys. Chem. Lett. **10**, 5117 (2019).

Authors
K. Inoue, T. Nagata, and H. Yawo

Electrical Manipulation of a Topological Antiferromagnetic State

Nakatsuji, Otani, and Miwa Groups

Recently, materials with nontrivial band topology have attracted considerable attention due to their novel physical properties. One such example is a Weyl semimetal, in which two non-degenerate bands linearly touch in momentum space, forming gapless Weyl fermions with different chiralities in a time-reversal-symmetry (TRS) or inversion-symmetry breaking state. These touching points or Weyl nodes act as topologically protected, unit-strength monopoles or antimonopoles of underlying Berry curvature such as a large anomalous Hall effect (AHE) and chiral anomaly. The electrical manipulation of these novel properties becomes an important topic for developing new technologies utilizing novel topological state. For this purpose, TRS-breaking or magnetic Weyl semimetals would be suitable owing to their magnetic texture. Moreover, given the prospects of antiferromagnetic (AF) spintronics for realizing high-density devices with ultrafast operation [1], electrical manipulation of an AF Weyl metal is ideal, but have not yet been reported. In this study, we demonstrate the electrical switching of a topological AF state and its detection by AHE at room temperature in a Weyl antiferromagnet Mn_3Sn by using spin-orbit torque (SOT) switching method.

Mn_3Sn has a hexagonal $D0_{19}$ structure with the ABAB-stacking sequence of a (0001)-kagome layer of Mn, and the geometrical frustration leads to a three-sublattice non-collinear AF ordering of Mn spins below the Néel temperature T_N ~ 430 K (Fig. 1(a)) [2]. The magnetic octupole's polarization direction determines the location of Weyl nodes and the associated distribution of the Berry curvature in the momentum space (Fig. 1(b) right). To induce possible SOT switching in Mn_3Sn, we prepared the Mn_3Sn/nonmagnetic metal (NM = Pt, W, Cu) bilayer devices. Figure 2(a) shows the schematic image of the SOT switching in Mn_3Sn/Pt bilayer devices. When an electrical current flows into the Pt layer, a spin polarized current generated by the spin Hall effect of Pt induces the SOT on the Mn_3Sn layer and causes the switching of the polarization direction of the magnetic octupole. The measurement configuration and optical micrograph of the fabricated bilayer Hall bar devices are shown in Fig. 2(b). In our study, we first perform the magnetic field switching of the Hall voltage V_H by using an out-of-plane magnetic field H_z with a read current of 0.2 mA. A clear hysteresis of V_H with the zero-field change of ΔV_H^{field} (= $V_H(+H_z \to 0) - V_H(-H_z \to 0)$) is observed (Fig. 2(c)). To examine the possible SOT switching of

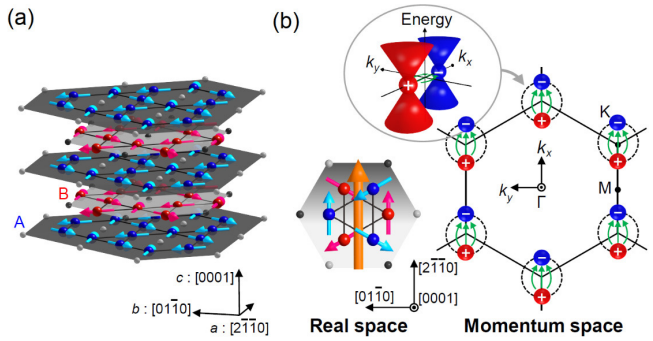

Fig. 1. (a) Mn_3Sn crystal structure and inverse triangular spin (ITS) structure. The large blue and red spheres (small gray and black spheres) represent Mn atoms (Sn atoms) at z = 0 and 1/2, respectively. The Mn magnetic moments (light blue and pink cylindrical arrows) lie within the kagome-layer with the AB-AB stacking sequence and form the ITS structure at room temperature. The spin structure on the kagome bilayers can be viewed as a ferroic ordering of a cluster magnetic octupole. (b) Left: cluster magnetic octupole (orange cylindrical arrow) consisting of the six spins on the kagome bilayer. Right: schematic distribution of the Weyl points near the Fermi energy in the momentum space (k_x-k_y plane at k_z = 0) for the magnetic structure shown in the left-side figure. Red and blue spheres correspond to Weyl nodes, which respectively act as sources (+) and drains (-) of the Berry curvature (green arrows). Inset: three-dimensional schematic picture of a pair of Weyl nodes.

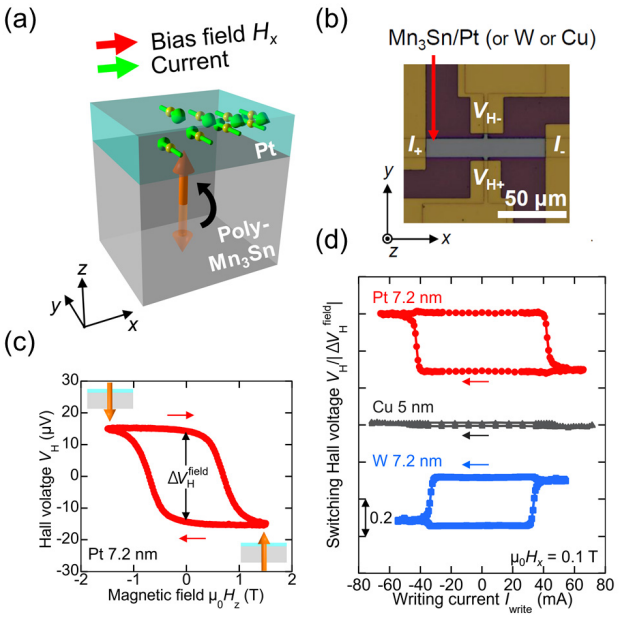

Fig. 2. (a) Schematic image for the spin-orbit torque switching. The spin-polarized current (green cylindrical arrows on yellow spheres) generated in Pt exerts a spin-orbit torque, causing the switching of the polarization axis of the cluster magnetic octupole (orange cylindrical arrow) in the polycrystalline Mn_3Sn under a write current and a bias field along the x-direction. (b) Measurement configuration and optical micrograph of the fabricated Mn_3Sn-nonmagnet bilayer Hall bar devices. (c) Hall voltage V_H vs. magnetic field along the z-direction H_z for the Mn_3Sn/Pt 7.2 nm device at room temperature. Inset: Schematic figures illustrating the direction of the cluster magnetic octupole. (d) Hall voltage V_H vs. write current I_{write} for the Pt 7.2 nm, Cu 5 nm, and W 7.2 nm devices at room temperature. The Hall voltage is normalized by the zero-field Hall voltage $|\Delta V_H^{field}|$ in the magnetic field dependence for each sample.

Mn_3Sn, we pass a 100 ms write-pulse current I_{write} along the x-direction; then, we wait for 600 ms after the pulse current and measure V_H with a 0.2 mA read current. Fig. 2(d) shows V_H as a function of I_{write} in Pt, W, and Cu devices. For the NM = Pt (spin Hall angle $\theta_{SH} > 0$), a clear negative (positive) jump appeared in the Hall voltage under a positive (negative) current larger than a critical threshold write-current I_c with a bias field H_x along the current direction x. The magnitude of the jump reaches ~30 % of the total Hall voltage change $|\Delta V_H^{field}|$ in the field sweep measurements. To confirm that this switching of V_H is related to the SOT from the spin Hall effect in the NM layer, we prepared NM = W ($\theta_{SH} < 0$) and Cu ($\theta_{SH} \sim 0$) instead of Pt. For NM = W, the switching polarity is opposite to the Pt one, while for NM = Cu, there is almost no hysteresis with the electrical current cycle. The difference in switching polarity between Pt and W devices and the absence of switching in Cu devices cannot be accounted for by the Oersted field generated by the electrical current but agree well with the sign of θ_{SH} of the NM layer. These results demonstrate that SOT from the NM layer induces the perpendicular switching of the AF domain and thus manipulates the direction of Weyl nodes.

In recent years, utilizing antiferromagnets in spintronics devices have attracted significant attention as its vanishing small stray fields and much faster spin dynamics than ferromagnets [1]. Our electrical switching measurement of AF Weyl metals is made by using the same protocol as the one used for ferromagnetic metals [3,4]. Moreover, the switching or critical write current density J_c in the NM layer is found reasonably small. It is estimated to be 2×10^{11} A/m^2 for 7.2 nm thick Pt and 5×10^{10} A/m^2 for 7.2 nm thick W devices, which are smaller than the original values reported for the first observations of the electrical switching in the NM/FM devices ($J_c \sim 10^{12}$ A/m^2) [3,4]. These results indicate that topological antiferromagnets may replace ferromagnets in spintronics devices.

In summary, we demonstrated the electrical switching of Weyl antiferromagnets Mn_3Sn by using Mn_3Sn/NM bilayer devices. Our findings indicate that SOT switching is a useful tool for electrically manipulating the distribution of Weyl points and Berry curvature in momentum space. These observations may lead to further scientific and technological advances in topological magnetism and antiferromagnetic spintronics [5].

References

[1] T. Jungwirth *et al*., Nat. Nanotechnol. **11**, 231 (2016).
[2] S. Nakatsuji, N. Kiyohara, and T. Higo. Nature **527**, 212 (2015).
[3] I. M. Miron *et al*., Nature **476**, 189 (2011).
[4] L. Liu *et al*., Science **336**, 555 (2012).
[5] H. Tsai, T. Higo, K. Kondou, T. Nomoto, A. Sakai, A. Kobayashi, T. Nakano, K. Yakushiji, R. Arita, S. Miwa, Y. Otani, and S. Nakatsuji, Nature **580**, 608 (2020).

Authors

H. Tsai, T. Higo, K. Kondou[a], T. Nomoto[b], A. Sakai, A. Kobayashi, T. Nakano[c], K. Yakushiji[c], R. Arita[a], S. Miwa, Y. Otani, and S. Nakatsuji

[a]RIKEN CEMS
[b]University of Tokyo
[c]AIST

Large Transverse Thermoelectric Effect in Iron-Based Binary Ferromagnets

Nakatsuji and Miwa Groups

Thermoelectricity, conversion of heat current into electric energy, provides key technology for versatile energy harvesting and heat current sensors. To date, the technology has relied on the longitudinal thermoelectric response known as the Seebeck effect. Its transverse counterpart in ferromagnets, the anomalous Nernst effect (ANE), has gained significant attention, as it has a number of potential benefits [1,2]. For example, the transverse geometry of the Nernst effect enables the efficient, large area and flexible coverage of a curved heat source (Fig. 1(a)). Moreover, the transverse geometry is hypothetically better suited for thermoelectric conversion, as the Ettingshausen heat current should support the Nernst voltage while the Peltier heat current may suppress the Seebeck voltage [3]. However, the anomalous Nernst effect is too small compared to the Seebeck effect for any thermoelectric application. Thus, it is essential to design a new class of materials that exhibit a large ANE at zero magnetic field.

To find candidate compounds efficiently, we carried out a high-throughput calculation to screen materials without synthesizing them first. Here we found two iron-based cubic compounds Fe_3X (where X is Ga or Al) as materials suitable for designing such low-cost, flexible thermoelectric devices, reaching about 6 μVK^{-1} and 4 μVK^{-1} at room temperature, respectively, close to the highest value reported so far. Our successful fabrication of epitaxial Fe_3Ga and Fe_3Al thin films enables us to obtain a large ANE of about 4 μVK^{-1} and 2 μVK^{-1} at room temperature using an in-plane temperature gradient. Moreover, these Fe_3Ga and Fe_3Al films have in-plane magnetization with a coercivity B_C of about 40 Oe and 20 Oe, respectively, and exhibit a spontaneous ANE at zero field (Fig. 1(b)) for the out-of-plane temperature gradient. These features enable us to design a much simpler thermoelectric device than the conventional Seebeck analogues.

The comparison between experiment and theory indicates that the Fermi energy tuning to the nodal web is the key for the substantial enhancement in the transverse thermoelectric coefficient, reaching a value of about 5 AK^{-1}m^{-1} with logarithmic temperature dependence. Figure 2(a) shows a schematic of the nodal web, a flat band structure made of interconnected nodal lines. The Berry curvature

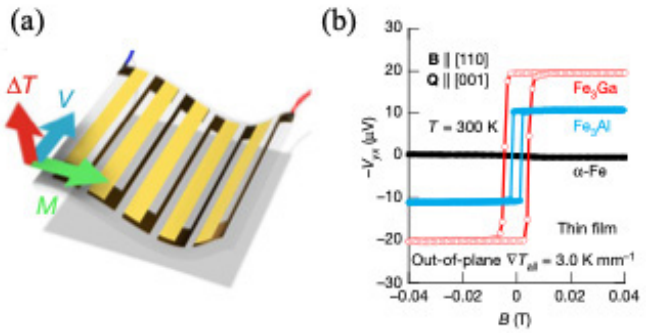

Fig. 1. (a) Thermopiles based on the ANE. V, M, and ΔT is the voltage, magnetization, and temperature difference, respectively. (b) Magnetic field dependence of the Nernst voltage $-V_{yx}$ for the thin films of Fe_3Ga, Fe_3Al and α-Fe. The temperature gradient in the sample (MgO substrate/Fe_3Ga, Fe_3Al, or α-Fe /MgO), ∇T_{all}, is monitored to be 3.0 Kmm^{-1}. The temperature gradient in the Fe_3Ga (Fe_3Al) layer is estimated to be $\nabla T \approx 0.86$ K mm^{-1} (1.0 K mm^{-1}).

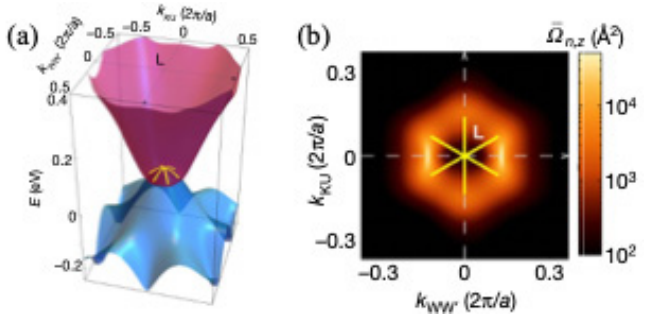

Fig. 2. (a) Energy dispersion of the conduction band (red) and the valence band (blue) around the L point on the BZ boundary for Fe_3Ga. The nodal web is made of nodal lines, shown by the yellow lines (the same as in Fig. 2(b)), along which the flat portions of the conduction and the valence bands touch around the L point. (b) Contour plot of the Berry curvature $\Omega_{n,z}$ of the lower-energy band n around the L point and nodal lines. The z direction is along [001] parallel to the magnetization.

is particularly enhanced at the momenta connecting the edge of the nodal web around the L point on the Brillouin zone boundary, extending over a quasi-2D area spanned by the web (Fig. 2(b)). These results suggest that the strongly enhanced Berry curvature occurs near the momenta originally belonging to the flat nodal web, such as the one around the L point.

Our discovery of the significant spontaneous transverse thermoelectric effects indicates that two iron-based compounds, Fe_3Ga and Fe_3Al, should be suitable for designing low-cost, flexible thermos electric generator by using their thin-film form. It is vital to enhance the coercivity further to achieve stable performance in daily use. Finally, it would be an interesting future direction to look for an enhanced output by combining the ANE with the spin Seebeck effect, both of which occur in the same transverse geometry [4].

References

[1] A. Sakai *et al*., Nat. Phys. **14**, 1119 (2018).
[2] M. Ikhlas, T. Tomita *et al*., Nat. Phys. **13**, 1085 (2017).
[3] M. Mizuguchi and S. Nakatsuji, Sci. Technol. Adv. Mater. **20**, 262 (2019).
[4] A. Sakai *et al*., Nature **581**, 53 (2020).

Authors

A. Sakai, S. Minami[a], T. Koretsune[b], T. Chen, T. Higo, Y. Wang, T. Nomoto[c], M. Hirayama[d], S. Miwa, D. Nishio-Hamane, F. Ishii[a], R. Arita[c,d], and S. Nakatsuji
[a]Kanazawa University
[b]Tohoku University
[c]The University of Tokyo
[d]RIKEN CEMS

Strain-Induced Magnetic Weyl Semimetal in an Epitaxial Thin Film of a Luttinger Semimetal

Nakatsuji, Lippmaa, Katsumoto, and Kindo Groups

Strong electronic correlations serve as a central thread of highly unusual behaviors in quantum materials, ranging from metal-insulator transitions to unconventional superconductivity. The interplay of correlated electron physics with recently discovered novel topological phases establishes a new, fascinating research direction that awaits a full exploration. A vital example of this kind is the magnetic Weyl semimetal (WSM), in which the strongly enhanced Berry curvature inherent to the linearly dispersing crossing points between two electronic bands (i.e., the Weyl points) allows for the emergence of surprisingly large anomalous transport effects even in antiferromagnets or spin-liquid candidates. While the WSM is earlier identified experimentally in nonmagnetic materials with breaking inversion symmetry [1,2], the search for magnetic WSM states in strongly correlated systems remains challenging yet of great importance, due to their excellent tunability and appealing potential for innovative technological applications.

The earliest predicted magnetic WSM is the family of pyrochlore iridates $R_2Ir_2O_7$ (where R is a lanthanoid or yttrium) [3], a 5*d* electron system featuring noncoplanar spin configurations in both 5*d* and 4*f* electron sectors. The 5*d* series provides an ideal ground for realizing exotic topological phases, owing to the comparable strength of the spin-orbit interaction relative to the Coulomb repulsion, allowing the correlation physics to play a critical role. Indeed, recent experiments identified $Pr_2Ir_2O_7$, the metallic end-member of the $R_2Ir_2O_7$ family, as a Luttinger semimetal comprising quadratic band touching of doubly degenerate valence and conduction bands at the Brillouin zone center Γ near the Fermi level E_F (Fig. 1a) [4]. Lattice strain or magnetic field tuning of the Luttinger semimetal may engender a rich topological phase diagram, and is considered a promising route towards realization of a magnetic WSM [5,6].

Recent studies on $Pr_2Ir_2O_7$ have focused on its bulk properties, yet the difficulties of applying uniaxial strain on bulk single crystals leave the magnetic WSM shrouded in mystery. In contrast, thin films allow for control over the crystal growth orientation and lattice deformation via compressive or tensile strain imposed by epitaxial lattice mismatch with a substrate. Here, we report the transport properties of our epitaxial $Pr_2Ir_2O_7$ thin films, which provide firm evidence for a magnetic WSM state induced by the tensile strain along the surface normal [111] direction [7].

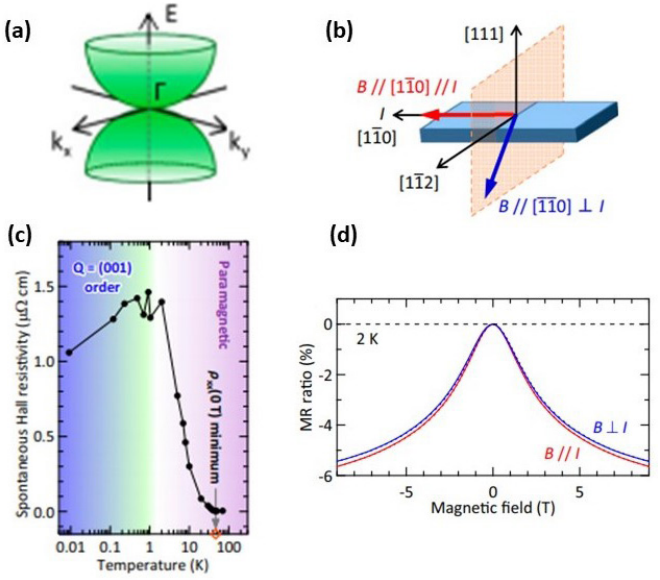

Fig. 1. (a) Band structure of a Luttinger semimetal consisting of quadratic band touching of 5d electrons at the Γ point near EF (b) Schematic for experimental configurations of magnetotransport measurements. (c) Temperature dependence of the spontaneous Hall resistivity. (d) Magnetoresistance curves as a function of the magnetic field B measured at 2 K for $B \parallel I$ and $B \perp I$ configurations. The solid and dotted lines are up and down sweeps of B, respectively. The difference between the two curves arises from the chiral anomaly and indicates that the film is in the Weyl semimetal state.

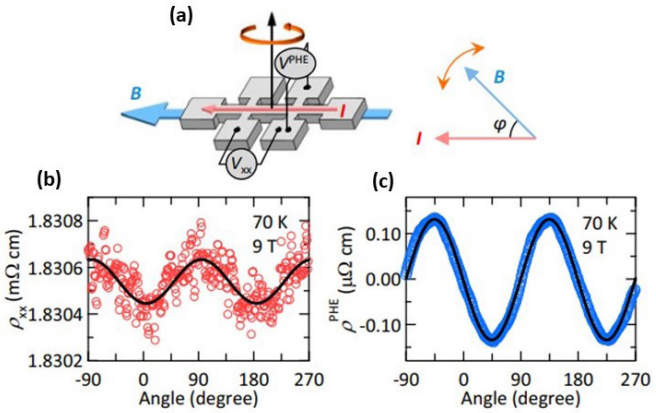

Fig. 2. (a) Schematic for the experimental configuration of the planar Hall effect measurements. (b) and (c) Angle dependence of longitudinal and planar Hall resistivities, respectively, obtained at 70K and 9T

Using strained $Pr_2Ir_2O_7$ thin films, we observed a zero-field Hall effect persisting up to about 50K without detectable spontaneous magnetization (Fig.1c). This onset temperature of the spontaneous Hall effect is much higher than the value (~ 1.5K) observed in bulk single crystals and is nearly two orders of magnitude higher than the exchange coupling (J ~ 0.7K) of Pr 4*f* moments [8], indicating the breaking of time-reversal symmetry induced by the magnetic order of Ir 5*d* electrons. Thus, the condition for realizing a magnetic WSM state is fulfilled in the strained thin film. Moreover, we identified a negative contribution to the magnetoresistance specific to the chiral anomaly (Fig. 1 b and d) and the planar Hall effect (Fig. 2); both phenomena are considered the fingerprints of Weyl points lying close to E_F [9, 10, 11].

In summary, we succeeded in synthesizing epitaxial thin films of $Pr_2Ir_2O_7$ and revealed key transport signatures of the WSM under strain tuning. The discovery of strain-induced magnetic Weyl semimetal state in pyrochlore iridates thin films paves a new avenue to explore topological phases in strongly correlated materials.

References
[1] B. Q. Lv *et al.*, Phys. Rev. X **5**, 031013 (2015).
[2] S.-Y. Xu *et al.*, Science **349**, 613 (2015).
[3] X. Wan *et al.*, Phys. Rev. B **83**, 205101 (2011).
[4] B. Cheng, T. Ohtsuki *et al.*, Nat. Commun. **8**, 2097 (2017).
[5] E.-G. Moon *et al.*, Phys. Rev. Lett. **111**, 206401 (2013).
[6] T. Kondo *et al.*, Nat. Commun. **6**, 10042 (2015).
[7] T. Ohtsuki *et al.*, Proc. Natl. Acad. Sci. U.S.A. **116**, 8803 (2019).
[8] Y. Machida *et al.*, Nature **463**, 210 (2010).
[9] D. T. Son and B. Z. Spivak, Phys. Rev. B **88**, 104412 (2013).
[10] A. A. Burkov, Phys. Rev. B **96**, 041110(R) (2017).
[11] S. Nandy *et al.*, Phys. Rev. Lett. **119**, 176804 (2017).

Authors
T. Ohtsuki, Z. Tian, A. Endo, M. Halim, S. Katsumoto, Y. Kohama, K. Kindo, M. Lippmaa, and S. Nakatsuji

Evidence for the Quadrupolar Kondo Effect in the Heavy Fermion Superconductor PrV_2Al_{20}

Nakatsuji Group

The non-Fermi liquid (NFL) phase holds abiding fascination owing to its prime connections with unconventional superconductivity and other intriguing emergent quantum states in itinerant electron systems. Magnetic heavy-fermion metals offer some prototypical examples of the NFL as a

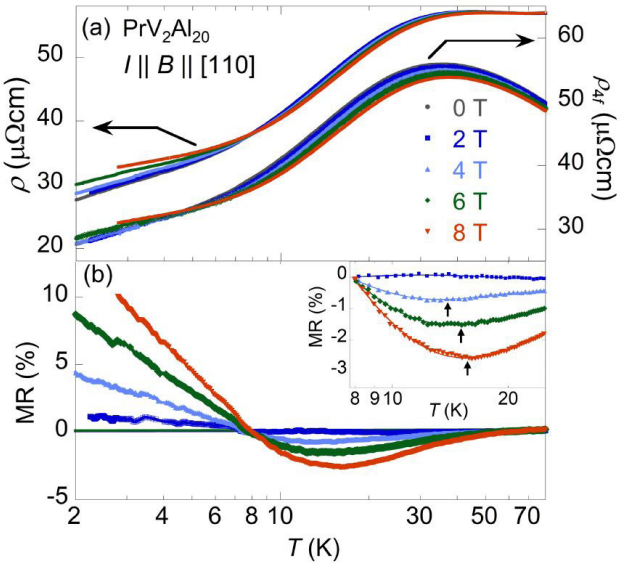

Fig. 1. (a) Temperature dependence of the electric resistivity (left axis) and 4*f*-electron contribution (right axis) of PrV_2Al_{20} under various magnetic fields along [110]. (b) Temperature dependence of the longitudinal magnetoresistance MR of PrV_2Al_{20}.

result of the competing interplay between the magnetic Kondo effect and the Ruderman-Kittle-Kasuya-Yosida (RKKY) interaction among local dipolar moments. Such NFL often appears at the boundary of magnetic instability and is attributed to quantum criticality.

Heavy fermion metals hosting multipolar local moments entail a new route to exotic spin-orbital entangled quantum phases. In the case of quadrupolar systems, the conventional Kondo effect is replaced by a two-channel Kondo mechanism, known as the quadrupolar Kondo effect. Here Kondo entanglement takes place between the quadrupolar moments of f-electrons and the orbital fluctuations of the conduction electrons, while the conduction electron spins offer two separated scattering channels. This effect is considered a key mechanism behind the orbital-driven NFL behavior and quantum critical phenomena. The heavy fermion superconductor PrV_2Al_{20} possesses a nonmagnetic ground-state doublet, featuring both electric quadrupoles

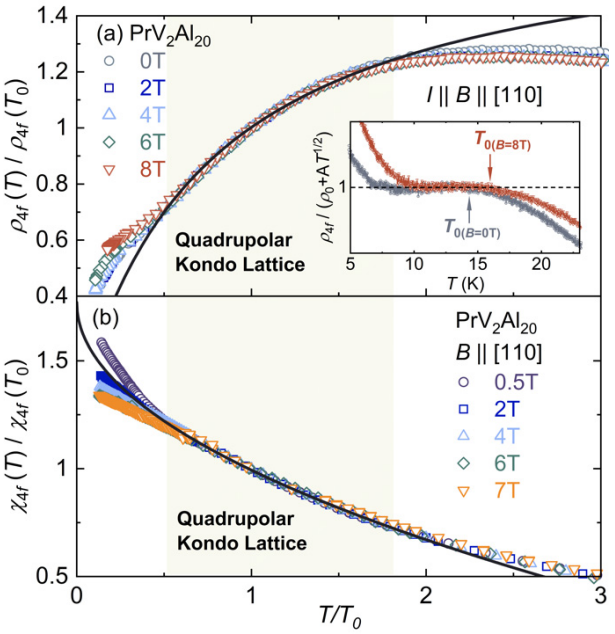

Fig. 2. Universal scaling behavior of (a) the 4*f*-electron contribution to the resistivity and of (b) the magnetic susceptibility measured under a [110] magnetic field.

and magnetic octupoles. It exhibits novel NFL behavior above the antiferroquadrupolar ordering transition at ambient pressure, with ~ $\sqrt{T}$ dependent resistivity and ~ $-\sqrt{T}$ magnetic susceptibility. The relation of this NFL phase with the quadrupolar Kondo effect is yet to be explored.

We report a comprehensive study of the NFL phenomena in PrV_2Al_{20} single crystals based on magnetoresistance (MR), magnetic susceptibility, and specific heat measurements obtained under a [110] magnetic field. Upon entering the NFL regime, we observed a universal scaling behavior expected for the quadrupolar Kondo lattice, which reveals the vital role of the quadrupolar Kondo effect in shaping the NFL phase of PrV_2Al_{20}. Deviations from this scaling relation occur below about 8 K, accompanied by a negative MR and a power-law divergent specific heat. Such behavior signifies the emergence of an anomalous low-temperature state, which is likely driven by heavy-fermion coherence in the quadrupolar Kondo lattice or critical quantum fluctuations of multipolar moments.

References
[1] P. Gegenwart, Q. Si, and F. Steglich, Nat. Phys. **4**, 186 (2008).
[2] D. L. Cox and A. Zawadowski, Adv. Phys. **47**, 599 (1998).
[3] A. Sakai and S. Nakatsuji, J. Phys. Soc. Jpn. **80**, 063701 (2011).
[4] M. Fu *et al*., J. Phys. Soc. Jpn. **89**, 013704 (2020).

Authors
M. Fu, A. Sakai, N. Sogabe, M. Tsujimoto, Y. Matsumotoa, and S. Nakatsuji
[a]Max Planck Institute for Solid State Research

Orbital-Driven Giant Anisotropic Magnetoresistance in the Quadrupolar Heavy Fermion Superconductor PrV_2Al_{20}

Nakatsuji and Sakakibara Groups

The quest for a mechanism that realizes significant transport anomalies in non-ferromagnetic materials may spark a breakthrough in developing ultrafast and energy-efficient memory devices [1,2]. An example of such transport anomaly is anisotropic magnetoresistance (AMR), defined as the difference between the resistance with current applied parallel and perpendicular to the ordered spin direction. To date, however, the AMR effect found in antiferromagnetic materials is limited to a small value of 1% - 2% [3,4]. Rearrangement of electron orbitals may hold the key to further enhancing the AMR in non-ferromagnetic systems, as it should generate anisotropy in the electronic band structure, thereby inducing dramatic effects on the transport properties. A promising discovery along this line is the strongly anisotropic magnetoresistance appearing within the nematic order phase in iron-based superconductors.

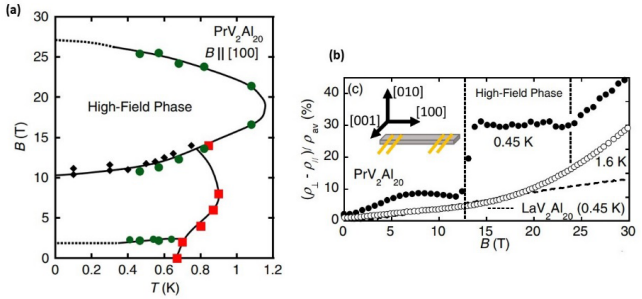

Fig. 1. (a) Temperature-magnetic field (T-B) phase diagram for a [100] magnetic field obtained from the magnetoresistance data. (b) The anisotropic magnetoresistance ratio as a function of magnetic field measured at 0.45K and 1.6K

Here, we focus on a cubic heavy fermion compound PrV_2Al_{20}. A unique feature of this material is its nonmagnetic Γ_3 ground-state doublet, in which the magnetic dipole moment is absent, whereas the quadrupole and octupole moments are active [5], offering an ideal stage for investigating transport phenomena driven solely by electron orbitals. The strong hybridization of these multipolar moments with conduction electrons leads to a rich phase diagram involving a two-stage multipolar order below 0.6–0.7K, non-Fermi-liquid behavior driven by multipolar Kondo effect, and heavy-fermion superconductivity below about 0.05K at ambient pressure [6]. Under a [100] magnetic field, earlier magnetization measurements revealed a high-field phase lying between ~11 – 24T below about 1K [7] (Fig. 1a). This high-field phase is likely the result of rearrangement of the quadrupole moments and therefore is a promising place to explore anisotropic transport properties.

We carried out magnetoresistance measurements under high magnetic fields up to 31.4T at the National High Magnetic Field Laboratory, Tallahassee, USA [8]. Under a [100] magnetic field, we found that, on entering the high-field phase at about 12 T, the rearrangement of quadrupolar moments yields a sharp jump in the magnetoresistance (ΔMR~100%), with a substantial AMR effect of about 30% (Fig. 1b). This feature signifies a Fermi surface reconstruction within the high-field quadrupolar ordered phase, owing to the strong hybridization between the local quadrupolar moment and the conduction electrons. This giant anisotropic magnetoresistance induced by quadrupole rearrangement may form the basis of conceptually new memories and information storage using multipolar states.

References
[1] S. Nakatsuji, N. Kiyohara, and T. Higo, Nature **527**, 212 (2015).
[2] T. Jungwirth *et al*., Nat. Nanotechnol. **11**, 231 (2016).
[3] D. Kriegner *et al*., Nat. Commun. **7**, 11623 (2016).
[4] X. Marti *et al*., Nat. Mater. **13**, 367 (2014).
[5] A. Sakai and S. Nakatsuji, J. Phys. Soc. Jpn. **80**, 063701 (2011).
[6] M. Tsujimoto *et al*., Phys. Rev. Lett. **113**, 267001 (2014).
[7] Y. Shimura *et al*., J. Phys. Soc. Jpn. **82**, 043705 (2013).
[8] Y. Shimura *et al*., Phys. Rev. Lett. **122**, 256601 (2019).

Authors
Y. Shimura[a], Q. Zhang[b], B. Zeng[b], D. Rhodes[b], R. Schönemann[b], M. Tsujimoto, Y. Matsumoto[c], A. Sakai, T. Sakakibara, K. Araki[d], W. Zheng[b], Q. Zhou[b], L. Balicas[b], and S. Nakatsuji
[a]Hiroshima University
[b]National High Magnetic Field Laboratory
[c]Max Planck Institute for Solid State Research
[d]National Defense Academy

Magnetic Field Induced Quantum Phases in a Tensor Network Study of Kitaev Magnets

Kawashima Group

Tensor network (TN) is a useful concept in various fields, not only in the condensed matter theory, but also in data science and machine learning. Even in the condensed matter theory alone, the application of the TN concept is multi-fold. In variational principles calculation, the TN is used as a new type of variational wave function. In the real-space renormalization group (RG) theory, it serves as a natural representation of a renormalized system. In the pure mathematical physics, it is used as a new language for discussing the

topological nature of the quantum states.

In our previous study [Lee, Kaneko, Okubo and Kawashima: Phys. Rev. Lett. **123**, 087203 (2019)], we studied the Kitaev model by the TN representation. We proposed a new wave function that is extremely simple in the TN representation but still shares many essential properties with the ground state of the Kitaev model, such as the quasi-long-range correlation, the short-range magnetic correlation, the flux-free property, the Z_2 gauge structure, and the 2D Ising universality. We call this state the "loop gas state" because of its mathematical equivalence to the loop gas model, one of the standard and solvable statistical physical models. We showed that the loop gas state is adiabatically connected to the ground state of the Kitaev model, indicating a similar role to the AKLT state for the S = 1 AFH chain.

We then extended our method to several other models: S = 1 Kitaev model, and Kitaev-Gamma model. In this study, we studied field-induced quantum phases in the theoretical model of a real candidate material of Kitaev magnets, i.e., α-$RuCl_3$. For this compound, there was an experimental discovery of the half quantized thermal Hall conductivity, which initiated a series of theoretical investigations aiming at finding a concrete connection between the observed quantum phenomena and the theoretical developments of the Kitaev spin liquid. Our TN calculation suggested that a field-induced phase appears between the low field zig-zag magnetic order and the high field polarized state. We found that the chiral Kitaev spin liquid occupies an area in the phase diagram, smaller than predicted by other groups.

Specifically, we studied the K-Γ-Γ' model on the honeycomb lattice represented by the following Hamiltonian,

$$H = \sum_{ij} H_{ij}^{\alpha_{ij}}$$

$$H_{ij}^{\alpha} = \frac{\mathbf{h}}{3}\cdot(\mathbf{S}_i + \mathbf{S}_j) + \mathbf{S}_i^{\mathrm{T}} G^{\alpha} \mathbf{S}j$$

where α_{ij} = x,y,z depending on the direction of the bond (ij). The magnetic field is along the [111] direction. The matrix G_α characterizes the two-body anisotropic interaction, e.g, for α = z,

$$G^z \equiv \begin{pmatrix} 0 & \Gamma & \Gamma' \\ \Gamma & 0 & \Gamma' \\ \Gamma' & \Gamma' & K \end{pmatrix}$$

The matrices for other directions are defined similarly.

In Fig. 1, the obtained phase diagram is presented. The KSL ground state survives only in a small corner of the phase diagram. It disagrees with the previous results obtained by 24-site exact diagonalization and DMRG studies, which suggested a largely extended KSL phase. The discrepancy

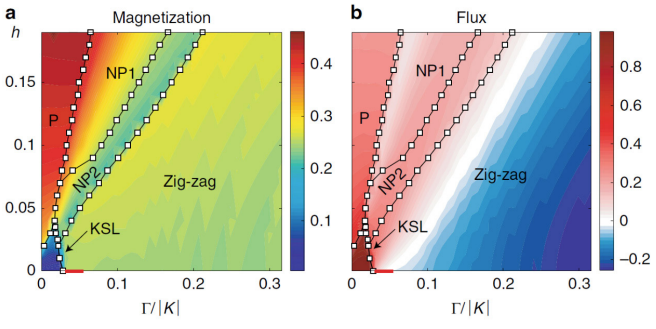

Fig. 1. (a) The magnetization and (b) the flux expectation value of the K-Γ-Γ' model at Γ'= - 0.03. Here "KSL" stands for the chiral Kitaev spin liquid, "P" for a spin-polarized phase, and "NP1" and "NP2" for nematic paramagnet phase. The red solid line at h = 0 denotes a ferromagnetic phase.

may imply the importance of the thermodynamic limit. The tensor network method provides us results for infinite system in contrast to the methods used in the previous ones. At zero field, there is a transition from KSL to a FM (ferromagnetic) phase where spins are aligned in the $[1\bar{1}\bar{1}]$ direction. However, with a very weak magnetic field (h = 0.005), the FM phase disappears, and a direct phase transition from KSL to ZZ (zigzag magnetic ordered) occurs. With increasing the magnetic field, the transition from KSL to the P (polarized) phase occurs at a finite h, where spins start aligning in the [111]-direction.

Apart from the KSL phase, we discovered two non-magnetic states, NP1 and NP2. These phases are characterized by spontaneously-broken 120-degree-lattice-rotational symmetry. When the magnetic field is tilted so that the lattice-rotational symmetry is broken by the Hamiltonian, we found that the phase transition between the KSL and NP2 is continuous in spite that both phases have the same symmetry. This may indicate the non-trivial topological nature of the NP2 phase, which should be clarified in the future study.

Reference

[1] H.-Y. Lee, R. Kaneko, L. E. Chern, T. Okubo, Y. Yamaji, N. Kawashima, and Y. B. Kim, Nature Communications **11**, 1639 (2020)

Authors
H.-Y. Lee[a], R. Kaneko[b], L. E. Chern[c], T. Okubo[d], Y. Yamaji[d], N. Kawashima, and Y. B. Kim[c][e]
[a]ISSP and Korea University
[b]ISSP and Kindai University
[c]University of Toronto
[d]The University of Tokyo
[e]Perimeter Institute

Quantum Criticality of Valence Transition for the Antiferromagnetic Compound $EuCu_2Ge_2$ under Pressure

Uwatoko Group

Most Eu compounds order magnetically because of a divalent electronic state Eu^{2+}. And, valence instability often occurs in Eu compounds, from the divalent electronic state of Eu^{2+} at high temperatures to the nearly nonmagnetic electronic state Eu^{3+} at low temperatures, upon changing the magnetic field and pressure. These compounds can be used to construct a conventional pressure phase diagram with very similar to the Doniach phase diagram for the Ce compounds.

Recently, chemical- and high-pressure measurements have been carried out on single crystals of $EuCu_2(Si_xGe_{1-x})_2$ with the $ThCr_2Si_2$-type tetragonal structure, which undergoes two successive transitions at T_N ~ 15 K and T'_N ~ 9 K on x = 0, and no magnetic orderings on x = 1, at ambient pressure. T_N slightly increases with increasing x and starts decreasing at x = 0.5. and T_N disappears around x ~ 0.7, revealing a mixed-valence or valence-fluctuating state.

In this report, we present the results of electrical resistivity measurements under pressure that revealed a new aspect of the quantum criticality on Eu valence transition[1].

Figure 1 shows the temperature dependence of the electrical resistivity ρ of $EuCu_2Ge_2$ under several pressures. With increasing pressure, the resistivity at room temperature increases because the c - f hybridization between conduction electrons and 4f electrons is enhanced. T_N substantially

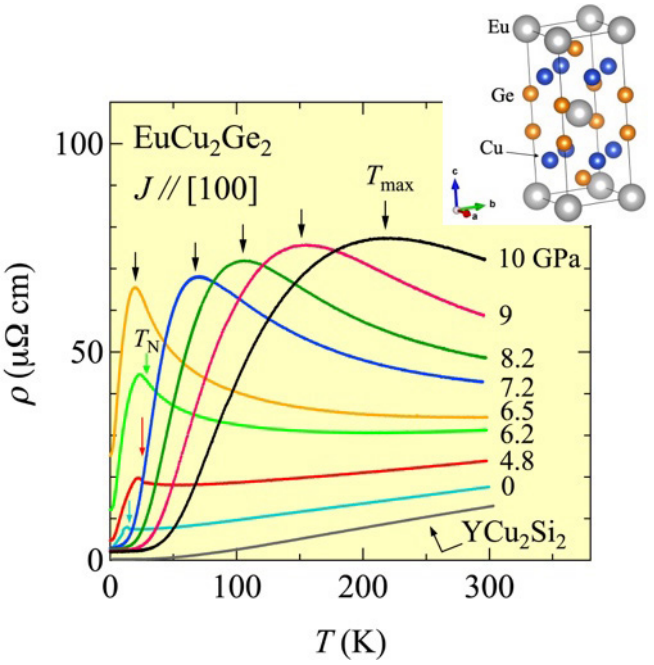

Fig. 1. Temperature dependence of electrical resistivity in $EuCu_2Ge_2$ under several pressures together with the data for YCu_2Si_2 as a reference of the phonon parts of $EuCu_2Ge_2$. The inset shows the tetragonal crystal structure of $EuCu_2Ge_2$.

increases from 15 K and becomes maximum at about 27 K at 6.2 GPa and then it is unclear in a wide temperature region. These results suggest that the valence of Eu increases continuously from nearly divalent to trivalent with increasing pressure. The resistivity at 6.5 GPa indicates no clear magnetic ordering and is typical for a moderate heavy-fermion state. T_{max} remains up to 6.5 GPa and shifts to higher temperatures with further increasing pressure.

Figure 2 shows the P vs Néel temperature T_N phase diagram of $EuCu_2Ge_2$. With increasing pressure, T_N substantially increases from 15 K and becomes maximum at about 27 K at 6.2 GPa. The resistivity at 6.5 GPa indicates no clear magnetic ordering. Note that T'_N disappears rapidly under pressure. In the present case, the Neel temperature became zero abruptly at around 6.5 GPa. This suggests that the valence of Eu increased continuously up to 6.2 GPa, and then the quantum critical point(QCP) of the valence transition arises abruptly at around P_c = 6.5 GPa. The electronic specific heat coefficient, estimated from

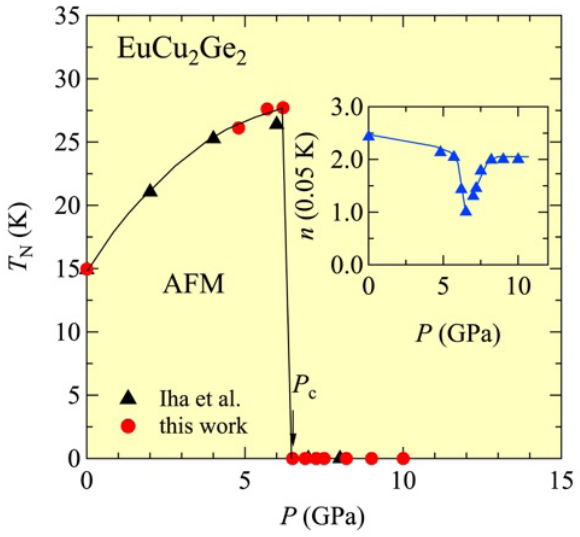

Fig. 2. Pressure-Néel temperature phase diagram in EuCu2Ge2. The inset shows pressure dependence of exponent n of the power law $\rho_{mag} = \rho_{mag0} + BT^n$ of the magnetic resistivity at 0.05 K.

the generalized Kadowaki-Woods plot, was about 510 mJ/(mol K^2), suggesting that the effective mass of the quasiparticles is highly enhanced around P_c. From the analysis of the pressure effect on the exponent n of the power law dependence of the resistivity: $\rho_{mag} = \rho_{mag0} + BT^n$, the fit of the power law to the resistivity data provides valuable information on the pressure dependences of the exponent n of $EuCu_2Ge_2$. It is predicted that n reaches 1.5 for the AF-QCP, while it reaches 1 for the QCP of the valence transition. Inset of Fig. 2 shows the pressure dependence of exponent n. In the magnetic region n is larger than the Fermi liquid value n = 2, probably due to electron-magnon scattering. Approaching P_c, the exponent n decreases as a function of pressure and approaches n = 1. It suggests that the case can be explained as QCP of the valence transition while the scenario based on critical AF-QCP cannot be applied to the present case [1]. This is the first observation of this phenomenon among the Eu compounds.

Reference

[1] J. Gouchi, K. Miyake, W. Iha, M. Hedo, T. Nakama, Y. Ōnuki, and Y. Uwatoko, J. Phys. Soc. Jpn. **89,** 053703 (2020).

Authors
J. Gouchi, K. Miyake[a], W. Iha[b], M. Hedo[b], T. Nakama[b], Y. Ōnuki[b], and Y. Uwatoko
[a]Osaka University
[b]University of the Ryukyus

Kármán-Vortex Cavitation behind Circular-Cylinder Arrays

Noguchi Group

Cavitation is a phenomenon in which bubbles are generated by local pressure changes in a liquid flow. Since cavitation has adverse effects on fluid machinery such as performance degradation, vibration and noise, and erosion, the elucidation of its mechanism is of great engineering importance. Numerically, cavitation has been mainly studied by simulations based on the Navier–Stokes equation. However, it requires a bubble seed to simulate a vapor phase so that it cannot treat the cavitation inception. Here, we directly simulated the cavitation using molecular dynamics (MD) that

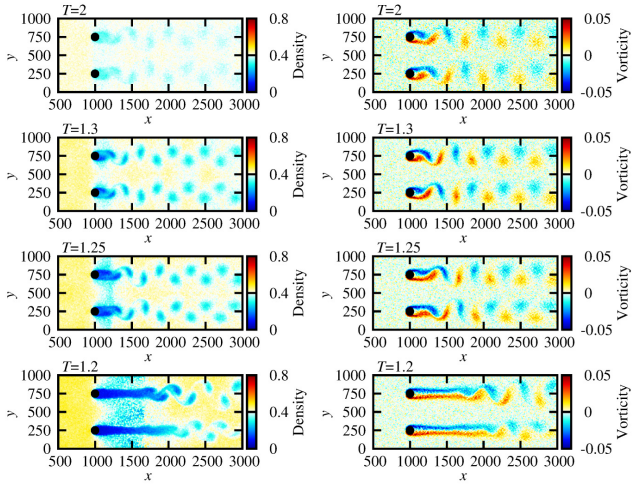

Fig. 1. Snapshots of density (left panels) and vorticity (right panels) fields. The black circles in the figure represent cylinders. At the high temperature, T = 2, Kármán vortex is formed without bubble generation. At the lower temperatures, cavitation occurs. A gas phase (the low-density region in blue color) appears behind the cylinders.

does not require the assumption of a phase transition model or an equation of state for the bubble generation.

We employed Lennard-Jones fluids around periodically aligned side-by-side cylindrical objects at Reynolds number Re~100. As shown in the top panels in Fig. 1, a Newtonian fluid exhibits a Kármán vortex, in which vortexes are periodically generated behind the objects. The neighboring Kármán vortex is synchronized in the antiphase. This synchronization amplifies the vibrations acting on the cylinder. We decrease the temperature to observe the cavitation. At the temperatures T = 1.3 and 1.25, bubbles are generated in conjunction with the shedding cycle of the Kármán vortex (the middle panels in Fig. 1). The Kármán vortex remains synchronized in the anti-phase as in the non-cavitating flow. As the temperature is further reduced to T = 1.2, the gas-phase region behind the cylinder is further expanded, and the upper and lower Kármán vortices become asymmetric (the bottom panels in Fig. 1). This asymmetric structure is switched by a long period of time. A similar dynamics is seen at more closely packed cylindrical arrays in a Newtonian fluid. Thus, the bubbles give an effective increase in the cylindrical diameter.

The change in the vortex structure alters the vibrations excited by the vortex. Because the generated bubbles inhibit the propagation of the vibration associated with the ejection of the vortex, the vibration amplitude decreases and eventually disappears as the cavitation develops.

In summary, the molecular-scale analysis reveals that bubbles generated near the cylinder significantly change the properties of the lift and flow fields.

Reference
[1] Y. Asano, H. Watanabe, and H. Noguchi, J. Chem. Phys. 152, 034501 (2020).

Authors
Y. Asano, H. Watanabe[a], and H. Noguchi
[a]Keio University

Highly Homogeneous Gel without Spatial Heterogeneity

Shibayama Group

Fabrication of ordered nanostructure is a crucial step in a wide range of fields, although the typical size of these objects is still limited to a scale of μm^3 even with current technologies. Polymer gels are a familiar soft material consisting of a nanoporous three-dimensional network that is readily prepared in a large scale, in principle unlimited. However, application of gels as a nanostructured object is obstructed by the fact that gel networks inevitably have a significant level of defects including dangling ends, loops, entanglements, and nonuniform pore sizes, as a result of the fully stochastic gelation reaction. Numerous attempts have been made to remove these defects from polymer gels, including by synthesizing them from monodisperse polymer chains, by using a relatively uniform cross-linking process such as a photoreaction, by limiting unfavorable intramolecular reactions via the A-B type cross-coupling of star polymers, and even by cross-linking polymer chains with movable cross-linkers. Nevertheless, discernible signs of spatial defects have been persistently observed in gels. Gels have been believed to be inherently dis-ordered as a result of the stochastic reaction.

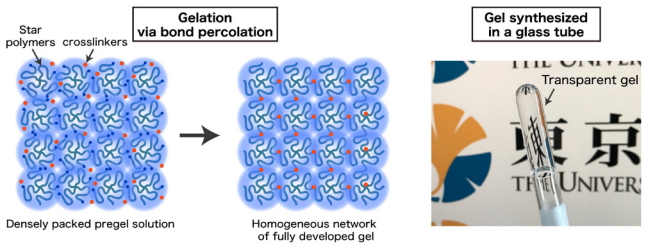

Fig. 1. Illustration of synthesis scheme of highly homogeneous gel via bond percolation. Four-armed star polymer units were dissolved in a good solvent at a concentration much higher than the chain overlapping limit of the polymers. Small crosslinkers were added into the polymer solution. The crosslinkers gradually connect the star polymers and eventually percolate the system. Because there is almost no spatial defect in this polymer gel, the transparency of this material is extremely high.

In this study, we broke this preconception: we present a simple but yet universal scheme to fabricate polymer gels with a highly ordered network. Our strategy is to bring a geometric constraint into the pregel solution so that the space is always uniformly filled with the starting polymer units throughout the gelation reaction (Fig. 1). This gelation framework is known as “bond-percolation” in the classical percolation theory. The spatial and temporal heterogeneity of the synthesized gel network is investigated in the Fourier space by using scattering techniques. Our gel did not show any signatures of heterogeneity: no static laser speckles (Fig. 2), no anomalous small angle scattering, and fully ergodic concentration fluctuations (Fig. 3) and ideal rubber elasticity were observed. These results are completely different from the widely accepted picture of gels. Because both the spatial and temporal correlations of polymer chains in our gels are identical to those of non-crosslinked pre-gel solutions, we cannot even determine the physical state (sol or gel) of our sample by scattering techniques.

Gels have often been discussed in analogy with glass because both gels and glass have a highly disordered structure. However, our results suggest that the bond percolation gel is more like a crystal than glass because almost identical star polymers are closely packed in the space and no spatial defects were detected. The Bragg peaks of the neighboring polymer units were not observed in this gel because the polymer chains can fluctuate much more than atoms in the crystals. This fluctuation of the polymer chains would lead to substantial blurring of the observable correlation between chains.

The simplicity of our gel preparation scheme will enable us to synthesize homogeneous gels with highly ordered network from a variety of polymers with different chemical structures and functionalities (e.g. polydimethylsiloxane, poly(acrylic acid), and poly(N-isopropylacrylamide)), which will open the door to a wide range of new applications.

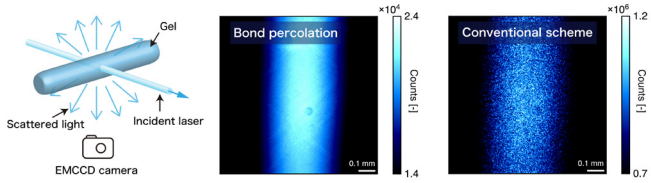

Fig. 2. Static laser speckle test to visualize the spatial defects in the gels synthesized via the bond percolation and conventional scheme. A coherent laser beam was directed to the gel samples and the scattered light was collected using an EMCCD camera. Each image was accumulated for 30 sec to obtain a time-averaged intensity. The bright spots (static laser speckles) in the images denote the static interference from the heterogeneous structures in the gels.

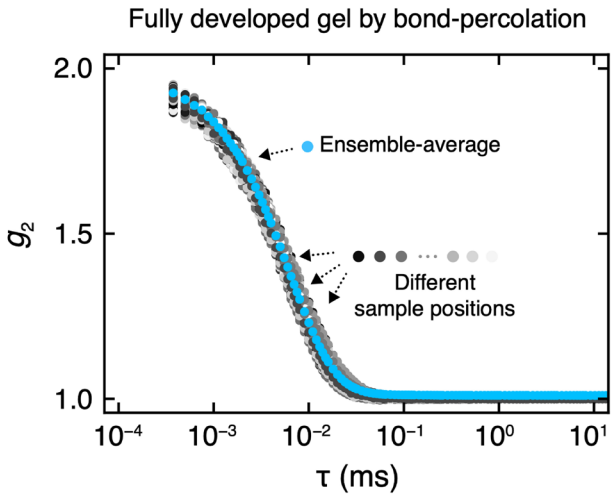

Fig. 3. Intensity time correlation function of the highly homogeneous gel measured with dynamic light scattering at 100 randomly chosen sample positions. All the intensity correlation functions well overlap, indicating the high temporal homogeneity in this gel. The calculated ensemble-averaged intensity correlation function were in perfect consistence with the individual local correlation function, suggesting the ergodic concentration fluctuations of polymer chains in the highly homogeneous gel.

Reference
[1] X. Li, S. Nakagawa, Y. Tsuji, N. Watanabe, and M. Shibayama, Science Advances. **5**, eaax8647 (2019).

Authors
X. Li and M. Shibayama

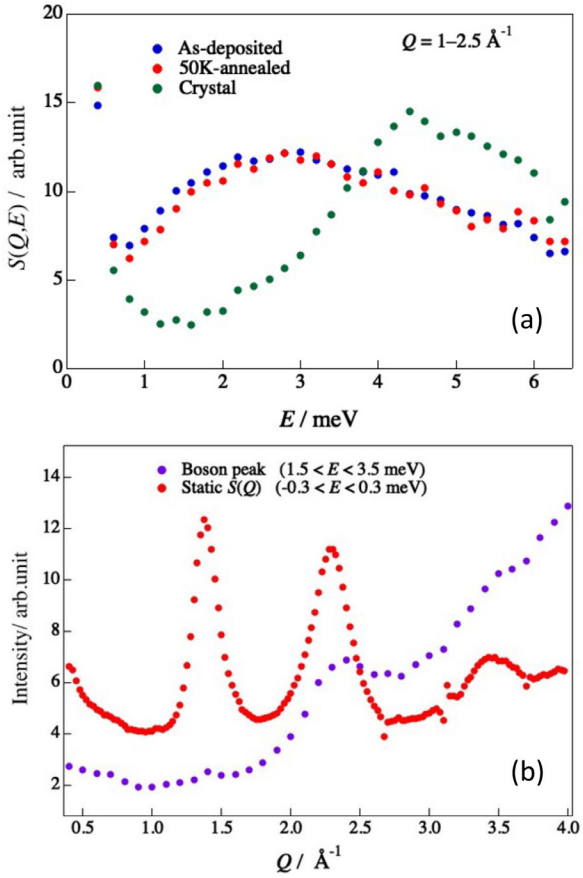

Fig. 1. (a) Inelastic neutron scattering spectra of two glassy and one crystalline states of CCl_4 at 6 K. (b) Q dependence of the boson peak intensity integrated over E = 1.5–3.5 meV. Structure factor $S(Q)$ of glassy CCl_4 is also plotted.

Low-energy Excitations of Glassy Carbon Tetrachloride

Yamamuro Group

There remain many unsolved problems in physical properties of glasses. One of the most important problems is the low-energy excitations (LEE) characteristic to glasses. A broad excitation peak appears around 2-5 meV in most of Raman and inelastic neutron scattering (INS) spectra of glasses. This peak is usually called "boson peak" since the temperature dependence of the peak intensity is scaled well by Bose factors. This peak is basically due to a local excitation since the peak position does not depends on momentum transfer Q. Another interesting phenomenon is the phonon dispersion which has been observed in network glasses [1]. It seems strange that the glasses have phonon dispersion relations since they do not have periodicity. Nevertheless, broad dispersion-like excitations actually exist on dynamic structure factor $S(Q,E)$ planes of glasses. The origins of the above phenomena should be associated with disordered (non-periodic) but locally-ordered structures of glasses. However, their microscopic mechanisms are still unknown.

An essential approach to the LEE problems is the INS study of molecular glasses with simple structures. The study enables us to make direct comparison with the results of various theoretical and computer simulation studies. Vitrification of simple molecules is not easy owing to their prompt crystallization on cooling. Hence we utilize the vapor-deposition (VD) technique whose cooling rate is estimated to be more than 10^7 Ks^{-1}.

We have measured the INS spectra of VD carbon tetrachloride (CCl_4) glass on AMATERAS, J-PARC. Fig. 1(a) shows the $S(Q,E)$ data in the boson peak energy region. A clear boson peak appeared at around 2.5 meV in the glassy state while a sharper peak, which corresponds to the Debye cut-off of the acoustic phonon, at 4.5 meV in the crystalline state. The annealing at 50 K slightly reduced the intensity of the boson peak in the lower-energy side as observed in VD molecular glasses [2]. Fig. 1(b) gives the Q dependence of the boson peak intensity. The intensity has a clear hump at 2.3 Å^{-1} and 3.4 Å^{-1} which coincides with the second and third peak positions in $S(Q)$. This is a similar Q dependence

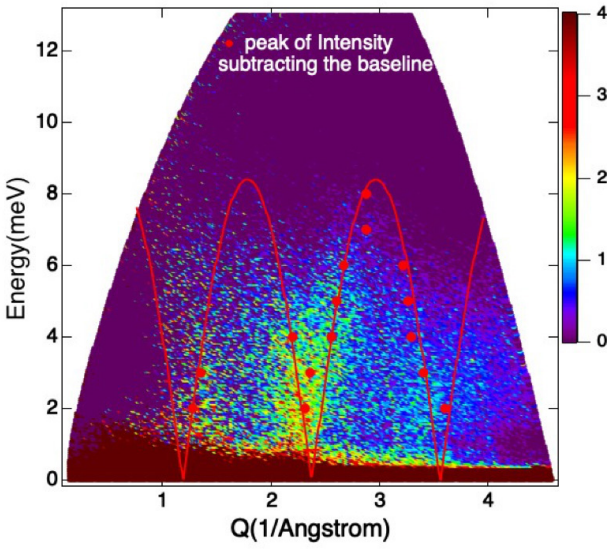

Fig. 2. $S(Q,E)/Q^2$ color contour map of the glassy CCl_4 data at 6 K from which normal phonon contribution proportional to Q^2 has been subtracted in advance.

to that of the boson peak of SiO_2 glass [3]. The phenomenon is roughly explained by a coupled rotation model of the SiO_4 tetrahedral unit. Fig. 3 shows the $S(Q,E)/Q^2$ color contour map of the data in which normal phonon contribution proportional to Q^2 has been subtracted. It is of interest that, as shown by red curves, the phonon excitation has a clear dispersion relation starting at Q = 2.3 Å^{-1} where the boson peak intensity has a maximum and $S(Q)$ exhibits the second peak. This is the first observation of the dispersion-like excitation in molecular glasses. We are now trying a normal mode analysis based on the local structure determined by the reverse Monte Carlo analysis on the X-ray diffraction data which was obtained in SPring-8.

References

[1] M. Arai, Y. Inamura, T. Otomo, N. Kitamura, S. M. Bennington, and A. C. Hannon, Physica B **263**, 268 (1999).
[2] O. Yamamuro, I. Tsukushi, T. Matsuo, K. Takeda, T. Kanaya, and K. Kaji, J. Chem. Phys. **106**, 2997 (1997).
[3] U. Buchenau, M. Prager, N. Nücker. A. J. Dianoux, N. Ahmad, and W. A. Phillips, Phys. Rev. B **34**, 5665 (1986).

Authors

X. Wu, M. Kofu[a], Y. Mizuno, H. Akiba, T. Kikuchi[a], S. Kawamura[a], K. Nakajima[a], and O. Yamamuro

[a]J-PARC, JAEA

Novel Excitations near Quantum Criticality in Geometrically Frustrated Antiferromagnet $CsFeCl_3$

Masuda Group

For understanding condensed matter, the investigation of the collective excitation in low energy range is indispensable. According to the quantum field theory, the excitation in the system with spontaneously symmetry broking is characterized by phase and amplitude fluctuations of order parameters. The former is known as the Nambu-Goldstone (NG) mode, and the latter is called as the amplitude mode. Even though these modes are usually separated, they are hybridized under some conditions, and interesting phenomena are induced; for example in a crystal lattice system, acoustic phonon (NG mode) and optical phonon (amplitude mode) are hybridized through anharmonic terms in a thermoelectric material PbTe, which renormalizes the phonon spectrum and leads to low thermal conductivity and high figure of merit in thermoelectric property [1]. Such a hybridization effect could exist in other types of elementary excitations, however, no research has been reported to our knowledge partially because longitudinal mode itself is not trivial.

Spin S = 1 easy-plane antiferromagnet is one of the prototypical quantum spin systems that allows to explore the quantum phase transition (QPT) [2]. When the anisotropy D is large, the ground state is a quantum disordered (QD) singlet as shown in Fig. 1 left panel. When D is small and the exchange interaction is large, the ground state is magnetically long-range ordered state. A remarkable feature in the renormalized energy scheme in Fig. 1 right panel is that the second excited state can be excited only by the longitudinal component of spin operator $S^{\parallel}$, meaning that the longitudinal mode is allowed in the system. Because the geometrical frustration in magnets could induce the hybridization of the transverse (T) and longitudinal (L) modes, spin S = 1 easy-plane antiferromagnet having geometrically frustrated lattice is the best playground for the research of hybridized modes in magnetic material.

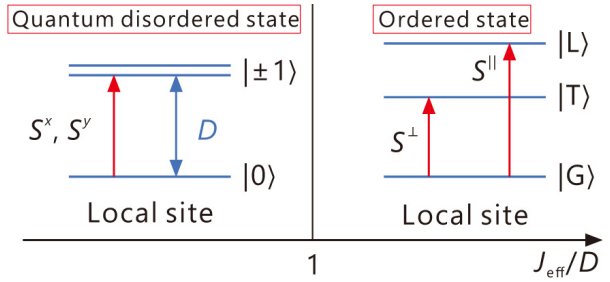

Fig. 1. Schematic diagram of the S = 1 easy-plane antiferromagnet. In the ordered state, the doublet excited states |±1> splits into |*L*> and |*T*>. Here, the former and latter have longitudinal and transverse fluctuations, respectively.

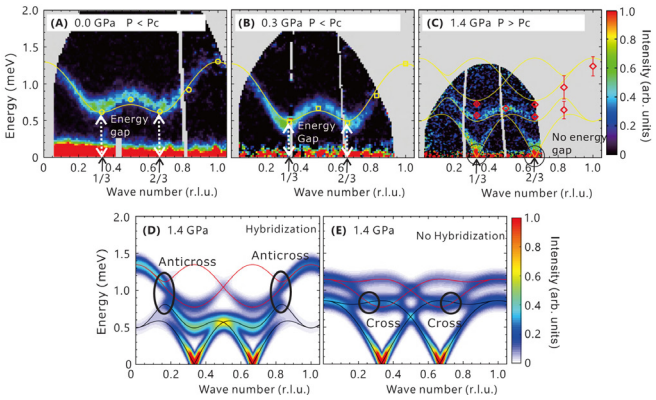

Fig. 2. Inelastic neutron scattering spectra. The spectra obtained at a chopper spectrometer under (A) 0.0 GPa at 6 K, (B) 0.3 GPa at 2.7 K and (C) 1.4 GPa at 0.9 K sliced by the energy transfer - wave vector ($\hbar\omega$ – $\boldsymbol{q}$) plane for q = (-k, 2k, 0). The yellow circles, squares, and red diamonds are the peak positions of the excitations obtained from the constant-q scans using a triple-axis spectrometer. The solid yellow curves are the dispersions calculated by ESW. Calculated neutron cross-section by the ESW under (D) 1.4 GPa at 0 K. Calculated neutron cross-section in the absence of the off-diagonal elements under (E) 1.4 GPa at 0 K. The black and red solid curves in (D) and (E) are gapless and gapped modes, respectively.

$CsFeCl_3$ is the S = 1 easy-plane triangular antiferromagnet. The inelastic neutron scattering (INS) study at ambient pressure revealed that the ferromagnetic chains along the crystallographic c axis are antiferromagnetically coupled in the ab plane [3]. The ground state is the QD state because of large single-ion anisotropy. The magnetic susceptibility measurement under pressures exhibited a pressure-induced magnetic order above a critical pressure of about 0.9 GPa [4]. Owing to the strong easy-plane anisotropy, the ordered moment aligns in the ab plane; the neutron diffraction evidenced the noncollinear 120° structure in the LRO phase [5]. $CsFeCl_3$ is, thus, a promising host for the pressure-induced QPT in the geometrically frustrated lattice. In 2019 our group reported a new hybridization of the phase and amplitude fluctuations of the order parameter near QCP in $CsFeCl_3$ [6].

The INS spectrum measured at 0.0 GPa by using chopper spectrometer in Fig. 2A exhibits a single dispersive excitation with the energy gap of 0.6 meV at the wave vectors $\boldsymbol{q}$ = (-k, 2k, 0) for k = 1/3 and 2/3. The energy gap at 0.3 GPa in Fig. 2B becomes softened when approaching the ordered state. A qualitatively different spectrum is observed in the ordered state at 1.4 GP in Fig. 2C. A well-defined gapless excitation emerges at k = 1/3 and 2/3 and another dispersive excitation are observed in the higher energy range. The INS spectra were collected also by using a triple-axis spectrometer in order to cover wide $\hbar\omega$ – $\boldsymbol{q}$ range, and the

extracted peak energies are overplotted by open symbols in Figs 2A-2C. At 1.4 GPa, the spectral lineshape at k = 5/6 was reproduced by double Lorentzians with broad widths which is reflected by large errorbars. The dispersion relations calculated by the extended spin-wave theory (ESW) [7] are indicated by the solid yellow curves. The calculation is consistent with the experiment both in the QD and LRO phases.

In ESW calculation one can notice that noncollinearity of the magnetic structure makes off-diagonal elements in the Hamiltonian nonzero, leading to the hybridization of L and T modes in one-magnon process. To understand the effects of LT-hybridization, we demonstrate the INS spectra after dropping the off-diagonal element. The results are shown in Figs. 2E, where the black-gapless (red-gapped) modes are pure transverse (longitudinal) modes in this case. The result is inconsistent with the experiment in Fig. 2C. When LT-hybridization is taken into account, the off-diagonal elements lead to anticross of the modes at k~ 5/6 in Fig. 2D, and novel magnetic excitations are formed; both gapless and gapped modes are accompanied by strong longitudinal and transverse fluctuations. The result is consistent with the experiment, and, thus, the LT-hybridization plays an important role in magnon dynamics in noncollinear magnet near QCP.

Since the newly found excitation exists in a noncollinear spin structure, the search of the excitation in different types of noncollinear structures such as cycloidal structure, all-in-all-out structure, and skyrmion lattice would be interesting topics. The search of the hybridized mode in other systems including charge density wave, spin density wave, and ultracold atoms would be important. Finally, the effect of hybridization to the lifetime of the magnon and other elementary excitations would be also interesting.

References

[1] O. Delaire, J. Ma, K. Marty, A. F. May, M. A. McGuire, M. H. Du, D. J. Singh, A. Podlesnyak, G. Ehlers, M. D. Lumsden, and B. C. Sales, Nat. Mat. **10**, 614 (2011).
[2] M. Matsumoto and M. Koga, J. Phys. Soc. Jpn. **76**, 073709 (2007).
[3] H. Yoshizawa,W. Kozukue, and K. Hirakawa, J. Phys. Soc. Jpn. **49**, 144 (1980).
[4] N. Kurita and H. Tanaka, Phys. Rev. B **94**, 104409 (2016).
[5] S. Hayashida, O. Zaharko, N. Kurita, H. Tanaka, M. Hagihala, M. Soda, S. Itoh, Y. Uwatoko, and T. Masuda, Phys. Rev. B **97**, 140405 (2018).
[6] S. Hayashida, M. Matsumoto, M. Hagihala, N. Kurita, H. Tanaka, S. Itoh, T. Hong, M. Soda, Y. Uwatoko, and T. Masuda, Sci. Adv. **5**, eaaw5639 (2019).
[7] R. Shiina, H. Shiba, P. Thalmeier, A. Takahashi, and O. Sakai, J. Phys. Soc. Jpn. **72**, 1216 (2003).

Authors
S. Hayashida, M. Matsumoto[a], M. Hagihala, N. Kurita[b], H. Tanaka[b], S. Itoh[c], T. Hong[d], M. Soda, Y. Uwatoko and T. Masuda
[a]Shizuoka University
[b]Tokyo Institute of Technology
[c]KEK
[d]Oak Ridge National Laboratory

Magnetic Structure and Excitation of Quasi One-Dimensional Antiferromagnet $Ba_2CoSi_2O_7$

Masuda Group

The relationship between magnetism and dielectricity has been extensively studied. In the multiferroics, the ferroelectrics with the cycloidal and proper-screw magnetic structures are explained by the spin-current mechanism and the spin-dependent d–p hybridization mechanism, respectively [1,2]. On the other hand, the multiferroic property has been reported even on a collinear antiferromagnet. One of the maultiferroics with the collinear magnetic structure is an antiferromagnet $Ba_2CoGe_2O_7$. $Ba_2CoGe_2O_7$ with the Co-square lattice shows multiferroic properties, and the local electric polarization of CoO_4 tetrahedra is explained by the spin-dependent d-p hybridization mechanism [3,4]. In contrast, the anomaly of the dielectric constant in similar material $Ba_2CoSi_2O_7$ is not observed at the antiferromagnetic transition temperature T_N =6 K [5]. $Ba_2CoSi_2O_7$ has a distorted crystal structure formed by CoO_4 and SiO_4 networks, as shown in Fig. 1(a), and two kinds of Co-Co bonds exist within the b-plane. In order to clarify the magnetic model of $Ba_2CoSi_2O_7$, the magnetization and neutron scattering measurements have been performed.

In the neutron powder diffraction measurement using the high-resolution powder diffractometer ECHIDNA installed at OPAL, ANSTO, Australia, the magnetic reflections indexed by the propagation vector (1/2, 1/2, 1/2) was observed below T_N = 6 K. By analyzing the powder neutron profile, we found that a collinear antiferromagnetic structure shown in Fig. 1(b) was realized below T_N = 6 K. The magnetic moments with the easy axis along the [10-1] form an antiferromagnetic arrangement along [101] and a ferromagnetic arrangement along [10-1]. In the spin-dependent d-p hybridization mechanism, the local electric polarization of the CoO_4 tetrahedron is almost zero with the magnetic moment along [10-1]. This is consistent with the dielectric property where the temperature dependence of the dielectric constant has no anomaly at T_N = 6 K.

We have also measured the $\boldsymbol{Q}$-dependencies of the magnetic excitations along the b^*, [10-1], and [101] directions at 1.5 K to clarify the magnetic correlation of $Ba_2CoSi_2O_7$ by using a cold-neutron triple-axis spectrometer (CTAX) installed at HFIR, ORNL, USA. Figure 2(a) shows the constant-$\boldsymbol{Q}$ scan profiles measured at (h, 1/2, h). Figure 2(b) shows the h-dependence of integrated intensities and peak energies obtained by Gaussian fitting of the constant-$\boldsymbol{Q}$ profiles at (h, 1/2, h), which corresponds to the $\boldsymbol{Q}$-dependence along the [101] direction. The excitation observed at $\hbar w$ = 2.9 meV is almost dispersionless, but the integrated

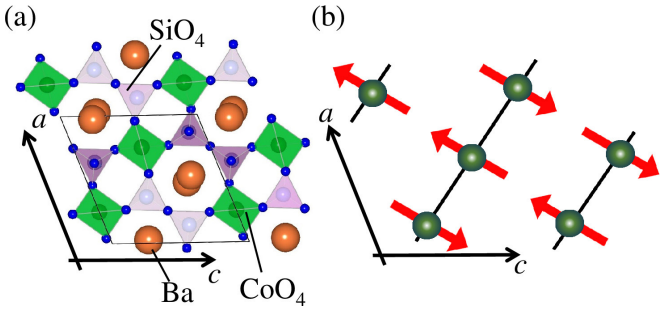

Fig. 1. (a) Crystal structure of $Ba_2CoSi_2O_7$. (b) Schematic magnetic structure of $Ba_2CoSi_2O_7$.

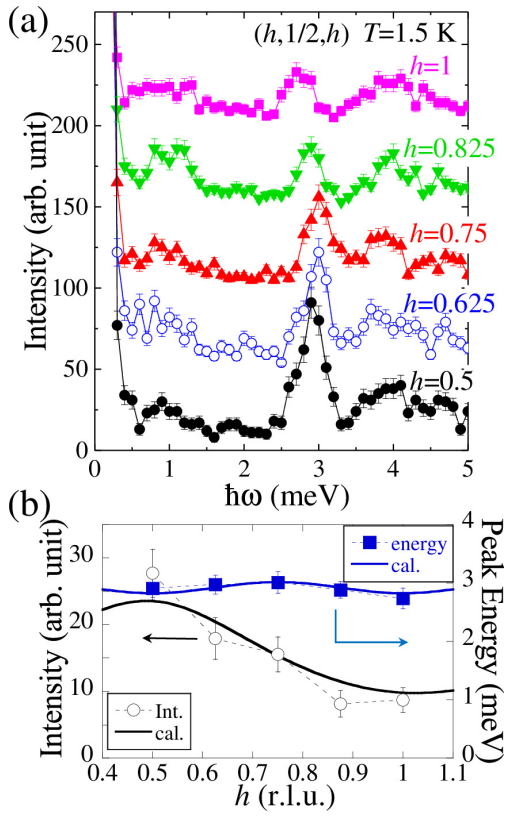

Fig. 2. (a) Constant-$\boldsymbol{Q}$ scans at (h, 1/2, h) measured at 1.5 K. Data are shifted by vertical offsets. (b) Integrated intensities and the peak energies at (h, 1/2, h). Solid lines are the calculated values with the classical spin-wave theory.

intensity exhibits a clear modulation along the [101] direction. In the measurements along the b^* and [10-1] directions, on the other hand, both the neutron intensity and peak energy show less change. (not shown)

We analyzed the magnetic excitation by using the spin Hamiltonian in order to clarify the magnetic model including the magnetic interaction in $Ba_2CoSi_2O_7$. To explain the observed magnetic excitation, we consider the one-dimensional antiferromagnet in which the antiferromagnetic chain is along the [101] direction. We performed the calculations of the neutron intensity and the dispersion energy for both the easy-axis and Ising-like antiferromagnet models; two models cannot be distinguished in the classical spin-wave theory. The magnetic dispersion relation shown in Fig. 2(b) is reproduced by the one-dimensional antiferromagnet model, as shown by solid curves.

Our results of the neutron scattering suggest that the $Ba_2CoSi_2O_7$ is the one-dimensional antiferromagnet with the easy-axis spin anisotropy or the Ising-like spin. On the other hand, $Ba_2CoGe_2O_7$ with the tetragonal structure is two-dimensional easy-plane antiferromagnet. The neutron results suggest that the crystal structure affects both the magnetic interaction dimensionality and anisotropy in åkermanite-type materials.

References

[1] T. Kimura, T. Goto, H. Shintani, K. Ishizaka, T. Arima, and Y. Tokura. Nature **426**, 55 (2003).
[2] S. Seki, Y. Onose, and Y. Tokura. Phys. Rev. Lett. **101** 067204 (2008).
[3] H. Murakawa, Y. Onose, S. Miyahara, N. Furukawa, and Y. Tokura. Phys. Rev. Lett. **105**, 137202 (2010).
[4] M. Soda, M. Matsumoto, M. Månsson, S. Ohira-Kawamura, K. Nakajima, R. Shiina, and T. Masuda, Phys. Rev. Lett. **112**, 127205 (2014).
[5] M. Akaki, J. Tozawa, D. Akahoshi, and H. Kuwahara, J. Phys.: Conf. Ser. **150**, 042001 (2009).

Authors

M. Soda[a], T. Hong[b], M. Avdeev[c], H. Yoshizawa[a], T. Masuda, and H. Kawano-Furukawa[a,d]

[a]RIKEN
[b]ORNL
[c]ANSTO
[d]Ochanomizu University

High-Field Ultrasonic Study of Quadrupole Ordering and Crystal Symmetry Breaking in $CeRhIn_5$

Tokunaga Group

In a number of strongly correlated electron systems, the electronic nematic (EN) state characterized by the lacking of the $C_4^{\pm}$-rotational operations has been focused because the EN contribution to superconductivity and other exotic phenomena have been proposed. Recently, the field-induced EN phase above 30 T has been proposed in the D_{4h}[1] tetragonal compound of $CeRhIn_5$ [1,2], which was well known as a pressure-induced heavy-fermion superconductor.

To investigate the active representation and the order parameter of the field-induced EN phase, we performed an ultrasonic measurement for $CeRhIn_5$ in pulsed magnetic fields up to 56 T [3]. The ultrasound technique is a powerful tool to determine the active representation of a phase transition related to the crystal symmetry breaking because sound waves can induce the symmetry strain belonging to the irreducible representation (IR) of the space group. Furthermore, we can propose the electric quadrupole as an order parameter of the crystal symmetry breaking and the EN state in terms of the electric quadrupole-strain interaction, which is based on the selection rule of group theory.

To identify the active representation of the symmetry breaking at the EN state, we measured all the elastic constants of $CeRhIn_5$ that can be detected in the tetragonal system. As shown in Fig. 1, the transverse elastic constant $C_T = (C_{11} - C_{12})/2$ with the B_{1g} IR of D_{4h} shows the anomaly at B_{IM} = 28.5 T at 1.4 K and 2.1 K. This B_{IM} is consistent with the previous studies [1, 2]. While C_T shows an anomaly, other elastic constants, which can identify the symmetry breaking of B_{2g} and E_g IR, do not exhibit anomaly at B_{IM}. Therefore, our ultrasonic measurements demonstrate the B_{1g}-type crystal symmetry breaking. Furthermore, the

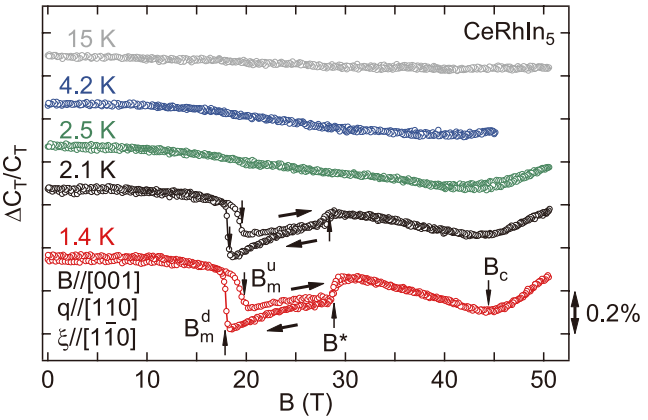

Fig. 1. Magnetic field dependence of the transverse elastic constant $\Delta C_T/C_T$ at several temperatures for B//[001]. The vertical arrows indicate the metamagnetic transition field $B_m^{u(d)}$ for field up(down) sweep, the EN transition field B^*, and the critical field B_c. The right and left arrows show hysteresis direction. The propagation direction $\boldsymbol{q}$ and polarization direction $\boldsymbol{\xi}$ of ultrasound are indicated.

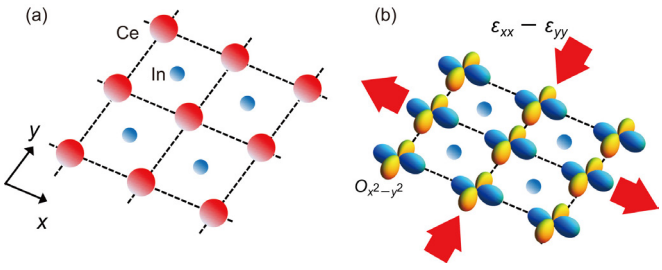

Fig. 2. Schematic view of the B_{1g}-type quadrupole ordering and crystal symmetry breaking. (a) Crystal structure in the xy plane of $CeRhIn_5$ in the normal phase. (b) High-field symmetry breaking state of $CeRhIn_5$. The red arrows indicate the deformation direction of the crystal lattice due to the strain $\varepsilon_{x^2-y^2} = \varepsilon_{xx} - \varepsilon_{yy}$.

electronic degree of freedom with the B_{1g} IR, namely the electric quadrupole $O_{x^2-y^2} \propto (x^2 - y^2)/r^2$, can be the order parameter of the EN state. This symmetry breaking is attributed by the electric quadrupole-strain coupling written as $H_{QS} = -g_{x^2-y^2} O_{x^2-y^2} \varepsilon_{x^2-y^2}$.

We show the schematic view of the B_{1g}-type ferroic electric quadrupole ordering and crystal symmetry breaking in Fig. 2. The square lattice of $CeRhIn_5$ with the tetragonal crystal structure of D_{4h}^1 is drawn in Fig. 2(a). In the field-induced EN state, the electric quadrupole $O_{x^2-y^2}$ appears on the Ce site. The lattice changes from the square of the tetragonal structure to the rectangle of orthorhombic one due to the quadrupole-strain coupling H_{QS} accompanying the lattice distortion $\varepsilon_{x^2-y^2} = \varepsilon_{xx} - \varepsilon_{yy}$. A maximal nonisomorphic orthogonal subgroup D_{2h}^1 is an appropriate space-group for this symmetry lowering from D_{4h}^1.

Furthermore, we found the acoustic de Haas-van Alphen (AdHvA) oscillation in C_T with the frequency 690 T, which has not been observed experimentally. On the other hand, the theoretical study treating 4*f* electrons as itinerant has shown a hole Fermi surface with the frequency ~ 690 T [4]. Thus, we proposed the origin of the AdHvA oscillation in terms of the quadrupole-strain coupling in the *k*-space based on the deformation potential theory [5].

We also discussed the quantum state possessing the electric quadrupole. The delocalization of 4*f* electrons and the in-plane type *p*-*f* hybridization are candidate interactions constructing the quantum state in high fields.

References
[1] P. J. Moll *et al*., Nat. Commun. **6**, 6663 (2015).
[2] F. Ronning *et al*., Nature (London) **548**, 313 (2017).
[3] R. Kurihara *et al*., Phys. Rev. B **101**, 115125 (2020).
[4] D. Hall *et al*., Phys. Rev. B **64**, 064506 (2001).
[5] M. Kataoka and T. Goto, J. Phys. Soc. Jpn. **62**, 4352 (1993).

Authors
R. Kurihara, A. Miyake, M. Tokunaga, Y. Hirose[a], and R. Settai[a]
[a]Niigata University

Discovery of Metamagnetic Transition in New Unconventional Superconductor UTe_2

Tokunaga Group

News of the discovery of unconventional superconductivity in a paramagnetic heavy-fermion system UTe_2 at the end of 2018 has excited strongly the researchers working on the condensed matter physics. Within a few years since the first report in arXiv, many new aspects have been unveiled both experimentally and theoretically. One of the intriguing phenomena in UTe_2 recognized in the very early stage is its large superconducting critical fields. For the magnetic fields applied along the hard magnetization *b*-axis, the superconducting transition can survive well above the Pauli paramagnetic limit [1,2]. This fact suggests the realization of the long-sought spin-triplet superconductivity. Such unconventional superconductivity is believed to realize in the ferromagnetic superconductors (FMSCs), such as URhGe and UCoGe. In the case of UTe_2, however, the ground state is paramagnetic. Here, we introduce our observation of metamagnetic transition in UTe_2 and discuss the relation between metamagnetism and superconductivity by compared to FMSCs [3].

The high-field magnetization was measured by using the pulse magnets installed in the International MegaGauss Science Laboratory. Figure 1(b) shows the magnetization curve for the field along the *b* axis at 1.4 K. At $\mu_0 H_m$ ~ 35 T, magnetization suddenly increases with a large step of ~0.6 μ_B. Because of the hysteric behavior against the magnetic field, this metamagnetic transition is of first-order. From the magnetization curves at various temperatures, we summarized a magnetic phase diagram of UTe_2 in Fig. 1(a). The field hysteresis disappears above 11 K, indicating the existence of the critical end point (CEP), and the transition changes to crossover. As known in many paramagnets, the energy scale of metamagnetic transition, $\mu_0 H_m$, corresponds to T_χ^{max}, where the temperature dependence of magnetic susceptibility shows a broad maximum. This relation is further supported by the fact that $\mu_0 H_m(T)$ connects to $T_\chi^{max}(\mu_0 H)$. At almost the same time, the high-field magnetoresistance measurements independently revealed a similar phase diagram [4]. A sharp step-like increase in the resistance across the H_m may reflect the modification of the Fermi surface, although it is not clear yet. More interestingly, the superconducting (SC) phase shows a reentrant behavior above 16 T and is suddenly suppressed above $\mu_0 H_m$ [5] [see

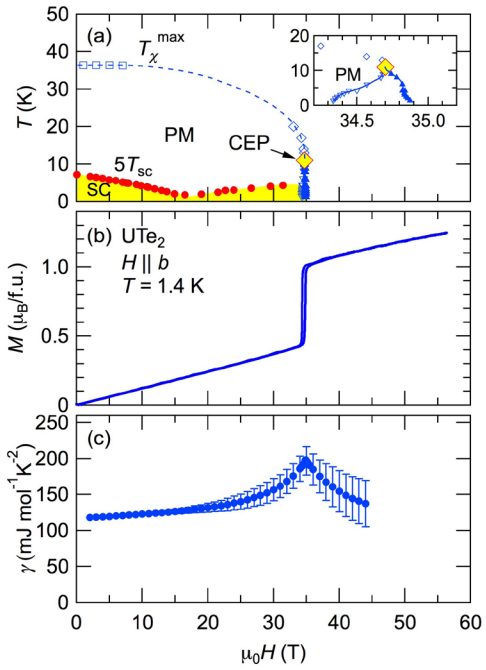

Fig. 1. (a) Magnetic phase diagram of UTe_2 for $H \parallel b$ determined by H_m and T_c^{max}. CEP denoted by a diamond is critical end point. (b) Magnetization curve for $H \parallel b$ at 1.4 K. (c) Magnetic field dependence of the electronic specific heat derived from magnetization curves by the Maxwell relation.

Fig. 1(a)]. This unusual T_c enhancement can be explained qualitatively by a simple mass-enhancement model as follows. Figure 1(c) represents the magnetic-field evolution of the electronic specific heat g, derived by the thermodynamic Maxwell relation using the temperature dependencies of magnetization at constant fields [3]. With increasing fields, the γ increases and shows a maximum at H_m. This enhancement is also confirmed by the direct specific heat measurement using a pulse magnet in ISSP [6]. This enhancement on going to metamagnetic transition indicates that the development of the fluctuation evolves around H_m. This fluctuation may stabilize the SC phase even at high magnetic fields as has been adapted to explain the reentrant superconductivity in URhGe. Using a simplified McMillan-type formula, the field-enhancement of the superconducting transition temperature can be reproduced qualitatively [see Refs. 3 and 6 for more detail and references therein].

Now, it is no doubt that the high-field studies make an important role to reveal the superconductivity on UTe_2. Soon after our work [4], more exciting phenomena in high fields were reported [7]: Surprisingly, another SC phase appears at H_m when the field is applied intermediate angles between the a and c axis. This is in stark contrast to the fact of suppression of SC at H_m for the b axis. Our struggles continue.

References

[1] S. Ran, C. Eckberg, Q.-P. Ding, Y. Furukawa, T. Metz, S. R. Saha, I.-L. Liu, M. Zic, H. Kim, J. Paglione, and N. P. Butch, Science **365**, 684 (2019).
[2] D. Aoki, A. Nakamura, F. Honda, D. X. Li, Y. Homma, Y. Shimizu, Y. J. Sato, G. Knebel, J.-P. Brison, A. Pourret, D. Braithwaite, G. Lapertot, Q. Niu, M. Vališka, H. Harima, and J. Flouquet, J. Phys. Soc. Jpn. **88**, 043702 (2019).
[3] A. Miyake, Y. Shimizu, Y. J. Sato, D. Li, A. Nakamura, Y. Homma, F. Honda, J. Flouquet, M. Tokunaga, and D. Aoki, J. Phys. Soc. Jpn. **88**, 063706 (2019).
[4] W. Knafo, M. Vališka, D. Braithwaite, G. Lapertot, G. Knebel, A. Pourret, J.-P. Brison, J. Flouquet, and D. Aoki, J. Phys. Soc. Jpn. **88**, 063705 (2019).
[5] G. Knebel, W. Knafo, A. Pourret, Q. Niu, M. Vališka, D. Braithwaite, G. Lapertot, M. Nardone, A. Zitouni, S. Mishra, I. Sheikin, G. Seyfarth, J.-P. Brison, D. Aoki, and J. Flouquet, J. Phys. Soc. Jpn. **88**, 063707 (2019).
[6] S. Imajo, Y. Kohama, A. Miyake, C. Dong, J. Flouquet, K. Kindo, and D. Aoki, J. Phys. Soc. Jpn. **88**, 083705 (2019).
[7] S. Ran, I.-L. Liu, Y. S. Eo, D. J. Campbell, P. Neves, W. T. Fuhrman, S. R. Saha, C. Eckberg, H. Kim, J. Paglione, D. Graf, J. Singleton, and N. P. Butch, Nat. Phys. **15**, 1250 (2019).

Authors

A. Miyake, Y. Shimizu[a], Y. J. Sato[a], D. Li[a], A. Nakamura[a], Y. Homma[a], F. Honda[a], J. Flouquet[b], M. Tokunaga, and D. Aoki[a, b]
[a]Tohoku University
[b]CEA-Grenoble

High-Magnetic-Field X-Ray Diffraction Study in Solid Oxygen

Y. Matsuda Group

Molecular oxygen is a unique homonuclear diatomic molecule because it possesses a spin quantum number S = 1. After M. Faraday had noticed that gaseous oxygen exhibits magnetism, condensed phases, namely liquid and solid phases have been extensively studied as intriguing magnetic materials. Solid oxygen undergoes successive phase transitions with lowering temperature, and three distinct phases, γ-phase, β-phase, and α-phase appear at 54, 44, and 24 K, respectively. One of the most intriguing findings on these three phases is that they have different crystal symmetries,

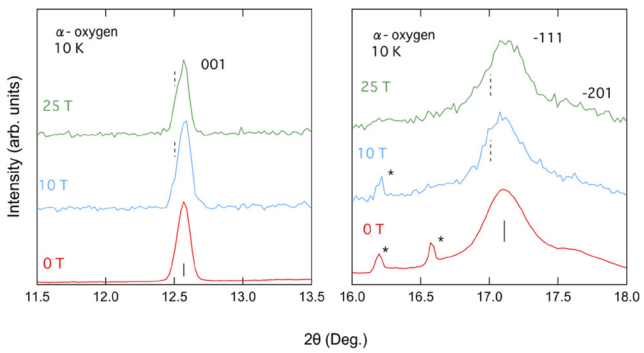

Fig. 1. High-magnetic-field X-ray diffraction profiles of the α-phase of solid oxygen at 10 K. Vertical dashed lines indicate the positions that are expected from the previous report [2]. (a) 001 reflection peaks are shown. (b) -111 and -201 peaks are shown. Peaks with * are considered to be due to impurities on the window of the sample cell.

meaning that the successive phase transitions are not merely magnetic phase transitions but structural phase transitions. The γ-phase, β-phase, and α-phase have a cubic, rhombohedral, and monoclinic crystal structure, respectively. The lowest temperature phase, the α-phase is an antiferromagnet at a low temperature below 24 K, while the β-phase only exhibits a short-range antiferromagnetic correlation and the γ-phase is paramagnetic. We have been sharing the idea that magnetic energy between oxygen molecules should play an important role for having different crystal structure for a long time. However, no direct experimental evidence of the strong spin-lattice coupling had ever been obtained before the discovery of the novel magnetic-field-induced θ-phase at 120 T [1]. It has been proved that controlling spins induces a novel oxygen crystal.

Microscopic investigation of the crystal lattice of solid oxygen in magnetic fields is important. Actually, there was a report of the high magnetic field x-ray diffraction of the solid oxygen using a synchrotron x-rays up to 8 T and significantly large magnetostriction was likely to occur in the α-phase of solid oxygen [2]. The volume striction $\Delta V/V$ was found to reach around 10^{-2}. In the present study, we have extended the magnetic field range to 25 T for the x-ray diffraction experiment.

The high-field XRD experiments have been performed at the Institute for Materials Research of Tohoku University with a DC magnet up to 5 T, and at BL22XU in SPring- 8 up to 25 T using a pulsed magnet. Pure oxygen gas (purity > 99.99995%) was liquified by cooling into a sample cell designed for each experiment. For the 5 T DC-magnet experiment, a CuKα (1.54 Å) characteristic emission line

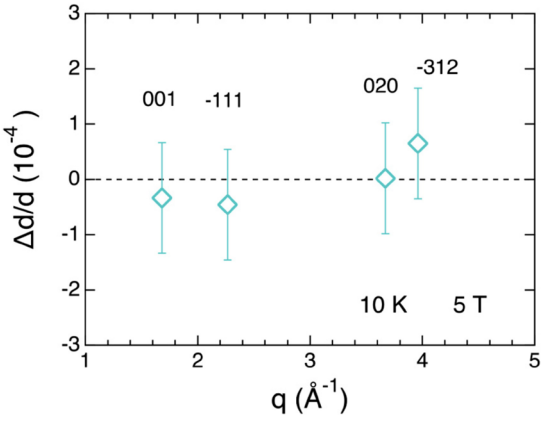

Fig. 2. The relative changes of the diffraction plane spacing at 5 T are shown at different reciprocal vectors.

was used as the x-ray source. The measurement temperature was controlled to be 10 K. In the 25 T pulse-magnet experiments, the photon energy (wavelength) of the synchrotron x-ray used is 15 keV (0.8266 Å). The time interval of the successive pulsed magnetic field measurements is 10–20 min, which is necessary for cooling the magnet after heating due to the discharge for field generation. The variation of the magnetic field ΔB/B during the measurement time (100 μs) is around 2% [3].

The measured XRD profiles in pulsed magnetic fields at 10 and 25 T are shown in Fig. 1 along with the zero-field profile. The XRD at 0 T is measured with an exposure time of 10 ms. The profiles at 10 and 25 T are obtained by averages of six times and five times the repetition of the measurements, respectively. The obtained XRD profiles at different magnetic fields seem to be identical at first glance.

In order to confirm the unexpectedly small magnetic field effect, we have also analyzed the steady field XRD data that have higher precision in terms of the longer accumulation time. And also, we need to exclude a possibility that the dynamics of the crustal lattice is slower than the pulsed magnetic field of which duration time is 1 ms in this study.

Figure 2 shows the obtained linear magnetostriction Δd/d at 5 T. The Δd/d of several diffraction plane spacing is found to be as small as 10^{-4} which is more than one order of magnitude smaller than the values reported previously [2].

The reason for the contradiction between our results and the previous study is not very clear. One of the possible causes for the contradiction is that there had been some mechanical influence on the experimental configuration by applying DC magnetic fields. Small mechanical movements of measurement apparatuses can cause a change in the observed XRD peak positions [3].

The high-field XRD experiments on α oxygen at 10 K has revealed that the linear magnetostriction Δd/d is smaller than 10^{-4} T^{-1} in magnetic fields of up to 25 T [3]. The absence of the giant magnetostriction in α oxygen is also in agreement with the experimental fact that the magnetic field induced α-θ transition is first order [1]. The deformation of the crystal lattice in a magnetic field is not significant below the critical magnetic field around 100 T. It is likely that a drastic symmetry change in the crystal lattice takes place discontinuously at the phase transition.

References

[1] T. Nomura, Y. H. Matsuda, S. Takeyama, A. Matsuo, K. Kindo, J. L. Her, and T. C. Kobayashi, Phys. Rev. Lett. **112**, 247201 (2014).
[2] K. Katsumata, S. Kimura, U. Staub, Y. Narumi, Y. Tanaka, S. Shimomura, T. Nakamura, S. W. Lovesey, T. Ishikawa, and H. Kitamura, J. Phys.: Condens. Matter **17**, L235 (2005).
[3] Y. H. Matsuda, A. Shimizu, A. Ikeda, T. Nomura, T. Yajima, T. Inami, K. Takahashi, T. C. Kobayashi, Phys. Rev. B **100**, 214105 (2019).

Authors

Y. H. Matsuda, A. Shimizu, A. Ikeda, T. Nomura, T. Yajima, T. Inami[a], K. Takahashi[b], and T. C. Kobayashi[c]

[a]National Institutes for Quantum and Radiological Science and Technology
[b]Tohoku University
[c]Okayama University

Observation of Quantum Spin-Nematic Phase in Volborthite

Kohama, Kindo and Hiroi Groups

For a long time, it was believed that matter could exist in only three different forms, solid, liquid and gas. However, in the second half of the nineteenth century, it became clear that not all substances could be described as solid, liquid or gas. Liquid crystals came of age in the twentieth century, as both a subject of fundamental research and the basis for modern display technology. Since we know examples of quantum gases, liquids and solids, it is natural to ask, *are there quantum liquid crystals, too*? For a long time, this question remained a mathematical curiosity. However, in recent years, potential quantum analogues of a liquid crystal state have been discussed in real material, which is called a quantum spin-nematic state. Its experimental observation has proved much more challenging, since the order parameter of the spin nematic state, spin quadrupole moment, is hard to detect with conventional magnetic probes.

In this research, with an exotic frustrated magnet, volborthite, we provided the possible evidence of quantum analogue of the nematic crystal, and resolved a long-standing mystery about the magnetism of volborthite [1]. Here we applied thermodynamic measurement techniques, the magnetocaloric effect (MCE) and specific heat(C) measurements, which measure entropy and sensitive to any phase transition irrespective of the type of the order parameter. The state-of-art experimental capability in IMGSL; high-field calorimetry in magnetic fields up to 60 T and low temperatures down to 0.5 K, enabled observation of quantum spin-nematic state in volborthite.

First, we show the MCE curves obtained in the adiabatic condition, $T(H)$, in Fig. 1(a). The adiabat $T(H)$ initially decreases with increasing fields, before passing a broad minimum at ~25 T and then increases at higher fields. Below 1.7 K, a notable change occurs as seen in the enlarged plot (Fig. 1(b)). The broad minimum in $T(H)$ acquires small dips, indicative of phase transitions at 22.5, 25.5 and 27.5 T. Each of these three critical fields has also been found in measurements of MCE under nearly isothermal conditions

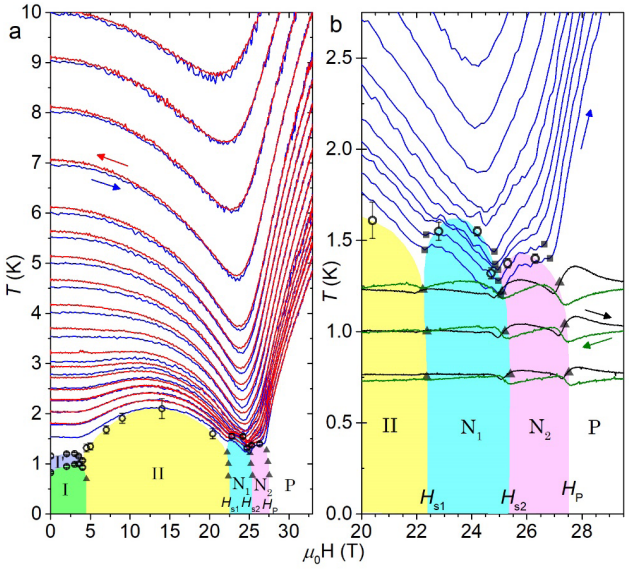

Fig. 1. Magnetocaloric effect and magnetic phase diagram of volborthite. (a) Experimental data of the MCE in volborthite. (b) Enlarged plot of MCE curve. The phase boundaries deduced from the MCE and $C(T)$ measurements were plotted by solid symbols and open circles.

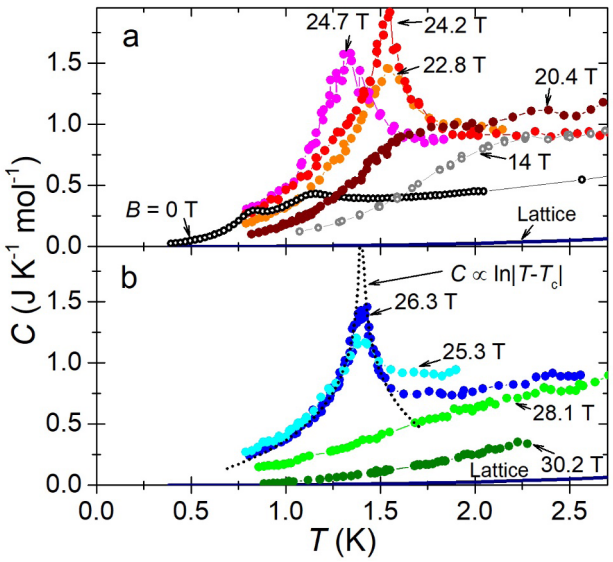

Fig. 2. Specific heat in volborthite. (a) Experimental results for specific heat $C(T)$ for magnetic fields spanning the low-field phase I, phase II (SDW), and phase N_1. (b) Specific heat within the hidden-order phase N_2 and the plateau state P.

as shown in Fig. 1(b) as black and green curves. In Fig. 1(b), we also plot the phase boundary deduced from MCE and $C(T)$ measurements.

We have further investigated the temperature-dependence of C in magnetic fields up to 30.2 T as seen in Fig. 2. In the absence of magnetic field, $C(T)$ exhibits small peaks as reported previously (See Fig. 2(a)). The onset of SDW order (Phase II) is also revealed as a broad shoulder in $C(T)$. Different behavior is observed above 22.5T where the transition is marked by a substantial λ-shaped anomaly. An extremely sharp peak (Fig. 2(b)) is developed above 25.5 T, consistent with the phase boundary identified in MCE. Above the crossover field to the plateau state (P) at 27.5T, no anomaly is observed in $C(T)$. These observations provide unequivocal evidence that there are two different magnetic states between SDW and plateau states, i.e., Phases N_1 and N_2 as seen in Fig. 1(b). It is important to note that the earlier NMR results [2], however, failed to resolve the phase N_2. Since the spin quadrupole moment cannot be detected by conventional magnetic probes such as NMR, it is reasonable to consider the phase N_2 between 25.5 and 27.5 T is the ordered state of the quadruple moment that is so-called a quantum spin nematic state.

References

[1] Y. Kohama, H. Ishikawa, A. Matsuo, K. Kindo, N. Shannon, and Z. Hiroi, PNAS **116**(22) 10686 (2019).

[2] H. Ishikawa, M. Yoshida, K. Nawa, M. Jeong, S. Kramer, M. Horvatic, C. Berthier, . Takigawa, M. Akaki, A. Miyake, M. Tokunaga, K. Kindo, J. Yamaura, Y. Okamoto, and Z. Hiroi, Phys. Rev. Lett. **114**, 227202 (2015).

[3] O. Janson, S. Furukawa, T. Momoi, P. Sindzingre, J. Richter, and K. Held, Phys. Rev. Lett. **117**, 037206 (2016).

Authors

Y. Kohama, H. Ishikawa, A. Matsuo, K. Kindo N.Shannon[a], and Z. Hiroi

[a]Okinawa Institute of Science and Technology Graduate University

Magnetization Process of the Breathing Pyrochlore Magnet $CuInCr_4S_8$ in Ultrahigh Magnetic Fields up to 150 T

Kohama Group

Breathing pyrochlore magnets with an alternating array of small and large tetrahedra have recently attracted attention because of their potential realization of exotic magnetic states. One promising candidate is the S = 3/2 chromium spinel oxide, $LiInCr_4O_8$, characterized by the small breathing factor J'/J~0.1, where J and J' are the exchange interactions on the small and large tetrahedra, respectively (inset of Fig. 1) [1]. In this system, the spin-lattice coupling (SLC) as well as the breathing factor govern its magnetic properties, as represented by a tetramer-singlet formation [1] and a field-induced transition to a 1/2-magnetization plateau phase [2]. Another intriguing system is the sulfide, $CuInCr_4S_8$, where the antiferromagnetic (AFM) J and the ferromagnetic (FM) J' coexist [3]. As shown in Fig. 1, the previously reported M-H curves at 1.4 K (orange and cyan lines for up and down sweeps, respectively) show a metamagnetic behavior with a large hysteresis loop at around H_{c1}=20~40 T, while M reaches only 45 % of the saturation magnetization of ~3.06 μ_B/Cr at 73 T [3].

In this work, we performed magnetization measurements on a polycrystalline powder sample of $CuInCr_4S_8$ by using a single-turn coil system. The observed M-H curve and its derivative dM/dH at 5 K up to 150 T are shown in Fig. 1 (red and blue lines for up and down sweeps, respectively) [4]. Remarkably, a wide 1/2-plateau emerges from H_{c2} ~ 65 T

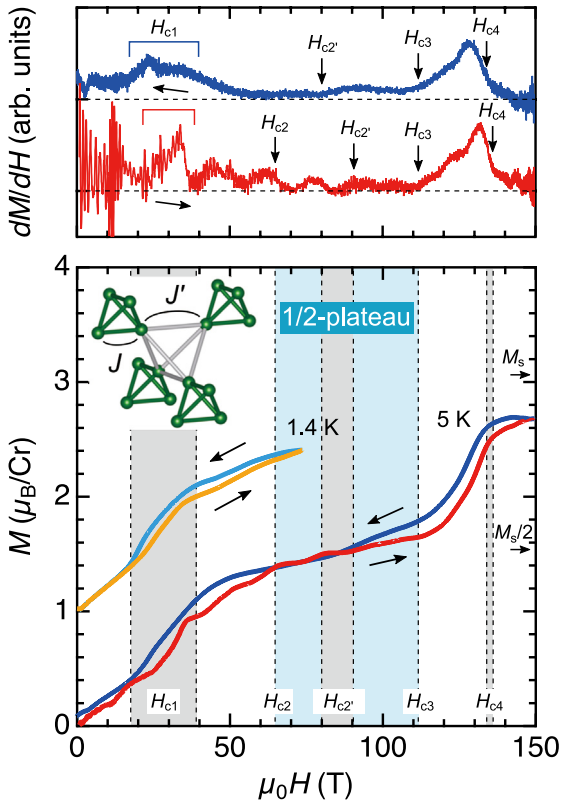

Fig. 1. M-H curves of $CuInCr_4S_8$ measured at ~5 K in a single-turn coil megagauss generator up to 150 T (red and blue curves for up and down sweeps, respectively). Derivatives dM/dH are shown in the upper panel. The previously reported M-H curve measured at 1.4 K up to 73 T are also shown (orange and cyan curves for up and down sweeps, respectively) [3]. Transition fields are denoted by brackets or arrows in the upper panel, and drawn by the shaded areas (first order) or dashed lines (second order) in the lower panel. Inset shows the schematic of the breathing pyrochlore lattice.

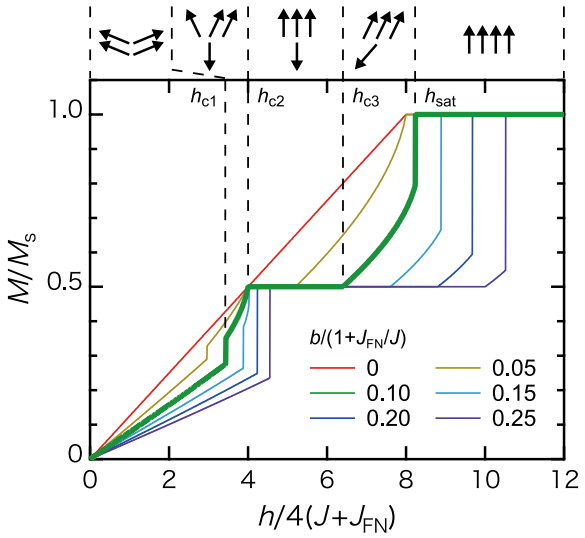

Fig. 2. Calculated magnetization curves as a function of magnetic field h for $b/(1 + J_{FN}/J) = 0$ to 0.25 in steps of 0.05. The spin structures corresponding to the curve for $b/(1 + J_{FN}/J) = 0.10$ (thick green line) are shown in the upper part of the figure.

to H_{c3} ~ 112 T as in Cr spinel oxides. Besides, two inherent features are observed: A slight change in the slope of the *M-H* curve at $H_{c2'}$ ~ 85 T and a shoulder like shape at H_{c4} ~ 135 T. Both are accompanied by a hysteresis, suggesting first-order transitions. The saturation is estimated to H_{sat} ~ 180 T under the assumption that *M* increases linearly above 150 T, where *M* already reaches ~2.7 μ_B/Cr.

For interpreting the observed magnetization process, we constructed an effective spin model mapped onto the fcc lattice, which is derived from the microscopic spin model on the breathing pyrochlore lattice with the SLC as proposed in Ref. [5]. Figure 2 summarizes the calculated *M-H* curves for given values of the SLC parameter *b* and the corresponding spin structures. In spite of the simplification in our model, the calculation well reproduces the main feature of the *M-H* curve of $CuInCr_4S_8$, including a relatively wide intermediate (canted 2:1:1) phase as well as the 1/2-plateau phase with collinear 3:1 spin configuration.

It is noteworthy that the *M-H* curves of $LiGaCr_4S_8$ and $LiInCr_4S_8$, where the FM interaction *J'* is expected to be strong, do not exhibit the 1/2-plateau [3]. Bearing this in mind, the exotic magnetic behaviors on $CuInCr_4S_8$ can be attributed to the relatively dominant AFM interactions $J+J_{FN}$ compared to the FM *J'*, which is achieved only by the moderate breathing distortion in the Cr spinel sulfide. On the other hand, the origins of the hysteretic behaviors on $CuInCr_4S_8$ at $H_{c2'}$ and H_{c4} remain unsolved at the moment. They might originate from the interplay between the SLC and the further neighbor interactions J_{FN}, or the thermal and quantum effects, which are not considered in the present theory. The macroscopic spin structures beyond four sites within small tetrahedra should also be clarified, which is crucial to prove the novelty of the magnetic properties in $CuInCr_4S_8$. Further experimental investigations such as magnetostriction, ESR, and magnetocaloric effect measurements in high magnetic fields are ongoing to elucidate the essence of the successive phase transitions.

References

[1] Y. Okamoto, G. J. Nilsen, J. P. Attfield, and Z. Hiroi, Phys. Rev. Lett. **110**, 097203 (2013).
[2] M. Gen, D. Nakamura, Y. Okamoto, and S. Takeyama, J. Magn. Magn. Mater. **473**, 387 (2019).
[3] Y. Okamoto, M. Mori, N. Katayama, A. Miyake, M. Tokunaga, A. Matsuo, K. Kindo, and K. Takenaka, J. Phys. Soc. Jpn. **87**, 034709 (2018).
[4] M. Gen, Y. Okamoto, M. Mori, K. Takenaka, and Y. Kohama, Phys. Rev. B **101**, 054434 (2020).
[5] K. Aoyama and H. Kawamura, Phys. Rev. B **99**, 144406 (2019).

Authors

M. Gen, Y. Okamoto[a], M. Mori[a], K. Takenaka[a], and Y. Kohama
[a]Nagoya University

Femtosecond Laser Pulse Generation with 20-GHz Repetition Rate

Kobayashi Group

Femtosecond laser pulses have widely used in the field of spectroscopy, metrology and material processing. Especially, material processing using the femtosecond laser has played an important role in the manufacturing because it does not induce thermal damages around the processing area, resulting in the high-quality micro-processing. One important laser parameter for these applications is a pulse repetition rate, which is typically in the range of 1 kHz to 100 MHz. Recent progress of the laser technologies has succeeded to generate femtosecond laser pulses with the gigahertz repetition rate. These high repetition rate pulses have performed efficient material processing compared with the low repetition rate laser pulses. Although the high repetition rate pulses are one candidate of the next-generation laser processing, mechanisms of the efficient material removal have not understood ever before. One reason is a lack of the multi-GHz femtosecond laser sources. Especially, material removal via laser pulses with the repetition rate above 10-GHz have not examined due to the difficulty of generating the multi-GHz laser pulses. We are interested in the generation of such kind of laser pulses.

Several methods have been used to generate multi-GHz repetition rate pulses. We focused on the Kerr-lens mode locked laser (KML), which provides the shortest pulse duration in the femtosecond lasers. The repetition rate of the KML is determined by the cavity length, with the relation of $f = c/L$, where f denotes the pulse repetition rate, c is the speed of the light and L is the cavity length. Therefore, the higher repetition rate is achieved with a shorter cavity length. To date, KML has realized up to 15 GHz repetition frequencies with a pulse duration of 150 fs. This repetition frequency corresponds to a cavity length of 20 mm. To increase the repetition rate above, the cavity length must be shorter than 20 mm. However, the cavity length is limited by the size of the optical element. In addition, typical KML is configured with 5 to 7 optical component, resulting in a large cavity.

In this work [1], we developed the KML with the repletion rate above 20 GHz only using three optical components. This was achieved by designing new cavity geometry, which includes a triangle-cut laser gain medium and multi-

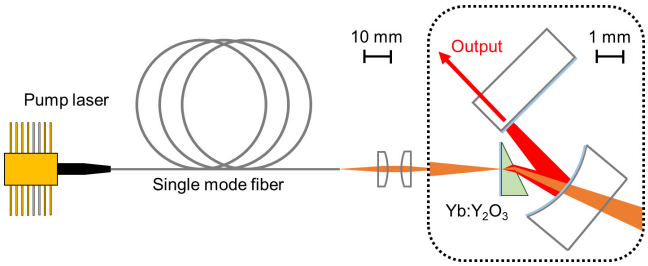

Fig. 1. The cavity geometry

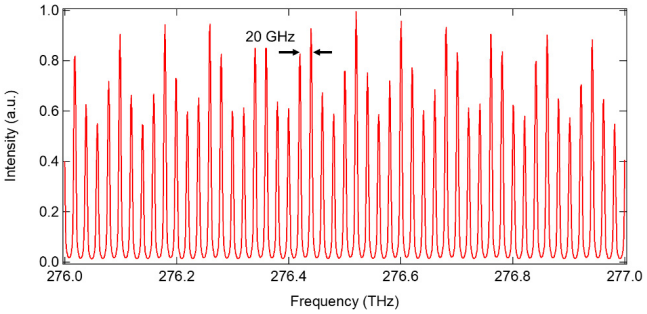

Fig. 2. A part of the output spectrum

functional dielectric coating. The detail cavity configuration is described in Figure 1. We use a gain medium of Yb:Y2O3 ceramic because an output light can be easily amplified by using a Yb-doped fiber amplifier. The pump source was an wavelength-stabilized laser diode coupled to a single mode fiber. One side of the gain medium was coated with a dichroic chirped mirror, while the other side was wedged at the Brewster angle. The concave mirror was dichroic-coated and its angle compensated an astigmatism that was introduced by the Brewster-cut gain medium. The plane mirror was high-reflection coated and was used as the output coupler.

Femtosecond pulse generation was achieved with the cavity length of 15 mm, which determines the pulse repetition rate as 20 GHz. A pulse duration was measured as 120 fs. The pulse repetition rate corresponds to the spacing of longitudinal cavity mode, which can be identified from the optical spectrum. Figure 2 shows a part of the optical spectrum. Each longitudinal mode is clearly observed because the mode spacing is wider than a spectrometer resolution of 4 GHz. To the best of our knowledge, the repetition rate of 20 GHz is the highest frequency in KMLs. Our results will enable the investigation of the material processing above the 10-GHz repetition rate.

Reference
[1] S. Kimura, S. Tani, and Y. Kobayashi, Optica **6**, 532 (2019).

Authors
S. Kimura S. Tani, and Y. Kobayashi

Geometrical Frustration of B-H Bonds in Layered Hydrogen Borides Accessible by Soft Chemistry

I. Matsuda Group

Electrically conducting materials have been essential elements for devices and also for redox reactions on electrodes to sustain our electronic and information society. Miniaturizations in nanotechnology have demanded to reduce the material size down to the atomic limit, however, there are only a few conducting atomic layers, such as graphene, up to now. A search of a novel atomic layer is significant to produce new physical/chemical properties and also to promote various functionalities by combining different types of layers.

In 2017, atomic sheets of hydrogen boride (HB) or borophene are synthesized by the ion-exchange process [1]. The HB sheet has been theoretically predicted to be conducting. However, preliminary experiments of the transport measurement have resulted in insulating properties. This fact has lead experimentalists to take great efforts of improving the purity of the samples to develop the conductivity. Eventually, in the present research [2], high-purity HB sheets were successfully synthesized, as shown in Fig. 1(a), and achieved the highest conductivity in hydrogen borides (0.13 S/cm). Moreover, suppression of the conductivity in previous samples were found to be due to adsorption of residual organic molecules on the sheet. Interestingly, the HB sheet becomes insulating at 30 °C when there are residual molecules and, reversely, returns to have high conductivity below the temperature, as shown in Fig. 1(b).

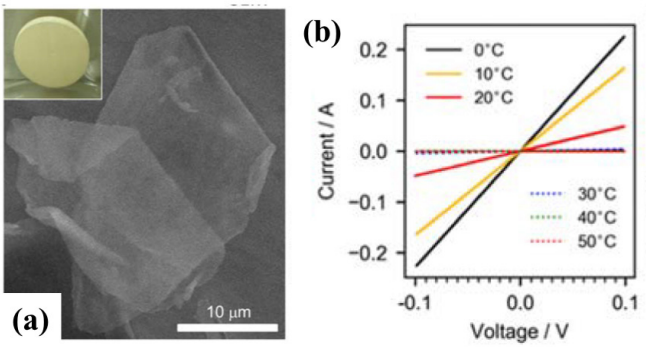

Fig. 1. (a) An image of scanning electron microscope of the hydrogen boride sheet. (b) Current-voltage curves acquired at various temperatures of the sheet [2].

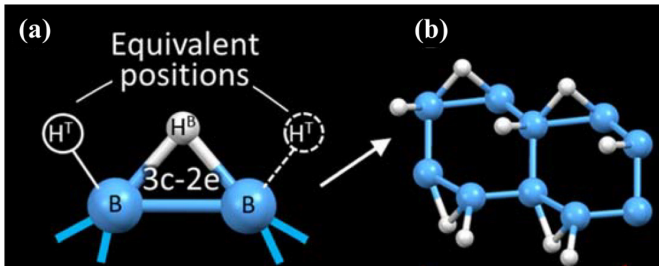

Fig. 2. Atomic structure model of the special local structure in the hydrogen boride sheet [2].

To reveal the intriguing phenomena in terms of the atomic structure, an X-ray scattering experiment was carried out at the synchrotron radiation facility, SPring-8. By analyzing the experimental pair distribution function with the Bayesian optimization, it became clear that there are locally special arrangements of hydrogen atoms in the sheet that allow adsorptions of the residual organic molecules. Figure 2 shows the atomic model. The structure consists of three-center, two-electron (3c-2e) B-H-B bridging bonds as well as ordinary two-center, two-electron (2c-2e) B-H terminal bonds. The present research revealed that conductivity of atomic sheets of hydrogen boride can be regulated by the tiny number of molecules, indicating promising functionalities in sensors or in catalysts.

References
[1] H. Nishino, T. Fujita, N. T. Cuong, S. Tominaka, M. Miyauchi, S. Iimura, A. Hirata, N. Umezawa, S. Okada, E. Nishibori, A. Fujino, T. Fujimori, S. Ito, J. Nakamura, H. Hosono, and T. Kondo, J Am Chem Soc. **139**, 13761 (2017).
[2] S. Tominaka, R. Ishibiki, A. Fujino, K. Kawakami, K. Ohara, I. Matsuda, H. Hosono, and T. Kondo, Chem **6**, 406 (2020).

Authors
S. Tominaka[a,b], I. Matsuda, and T. Kondo[c,d]
[a]International Center for Materials Nanoarchitectonics (MANA), National Institute for Materials Science (NIMS)
[b]Japan Synchrotron Radiation Research Institute
[c]Tokyo Institute of Technology
[d]University of Tsukuba

Ultrafast Unbalanced Electron Distributions in Quasicrystalline 30° Twisted Bilayer Graphene

I. Matsuda, Okazai, and Komori Groups

Layers of twisted bilayer graphene exhibit varieties of exotic quantum phenomena and the twist angle Θ has become an important degree of freedom for exploring novel states of matters. At Θ = 1.1°, the two-dimensional superconductivity was observed, while, at Θ = 30°, a two-dimensional quasicrystal is synthesized. For the quasi-crystalline twisted bilayer graphene (QCTBG), the interlayer interaction is the minimum due to the 30° twisted angle and the massless Dirac Fermions remain in the two layers. The electronic state results in the twelve-fold (dodecagonal) structure and it is composed of upper- and lower-layer Dirac cones, ULDs and LLDs, as shown in Fig. 1.

We explored this electronic structure by focusing on the ultrafast dynamics through time- and angle-resolved photoemission spectroscopy (TARPES), which allows us to directly observe the temporal evolution of fermions in the Dirac cones [1]. The measurement used the pump-probe approach with an infrared pulse with $h\nu$ = 1.55 eV serving as pump and an extreme-ultraviolet pulse with $h\nu$ = 21.7 eV serving as a probe to cover the entire two-dimensional Brillouin zone. Figure 2 shows a summary of the TARPES band diagrams taken at selected delay time for the ULD and LLD bands in a TBG quasicrystal. The results of the periodic non-twisted bilayer graphene (NTBG) are also shown for comparisons. After the pump pulse (intensity ~0.7 mJ/cm^2), the TARPES band diagram of individual bands of bilayers evolves on the femtosecond time scale. To enhance the temporal variations, the band diagrams are shown as the difference between the spectra before and after photoexcitation. The spectral weights for all bands decrease immediately below μ_{eq} and increase above μ_{eq} at Δt= 0.05 ps. This reflects the excitation of electrons from the occupied bands to the unoccupied bands. At Δt= 0.16 and 0.32 ps, the difference intensity decreases with delay time, which corresponds to the relaxation of photoexcited carriers.

To evaluate the occupation of Dirac cones by nonequilibrium carriers, we made energy distribution curves of the Dirac bands by integrating over momentum space and summarized the chemical-potential shift or the photo-induced potential as Fig. 3. As shown in the figure, the different time evolution for potential indicates that the ULD and LLD bands have the opposite behavior after Δt = 0.2 ps (*i.e.* the ULD undergoes a negative shift whereas the LLD undergoes a positive shift). Interestingly, the photo-induced potential for the NTBG band remains constant at essentially zero over the same time delay. The striking difference among the three types of the Dirac cones provides clear evidence of a carrier imbalance between the ULD and LLD bands of the QCTBG on the ultrafast time scale. Through the kinetic analysis, the key mechanism was found to involve the carrier transport between layers and the transient doping from the substrate interface. Our TARPES measurements on replicas of the ULD and LLD bands, shown in Fig.1, revealed that the ultrafast dynamics scheme continues after the Umklapp scattering. The dynamics in the atomic layer opens the possibility of new applications and creates interdisciplinary links in the optoelectronics of van der Waals crystals.

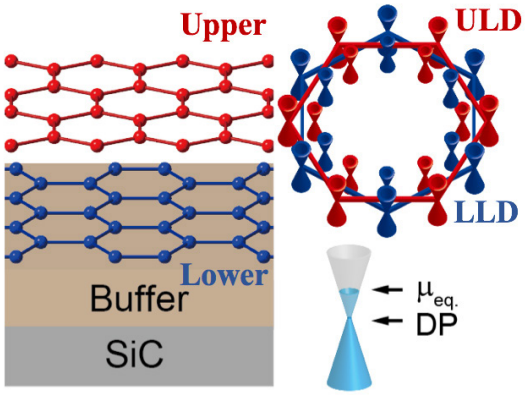

Fig. 1. Crystal and electronic structure of a twisted bilayer graphene quasicrystal on the SiC substrate. The upper- and lower-layer graphene sheets are twisted by 30 degrees with respect to each other. In the momentum space, electronic structure of a TBG quasicrystal is composed of the upper-layer Dirac (ULD) and lower-layer Dirac (LLD) bands. The inner-red and blue Dirac cones represent the replica bands of ULD and LLD bands by the umklapp scattering induced by the incommensurate interlayer stacking of the quasi-crystallinity. The quasi-crystalline twisted bilayer graphene was n-type: Dirac point and equilibrium chemical potential are denoted as DP and μ_{eq}, respectively.

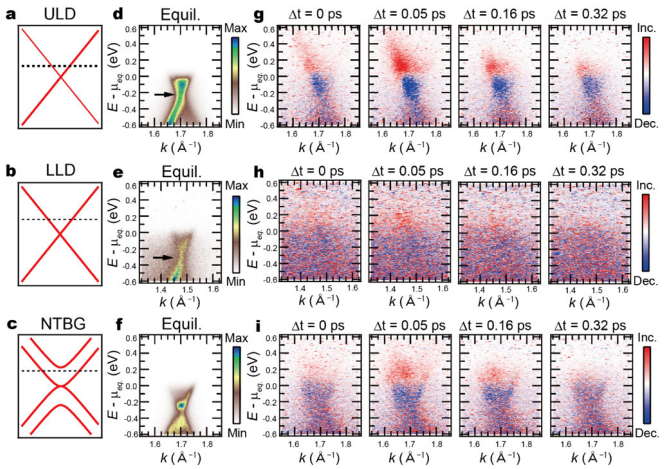

Fig. 2. Calculated band structures for the ULD and LLD bands in QCTBG and for non-twisted bilayer graphene (NTBG) band, respectively. Dashed lines indicate the μ_{eq} level. **d–f,** Equilibrium angle-resolved photoemission spectra for ULD, LLD, and NTBG bands. DP is indicated by an arrow. **g–i,** Difference images of TARPES for the ULD, LLD, and NBLG bands. Red and blue points represent increasing and decreasing photoemission intensity, respectively.

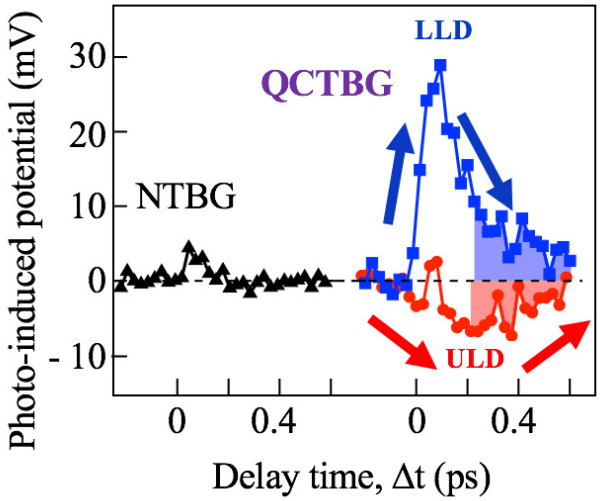

Fig. 3. Chemical-potential shift as a function of pump-probe delay time for LLD and ULD bands for QCTBG. For comparison, the result for NTBLG is also shown.

Reference
[1] T. Suzuki, T. Iimori, S. J. Ahn, Z. Yuhao, M. Watanabe, J. Xu, M. Fujisawa, T. Kanai, N. Ishii, J. Itatani, K. Suwa, H. Fukidome, S. Tanaka, J. R. Ahn, K. Okazaki, S. Shin, F. Komori, and I. Matsuda, ACS Nano **13**, 11981 (2019).

Authors
I. Matsuda, T. Suzuki, K. Okazaki, and F. Komori

Photoinduced Hydrogen Release from Hydrogen Boride Sheets

I. Matsuda Group

Materials consisting of one atomic layer, such as graphene, are one of the two-dimensional materials that have shown various physical and chemical properties that are different from ordinary ones. Recently, novel atomic layers of boron, so-called "borophene", were reported and the materials were found to surpass the performance of graphene by theoretical works. However, the growth requires special conditions such as appropriate metal substrates, high temperature and ultra-high vacuum.

Under these circumstances, we have succeeded in synthesizing a hydrogen boride (HB) sheet (Fig. 1(a)), which is hydrogenated borophene or borophane, under the ambient condition. Since the HB sheet is composed only of the light elements, boron and hydrogen, the mass hydrogen density is as high as 8.5%, and it was expected to be applied as a safe and lightweight material for the hydrogen carrier that replaces the conventional high-pressure hydrogen gas cylinder with a risk of explosion. However, it has required to consider a procedure to extract hydrogen atoms/molecules from the sheet before the actual use. In the present research, we designed and verified the hydrogen release by the light irradiation [1].

According to the first-principles calculation of the hydrogen boride sheet, the optical transition ($\alpha \rightarrow \beta$) occurs from the bonding orbital of boron to the antibonding orbital, as shown in Fig. 1(b). On the other hand, there is also an optical transition ($\alpha \rightarrow \gamma$) to the antibonding orbital of hydrogen. Since this transition energy corresponds to a photon energy of ultraviolet (UV) ray, it is hypothesized that hydrogen could be released from a hydrogen boride sheet only by the UV irradiation even under the ambient condition.

The experimental verification was made by analyzing the gas molecules emitted from the hydrogen boride sheets with using two types of light sources. One type of the sources irradiates visible light that can cause the optical transition ($\alpha \rightarrow \gamma$), while the other type irradiates ultraviolet light that can induce the optical transition ($\alpha \rightarrow \beta$). As shown in Fig. 2, it was confirmed that the hydrogen gas was generated by exposure of the ultraviolet ray. By quantifying the amount

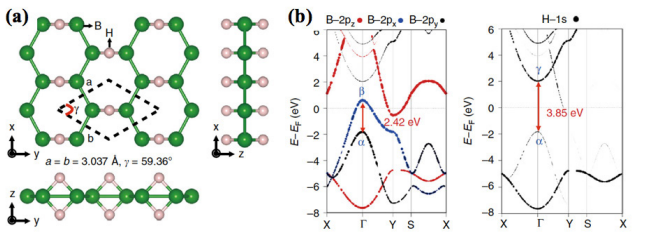

Fig. 1. (a) Top and side views of the atomic structure of the HB sheet. The unit cell is indicated by the dashed lines. (b) Projected band structures of B- and H-originated orbitals [1].

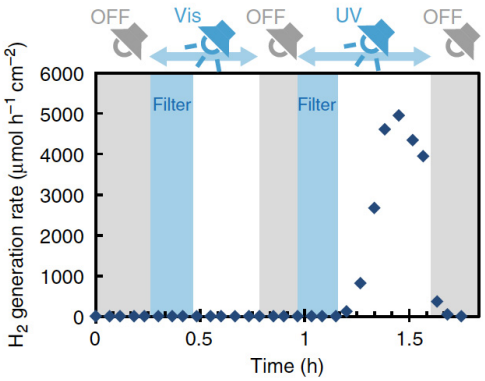

Fig. 2. A amount of H_2 production by the light irradiation with two different light sources [1].

of the hydrogen production, it was found that 8% of the mass of the hydrogen boride sheet was consumed for the hydrogen release. For conventional hydrogen storage alloys, the mass hydrogen density is up to 2%. Even a promising hydrogen carrier of the organic hydrides reaches mass hydrogen density of 6.2% with heating above 300 °C. Thus, the hydrogen boride sheet can be a safe, lightweight and simple portable hydrogen carrier with a simple light operation of the extremely high hydrogen release.

Reference
[1] R. Kawamura, N. T. Cuong, T. Fujita, R. Ishibiki, T. Hirabayashi, A. Yamaguchi, I. Matsuda, S. Okada, T. Kondo, and M. Miyauchi, Nature Commun. **10**, 4880 (2019).

Authors
I. Matsuda, T. Kondo[a,b], and M. Miyauchi[c]
[a]Tokyo Institute of Technology,
[b]University of Tsukuba
[c]Tokyo Institute of Technology

Surface-State Coulomb Repulsion Accelerates a Metal-Insulator Transition in Topological Semimetal Nanofilms

I. Matsuda, Sugino, and Komori Groups

By reducing the size of materials in the microscopic scale, the electronic states are governed by the rules of quantum mechanics and the various quantities, such as energy levels, take discrete values (the quantum size effect, QSE). Thus, there can be a case that gapless metal films become insulating at the nanoscale. Such a QSE-induced transition into an insulating phase in semimetallic nanofilms was predicted more than half a century ago on bismuth (Bi) films [1]. Despite the researches of spectroscopy and transport experiments, the previous results have remained contradictions, indicating an interesting mechanism behind.

In the present research, we revealed an unexpected mechanism of the transition in Bi by combining of high-resolution measurements of angle-resolved photoemission spectroscopy (ARPES) on high-quality films and the density-functional theory (DFT) calculations [2]. Figure 1 (a) shows peak-enhanced ARPES images resolving all quantized bulk bands and surface bands. One can see that the top quantized levels are clearly shifting below the Fermi level with decreasing thickness. This is the first direct observation of the QSE-induced transition into an insulating phase in Bi films.

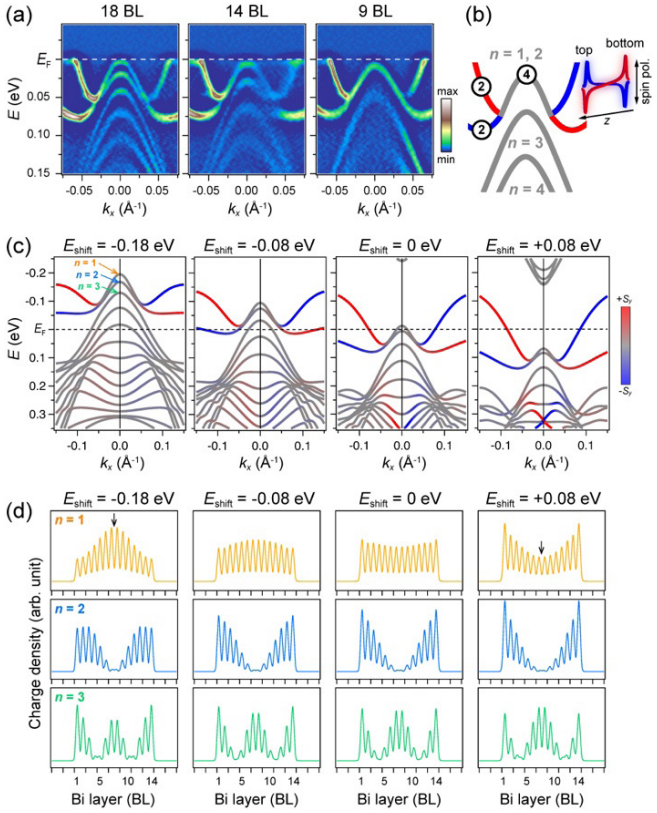

Fig. 1. (a) Peak-enhanced ARPES images measured on atomically thin Bi films. 1 bilayer (BL) of Bi corresponds to 3.9 Å. (b) Schematic of unusual band connections. The number indicates degeneracy of each band. (c) DFT band structures calculated on a 14 BL Bi slab with energy shifts manually induced. (d) Wave function characters calculated for n = 1, 2, 3 quantized states.

The high-resolution ARPES observation reveals an unusual signature: both of two surface bands connect to the top quantized bulk band. Because of the presence of surface states at the top and bottom of a film, these surface bands are doubly degenerate. Thus, this band connection readily means that the top quantized level must be quadruply degenerate. Although this breakup of conventional quantization rule was totally unexpected, our first-principles calculations reproduced the behavior. In Fig. 1(c) shows band structures that are intentionally shifted via modulation of lattice parameters. In the leftmost panel, quantized energy levels are regularly ordered, and n = 1, 2, 3 states possess wave function characters expected for ones confined in an ideal quantum well. From the leftmost to the rightmost panels, the separation between n = 1 and 2 levels is gradually reduced, and the wave function characters divert from the ideal cases and get localized near surfaces.

What is the essential mechanism for the unexpected level degeneracy and the bulk-to-surface transformation of quantized wave functions? In the DFT framework, an effective one-body potential and a total charge density are determined by a self-consistent cycle reflecting Coulomb interaction. From left to right in Fig. 1(c), the occupation of the surface bands increases and their relative contributions to the total charge density increase.

This tendency makes Coulomb repulsion among electrons compress the total charge density toward the film center. In the one-body picture of the DFT framework, a potential barrier around the film center is induced by this compressed total charge, which creates a double-well potential, as illustrated in Fig. 2(a). Such a double-well potential supports degenerate ground states whose wave functions are localized in both wells with opposite parity, which explains

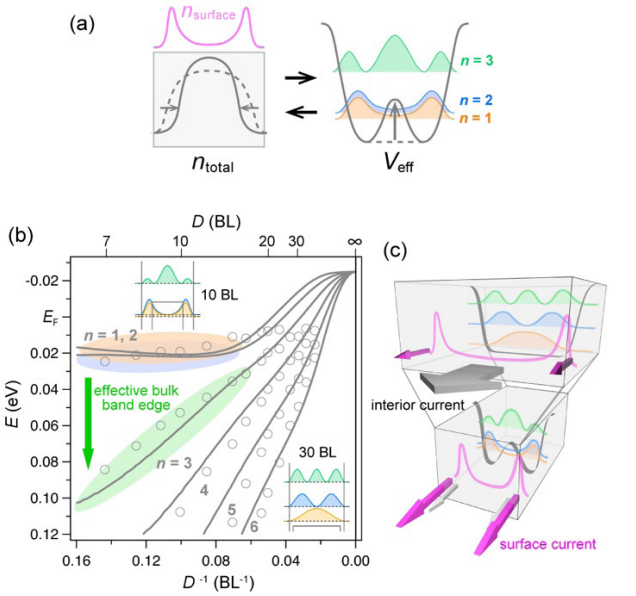

Fig. 2. (a) Schematic of a self-consistent cycle for a total charge density and an effective confinement potential. (b) Comparison of experimental thickness dependence of quantized levels (markers) and a numerical simulation (solid lines). The inset depicts wave function characters obtained in the simulation. (c) Schematics of the new class of size effects driven by increased Coulomb repulsion from surface states.

observations above. Furthermore, experimental thickness dependence of quantized levels was excellently reproduced by a numerical simulation using a single-well potential which gradually deforms into a double well (Fig. 2(b)).

This unprecedented picture naturally reconciles the strange contradiction observed in previous studies: even if the top quantized levels can cross the Fermi level, the states effectively behave as surface-conducting states, and the film interior is insulating as observed in transport experiments, as shown in Fig.2(c). Thus, we established the complete picture of the half-century problem in Bi, which demonstrates a new class of size effects driven by increased Coulomb repulsion from surface states.

References

[1] V. B. Sandomirskii, Quantum size effect in a semimetal film. *Soviet Physics JETP* **25**, 101 (1967).
[2] S. Ito, M. Arita, J. Haruyama, B. Feng, W.-C. Chen, H. Namatame, M. Taniguchi, C.-M. Cheng, G. Bian, S.-J. Tang, T.-C. Chiang, O. Sugino, F. Komori, and I. Matsuda, Science Advances **6**, eaaz5015 (2020).

Authors
S. Ito, O. Sugino, F. Komori, and I. Matsuda

Real-Time Observation of Electronic, Vibrational, and Rotational Dynamics in Nitric Oxide with Attosecond Soft X-Ray Pulses at 400 eV

Itatani Group

Attosecond science has made tremendous progress in the past two decades along with the advance of Ti:sapphire-based ultrafast laser technologies. Intense ultrashort pulses in visible and near infrared regions are now routinely produced, which allow to produce attosecond pulses in the extreme ultraviolet (EUV, photon energy <200 eV) by using the physics of high harmonic generation (HHG). Since the

maximum photon energy (or the high harmonic cut off) is scaled by the ponderomotive potential that is proportional to the square of laser wavelength, intense ultrashort-pulse IR sources are required to extend the spectral range of attosecond pulses towards the soft X-ray (SX) range. Such spectral extension of high harmonics paves a way to element-specific ultrafast spectroscopy using atomic absorption edges. The features of atomic selectivity, photon-in/photon-out methodology, and the preservation of temporal resolution on the attosecond time scale are attractive to construct attosecond transient spectroscopy that can generally be applicable to atoms, molecules, and condensed matters even in the presence of strong external fields.

Since 2008, Our group developed a carrier-envelope phase-stable ultrashort-pulse IR source that used BiB_3O_6 (BiBO) crystals as an optical parametric chirped-pulse amplification (OPCPA) medium. Because of the extremely broadband gain of BiBO-OPCPA in 1.2-2.2 μm, we successfully produced CEP-stable sub-two-cycle IR pulses (1.5 mJ, 10 fs) at a repetition rate of 1 kHz [1]. The high pressure gas cell that is filled with Ne or He gases allow to generate attosecond continua that cover nearly all of the water window.

Using the BiBO-OPCPA and a high-pressure He target (2.4 bar), we demonstrated attosecond SX spectroscopy of NO molecules that were exposed to intense IR fields as shown in Fig. 1 [2]. The output from BiBO-OPCPA (1.6 μm, 10 fs, 1.5 mJ, 1 kHz, CEP stable) was split to pump and probe pulses. The pump pulses induced field ionization, followed by multi-scale coherent dynamics in NO molecules. The probe pulses produced attosecond SX pulses that monitored the unoccupied energy levels by inner shell excitation. The transmitted SX spectra were then recorded with a grating-based spectrometer with a back-illuminated x-ray CCD camera.

Figure 2(a) shows the measured transient differential absorbance of NO (pump intensity: ~1×10^{14} W/cm^2). The static absorbance of NO without the pump pulses is shown in Fig. 2(b). The main feature in Fig. 2(a) is the appearance of upshifted absorbance of the 1s-2π peak at 402.5 eV when the IR pulse precedes the SX pulse. This upshift comes from NO^+ generated by tunnel ionization. Figure 2(c) shows the differential absorbance at 403.1 eV around the time origin (pump intensity: ~2×10^{14} W/cm^2). A step-like absorbance increase with a period of 2.7 fs (half cycle of the pump IR pulse) was observed. These steps are characteristic of tunnel ionization. Figure 2(d) shows the oscillation of the central energy of the NO^+ 1s-2π peak with a period of 14.5 ± 0.1 fs. Figure 2(e) shows the differential absorbance of the NO 1s-2π peak (pump intensity: ~1×10^{14} W/cm^2). The peak structure around 100 fs can be explained by laser-induced molecular alignment. As far as we know, this attosecond

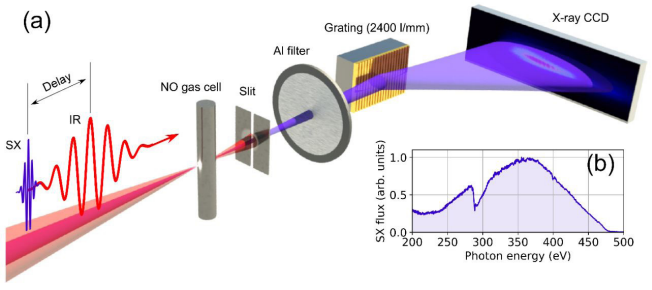

Fig. 1. (a) Schematic of the experimental setup. (b) Typical SX spectrum obtained by HHG in Helium.

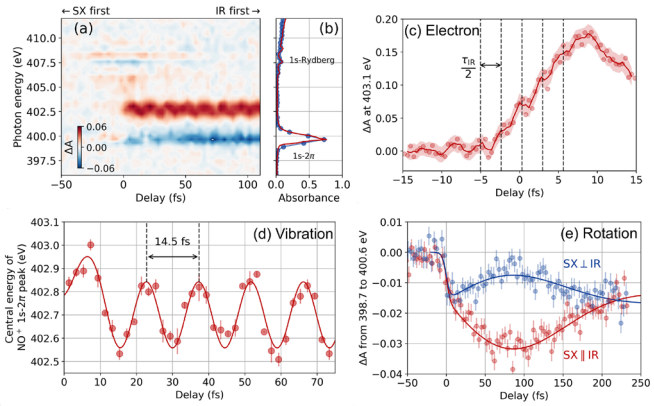

Fig. 2. (a) Time-resolved absorption spectra of NO. (b) Static absorbance of NO without the pump pulses measured in our experiment (blue circles) and a synchrotron (red curve). (c) Absorbance change of the NO^+ 1s-2π peak at 403.1 eV (red circles) and its 3-point rolling average (red curve). (d) Central energy of the NO^+ 1s-2π peak (red circles) and the fitting by a cosine and Gaussian function (red curve). (d) Absorbance change of the NO 1s-2π peak (398.7 to 400.6 eV) with parallel (red circles) and perpendicular (blue circles) IR and SX polarizations. The solid curves are calculation results considering molecular alignment. The pump intensity is ~1×10^{14} W/cm^2 for (a, b, d, e) and ~2×10^{14} W/cm^2 for (c). The polarizations of the IR and SX are parallel for (a, c, d).

transient spectroscopy is at the highest photon energy, and the first experiment to measure the field-induced alignment of molecular ions.

Attosecond transient spectroscopy of NO molecules reveals that the absorption spectra near the nitrogen K-edge (~400 eV) allow to capture full quantum dynamics (i. e., electronic, vibrational, and rotational dynamics) with a single spectrogram. These results show that attosecond soft-x-ray absorption spectroscopy is a powerful technique to trace the molecular dynamics of various freedoms in a different time and energy scales.

References
[1] N. Ishii, K. Kaneshima, T. Kanai, S. Watanabe, and J. Itatani, J. Opt. **20**, 014003 (2018).
[2] N. Saito, H. Sannohe, N. Ishii, T. Kanai, N. Kosugi, Y. Wu, A. Chew, S. Han, Z. Chang, and J. Itatani, Optica **6**, 1542 (2019).

Authors
N. Ishii, K. Kaneshima, T. Kanai, S. Watanabe[a], N. Saito, H. Sannohe, N. Kosugi[b], Y. Wu[c], A. Chew[c], S. Han[c], Z. Chang[c], and J. Itatani
[a]Tokyo University of Science
[b]Institute of Materials Structure Science, High Energy Accelerator Research Organization
[c]University of Central Florida

Efficient Terahertz Harmonic Generation with Coherent Acceleration of Electrons in the Dirac Semimetal Cd_3As_2

Matsunaga, Tsunetsugu, and Itatani Groups

Intense waveform-controlled light field has revealed highly-intriguing nonlinear and nonperturbative light-matter interactions such as high-order harmonic generation (HHG). Recently, HHG in solids with mid-infrared (IR) excitation has been reported, opening a new route toward laser-based stable and compact extreme ultraviolet (EUV) sources. Meanwhile, in the long wavelength limit, efficient third harmonic generation (THG) in the terahertz (THz) frequency regime has also been reported in a superconducting film [1]. Realization of such extreme nonlinear photonics in the

THz region at room temperature is highly desired for high-speed THz electronics and for nonlinear frequency mixing in sensitive detection of cosmic microwave background. From these perspectives, graphene has attracted tremendous attention as a candidate for efficient THz frequency multiplication using massless Dirac electrons because the current flow across the Dirac node in the momentum space is expected to exhibit remarkably large nonlinearity [2], as schematically shown in Fig. 1(a). Very recently, HHG in the THz frequency range in graphene was clearly demonstrated by using a very intense light source that is based on a large-scale electron accelerator [3]. In their experiment, the nonlinear coefficients in graphene were found to be much larger than typical materials, whereas the conversion efficiency is still limited by its monolayer nature.

In our work [4], we investigated THz nonlinear spectroscopy for thin films (thickness of 240 nm) of the three-dimensional Dirac semimetal Cd_3As_2 at room temperature using a laboratory-scale laser source. We have observed intense THz pulse generation using this laser-based setup and performed nonlinear transmission spectroscopy of quasi-monochromatic intense THz pulse with the center frequency of 0.8 THz [4]. Figure 1(b) shows the results of the spectral amplitude for transmitted pulses. A sharp peak of THG is clearly observed at 2.4 THz, which demonstrates the efficient nonlinear frequency conversion of the THz light. For comparison, we examined monolayer graphene with the same excitation condition, and also observed the THG signal. The nonlinear coefficient for graphene was estimated as ~10^{-9} m^2V^{-2}, which is consistent with the previous literature, and several orders of magnitude larger than typical materials. Compared to graphene, the conversion efficiency in Cd_3As_2 is much larger due to the film thickness, and the observed THG field amplitude is ~100 V/cm under the pump field of 6.5 kV/cm inside the film. In the next step, we can reduce the Fresnel reflection loss at the sample surface by using an antireflection coating on the film or directly applying the field via contact electrodes, which will allow to generate further stronger harmonics for realistic applications in ultrafast electronics.

To understand the efficient HHG mechanism in Cd_3As_2 in a microscopic picture, we also performed THz pump-THz probe spectroscopy. In the case of graphene, the origin of the THz HHG was successfully explained by a thermodynamic model where electrons were assumed to be in quasi-equilibrium with repeating heating and cooling processes very rapidly within the THz timescale [3]. However, such a picture of incoherent electron dynamics is essentially different from the originally proposed scheme to induce large nonlinearity in massless Dirac systems [2]. Our time-resolved THz spectroscopy in this work has revealed that the relaxation rate of the carriers in Cd_3As_2 is ~8 ps, which

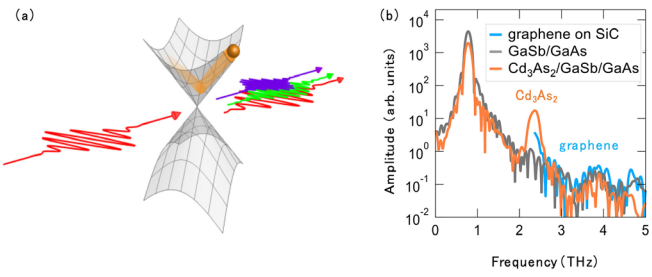

Fig. 1. (a) A schematic of high harmonic generation due to the coherent acceleration of Dirac electrons. (b) Amplitude spectra of the transmitted intense THz pulse with appearance of the THz THG in Cd_3As_2 thin film.

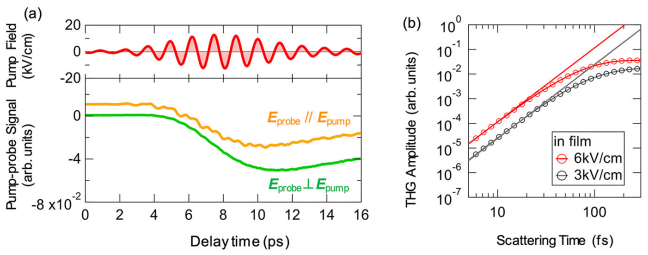

Fig. 2. (a) Pump THz field waveform (upper). THz pump-THz probe signal as a function of the pump-probe delay time with different polarization configurations. (b) Calculated THG amplitude in the intraband acceleration model as a function of the scattering time.

is much longer than one optical cycle of the pump field (1.25 ps) in contrast to the rapid cooling in graphene (<< 1 ps). We performed the thermodynamic-model calculation and confirmed that this model cannot reproduce the efficient THG with realistic parameters.

In addition, we experimentally investigated the electron dynamics during the THz wave irradiation and found that the nonlinear response manifests itself almost only for the pump polarization direction, as shown in Fig. 2(a). The result can be well explained by the intraband current model [2]. When electrons are accelerated by the pump field, the electron distribution function in the momentum space moves rapidly back and forth along with the pump polarization direction, but it appears as if "nothing happens" in other probe polarization directions, which was observed as the anisotropic nonlinearity. We also calculated the nonlinear current by considering the intraband acceleration in a simple linear dispersion model and confirmed that the intraband acceleration model can reproduce the value of the THG amplitude and its saturating behavior which we observed.

Our results show that, even though the scattering time of ~145 fs in Cd_3As_2 is still shorter than the pump field cycle of 1.25 ps, the nonlinear response is well described by the intraband current by coherent acceleration of electrons. It can be explained by the fact that asymmetric non-thermal electron population distribution in momentum space can be developed as rapidly as in ~85 fs. Figure 2(b) shows the calculated result of the THG amplitude as a function of the scattering time. If the scattering time is as long as 100 fs, the THG amplitude strongly saturates. Therefore, the scattering time of 145 fs in this material is "long enough" for nonperturbative intraband acceleration driven by the optical field of a few-kV/cm.

In future, even longer scattering times might be achieved in other topological semimetals with massless dispersion, which will allow us more efficient frequency conversion, perhaps at sub-kV/cm field strength. Our results will open a new pathway towards a novel frequency convertor in the THz frequency based on Dirac semimetals.

References

[1] R. Matsunaga *et al.*, Science **345**, 1145 (2014).
[2] S. A. Mikhailov, Europhys. Lett. (EPL) **79**, 27002 (2007).
[3] H. A. Hafez *et al.*, Nature **561**, 507 (2018).
[4] B. Cheng†, N. Kanda†, T. N. Ikeda, T. Matsuda, P. Xia, T. Schumann, S. Stemmer, J. Itatani, N. P. Armitage, and R. Matsunaga, Phys. Rev. Lett. **124**, 117402 (2020). (†: equal contribution)

Authors

B. Cheng[a,†], N. Kanda[†], T. N. Ikeda, T. Matsuda, P. Xia, T. Schumann[b], S. Stemmer[b], J. Itatani, N. P. Armitagea, and R. Matsunag[a] ([†]: equal contribution)
[a]The Johns Hopkins University
[b]University of California

Observation of Terahertz Anomalous Hall Effect in Weyl Antiferromagnet Mn_3Sn Thin Films

Matsunaga and Nakatsuji Groups

Control of magnetism has been a key issue for modern data processing and recording in spintronic devices. From the viewpoint of manipulation speed, antiferromagnets are promising materials because spin precession motion occurs typically at terahertz (THz = 10^{12} per second) frequencies, a few orders of magnitude higher than ferromagnets. Readout of the magnetization information in antiferromagnets is, however, still very difficult since they are generally not sensitive to the external field because of the much smaller net magnetization than in ferromagnets, which has made their practical application challenging. In 2015, Nakatsuji group in ISSP has discovered large anomalous Hall effect (AHE) in an antiferromagnet Mn_3Sn at room temperature comparable to ferromagnets in spite of the vanishingly-small net magnetization [1]. The exceptionally-large response originates from an inverse-triangular spin structure where the spins form a 120-degree order with negative vector chirality in the ab plane. Such noncollinear antiferromagnetic spin order in the Kagome bilayer is characterized by cluster magnetic octupole moments, which macroscopically breaks time-reversal symmetry. Deep understanding of the dynamical properties of Mn_3Sn in the THz frequency range is highly desired for ultrafast readout of the antiferromagnetic spin order to develop novel functional devices.

In another point of view, Mn_3Sn has also been interested as a possible candidate for Weyl semimetals with broken time-reversal symmetry, or "Weyl (antiferro)magnets", which host massless electron dispersions with opposite chirality in the vicinity of the Fermi energy [2]. Since the ac anomalous Hall effect is directly related to the interband excitation across the Weyl nodes, a number of theoretical efforts have been recently devoted to investigating the ac anomalous Hall conductivity in $\sigma_{xy}(\omega)$ Weyl semimetals. Investigating $\sigma_{xy}(\omega)$ experimentally is therefore important for understanding novel electromagnetic responses related with the Berry curvature in Weyl semimetals.

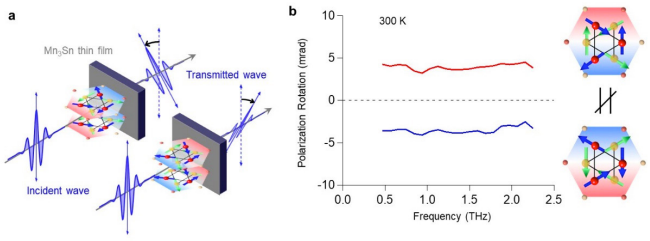

Fig. 1. (a) A schematic of THz wave polarization rotation in Mn3Sn thin films depending on the antiferromagnetic spin order. (b)The experimental results of the polarization rotation spectra with different antiferromagnetic spin orders.

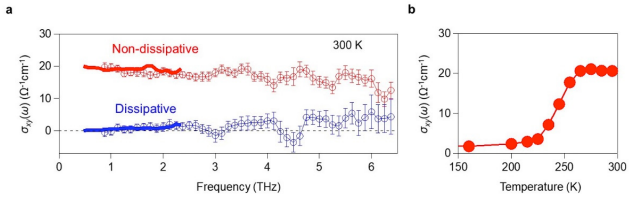

Fig. 2. (a) Frequency dependence of real- and imaginary-part anomalous Hall conductivity, indicating non-dissipative and dissipative part, respectively. (b) Temperature dependence of the real-part anomalous Hall conductivity.

Frequency dependence of the AHE can be observed in an optical method by measuring the polarization rotation of transmitted light. It is based on the relation between $\sigma_{xy}(\omega)$ and the polarization rotation angle $\theta(\omega)$:

$$\theta(\omega) + i\eta(\omega) = \frac{\sigma_{xy}(\omega)Z_0 d}{1 + n_s + \sigma_{xy}(\omega)Z_0 d}$$

where $\eta(\omega)$ an ellipticity angle, d the film thickness, Z_0 the vacuum impedance, n_s the substrate refractive index, and σ_{xx} the longitudinal conductivity. In the present work, we developed polarization-resolved THz time-domain spectroscopy setups with precise polarization resolution up to 0.05 mrad in 0.5-2.0 THz frequency window for 20-min accumulation time [3]. Figure 1(a) shows a schematic of our measurement. Using Mn_3Sn thin films with 50-200 nm thicknesses [4], we clearly observed the polarization rotation of transmitted THz wave at room temperature and zero magnetic field as shown in Fig. 1(b), depending on the direction of the cluster magnetic octupole moments. The result quantitatively agrees with the large AHE previously reported in the DC resistivity measurement.

We also performed the polarization-resolved THz spectroscopy with broad band frequency range up to 6 THz (25 meV) [3]. Figure 2(a) shows the result of real- and imaginary-part $\sigma_{xy}(\omega)$, corresponding to the non-dissipative and dissipative Hall current, respectively. The results demonstrate small dissipation in the AHE up to THz frequencies, which is consistent with an intrinsic origin of it. Figure 2(b) shows the temperature dependence of $\sigma_{xy}(\omega)$. The strong suppression of $\sigma_{xy}(\omega)$ below 250 K is consistent with the spin-reorientation phase transition from the inverse-triangular structure to a helical spin ordering along the c-axis. The development of the helical spin ordering along the c-axis recovers the macroscopic time-reversal symmetry, which results in the disappearance of the AHE.

The observation of the THz AHE at room temperature demonstrates the ultrafast readout for the antiferromagnetic spintronics using Mn_3Sn. Our all-optical approach in a noncontact way with picosecond time resolution also opens a new avenue for studying nonequilibrium dynamics in Weyl antiferromagnets.

References

[1] S. Nakatsuji, N. Kiyohara, and T. Higo, Nature **527**, 212 (2015).
[2] K. Kuroda *et al.*, Nature Mater. 16, 1090 (2017).
[3] T. Matsuda, N. Kanda, T. Higo, N. P. Armitage, S. Nakatsuji, and R. Matsunaga, Nature Commun. **11**, 909 (2020).
[4] T. Higo, D. Qu, Y. Li, C. L. Chien, Y. Otani, and S. Nakatsuji, Appl. Phys. Lett. **113**, 202402 (2018).

Authors

T. Matsuda, N. Kanda, T. Higo[a], N. P. Armitage[b], S. Nakatsuji, and R. Matsunaga
[a]CREST, Japan Science and Technology Agency
[b]The Johns Hopkins University

Photoinduced Possible Superconducting State with Long-Lived Disproportionate Band Filling in FeSe

Okazaki Group

Photoexcitation is a very powerful way to instantaneously drive a material into a novel quantum state without any fabrication, and variable ultrafast techniques have been developed to observe how electron, lattice, and spin degrees of freedom change. One of the most spectacular phenomena is photoinduced superconductivity, and it has been suggested in cuprates that the transition temperature T_c can be enhanced from the original T_c with significant lattice modulations.

Here, we demonstrate the possibility for another photo-induced high-T_c superconducting state in the iron-based superconductor FeSe using time- and angle-resolved photoemission spectroscopy (TARPES) [1]. We find that a photo-induced superconducting gap appears as a result of significant lattice modulation. Our demonstration of how we can change electron- as well as lattice-structure in FeSe by strong photo-excitation provides important insight into the next-generation devices using photo-induced superconductors, e.g. ultrafast switches or quantum engineering.

Figures 1**a** and 1**b** show the time-dependent oscillatory components of the photoemission intensity integrated above the Fermi level (E_F) after photo-excitation for the hole and electron Fermi surfaces (FSs), respectively. The fits by sinusoidal functions are shown as black solid lines. The clear appearance of single cosine-like signature is noticed both for the hole and electron FSs. The frequency of this oscillation is 5.3 THz, which corresponds to the A_{1g} coherent phonon mode shown in Fig. 1**c**. Moreover, the amplitude of the oscillation significantly increases with the increase of pump fluence shown in Fig. 1**d**. These signatures indicate that the observed coherent phonons is explained by the displacive excitation mechanism, in which coherent phonons are generated as a result of the photo-induced modulation of the lattice structure.

In order to study the photo-induced electronic state in more detail, we further conducted long time-scale measurements. Figures 2**a** and 2**b** show the photo-induced leading-edge midpoint (LEM) shifts for the electron and holes FSs as a function of time and pump fluence, respectively. One can notice that the LEM shift at the hole FS is negative, while the LEM shift at the electron FS is negligibly small. This unbalanced shift is due to disproportionate band filling schematically shown in Fig. 2**c**. It is of note that the disproportionate band filling lasts for a quite long time of ~1ns owing to the indirect semimetallic band structure, where the electron-hole recombination must accompany the assistance of phonons with a large momentum.

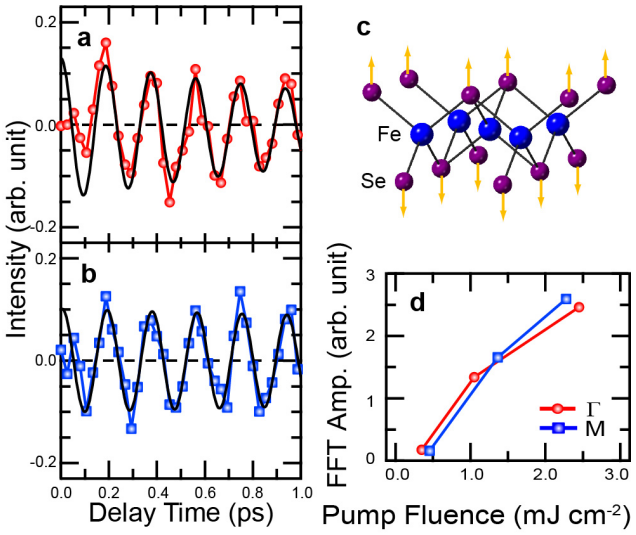

Fig. 1. **a**, **b**. Oscillatory components for the time-dependent photoemission intensities integrated above Fermi Energy for the hole and electron Fermi surfaces. **c**. Illustration of lattice modulation by photoexcitation, corresponding to A_{1g} phonon mode. **d**. Fast Fourier transform (FFT) amplitude at 5.3 THz for the hole and electron FSs as a function of the pump fluence.

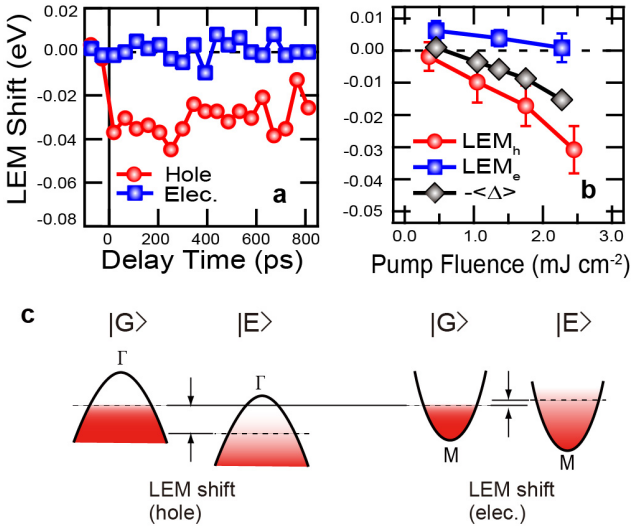

Fig. 2. **a**, **b**. Shifts of the leading-edge midpoints (LEM) as a function of time and pump fluence for the hole and electron FSs. In Fig. 2b, the averaged superconducting gap, <Δ> is shown as black solid lines and markers. **c**. Illustration of photoinduced LEM shifts for the hole (Γ) and electron (M) bands. |G> and |E> represent the ground and photoexcited states, respectively.

The origin of the disproportionate band filling is most likely ascribed to the emergence of photo-induced superconducting gap because FeSe has no other competing orders such as the anti-ferromagnetic order in the equilibrium state. To further investigate the photo-induced superconducting gap, we extract the superconducting gap and performed photo-intensity dependent measurements, as shown in Fig. 2**b**. We find that with increasing photo intensity, the superconducting gap also increases, which suggests that the enhancement of superconducting order is enabled by tuning light intensity.

In summary, our finding of the possible photo-induced superconducting state for FeSe can provide another platform of photo-induced superconductivity. The significant property in this system is the longevity of the photo-induced state, which is also called metastable. According to the report in photo-induced superconducting state in cuprates, the carrier lifetime of FeSe is more than two orders of magnitude longer than that of cuprates. In terms of device applications, this signature is quite powerful because one can perform multiple and complicated processes during this metastable state.

Reference

[1] T. Suzuki, T. Someya, T. Hashimoto, S. Michimae, M. Watanabe, M. Fujiwara, T. Kanai, N. Ishii, J. Itatani, S. Kasahara, Y. Matsuda, T. Shibauchi, K. Okazaki, and S. Shin, Communications Physics, **2**, 115 (2019).

Authors

T. Suzuki, T. Someya, T. Hashimoto, S. Michimae, M. Watanabe, M. Fujiwara, T. Kanai, N. Ishii, J. Itatani, S. Kasahara[a], Y. Matsuda[a], T. Shibauchi[b], K. Okazaki, and S. Shin

[a]Kyoto University

[b]The University of Tokyo

Heavy Fermion State of $YbNi_2Si_3$ without Local Inversion Symmetry

S. Nakamura, T. Sakakibara, and M. Yamashita

Various fascinating phenomena often appear in the materials without the global inversion symmetry. It is theoretically suggested that both global and local inversion-symmetry-breaking host an exotic superconductivity. This study focuses on the materials in which only the local inversion symmetry is broken. There are not much examples showing superconductivity in the materials without the local inversion symmetry, but the local inversion symmetry is broken in high temperature superconductors such as iron-based and copper-oxide superconductors.

We discover a new heavy-fermion compound $YbNi_2Si_3$ in which the local inversion symmetry at ytterbium site is broken (Fig. 1(a) and (b)), whereas the global inversion symmetry is retained. The space group of this material is *I*4/*mmm*, and the site symmetry at Yb-ion is 4*mm*. This crystal structure is partially similar to tetragonal $ThCr_2Si_2$-type crystal structure; $CeCu_2Si_2$ and URu_2Si_2 are well known as heavy-fermion superconductors. Rare-earth metal, transition metal, and silicone atoms form a square lattice on the *c* plane both in these two crystal structures.

The electrical resistivity, the magnetization, the magnetic torque and the heat capacity measurements have been performed in $YbNi_2Si_3$, and we check if there is a superconducting state without the local inversion symmetry. We

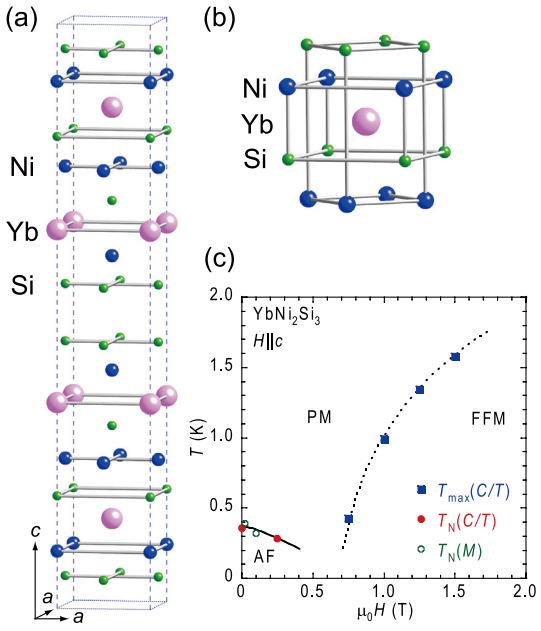

Fig. 1. (a) The crystal structure of $YbNi_2Si_3$ in which the local inversion symmetry around the Yb ions is broken as shown in (b). (c) The *H*-*T* phase diagram, where T_N and T_{max} denote the Néel temperature and a crossover line between paramagnetic and forced ferromagnetic regions, respectively.

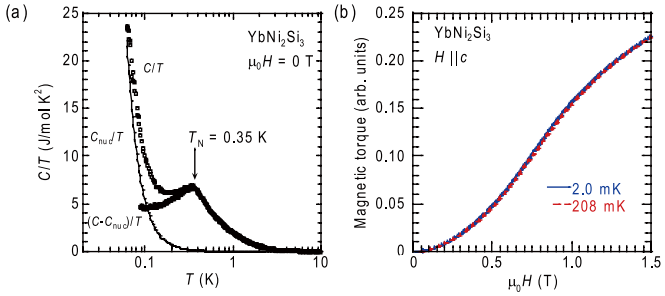

Fig. 2. (a) The temperature dependence of the heat capacity of $YbNi_2Si_3$ at zero magnetic field. (b) The magnetic field dependence of the magnetic torque of $YbNi_2Si_3$ at 208 and 2 mK.

determine the *H*–*T* phase diagram of $YbNi_2Si_3$ by the magnetization and the heat capacity measurements (Fig. 1(c)). We find an antiferromagnetic state appears below 0.35 K at zero magnetic field, and it is suppressed by applying a magnetic field of 0.7 T. The temperature dependence of the electrical resistivity shows a typical heavy-fermion behavior with the Kondo temperature of ~ 2 K. Remarkably, a large electronic specific heat coefficient of γ = 5 J/mol K^2 is found to remain down to 0.08 K in the antiferromagnetic state (Fig. 2(a)), demonstrating a heavy-fermion state in $YbNi_2Si_3$. Such large entropy is often released by a superconducting transition at a lower temperature. To this end, we have carried out the magnetic torque measurements down to ultralow temperatures. However, no discernible change is observed down to 2 mK (Fig. 2(b)), showing the persistence of the heavy-fermion state. We further check the valence state of the Yb ions via hard X-ray photoemission spectroscopy, and find that almost all the Yb-ions are in the Yb^{3+} state, showing the absence of the valence fluctuation between Yb^{2+} and Yb^{3+}. This absence would suggest that the origin of the heavy-fermion state is a magnetic fluctuation rather than a valence-fluctuation, which often expected in Yb compounds. It remains as a important future issue to reveal the origin of the heavy-fermion state in $YbNi_2Si_3$ by microscopic measurements such as NMR.

Reference

[1] S. Nakamura, K. Hyodo, Y. Matsumoto, Y. Haga, H. Sato, S. Ueda, K. Mimura, K. Saiki, K. Iso, M. Yamashita, S. Kittaka, T. Sakakibara, and S. Ohara, J. Phys. Soc. Jpn. **89**, 024705 (2020).

Authors
S. Nakamura[a], T. Sakakibara, and M. Yamashita
[a]Nagoya Institute of Technology

Patterning of Topological Insulator on Thin Film

H. Mine, J. Haruyama and T. Nakamura

Because topological insulators (TIs) have their conducting channels at the sample edges, shapes of them play crucial roles in device applications. Hence it can be a very convenient tool if we can "draw" spatial patterns of TI just like drawing a picture. Members of two-dimensional (2D) transition metal dichalcogenides (TMDCs) have been predicted and experimentally confirmed as a new class of 2D TI materials though the edge conduction is fragile in most cases. Here, we realize the controlled patterning of a TI phase embedded in an insulating phase of thin molybdenum-disulfide (MoS_2) by laser beam irradiation.

MoS_2 is known to have various metastable lattice structures according to the freedom in the stacking angle of the chalcogen layer. In so called H-phase, the chalcogens form triangle poles or trigonal prism. In single crystal, two-layers form a unit and called 2H phase. This is semiconducting.

In so called T-phase, the two-triangles are in the twisted relation. The stacking unit is single and called 1T phase. This is metallic. These two are the representative phases but there are many other metastable phases.

An interesting is the one called 1T' phase, which is somewhat intermediate between these two. In this 1T' phase, for example this upper chalcogen atoms shift in this way and stop at some intermediate position. Some theories predict this 1T' phase should be a topological phase. So if we can cause local phase transition between these three, we can make up desired circuits with semiconductors, metals and topological insulators. We showed that 1T' phase can be actually created in 2H MoS_2 and also it works as a TI [1].

In order to obtain 1T', we used the excitation by Ar laser beam of energy 2.5 eV and simply drew some patterns on 2H MoS_2. From an atomic force microscope topography, it

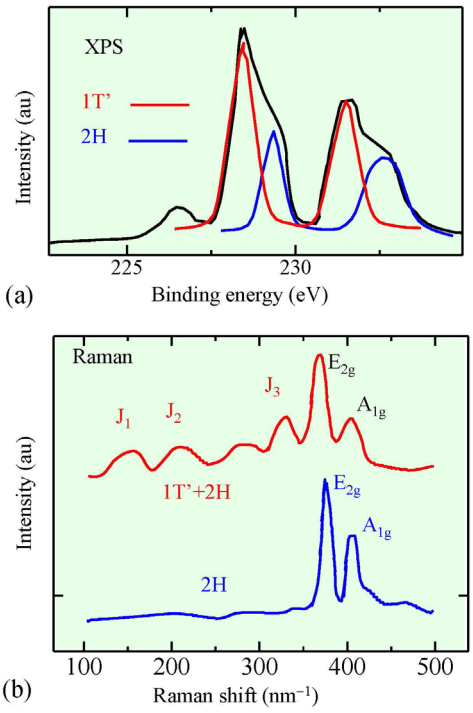

Fig. 1. (a) X-ray photoelectron spectroscopy taken at a laser-irradiated region (black line). Red and blue lines are those expected for 1T' and 2H phases respectively.(b) Raman shift spectra. Blue: 2H phase before laser irradiation. Red: mixture of 1T' phase and 2H phase after irradiation.

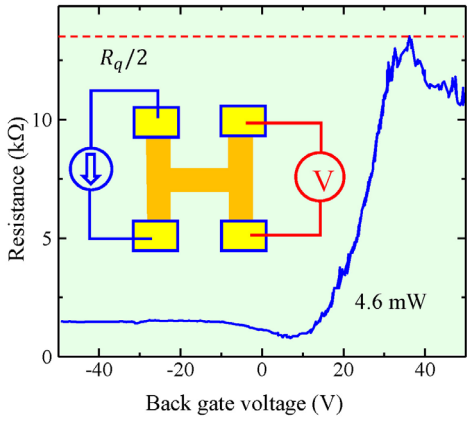

Fig. 2. Resistance of laser irradiated pattern on MoS_2 as a function of back gate voltage. In the inset we illustrate the setup of resistance measurement.

turned out that the irradiated region is a bit thinner than the surrounding region. This is probably due to some evaporation of atoms and the phase transition is not due to the direct energy transfer from photon to lattice but some heating effect causes the transition. The appearance of 1T' phase was confirmed in the Raman and the XPS spectra as shown in Fig. 1 (a) and (b).

The pattern of 1T' phase we used for the measurement of edge channel conduction is a simple H-shape as illustrated in the inset of Fig. 2. The size is about 2 μm, which is comparatively large compared with ordinary reported coherence length of edge conductions in TIs. The flake of MoS_2 was placed on a metallic doped Si substrate covered with SiO_2, hence we can tune the position of Fermi energy in MoS_2 wtih the back gate voltage. Figure 2 shows the resistance of H-shaped sample in the measurement geometry drawn in the inset, as a function of the back gate voltage. The resistance R took a peak structure around at $R = R_q/2 = h/2e^2 =$ 12.6 kΩ. This is the value calculated for ideal helical edge states and clearly tells that the patterned 1T' was working as a TI. The resistance quantization persisted surprisingly up to room temperature manifesting an opening of large spin-orbit energy gap. The gap closing around the sample edges was also confirmed with a scanning tunneling spectroscopy.

Reference

[1] H. Mine, A. Kobayashi, T. Nakamura, T. Inoue, S. Pakdel, D. Marian, E. Gonzalez-Marin, S. Maruyama, S. Katsumoto, A. Fortunelli, J. J. Palacios, and J. Haruyama, Phys. Rev. Lett. **123**, 146803 (2019).

Authors

H. Mine[a], J. Haruyama[a], T. Nakamura, and S. Katsumoto

[a]Aoyama Gakuin University

Electronic Structures of 4°-Twisted Bilayer Graphene Fabricated in a Vacuum

S. Tanaka and F. Komori

Twisted bilayer graphene (TBG) is a stacked two graphene sheets with mutually in-plane rotation, and exhibits electronic states different from those observed in a typical bilayer graphene with Bernal stacking. Its Fermi velocity in the vicinity of the Dirac point strongly depends on the twist-angle θ below 10° [1], and vanishes around a magic angle of θ ~ 1.1° [2]. At this magic angle, a flat band with extremely sharp density of states is thus realized, and its electronic

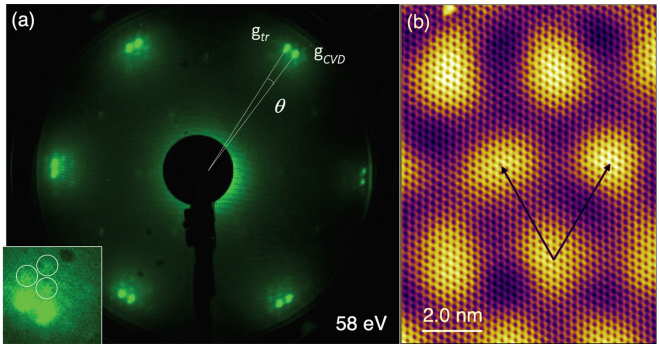

Fig. 1. (a) LEED pattern at the area with TBG. Bright 12 spots are identified as two sets of 6-fold symmetric graphene diffraction spots from the lower (g_{CVD}) and upper (g_{tr}) layers. Inset shows the magnified image of the graphene diffraction including satellite spots (circles) due to the moiré structure. (b) STM image taken at the TBG area, showing graphene atomic image and moiré lattices. Moiré unit cell of the lattice is indicated by arrows. The image was taken at the sample bias voltage 0.8 *V* and tunneling current 0.5 nA at 80 K [3].

properties have attracted much attention. TBG is usually prepared by stacking mechanically-exfoliated graphene sheets in air, and thus it is difficult to prepare a millimeter-scale samples with clean interface between the sheets for using standard surface analysis techniques such as various diffraction methods and high-resolution photoemission spectroscopy. To prepare wide TBG's with clean interface, we have developed a new method of directly bonding clean graphene sheets in a vacuum without any chemical adhesion and transmission media. For this purpose, we use monolayer graphene that can be easily exfoliated from the SiC substrate [3]. The band structure observed by angle resolved photoemission spectroscopy (ARPES) exhibits changes of the electronic states due to the interlayer interaction [1].

Graphene sheets are made on a 4H-SiC (0001) substrate

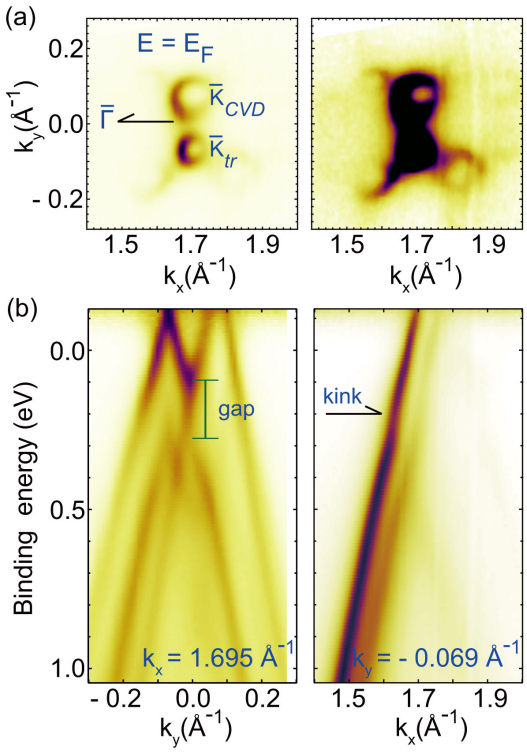

Fig. 2. ARPES constant energy and band dispersion maps. The k_x axis is on the line between the middle of the two K points of the graphene layers (K_{CVD}, K_{tr}) and Γ point. (a) Constant energy maps at E_F without (left) and with (right) image enhancement. Replica bands are seen at this energy as in left. (b) Band dispersions along k_y axis at k_x = 1.695 Å^{-1} (left) and along k_x axis at k_y = - 0.069 Å^{-1} (right). Here, the ARPES intensity is normalized by the Fermi-Dirac distribution function at 300 K. Two Dirac bands of the transferred graphene are seen at negative k_y in the left figure [3].

by chemical vapor deposition (CVD) using ethylene. A buffer layer with a 3 × 3 periodicity is formed at the interface between the graphene and substrate, and allows us to exfoliate the graphene layer easily. It is noted that graphene on the thermally decomposed $6\sqrt{3} \times 6\sqrt{3}$ -R30° buffer layer (6R3) coexists. The TBG samples are prepared at 200 ºC in a vacuum by pressing together for 1 hour and detached at the same temperature. The samples were then evaluated by optical microscope, μ-Raman spectroscopy, low energy electron diffraction (LEED), scanning tunneling microscopy (STM) and ARPES. Sub-millimeter areas with TBG were confirmed on the substrate.

Observed LEED and STM images of a 4º-rotated TBG are shown in Fig. 1. Two sets of 6-fold bright graphene spots with surrounding satellite spots are seen in Fig. 1(a), and correspond to lower-layer (g_{CVD}) and upper-layer transferred (g_{tr}) graphene. In the STM image, a moiré pattern due to the twisted layers is observed with the graphene lattice. The twist angle θ is estimated from the satellite-spot periodicity and the moiré image. Graphene band structures measured by ARPES at 300 K using 52 eV synchrotron light (KEK-PF, BL13) are shown in Fig. 2. Two graphene Dirac cones appear at Fermi energy (E_F) as in Fig. 2(a). The band structure shown in Fig. 2(b) indicates the both graphene layers are p-doped. The cone at negative k_y originates from the transferred graphene on the 3 × 3 substrate. In addition, an n-doped Dirac band is seen in Fig. 2(b), which originates from the transferred graphene on the 6R3 substrate. Energy gap of the bands due to the interlayer interaction is found at k_y = 0 in the same figure. The Dirac band shown in Fig. 2(b, right) has a kind structure at 0.2 eV.

References

[1] J. M. B. Lopes dos Santos *et al.*, Phys. Rev. Lett. **99**, 256802 (2007).
[2] R. Bistritzer, and A.H. MacDonald, Proc. Natl. Acad. Sci. U. S. A. **108**, 12233 (2011).
[3] H. Imamura *et al.*, Appl. Phys. Express **13**, 075004 (2020).

Authors
H. Imamura[a], A. Visikovskiy[a], R. Uotani[a], T. Kajiwara[a], H. Ando[a], T. Iimori, K. Iwata, T. Miyamachi, K. Nakatsuji[b], K. Mase[c], T. Shirasawa[d], S. Tanaka[a], F. Komori
[a]Kyushu University
[b]Tokyo Institute of Technology
[c]KEK & SOKENDAI
[d]AIST

Pulsed Laser Deposition with Rapid Target Switching

Y. Matsumoto and M. Lippmaa

Pulsed laser deposition (PLD) is one of the most common techniques for growing complex oxide thin films. The biggest merit of PLD is the near-stoichiometric transfer of material from a polycrystalline ceramic target to a single-crystalline thin film, which means that it is usually not necessary to tune individual cation ratios during the crystal growth process. Indeed, PLD became the method of choice for developing high-temperature superconductor thin films and devices due to the simplicity of phase and stoichiometry control.

The PLD process is based on the use of a high-intensity pulsed laser that momentarily heats the surface of a ceramic source material pellet, forming a rapidly expanding plasma cloud in vacuum or in a low-pressure reactive gas ambient.

Due to the pulsed nature of the process, the surface of a growing film reaches a high level of supersaturation when the plasma plume arrives, but this very high instantaneous deposition rate is followed by a long relaxation period of up to about a second. The dynamic aspect of the crystal growth is therefore also important in determining the growth mode and crystallinity of a film.

In recent years, there is increasing interest in materials property mapping and the use of combined computational and experimental materials data to feed machine learning models for aiding materials discovery and optimization. In thin film property mapping experiments, it is necessary to grow large numbers of thin film samples with slightly different compositions. In a traditional PLD process, this would require the synthesis of a large number of bulk compositions for use as PLD ablation targets, which is technically difficult. Multi-target PLD has been used to avoid this problem by using just two ablation targets to grow mixed-composition phases. For example, by alternating ablation from $SrTiO_3$ and $BaTiO_3$ targets, it is possible to grow any intermediate composition in the $Ba_{1-x}Sr_xTiO_3$ phase space. Since each unit cell layer usually requires up to a hundred ablation pulses to grow, it is easy to adjust compositions on a percent scale. However, switching between two targets generally requires mechanical motion of the target stage, which is a slower process than the normal ablation pulse period. Since adatom surface migration during the interpulse period affects the film microstructure, the longer time delay of target exchange may lead to a nanoscale multiphase film of, e.g., $SrTiO_3$ and $BaTiO_3$ domains instead of a mixed $Ba_{1-x}Sr_xTiO_3$ crystal.

In this project, supported by the Joint Use program, a rapid beam deflection system was developed to switch ablation between two target materials on a millisecond scale. [1] The experimental setup is illustrated in Figs. 1(a,b). A galvanometer mirror is used to direct ablation laser pulses on one of two targets without having to move the target stage. The mirror motion is fast enough to interleave depositions from two targets in a 1:1 pulse sequence at laser pulse rates of up to 200 Hz.

Various film synthesis experiments were used to test the benefits of rapid sequential deposition of various mixed-composition oxide films. The experiments clearly showed the benefit of rapid target switching in synthesizing $(Ba,Sr)TiO_3$, $(Bi,Sm)FeO_3$, (Mg,Zn)O, Ni-Ge, and Ni-Si films. A particularly interesting capability of this new rapid target switching PLD system is depth direction grading of film composition for tuning the lattice parameter, doping level, crystal symmetry, or other properties without sacrificing the deposition rate or risking phase segregation when slower mechanical target stage motion is used for multi-target deposition.

An example of a depth-graded $Ba_{1-x}Sr_xTiO_3$ film composition is shown in Fig. 1(c). The Ba content was adjusted over the 100 nm thickness of the film from 0 to 30% as shown by the design plot (blue) and verified by Secondary Ion Mass Spectrometry (SIMS) as shown in red. The continuous change of the lattice parameter can be seen in the x-ray diffraction pattern for a gradient film grown on a $SrRuO_3$ electrode layer on a $SrTiO_3$ substrate. The spread of the $(Ba,Sr)TiO_3$ film peak corresponds to the continuous composition gradient in the film. This type of gradient films can be used in novel types of photoelectrochemical electrodes and for constructing polar films with an internal electric field gradient related to the depth-variable polarization of the lattice.

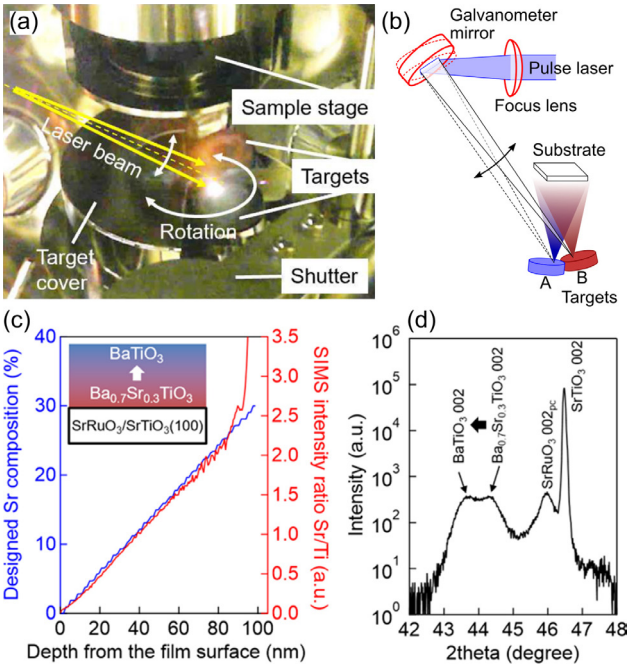

Fig. 1. (a) Photograph of the ablation target stage, showing the ablation spot on the lower target. (b) Schematic diagram of the rapid galvanometer beam switching between two targets. (c) Design (blue) and measured (red) composition of a $(Ba,Sr)TiO_3$ film. The x-ray diffraction pattern in (d) shows that the film lattice parameter varied continuously in the film.

References

[1] S. Maruyama, N. Sannodo, R. Harada, Y. Anada, R. Takahashi, M. Lippmaa, and Y. Matsumoto, Rev. Sci. Instrum. **90**, 093901 (2019).

Authors

S. Maruyama[a], N. Sannodo[a], R. Harada[a], Y. Anada[a], R. Takahashi, M. Lippmaa, and Y. Matsumoto[a]

[a]Tohoku University

Density Functional Theory with Machine Learned Functional

R. Nagai, R. Akashi, and O. Sugino

Modern electronic structure theory of materials is most frequently based on the Kohn-Sham density functional theory (KS-DFT), where the accuracy depends on the quality of the density-to-energy mapping called exchange-correlation (xc) functional. The mapping has extremely large degrees of freedom that are too complex to determine manually. In this context, we have proposed a machine learning approach [1]. We have prepared the atomization energy (E_a) and electron density $n(\boldsymbol{r})$ of reference molecules using a quantum chemical simulation and let neural network (NN) learn the data. In the learning, the energy E_a and the density $n(\boldsymbol{r})$ are related via a functional of the density called the xc potential $\varepsilon_{xc}[n](\boldsymbol{r})$, and the parameters characterizing the functional are optimized to best reproduce the input data. The mapping thus established depends on the form of the functional, such as the point-to-point mapping called local density approximation (LDA) and the mapping reinforced using the density gradient called generalized gradient approximation (GGA) or meta-GGA. Quality of the functionals was tested for a ten dozen of unreferenced molecules and was found superior to existing ones for each form, suggesting possibility to systematically develop accurate functionals.

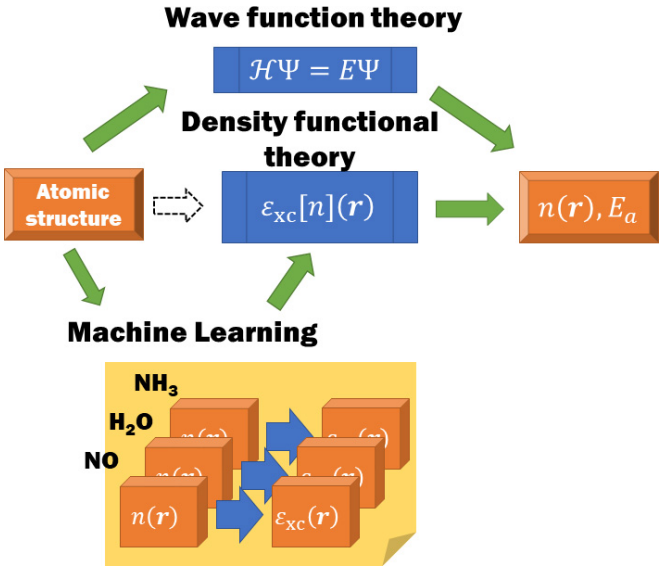

Fig. 1. Machine learning scheme for developing exchange correlation (xc) functional. Referring to electron density $n(\boldsymbol{r})$ and atomization energy E_a of a few molecules, the xc energy was related to the density as a functional $\varepsilon_{xc}[n](\boldsymbol{r})$. With this machine learned functional, $n(\boldsymbol{r})$ and E_a of unrefernced materials were found to be predicted more accurately than with conventional functionals.

In our study, we have used three molecules, H_2O, NH_3, and NO, that contain different bonding property and spin polarization, as the reference. The NN successfully determined the parameters without overtraining owing large number of data contained in the density, which amounts to 100,000. We further tried to include nonlocality into the functional beyond the gradient approximations by considering the electron density averaged in the vicinity of an electron. The resulting functional form, called near region approximation (NRA), improves the accuracy equivalent to that achieved using the nonlocal exchange, allowing thereby significantly to reduce the computational complexity.

In view of the ability of artificial intelligence to recognize a picture, it is likely to be possible to learn the chemical bonds without explicitly indicating a descriptor. Such advance in the method will enable a researcher to develop a high-quality functional dedicated to the target materials of interest with an effect of speed-up of material design. Impact of systematic functional development is thus expected to be large in the computational materials science.

Reference
[1] R. Nagai, R. Akashi, and O. Sugino, npj Compt. Mater. **6**, 43 (2020).

Authors
R. Nagai, R. Akashi[a] and O. Sugino
[a]The University of Tokyo

Predicting and Understanding Structural Phase Transition of Solids from Finite-Temperature Phonon Calculations

T. Tadano and W. A. Saidi

The study of structural phase transition has been an active research subject in condensed matter physics and materials science because a variety of materials' properties, including but not limited to transport, optical, and superconducting properties, often changes sensitively with the crystal structure. So far, first-principles calculations based on density functional theory (DFT) have been performed extensively for identifying (meta-)stable structures at $T = 0$ K. On the other hand, predicting finite-temperature structures based on DFT is still challenging because it requires a proper treatment of entropic effects of phonons and magnons. In particular, the vibrational entropy plays a central role in realizing structural phase transitions of nonmagnetic materials, including perovskite oxides such as $BaTiO_3$. However, the conventional phonon calculation method based on the harmonic approximation (HA) often yields unstable phonon modes for high-temperature phases of phase change materials, which hinders an estimation of vibrational entropy.

To overcome the limitation of the conventional phonon calculation method, we have recently developed a new approach that is applicable to high-temperature phases [1]. Our method is based on the self-consistent phonon (SCP) theory, which incorporates the anharmonic renormalization of phonons at the mean-field level. We have so far employed the developed SCP scheme to compute finite-temperature phonons of cubic $SrTiO_3$ [1], thermoelectric clathrate [2], and ScF_3 [3], where we have obtained an excellent agreement with the experimental data. Also, it can be used to compute the vibrational free energy of solid whose structure is dynamically unstable within the HA, as has been demonstrated for ScF_3 [3] and hydrogen-rich superconductors [4].

To further test and improve the prediction accuracy of our approach, we have recently applied the SCP method to an all-inorganic halide perovskite $CsPbBr_3$, which has been actively studied in recent years as an efficient photovoltaic material. $CsPbBr_3$ shows a successive structural phase transition with cooling from cubic α phase ($Pm\bar{3}m$) to the tetragonal β phase ($P4/mbm$) at 403 K and then to the orthorhombic γ phase ($Pnma$) at 361 K. When the HA was used, we obtained unstable phonon modes for the high-temperature phases as shown in Fig. 1. These phonon modes involve a distortive motion of the bromine octahedra; therefore, these soft modes, particularly those at the M (1/2,1/2,0) point of the α phase and the Z (0,0,1/2) point of the β phase, may act as the soft modes of the structural phase transition. After including the effect of finite-temperature renormalization by the SCP theory, all phonon modes were stabilized, as shown by solid lines in Fig.1. After that, we calculated the vibra-

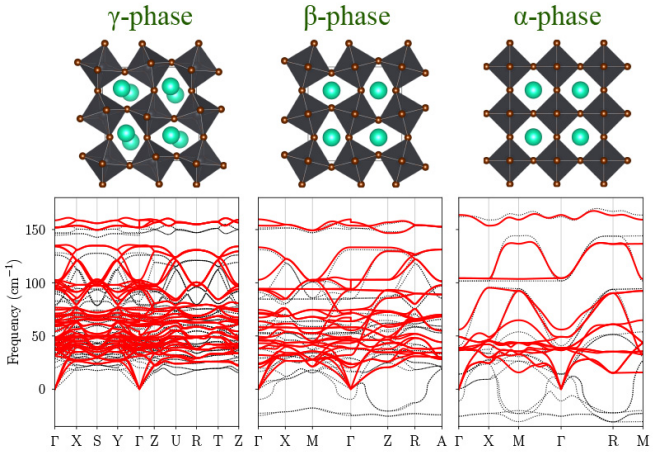

Fig. 1. (Top) Crystal structures of α, β, and γ phases of halide perovskite $CsPbBr_3$. (Bottom) Phonon dispersion curves of three different phases of $CsPbBr_3$ calculated within the harmonic approximation (dotted lines) and self-consistent phonon method at 500 K (solid lines). The unstable phonon modes in the high-temperature phases (β, γ) are stabilized by anharmonic renormalization at finite temperature.

tional free energies with including the effect of the quartic anharmonicity [3] and predicted the phase transition temperature (T_c) based on the calculated Helmholtz free energies. When we used the PBEsol exchange-correlational functional, the T_c values of the cubic-to-tetragonal and tetragonal-to-orthorhombic phase transitions were predicted as T_c ~ 280 K and T_c ~ 180 K, respectively, both of which underestimate the experimental results. To improve the prediction accuracy, we have further considered the higher-order correction to the vibrational free energy that originates from the cubic anharmonicity. Then, the T_c value of the cubic-to-tetragonal phase transition changed as T_c ~ 400 K, which shows better agreement with the experimental value.

We are also interested in how the structural phase transition affects thermal transport properties. To investigate this point quantitatively, we have calculated the lattice thermal conductivity of $CsPbBr_3$ for the three different phases. To this end, we calculated the phonon lifetimes by considering the three-phonon scattering process on top of the SCP calculations. After that, the lattice thermal conductivity was estimated, where both of the particle-like transport and coherent transport terms were calculated following Ref. [5]. For all phases, the thermal conductivity values were smaller than 1 W/mK, indicating the strong lattice anharmonicity of $CsPbBr_3$. We found that the lattice thermal conductivity of the high-temperature α phase was larger than those of the low-temperature phases due to the longer phonon lifetimes in the highly symmetric α phase, which can be attributed to the smaller scattering phase space of the three-phonon process. Interestingly, unlike the conventional semiconductors where most of the thermal transport is accounted for by the highly dispersive acoustic phonons, more than ~60% of the total thermal conductivity was carried by optical phonons above 30 cm^{-1} in $CsPbBr_3$.

The computational results on $CsPbBr_3$ again highlight the versatility and efficiency of the SCP theory for studying lattice dynamics in solids. While it is tempting to state that the SCP-based approaches are already reliable enough to make a quantitative prediction of structural phase transitions, many effects are yet to be investigated, including thermal expansion and choice of the exchange-correlation functionals. Investigating these effects on a T_c value would be an important future direction for our forthcoming studies.

References

[1] T. Tadano and S. Tsuneyuki, Phys. Rev. B **92**, 054301 (2015); J. Phys. Soc. Jpn. **87**, 041015 (2018); J. Ceram. Soc. Jpn. **127**, 404 (2019).
[2] T. Tadano and S. Tsuneyuki, Phys. Rev. Lett. **120**, 105901 (2018).
[3] Y. Oba, T. Tadano, R. Akashi, and S. Tsuneyuki, Phys. Rev. Materials **3**, 033601 (2019).
[4] I. Errea, F. Belli, L. Monacelli, A. Sanna, T. Koretsune, T. Tadano, R. Bianco, M. Calandra, R. Arita, F. Mauri, and J. A. Flores-Livas, Nature **578**, 66-69 (2020).
[5] M. Simoncelli, N. Marzari, and F. Mauri, Nature Phys. **8**, 809-813 (2019).

Authors
T. Tadano[a], W. A. Saidi[b]
[a]National Institute for Materials Science
[b]University of Pittsburgh

Neutron Spin Resonance and Horizontal Line Nodes in Sr_2RuO_4

K. Iida, K. Suzuki, and T. Masuda

Sr_2RuO_4 with T_c = 1.5 K has attracted a great deal of interest as the prime candidate for the chiral *p*-wave superconductor. Recently, however, experimental and theoretical studies under an application of uniaxial pressure along <100> reported a factor of 2.3 enhancement of T_c, raising the possibility of an even-parity spin-singlet order parameter in Sr_2RuO_4 [1]. More recently, new NMR results demonstrated that the spin susceptibility substantially drops below T_c, ruling out the chiral-*p* spin-triplet superconductivity [2]. As such, these recent works turn the research on Sr_2RuO_4 towards a fascinating new era. So far, various experimental techniques reported that the superconducting gaps of Sr_2RuO_4 have line nodes, but the details of the line nodes, *e.g.* of the vertical or horizontal nature, are not uncovered yet. Since the complete information of the superconducting gaps can shed light on the symmetry of the pairing, exclusive determination of the direction of the line nodes in Sr_2RuO_4 is highly desirable. To investigate in detail the superconducting gap, we performed the high-resolution inelastic neutron scattering (INS) measurements and random phase approximation (RPA) calculations.

Three single crystals were co-aligned with the (*HHL*) plane been horizontal to the scattering plane using the high-energy x-ray Laue diffractometer installed at ISSP. We performed INS measurements at 0.3 and 1.8 K using the disk chopper time-of-flight neutron spectrometer AMATERAS installed at J-PARC.

The most pronounced magnetic signal in the normal state of Sr_2RuO_4 is nearly two-dimensional incommensurate (IC) magnetic fluctuations at $\mathbf{Q}_{IC}$ = (0.3, 0.3, *L*) owing to the Fermi surface nesting between (or within) the quasi-one-dimensional α and β sheets [3]. We focused on the

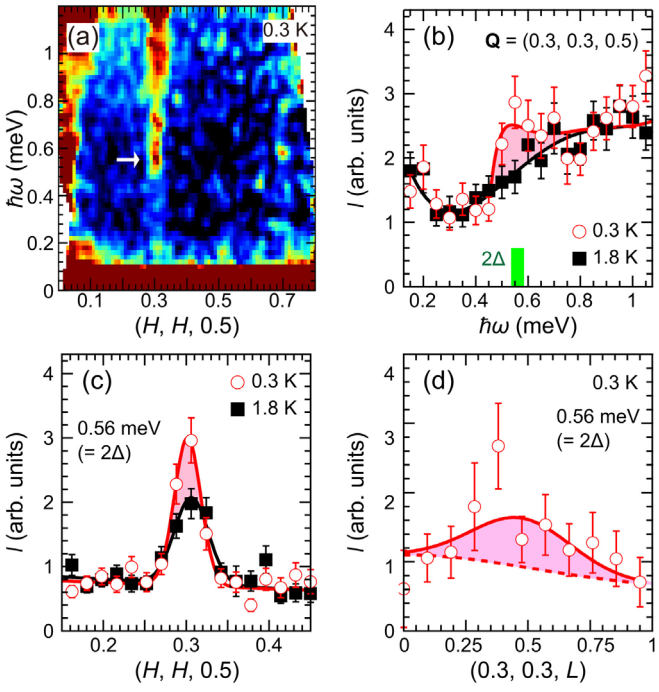

Fig. 1. (a) Low-energy INS intensity maps regarding the IC magnetic fluctuations in Sr_2RuO_4 along (*H*, *H*, 0.5). (b) $I(\hbar\omega)$ cuts at **Q** = (0.3, 0.3, 0.5) below and above T_c. (c) $I(\mathbf{Q})$ cuts along **Q** = (*H*, *H*, 0.5) at 0.3 and 1.8 K with the energy window of 0.56 meV. (d) $I(\mathbf{Q})$ cut along **Q** = (0.3, 0.3, *L*) at 0.3 K with the energy window of 0.56 meV.

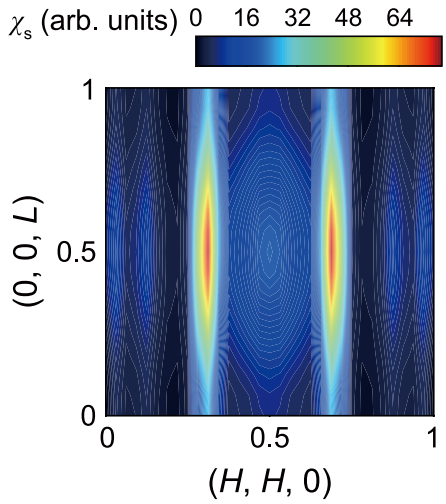

Fig. 2. Calculated density maps of the dynamical spin susceptibility assuming the horizontal line nodes in Sr_2RuO_4 for energy $\hbar\omega = 2\Delta_0$.

low-energy IC magnetic fluctuations in Sr_2RuO_4 below and above T_c to search a spin resonance as the feedback effect from the superconducting gaps. We observed a spin resonance with energy of $\hbar\omega_{res}$ = 0.56 meV centered at a characteristic wavevector $\mathbf{Q}_{res}$ = (0.3, 0.3, 0.5) (Figs. 1(a)–1(c)). The resonance energy corresponds well to the superconducting gap 2Δ = 0.56 meV estimated by the tunneling spectroscopy. In addition, the spin resonance shows the L modulation with a maximum at around L = 0.5 (Fig. 1(d)), indicating the three-dimensional gap structure.

To theoretically elucidate the origin of the L modulated intensity of the spin resonance in Sr_2RuO_4, RPA calculations assuming the horizontal line nodes at the superconducting gaps were also performed. Figure 2 illustrates the calculated dynamical spin susceptibilities for energy $\hbar\omega = 2\Delta_0$. The dynamical spin susceptibility shows the maximum at Q = (1/3, 1/3, 0.5) and (2/3, 2/3, 0.5). The superconducting gaps with the horizontal line nodes give such the feature along L, which is indeed observed in our INS measurements (Fig. 1(d)).

The L modulation of the spin resonance and our RPA calculations indicate that the superconducting gaps regarding the quasi-one-dimensional α and β sheets at the Fermi surfaces have the horizontal line nodes [4]. These results may set a strong constraint on the pairing symmetry of Sr_2RuO_4.

References
[1] A. Steppke *et al.*, Science **355**, eaaf9398 (2017).
[2] A. Pustogow *et al.*, Nature (London) **574**, 72 (2019).
[3] K. Iida *et al.*, Phys. Rev. B **84**, 060402(R) (2011).
[4] K. Iida *et al.*, J. Phys. Soc. Jpn. **89**, 053702 (2020).

Authors
K. Iida[a,b], M. Kofu[a,c], K. Suzuki[d], N. Murai[c], S. Ohira-Kawamura[c], R. Kajimoto[c], Y. Inamura[c], M. Ishikado[b], S. Hasegawa, T. Masuda, Y. Yoshida[e], K. Kakurai[b], K. Machida[d], and S.-H Lee[a]
[a]University of Virginia
[b]CROSS
[c]J-PARC Center
[d]Ritsumeikan University
[e]AIST

Large Enhancement of Thermoelectric Efficiency Due to Pressure-Induced Lifshitz Transition in SnSe

H. Sakai, M. Tokunaga, and Y. Uwatoko

Control of the number of Fermi pockets, i.e., electronic valleys, in conductive materials has recently attracted a great deal of attention in terms of the emerging electronics utilizing valley degrees of freedom. An important physical aspect of the valley engineering is that the emergence and annihilation of the valleys are described by a topological electronic transition known as Lifshitz transition. The Lifshitz transition is totally different from the conventional Landau-type phase transition, because it is not accompanied by any symmetry breaking. Despite many predictions of its important roles on various quantum phenomena, the experimental verification has remained challenging.

In this study [1], we have revealed a marked influence of the pressure-induced Lifshitz transition on thermoelectric efficiency in SnSe (Fig. 1(a)), which has recently become the focus of attention for its high thermoelectric performance [2]. Thermopower, which is proportional to the energy derivative of density of states, is anticipated to be an ideal probe for the Lifshitz transition. However, it has been overlooked so far owing to the lack of a model thermoelectric material, where the valley state is controllable. Here we have discovered that the band structure as well as thermoelectric performance for SnSe is highly sensitive to the external pressure by measuring the quantum oscillation of magneto-resistivity concurrently with the thermopower in a piston cylinder type high pressure cell (Fig. 2).

The obtained pressure dependence of the quantum oscillation frequencies clearly indicates that the number of the valleys increases from two to four at ~1 GPa with increasing pressure (Fig. 1(b) upper panel), as is semi-quantitatively reproduced by the first-principles calculations. At around 1.6 GPa, the four valleys are almost equivalent in size, where the thermoelectric power factor is more than 100% higher than that at ambient pressure over a wide temperature range (10–300 K) (Fig. 1(b) lower panel).

The present result demonstrates the multi-valley state is of great importance for achieving high thermoelectric performance, providing a guide for band engineering for the SnSe-based thermoelectric materials. Furthermore, since atomically thin SnSe films have recently attracted much attention

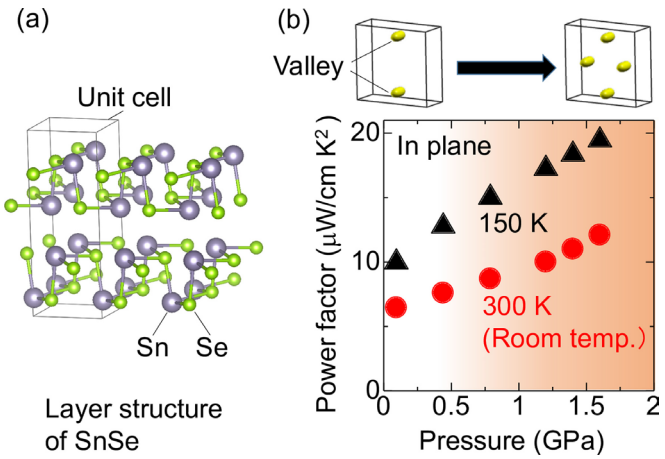

Fig. 1. (a) Schematic of the layered crystal structure of SnSe. (b) (upper panel) A schematic illustration of the pressure variation in the valley topology for SnSe. (lower panel) Pressure dependence of the thermoelectric power factor at 150 and 300 K for SnSe.

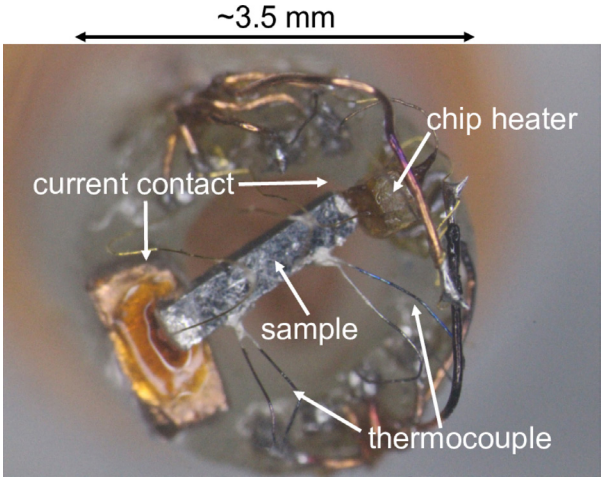

Fig. 2. Setup of the thermopower and resistivity measurements under pressure.

as a new 2D material, the controllability of valley structure presented here may help for exploring their novel functions in the future electronics.

References

[1] T. Nishimura, H. Sakai, H. Mori, K. Akiba, H. Usui, M. Ochi, K. Kuroki, A. Miyake, M. Tokunaga, Y. Uwatoko, K. Katayama, H. Murakawa, and N. Hanasaki, Phys. Rev. Lett. **122**, 226601 (2019).

[2] L.-D. Zhao, S.-H. Lo, Y. Zhang, H. Sun, G. Tan, C. Uher, C. Wolverton, V. P. Dravid, and M. G. Kanatzidis, Nature (London) **508**, 373 (2014).

Authors

T. Nishimura[a], H. Sakai[a,b], H. Mori[a], K. Akiba, H. Usui[a], M. Ochi[a], K. Kuroki[a], A. Miyake, M. Tokunaga, Y. Uwatoko, K. Katayama[a], H. Murakawa[a], and N. Hanasaki[a]

[a]Osaka University

[b]PRESTO, JST

Cyclotron Resonance in Near Surface of InAs Quantum Well

G. A. Khodaparast, B. A. Magill, and Y. H. Matsuda

Electronic states of semiconductor nanostructure near surface has been attracting much attention in terms of controlling quantum effects that can emerge through correlation with a superconductor. Josephson junctions made from Al-InAs have been used to create tunable superconducting qubits [1]. The key feature of the superconductor (Al) and semiconductor (InAs) nanostructure is that the two-dimensional gas (2DEG) is confined near the surface, in close proximity to the superconductor.

Although the electronic state of a bulk InAs is well understood, it is expected that the quantum confinement effect modifies the electronic state. Moreover, a narrow gap semiconductor exhibits small effective mass and large g factor, and the non-parabolicity of the band due to the confinement affects these fundamental parameters. Investigation of the electronic state of the 2DEG in InAs quantum well is essential for development of the novel semiconductor-superconductor device. In the present study, the cyclotron resonance (CR) of an InAs quantum well has been investigated. Clear spin-split cyclotron resonance has been observed and the effective mass and the g factor are deduced as a function of magnetic field.

The CR experiment was performed with the single-turn coil (STC) at the ISSP for magnetic field generation and an infrared CO_2 gas laser as the light source. The wavelengths used were 9.22, 10.48, and 10.6 μm. The laser light shines the sample and the transmitted light intensity was measured as a function of time during a pulse of a magnetic field ($\boldsymbol{B}$) generated by the STC. A high speed HgCdTe PIN photo diode was used for detection of the light signal. The samples were grown on a semi-insulating InP (100) substrate, using a molecular beam epitaxy system. The $In_xAl_{1-x}As$ buffer is grown at low temperature to help mitigate formation of dislocations originating from the lattice mismatch between the InP substrate and higher levels of the heterostructure [2]. The indium content of $In_xAl_{1-x}As$ is step-graded from x = 0.52 to 0.81. Next, a delta-doped Si layer of ~ 7.5 × 10^{11} cm^{-2} density is placed here followed by 6 nm of $In_{0.81}Al_{0.19}As$. The quantum well is grown next, consisting of a 4 nm thick layer of $In_{0.81}Ga_{0.19}As$ layer, a 4 nm thick layer of InAs, and finally a 10 nm thick top layer of $In_{0.81}Ga_{0.19}As$.

Figure 1 shows the CR spectra at 300 and 20 K. In the upper panel, the CR peaks around 40 T indicated by solid allows are interpreted as the spin-split resonances : They are the inter-Landau level transitions between n = 0 and n = 1 with different spin polarization, where n is the Landau level index. Another CR peak at around 55 T is, on the other hand, due to the transition between n =1 and n = 2 levels. When the temperature is lowered to 20 K, only one of the spin-split CR peaks is observed, which can be explained in terms of the population of carriers. They populate only in the lowest level at a low temperature. Remaining 55-T CR peak confirm that this resonance is due to non-equilibrium distributed carriers.

The effective mass of electrons (m^*) is directly deduced from the peak position B_c. The left-panel of Fig. 2 shows the magnetic field dependence of m^*. It is found that they are considerably larger than the band-edge effective mass of a bulk InAs $0.023m_0$, where m_0 is the mass of a free electron. The large effective mass is due to the quantum confinement

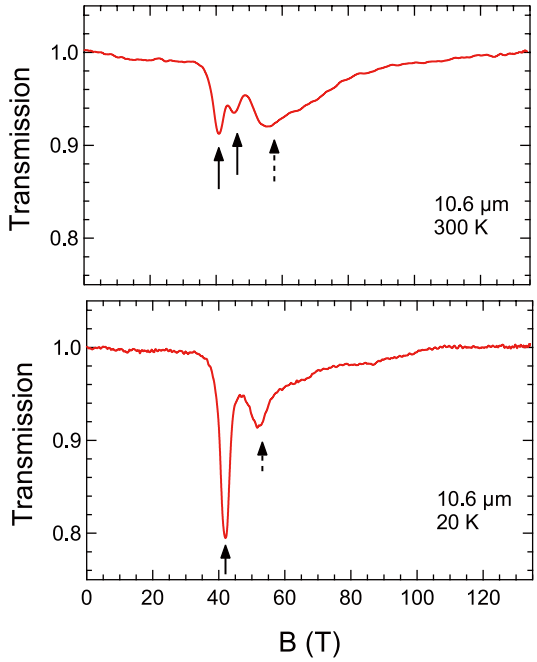

Fig. 1. Cyclotron resonance (CR) in the InAs quantum well. The upper panel shows the resonance spectrum at 300 K. The two solid arrows suggest the spin-split CR. The broad CR indicated by the dashed arrow is due to the inter-Landau level transition between n = 1 and n = 2. The lower panel shows the CR at 20 K. Observation of only single peak near 40 T indicates effect of the thermal population of carriers. Since the CR around 55 T is considered to be due to the non-equilibrium of electrons, it remains at a low temperature.

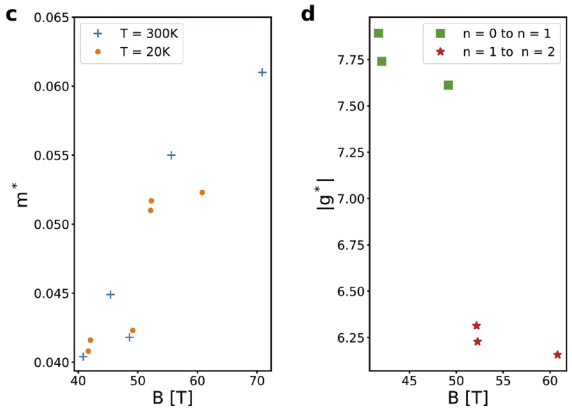

Fig. 2. Left-side panel: The obtained effective mass of electrons. The rather large field variation indicates the strong non-parabolicity of the energy band. The right-side panel: The g-factor deduced from the experiment and numerical analysis. It is clear that g-factor is also affected by the non-parabolicity.

effect and the cyclotron energy. The enhancement of m^* with increasing magnetic field is interpreted as a result of the non-parabolicity of the band due to the cyclotron energy. The g factor can also be obtained by comparison between the CR peak position and the calculated inter-Landau level energies. It has been found that the g factor becomes small with increasing cyclotron energy. The g factor of a bulk InAs is known to be -14.

The magnetic field dependences of the m^* and g leads us to the values at zero magnetic fields and they are found to be $0.027m_0$ and -12, respectively [3]. Determination of these quantum parameters will significantly contribute development of the novel Josephson-junction devices.

References

[1] T. W. Larsen, K. D. Petersson, F. Kuemmeth, T. S. Jespersen, P. Krogstrup, J. Nygard, and C. M. Marcus, Phys. Rev. Lett. **115**, 127001 (2015).
[2] J. Shabani, S. Das Sarma, and C. J. Palmstrøm, Phys. Rev. B **90**, 161303 (2014).
[3] J. Yuana, M. Hatefipoura, B. A. Magillb, W. Mayera, M. C. Dartiailha, K. Sardashtia, K. S. Wickramasinghea, G. A. Khodaparastb, Y. H. Matsuda, Y. Kohama, Z. Yang, S. Thapac, C. J. Stantonc, and J. Shabania, Phys, Rev. B **101**, 205310 (2020).

Authors

J. Yuan[a], M. Hatefipour[a], B. A. Magill[b], W. Mayer[a], M. C. Dartiailh[a], K. Sardashti[a], K. S. Wickramasinghe[a], G. A. Khodaparast[b], Y. H. Matsuda, Y. Kohama, Z. Yang, S. Thapa[c], C. J. Stanton[c], and J. Shabani[a]

[a]New York University
[b]Virginia Tech
[c]University of Florida

Many-Body String Excitations in the Antiferromagnetic Ising Spin Chain Compound $BaCo_2V_2O_8$

Z. Wang, Y. Kohama, and K. Kindo

The one-dimensional (1D) spin-1/2 Heisenberg-Ising model is the paradigmatic model for the study of quantum phase transitions and spin dynamics. However, the realization of this spin model in a solid-state material and its study are quite challenging. Several criteria must be fulfilled simultaneously: 1. the intrachain coupling should be dominant over the interchain coupling. 2. A significant Ising-like anisotropy should be present. 3. The required experimental conditions, such as high magnetic fields, should be available.

These criteria were found to be realized in the spin-1/2 Heisenberg-Ising chain antiferromagnetic material $BaCo_2V_2O_8$. Our recent work has revealed a unique quantum critical behaviors under a strong *transverse* magnetic field ($B\perp c$) of 40 T [1], which is characteristic for the transverse-field Ising quantum critical point. In contrast, in an applied *longitudinal* field ($B//c$), the phase diagram of the Heisenberg-Ising antiferromagnetic chain is completely different. Two phase transitions can be induced, and the different phases are characterized by different quantum spin excitations. In this work, we performed high-resolution terahertz spectroscopy and magnetocaloric-effect (MCE) measurements in $BaCo_2V_2O_8$ as a function of temperature and applied longitudinal magnetic field [2]. We found characteristic features revealing the field-induced quantum phase transitions, and observed the characteristic spin dynamics for the various phases. In particular, many-body string excitations as well as low-energy fractional excitations [3] were identified in the field-induced gapless phase, by comparing to the Bethe-Ansatz calculations [2]. Moreover, approaching the field-induced quantum phase transition from higher field, we observed a dominant contribution of the higher-energy string states than the lower-lying fractional excitations, in contrast to the conventional belief.

Figure 1(a) shows the MCE data, $T(B)$, measured at different initial temperatures. The $T(B)$ starting from 1.7 K at zero field reaches a minimum at the critical field (B_c) of 3.8 T, following by a slight increase towards higher fields. Before the temperature jump above the saturation fields of 22.9 T, the MCE detect a weak minimum at about 19.5 T. The weak minimum corresponds to the half-saturated magnetization as seen in Figure 1(b) and possibly reflects commensurate fluctuations. In down-sweeping data, the $T(B)$ curve matches with the up-sweeping curve, except for a (irreversible) heating effect at the phase boundary. At higher temperatures, the anomalies at the critical and the half-saturated fields broaden and smear out, whereas the minimum at saturation fields remains and becomes the dominant feature. These observations qualitatively agree with the calculated phase diagram for the 1D Heisenberg-Ising

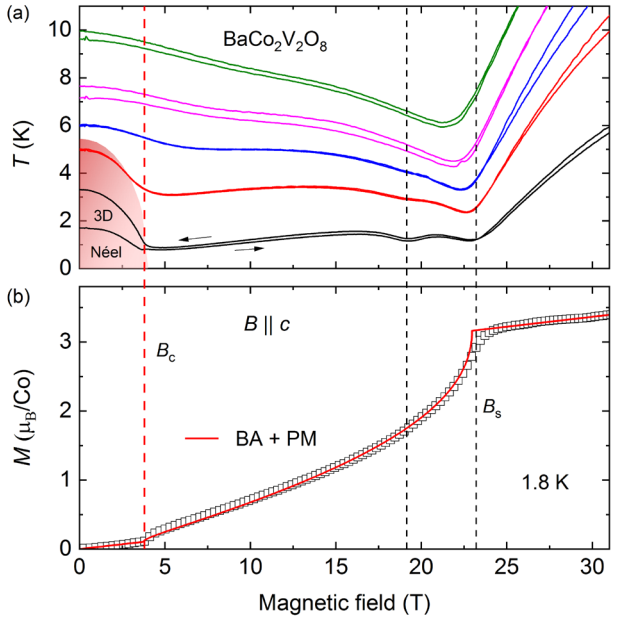

Fig. 1. (a) Magnetocaloric effect $T(B)$, (b) magnetization of $BaCo_2V_2O_8$ measured in the longitudinal configuration ($B//c$). The solid red line in (b) is calculated from the Bethe ansatz solution of the Heisenberg-Ising model with a paramagnetic background.

model, confirming that the $BaCo_2V_2O_8$ is a suitable system for investigating the string and the additional fractional magnetic excitations. This conclusion is also checked by the magnetization data, which shows quantitatively agreement with the 1D Heisenberg-Ising model (Red curve in Fig.1(b)).

We investigated the dynamical properties with THz transmission spectra in the applied longitudinal magnetic field. These data are available in Ref. [2] which tracked the field dependence of exotic spin excitations, i.e., many-body string and fractional excitations. We have revealed their selection rule in the vicinity of a field induced QCP in the Ising-like spin-½ chain compound. While the gapped fractional excitations are dominant in the 3D ordered state, we found that the high-energy string excitations plays an important role in quantum critical dynamics, which is consistent with Bethe-Ansatz calculations [2].

References

[1] Zhe Wang *et al*., Phys. Rev. Lett. **120**, 207205 (2018).
[2] Zhe Wang *et al*., Phys. Rev. Lett. **123**, 067202 (2019).
[3] Zhe Wang *et al*., Nature **554**, 219 (2018).

Authors

Zhe Wang[a,b,c], A. Loidl[a], Y. Kohama and K. Kindo
[a]University of Augsburg
[b]Helmholtz-Zentrum Dresden-Rossendorf
[c]University of Cologne

Operando Soft X-ray Emission Spectrosopy of Fe_2O_3 Anode for Li-Ion Battery

D. Asakura, E. Hosono, J. Miyawaki, and Y. Harada

Improving the energy and power density of electrode materials for Li-ion batteries (LIBs) is highly important to further develop electric vehicles. For the improvements of battery performance, understanding the charge (Li-extraction) and discharge (Li-insertion) mechanisms from the viewpoint of the electronic structure is indispensable. Here, we demonstrate *operando* Fe L_3-edge resonant XES for Fe_2O_3 which is an anode material of LIB [1]. It is known that the discharge/charge mechanism is based on conversion reaction denoted as $Fe_2O_3 + 6Li^+ + 6e^- \Leftrightarrow 3Li_2O + 2Fe$ [2,3]. To confirm the conversion reaction and further investigate the electronic-structure charge, we analyzed the *operando* XES spectra using full-multiplet calculation [4,5].

The *operando* cell consists of Fe_2O_3 poly-crystalline thin film (~100 nm), a Li-metal counter electrode, and an electrolyte solution [1,6]. The *operando* XES experiments were carried out with the HORNET XES spectrometer at BL07LSU of SPring-8 [7]. The electrochemical discharge/charge was performed by cyclic voltammetry. The *operando* XES measurements were at an open-circuit voltage (OCV), discharged state and charged state on the second discharge-charge cycle.

Figure 1 shows the XES results [1]. The XES spectrum for the initial state is attributed to Fe^{3+} state because the XES line shape is almost the same as that for Fe_2O_3 in previous reports [8]. On the other hand, the valence of Fe at the OCV before the second cycle was not Fe^{3+}, but Fe^{2+} with a weak *p-d* hybridization, suggesting considerable irreversibility on the first discharge-charge cycle and a weakened Fe-O bond after the first cycle. Moreover, we revealed that

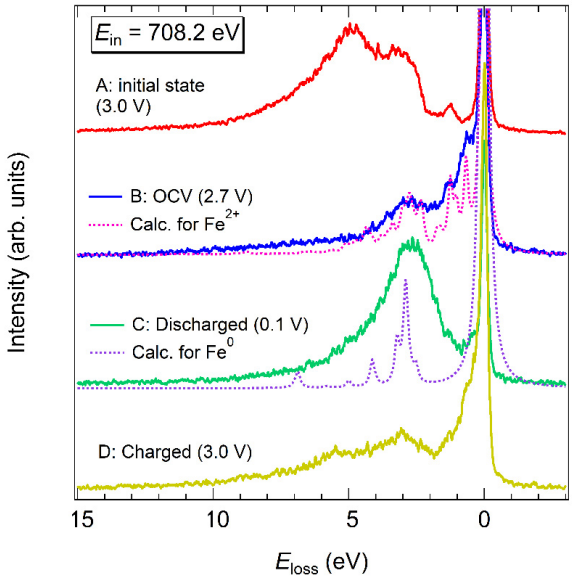

Fig. 1. *Operando* Fe L_3-edge resonant XES spectra for the Fe_2O_3 on the second cycle taken with the excitation energy E_{in} = 708.2 eV [1]. The Fe L_3-edge XES spectrum for the initial state is also displayed. All the spectra are plotted as a function of energy loss (E_{loss}).

the Fe 3*d* electronic-structure change during the second cycle was to some extent reversible as Fe^{2+} (2.7 V vs. Li/Li^+: OCV) → Fe^0 (0.1 V vs. Li/Li^+: discharged) → $Fe^{(2+d)+}$ (3.0 V vs. Li/Li^+: charged). This *operando* Fe L_3-edge resonant XES in combination with the full-multiplet calculation provides detailed information for redox chemistry during a discharge-charge operation that cannot be obtained by other methods such as crystal-structure and morphology analyses. XES is thus very powerful to investigate the origin and limitation of the lithiation function of anodes involving conversion reaction.

References

[1] D. Asakura *et al*., Phys. Chem. Chem. Phys. **21**, 26351 (2019).
[2] S. Morzilli *et al*., Electrochem. Acta **30**, 1271 (1985).
[3] J. Chen *et al*., Adv. Mater. **17**, 582 (2005).
[4] D. Asakura *et al*., J. Phys. Chem. Lett **5**, 4008 (2014).
[5] D. Asakura *et al*., Phys. Chem. Chem. Phys. **21**, 18363 (2019).
[6] D. Asakura *et al*., Electrochem. Commun. **50**, 93 (2015).
[7] Y. Harada *et al*., Rev. Sci. Instrum. **83**, 013116 (2012).
[8] J. Miyawaki *et al*., Phys. Rev. B **96**, 214420 (2017).

Authors

D. Asakura[a], Y. Nanba[a], M. Okubo[a], H. Niwa, H. Kiuchi[b], J. Miyawaki, M. Oshima[b], E. Hosono[a], and Y. Harada
[a]National Institute of Advanced Industrial Science and Technology (AIST)
[b]The University of Tokyo

Mass Transport in the PdCu Phase Structures during Hydrogen Adsorption and Absorption Studied by Ambient-Pressure XPS under Hydrogen Atmosphere

J. Tang, I. Matsuda, and J. Yoshinobu

Pd-based alloys have been the attractive materials for the hydrogen permeation process, because they possess higher hydrogen permeability and suppress the hydrogen embrittlement compared to pure Pd bulk. It was reported that the PdCu alloy, especially so-called "$PdCu_{40}$ alloy", has a relatively higher hydrogen diffusivity than the other Pd-alloys (PdAg, PdAu, PdRh, etc.). Industrial usages of

the $PdCu_{40}$ alloys with the high Cu content also improve the economic perspectives because of the lower Cu cost. Although there are advantages of PdCu alloys in the application fields, it requires further improvements in microscopic aspects. For example, hydrogen solubility of the face-centered cubic (fcc) structure of a PdCu alloy is approximately one order of magnitude higher than that of body-centered cubic (bcc) structure.

In the present research, we traced Pd and Cu atoms during hydrogen adsorption and absorption processes at the elemental steps, dissociative adsorption of H atoms on the surface and dissolution of H atoms into the bulk, by the individual core-level photoelectron spectroscopies under the hydrogen atmosphere [1]. The absorption process is investigated by the Ambient Pressure (AP)-XPS measurements at the soft X-ray undulator beamline BL07LSU at SPring-8. The $PdCu_{40}$ sample, provided from Tanaka Kikinzoku Kogyo K.K., was annealed at 673 K to form the B2 phase structure. Then, the B2/fcc phase structure was prepared by subsequent annealing at 1000 K. Figures 1(a) and (b) show the

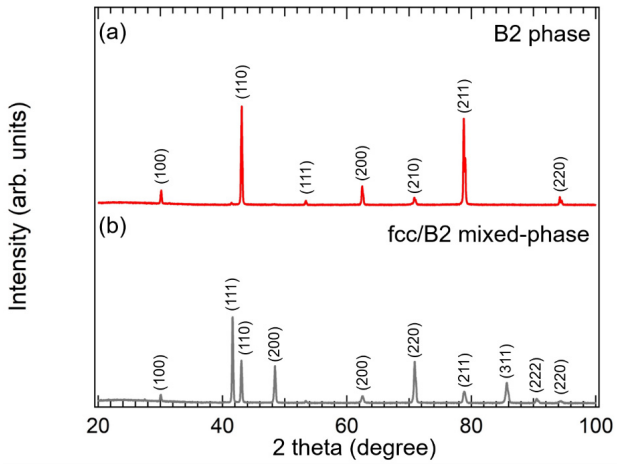

Fig. 1. XRD patterns of (a) B2 and (b) fcc/B2 mixed-phase PdCu alloys.

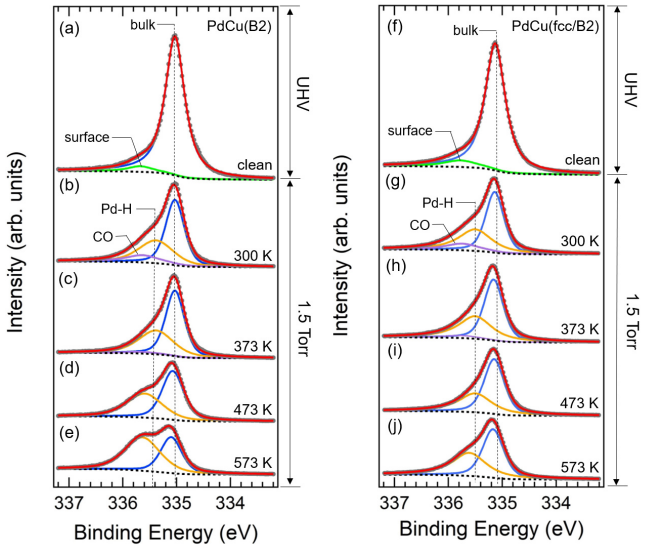

Fig. 2. Pd $3d_{5/2}$ spectra measured on (a) clean surface, and under H_2 exposure at 1.5 Torr at (b) 300 K, (c) 373 K, (d) 473 K, (e) 573 K with photon energy of 680 eV on PdCu(B2) alloy. Pd $3d_{5/2}$ spectra measured on (f) clean surface, and under H_2 exposure at 1.5 Torr at (g) 300 K, (h) 373 K, (i) 473 K, (j) 573 K with photon energy of 680 eV on PdCu(fcc/B2) alloy. Surface Pd component, bulk Pd component, CO adsorption component and Pd-H component are presented with green, blue, purple, and yellow solid lines, respectively.

XRD patterns of the B2- and fcc/bcc- phased PdCu alloys, respectively. Figures 2 and 3 show the temperature dependence of hydrogen absorption reactions on the B2 and fcc/bcc phases, observed by measuring the Pd $3d_{5/2}$ and Cu $2p_{3/2}$ XPS spectra during the hydrogen exposure at 1.5 Torr at 300-573 K. The temperature-dependent data show that a number of the Pd-H bond increased accompanied with the decrease of the Cu-H bond with temperature. The Pd hydride formation in the B2 and fcc/bcc structures show the same behavior at 300-373 K, however, more Pd hydride was formed in the B2 structure than in the fcc/bcc structure at 473-573 K. The decrease rate of Cu-H component is higher in the B2 phase than fcc/bcc phase. These results indicate that the interstitial hydrogen occupied the different sites in the PdCu alloy bulk at different temperature and confirms the difference in absorption between the two phases. Comparing with the previous calculation [2], the significant enhancement of the hydride formation at 473 K can consistently be described in terms of variation of the hydrogen diffusion paths from the Cu-rich octahedral site to the energetically favorable Pd-rich octahedral site. Furthermore, the activation energy of the hydrogen diffusion is found to be lower in the B2 phase than that in the fcc/B2 phase. Our elucidation of hydrogen diffusion mechanisms on the different phase structures gives a new understanding of the hydrogen absorption process, which could be the critical point for the rate-limiting process in the hydrogen permeation through the PdCu alloy.

Similar investigation on hydrogen permeation process was carried out for the PdAg alloy[3]. The measurements of AP-XPS revealed that Pd atoms were also found to reactive sites during hydrogen absorption. On the other hand, the process is likely promoted by the Pb segregation. It is of interest to make systematic investigations of individual Pd-alloys to capture the whole picture.

References

[1] J. Tang, S. Yamamoto, T. Koitaya, A. Yoshigoe, T. Tokunaga, K. Mukai, I. Matsuda, and J. Yoshinobu, Appl. Surf. Sci. **480**, 419 (2019).
[2] L. C. Liu, J. W. Wang, Y. H. He, and H. R. Gong, J. Membr. Sci. **542** , 24 (2017).
[3] J. Tang, S. Yamamoto, T. Koitaya, Y. Yoshikura, K. Mukai, S. Yoshimoto, I. Matsuda, and J. Yoshinobu, Appl. Surf. Sci. **463**, 1161 (2019) .

Authors
J. Tang[a], I. Matsuda, and J. Yoshinobu
[a]University of Hyogo

Sub-Cycle Spectroscopy of Proton Transfer in Ferroelectric Cocrystals Driven by Intense THz and MIR Fields

T. Umanodan, Y. Okimoto, and J. Itatani

Ferroelectricity in organic materials is one of the most important topics in condensed matter physics. It has a wide range of practical applications because organic systems possess advantages such as mechanical flexibility, printability, disposability, and cost-effectiveness. Very recently, proton-mediated co-crystals have been developed as novel organic ferroelectric materials [1]. In these co-crystals, proton ordering along the hydrogen bonds between the proton-donor and -acceptor molecules leads to the emergence of ferroelectricity, leading to the lack of inversion symmetry. We focused on a proton-mediated co-crystal [H-dppz][Hca] (dppz = 2,3-di(2-pyridinyl)pyrazine, Hca = chloranilate) that

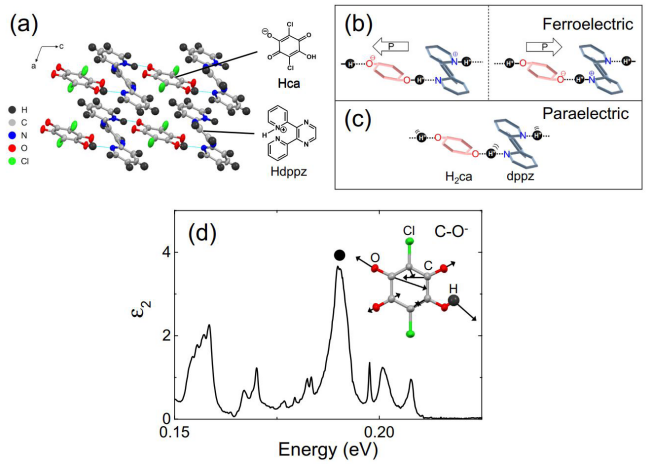

Fig. 1. (a) Crystal structure of Hdppz-Hca cocrystal. (b, c) Schematic illustrations of the (b) ferroelectric and (c) paraelectric phases.

shows ferroelectricity at room temperature (T_c = 402 K). Figure 1 shows the crystal structure (a), the ferroelectric and paraelectric origins due to the position of protons (b, c), and the imaginary part of dielectric constant at room temperature (d).

In this study [2], we investigated the ultrafast dielectric response of [H-dppz][Hca] by sub-cycle spectroscopy where carrier-envelope phase-stable intense optical pulses at 1 or 40 THz drove the ferroelectricity, then sub-cycle visible pulses probes the field-driven dynamics.

First, we irradiated the co-crystal with a single-cycle THz pulse at a center frequency around 1 THz with a maximum electric field of ~1 MV/cm, and measured the second harmonic (SH) of 100-fs laser pulses at 800 nm as a function of the relative delay between the THz and 800-nm pulses. The modulation of SH intensity exactly followed the waveform of the applied THz electric field, and the magnitude of the relative SH change reached up to 10%. This result indicates that the ultrafast change of the ferroelectricity was directly driven by the THz electric field.

Second, we irradiated the crystal with an intense mid-infrared (MIR) pulse (center frequency ~40 THz, maximum electric field ~30 MV/cm), and found that the induced SH change occurred very differently. The time profile of observed change of SH intensity was not scaled by the field profile of the 40 THz pulse as shown in Fig. 2(b). The SH change contained a component proportional to the square of the applied electric field in addition to the linear component that is proportional to the field as observed in the 1-THz case. These results suggest that the change of the polarity of the co-crystal cannot follow the oscillation of the electric field at 40 THz.

To understand these field effects, we analyzed the following nonlinear equation of motion that contains the C-O$^-$ stretching mode,

$$\mu\frac{d^2X(t)}{dt^2}+\mu\gamma\frac{dX(t)}{dt}+\mu\Omega^2X(t)+a\mu X^2(t)=aE_{MIR}(t),$$

where $\chi(t)$ is the change in amplitude of the normal mode, which can be viewed as an index of the displacement of the atoms including the protons caused by the intense MIR electric field $E_{MIR}(t)$. We used the experimental data for $E_{MIR}(t)$ that was obtained by EO sampling with 6-fs visible pulses. The values μ, Ω, q, are the reduced mass, frequency, and effective charges of the C-O$^-$ mode derived from a DFT calculation and reflectivity data. We fit the observed time profile of $\Delta I_{SH}/I_{SH}$ by numerically solving the above

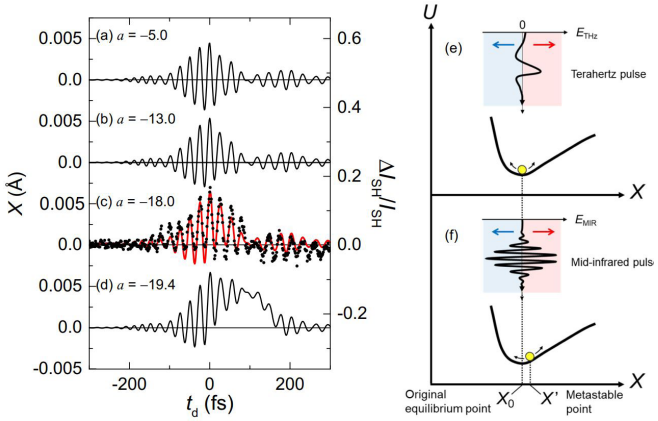

Fig. 2. (a-d) Calculated amplitudes of C-O$^-$ stretching mode for various anharmonic parameter a. The black circles in (c) denote the observed time profile of the SH intensity. (e, f) Schematic illustrations of the proton motion in the binding potential of the cocrystal when a THz or MIR pulse is applied. X_0, X' denote the equilibrium position and a metastable position with excitation pulses, respectively.

equation, and found that the observed signal $\Delta I_{SH}/I_{SH}$ were well reproduced when $a \approx -18$ Å^{-1}fs^{-2}, $\gamma \approx 0.75$ eV, and $k \approx 26$ Å^{-1} as shown by the solid line in Fig. 2. This result reveals the importance of phonon excitation in our observation of unconventional positive shift of $\Delta I_{SH}/I_{SH}$.

Figures 2(e, f) summarize the origins of the observed SH changes for THz and MIR excitation. In the presence of a strong MIR field that resonantly excites the C-O$^-$ stretching mode, dynamical repositioning of protons occurs, which leads to the asymmetric polarization. These results can be viewed as an example of ultrafast control of organic ferroelectric cocrystals using intense ultrafast laser pulses at room temperature.

References

[1] S. Horiuchi, F. Ishii, R. Kumai, Y. Okimoto, H. Tachibana, N. Nagaosa, and Y. Tokura, Nat. Mater. **4**, 163 (2005).
[2] T. Umanodan, K. Kaneshima, K. Takeuchi, N. Ishii, J. Itatani, H. Hirori, Y. Sanari, K. Tanaka, Y. Kanemitsu, T. Ishikawa, S. Koshihara,S. Horiuchi, and Y. Okimoto, J. Phys. Soc. Jpn. **88**, 013705 (2019).

Authors

T. Umanodan[a], K. Kaneshima, K. Takeuchi, N. Ishii, J. Itatani, H. Hirori[b], Y. Sanari[b], K. Tanaka[b], Y. Kanemitsu[b], T. Ishikawa[a], S. Koshihara[a], S. Horiuchi[c], and Y. Okimoto[a]
[a]Tokyo Institute of Technology
[b]Kyoto University
[c]National Institute of Advanced Industrial Science and Technology (AIST)

Progress of Facilities

Supercomputer Center

The Supercomputer Center (SCC) is a part of the Materials Design and Characterization Laboratory (MDCL) of ISSP. Its mission is to serve the whole community of computational condensed-matter physics of Japan, providing it with high performance computing environment. In particular, the SCC selectively promotes and supports large-scale computations. For this purpose, the SCC invites proposals for supercomputer-aided research projects and hosts the Steering Committee, as mentioned below, that evaluates the proposals.

The ISSP supercomputer system consists of two subsystems: System B is intended for larger total computational power and has more nodes with relatively loose connections whereas System C is intended for higher communication speed among nodes. System B is SGI ICE XA / UV hybrid system that consists of FAT nodes with large memory, CPU nodes based on Intel Xeon, and ACC node enhanced by GPGPU accelerator. Its theoretical performance is 2.6 PFLOPS. System C is HPE SGI 8600 with 0.77 PFLOPS. Replacement of the System B is scheduled in Autumn 2020. The new machine will be much more powerful (more than by the factor of 2) than the current System B in its peak performance.

In addition to the hardware administration, the SCC puts increasing effort on the software support. Since 2015, the SCC has been conducting “Project for advancement of software usability in materials science (PASUMS)”. In this project, for enhancing the usability of the ISSP supercomputer system, we perform some software-advancement activity such as developing new application software that runs efficiently on the ISSP supercomputer system, adding new functions to existing codes, helping in releasing private codes for public use, and writing/improving manuals for public codes. Two target programs were selected in fiscal year 2019 and developed software were released as abICS (proposal made by S. Kasamatsu (Yamagata U.)) and TeNeS (proposal made by N. Kawashima (ISSP)).

All staff members of university faculties or public research institutes in Japan are invited to propose research projects (called User Program). The proposals are evaluated by the Steering Committee of SCC. Pre-reviewing is done by the Supercomputer Project Advisory Committee. In fiscal year 2019, totally 276 projects were approved. The total points applied and approved are listed on Table. 1 below. Additionally, we supported post-K and other computational-materials-science projects through Supercomputing Consortium for Computational Materials Science (SCCMS).

The research projects are roughly classified into the following three (the number of projects approved):

First-Principles Calculation of Materials Properties (145)
Strongly Correlated Quantum Systems (36)
Cooperative Phenomena in Complex, Macroscopic Systems (128)

In all the three categories, most proposals involve both methodology and applications. The results of the projects are reported in 'Activity Report 2019' of the SCC. Every year 3-4 projects are selected for “invited papers” and published at the beginning of the Activity Report. In the Activity Report 2019, the following three invited papers are included:

1. "Development of Open-Source Parallelized Tensor Network Softwares: mptensor and TeNeS", Satoshi MORITA (ISSP) and Naoki KAWASHIMA (ISSP)
2. "Disorder-Free Glass Transitions of Spins and Orbitals in a Frustrated Pyrochlore Magnet", Kota Mitsumoto (Osaka U.), Chisa Hotta (U. Tokyo), and Hajime Yoshino (Osaka U.)
3. "First-principles calculation of thermophysical properties of solids with strong phonon anharmonicity", Terumasa TADANO (NIMS)

Class	Max Points		Application	Number of Projects	Total Points			
					Applied		Approved	
	System B	System C			System B	System C	System B	System C
A	100	100	any time	17	1.7k	0.9k	1.7k	0.9k
B	1k	500	twice a year	88	82.8k	4.7k	58.3k	4.1k
C	10k	2.5k	twice a year	183	1446.2k	91.2k	612.0k	63.7k
D	10k	2.5k	any time	5	26.9k	2.0k	26.9k	2.0k
E	30k	2.5k	twice a year	16	445.0k	41.0k	249k	34.7k
S			twice a year	0	0	0	0	0
SCCMS				32	218.9k	103.5k	218.9k	103.5k
Total				276	2058.3k	312.3k	1180.7k	267.8k

Table 1. Research projects approved in 2019
The maximum points allotted to the project of each class are the sum of the points for the two systems; Computation of one node for 24 hours corresponds to one point for the CPU nodes of System B and System C. The FAT and ACC nodes require four and two points for a 1-node 24-hours use, respectively.

Neutron Science Laboratory

The Neutron Science Laboratory (NSL) has been playing a central role in neutron scattering activities in Japan since 1961 by performing its own research programs as well as providing a strong General User Program for the university-owned various neutron scattering spectrometers installed at the JRR-3 (20 MW) operated by Japan Atomic Energy Agency (JAEA) in Tokai, Ibaraki (Fig. 1). In 2003, the Neutron Scattering Laboratory was reorganized as the Neutron Science Laboratory to further promote the neutron science with use of the instruments in JRR-3. Under the General User Program supported by NSL, 12 university-group-owned spectrometers in the JRR-3 reactor are available for a wide scope of researches on material science. The submitted proposals were about 300 and the visiting users reached over 6000 person-day in FY2010. In 2009, NSL and Neutron Science Division (KENS), High Energy Accelerator Research Organization (KEK) built a chopper spectrometer, High Resolution Chopper Spectrometer, HRC, at the beam line BL12 of MLF/J-PARC (Materials and Life Science Experimental Facility, J-PARC) (Fig. 2). HRC covers wide energy transfer (100 μeV < $\hbar\omega$ < 0.5 eV and 0.03 Å^{-1} < Q < 30 Å^{-1}) ranges, and therefore becomes complementary to the existing inelastic spectrometers at JRR-3. HRC has accepted general users through the J-PARC proposal system since FY2011.

Triple axis spectrometers, HRC, a four-circle diffractometer, and a high resolution powder diffractometer are utilized for a conventional solid state physics and a variety of research fields on hard-condensed matter, while in the field of soft-condensed matter science, researches are mostly carried out by using a small angle neutron scattering (SANS-U) and/or neutron spin echo (iNSE) instruments. The upgraded time-of-flight (TOF) inelastic scattering spectrometer, AGNES, is available both for hard- and soft-matter science. Our General User Program has produced 2064 publications and 284 dissertations until Jan. 29, 2020. Their lists for the last 10 years is given in Activity Report on Neutron Scattering Research which is available in ISSP and NSL web pages.

Since the Great East Japan Earthquake on March 11, 2011, JRR-3 has been closed mainly from safety issues. Hence, our domestic activity is only on HRC. To take recent research examples, well-defined spin wave was successfully measured in the pressure-induced magneticphase in $CsFeCl_3$, and novel excitations near quantum criticality was identified [1]. Another progress on HRC was that usage of superconducting magnet up to 5 T became available.

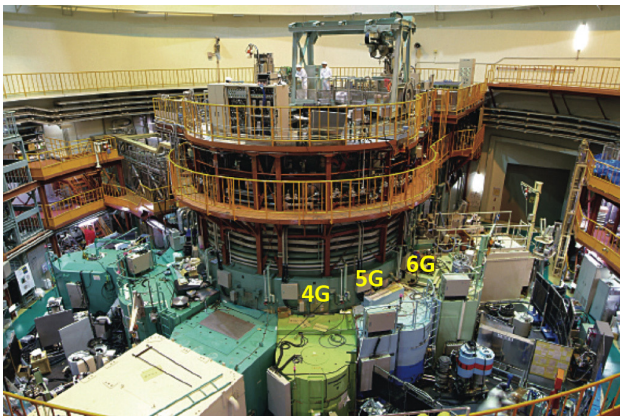

Fig. 1. Reactor hall of JRR-3. Three triple axis spectrometers are shown in the photo.

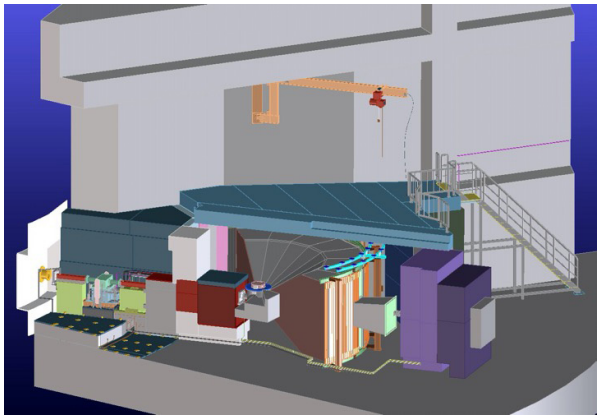

Fig. 2. Schematic view of HRC.

Field dependence of spin-wave spectra in 2D antiferromagnet $Ba_2MnGe_2O_7$ was measured. Since 2012, NSL have managed User-Program Supports for Overseas Experiments. Until March 30, 2020, 398 people (for 297 proposals) have performed their experiments in various foreign facilities and published 106 papers. The lists for User-Program Supports for Overseas Experiments are also available in Activity Report on Neutron Scattering Research mentioned above.

As for international cooperative programs, NSL operates the U.S.-Japan Cooperative Program on neutron scattering, providing further research opportunities to material scientists who utilize the neutron scattering technique for their research interests. In 2010, relocation of the U.S.-Japan triple-axis spectrometer, CTAX, was completed, and it is now open to users. NSL has another agreement with Australian Centre for Neutron Scattering (ANSTO), which is the main foreign facility for the User-Program Supports for Overseas Experiments.

JRR-3 will restart in February 2021 after long shutdown. During the shutdown period, we have been concentrating our efforts on upgrading the instruments and neutron beam circumstances. Specific actions taken include: the installation of focusing collimation systems, such as focusing monochromator and focusing analyzer, and material lens; and the introduction of polarization optics together with the installation of non-magnetization neutron shield. The neutron guides in the Guide Hall have also been upgraded by replacing the existing ones with super-mirror guides. These upgrades should result in increase in neutron beam flux several times. The sample environments such as cryostat and pressure cells have also been upgraded. Of course, the normal General User Program will also restart from FY2021. We are eagerly waiting for that.

[1] S. Hayashida *et al.*, Phys. Rev. B **97**, 140405(R) (2018).

International MegaGauss Science Laboratory

The objective of this laboratory (Fig. 1) is to study the physical properties of solid-state materials (such as semiconductors, magnetic materials, metals, insulators, superconducting materials) under ultra-high magnetic field conditions. Such a high magnetic field is also used for controlling the new material phase and functions. Our pulse magnets, at moment, can generate up to 87 Tesla (T) by non-destructive manner, and from 100 T up to 1200 T (the world strongest as an in-door record) by destructive methods. The laboratory

is opened for scientists both from Japan and from overseas, especially from Asian countries, and many fruitful results are expected to come out not only from collaborative research but also from our in-house activities. One of our ultimate goals is to provide the scientific users as our joint research with magnets capable of a 100 T, millisecond long pulses in a non-destructive mode, and to offer versatile physical precision measurements. The available measuring techniques now involve magneto-optical measurements, cyclotron resonance, spin resonance, magnetization, and transport measurements. Recently, specific heat and calorimetric measurements are also possible to carry out with sufficiently high accuracy.

Our interests cover the study on quantum phase transitions (QPT) induced by high magnetic fields. Field-induced QPT has been explored in various materials such as quantum spin systems, strongly correlated electron systems and other magnetic materials. Non-destructive strong pulse magnets are expected to provide us with reliable and precise solid state physics measurements. The number of collaborative groups for the research is almost 50 in the FT of 2019.

A 210 MJ flywheel generator (Fig. 2), which is the world largest DC power supply (recorded in the Guinness Book of World Records) has been installed in the DC flywheel gener-

Fig. 1. Signboard at the entrance of the IMGSL.

Fig. 2. The building for the flywheel generator (left hand side) and a long pulse magnet station (right hand side). The flywheel giant DC generator is 350 ton in weight and 5 m high (bottom). The generator, capable of a 51 MW output power with the 210 MJ energy storage, is planned to energize the long pulse magnet generating 100 T without destruction.

	Alias	Type	B_{max}	Pulse width Bore	Power source	Applications	Others
Building C Room 101-113	Electro- Magnetic Flux Compression	destructive	1200 T	μs 10 mm	5 MJ, 50 kV 2 MJ, 50 kV	Magneto-Optical Magnetization	5 K – Room temperature
	Horizontal Single-Turn Coil	destructive	300 T 200 T	μs 5 mm 10 mm	0.2 MJ, 50 kV	Magneto-Optical measurements Magnetization	5 K – 400 K
	Vertical Single-Turn Coil	destructive	300 T 200 T	μs 5 mm 10 mm	0.2 MJ, 40 kV	Magneto-Optical Magnetization	2 K – Room temperature
Building C Room 114-120	Mid-Pulse Magnet	Non-destructive	60 T 70 T	40 ms 18 mm 40 ms 10 mm	0.9 MJ, 10 kV	Magneto-Optical measurements Magnetization Magneto-Transport Hall resistance Polarization Magneto-Striction Magneto-Imaging Torque Magneto- Calorimetry Heat Capacity	Independent Experiment in 5 site Lowest temperature 0.1 K
Building C Room 121	PPMS	Steady State	14 T			Resistance Heat Capacity	Down to 0.3 K
	MPMS	Steady State	7 T			Magnetization	
Building K	Short-Pulse Magnet	Non-destructive	87 T (2-stage pulse) 85 T	5 ms 10 mm 5 ms 18 mm	0.5 MJ, 20 kV	Magnetization Magneto-Transport	2 K – Room temperature
	Long-Pulse Magnet	Non-destructive	43.5 T	1 s 30 mm	210 MJ, 2.7 kV	Resistance Magneto-Calorimetry	2 K – Room temperature

Table 1. Available Pulse Magnets, Specifications

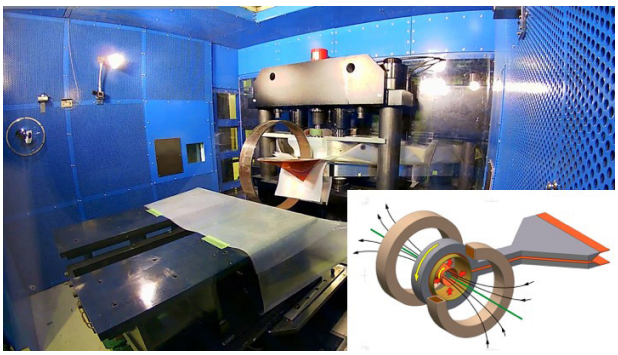

Fig. 3. (Build. C) A view of the electro-magnetic flux compression 1000 T-class megagauss generator set in side of an anti-explosive house. 1000 T project started since 2010, and finally condenser banks of 9 MJ (5 MJ + 2 MJ +2 MJ) as a main system with the 2 MJ sub bank system for the seed field have been installed, and settled in the year of 2014.

ator station at our laboratory, and used as an energy source of super-long pulse magnets. The magnet technologies are intensively devoted to the quasi-steady long pulse magnet (an order of 1-10 sec) energized by the giant DC power supply. The giant DC power source will also be used for the giant outer-magnet coil to realize a 100 T nondestructive magnet by inserting a conventional pulse magnet coil in its center bore.

Magnetic fields exceeding 100 T can only be obtained with destruction of a magnet coil, where ultra-high magnetic fields are obtained in a microsecond time scale. The project, financed by the ministry of education, culture, sports, science and technology aiming to generate 1000 T with the electromagnetic flux compression (EMFC) system (Fig. 3), has been proceeded. Our experimental techniques using the destructive magnetic fields have intensively been developed. The system which is unique to ISSP in the world scale is comprised of a power source of 5 MJ main condenser bank and 2 MJ condenser bank. Two magnet stations are constructed and both are energized from each power source. Both systems are fed with another 2 MJ condenser bank used for a seed-field coil, of which magnetic flux is to be compressed. The 2 MJ EMFC system is currently under the process for optimizing several mechanical and electrical parameters such as dimensions of coils and liners. And so far, generation of 450 T was successfully done using 1.6 MJ energy. The 5 MJ EMFC system is under conditioning the main gap switches by finely tuning control parameters. And so far, generation of 1200 T was successfully done using 3.2 MJ energy. As an easy

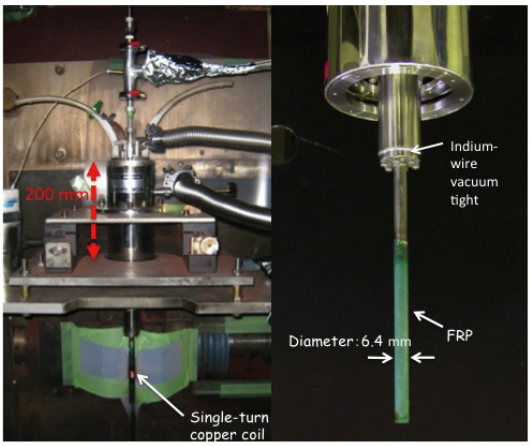

Fig. 4. Schematic picture of the H-type single-turn coil equipped with 50 kV, 200 kJ fast operating pulse power system, capable of generating 300 T within 3 mm bore coil.

access to the megagauss science and technology, we have the single-turn coil (STC) system capable of generating the fields of up to 300 T by a fast-capacitor of 200 kJ. We have two STC systems, one is a horizontal type (H-type, Fig. 4) and the other is a vertical type (V-type). Various kinds of laser spectroscopy experiments such as the cyclotron resonance and the Faraday rotation are possible using the H-type STC.

Center of Computational Materials Science

The goal of the computational materials science is to understand and predict properties of complicated physical systems with a vast number of degrees of freedom and to design new useful materials before actual experiments. Since such problems cannot be solved with bare hands, it is quite natural to use computers in computational materials science. In fact, computer-aided science has been providing answers to many problems ranging from the most fundamental ones to the ones with direct industrial applications. In the recent trends of the hardware developments, however, the growth of computer power is mainly due to the growth in the number of the units. This fact poses a very challenging problem in front of us --- how can we parallelize computing tasks? In order to solve this problem in an organized way, we coordinate the use of the computational resources available to our community, and support community members through various activities such as administrating the website "MateriApps" for information on application software in computational science. These activities are supported by funds for various governmental projects in which CCMS is involved. In particular, we acted as the headquarters of Priority Area 7 of MEXT FLAGSHIP2020 Project (so-called "post-K computer project") in the last project year of 2019. In addition to this, CCMS was involved in Priority Area 5 and Pioneering Area (CBSM2) of FLAGSHIP2020 project, Element Strategy Initiative, and Professional Development Consortium for Computational Materials Scientists (PCoMS).

The following is the selected list of meetings organized by CCMS in FY2019:

- 4/2-4/3 Joint Research Meeting of ISSP Supercomputer Joint Use and CCMS Annual Activity Report 2019, ISSP, Kashiwa
- 5/17 PCoMS Matching Workshop for industries & graduate students/postdocs The University of Tokyo, ISSP, Kashiwa
- 7/16-8/8 Computational Approaches to Quantum Many-body Problems 2019 (CAQMP 2019), ISSP, Kashiwa

Fig. 1. Members of CCMS.

- 8/9 Post-K Project Priority Issue 7, The 5th Annual Meeting, Ito-Hall, Hongo, Tokyo
- 10/8-10/10 The 3rd Innovation Camp for Computational Materials Science (3rd ICCMS) The Hohoemi-no-Yado, Yamagata
- 12/6 TIA-Kakehashi Poster Workshop 2019, The University of Tokyo, Kashiwa Campus Station Satellite, Kashiwa
- 2/17-2/18 The 9th Materials Simulation Workshop, Akihabara
- 2/25 PCoMS Skill improvement training for graduate students & postdocs ISSP, Kashiwa

Laser and Synchrotron Research Center (LASOR Center)

Laser and synchrotron research center (LASOR Center) was established in October 2012 to push the frontiers of the photon and materials science. LASOR has 10 groups in 2019, which is the biggest division in ISSP. Most of the research activities on the development of new lasers with an extreme performance and the application to materials science are studied in specially designed buildings D and E with large clean rooms and the isolated floor from the vibrations in Kashiwa Campus. On the other hand, the experiments utilizing the synchrotron radiation are performed at beamline BL07LSU in SPring-8 (Hyogo).

The development of novel laser-based light sources in the vacuum-ultraviolet to soft-X-ray regions innovated materials investigations as represented by the highest-energy-resolution photoemission, ultrafast time-domain, and ultra-fast non-linear spectroscopies. Materials science research powered by lasers thus has entered a new era. The ultra-short and high-power lasers are more and more attractive light source for both basic science and industry. The state-of-the-art laser source and spectroscopy are intensively explored.

Another stream pursued at ISSP is the synchrotron-based research. The drastic advance in brilliance of the synchrotron radiation has also opened a new field of its own in photon science. The soft-X-ray beam-line in SPring-8 (BL07LSU) was implemented with the longest undulator in the world: The end stations illuminated by the brilliant soft-X-rays are used to output innovative achievements based on high-resolution spectroscopy data. In 2018, Japanese government has made a statement to construct a new synchrotron facility in Tohoku. LASOR has decided to subjectively contribute to this facility from the design to the operation.

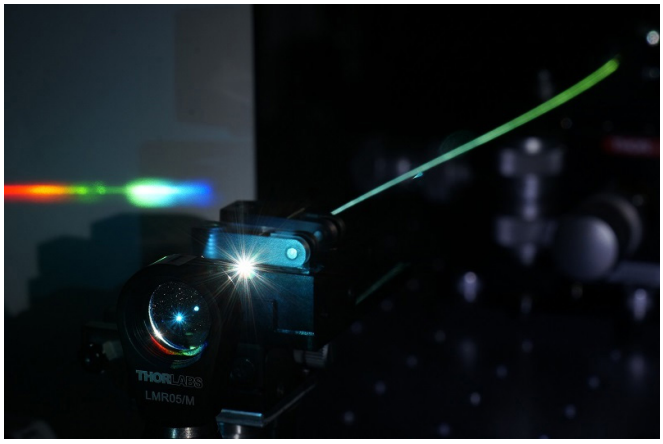

Fig. 1. Optical frequency comb

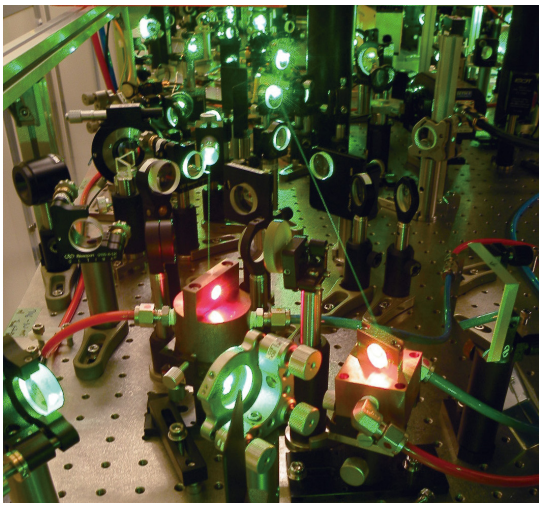

Fig. 2. Close look of a high-peak-power ultrashort-pulse laser

Lasers and synchrotrons have developed independently; now both light sources cover a wide photon-energy range with an overlap in the vacuum-ultraviolet to soft-X-ray regions. Foreseeing their common interests in research fields and technologies, ISSP integrated the two streams, namely the extreme lasers and synchrotron radiations, into the common platform. Through the mutual interactions between the forefronts of lasers and synchrotrons, LASOR will be the center of innovations in light and materials science, with the aid of world-wide joint research and close collaborations with other divisions in ISSP such as New Materials Science, Nanoscale Science, and Condensed Matter Theory.

The mission of LASOR is to cultivate and propel the following three scientific fields:
1. Laser Science,
2. Synchrotron radiation Science,
3. Extreme Spectroscopy,

• Laser science group

We were committed to continuing to developed various state-of-the-art laser systems such as high-power solid-state or gas lasers, high-intensity lasers, ultra-short pulse lasers down to attosecond time scale (Peta Hz linewidth), ultra-stable lasers with 1-Hz linewidth, optical frequency combs, mid-infrared lasers, THz light source, and semiconductor lasers.

High-power and ultrashort pulse laser technology has progressed for this 10 years. It opened two directions of

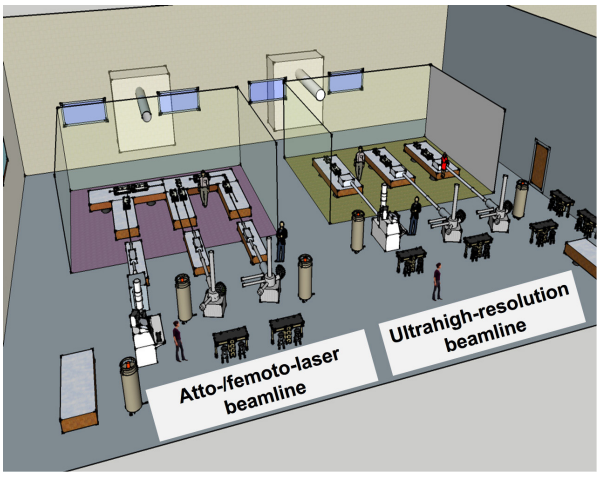

Fig. 3. Design of E building for extreme VUV- and SX-lasers and new spectroscopy.

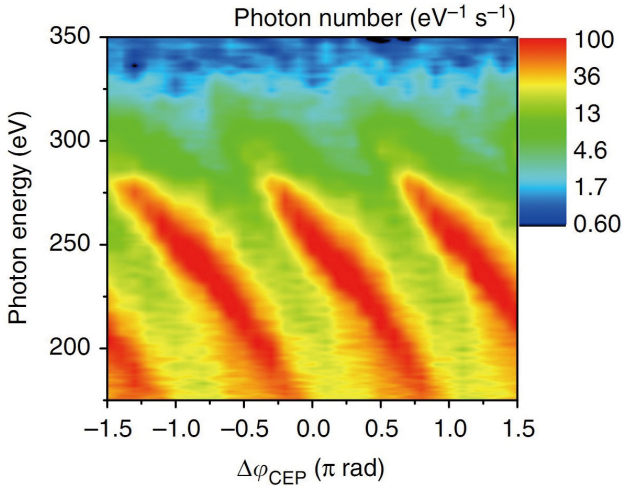

Fig. 4. Phase-dependence of high harmonic spectra in soft X rays.

research. One is a coherent extreme ultraviolet light source realized by a high-harmonic generation (HHG) scheme. The average power of HHG became high enough to use it for a photoemission spectroscopy. The photon energies of 7 eV to 60 eV are now available. They can be either very narrow band width or ultrashort pulse. The other is an industrial science such as a laser processing. Pulse duration variable, 100-W average power, femtosecond laser is now available in LASOR for any collaborative research including companies.

We also aim to develop novel laser spectroscopy and coherent non-linear optical physics, enabled via emerging lasers and optical science/technology, and extensively study basic light-matter physics, optical materials science, and applied photonics. Such researches include ultrafast spectroscopy for excited state dynamics, terahertz magnetic-field spectroscopy for spin dynamics, quantitative micro-spectroscopy on semiconductor lasers and nano-structure photonics devices, such as quantum wire lasers, gain-switch semiconductor laser, multi-junction solar cells, and bio-luminescent systems.

• Synchrotron radiation science group

By inheriting and developing the synchrotron techniques cultivated for more than 20 years, we continuously develop world cutting-edge spectroscopies such as time-resolved photoemission /diffraction, ultrahigh resolution soft X-ray emission, 3D (depth + 2D microscopy) nano ESCA and X-ray magneto-optical effect and provide these techniques both for basic material science and for applied science, which contributes to the device applications in collaboration

Fig. 5. 10-MHz high harmonic generation in an enhancement cavity.

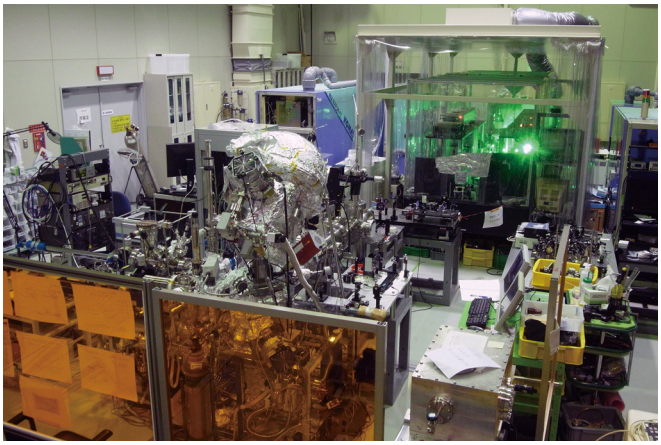

Fig. 6. Pump-probed photoemission system using 60-eV laser

with outside researchers. In order to pioneer new spectroscopies for the next-generation light sources, we upgrade fast polarization switching of the undulator light source in cooperation with SPring-8. In addition, we promote frontier works on the use of X-ray free electron lasers, SACLA with high spatial and temporal coherence comparable to optical lasers in collaboration with scientists of laser light sources and spectroscopies.

• Extreme spectroscopy group

The advent of laser-based light sources in the soft-X-ray region is opening a new stage in the field that has been cultivated by the synchrotron radiations. One of the milestones is to develop a laser-based light source of ~7 eV for the sub-meV-resolution photoemission spectroscopy. In this five years, available photon energy became 11 eV with help of Yb-fiber laser technology. It has high photon flux (10^{14} photons/sec) with sub picosecond time resolution. Laser-based spin-resolved ARPES is realizing in LASOR. This technology would open brand-new spectroscopy. High-harmonic generation based photoemission spectroscopy in the 20-60 eV region is another direction to be pursued. Time-domain spectroscopy in the femtosecond region was achieved. Combined with the picosecond time-domain spectroscopy utilizing the pulsed light delivered from synchrotrons, we investigate the electronic structures and dynamics of matter in bulk, on surface, and into the nano-scale. The ultimate objective is to expand the soft-X-ray operando methodologies by lasers. Diffractions, magneto-optical effects, and inelastic scatterings now done at synchro-

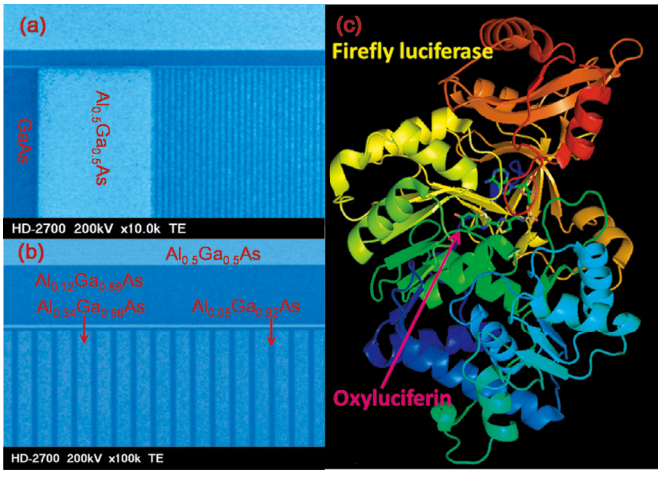

Fig. 7. Photonics devices under study: (left panel) semiconductor quantum wires and (right panel) firefly-bioluminescence system consisting of light emitter (oxyluciferin) and enzyme (luciferase)

trons will be performed by lasers, to access the real-time dynamics of chemical reactions and phase transitions down to the femtoseconds.

State-of-the-art laser based organism spectroscopy is new direction in LASOR. ISSP research area is shifting from simple material and science to complex one including living body and functional material with excited state physics.

Synchrotron Radiation Laboratory

The Synchrotron Radiation Laboratory (SRL) was established in 1975 as a research division dedicated to solid state physics using synchrotron radiation (SR). Currently, SRL is composed of two research sites, the Harima branch and the E-building of the Institute for Solid State Physics.

• Brilliant soft X-ray beamline at Harima branch

In 2006, the SRL staffs have joined the Materials Research Division of the Synchrotron Radiation Research Organization (SRRO) of the University of Tokyo and they have played an essential role in constructing a new high brilliant soft X-ray beamline, BL07LSU, in SPring-8. The light source is the polarization-controlled 25-m long soft X-ray undulator with electromagnetic phase shifters that allow fast switching of the circularly (left, right) and linearly (vertical, horizontal) polarized photons.

The monochromator is equipped with a varied line-spacing plain grating, which covers the photon energy range from 250 eV to 2 keV. At the downstream of the beamline, a lot of experimental stations have been developed for frontier spectroscopy researches: five endstations, i.e. time-resolved soft X-ray spectroscopy (TR-SX) equipped with a two-dimensional angle-resolved time-of-flight (ARTOF) analyzer (Fig. 1), three-dimensional (3D) nano-ESCA station equipped with the Scienta R-3000 analyzer (Fig. 2), high resolution soft X-ray emission spectroscopy (XES) stations (Fig. 3) are regularly maintained by the SRL staffs and open for public use, and at free-port station many novel spectroscopic tools have been developed and installed such as ambient pressure photoemission (Fig. 4) and soft X-ray diffraction (Fig. 5) which are also open for public use from 2018, and soft X-ray resonant magneto-optical Kerr effect (MOKE) and so on. The beamline construction

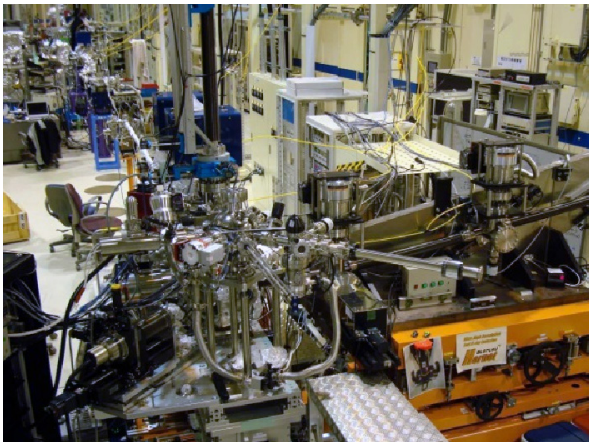

Fig. 3. Soft X-ray emission station

was completed in 2009 and SRL established the Harima branch laboratory in SPring-8. At SPring-8 BL07LSU, each end-station has achieved high performance: the TR-SX station have established the laser-pump and SR-probe method with the time-resolution of 50 ps which corresponds to the SR pulse-width; the 3D nano-ESCA station reaches the spatial resolution of 70 nm; the XES station provides spectra with the energy resolution around 70 meV at 400 eV and enabled real ambient pressure experiments. Soft X-ray resonant MOKE station has been developed to make novel magneto-optical experiment using fast-switching of the polarization-controlled 25-m long soft X-ray undulator. The soft X-ray diffraction station has been fully constructed and the time-resolved measurement is available by using lasers at the TR-SX station. In 2019, 240 researchers made their experiments during the SPring-8 operation time of 4584 hours.

• High-resolution Laser SARPES at E-building

Spin- and angle-resolved photoelectron spectroscopy (SARPES) is a powerful technique to investigate the spin-dependent electronic states in solids. In FY 2014, LASOR and SRL staffs constructed a new SARPES apparatus (Fig. 6), which was designed to provide high-energy and -angular resolutions and high efficiency of spin detection using a laser light at E-building. The achieved energy resolution of 1.7 meV in SARPES spectra is the highest in the world at present. From FY 2015, the new SARPES system has been opened to outside users.

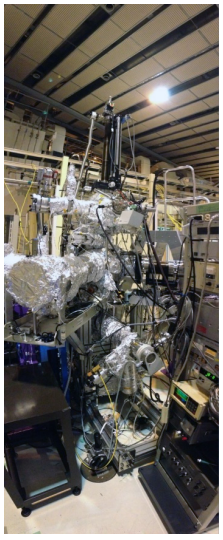

Fig. 1. TR-SX station

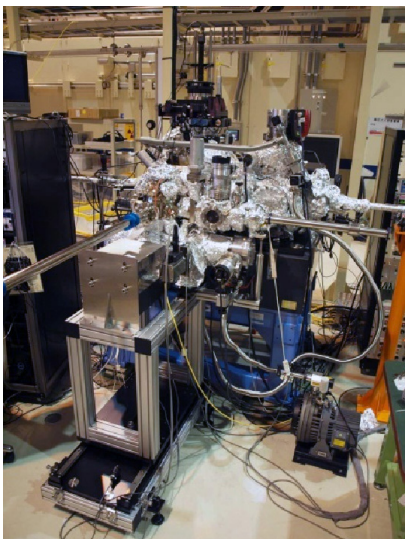

Fig. 2. 3D-nano ESCA station

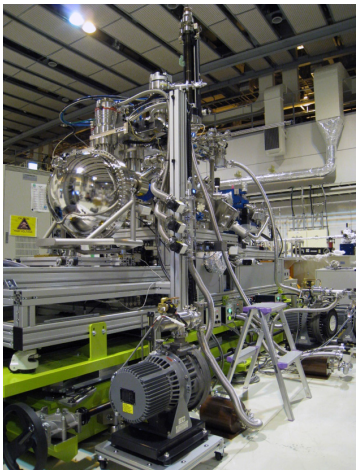

Fig. 4. Ambient pressure photoemission

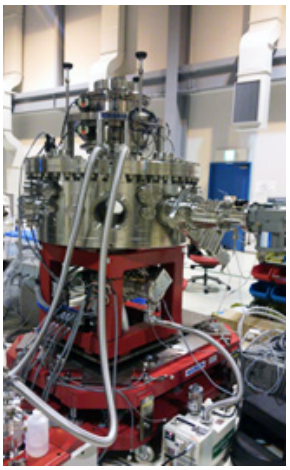

Fig. 5. Soft X-ray diffraction station

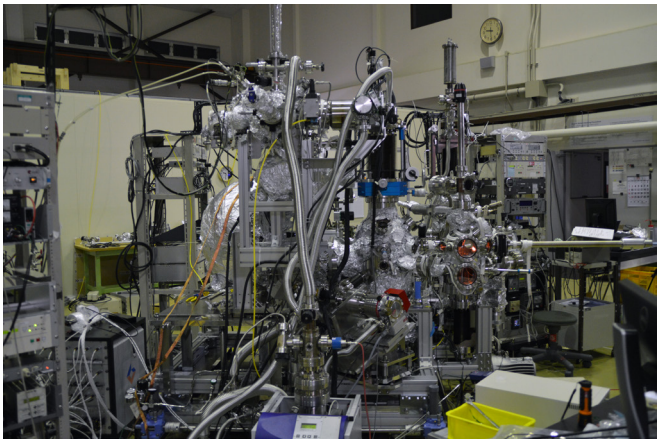

Fig. 6. Laser-SARPES system at E-building

The Laser-SARPES system consists of an analysis chamber, a carousel chamber connected to a load-lock chamber, and a molecular beam epitaxy chamber, which are kept ultra-high vacuum (UHV) environment and are connected each other via UHV gate valves. The electrons are excited with 6.994-eV photons, yielded by 6th harmonic of a Nd:YVO_4 quasi-continuous wave laser with repetition rate of 120 MHz and 10.7 eV photons, driven by the third harmonic radiation at 347 nm of an Yb:fiber chirped pulse amplifier laser, which was developed by Kobayashi's lab in LASOR. The hemispherical electron analyzer is a custom-made ScientaOmicron DA30-L, modified for installing the spin detectors. The spectrometer is equipped with two high-efficient spin detectors associating very low energy electron diffraction are orthogonally placed each other, which allows us to analyze the three-dimensional spin polarization of electrons. At the exit of the hemispherical analyzer, a multi-channel plate and a CCD camera are also installed, which enables us to perform the angle-resolved photoelectron spectroscopy with two-dimensional (energy-momentum) detection. The laser-SARPES machine can provide both high-resolution spin-integrated and spin-resolved photoemission spectra in various types of solids, such as spin-orbit coupled materials and ferromagnetic materials.

Conferences and Workshops

Spectroscopies in Novel Superconductors (SNS2019)

June 16-21, 2019
K. Okazaki and H. Wadati

SNS 2019 follows a successful series of international conferences in Argonne (1991), Sendai (1992), Santa Fe (1993); Stanford (1995), Cape Cod (1997), Chicago (2001), Sitges (2004), Sendai (2007), Shanghai (2010), Berkeley (2013), and Stuttgart (2016). Leading experts in spectroscopy, transport, materials, and theory meet to address current issues in the frontier of superconductivity research. Highlights to be discussed include the pairing mechanisms of cuprates, ruthenates, iridates, iron compounds, heavy-fermion systems, organic compounds, and low-dimensional materials; interplay between superconductivity and competing orders; topological superconductivity; superconductivity in 2D materials, at surfaces, and interfaces; non-equilibrium superconductivity and its dynamical control; experiments under extreme conditions; new experimental methods; and the design and discovery of novel superconductors with higher transition temperatures. This conference was held at Ito international research center, the University of Tokyo, and organized by the international steering committee, of which chair is Professor Arun Bansil (Northeastern University, USA), the program committee, of which chair is Professor Takami Tohyama, and the organizing committee, of which chairs are Professor Atsushi Fujimori and Professor Shik Shin, and advised from the international advisory committee. There are 208 participants from 21 countries mainly from Japan, China, and USA. As main topics, the recent progress in charge ordering and physical properties under uniaxial pressure of cuprate high-Tc superconductors, nematic electronic states of cuprates and iron-based superconductors, non-equilibrium superconductivity, superconductivity in magic-angle bilayer graphene, topological superconductivity, and Higgs mode in superconductors were presented. The programs proceeded in a single track without parallel sessions, and there were 193 presentations including 75 oral presentations (47 invited presentations) and 118 poster presentations. During the conference, discussions were actively conducted every day. In the closing session, it was announced that the next conference will be held at Bangalore in India, and 6 young researchers were awarded the young researcher's prize.

Computational Approaches to Quantum Many-body Problems (CAQMP2019)

July 16 - Aug. 8, 2019

K. Harada, K. Ido, R. Kaneko, N. Kawashima, Y. Kuramashi, T. Misawa, S. Morita, Y. Motoyama, T. Nishino, T. Okubo, T. Sakurai, T. Suzuki, K. Tamai, S. Todo, and K. Yoshimi

This event is one of the series of long-term annual international workshops started in 2006, in which a theoretical staff member serves as the principal organizer. A relatively small number of researchers stay in one place for a longer period than ordinary meetings, focusing on the subjects of remarkable recent progress. The 2019 workshop (CAQMP2019) was the 13th in the series. The theme of CAQMP2019 was the tensor network and its application. The 2016 workshop (TNQMP2016) was also dedicated to this subject. Between two workshops, there have been many advances in the methodology and application. Also, researchers recently became aware of connection between the tensor network and information science. Reflecting them, in the first week of the workshop, we discussed new numerical calculation methods, in the second week, the tensor network method, and in the third week, we focused on the connection with information science. The 4th week was dedicated to the comparison between calculations and experiments. We used the same format as in TNQMP2016, *i.e.*, on Mondays, we have symposia, each consisting of 30-minute talks, and from Tuesday to Friday, there was a lecture in the morning and a seminar in the afternoon. The list of the participants included: Anders Sandvik (Boston), Tao Xiang (CAS, Beijing), Laurence Vanderstraeten (Ghent), Yoshinobu Kuramasu (Univ. Of Tsukuba), Guangming Zhang (Tsinghua), Qibin Zhao (RIKEN), Hyun-Yong Lee (ISSP), Lei Wang (CAS, Beijing) and Cristian Batista (Tennessee). The total number of participants, including lectures and symposia, was 538 (of which 380 were lectures and 158 were symposia). Many lectures held this time were all recorded and uploaded to YouTube.

New Perspective in Spin Conversion Science (NPSCS2020)

February 3-4, 2020
Y. Otani, E. Saitoh, M. Shiraishi, S. Murakami, and A. Oiwa

Spin conversion is a generic term for the phenomena associated with the interconversion between different physical entities such as electricity, light, sound, vibration, and heat that are mediated by spins. Most spin-conversion phenomena take place at the nanoscale in the regions near the interface of two diverse varieties of materials, such as magnets, non-magnets, semiconductors, and insulators. The fundamental understanding of the spin conversion phenomena will thus allow us to develop novel functionalities applicable to practical energy-efficient spintronics as well as thermoelectric devices.

Therefore, we set the purpose of this workshop is for the international spintronics research community, especially for the world-leading foreign and domestic researchers working on the spin conversion phenomena, to exchange the most recent experimental and theoretical achievements on the spin conversion science. This workshop was also held as a concluding meeting of the Grant in Aid for Scientific Research in Innovative Areas, "Nano-Spin Conversion Science" conducted from 2014 to 2020.

The workshop was a great success. The 21 invited talks covered a variety of research topics such as spin-charge interconversion at the topological surface and Rashba interface states, the magnon-phonon coupling, antiferromagnet spintronics, superconducting spintronics, and also neuromorphic computing using spin conversion phenomena. Young researchers and graduate course students gave 53 poster presentations and participated in animated discussions at the workshop. The total number of participants was 183. Lastly, we much appreciate everyone's generous support, including the organizers, judges, directors, secretaries, and student part-timers. Without any help from the members, this could not have been accomplished.

Computational Materials Science —New Perspectives—

April 2-3, 2019

T. Ozaki, N. Kawashima, O. Sugino, H. Noguchi, Y. Higuchi, S. Morita, H. Watanabe, H. Kawamura, J. Haruyama, T. Hoshi, T. Tohyama, and H. Okuyama

This workshop was organized for the computational condensed matter research community, especially for the users of the ISSP supercomputers, to exchange the most recent research progress and related information on the computational condensed matter research and on the high-performance computation of related research areas. This was held as a series of annual workshop of ISSP supercomputer that has been held every year. The selected topics include the target of the post-K supercomputer project, the progress made in the elements strategy projects, the emergent data-driven material research, and "the Project for advancement of software usability in materials science" that in 2019 developed abICS, which is a software framework for performing configurational sampling in disordered systems, with a specific emphasis on multi-component solid state systems such as metal and oxide alloys, and TeNes, which is a solver for 2D quantum lattice system based on a PEPS wave function and the CTM method. In addition to 16 invited talks and 30 poster presentations, two special lectures were given by Prof. Miyashita and Prof. Fujii for quantum states of photons and quantum computing, respectively.

Joint Workshop of Novel Material Development and Measuring Technique by Using High-Pressure

July 5-6, 2019

F. Iga, Y. Uwatoko, and C. Sekine

Much novel and interesting physical properties such as superconductivity, metal-insulator transition and multipole transition induced under high-pressure condition have been found in recent years. Furthermore, much novel interesting materials by using high pressure synthesis have been also developed recently. High-pressure technology in Japan is historically on the top class in the world, but it becomes severe in international competition in recent years. Researchers of condensed matter physics and geophysics fields have carried development of high-pressure synthetic technology together, while sometimes influencing some degree independence each other, up to date. This joint workshop at ISSP has been organized for the high-pressure community to discuss the recent interesting physics and exchange the most recent information on each measurement technique.

In the workshop, 19 of oral and 25 poster presentations in total have been held for 2 days, and the participants had fruitful discussion, especially including a topic of room temperature superconductivity. The 1st day participants were 75 people (47 people from outside ISSP and 28 from the campus) and the number of the participants of the 2nd day were 49 (36 from outside and 28 from the ISSP). It can be said that this workshop has succeeded in accomplishing purposes as expected.

Physics and Chemistry of Light-induced Functions of Retinylidene Proteins

September 5-6, 2019
K. Inoue

Retinal proteins (rhodopsins) are photoreceptive membrane proteins that exist in an extremely wide range of biological species, from bacteria to animal, and giant viruses. When the retinal protein absorbs light, the retinal chromophore is isomerized and various physiological functions such as ion transport, enzymatic reaction and intracellular signal transduction are expressed. To achieve common understanding of the current situation of the study on retinal proteins, we held an ISSP workshop presenting cutting-edge researches by representative retinal protein researchers in Japan. This workshop was also positioned as a satellite symposium of the International Conference on Retinal Proteins, which is held in Ise-Shima in 2020. Totally, 111 people participated, and one keynote speech, 22 invited speeches, and 24 poster presentations from the general public were given. They presented recent studies on non-equilibrium processes in expression of the biological functions using advanced laser spectroscopy, structural studies by synchrotron x-ray radiation and free electron laser, and NMR, large-scale computational study, and so on. Throughout the workshop, many opinions on the current situation in the discipline and new problems to be solved were actively exchanged.

Helium Crisis: Present and Future

November 6, 2019
S. Ohara, H. Kawamura, H. Mori, S. Katsumoto, K. Kindo, T. Kondo, H. Tsuchiya, R. Sagiyama, and M. Yamashita

Shortage of helium supply directly hits researchers and is threatening sustainability of current academic studies all over the world. Helium is indispensable not only for condensed-matter scientists, but also for those in various research fields including elementary-particle physics, astronomy, and chemistry. Moreover, helium is unsubstitutable gas for many industrial uses, such as medical MRI examinations, productions of semiconductors and optical fibers, etc. Helium supply in Japan totally depends on imports from unstable suppliers in limited production areas, resulting "Helium Crisis" frequently. The present Helium Crisis is more serious than ever before because the demands from developing countries increase rapidly despite the decrease of supplies from United States.

In this workshop, we assembled academic scientists from different research area and participants from relevant companies to discuss the present status and possible future perspectives. We first discussed the current situations happening in research institutions. A review regarding the situation of gas supplying companies was also given by Y. Koizumi, president of Gas Review. Discussions about the restrictions applied to liquid helium and subjects to form the urgent proposals were also given.

One of the focus topics of this workshop was a helium-recycle framework by utilizing helium liquefying facilities of academic places. Recycling helium from vaporized helium gas is limited in research institutions equipped with expensive helium-liquefaction facility. Therefore, sharing a liquefaction facility with neighboring sites can considerably save the cost for recycling helium. Successful cases were reported from the collaborations between OIST and University of the Ryukyus and those between JAXA and Osaka University. It was also pointed out as an important future issue to build stockpiles of helium gas for preparing shortage. We hope that this workshop will be taken as an opportunity to enhance helium recycle in Japan.

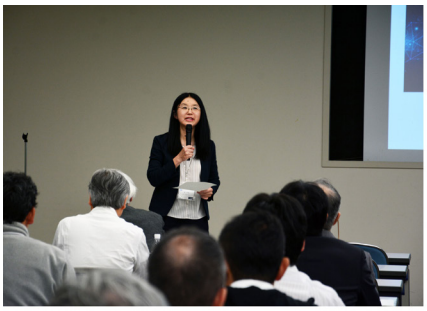

New Development of High Magnetic Field Science by HMF Collaboratory —Associated with Optical Science—

December 3-5, 2019

M. Hagiwara, K. Kindo, M. Tokunaga, Y. H. Matsuda, H. Nojiri, T. Sasaki, S. Tajima, N. Hanasaki, and Y. Narumi

This workshop was organized by high magnetic field (HMF) forum, the members of which are HMF users and providers, to exchange the most recent information on the development of measurement techniques and scientific research in high magnetic fields, and to aim at the association with optical science. This was held for the first time outside ISSP, namely Osaka University where the Joint-usage program of HMF research is conducted by the Center for Advanced High Magnetic Field Science with International MegaGauss Science Laboratory at ISSP as a new network-type Joint Usage/Research Center. A variety of scientific topics including optical science (magnetic alloy, multiferroics, heavy fermions, frustrated magnets, quantum magnets, topological materials, magnetic semiconductors, measurement techniques, theory and so on.) were presented at this workshop. In addition to 20 talks and 57 poster presentations, 6 invited talks by optical scientists were given. The number of registered participants was 112. During the workshop, present status and future plan of HMF facilities in Japan and a western Japan HMF network named KOFUC network were also provided.

Innovations to the Next-Generation Synchrotron Radiation

February 14, 2020

I. Matsuda, T. Arima, F. Komori, Y. Harada, H. Mimura, and T. Kondo

A plan for the next-generation synchrotron radiation facility was launched in Japan and the user-experiments are expected from 2023. Ten beamlines are planned by the Photon Science Innovation Center (PhoSIC) and the National Institutes for Quantum and Radiological Science and Technology (QST). There have been vigorous discussions on experimental methods for the individual beamlines that are expected to innovate our science and technology, including novel X-ray optics, advanced measurements, informatics analyses and automatic controls by AI robots.

To promote our project toward the new synchrotron radiation facility, we organized this workshop at the ISSP lecture room with broadcast live at SPring-8. It has successfully brought together 91 participants with fruitful discussion on these new technologies and foresights of the coming science. The program started with invite talks by Dr. Tetsuya Nakamura (PhoSIC) and Dr. Masamitsu Takahashi (QST), introducing their beamlines. In the following, there were invited talks by leading young researchers who made presentations on technical innovations for synchrotron radiation. We had a poster session by graduate students and postdocs who shared their new results and actively discussed with each other. Participants were confident to find that our next-generation synchrotron radiation facility would be developed by our next generations.

Subjects of Joint Research

令和元年度 共同利用課題一覧（前期）/ Joint Research List (2019 First Term)

嘱託研究員 / Commission Researcher

No.	課題名	氏名	所属		Title	Name	Organization
担当所員：森　初果							
1	水素結合型分子性無水プロトン伝導体におけるダイナミクスの研究	水野　元博	金沢大学	大学院自然科学研究科	Dynamics study of moleclar anhydrous proton conductors with hydrogen bonds	Motohiro Mizuno	Kanazawa University
担当所員：長谷川　幸雄							
2	極低温走査トンネル顕微鏡を用いた鉄カルコゲナイド超伝導体 FeSeTe の研究	吉田　靖雄	金沢大学	理工学域	Lo w -temperature STM study on iron-chalcogenide superconductor FeSeTe	Yasuo Yoshida	Kanazawa University
3	走査トンネル顕微鏡による局所強磁性共鳴法の開発	安　東秀	北陸先端科学技術大学院大学	先端科学技術研究科	Development of local ferromagnetic resonance in scanning tunneling microscopy	Toshu Ann	Japan Advanced Institute of Science and Technology
担当所員：川島　直輝							
4	スーパーコンピュータの調達に関する意見交換	渡辺　宙志	慶應義塾大学	理工学部	Procurement of Supercomputer System	Hiroshi Watanabe	Keiyo University
担当所員：上床　美也							
5	希土類 122 化合物における圧力効果	繁岡　透	山口大学	大学院理工学研究科	Pressure effect of rare earth 122 compounds	Toru Shigeoka	Yamaguchi University
6	低温用マルチアンビル装置の開発	辺土　正人	琉球大学	理学部	Development of multi-anvil apparatus for low temperature	Masato Hedo	University of the Ryukyus
7	ターンバックル式小型 DAC を利用した多重環境下電気抵抗測定	狩野　みか	日本工業大学	共通教育群	Electrical resistivity measurements under multi-extreme conditions by using a micro-turnbuckle DAC	Mika Kano	Nippon Institute of Technology

No.	課題名	氏名	所属		Title	Name	Organization
8	3d 遷移化合物に関する圧力効果	鹿又　武	東北学院大学	工学総合研究所	Effect of pressure on the 3d transition compounds	Takeshi Kanomata	Tohoku Gakuin University
9	擬一次元有機物質の圧力下物性研究	糸井　充穂	日本大学	医学部	Study on pressure induced superconductivity of quasi organic conductor	Miho Itoi	Nihon University
10	高圧下 X 線回折法の開発	江藤　徹二郎	久留米工業大学	工学部	Development of High Pressure X-ray diffraction measurements	Tetsujiro Eto	Kurume Institute of Technology
11	多重極限関連圧力装置の調整	高橋　博樹	日本大学	文理学部	Adjustment of Cubic Anvil apparatus	Hiroki Takahashi	Nihon University
12	磁性体の圧力効果	巨海　玄道	久留米工業大学	工学部	Effect of pressure on the Magnetic Materials	Gendo Oomi	Kurume Institute of Technology
13	希釈冷凍機温度で使用可能な 10GPa 級超高圧発生装置の開発	松林　和幸	電気通信大学	大学院情報理工学研究科	Development of 10 GPa class high pressure apparatus for low temperature	Kazuyuki Matsubayashi	The University of Electro-Communications
14	高圧下量子振動観測システムの開発	摂待　力生	新潟大学	理学部	Development of quantum oscillation under high pressure	Rikio Settai	Niigata University
15	酸化物試料の作製と高圧下物性測定	川中　浩史	産業技術総合研究所	電子光技術研究部門	Sample preparation and high pressure experiments	Hirofumi Kawanaka	National Institute of Advanced Industrial Science and Technology
16	カンチレバーを用いたトルク測定法の開発	鳥塚　潔	日本工業大学	共通教育群	Development of torque measurement method	Kiyoshi Torizuka	Nippon Institute of Technology
17	圧力下 NMR 測定法に関する開発	藤原　直樹	京都大学	大学院人間・環境学研究科	Development of NMR measurement method under high pressure	Naoki Fujiwara	Kyoto University
18	有機伝導体の圧力効果	村田　恵三	大阪経済法科大学	２１世紀社会総合研究センター	Effect of pressure on the organic conductor	Keizo Murata	Osaka University
担当：中性子科学研究施設							
19	4G における共同利用推進	佐藤　卓	東北大学	多元物質科学研究所	Research and Support of General-Use at 4G	Taku Sato	Tohoku University
20	〃	奥山　大輔	東北大学	多元物質科学研究所	〃	Daisuke Okuyama	Tohoku University
21	〃	那波　和宏	東北大学	多元物質科学研究所	〃	Kazuhiro Nawa	Tohoku University
22	6G における共同利用推進	富安　啓輔	東北大学	大学院理学研究科	Research and Support of General-Use at 6G	Keisuke Tomiyasu	Tohoku University
23	6G、T1-1 における共同利用推進	岩佐　和晃	茨城大学	フロンティア応用原子科学研究センター	Research and Support of General-Use at 6G, T1-1	Kazuaki Iwasa	Ibaraki University

No.	課題名	氏名	所属		Title	Name	Organization
24	T1-1、T1-3 における共同利用推進	大山　研司	茨城大学	大学院理工学研究科	Research and Support of General-Use at T1-1, T1-3	Kenji Ohyama	Ibaraki University
25	T1-1 における共同利用推進	桑原　慶太郎	茨城大学	大学院理工学研究科	Research and Support of General-Use at T1-1	Keitaro Kuwahara	Ibaraki University
26	〃	横山　淳	茨城大学	理学部	〃	Makoto Yokoyama	Ibaraki University
27	〃	伊賀　文俊	茨城大学	大学院理工学研究科	〃	Fumitoshi　Iga	Ibaraki University
28	T1-2、T1-3 における共同利用推進	藤田　全基	東北大学	金属材料研究所	Research and Support of General-Use at T1-2, T1-3	Masaki Fujita	Tohoku University
29	T1-2、T1-3、６G における共同利用推進	南部　雄亮	東北大学	金属材料研究所	Research and Support of General-Use at T1-2, T1-3, 6G	Yusuke Nambu	Tohoku University
30	〃	池田　陽一	東北大学	金属材料研究所	〃	Yoichi Ikeda	Tohoku University
31	T2-2、T1-3 における共同利用推進	木村　宏之	東北大学	多元物質科学研究所	Research and Support of General-Use at T2-2, T1-3	Hiroyuki Kimura	Tohoku University
32	〃	坂倉　輝俊	東北大学	多元物質科学研究所	〃	Terutoshi Sakakura	Tohoku University
33	T2-2、T1-3 における共同利用推進	山本　孟	東北大学	多元物質科学研究所	Research and Support of General-Use at T2-2, T1-3	Hajime Yamamoto	Tohoku University
34	C1-2 における共同利用推進	杉山　正明	京都大学	複合原子力科学研究所	Research and Support of General-Use at C1-2	Masaaki Sugiyama	Kyoto University
35	C1-2、C2-3-1 における共同利用推進	井上　倫太郎	京都大学	複合原子力科学研究所	Research and Support of General-Use at C1-2, C2-3-1	Rintaro Inoue	Kyoto University
36	C2-3-1 における共同利用推進	守島　健	京都大学	複合原子力科学研究所	Research and Support of General-Use at C2-3-1	Ken Morishima	Kyoto University
37	C3-1-2、C2-3-1 における共同利用推進	日野　正裕	京都大学	複合原子力科学研究所	Research and Support of General-Use at C3-1-2, C2-3-1	Masahiro Hino	Kyoto University
38	C3-1-2 における共同利用推進	田崎　誠司	京都大学	大学院工学研究科	Research and Support of General-Use at C3-1-2	Seiji Tasaki	Kyoto University
39	〃	小田　達郎	京都大学	複合原子力科学研究所	〃	Tatsuro Oda	Kyoto University
40	〃	北口　雅暁	名古屋大学	現象解析研究センター	〃	Masaaki Kitaguchi	Nagoya University

No.	課題名	氏名	所属		Title	Name	Organization
担当所員：原田　慈久							
41	時間分解光電子顕微分光実験の技術開発	木下　豊彦	高輝度光科学研究センター	利用研究推進部門	Technical development of time-resolved photoemission microscopy measurement	Toyohiko Kinoshita	JASRI
42	有機化合物の光電子分光	金井　要	東京理科大学	理工学部	Photoemission study on organic compounds	Kaname Kanai	Tokyo University of Science
43	トポロジカル絶縁体の電子状態の解明	木村　昭夫	広島大学	大学院理学研究科	Electronic-structure study of topological insulators	Akio Kimura	Hiroshima University
44	Si(111）上単層タリウムの高次高調波を用いた時間分解光電子分光	坂本　一之	大阪大学	大学院工学研究科	Time-resolved ARPES investigation of monolayer Thallium on Si(111)	Kazuyuki Sakamoto	Chiba University
45	液中プラズマ印加水の軟Ｘ線吸収 / 発光分光技術開発	寺嶋　和夫	東京大学	大学院新領域創成科学研究科	Technical development of soft X-ray absorption/emission spectroscopy for water processed by in-liquid plasma	Kazuo Terashima	The University of Tokyo
46	液中プラズマ印加によるナノ粒子分散特性評価と軟Ｘ線分光	伊藤　剛仁	東京大学	大学院新領域創成科学研究科	Characterization of nano-particle distribution in water processed by in-liquid plasma and soft X-ray spectroscopy	Tsuyohito Ito	The University of Tokyo
47	軟Ｘ線発光・共鳴非弾性散乱分光の磁気円・線二色性測定システムの構築	菅　滋正	大阪大学	産業科学研究所	Construction of a noble system for circular and linear dichroism in soft X-ray emission and RIXS spectroscopy	Shigemasa Suga	Osaka University
48	軟Ｘ線吸収／発光分光法によるリチウムイオン電池電極材料の電子物性研究	細野　英司	産業技術総合研究所	省エネルギー研究部門	Study on the electronic property of electrode materials for Li-ion batteries by soft X-ray absorption/emission spectroscopy	Eiji Hosono	National Institute of Advanced Industrial Science and Technology
49	〃	朝倉　大輔	産業技術総合研究所	エネルギー技術研究部門	〃	Daisuke Asakura	National Institute of Advanced Industrial Science and Technology
50	高分解能光電子分光による酸化バナジウムの研究	藤原　秀紀	大阪大学	大学院基礎工学研究科	Study on vanadium oxides by high resolution Photoemission	Hidenori Fujiwara	Osaka University
51	省エネ・創エネ・蓄電デバイスのオペランド分光	尾嶋　正治	東京大学	大学院工学系研究科	Operando nano-spectroscopy for energy efficient, power generation and energy storage devices	Masaharu Oshima	The University of Tokyo
52	原子レベルで制御されたモデル有機分子表面上の界面水の電子状態観測	林　智広	東京工業大学	総合理工学研究科	Analysis of the electronic structure of interfacial water formed on model organic surfaces	Tomohiro Hayashi	Tokyo Institute of Technology
53	三次元 nanoESCA による実デバイスのオペランド電子状態解析	永村　直佳	物質・材料研究機構	先端材料解析研究拠点	Operando analysis of the electronic structure of actual devices by 3DnanoESCA	Naoka Nagamura	National Institute for Materials Science
担当所員：松田　巌							
54	スピン分解光電子分光の測定技術開発	木村　真一	大阪大学	大学院生命機能研究科	Technical development of spin-resolved photoemission spectroscopy measurement	Shin-ichi Kimura	Osaka University
55	時間分解磁気光学実験の技術開発	小嗣　真人	東京理科大学	基礎工学部	Technical development of time-resolved magneto-optical experiment	Masato Kotsugi	Tokyo University of Science

No.	課題名	氏名	所属		Title	Name	Organization
56	超高速磁化応答による磁性波動関数の制御	小林　正起	東京大学	大学院工学系研究科	Regulation of magnetic wave functions by	Masaki Kobayashi	The University of Tokyo
57	時間分解吸収分光による $EuNi_2(Si_{1-x}Ge_x)_2$ の価数転移ダイナミクスの解明	三村　功次郎	大阪府立大学	大学院工学研究科	Dynamics of valence transition in $EuNi_2(Si_{1-x}Ge_x)_2$ revealed by time-resolved XAS	Kojiro Mimura	Osaka Prefecture University
58	コヒーレント共鳴軟 X 線散乱による磁気ドメイン構造の観測	山崎　裕一	物質・材料研究機構	統合型材料開発・情報基盤部門	Observation of magnetic domain structure for ferromagnetic thin films by means of resonant scatterin	Yuichi Yamasaki	National Institute for Materials Science
59	遷移金属化合物の時間分解 X 線分光と回析	和達　大樹	兵庫県立大学		Time-resolved x-ray spectroscopy and diffraction of transition-metal-compounds	Hiroki Wadati	University of Hyogo
担当所員：近藤　猛							
60	トポロジカル超伝導体の探索	坂野　昌人	東京大学	大学院工学系研究科	Search for topological insulators	Masato Sakano	The University of Tokyo
61	高分解能光電子分光による強相関物質の研究	横谷　尚睦	岡山大学	異分野基礎科学研究所	ultra-high resolution study on strongly correlated materials	Takayoshi Yokoya	Okayama University
62	レーザー励起光電子顕微鏡を使った抵抗変化メモリ材料の研究	木下　健太郎	東京理科大学	理学部	Study on Materials for Resistive Switching Memories using laser-PEEM	Kentaro Kinoshita	Tokyo University of Science
63	60-eV レーザーを用いた時間分解光電子分光の開発	石坂　香子	東京大学	大学院工学系研究科	The development of time-resolved photoemission using 60eV laser	Kyoko Ishizaka	The University of Tokyo
64	収差補正型光電子顕微鏡の建設と利用研究	小嗣　真人	東京理科大学	基礎工学部	Construction and utilization research of aberration correction photoelectron emission microscopy	Masato Kotsugi	Tokyo University of Science
65	鉄系超伝導体のレーザー光電子分光	下志万　貴博	理化学研究所	創発物性科学研究センター	Laser-ARPES on Fe superconductor	Takahiro Shimojima	RIKEN
66	光電子分光法を用いた各種分子性結晶の電子状態の研究及び装置の低温化	木須　孝幸	大阪大学	大学院基礎工学研究科	Research on electron state of molecular crystals using photoemission spectroscopy	Takayuki Kisu	Osaka University
担当所員：岡崎　浩三							
67	時間分解光電子分光や超高分解能光電子分光を用いた超伝導体や強相関物質の研究	吉田　鉄平	京都大学	大学院人間・環境学研究科	Laser ARPES study on superconductors and strongly-correlated materials	Teppei Yoshida	Kyoto University
68	固体中のマヨラナ粒子の研究	松田　祐司	京都大学	大学院理学研究科	Study of Majorana Fermion in Solids by Laser Photoemission Spectroscopy	Yuji Matsuda	Kyoto University
69	〃	佐藤　昌利	京都大学	基礎物理学研究所	〃	Masatoshi Sato	Kyoto University
70	FeSe 超伝導体における BCS-BES クロスオーバーの研究	紺谷　浩	名古屋大学	大学院理学研究科	Study of BCS-BES crossover in FeSe superconductors	Masatoshi Sato	Kyoto University

No.	課題名	氏名	所属		Title	Name	Organization
71	時間分解光電子分光を用いた強相関物質の研究	溝川　貴司	早稲田大学	理工学術院	Time-resolved photoemmission study on strongly-correlated materials	Takashi Mizokawa	Waseda University
72	超高分解能レーザー光電子分光による高温超伝導体の研究	チャン　ウェイル	上智大学	機能創造理工学科	Study of high - Tc superconductors by high-resolution laser ARPES	Zhang Weilu	Sopia University

一般研究員 / General Researcher

No.	課題名	氏名	所属		Title	Name	Organization
担当所員：瀧川　仁							
1	有機三角スピン系の核磁気共鳴による磁気誘電現象の解明	細越　裕子	大阪府立大学	大学院理学系研究科	NMR study on the magnetodielectric properties of organic triangular spin system	Yuko Hosokoshi	Osaka Prefecture University
2	〃	三好　克典	大阪府立大学	大学院理学系研究科	〃	Katsunori Miyoshi	Osaka Prefecture University
3	〃	瀬戸川　大喜	大阪府立大学	大学院理学系研究科	〃	Hiroki Setogawa	Osaka Prefecture University
4	YbH_{2+x} の磁性と伝導	中村　修	岡山理科大学	研究・社会連携センター	Magnetic and transport properties in YbH_{2+x}	Osamu Nakamura	Okayama University of Science
担当所員：榊原　俊郎							
5	重い電子系超伝導体の対称性の決定	町田　一成	立命館大学	理工学部	Determination of the pairing symmetry of heavy Fermion superconductors	Kazushige Machida	Ritsumeikan University
6	重い電子系化合物が示す非従来型超伝導と磁性の相関	横山　淳	茨城大学	理学部	Interplay between unconventional superconductivity and magnetism in heavy-fermion compounds	Makoto Yokoyama	Ibaraki University
7	〃	ラフマント	茨城大学	理学部	〃	Rahmanto	Ibaraki University
8	特異な強磁性転移を示す $Yb_2Ti_2O_7$ の誘電特性	安井　幸夫	明治大学	理工学部	Dielectric properties of $Yb_2Ti_2O_7$ with anomalous ferromagnetic transition	Yukio Yasui	Meiji University
9	トポロジカル超伝導のネマチック相研究	孫　悦	青山学院大学	理工学部	Study of the nematic phase of topological superconductors	Yue Sun	Aoyama Gakuin University
10	フラストレート系有機磁性体の低温物性測定	山口　博則	大阪府立大学	大学院理学系研究科	Low temperature physical properties of frustrated organic radical compounds	Hironori Yamaguchi	Osaka Prefecture University
11	〃	沖田　大輝	大阪府立大学	大学院理学系研究科	〃	Taiki Okita	Osaka Prefecture University

No.	課題名	氏名	所属		Title	Name	Organization
12	$SmPt_2Cd_{20}$ の低温磁化測定	広瀬　雄介	新潟大学	理学部	Low temperature magnetization measurements of $SmPt_2Cd_{20}$	Hirose Yusuke	Niigata University
13	Ba^{2+}-Fe^{3+}-Ti^{4+} 酸化物磁性体の磁場中誘電特性	神島　謙二	埼玉大学	大学院理工学研究科	Dielectric properties of Ba^{2+}-Fe^{3+}-Ti^{4+} magnetic oxides under magnetic field	Kenji Kamishima	Saitama University
14	〃	安田　直生	埼玉大学	大学院理工学研究科	〃	Naoki Yasuda	Saitama University
15	〃	神　治樹	埼玉大学	大学院理工学研究科	〃	Haruki Kan	Saitama University
16	〃	高橋 久由	埼玉大学	大学院理工学研究科	〃	Hisayoshi Takahashi	Saitama University
17	純良単結晶を用いた新規遷移金属超伝導体の精密比熱測定	加瀬　直樹	東京理科大学	理学部	Superconducting state of the transition-metal based compounds elucidated through specific heat measurements	Kase Naoki	Tokyo University of Science
18	フラストレート系有機磁性体の低温物性測定	河野　洋平	大阪府立大学	大学院理学系研究科	Low temperature physical properties of frustrated organic radical compounds	Yohei Kono	Osaka prefecture University
担当所員：山下　穣							
19	三角格子反強磁性体の低温比熱測定	柄木　良友	琉球大学	教育学部	Low temperature specific heat measurements of triangular antiferromagnets.	Yoshitomo Karaki	University oy The Ryukyus
20	重い電子系超伝導体 $CeCoIn_5$ の超低温における dHvA 効果の角度依存性	宍戸　寛明	大阪府立大学	大学院工学研究科	Angular dependence of the dHvA effect at ultra-low temperatures in a heavy fermion superconductor $CeCoIn_5$	Hiroaki Shishido	Osaka Prefecture University
21	磁場角度分解熱輸送測定による新規超伝導の研究	水上　雄太	東京大学	大学院新領域創成科学研究科	Studies on novel superconductors by field-angle-resolved thermal transport measurements	Yuta Mizukami	The University of Tokyo
22	重い電子系化合物 $YbNi_2Si_3$ の超低温磁気トルク測定	大原　繁男	名古屋工業大学	物理工学科	Magnetic torque meansurements of heavy fermion $YbNi_2Si_3$ at ultra low temperature	Shideo Ohara	Nagoya Institute of Technology
23	〃	中村　翔太	名古屋工業大学	物理工学科	〃	Shota Nakamura	Nagoya Institute of Technology
担当所員：勝本　信吾							
24	ナノセンシングデバイスの開発	米谷　玲皇	東京大学	大学院新領域創成科学研究科	Development of nanosensing device	Reo Kometani	The University of Tokyo
25	〃	西田　裕信	東京大学	大学院新領域創成科学研究科	〃	Nishida Hironobu	The University of Tokyo
26	〃	ペンエークウォン　ケーマナット	東京大学	大学院新領域創成科学研究科	〃	Penekwong Khemnat	The University of Tokyo

No.	課題名	氏名	所属		Title	Name	Organization
27	〃	ゴ　チャウ	東京大学	大学院新領域創成科学研究科	〃	Gu Chao	The University of Tokyo
28	遷移金属ダイカルコゲナイド層状物質半導体 / 金属界面状態の電気輸送特性による研究	石黒　亮輔	日本女子大学	理学部	Sutudy of electrical transport property in transition metal dichalcogenide layered material semiconductor /metal interface state	Ryosuke Ishiguro	Japan Women's University
29	量子ホール効果測定のための高移動度半導体試料作成	福田　昭	兵庫医科大学	物理学教室	Development of the hogh mobility semiconductor sample for the measurements in the meansurements in the quantum Hall	Akira Fukuda	Hyogo College of Medicine
担当所員：大谷　義近							
30	5d 電子系酸化物薄膜におけるスピンホール効果	木俣　基	東北大学	金属材料研究所	Spin Hall effect in 5d oxide thin films	Motoi Kimata	Tohoku university
31	空間反転対称性の破れた結晶構造に発現する電流誘起磁化の電気的検出	木俣　基	東北大学	金属材料研究所	Electrical detection of current induced magnetization in non-centrosymmetric crystal structure	Motoi Kimata	Tohoku university
32	希土類金属間化合物の強磁場低温物性研究	海老原　孝雄	静岡大学	学術院理学領域	Physical properties in rare earth intermetallic compounds at high magnetic fields in low temperature	Takao Ebihara	Shizuoka University
33	〃	ジュマエダ・ジャトミカ	静岡大学	大学院自然科学教育部	〃	Jumaeda Jatmika	Shizuoka University
担当所員：小森　文夫							
34	Al-Pd-Ru 準結晶・近似結晶における空孔濃度の研究	金沢　育三	東京学芸大学	自然科学系	Positron-annihilation studies of Al-Pd-Ru quasicrystal and its approximant crystals	Ikuzo Kanazawa	Tokyo Gakugei University
35	〃	高橋　潤	東京学芸大学	大学院教育学研究科	〃	Jun Takahashi	Tokyo Gakugei University
36	単層グラフェンの電子状態の解析	大野　真也	横浜国立大学	大学院工学研究院	Analysis of electronic states of monolayer graphene	Shinya Ohno	Yokohama National University
37	〃	青柳 良英	横浜国立大学	大学院理工学府	〃	Yoshihide Aoyagi	Yokohama National University
38	$Si(111)_4 \times 1$-In 基板上における Bi-In 表面合金の電子状態	中辻　寛	東京工業大学	物質理工学院	Electronic structure of Bi-In surface alloy grown on $Si(111)_4 \times 1$-In substrates	Kan Nakatsuji	Tokyo Institute of Technology
39	〃	金野　達	東京工業大学	物質理工学院	〃	Tatsu Konno	Tokyo Institute of Technology
40	酸素サーファクタントを用いた Fe 薄膜の成長過程と電子状態	中辻　寛	東京工業大学	物質理工学院	Oxygen surfactant assisted growth of Fe thin-films and their electronic states	Kan Nakatsuji	Tokyo Institute of Technology
41	レアメタルフリー磁性材料 L10-FeCo の磁気特性の解析	小嗣　真人	東京理科大学	基礎工学部	Analysis of magnetic properties of rare-metal-free super magnet	Kotsugi Masato	Tokyo University of Science

No.	課題名	氏名	所属		Title	Name	Organization
42	〃	高橋　優樹	東京理科大学	基礎工学部	〃	Yuuki Takahashi	Tokyo University of Science
43	金属／半導体表面上への超薄膜およびナノ構造薄膜の形成とその磁化ダイナミックスの観測	河村　紀一	放送技術研究所	新機能デバイス研究部	Study on magnetic dynamics of ultra-thin films and nano-structures on metal / semiconductor surfaces	Norikazu Kawamura	NHK Science and Technology Research Laboratories
44	STM を用いた L10-FeNi 表面における N サーファクタント効果の解析	小嗣　真人	東京理科大学	基礎工学部	Study of N surfactant effect on L10-FeNi by using STM	Masato Kotsugi	Tokyo University of Science
45	〃	高橋　優樹	東京理科大学	基礎工学部	〃	Yuuki Takahashi	Tokyo University of Science
46	面内圧縮された Cu(001) 表面における局所構造緩和 (2)	山田　正理	中央大学	理工学部	Local structural rearrangement on a compressed Cu(001) surface (2)	Masamichi Yamada	Chuo University
47	真空転写法により形成した積層グラフェンの電子状態評価	田中　悟	九州大学	大学院工学研究院	Evalution of electronic structures of stacked graphene fabricated by vacuum transfer technique.	Satoru Tanaka	Kyushu University
48	〃	今村　均	九州大学	大学院工学研究院	〃	Hitoshi Imamura	Kyushu University
49	酸素サーファクタントを用いた Fe 薄膜の成長過程と電子状態	木村　彰博	東京工業大学	物質理工学院	Oxygen surfactant assisted growth of Fe thin-films and their electronic states	Akihiro Kimura	Tokyo Institute of Technology
担当所員：長谷川　幸雄							
50	エピタキシャルシリセン、ゲルマネン及びそのヘテロ構造の低温走査トンネル顕微鏡観察	高村　由起子	北陸先端科学技術大学院大学	マテリアルサイエンス系	STM investigation of epitaxial silicene, germanene, and their heterostructures	Yukiko Takamura	JAIST
担当所員：リップマー　ミック							
51	機械学習を用いた高効率薄膜作成手法の開発	大久保　勇男	物質・材料研究機構	機能性材料研究拠点	Development of an efficient thin film growth thechnique using a mechine learning approach	Isao Ohkubo	National Institute for Materials Science
担当所員：吉信　淳							
52	IRAS による環状分子膜の構造評価	川井　茂樹	物質・材料研究機構	国際ナノアーキテクトニクス研究拠点	Structual analysis of cyclic moneculay layer by IRAS	Shigeki Kawai	Natuinal Institute for Materials Science
担当所員：秋山　英文							
53	オキナワマドホタルルシフェラーゼを用いた生物発光における pH 依存性の定量的評価	樋山　みやび	群馬大学	大学院理工学府	Quantitative evaluation of pH dependence in Pyrocoelia-matsumurai-firefly bioluminescence	Miyabi Hiyama	Gunma University
54	〃	小野　稜平	群馬大学	理工学部	〃	Ryohei Ono	Gunma University

No.	課題名	氏名	所属		Title	Name	Organization
55	北米産ホタルを用いた生物発光スペクトルにおける重金属の影響調査	樋山　みやび	群馬大学	大学院理工学府	Effects on heavy metals in Photinus pyralis firefly bioluminescence spectra	Miyabi Hiyama	Gunma University
56	〃	手塚　大輔	群馬大学	理工学部	〃	Daisuke Tezuka	Gunma University
57	多波長励起フォトルミネッセンス測定による GaPN 混晶のアップコンバージョン発光に関する研究	矢口　裕之	埼玉大学	大学院理工学研究科	Multiple wavelength excited photoluminescence measurements of up-conversion luminescence of GaPN alloys	Hiroyuki Yaguchi	Saitama University
58	多波長励起による GaPN 混晶のアップコンバージョン発光に関する研究	古田　和	埼玉大学	大学院理工学研究科	Multiple wavelength excited photoluminescence measurements of up-conversion luminescence of GaPN alloys	Kazu Furuta	Saitama University
59	〃	高宮　健吾	埼玉大学	総合技術支援センター	〃	Kengo Takamiya	Saitama University
60	希薄磁性半導体超格子 GaGdAs:Si/GaAs におけるバースタイン・モスシフトの測定によるフェルミ面位置とキャリア誘起強磁性の関係解明	宮川　勇人	香川大学	創造工学部	Relationship between Fermi surface position and carrier induced ferromagnetism by measuring Burstein-Moss Shift in diluted magnetic semiconductor superlattice GaGdAs:Si/GaAs	Hayato Miyagawa	Kagawa University
61	〃	高藤　誠	香川大学	大学院工学研究科	〃	Makoto Takafuji	Kagawa University
62	希薄磁性半導体 GaGdAs を用いたスピン LED における円偏光度制御の検証	宮川　勇人	香川大学	創造工学部	Control of circular polarization light of spin-polarized light-emitting diodes using diluted magnetic semiconductor	Hayato Miyagawa	Kagawa University
63	〃	船曳　晃弘	香川大学	大学院工学研究科	〃	Akihiro Funabiki	Kagawa University
64	宇宙線望遠鏡の焦点面ライトガイドの反射率測定	吉田　龍生	茨城大学	理学部	Reflectance measurement of focal plane light concentrators for cosmic-ray telescopes	Tatsuo Yoshida	Ibaraki University
65	超伝導転移端センサ用金属薄膜の光学測定	遠藤　護	東京大学	大学院工学系研究科	Optical property measurement of metal membrene for superconducting transition edge sensor	Mmoru Endo	The University of Tokyo
66	〃	松山　幹尚	東京大学	大学院工学系研究科	〃	Mikihisa Matsuyama	The University of Tokyo
担当所員：川島　直輝							
67	層状構造を有する金属間化合物のディインターカレーションと低温物性	山田　高広	東北大学	多元物質科学研究所	Ground-state phase diagram and magnetic excitations of theKitaev-J- Γ model on a honeycomb lattice	Takafumi Suzuki	University of Hyogo
68	物性における数値繰り込み群法の応用	原田　健自	京都大学	大学院情報学研究科	Application of numerical renormalization group method in condensed-matter physics	Kenji Harada	Kyoto University
担当所員：廣井　善二							
69	蜂の巣格子 Kitaev-J- Γ 模型の基底状態相図と磁気励起	鈴木　隆史	兵庫県立大学	大学院工学研究科	Characterization of electric and magnetic properties of intermetallic compounds with layered structures	Takahiro Yamada	Tohoku University

No.	課題名	氏名	所属		Title	Name	Organization
70	基板上に成膜した CoPt 規則化強磁性体の磁化測定	山浦　淳一	東京工業大学	元素戦略研究センター	Magnetization measurement of CoPt ordered ferromagnet fabricated on substrate	Junichi Yamaura	Tokyo Institute of Technology
71	〃	真島　豊	東京工業大学	科学技術創成研究院・フロンティア材料研究所	〃	Yutaka Majima	Tokyo Institute of Technology
72	〃	遠山　諒	東京工業大学	物理工学院	〃	Ryo Toyama	Tokyo Institute of Technology
73	希土類４ｆ電子数制御による新規アクチュエータ材料の創製	竹中　康司	名古屋大学	大学院工学研究科	Development of novel volume-change-driven actuator materials by control of rare earth 4f electron number	Koshi Takenaka	Nagoya University
74	〃	横山　泰範	名古屋大学	大学院工学研究科	〃	Yasunori Yokoyama	Nagoya University
75	〃	水野　陽介	名古屋大学	大学院工学研究科	〃	Yosuke Mizuno	Nagoya University
76	〃	長谷川　遥加	名古屋大学	大学院工学研究科	〃	Haruka Hasegawa	Nagoya University
77	新規ハイパーハニカム格子磁性体β -$ZnIrO_3$ の磁化測定	原口　祐哉	東京農工大学	物理システム工学科	Magnetization measurement of the novel hyperhoneycomb lattice magnet β -$ZnIrO_3$	Yuya Haraguchi	University of Agriculture anf Technology
担当所員：上床　美也							
78	キュービックアンビルセルを用いた NMR 測定開発	藤原　直樹	京都大学	大学院人間・環境学研究科	Development of NMR measurements under pressure using a cubic-anvil cell	Naoki Fujiwara	Kyoto University
79	〃	桑山　昂典	京都大学	大学院人間・環境学研究科	〃	Takanori Kuwayama	Kyoto University
80	$FeSe_{1-x}Te_x$ の単結晶試料における高圧下物性研究	松浦　康平	東京大学	大学院新領域創成科学研究科	The high pressure study on single-crystalline$FeSe_{1-x}Te_x$	Kouhei Matsuura	The University of Tokyo
81	三角格子反強磁性体の低温磁性	柄木　良友	琉球大学	教育学部	Low temperature magnetism of triangular antiferromagnets	Yoshitomo Karaki	University oy The Ryukyus
82	重い電子系希土類化合物の dHvA 効果	摂待　力生	新潟大学	理学部	de Haas-van Alphen effect in heavy fermion cerium compounds	Rikio Settai	Niigata University
83	〃	佐野　純佳	新潟大学	理学部	〃	Sumika Sano	Niigata University
84	多形化合物 RIr_2Si_2(R= 希土類）の結晶育成と物質評価 6	繁岡　透	山口大学	大学院創成科学研究科	Crystal growth and characterization of polymorphic compounds RIr_2Si_2 (R=rera earth) 6	Toru Shigeoka	Yamaguchi University
85	〃	内間　清晴	沖縄キリスト教短期大学	総合教育系	〃	Kiyoharu Uchima	Okinawa Christian Junior College

No.	課題名	氏名	所属		Title	Name	Organization
86	擬三元化合物 $Ce_{1-x}M_xNiC_2$(M = Y, La) の結晶育成と物質評価 2	繁岡　透	山口大学	大学院創成科学研究科	Crystal growth and characterization of pseudo-ternary compounds $Ce_{1-x}M_xNiC_2$(M = Y, La) 2	Toru Shigeoka	Yamaguchi University
87	〃	Shunnsuke Yamada	沖縄キリスト教短期大学	総合教育系	〃	Kiyoharu Uchima	Okinawa Christian Junior College
88	多形化合物 RIr_2Si_2(R= 希土類）磁気特性 4	繁岡　透	山口大学	大学院創成科学研究科	Magnetic characteristics of polymorphic compounds RIr_2Si_2(R=rare earth) 4	Toru Shigeoka	Yamaguchi University
89	〃	内間　清晴	沖縄キリスト教短期大学	総合教育系	〃	Kiyoharu Uchima	Okinawa Christian Junior College
90	高圧下における Eu 化合物の価数転移の探索	大貫　惇睦	琉球大学	理学部	Investigation of valence transition on Eu compounds under high pressure	Yoshichika Onuki	University of the Ryukyus
91	〃	本多　史憲	東北大学	金属材料研究所	〃	Fuminori Honda	Tohoku University
92	ウラン化合物の磁性の圧力効果	本多　史憲	東北大学	金属材料研究所	Effect of Pressure on the magnetism of uranium compounds	Fuminori Honda	Tohoku University
93	Ce_2MgGe_2 の高圧力下電気抵抗測定	広瀬　雄介	新潟大学	理学部	Electrical resistivity measurement under pressure of Ce_2MgGe_2	Yusuke Hirose	Niigata University
94	〃	山田　峻輔	新潟大学	理学部	〃	Shunnsuke Yamada	Niigata University
95	カミオカイト型酸化物 $(Fe_{1-x}Zn_x)_2Mo_3O_8$ の高圧下における物性	赤星　大介	東邦大学	理学部	Physical properties of $(Fe_{1-x}Zn_x)_2Mo_3O_8$ under high pressure	Daisuke Akahoshi	Toho University
96	六方晶 $Hf_{1-x}Ta_xFe_2$ の磁気特性	松本　圭介	愛媛大学	大学院理工学研究科	Magnetic properties of hexagonal $Hf_{1-x}Ta_xFe_2$	Keisuke Matsumoto	Ehime University
97	〃	石原　憲	愛媛大学	大学院理工学研究科	〃	Ken Ishihara	Ehime University
98	SQUID 磁束計用 ^{3}He インサートの開発および低温磁化測定	河江　達也	九州大学	大学院工学研究院	Development of ^{3}He insert for SQUID magnetometer	Tatsuya Kawae	Kyushu University
99	〃	司　文	九州大学	大学院工学府	〃	Si Wen	Kyushu University
100	直方晶 $Co_{1-x}Ni_xMnSi$ の磁気熱量効果	松本　圭介	愛媛大学	大学院理工学研究科	Magnetocaloric properties of orthorhombic $Co_{1-x}Ni_xMnSi$	Keisuke Matsumoto	Ehime University
101	〃	今田　敦士	愛媛大学	工学部	〃	Atsushi Imada	Ehime university
102	〃	高畦　恋	愛媛大学	工学部	〃	Ren Takaaze	Ehime University

No.	課題名	氏名	所属		Title	Name	Organization
103	CeCoSi の圧力下電気抵抗測定	川村　幸裕	室蘭工業大学	大学院工学研究科	Measurement of electrical resistivity under pressure of CeCoSi	Yukihiro Kawamura	Muroran Institute of Technology
104	ハーフメタルホイスラー合金の磁気体積効果に関する研究	重田　出	鹿児島大学	大学院理工学研究科	Study on the magneto-volume effect of half-metallic Heusler alloys	Iduru Shigeta	Kagoshima University
105	重い電子系物質における ^{3}He 温度領域での磁化測定	志賀　雅亘	九州大学	大学院工学府	Magnetization measurements in ^{3}He temperature region for heavy fermion systems	Masanobu Shiga	Kyushu University
106	$HoRh_2Si_2$ の Co 置換系化合物の単結晶育成　(2)	藤原　哲也	山口大学	大学院創成科学研究科	Single crystal growth of Co substituted $HoRh_{2-x}Co_xSi_2$ compounds II	Tetsuya Fujiwara	Yamaguchi University
107	〃	山本　嵩	山口大学	大学院創成科学研究科	〃	Shu Yamamoto	Yamaguchi University
108	$Ho_{1-x}La_xRh_2Si_2$ 単結晶の磁場中比熱測定	藤原　哲也	山口大学	大学院創成科学研究科	Specific heat measurement under magnetic field of $Ho_{1-x}La_xRh_2Si_2$ single crystal	Tetsuya Fujiwara	Yamaguchi University
109	〃	山本　嵩	山口大学	大学院創成科学研究科	〃	Shu Yamamoto	Yamaguchi University
110	$EuMn_2Ge_2$ 単結晶の磁場中比熱測定	藤原　哲也	山口大学	大学院創成科学研究科	Specific heat measurement under magnetic field of $EuMn_2Ge_2$ single crystal	Tetsuya Fujiwara	Yamaguchi University
111	〃	山本 嵩	山口大学	大学院創成科学研究科	〃	Shu Yamamoto	Yamaguchi Univ
112	混晶系 $HoRh_{2-x}Co_2Si_2$ の磁化測定	藤原　哲也	山口大学	大学院創成科学研究科	Magnetization measurements of pseudo-ternary system $HoRh_{2-x}Co_2Si_2$	Tetsuya Fujiwara	Yamaguchi University
113	〃	山本　嵩	山口大学	大学院創成科学研究科	〃	Shu Yamamoto	Yamaguchi University
114	希土類強相関物質における新奇揺らぎの探索と圧力効果	中野　智仁	新潟大学	大学院自然科学研究科	Investigation novel fluctuation in rare earth strongly correlated electron system	Tomohito Nakano	Niigata University
115	〃	名坂　直紀	新潟大学	工学部	〃	Naoki Nasaka	Niigata University
116	$Yb(Co_{1-x}Ir_x)_2Zn_{20}$ の 基本物性評価 IV	阿曽　尚文	琉球大学	理学部	Evaluation of fundamental physical properties in $YbYb(Co_{1-x}Ir_x)_2Zn_{20}$ IV	Naofumi Aso	University of the Ryukyus
117	遷移金属カルコゲナイドの圧力下 dHvA 効果の研究	摂待　力生	新潟大学	理学部	de Haas-van Alphen effect under pressure in transition metal chalcogenide	Rikio Settai	Niigata University
118	〃	武藤　研太	新潟大学	大学院自然科学研究科	〃	Kenta Muto	Niigata University
119	鉄セレン系化合物の合成および圧力効果	久田　旭彦	徳島大学	大学院社会産業理工学研究部	Synthesis and pressure-effect study of iron-selenide compound	Akihiko Hisada	Tokushima University

No.	課題名	氏名	所属		Title	Name	Organization
120	$MnCo_{1-x}Ge$ 合金の磁気特性に関する研究	江藤　徹二郎	久留米工業大学	建築・設備工学科	Study of magnetic properties in $MnCo_{1-x}Ge$ alloys	Tetsujiro Eto	Kurume Institute of Technology
121	高圧下電気抵抗による CeT_2X_8(T: 遷移金属元素, X:Al,Ga) の磁性研究	中島　美帆	信州大学	理学部	Magnetism of CeT_2X_8 (T: transition metal element, X: Al, Ga) by electrical resistivity under high pressure.	Miho Nakashima	Shinshu University
122	〃	矢口　達志	信州大学	大学院総合理工学研究科	〃	Tatsushi Yaguchi	Graduate School Shinshu University
123	遷移金属化合物の高圧力下の輸送特性	仲間　隆男	琉球大学	理学部	Pressure effect on transport properties of transition metal compounds	Takao Nakama	University of the Ryukyus
124	〃	太田　譲二	琉球大学	大学院理工学研究科	〃	Jouji Ota	University of the Ryukyus
125	10 GPa を超えた圧力領域まで拡張した有機導体の圧力下物性の探索	村田　惠三	大阪経済法科大学	２１世紀社会総合研究センター	Pressure Effect of Organic Conductors in the pressure region beyond 10 GPa.	Keizo Murata	Osaka　University of Economics and Law
126	磁場で合成した $Sm_2Fe_{17}N_3$ の磁気特性	小山　佳一	鹿児島大学	大学院理工学研究科	Magnetic properties of $Sm_2Fe_{17}N_3$ prepared under magnetic fields	Keiichi Koyama	Kagoshima University
127	〃	尾上　昌平	鹿児島大学	研究推進機構研究支援センター	〃	Masahira Onoue	Kagoshima University
128	Mn_2Sb 基化合物のスピン再配列	三井　好古	鹿児島大学	大学院理工学研究科	Spin-reorientation in Mn_2Sb-based compounds	Yoshifuru Mitsui	Kagoshima University
129	〃	野口　滉平	鹿児島大学	大学院理工学研究科	〃	Kohei Noguchi	Kagosima University
130	強相関電子系化合物における圧力および磁場誘起量子相転移の探索	大橋　政司	金沢大学	理工研究域	Pressure and field induced quantum phase transition in strongly correlated electron systems	Masashi Ohashi	Kanazawa University
131	〃	稲森　庸介	金沢大学	大学院自然科学研究科	〃	Yosuke Inamori	Kanazawa University
132	Fe 置換 Ni_2MnGa ホイスラー合金の磁化および相転移温度の高圧効果	安達　義也	山形大学	大学院理工学研究科	Pressure effect of the magnetization and phase transition temperature for the Fe-substituted Ni_2MnGa Heusler alloys	Yoshiya Adachi	Yamagata University
133	〃	吉田　圭吾	山形大学	工学部	〃	Keigo Yoshida	Yamagata University
134	層状硫化ビスマス超伝導体 $LaOBiS_2$ の圧力誘起超伝導の検証	加瀬　直樹	東京理科大学	理学部	Pressure-induced superconductivity of the BiS_2-based superconductors	Naoki Kase	Tokyo University of Science
135	圧力誘起価数転移の探索と高圧下輸送特性	辺土　正人	琉球大学	理学部	Searching of pressure-induced valence transition and transport properties under high pressure	Masato Hedo	University of the Ryukyus
136	〃	仲井間　憲李	琉球大学	大学院理工学研究科	〃	Kenri Nakaima	University of the Ryukyus

No.	課題名	氏名	所属		Title	Name	Organization
137	Eu 化合物の圧力誘起近藤状態の探索	辺土　正人	琉球大学	理学部	Searching for pressure-induced Kondo state on Eu compounds	Masato Hedo	University of the Ryukyus
138	〃	伊覇　航	琉球大学	大学院理工学研究科	〃	Wataru Iha	University of the Ryukyus
139	〃	松田　進弥	琉球大学	大学院理工学研究科	〃	Shinya Matsuda	University of the Ryukyus
140	スピングラスを持つ $Mn_{1-x}Co_xNiGe$ 系化合物の高圧化磁化測定	伊藤　昌和	鹿児島大学	総合科学域	Magnetization of $Mn_{1-x}Co_xNiGe$ with spin glass system under high pressure	Masakazu Ito	Kagoshima University
141	〃	白濱　透	鹿児島大学	大学院理工学研究科	〃	Toru Shirahama	Kagoshima University
142	アクチノイド強磁性化合物の圧力効果	芳賀　芳範	日本原子力研究開発機構	先端基礎研究センター	Pressure effect on actinide ferromagnetic compounds	Yoshinori Haga	Japan Atomic Energy Agency
143	λ-$(BEST)_2GaCl_4$ の超高圧下電気抵抗測定による λ型塩における分子置換効果の研究	小林　拓矢	埼玉大学	大学院理工学研究科	Study of molecular substitution effect on λ-type organic conductor in λ-$(BEST)_2GaCl_4$ by electric resistivity measurements under ultra-high pressures	Takuya Kobayashi	Saitama University
144	〃	谷口　弘三	埼玉大学	大学院理工学研究科	〃	Hiromi Taniguchi	Saitama University
145	〃	綱川　仁志	埼玉大学	大学院理工学研究科	〃	Hitoshi Tsunakawa	Saitama University
146	〃	生沼　浩介	埼玉大学	大学院理工学研究科	〃	Kohsuke Oinuma	Saitama University
147	〃	小澤　宏彬	埼玉大学	大学院理工学研究科	〃	Hiroaki Ozawa	Saitama University
148	〃	伊藤　有咲	埼玉大学	理学部	〃	Arisa Ito	Saitama University
149	ターンバックル式小型 DAC を用いた多重極限下電気抵抗測定	狩野　みか	日本工業大学	共通教育学群・物理	Electrical resistivity measurements under multi-extreme conditions by using a micro-turnbuckle DAC	Mika Kano	Nippon Institute of Technology
150	RE_3TiBi_5(RE = 希土類元素) の圧力下比熱測定	本山　岳	島根大学	大学院自然科学研究科	Specific heat measurements of RE_3TiBi_5 (RE = rare earth) ternary compounds under pressure	Gaku Motoyama	Shimane University
151	〃	坪内　将紘	島根大学	大学院自然科学研究科	〃	Masahiro Tsubouchi	Shimane University
152	キュービックアンビルセルを用いた NMR 測定開発	中川　悟志	京都大学	大学院人間環境学研究科	Development of NMR measurements under pressure using a cubic-anvil cell	Satoshi Nakagawa	Kyoto University

担当所員：尾崎　泰助

No.	課題名	氏名	所属		Title	Name	Organization
153	実験と計算の協奏による二次元材料の構造・電子状態解析及び制御	アントワーヌ フロランス	北陸先端科学技術大学院大学	マテリアルサイエンス系	Analysis and control of crystal and electronic structures of 2D materials through concerted collaboration of experiment and theory	Antoine Fleurence	JAIST
154	〃	新田　寛和	北陸先端科学技術大学院大学	大学院先端科学技術研究科	〃	Hirokazu Nitta	JAIST
担当所員：益田　隆嗣							
155	高分解能チョッパー分光器による物質のダイナミクスの研究	伊藤　晋一	高エネルギー加速器研究機構	物質構造科学研究所	Studies on Dynamics in Condensed Matters by using the High Resolution Chopper Spectrometer	Shinichi Itoh	High Energy Accelerator Research Organization
156	〃	横尾　哲也	高エネルギー加速器研究機構	物質構造科学研究所	〃	Tetsuya Yokoo	High Energy Accelerator Research Organization
157	〃	羽合　孝文	高エネルギー加速器研究機構	物質構造科学研究所	〃	Takafumi Hawai	High Energy Accelerator Reserach Organization
158	〃	齋藤　開	高エネルギー加速器研究機構	物質構造科学研究所	〃	Hiraku Saito	High Energy Accelerator Research Organization
159	$(Yb_{1-x}Lu_x)Co_2Zn_{20}$ の極低温比熱測定　III	阿曽　尚文	琉球大学	理学部	Specific heat measurement at very low temperature on $(Yb_{1-x}Lu_x)Co_2Zn_{20}$ III	Naofumi Aso	University of the Ryukyus
160	空間反転対称性の破れた超伝導体の結晶性評価	古川　はづき	お茶の水女子大学	基幹研究院	Evaluation of single crystal quality of non-centrosymmetric superconductors	Hazuki Furukawa	Ochanomizu University
161	〃	左右田　稔	理化学研究所	創発物性科学研究センター	〃	Minoru Soda	RIKEN
162	フラストレーションの強い量子反強磁性体の結晶方位決定	田中　秀数	東京工業大学	理学院	Determination of the crystal orientations for strongly frustrated quantum magnets	Hidekazu Tanaka	School of Science
163	サイト選択アニオンドーピングによる $Ce(Te,Se)_3$ の比熱測定	植田　大地	沖縄科学技術大学院大学	量子物質科学ユニット	Specific heat meansurement of site selective anion doping $Ce(Te,Se)_3$	Daichi Ueta	Okinawa Institute of Science and Technology Granduate University
担当所員：金道　浩一							
164	イットリウム積層化合物 Y_4TGe_8(T: 遷移金属) 及びインターカレーション化合物 M_xTaS_2(M:Ni,Co) の強磁場磁化測定	道岡　千城	京都大学	大学院理学研究科	High-field magnetization measurements of Y_4TGe_8(T:transition metal) and M_xTaS_2(M:Ni,Co)	Chishiro Michioka	Kyoto University
165	〃	山中　俊介	京都大学	大学院理学研究科	〃	Shunsuke Yamanaka	Kyoto University
166	幾何学的フラストレート磁性体の強磁場磁化測定	菊池　彦光	福井大学	学術研究院工学系部門	Magnetization measurements of the frustrated magnets	Hikomitsu Kikuchi	University of Fukui
167	1/2 量子磁化プラトーを示す $Ni_2V_2O_7$ の強磁場磁化測定	長谷　正司	物質・材料研究機構	先端材料解析研究拠点	High-field magnetization measurements on 1/2 quantum magnetization plateau compound $Ni_2V_2O_7$	Masashi Hase	National Institute for Materials Science

No.	課題名	氏名	所属		Title	Name	Organization
168	BiS_2 系超伝導体で実現する巨大上部臨界磁場の検証	加瀬　直樹	東京理科大学	理学部	Upper critical field of the BiS_2-based superconductors	Naoki Kase	Tokyo University of Science
169	topological Kondo insulator SmB_6,YbB_{12} の磁化特性と比熱	伊賀　文俊	茨城大学	理学部	Magnetic and thermal properties of topological Kondo insulator SmB_6 and YbB_{12}	Fumitoshi Iga	Ibaraki University
170	〃	松浦　航	茨城大学	大学院理工学研究科	〃	Wataru Matsuura	Ibaraki university
171	高圧合成新規希土類 Ce_{12} ホウ化物の強磁場中の磁化と比熱	伊賀　文俊	茨城大学	理学部	Magnetic and thermal properties in high magnetic fields of rare earth hexa- and dodeca-borides produced by high pressure synthesis	Fumitoshi Iga	Ibaraki University
172	〃	中山　裕之	茨城大学	大学院理工学研究科	〃	Hiroyuki Nakayama	Ibaraki university
173	高圧合成による Y ベース Pr 置換 B_{12} の強磁場中の磁性と比熱，伝導	伊賀　文俊	茨城大学	理学部	Magnetic, transport and thermal properties in high magnetic fields of $Y_{1-x}Pr_xB_{12}$ produced by high pressure synthesis	Fumitoshi Iga	Ibaraki University
174	〃	山田　貴大	茨城大学	大学院理工学研究科	〃	Takahiro Yamada	ibaraki university
175	スピングラスを持つ MnNiGe-CoNiGe 系化合物の高磁場磁歪測定	伊藤　昌和	鹿児島大学	総合科学域	Magnetic strain of MnNiGe-CoNiGe with spin-glass system in high magnetic field	Masakazu Ito	Kagoshima University
176	〃	白濱　透	鹿児島大学	大学院理工学研究科	〃	Toru Shirahama	Kagoshima University
177	金属ナノ結晶集合体の磁化特性	稲田　貢	関西大学	システム理工学部	Magnetic properties of metal nanocrystal assemblies	Mitsuru Inada	Kansai University
178	〃	米澤　諒	関西大学	大学院理工学部	〃	Ryo Yonezawa	Kansai University Graduate School
179	フラストレーションの強い量子反強磁性体の強磁場磁化測定	田中　秀数	東京工業大学	理学院	Magnetization measurements on highly frustrated quantum magnets	Hidekazu Tanaka	School of Science
担当所員：徳永　将史							
180	重い電子系における強磁場中の電子状態研究	海老原　孝雄	静岡大学	学術院理学領域	Electronic states at high magnetic fields in Heavy Fermion systems	Takao Ebihara	Shizuoka University
181	〃	丸山　博史	静岡大学	大学院総合科学技術研究科	〃	Hiroshi Maruyama	Shizuoka University
182	磁気光学顕微鏡による超伝導体中の量子渦の実空間非平衡ダイナミクス観測手法の確立	黒川　穂高	東京大学	大学院総合文化研究科	Observing the real-space nonequilibrium dynamics of vortices in superconductor with a magneto-optical microscope	Hodaka Kurokawa	The University of Tokyo
183	PrT_2Cd_{20}(T=Ni,Pd) の強磁場磁化測定	広瀬　雄介	新潟大学	理学部	High-field magnetization of PrT_2Cd_{20}(T=Ni,Pd) (T=Ni and Pd)	Yusuke Hirose	Niigata University

No.	課題名	氏名	所属		Title	Name	Organization
184	〃	高山　昂己	新潟大学	理学部	〃	Koki Takayama	Niigata University
185	フラストレーションを有する磁性体の強磁場下での振る舞い	香取　浩子	東京農工大学	大学院工学研究院	Magnetic properties of frustrated materials in high magnetic fields	Hiroko Katori	Tokyo University of Agriculture and Technology
186	〃	羽鳥　滋	東京農工大学	大学院工学府	〃	Shigeru Hatori	Tokyou University of Agriculture and Technology
187	逆スピネル化合物の強磁場磁化過程	香取　浩子	東京農工大学	大学院工学研究院	High-field magnetization process of inverse spinel materials	Hiroko Katori	Tokyo University of Agriculture and Technology
188	〃	太田　寛人	東京農工大学	大学院工学研究院	〃	Hiroto Ohta	Tokyo University of Agriculture and Technology
189	〃	徳永　柊介	東京農工大学	大学院工学府	〃	Shusuke Tokunaga	Tokyo University of Agriculture and Technology
190	正四角台塔反強磁性体の強磁場中電気磁気特性の測定	木村　健太	東京大学	大学院新領域創成科学研究科	High-field magnetoelectric properties square-cupola-based antiferromagnets	Kenta Kimura	The University of Tokyo
191	多層ディラック電子系 $AMnX_2$ (A=Sr,Ba. X=Sb, Bi) における量子ホール効果の研究	酒井　英明	大阪大学	大学院理学研究科	Study of the quantum Hall effect in multilayered Dirac fermion systems $AMnX_2$ (A=Ba,Sr. X=Sb, Bi)	Hideaki Sakai	Osaka University
192	〃	近藤　雅起	大阪大学	大学院理学研究科	〃	Masaki Kondo	Graduate School of Science Osaka University
193	〃	中川　賢人	大阪大学	大学院理学研究科	〃	Nakagawa Kento	Osaka University
194	ランタノイド Kitaev 型量子スピン液体の探索のための強磁場磁化過程測定	北川　健太郎	東京大学	大学院学院理学系研究科	High-Field magnetization meansurement for Lanthanoid Kitaev-type quantum spin liquid	Kentaro Kitagawa	The University of Tokyo
195	水素終端ダイヤモンド表面の伝導キャリアの強磁場量子振動	山口　尚秀	物質・材料研究機構	国際ナノアーキテクト二クス研究拠点	High-field quantum oscillations in hydrogen-terminated diamond	Takahide Yamaguchi	National Institute for Materials Science
196	トーラス型フェルミ面を持つラシュバ型半導体の量子極限伝導性の研究	村川　寛	大阪大学	大学院理学研究科	High field studay for quantum limit transport properties of torus Fermi surface in Rashba semiconductor	Hiroshi Murakawa	Osaka university
197	3d-4 f 金属間化合物 Er_2Fe_{17} における磁気熱量効果の直接測定	木原　工	東北大学	金属材料研究所	Direct magnetocaloric effect measurement for 3d-4f intermetallic compound Er_2Fe_{17}	Takumi Kihara	Tohoku University
198	新奇トポロジカル磁性体の開拓	高橋　英史	大阪大学	大学院基礎工学研究科	Exploring of new topological magnet	Hidefumi Takahashi	Osaka University
199	〃	小野瀬　雅穂	東京大学	大学院工学系研究科	〃	Masaho Onoue	The University of Tokyo
担当所員：松田　康弘							

No.	課題名	氏名	所属		Title	Name	Organization
200	近藤半導体 (Yb,R)B_{12}、ほか新規高圧合成物質のワンターンコイル 120T 強磁場磁化と伝導	伊賀　文俊	茨城大学	理学部	Magnetization and transport properties by using one-turn coil in a 120 T pulse magnet of Kondo insulator (Yb,R)B_{12} and novel rare-earth borides producted by high-pressure synthesis	Fumitoshi Iga	Ibaraki University
201	〃	竹森　氷馬	茨城大学	理学部	〃	Hyouma Takemori	ibaraki university
202	遍歴電子強磁性体 $Ln_2Co_{12}P_7$ の強磁場磁化過程の研究	太田　寛人	東京農工大学	大学院工学研究院	Magnetic study under high magnetic field on itinerant ferromagnet $Ln_2Co_{12}P_7$	Hiroto Ohta	Tokyo University of Agriculture and Technology
担当所員：小濱　芳允							
203	Bi 系銅酸化物高温超伝導体における量子振動の観測	渡辺　孝夫	弘前大学	大学院理工学研究科	Observation of the quantum oscillation in Bi-based high-Tc superconductors	Takao Watanabe	Hirosaki University
204	〃	藤井　武則	東京大学	低温センター	〃	Takenori Fujii	University of Tokyo
205	〃	山口　隼平	弘前大学	大学院理工学研究科	〃	Shunpei Yamaguchi	Hirosaki　University
206	正四角台塔反強磁性体 $Pb(TiO)Cu_4(PO_4)_4$ における強磁場中での電気磁気光学効果の研究	木村　健太	東京大学	大学院新領域創成科学研究科	Optical magnetoelectric effect of the square-cupola-based antiferromagnet $Pb(TiO)Cu_4(PO_4)_4$ in a high magnetic field	Kenta Kimura	The University of Tokyo
207	パルス強磁場を用いた強磁場 NMR 測定による量子磁性体の磁場誘起相の研究	井原　慶彦	北海道大学	大学院理学研究院	Pulsed field NMR study for field induced magnetic state in quantum magnets	Yoshihiko Ihara	Hokkaido university
208	〃	荒島　洸樹	北海道大学	大学院理学院	〃	Koki Arashima	Hokkaido university
209	トポロジカル超伝導候補物質における強磁場下物性測定	芝内　孝禎	東京大学	大学院新領域創成科学研究科	Physical property measurements of topological superconductor candidates under high magnetic field	Takasada Shibauchi	The University of Tokyo
210	〃	水上　雄太	東京大学	大学院新領域創成科学研究科	〃	Yuta Mizukami	The University of Tokyo
211	〃	竹中　崇了	東京大学	大学院新領域創成科学研究科	〃	Takaaki Takenaka	The University of Tokyo
212	〃	石原　滉大	東京大学	大学院新領域創成科学研究科	〃	Kota Ishihara	The University of Tokyo
213	六方晶近藤格子系 $EuSn_2As_2$ 単結晶における位相幾何学的電子相の研究	神原　陽一	慶應義塾大学	理工学部	Research on topological electronic phases in a hexagonal Kondo-lattice, single crystalline $EuSn_2As_2$	Yoichi Kamihara	Keio University
担当所員：小林　洋平							
214	次世代レーザーとレーザー加工の基礎技術研究	吉富　大	産業技術総合研究所	電子光技術研究部門	Basic research on next generation laser systems and laser machining technology	Dai Yoshitomi	National Institute of Advanced Industrial Science and Technology

No.	課題名	氏名	所属		Title	Name	Organization
215	〃	高田　英行	産業技術総合研究所	電子光技術研究部門	〃	Hideyuki Takada	National Institute of Advanced Industrial Science and Technology
216	〃	佐藤　大輔	産業技術総合研究所	分析計測標準研究部門	〃	Daisuke Satoh	National Institute of Advanced Industrial Science and Technology
217	〃	澁谷　達則	産業技術総合研究所	分析計測標準研究部門	〃	Tatsunori Shibuya	National Institute of Advanced Industrial Science and Technology
218	次世代レーザーとレーサー加工の基礎技術的研究	盛合　靖章	産業技術総合研究所	先端オペランド計測技術オープンイノベーションラボラトリ	Basic research on next generation laser systems and laser machining technology	Yasuaki Moriai	National Institute of Advanced Industrial Science and Technology
219	〃	黒田　隆之助	産業技術総合研究所	先端オペランド計測技術オープンイノベーションラボラトリ	〃	Ryunosuke Kuroda	National Institute of Advanced Industrial Science and Technology
220	〃	鳥塚　健二	産業技術総合研究所	電子光技術研究部門	〃	Kenji Torizuka	National Institute of Advanced Industrial Science and Technology
221	青色半導体レーザー用ファイバ型光コンバイナの開発	藤本　靖	千葉工業大学	工学部	Development on fiber power combiner for GaN semiconductor lasers	Yasushi Fujimoto	Chiba Institute of Technology (CIT)
222	短波長パルスレーザーによる炭素繊維の改質	森山　匡洋	東京大学	大学院理学系研究科付属フォトンサイエンス研究機構	Laser modification of carbon fiber by short wavelength pusled laser	Masahiro Moriyama	The University of Tokyo
223	ファイバーレーザーの安定化	大間知　潤子	関西学院大学	理工学部	Stabilization of fiber laser	Junko Omachi	Kwansei Gakuin University
224	〃	松井　芳樹	関西学院大学	理工学部	〃	Yoshiki Matsui	Kwansei Gakuin University
225	〃	美世　将虎	関西学院大学	理工学部	〃	Masatora Mise	Kwansei Gakuin University
226	〃	藤田　滉平	関西学院大学	理工学部	〃	Kohei Fujita	Kwansei Gakuin University
227	超高速発光による金属表面の研究	末元　徹	豊田理化学研究所		Study on metal surfaces by ultrafast luminescence spectroscopy	Tohru Suemoto	Toyota Physical and Chemical Research Institute
担当所員：原田　慈久							
228	半導体基板上の金属的擬一次元表面状態におけるフェルミ準位近傍のスピン偏極構造	大坪　嘉之	大阪大学	大学院生命機能研究科	Spin texture of the metallic quasi-1D surface states around Fermi level fabricated on semiconductor substrates	Yoshiyuki Ohtsubo	Osaka University
229	〃	中村　拓人	大阪大学	大学院理学研究科	〃	Takuto Nakamura	Osaka university
230	〃	徳舛　直樹	大阪大学	大学院理学研究科	〃	Tokumasu Naoki	Osaka university

No.	課題名	氏名	所属		Title	Name	Organization
231	スピン分解角度分解光電子分光による V_2AlC のスピン偏極状態の研究	伊藤　孝寛	名古屋大学	シンクロトロン光研究センター	Spin- and angle-resolved photoemission study of Spin-polarized electronic structure of V_2AlC	Takahiro Ito	Nagoya University
232	〃	鍋平　直輝	名古屋大学	大学院工学研究科	〃	Naoki Nabehira	Nagoya University
233	トポロジカル絶縁体を用いたスピン軌道トルク磁気メモリの表面状態解明	小林　正起	東京大学	大学院工学系研究科	Unveiling the surface state of spin-orbital torque magnetic memory using topological insulator	Masaki Kobayashi	University of Tokyo
担当所員：板谷　治郎							
234	時間分解非線形分光法を用いた希土類酸化物のコヒーレントフォノンにおけるソリトン成分の観測	牧野　哲征	福井大学	学術研究院工学系部門	Soliton contribution in coherent phonons of rare-earth oxides studied by time-resolved nonlinear spectroscopy	Takayuki Makino	University of Fukui
235	〃	山出　拓史	福井大学	大学院工学研究科	〃	Takuji Yamade	University of Fukui
236	〃	竹内　智哉	福井大学	大学院工学研究科	〃	Tomoya Takeuchi	University of Fukui
237	〃	浅井　郁帆	福井大学	大学院工学研究科	〃	Takaho Asai	University of Fukui
担当所員：岡崎　浩三							
238	励起子絶縁体 Ta_2NiSe_5 における光誘起絶縁体 - 金属転移の研究	久保田　雄也	高輝度光科学研究センター	XFEL 利用研究推進室	Investigation of the photo-induced insulator-to-metal transition in an exitonic insulatorTa_2NiSe_5	Yuya Kubota	Japan Synchrotron Radiation Research Institute (JASRI)
239	T’ 構造をもつ銅酸化物高温超伝導体の角度分解光電子分光による研究	チャン ウェイル	上智大学	機能創造理工学科	Photoemission spectroscopy of electron-doped T'-cuprate superconductors	Zhang Weilu	Sopia University
240	時間分解 ARPES による Si(111) 基板上 Cu_2Si の電子状態の研究	高山　あかり	早稲田大学	先進理工学部	Electronic state of Cu_2Si on Si(111) studied by time-resolved ARPES	Akari Tkayama	Waseda University

一般研究員・大阪大学 先端強磁場科学研究センター / General Researcher・Center for Advanced High Magnetic Field Science Osaka University

No.	課題名	氏名	所属		Title	Name	Organization
担当：萩原　政幸（大阪大学）							
1	パルス強磁場を用いた強相関電子系物質の強磁場物性の研究	竹内　徹也	大阪大学	低温センター	Magnetic properties of strongly correlated electron systems under a pulsed high magnetic field	Tetsuya Takeuchi	Osaka University
2	〃	大貫　惇睦	琉球大学	理学部	〃	Yoshichika Onuki	University of the Ryukyus

No.	課題名	氏名	所属		Title	Name	Organization
3	クロミック化合物における強磁場磁化過程の粒径依存性	浅野　貴行	福井大学	学術研究院	Particle size dependence of high-field magnetization process in chromic compound	Takayuki Asano	University of Fukui
4	〃	西首　時夫	福井大学	工学部	〃	Tokio Nishikubi	University of Fukui
5	パルス強磁場によるマルテンサイト変態の時間依存性に関する研究	福田　隆	大阪大学	大学院工学研究科	Study on time dependence of martensitic transformation using pulsed high magnetic field	Takashi Fukuda	Osaka University
6	$CaBa(Ca_{1-x}Fe_x)_4O_7(x=0,1/2,3/4,1)$ 単結晶試料の強磁場下での磁化・電気分極・ESR 測定	桑原　英樹	上智大学	理工学部	Magnetization, electric polarization, and ESR measurements for $CaBa(Ca_{1-x}Fe_x)_4O_7(x=0,1/2,3/4,1)$ single crystals in pulsed high magnetic fields	Hideki Kuwahara	Sophia University
7	〃	遠藤　颯	上智大学	理工学部	〃	Hayate Endo	Sophia University
8	パルス強磁場高圧下 ESR 装置の開発と応用	櫻井　敬博	神戸大学	研究基盤センター	Development of pulsed high magnetic field high pressure ESR system and its application	Takahiro Sakurai	Kobe University
9	フェルダジル系電荷移動塩の強磁場磁性	山口　博則	大阪府立大学	大学院理学系研究科	High-field magnetic properties of new verdazyl-based charge-transfer salts	Hironori Yamaguchi	Osaka Prefecture University
10	〃	岩崎　義己	大阪府立大学	大学院理学系研究科	〃	Yoshiki Iwasaki	Osaka Prefecture University
11	フタロシアニン分子系伝導体で観測される巨大磁気抵抗に対する遷移金属置換の効果	花咲　徳亮	大阪大学	大学院理学研究科	Transition-metal-substitution Effect on Giant Magnetoresistance in Phthalocyanine-molecular Conductors	Noriaki Hanasaki	Osaka University
12	〃	清水　智可	大阪大学	大学院理学研究科	〃	Tomoka Shimizu	Osaka University
13	第二種ワイル半金属の強磁場中量子輸送特性の研究	村川　寛	大阪大学	大学院理学研究科	High magnetic fied study on transport properties of type II Weyl semimetals	Hiroshi Murakawa	Osaka university
14	〃	駒田 盛是	大阪大学	大学院理学研究科	〃	Komada Moriyoshi	Osaka university
15	〃	横井　滉平	大阪大学	大学院理学研究科	〃	Yokoi Kohei	Osaka university
16	〃	中岡　優大	大阪大学	大学院理学研究科	〃	Yudai Nakaoka	Osaka university
17	正四角台塔反強磁性体の強磁場中 ESR 測定	木村 健太	東京大学	大学院新領域創成科学研究科	High-field ESR measurements of square-cupola-based antiferromagnets	Kenta Kimura	The University of Tokyo
18	Ni_2MnGa 系及び Pd_2MnSn 系の新規ホイスラー合金の超磁歪の高速磁場応答性の研究	左近　拓男	龍谷大学	理工学部	Research on time dependences of magnetstriction of Ni_2MnGa type and Pd_2MnSn type Heusler alloys	Takuo Sakon	Ryukoku University
19	HFESR を用いた配位子場分裂した f 電子副準位構造の決定	福田　貴光	大阪大学	大学院理学研究科	Determination of f-electronic sublevels arising from ligand field splittings by means of HFESR	Takamitsu Fukuda	Osaka University

No.	課題名	氏名	所属		Title	Name	Organization
20	多孔構造スクアリン酸錯体の合成、構造及び磁性に関する研究	本多　善太郎	埼玉大学	大学院理工学研究科	Synthesis, structure, and magnetic properties of porous metal squarate complexes	Zentaro Honda	Saitama University
21	ディラック電子系磁性体 $BaMnX_2$ (X=Sb, Bi) のキャント反強磁性における元素置換効果	酒井　英明	大阪大学	大学院理学研究科	Impact of chemical substitution on the canted antiferromagnetic states for magnetic Dirac materials $BaMnX_2$ (X=Sb, Bi)	Hideaki Sakai	Osaka University
22	〃	近藤　雅起	大阪大学	大学院理学研究科	〃	Masaki Kondo	Graduate School of Science Osaka University
23	〃	中川　賢人	大阪大学	大学院理学研究科	〃	Nakagawa Kento	Osaka University
24	SmB_6/SrB_6 人工超格子の強磁場中輸送係数測定	宍戸　寛明	大阪府立大学	大学院工学研究科	Transport measurements for SmB_6/SrB_6 superlattices under high magnetic field	Hiroaki Shishido	Osaka Prefecture University
25	タイプ II ラインノード半金属候補物質 Mg_3Bi_2 及び $CaMg_2Bi_2$ の強磁場輸送特性解明	浦田　隆広	名古屋大学	大学院工学研究科	High-field magnetotransport properties of type-II nodal-line semimetal candidates Mg_3Bi_2 and $CaMg_2Bi_2$	Takahiro Urata	Nagoya University
26	強磁場電子スピン共鳴による有機磁性体の磁場誘起量子相の解明	細越　裕子	大阪府立大学	大学院理学系研究科	High-field ESR study on the field-induced quantum phases of organic radical crystals	Yuko Hosokoshi	Osaka Prefecture University
27	〃	三好　克典	大阪府立大学	大学院理学系研究科	〃	Katsunori Miyoshi	Osaka Prefecture University
28	〃	瀬戸川　大喜	大阪府立大学	大学院理学系研究科	〃	Hiroki Setogawa	Osaka Prefecture University
29	量子スピン系の電場励起 ESR	木村　尚次郎	東北大学	金属材料研究所	Electric dipole spin resonance of quantum spin systems	Shojiro Kimura	Tohoku University
30	水平磁場印加によるタンパク質結晶の磁場効果	牧　祥	大阪大谷大学	薬学部	Effect of protein crystallization by the application of horizontal magnetic force	Syou Maki	Osaka Ohtani University
31	2 次元三角格子反強磁性体 $Mn(OH)_2$ の強磁場 ESR および強磁場磁化	佐藤　博彦	中央大学	理工学部	High-field ESR and high-field magnetization of two-dimensional triangular-lattice antiferromagnet $Mn(OH)_2$	Hirohiko Sato	Chuo University
32	〃	大寺　翔也	中央大学	大学院理工学研究科	〃	Shoya Ohtera	Chuo University
33	新しい Eu 化合物の強磁場磁化過程	光田　暁弘	九州大学	大学院理学研究院	Magnetization in pulsed magnetic fields of new Eu-based compounds	Akihiro Mitsuda	Kyushu University
34	〃	大山　耕平	九州大学	理学府	〃	Kohei Oyama	Kyushu University
35	三角格子反強磁性体 $CsCuCl_3$ の圧力下強磁場磁化測定	櫻井　敬博	神戸大学	研究基盤センター	High pressure and high magnetic field magnetization measurement of triangular antiferromagnet $CsCuCl_3$	Takahiro Sakurai	Kobe University
36	キラル反強磁性体の強磁場磁化測定	井上　克也	広島大学	大学院理学研究科	High field magnetic measurements on Chiral Antiferromagnet	Katsuya Inoue	Hiroshima University

物質合成・評価設備 P クラス / Materials Synthesis and Characterization P Class Researcher

No.	課題名	氏名	所属		Title	Name	Organization
1	レアメタルフリー磁性材料 L10-FeCo の磁気特性の解析	小嗣　真人	東京理科大学	基礎工学部	Analysis of magnetic properties of rare-metal-free super magnet	Kotsugi Masato	Tokyo University of Science
2	Bi 系 misfit 単結晶の構造観察	小林　夏野	岡山大学	異分野基礎科学研究所	Observation of local structure on Bi-based misfit single crystal	Kobayashi Kaya	Okayama University

物質合成・評価設備 G クラス / Materials Synthesis and Characterization G Class Researcher

No.	課題名	氏名	所属		Title	Name	Organization
1	単結晶 $CaMn_{1-x}Sb_xO_3$ の熱物性の研究	谷口　晴香	岩手大学	理工学部	Study of thermophysical properties of single crystalline $CaMn_{1-x}Sb_xO_3$	Haruka Taniguchi	Iwate University
2	光ファイバーセンシング技術を利用した泥岩中の化学的浸透現象に伴う岩石の局所的変形の計測	廣田　翔伍	東京大学	大学院新領域創成科学研究科	Measurement of local deformation of mudstones caused by chemical osmosise with optical ber sensing technique	Shogo Hirota	The University of Tokyo
3	新しい希土類金属間化合物の結晶構造の決定	中村　翔太	名古屋工業大学	大学院物理工学科	Decision of crystal structure of new rare-earth intermetallic compounds	Nakamura Shota	Nagoya Institute of Technology
4	〃	矢田　達也	名古屋工業大学	大学院工学研究科	〃	Yada Tatsuya	Nagoya Institute of Technology
5	ナノ構造制御材料を用いた省エネルギーデバイス開発	細野 英司	産業技術総合研究所	省エネルギー研究部門	Development of devices for energy conservation by using nanostructure controlled materials	Eiji Hosono	National Institute of Advanced Industrial Science and Technology
6	〃	太田　道広	産業技術総合研究所	省エネルギー研究部門	〃	Michihiro Ohta	National Institute of Advanced Industrial Science and Technology
7	〃	ジュド　プリヤンカ	産業技術総合研究所	省エネルギー研究部門	〃	Jood Priyanka	National Institute of Advanced Industrial Science and Technology
8	新しい希土類磁石の探求	齋藤　哲治	千葉工業大学	工学部	Research of new rare-earth magnets	Tetsuji Saito	Chiba Institute of Technology
9	マイクロミキサを用いた機能性無機ナノ粒子の連続合成	陶　究	産業技術総合研究所	化学プロセス研究部門	Continuous synthesis of functional inorganic nanoparticles using a micromxer	Kiwamu Sue	National Institute of Advanced Industrial Science and Technology
10	$Nd_{1-x}Sr_xFeO_3$ $(0.1 \leqq x \leqq 0.9)$ の高温における磁性と熱電特性に関する研究	中津川　博	横浜国立大学	大学院工学研究院	Magnetism and thermoelectric properties at high temperature in $Nd_{1-x}Sr_xFeO_3$ $(0.1 \leqq x \leqq 0.9)$	Hiroshi Nakatsugawa	Yokohama National University
11	準結晶・近似結晶の磁性に関する研究 II	鈴木　慎太郎	東京理科大学	基礎工学部	Magnetism of quasicrystal and approximants II	Shintaro Suzuki	Tokyo University of Science
12	層状ロジウム酸化物の磁気相図	岡崎　竜二	東京理科大学	理工学部	Magnetic phase diagram of the layered rhodium oxides	Ryuji Okazaki	Tokyo University of Science

No.	課題名	氏名	所属		Title	Name	Organization
13	〃	栗田　寛士	東京理科大学	大学院理工学研究科	〃	Kanji Kurita	Tokyo university of science
14	〃	石井　まゆ	東京理科大学	大学院理工学研究科	〃	Mayu Ishii	Tokyo University Of Science
15	〃	坂林　北斗	東京理科大学	大学院理工学研究科	〃	Hokuto Sakabayashi	Tokyo University of Science
16	多形物質 M_2GeO_5(M=V,Cr,Fe) の磁化測定	香取　浩子	東京農工大学	大学院工学研究院	Magnetization measurements of polymorphism M_2GeO_5(M=V,Cr,Fe)	Hiroko Katori	Tokyo University of Agriculture and Technology
17	〃	柿本　和勇	東京農工大学	大学院工学府	〃	Kazuo Kakimoto	Tokyo University of Agriculture and Technology
18	〃	大木　祐明	東京農工大学	大学院工学府	〃	Yoshiaki Ohki	Tokyo University of Agriculture and Technology
19	スピネル酸化物 $GeFe_2O_4$ におけるスピングラス出現機構の解明	香取　浩子	東京農工大学	大学院工学研究院	Clarification of the appearance mechanism of spin glass in spinel oxide $GeFe_2O_4$	Hiroko Katori	Tokyo University of Agriculture and Technology
20	〃	太田　寛人	東京農工大学	大学院工学研究院	〃	Hiroto Ohta	Tokyo University of Agriculture and Technology
21	〃	小日置　隆	東京農工大学	工学部	〃	Yutaka Kobiki	Tokyo University of Agliculture and Technology
22	ハーフメタルホイスラー合金の遍歴電子磁性体のスピンゆらぎ理論による解析に関する研究	重田　出	鹿児島大学	大学院理工学研究科	Study on analysis of half-metallic Heusler alloys by the spin fluctuation theory for itinerant electron magnetism	Shigeta Iduru	Kagoshima University
23	ホイスラー化合物での反強磁性の研究	廣井　政彦	鹿児島大学	大学院理工学研究科	Study on antiferromagnetism in Heusler compounds	Masahiko Hiroi	Kagoshima University
24	〃	野々山　智仁	鹿児島大学	大学院理工学研究科	〃	Tomohito Nonoyama	Kagoshima University
25	触媒反応の insitu ラマン散乱測定	佐々木　岳彦	東京大学	大学院新領域創成科学研究科	in situ measurement of Raman scattering for　heterogeneous catalytic reactions	Takehiko Sasaki	The University of Tokyo
26	宇宙線望遠鏡の焦点面ライトガイドの反射率測定	吉田　龍生	茨城大学	理学部	Reflectance measurement of focal plane light concentrators for cosmic-ray telescopes	Tatsuo Yoshida	Ibaragi Univrsity
27	酸水素化物 SmHO における圧力誘起秩序無秩序相転移	山本　隆文	東京工業大学	フロンティア材用研究所	Pressure-induced order/disorder transition in SmHO	Takafumi Yamamoto	Kyoto University
28	ピストンシリンダーを用いた高温高圧下における有機化合物の重合反応の解明	篠崎　彩子	北海道大学	大学院理学研究院	Effect on pressure and temperature on the oligomerization organic compounds	Ayako Shiozaki	Hokkaido University
29	複数種の元素を充填した新規スクッテルダイト型熱電材料の高圧合成	関根　ちひろ	室蘭工業大学	大学院工学研究科	High-pressure synthesis of new multifilled skutterudite-type thermoelectric materials	Chihiro Sekine	Muroran Institute of Technology

No.	課題名	氏名	所属		Title	Name	Organization
30	〃	佐藤　雄也	室蘭工業大学	大学院工学研究科	〃	Yuya Sato	Muroran Institute of Technology
31	高温高圧下における下部マントル鉱物への窒素の取り込みに関する研究	福山　鴻	東京大学	大学院理学系研究科	The study on nitrogen incorporation into the lower-mantle minerals under high pressure and high temperature	Ko Fukuyama	The University of Tokyo
32	高圧下におけるアミノ酸のペプチド化反応の観察	藤本　千賀子	東京大学	大学院理学系研究科	Pressure-induced reaction of amino acids under high pressure	Chikako Fujimoto	The University of Tokyo
33	超高圧における窒素源前駆体の分解反応を利用した遷移金属窒化物の合成	丹羽　健	名古屋大学	大学院工学研究科	High pressure synthesis of transition metal nitrides via decomposition of nitrogen source precursor	Ken Niwa	Nagoya University
34	〃	生駒　鷹秀	名古屋大学	大学院工学研究科	〃	Takahide Ikoma	Nagoya University
35	層状酸化物の超高圧合成と結晶化学および物性	丹羽　健	名古屋大学	大学院工学研究科	High pressure synthesis, crystal chemistry and physical properties of layered oxides	Ken Niwa	Nagoya University
36	〃	高野　航一	名古屋大学	工学部	〃	Koichi Takano	Nagoya University
37	超高圧力合成法を用いた高窒素分圧下での窒化物蛍光体の合成	佐々木　拓也	名古屋大学	大学院工学研究科	High-pressure synthesis of nitride phosphors under high nitrogen partial pressure	Takuya Sasaki	Nagoya University
38	〃	近藤　信介	名古屋大学	工学部	〃	Shinsuke Kondo	Nagoya University
39	超高圧力合成法を用いたジルコニウム含有水素化物の創成	佐々木　拓也	名古屋大学	大学院工学研究科	High-pressure synthesis and crystal structure of novel zirconium-containing hydrides	Takuya Sasaki	Nagoya University
40	〃	市川　将成	名古屋大学	大学院工学研究科	〃	Masanari Ichikawa	Nagoya University
41	尿素経路を用いた新規金属窒化物の高圧合成	ニコ アレキサンダー ガイダ	名古屋大学	ベンチャー・ビジネス・ラボラトリー	High-pressure synthesis of novel transition metal nitrides using the urea approach	Nico Alexander Gaida	Nagoya University
42	ペロブスカイト関連化合物の高圧合成	稲熊　宜之	学習院大学	理学部	High-pressure synthesis of perovskite-related compounds	Yoshiyuki Inaguma	Gakushuin University
43	〃	植田　紘一郎	学習院大学	理学部	〃	Koichiro Ueda	Gakushuin University
44	〃	森　紘夢	学習院大学	大学院自然科学研究科	〃	Hiromu Mori	Gakushuin University
45	異相接合界面のバンド構造の解明と SOFC セルへの応用	大友　順一郎	東京大学	大学院新領域創成科学研究科	Elucidation of band diagram of hetero junction and application to SOFCs	Junichiro Otomo	The University of Tokyo
46	〃	那須　雄太	東京大学	大学院新領域創成科学研究科	〃	Yuta Nasu	The University of Tokyo

No.	課題名	氏名	所属		Title	Name	Organization
47	エネルギー貯蔵型燃料電池の電極活物質の開発	大友　順一郎	東京大学	大学院新領域創成科学研究科	Development of electrode materials of energy storage type - fuel cells	Junichiro Otomo	The University of Tokyo
48	〃	中西　泰介	東京大学	大学院新領域創成科学研究科	〃	Taisuke Nakanishi	The University of Tokyo
49	カルシウムルーピング法における二酸化炭素利用技術の開発	大友　順一郎	東京大学	大学院新領域創成科学研究科	Development of CO_2 utilization with calcium looping method	Junichiro Otomo	The University of Tokyo
50	〃	七瀬　浩希	東京大学	大学院新領域創成科学研究科	〃	Nanase Koki	The University of Tokyo
51	アンモニア電解合成における選択性向上の検討	大友　順一郎	東京大学	大学院新領域創成科学研究科	Study on promotion of selectivity in ammonia electrosynthesis	Junichiro Otomo	The University of Tokyo
52	〃	山本　和範	東京大学	大学院新領域創成科学研究科	〃	Kazunori Yamamoto	The University of Tokyo
53	熱化学サイクル型水素生成システムにおける高活性酸素キャリア複合粒子の開発	大友　順一郎	東京大学	大学院新領域創成科学研究科	Development of carrier materials and system design for chemical looping hydrogen production systems	Junichiro Otomo	The University of Tokyo
54	〃	甚野　幸一	東京大学	工学部	〃	Koichi Jinno	The University of Tokyo
55	プロトン伝導性固体電解質薄膜を用いた低温作動燃料電池・電解合成セルの開発	大友　順一郎	東京大学	大学院新領域創成科学研究科	Development of low-temperature solid oxide fuel cells and electrolysis cells using proton-conducting solid electrolyte thin films	Junichiro Otomo	The University of Tokyo
56	〃	松尾　拓紀	東京大学	大学院新領域創成科学研究科	〃	Hiroki Matsuo	The University of Tokyo
57	輸送現象の解明と燃料電池性能向上に向けたプロトン導電性固体電解質の合成	大友　順一郎	東京大学	大学院新領域創成科学研究科	Preparation of proton-conducting solid electrolytes for determination of charged-defect transport and improvement of solid oxide fuel cells.	Junichiro Otomo	The University of Tokyo
58	〃	オルティスコラレスフリアンアンドレス	東京大学	大学院新領域創成科学研究科	〃	Ortiz Corrales Julian Andres	The University of Tokyo
59	ケミカルループ法を用いた合成ガス製造システムの設計およびキャリア開発	大友　順一郎	東京大学	大学院新領域創成科学研究科	Development of carrier materials and system design for chemical looping syngas production systems	Junichiro Otomo	The University of Tokyo
60	〃	引間　脩	東京大学	大学院新領域創成科学研究科	〃	Shu Hikima	The University of Tokyo
61	イオン－電子混合伝導体の異相界面の作製と輸送現象の解明	大友　順一郎	東京大学	大学院新領域創成科学研究科	Formation of heterojunction of mixed ionic electronic conductors and clarification of its transport phenomena	Junichiro Otomo	The University of Tokyo
62	〃	福田　一峻	東京大学	工学部	〃	Fukuda Kazutaka	The university of Tokyo
63	プロトン伝導型固体酸化物燃料電池用新規メタルサポートセルデザインの開発	大友　順一郎	東京大学	大学院新領域創成科学研究科	Development of new metal supported cell design for PCFCs	Junichiro Otomo	The University of Tokyo

No.	課題名	氏名	所属		Title	Name	Organization
64	〃	阪田　一真	東京大学	大学院新領域創成科学研究科	〃	Kazuma Sakata	The University of Tokyo
65	プロトン伝導性固体酸化物を用いたアンモニア電解合成機構の解明	大友　順一郎	東京大学	大学院新領域創成科学研究科	The Mechanisms of Ammonia Electrosynthesis using proton-conducting solid oxide fuel cell	Junichiro Otomo	The University of Tokyo
66	〃	李　建毅	東京大学	大学院新領域創成科学研究科	〃	Chien-I Li	The University of Tokyo
67	カルシウムループ法による合成ガスプロセスの開発	大友　順一郎	東京大学	大学院新領域創成科学研究科	Development of Ca looping process for production of syngas	Junichiro Otomo	The University of Tokyo
68	〃	李　智漢	東京大学	大学院新領域創成科学研究科	〃	Jihan Lee	The University of Tokyo
69	メソポーラスマテリアル・グラフェンオキサイドに担持した金属触媒のキャラクタリゼーション	佐々木　岳彦	東京大学	大学院新領域創成科学研究科	Characterization of metal catalysts loaded on mesoporous materials and graphene oxide	Takehiko Sasaki	The University of Tokyo
70	超臨界水中でのニッケル鉄複合酸化物ナノ粒子合成に関する研究	布浦　鉄兵	東京大学	環境安全研究センター	Study on supercritical water synthesis of Ni-Fe composite oxide nanoparticles	Teppei Nunoura	The University of Tokyo
71	〃	周　暁雲	東京大学	大学院新領域創成科学研究科	〃	Zhou Xiaoyun	The University of Tokyo
72	バリウムフェライトの磁気異方性と元素置換効果	植田　浩明	京都大学	大学院理学研究科	Magnetic anisotropy and substitution effect of barium ferrites	Hiroaki Ueda	Kyoto university
73	〃	奥津　陽太	京都大学	理学部	〃	Yota Okutsu	Kyoto University
74	超臨界メタノール条件下でのエステル交換反応に固体触媒が与える影響	秋月　信	東京大学	大学院新領域創成科学研究科	The effect of solid catalysts on the ester exchange reaction in supercritical methanol	Makoto Akizuki	The University of Tokyo
75	〃	張　瑞子	東京大学	大学院新領域創成科学研究科	〃	Zhang Ruizi	The University of Tokyo
76	高温高圧条件下の水 - メタノール溶媒が固体触媒反応に及ぼす影響	秋月　信	東京大学	大学院新領域創成科学研究科	Investigation of the effect of hot compressed methanol-water mixed solvent on solid catalyzed reactions	Makoto Akizuki	The University of Tokyo
77	〃	島田　綾子	東京大学	工学部	〃	Ayako Shimada	The University of Tokyo
78	高温高圧水―アルコール混合溶媒が金属酸化物ナノ粒子の合成に与える影響の解明	大島　義人	東京大学	大学院新領域創成科学研究科	Research on the effect of water-alcohol mixture on metal oxide nanoparticle synthesis	Yoshito Oshima	The University of Tokyo
79	〃	劉　源	東京大学	大学院新領域創成科学研究科	〃	Yuan Liu	The University of Tokyo
80	高温高圧水中でのバイオマス変換に使用するマイクロポーラス材料	大島　義人	東京大学	大学院新領域創成科学研究科	Microporous material for biomass upgrading in sub- and supercritical water	Yoshito Oshima	The University of Tokyo

No.	課題名	氏名	所属		Title	Name	Organization
81	〃	アピバンボリラク　チャンウィット	東京大学	大学院新領域創成科学研究科	〃	Apibanboriak Chanwit	The University of Tokyo
82	超臨界水を利用したZnOナノ粒子の合成とその形態制御	大島　義人	東京大学	大学院新領域創成科学研究科	Synthesis and morphology control of zinc oxide nanoparticles using supercritical water	Yoshito Oshima	The University of Tokyo
83	〃	織田　耕彦	東京大学	大学院新領域創成科学研究科	〃	Yasuhiko Orita	The University of Tokyo
84	ブリージングパイロクロア磁性体の熱膨張と磁歪	岡本　佳比古	名古屋大学	大学院工学研究科	Thermal expansion and magnetostriction of breathing pyrochlore magnets	Yoshihiko Okamoto	Nagoya University
85	高温高圧下で多軽元素が鉄ー含水ケイ酸塩系に及ぼす影響の解明	飯塚　理子	東京大学	大学院理学系研究科	Behavior of multi light elements in iron-silicate-water system under high pressure and high temperature	Riko Iizuka	The University of Tokyo
86	高圧下での $MoSi_2$ 型構造の $FeAl_2$ 結晶の作製	木村　薫	東京大学	大学院新領域創成科学研究科	High pressure synthesis of $MoSi_2$ type iron aluminide, $FeAl_2$ crystal	Kaoru Kimjura	The University of Tokyo
87	〃	飛田　一樹	東京大学	大学院新領域創成科学研究科	〃	Kazuki Tobita	The University of Tokyo
88	希土類オルソフェライト単結晶成長とテラヘルツスピン分光	中嶋　誠	大阪大学	レーザー科学研究所	Single crystal growth for rare-earth orthoferrite and terahertz spin spectroscopy	Makoto Nakajima	Osaka University
89	〃	加藤　康作	大阪大学	レーザー科学研究所	〃	Kosaku Kato	Osaka University
90	〃	木本　翔大	大阪大学	レーザー科学研究所	〃	Shodai Kimoto	Osaka University
91	〃	上田　誠一郎	大阪大学	レーザー科学研究所	〃	Seiichiro Ueda	Osaka University
92	〃	小池　遥平	大阪大学	レーザー科学研究所	〃	Yohei Koike	Osaka University
93	マルチフェロイック物質における非自明な電子物性の探求に関する研究	木村　剛	東京大学	大学院新領域創成科学研究科	Exploration of nontrivial electronic properties in multiferroic materials	Tsuyoshi Kimjura	The University of Tokyo
94	〃	木村　健太	東京大学	大学院新領域創成科学研究科	〃	Kenta Kimura	The University of Tokyo
95	〃	三澤　龍介	東京大学	大学院新領域創成科学研究科	〃	Ryusuke Misawa	The University of Tokyo
96	〃	勝吉　司	東京大学	大学院新領域創成科学研究科	〃	Tsukasa Katsuyoshi	The University of Tokyo
97	〃	林田　健志	東京大学	大学院新領域創成科学研究科	〃	Takeshi Hayashida	The University of Tokyo

No.	課題名	氏名	所属		Title	Name	Organization
98	〃	八木　直輝	東京大学	大学院新領域創成科学研究科	〃	Naoki Yagi	The University of Tokyo
99	新奇超伝導体の物質合成と物性評価	水上　雄太	東京大学	大学院新領域創成科学研究科	Synthesis and physical property measurements of novel superconductors	Yuta Mizukami	The University of Tokyo
100	〃	竹中　崇了	東京大学	大学院新領域創成科学研究科	〃	Takaaki Takenaka	The University of Tokyo
101	〃	石田　浩祐	東京大学	大学院新領域創成科学研究科	〃	Kousuke Ishida	The University of Tokyo
102	〃	田中　桜平	東京大学	大学院新領域創成科学研究科	〃	Ohei Tanaka	The University of Tokyo
103	〃	辻井　優哉	東京大学	大学院新領域創成科学研究科	〃	Masaya Tsujii	The University of Tokyo
104	〃	石原　滉大	東京大学	大学院新領域創成科学研究科	〃	Kota Ishihara	The University of Tokyo
105	空間反転対称性を持たない新規磁性体の開発	有馬　孝尚	東京大学	大学院新領域創成科学研究科	Exploration of new noncentrosymmetric magnets	Taka-hisa Arima	The University of Tokyo
106	〃	徳永　祐介	東京大学	大学院新領域創成科学研究科	〃	Yusuke Tokunaga	The University of Tokyo
107	〃	阿部　伸行	東京大学	大学院新領域創成科学研究科	〃	Nobuyuki Abe	The University of Tokyo
108	〃	鷲見 浩樹	東京大学	大学院新領域創成科学研究科	〃	Hiroki Sumi	The University of Tokyo
109	〃	藤間　友理	東京大学	大学院新領域創成科学研究科	〃	Yuri Fujima	The University of Tokyo
110	〃	近江　毅志	東京大学	大学院新領域創成科学研究科	〃	Tsuyoshi Omi	The University of Tokyo
111	〃	荒木　勇介	東京大学	大学院新領域創成科学研究科	〃	Yusuke Araki	The University of Tokyo
112	〃	蘇　丹	東京大学	大学院新領域創成科学研究科	〃	Dan Su	The University of Tokyo
113	〃	渡辺　義人	東京大学	大学院新領域創成科学研究科	〃	Yoshito Watanabe	The University of Tokyo
114	〃	尾亦　恭輔	東京大学	大学院新領域創成科学研究科	〃	Kyosuke Omata	The University of Tokyo

No.	課題名	氏名	所属		Title	Name	Organization
115	〃	西　健太	東京大学	大学院新領域創成科学研究科	〃	Kenta Nishi	The University of Tokyo
116	〃	山本　圭祐	東京大学	大学院新領域創成科学研究科	〃	Keisuke Yamamoto	The University of Tokyo
117	バナジウムカルコゲナイドにおける Valence Bond 短距離秩序状態の研究	片山　尚幸	名古屋大学	大学院工学研究科	Study of Short-Ranged Valence Bond formation in vanadium chalcogenides	Naoyuki Katayama	Nagoya University
118	〃	小島　慶太	名古屋大学	工学部	〃	Keita Kojima	Nagoya University
119	バナジウムカルコゲナイドにおけるスピン軌道複合秩序状態	片山　尚幸	名古屋大学	大学院工学研究科	Spin-Orbital entangled ordered state in vanadium chalcogenides	Naoyuki Katayama	Nagoya University
120	〃	前田　秦	名古屋大学	大学院工学研究科	〃	Shin Maeda	Nagoya University

物質合成・評価設備 U クラス / Materials Synthesis and Characterization U Class Researcher

No.	課題名	氏名	所属		Title	Name	Organization
1	プラズマ風洞による宇宙往還機熱防護システムの動的酸化に関する研究	桃沢　愛	東京都市大学	工学部医用工学科	Investigation on dynamic oxidation of thermal protection system using plasma wind tunnel	Ai Momozawa	Tokyo City University
2	〃	田中　聖也	東京大学	大学院工学系研究科	〃	Seiya Tanaka	The University of Tokyo
3	〃	山田　慎	東京大学	大学院工学系研究科	〃	Shin Yamada	The University of Tokyo
4	オレイン酸の超臨界水ガス化工程におけるニッケル触媒の非活性化メカニズムの解明	布浦　鉄兵	東京大学	環境安全センター	Nickel catalyst deactivation in supercritical water gasification of oleic acid	Teppei Nunoura	The University of Tokyo
5	〃	ダイアン　グバタンガ	東京大学	大学院新領域創成科学研究科	〃	Diane Gubatanga	The University of Tokyo
6	積層型燃料電池の輸送特性制御と電解合成への応用	大友　順一郎	東京大学	大学院新領域創成科学研究科	Development of new electrochemical catalyst for ammonia electrolysis and evaluation of reaction mechanism at intermediate temperature	Junichi Otomo	The University of Tokyo
7	〃	田島　星也	東京大学	大学院新領域創成科学研究科	〃	Seiya Tajima	The University of Tokyo
8	中温域でのアンモニア電解合成における新規電極触媒開発及び反応機構解明	大友　順一郎	東京大学	大学院新領域創成科学研究科	Control of transport properties of stracked fuel cells and its application to electrochemical synthesis	Junichi Otomo	The University of Tokyo
9	〃	今田　佳那	東京大学	大学院新領域創成科学研究科	〃	Kana Imata	The University of Tokyo

No.	課題名	氏名	所属		Title	Name	Organization
10	静電浮遊法を用いた過冷却液体急冷法によるボロン系準結晶の探索	木村　薫	東京大学	大学院新領域創成科学研究科	Search for quasicrystalline boron using rapid quenching from super-cooled liquid by levitation technique	Kaoru Kimura	The University of Tokyo
11	〃	高橋　昂広	東京大学	大学院新領域創成科学研究科	〃	Takahiro Takahashi	The University of Tokyo
12	特異な形態を有するセラミック膜の加工と界面構造解析	小松　啓志	長岡技術科学大学	物質材料工学専攻	Microfabricated TEM sections of oxide film with unique morphology	Keiji Komatsu	Nagaoka University of Technology

長期留学研究員 / Long Term Young Researcher

No.	課題名	氏名	所属		Title	Name	Organization
1	有機半導体の分子吸着に伴って生じるトポロジカル表面状態の変化	北澤　辰也	東京理科大学	大学院理工学研究科	Modification of Topological surface states upon adsorption of organic semiconductors	Tatsuya Kitazawa	Tokyo University of Science
2	PdPc の表面吸着によって生じる Cu(111) ショックレー状態の変化	下澤　皐介	東京理科大学	理工学部	Modification of Cu(111)Shockley stateupon adsorption of PdPc	Kosuke Shimozawa	Tokyo University of Science

令和元年度 共同利用課題一覧（後期）/ Joint Research List (2019 Latter Term)

嘱託研究員 / Commission Researcher

No.	課題名	氏名	所属		Title	Name	Organization
担当所員：長谷川　幸雄							
1	低温走査トンネルポテンショメトリーの開発	江口　豊明	東北大学	大学院理学研究科	Development of low-temperature scanning tunneling potentiometry	Toyoaki Eguchi	Tohoku University
2	スピン偏極探針の作製・処理方法の開発	岡　博文	東北大学	材料科学高等研究所	Development of fabrication and treatment methods for spin-polarized tips	Hirofumi Oka	Tohoku University
3	走査トンネル顕微鏡による局所強磁性共鳴法の開発	安　東秀	北陸先端科学技術大学院大学	先端科学技術研究科	Development of local ferromagnetic resonance in scanning tunneling microscopy	Toshu An	Japan Advanced Institute of Science and Technology
4	極低温走査トンネル顕微鏡を用いた鉄カルコゲナイド超伝導体 FeSeTe の研究	吉田　靖雄	金沢大学	理工学域	Low-temperature STM study on iron-chalcogenide super conductor FeSeTe	Yasuo Yoshida	Kanazawa University
担当所員：リップマー　ミック							
5	Materials Foundry のための材料開発システム構築に向けた薄膜合成装置の開発	高橋　竜太	日本大学	工学部	Development of Film Deposition Systems for High-throughput Material Exploration	Ryota Takahashi	Nihon University
担当所員：上床　美也							
6	磁性体の圧力効果	巨海　玄道	久留米工業大学		Effect of pressure on the Magnetic Materials	Oomi Gendo	Kurume Institute of Technology
7	高圧下 X 線回折法の開発	江藤　徹二郎	久留米工業大学		Development of High Pressure X-ray diffraction measurements	Tetsujiro Eto	Kurume Institute of Technology
8	多重極限関連圧力装置の調整	高橋　博樹	日本大学	文理学部	Adjustment of Cubic Anvil apparatus	Hiroki Takahashi	Nihon University
9	3 d 遷移化合物に関する圧力効果	鹿又　武	東北学院大学	工学総合研究所	Effect of pressure on the 3d transition compounds	Takahashi Kanomata	Tohoku Gakuin University
10	酸化物試料の作製と高圧下物性測定	川中　浩史	産業技術総合研究所	電子光技術研究部門	Sample preparetion and high pressure experiments	Hirofumi Kawanaka	National Institute of Advanced Industorial Scuence and Technorogy
11	有機伝導体の圧力効果	村田　恵三	大阪経済法科大学		Effect of pressure on the organic conductor	Keizo Murata	Osaka University of economice and low
12	希土類 122 化合物における圧力効果	繁岡　透	山口大学	大学院理工学研究科	Pressure effect of rare earth 122compounds	Toru Shigeoka	Yamaguchi University

No.	課題名	氏名	所属		Title	Name	Organization
13	低温用マルチアンビル装置の開発	辺土　正人	琉球大学	理学部	Development of multi-anvil apparatus for low temperature	Masato Hedo	University of Ryukyu
14	カンチレバーを用いたトルク測定法の開発	鳥塚　潔	日本工業大学	共通教育学群	Development of torque measurement method	Kiyoshi Torizuka	Nippon Institute of technology
15	高圧下量子振動観測システムの開発	摂待　力生	新潟大学	理学部	Development of quantum oscillation under high pressure	Rikio Settai	Niigata University
16	希釈冷凍機温度で使用可能な 10GPa 級超高圧発生装置の開発	松林　和幸	電気通信大学		Development of 10GPa class high pressure apparatus for low temperature	Kazuyuki Matsubayashi	The University of Electro-Communications
17	DAC を用いた物性測定方法の開発	狩野　みか	日本工業大学		Development of physical property measurement method using DAC	Mika Kano	Nippon Institute of technology
18	擬一次元有機物質の圧力下物性研究	糸井　充穂	日本大学	医学部	Study on pressure induced superconductivity of quasi organic conductor	Miho Itoi	Nihon University
19	圧力下 NMR 測定法に関する開発	藤原　直樹	京都大学	大学院人間・環境学研究科	Development of NMR measurement method under high pressure	Naoki Fujiwarra	Kyoto University
担当所員：原田　慈久							
20	軟 X 線発光・共鳴非弾性散乱分光の磁気円・線二色性測定システムの構築	菅　滋正	大阪大学	産業科学研究所	Construction of a noble system for circularr and linear dichroism in soft X-ray emission and RIXS spectroscopy	Shigemasa Suga	Osaka University
21	軟 X 線吸収 / 発光分光法によるリチウムイオン電池電極材料の電子物性研究	細野　英司	産業技術総合研究所	省エネルギー研究部門	Study on the electronic property of electrode materials for Li-ion batteries by soft X-ray absorption /emission spectroscopy	Eiji Hosono	AIST
22	〃	朝倉　大輔	産業技術総合研究所	省エネルギー研究部門	〃	Disuke Asakura	AIST
23	高分解能光電子分光による酸化バナジウムの研究	藤原　秀紀	大阪大学	大学院基礎工学研究科	Study on vanadium oxides by high resolution Photoemission	Hidenori Fujiwara	Osaka University
24	省エネ・創エネ・蓄電デバイスのオペランド分光	尾嶋　正治	東京大学	大学院工学系研究科	Operando nano-spectroscopy for energy efficient, power,generation and energy storage devices	Masaharu Oshima	The University of Tokyo
25	原子レベルで制御されたモデル有機分子表面上の界面水の電子状態観測	林　智広	東京工業大学	大学院総合理工学研究科	Analysis of the electronic structure of interfacial water formed on model organic surfaces	Tomohiro Hayashi	Tokyo Institute of Technology
26	三次元 nanoESCA による実デバイスのオペランド電子状態解析	永村　直佳	物質・材料研究機構		Operando analysis of the electronic structure of actual devices by 3Dnano ESCA	Naoka Nagamura	National Institute of Material Science
27	時間分解光電子顕微分光実験の技術開発	木下　豊彦	高輝度光科学研究センター		Technical development of time-resolved photoemission microscopy measurement	Toyohiko Kinoshita	Japan Advanced Institute of Science and Technology
担当所員：松田　巌							

No.	課題名	氏名	所属		Title	Name	Organization
28	スピン分解光電子分光の測定技術開発	木村　真一	大阪大学	大学院生命機能研究科	Technical development of spin-resolved photoemmision spectroscopy measurement	Shinichi Kimura	Osaka University
29	時間分解磁気光学実験の技術開発	小嗣　真人	東京理科大学	基礎工学部	Technical development of time-resolved magneto-optical experiment	Masato Kotsugi	Tokyo University of Science
30	超高速磁化応答による磁性波動関数の制御	小林　正起	東京大学	大学院工学系研究科	Regulation of magnetic wave functions by ultrafast magnetization response	Masaki Kobayashi	The University of Tokyo
31	コヒーレント共鳴軟Ｘ線散乱による磁気ドメイン構造の観測	山崎　裕一	物質・材料研究機構	統合型材料開発・情報基盤部門	Observation of magnetic domain structure for ferromagnetic thin films by means of resonant soft x-ray scattering	Yuichi Yamasaki	National Institute for Materials Science
32	遷移金属化合物の時間分解Ｘ線分光と回析	和達　大樹	兵庫県立大学	大学院物質理学研究科	Time-resolved x-ray spectroscopy and diffraction of transition-metal-compounds	Hiroki Wadachi	University of Hyogo
担当所員：近藤　猛							
33	光電子分光法を用いた各種分子性結晶の電子状態の研究及び装置の低温化	木須　孝幸	大阪大学	大学院基礎工学研究科	Research on electron state of molecular crystals using photoemission spectroscopy	Takayuki Kisu	Osaka University
34	高分解能光電子分光による強相関物質の研究	横谷　尚睦	岡山大学	異分野基礎科学研究所	Ultra-high resolution study on strongly correlated materials	Takayoshi Yokoya	Okayama University
35	60-eV　レーザーを用いた時間分解光電子分光の開発	石坂　香子	東京大学	大学院工学系研究科	The development of time -resolved photoemission using 60eV laser	Kyoko Ishizaka	The University of Tokyo
36	トポロジカル超伝導体の探索	坂野　昌人	東京大学	大学院工学系研究科	Search for topological insulators	Masato Sakano	The University of Tokyo
37	有機化合物の光電子分光	金井　要	東京理科大学	理工学部	Photoemission study on organic compounds	Kaname Kanai	Tokyo University of Science
38	トポロジカル絶縁体の電子状態の解明	木村　昭夫	広島大学	大学院理学研究科	Electronic-structure study of topological insulators	Akio Kimura	Hiroshima University
39	Si(111) 上単層タリウムの高次高調波を用いた時間分解光電子分光	坂本　一之	大阪大学	大学院工学研究科	Time-resolved ARPES investigation of monolayer Thallium on Si(111)	Kazuyuki Sakamoto	Osaka University
担当所員：岡崎　浩三							
40	レーザー励起光電子顕微鏡を使った抵抗変化メモリ材料の研究	木下　健太郎	東京理科大学	理学部	Study on Materials for Resistive Switching Memories using laser-PEEM	Kentaro Kinoshita	Tokyo University of Science
41	収差補正型光電子顕微鏡の建設と利用研究	小嗣　真人	東京理科大学	基礎工学部	Construction and utilization research of aberration correction photoelectron emission microscopy	Masato Kotsugi	Tokyo University of Science
42	時間分解光電子分光を用いた強相関物質の研究	溝川　貴司	早稲田大学	理工学術院	Time-resolved photoemission study on strongly-correlated materials	Takashi Mizokawa	Waseda University

No.	課題名	氏名	所属		Title	Name	Organization
43	固体中のマヨラナ粒子の研究	松田　祐司	京都大学	大学院理学研究科	Study of Majorana Femion in Solids by Laser Photoemission Spectroscopy	Yuji Matsuda	Kyoto University
44	〃	佐藤　昌利	京都大学	基礎物理学研究所	〃	Masatoshi Sato	Kyoto University
45	FeSe 超伝導体における BCS-BES クロスオーバーの研究	紺谷　浩	名古屋大学	大学院理学研究科	Study of BCE-BES crossover in FeSe superconductors	Hiroshi Kontani	Nagoya University
46	時間分解光電子分光や超高分解能光電子分光を用いた超伝導体や強相関物質の研究	吉田　鉄平	京都大学	総合人間学部	Laser ARPPES study on superconductors and strongly-correlated materials	Teppei Yoshida	Kyoto University
47	超高分解能レーザー光電子分光による高温超伝導体の研究	チャン　ウェイル	上智大学	機能創造理工学科	Study of high-Tc superconductors by high-resolution laser ARPES	Weilu Zhang	Sophia University
48	鉄系超伝導体のレーザー光電子顕微鏡	下志万　貴博	理化学研究所	創発物性科学研究センター	Laser-PEEM on iron-based superconductor	Takahiro Shimojima	RIKEN

一般研究員 / General Researcher

No.	課題名	氏名	所属		Title	Name	Organization
担当所員：瀧川　仁							
1	三角スピン系有機ラジカルの核磁気共鳴による磁気誘電現象の解明	細越　裕子	大阪府立大学	大学院理学系研究科	NMR study on the magnetodielectric properties of organic triangular spin model compound	Yuko Hosokoshi	Osaka Prefecture University
担当所員：榊原　俊郎							
2	重い電子系超伝導体の対称性の決定	町田　一成	立命館大学	理工学部	Determination of pairing symmetry for heavy Fermion superconductors	Kazushige Machida	Ritsumeikan University
3	量子スピンアイス物質における量子モノポールの実験的検出	町田　洋	学習院大学	理学部	Experimental detection of quantum monopole in quantum spin ice systems	Yo Machida	Gakushuin University
4	重い電子系化合物における量子臨界現象	横山　淳	茨城大学	大学院理工学研究科	Quantum critical behavior in heavy-fermion compounds	Makoto Yokoyama	Ibaraki University
5	〃	ラフマント	茨城大学	大学院理工学研究科	〃	Rahmanto	Ibaraki University
6	有機ラジカルから成る新規量子スピン系の低温物性測定	山口　博則	大阪府立大学	大学院理学系研究科	Low temperature physical properties of quantum spin systems composed of organic radical	Hironori Yamaguchi	Osaka Prefecture University
7	〃	上本　菜央	大阪府立大学	大学院理学系研究科	〃	Nao Uemoto	Osaka Prefecture University

No.	課題名	氏名	所属		Title	Name	Organization
8	無機—有機ハイブリッド磁性体により実現する低次元量子スピン系の極低温物性測定	河野　洋平	大阪府立大学	大学院理学系研究科	Low temperature physical properties of low-dimensional quantum spin systems in metal--verdazyl complexes	Yohei Kono	Osaka Prefecture University
9	Ba^{2+}-Fe^{3+}-Ti^{4+}-Me^{2+} 酸化物磁性体の磁場中誘電特性	神島　謙二	埼玉大学	大学院理工学研究科	Dielectric properties of Ba^{2+}-Fe^{3+}-Ti^{4+}-Me^{2+} magnetic oxides under magnetic field	Kenji Kamishima	Saitama University
10	〃	安田　直生	埼玉大学	大学院理工学研究科	〃	Naoki Yasuda	Saitama University
11	〃	神　治樹	埼玉大学	大学院理工学研究科	〃	Haruki Kan	Saitama University
12	〃	高橋　久由	埼玉大学	大学院理工学研究科	〃	Hisayoshi Takahashi	Saitama University
13	トポロジカル超伝導のネマチック相研究	孫　悦	青山学院大学	理工学部	Study of the nematic phase of topological superconductors	Yue Sun	Aoyama Gakuin University
14	〃	宮沢　貴麿	青山学院大学	理工学部	〃	Miyazawa Takahiro	Aoyama Gakuin University
15	遍歴電子反強磁性体の磁化・比熱測定	加瀬　直樹	東京理科大学	理学部応用物理学科	Magnetization and specific heat measurements of the itinerant electron materials	Kase Naoki	Tokyo University of Science
16	新奇ウラン系奇パリティ超伝導における磁化・比熱・熱膨張測定	清水　悠晴	東北大学	金属材料研究所	Novel odd-parity uranium superconductors studied by magnetization, heat-capacity, and thermalexpansion meansurements	Yusei Shimizu	Tohoku University
担当所員：森　初果							
17	高対称性有機分子からなる新規分子性結晶の磁気的・電気的性質の解明	上田　顕	熊本大学	大学院先端科学研究部	Elucidation of magnetic and electrical properties of novel molecular crystals based on highly symmetric organic molecules	Akira Ueda	Kumamoto University
担当所員：山下　穣							
18	三角格子反強磁性体の低温比熱測定	柄木　良友	琉球大学	教育学部	Low temperature specific heat measurements of triangular antiferromagnets	Yoshimoto Karaki	University of the Ryukyus
19	Yb 化合物の超低温における dHvA 効果測定	宍戸　寛明	大阪府立大学	大学院工学研究科	dHvA effect measurements on Yb compounds at ultra-low temperatures	Hiroaki Shishido	Osaka Prefecture University
20	磁場角度分解熱輸送測定によるトポロジカル超伝導の研究	水上　雄太	東京大学	大学院新領域創成科学研究科	Studies on topological superconductors by field-angle-resolved thermal transport measurements	Yuta Mizukami	The University of Tokyo
担当所員：勝本　信吾							
21	量子ホール効果測定のための高移動度半導体試料作成	福田　昭	兵庫医科大学	物理学教室	Development of the high mobility semiconductor sample for the measurements in the quantum Hall	Akira Fukuda	Hyogo College of Medicine

No.	課題名	氏名	所属		Title	Name	Organization
22	二次元銅酸化物のホール測定と MPMS による磁化の測定	神戸　士郎	山形大学	大学院理工学研究科	Hall coefficient measurement of 2D curates and measurement of magnetic property by MPMS	Shiro Kanbe	Yamagata University
23	〃	三政　拓也	山形大学	大学院理工学研究科	〃	Takuya Mimasa	Yamagata University
24	ナノセンシングデバイスの研究開発	米谷　玲皇	東京大学	大学院新領域創成科学研究科	Research and development of nanosensing device	Reo Kometani	The University of Tokyo
25	〃	黎　学思	東京大学	大学院新領域創成科学研究科	〃	Xuesi Li	The University of Tokyo
26	〃	ペンエークウォン　ケーマナット	東京大学	大学院新領域創成科学研究科	〃	Penekwong Kehmnat	The University of Tokyo
27	〃	西田　裕信	東京大学	大学院新領域創成科学研究科	〃	Hironobu Nishida	The University of Tokyo
28	〃	齊藤　正樹	東京大学	大学院新領域創成科学研究科	〃	Masaki Saito	The University of Tokyo
29	〃	橋本　将	東京大学	大学院新領域創成科学研究科	〃	Sho Hashimoto	The University of Tokyo
30	〃	田中　駿太郎	東京大学	大学院新領域創成科学研究科	〃	Shuntaro Tanaka	The University of Tokyo
31	微細素子化した強相関酸化物における直流電流誘起された電子相の開拓	成田　秀樹	京都大学	大学院理学研究科	Investigation of electric current induced electronic phase in a microfabricated strongly correlated oxides	Hideki Narita	Kyoto University
担当所員：小森　文夫							
32	Si(111)4×1-In 基板上における Bi-In 表面合金の電子状態	中辻　寛	東京工業大学	物質理工学院	Electronic structure of Bi-In surface alloy grown on Si(111)4×1-In substrates	Kan Nakatsuji	Tokyo Institute of Thecnnology
33	〃	金野　達	東京工業大学	物質理工学院	〃	Tatsu Konno	Tokyo Institute of Thecnnology
34	酸素サーファクタントを用いた Fe 薄膜の成長過程と電子状態	中辻　寛	東京工業大学	物質理工学院	Oxygen surfactant assisted growth of Fe thin-films and their electronic states	Kan Nakatsuji	Tokyo Institute of Thecnnology
35	〃	木村　彰博	東京工業大学	物質理工学院	〃	Akihiro Kimura	Tokyo Institute of Thecnnology
36	窒素を飽和吸着させた Cu(001) 面における構造緩和	山田　正理	中央大学	理工学部	Structural relaxation on a Cu(001) surface saturated with adsorbed nitrogen	Masamichi Yamada	Chuo University
37	Al-Pd-Ru 準結晶・近似結晶における空孔濃度の研究	金沢　育三	東京学芸大学	自然科学系	Positron-annihilation studies of Al-Pd-Ru quasicrystal and its approximant crystals	Ikuzo Kanazawa	Tokyo Gakugei University

No.	課題名	氏名	所属		Title	Name	Organization
38	〃	高橋　潤	東京学芸大学	大学院教育学研究科	〃	Jun Takahashi	Gakugei University
39	特異なスピン状態を持つ希土類化合物表面及び吸着磁性原子電子状態のスピン状態の STS 解析	菅　滋正	大阪大学	産業科学研究所	Scanning Tunneling Spectroscopy of surfaces of exotic rare earth materials and adsorbed magnetic atoms	Shigemasa Suga	Osaka University
40	レアメタルフリー磁性材料 L10-FeCo の磁気特性の解析	小嗣　真人	東京理科大学	基礎工学部	Analysis of magnetic properties of rare-metal-free super magnet	Masato Kotsugi	Tokyo University of Science
41	〃	高橋　優樹	東京理科大学	基礎工学部	〃	Yuuki Takahashi	Tokyo University of Science
42	STM を用いた L10-FeNi 表面における N サーファクタント効果の解析	小嗣　真人	東京理科大学	基礎工学部	Study of N surfactant effect on L10-FeNi by using STM	Masato Kotsugi	Tokyo University of Science
43	〃	高橋　優樹	東京理科大学	基礎工学部	〃	Yuuki Takahashi	Tokyo University of Science
44	SiC ナノ周期表面上に転写したグラフェンの電子状態の観察	田中　悟	九州大学	大学院工学研究院	Electronic structure of graphene transferred on SiC periodic nanosurfaces	Satoru Tanaka	Kyushu University
45	〃	ビシコフスキー　アントン	九州大学	大学院工学研究院	〃	Visikovskiy Anton	Kyushu University
46	〃	魚谷　亮介	九州大学	大学院工学府	〃	Ryosuke Uotani	Kyushu University
47	真空転写法により形成したツイストグラフェンの電子状態評価	田中　悟	九州大学	大学院工学研究院	Evaluation of electronic structures of twisted graphene fabricated by vacuum transfer technique	Satoru Tanaka	Kyushu University
48	〃	ビシコフスキー　アントン	九州大学	大学院工学研究院	〃	Visikovskiy Anton	Kyushu University
49	〃	今村　均	九州大学	大学院工学府	〃	Hitoshi Imamura	Kyushu University
担当所員：長谷川　幸雄							
50	IV 族二次元材料及びそのヘテロ構造の低温走査トンネル顕微鏡観察	高村　由起子	北陸先端科学技術大学院大学	マテリアルサイエンス系	STM investigation of group IV 2D materials and their heterostructures	Yukiko Takamura	JAIST
担当所員：リップマー　ミック							
51	機械学習を導入した薄膜作製実験の高効率化	大久保　勇男	物質・材料研究機構	機能性材料研究拠点	An efficient thin film growth combined with a machine learning approach	Isao Ohkubo	National Institute for Materials Science
担当所員：吉信　淳							

No.	課題名	氏名	所属		Title	Name	Organization
52	有機金属構造体薄膜 - 超伝導体界面の構築	塚原　規志	群馬工業高等専門学校	電子メディア工学科	Building up the interface between a metal-organic framework film and a superconductor	Noriyuki Tsukahara	Gunma College
担当所員：秋山　英文							
53	顕微フォトルミネッセンス測定によるエルビウムドープ GaAs のスペクトル微細構造に関する研究	矢口　裕之	埼玉大学	大学院理工学研究科	Micro-photoluminescence study on the fine structure of spectral lines in Er doped GaAs	Hiroyuki Yaguchi	Saitama University
54	〃	高宮　健吾	埼玉大学	総合技術支援センター	〃	Kengo Takamiya	Saitama University
55	〃	清水　椋平	埼玉大学	大学院理工学研究科	〃	Ryohei Shimizu	Saitama University
56	北米産ホタルを用いた生物発光スペクトルにおける有害物質の濃度依存性調査	樋山　みやび	群馬大学	大学院理工学府	Concentration dependence of harmful substances in Photinus pyralis firefly bioluminescence spectra	Miyabi Hiyama	Gunma University
57	〃	手塚　大輔	群馬大学	大学院理工学府	〃	Daisuke Tezuka	Gunma University
58	合成ルシフェラーゼと結晶化ルシフェラーゼの絶対発光量比較	樋山　みやび	群馬大学	大学院理工学府	Comparative study of absolute bioluminescence between synthetic luciferase and crystallized luciferase	Miyabi Hiyama	Gunma University
59	〃	小野　稜平	群馬大学	大学院理工学府	〃	Ryohei Ono	Gunma University
60	宇宙線望遠鏡の焦点面ライトガイドの反射率測定	吉田　龍生	茨城大学	理学部	Reflectance measurement of focal plane light concentrators for cosmic-ray telescopes	Tetsuo Yoshida	Ibaraki University
担当所員：大谷　義近							
61	希土類金属間化合物の強磁場低温物性研究	海老原　孝雄	静岡大学	学術院理学領域	Physical properties in rare earth intermetallic compounds at high magnetic fields in low temperature	Takao Ebihara	Shizuoka University
62	〃	ジュマエダ・ジャトミカ	静岡大学	大学院自然科学教育部	〃	Jumaeda Jatmika	Shizuoka University
63	微細素子化した強相関酸化物における直電流誘起された電子相の開拓 2	成田　秀樹	京都大学	大学院理学研究科	Investigation of electric current induced electronic phase in a microfabricated strongly correlated oxides 2	Hideki Narita	Kyoto University
担当所員：廣井　善二							
64	希土類 4f 電子数制御による新規アクチュエータ材料の創製	竹中　康司	名古屋大学	大学院工学研究科	Development of novel volume-change-driven actuator materials by control of rare earth 4f electron number	Koshi Takenaka	Nagoya University
65	〃	横山　泰範	名古屋大学	大学院工学研究科	〃	Yasunori Yokoyama	Nagoya University

No.	課題名	氏名	所属		Title	Name	Organization
66	〃	水野　陽介	名古屋大学	大学院工学研究科	〃	Yosuke Mizuno	Nagoya University
67	〃	長谷川　遥加	名古屋大学	大学院工学研究科	〃	Haruka Hasegawa	Nagoya University
68	基板上に成膜した CoPt 規則化強磁性体の磁化測定	山浦　淳一	東京工業大学	元素戦略研究センター	Magnetization measurement of CoPt ordered ferromagnet fabricated on substrate	Junichi Yamaura	Tokyo Institute of Thecnnology
69	〃	真島　豊	東京工業大学	科学技術創成研究院	〃	Yutaka Majima	Tokyo Institute of Thecnnology
70	〃	遠山　諒	東京工業大学	物質理工学院	〃	Ryo Toyama	Tokyo Institute of Thecnnology
71	ラットリング原子を内包した金属間化合物の結晶構造と低温物性	山田　高広	東北大学	多元物質科学研究所	Characterization of crystal structures and magnetic properties of intermetallic compounds containing rattling atoms	Takahiro Yamada	Tohoku University
担当所員：川島　直輝							
72	テンソル繰り込み群法の改良	原田　健自	京都大学	大学院情報学研究科	Improvement of tensor network renormalization group method	Kenji Harada	Kyoto University
73	蜂の巣格子拡張 Kitaev- Γ 模型の基底状態相図	鈴木　隆史	兵庫県立大学	大学院工学研究科	Ground-state phase diagram of the extended Kitaev- Γ model on a honeycomb lattice	Takafumi Suzuki	University of Hyogo
担当所員：上床　美也							
74	高圧下における Eu 化合物の価数転移の探索	大貫　惇睦	琉球大学	理学部	Investigation of valence transition on Eu compounds under high pressure	Yoshichika Onuki	University of the Ryukyus
75	〃	本多　史憲	東北大学	金属材料研究所	〃	Fuminori Honda	Tohoku University
76	ウラン化合物の磁性の圧力効果	本多　史憲	東北大学	金属材料研究所	Effect of Pressure on the magnetism of uranium compounds	Fuminori Honda	Tohoku University
77	多形化合物 RIr_2Si_2(R= 希土類）の結晶育成と物質評価 7	繁岡　透	山口大学	大学院創成科学研究科	Crystal growth and characterization of polymorphic compounds RIr_2Si_2 (R=rera earth) 7	Toru Shigeoka	Yamaguchi University
78	〃	内間　清晴	沖縄キリスト教短期大学	総合教育系	〃	Kiyoharu Uchima	Okinawa Christian Junior College
79	擬三元化合物 $Ce_{1-x}M_xNiC_2$(M = Y, La) の結晶育成と物質評価 3	繁岡　透	山口大学	大学院創成科学研究科	Crystal growth and characterization of pseudo-ternary compounds $Ce_{1-x}M_xNiC_2$(M = Y, La) 2	Toru Shigeoka	Yamaguchi University
80	〃	内間　清晴	沖縄キリスト教短期大学	総合教育系	〃	Kiyoharu Uchima	Okinawa Christian Junior College

No.	課題名	氏名	所属		Title	Name	Organization
81	三角格子反強磁性体の低温磁性	柄木　良友	琉球大学	教育学部	Low temperature magnetism of triangular antiferromagnets.	Yoshitomo Karaki	University of the Ryukyus
82	〃	阿曽　尚文	琉球大学	理学部	〃	Naofumi Aso	University of the Ryukyus
83	多型化合物 RIr_2Si_2(R= 希土類）磁気特性 5	内間　清晴	沖縄キリスト教短期大学	総合教育系	Magnetic characteristics of polymorphic compounds RIr_2Si_2(R=rare earth）5	Kiyoharu Uchima	Okinawa Christian Junior College
84	〃	繁岡　透	山口大学	大学院創成科学研究科	〃	Toru Shigeoka	Yamaguchi University
85	YbH_{2+x} の磁性と伝導	中村　修	岡山理科大学	研究社会連携センター	Magnetic and transport properties in YbH_{2+x}	Osamu Nakamura	Okayama University
86	$MnCo_{1-x}Ge$ 合金の磁気特性に関する研究 (2)	江藤　徹二郎	久留米工業大学	共通教育科	Study of magnetic properties in $MnCo_{1-x}Ge$ alloys(2)	Tetsujiro Eto	Kurume Institute of Technology
87	遷移金属化合物の高圧力下の輸送特性	仲間　隆男	琉球大学	理学部	Pressure effect on transport properties of transition metal compounds	Takao Nakama	University of the Ryukyus
88	〃	太田　譲二	琉球大学	大学院理工学研究科	〃	Jouji Ota	University of the Ryukyus
89	ハーフメタルホイスラー合金の磁気体積効果に関する研究	重田 出	鹿児島大学	大学院理工学研究科	Study on the magneto-volume effect of half-metallic Heusler alloys	Iduru Shigeta	Kagoshima University
90	圧力誘起価数転移の探索と高圧下輸送特性	辺土　正人	琉球大学	理学部	Searching of pressure-induced valence transition and transport properties under high pressure	Masato Hedo	University of the Ryukyus
91	〃	仲井間　憲李	琉球大学	大学院理工学研究科	〃	Kenri Nakaima	University of the Ryukyus
92	Eu 化合物の圧力誘起近藤状態の探索	辺土　正人	琉球大学	理学部	Searching for pressure-induced Kondo state on Eu compounds	Masato Hedo	University of the Ryukyus
93	〃	伊覇　航	琉球大学	大学院理工学研究科	〃	Wataru Iha	University of the Ryukyus
94	〃	松田　進弥	琉球大学	大学院理工学研究科	〃	Shinya Matsuda	University of the Ryukyus
95	単結晶 $Ho_{1-x}La_xRh_2Si_2$ の電気抵抗測定 (2)	藤原　哲也	山口大学	大学院創成科学研究科	Resistivity measurements of $Ho_{1-x}La_xRh_2Si_2$ single crystal II	Tetsuya Fujiwara	Yamaguchi University
96	〃	山本　嵩	山口大学	大学院創成科学研究科	〃	Shu Yamamoto	Yamaguchi University
97	圧力誘起価数転移によって発生する Yb モーメントの磁気秩序についての検証	藤原　哲也	山口大学	大学院創成科学研究科	Evidence for the magnetic ordering of Yb moment accompanied by the valence transition	Tetsuya Fujiwara	Yamaguchi University

No.	課題名	氏名	所属		Title	Name	Organization
98	〃	西崎　裕哉	山口大学	大学院創成科学研究科	〃	Yuya Nishizaki	Yamaguchi University
99	$HoRh_{2-x}Co_xSi_2$ の比熱測定	藤原　哲也	山口大学	大学院創成科学研究科	Specific heat measurement of $HoRh_{2-x}Co_xSi_2$	Tetsuya Fujiwara	Yamaguchi University
100	〃	山本　嵩	山口大学	大学院創成科学研究科	〃	Shu Yamamoto	Yamaguchi University
101	$TmRh_2Si_2$ 化合物の単結晶育成	藤原　哲也	山口大学	大学院創成科学研究科	Single crystal growth of $TmRh_2Si_2$ compound	Tetsuya Fujiwara	Yamaguchi University
102	〃	西崎　裕哉	山口大学	大学院創成科学研究科	〃	Yuya Nishizaki	Yamaguchi University
103	高圧物性研究における圧力容器と媒体の影響	村田　恵三	大阪経済法科大学	２１世紀社会総合研究センター	Effect of Pressure Cell and Pressure Medium in High Pressure Study	Keizo Murata	Osaka University of Economics and Low
104	Fe を置換した Mn_2Sb 化合物のスピン再配列	三井　好古	鹿児島大学	大学院理工学研究科	Spin-reorientation in Fe-modified Mn_2Sb compounds	Yoshifuru Mitsui	Kagoshima University
105	〃	野口　滉平	鹿児島大学	大学院理工学研究科	〃	Kohei Noguchi	Kagoshima University
106	磁場で制御した $Sm_2Fe_{17}N_3$ の磁気特性	小山　佳一	鹿児島大学	大学院理工学研究科	Magnetic properties of $Sm_2Fe_{17}N_3$ prepared under magnetic fields	Keiichi Koyama	Kagoshima University
107	〃	尾上　昌平	鹿児島大学	研究推進機構研究支援センター	〃	masahira Onoue	Kagoshima University
108	磁場で制御された Mn-Ga 合金の磁気特性	小山　佳一	鹿児島大学	大学院理工学研究科	Magnetic properties of Mn-Ga alloys prepared under magnetic fields	Keiichi Koyama	Kagoshima University
109	〃	渡邊　有美	鹿児島大学	大学院理工学研究科	〃	Yumi Watanabe	Kagoshima University
110	銅オキシカルコゲナイドの高圧力下電気抵抗率測定	今井　良宗	東北大学	大学院理学研究科	Measurement of electrical resistivity in copper oxychalcogenides under high pressure	Yoshinori Imai	Tohoku University
111	〃	木村　遼太	東北大学	大学院理学研究科	〃	Ryota Kimura	Tohoku University
112	磁場中熱処理した Cu-Mn-Al の磁気特性	三井　好古	鹿児島大学	大学院理工学研究科	Magnetic properties of Cu-Mn-Al prepared by in-field annealing	Yoshifuru Mitsui	Kagoshima University
113	〃	中川　駿	鹿児島大学	大学院理工学研究科	〃	Shun Nakagawa	Kagoshima University
114	低次元化合物のクロスオーバー現象における超伝導	久田　旭彦	徳島大学	大学院社会産業理工学研究部	Superconductivity on a crossover phenomenon of low-dimensional compounds	Akihiko Hisada	Tokushima University

No.	課題名	氏名	所属		Title	Name	Organization
115	鉄系超伝導体 $Ba_{1-x}Rb_xFe_2As_2$ の高圧下電気抵抗率測定	芝内　孝禎	東京大学	大学院新領域創成科学研究科	Measurements of the electrical resistivity in $Ba_{1-x}Rb_xFe_2As_2$ under high pressure	Takasada Shibauchi	The University of Tokyo
116	〃	橋本　顯一郎	東京大学	大学院新領域創成科学研究科	〃	Kenichiro Hashimoto	The University of Tokyo
117	〃	松浦　康平	東京大学	大学院新領域創成科学研究科	〃	Kouhei Matsuura	The University of Tokyo
118	〃	向笠　清隆	東京大学	大学院新領域創成科学研究科	〃	Kiyotaka Mukasa	The University of Tokyo
119	〃	邱明瑋	東京大学	大学院新領域創成科学研究科	〃	Mingwei Qiu	The University of Tokyo
120	高圧下における $(Fe_{1-x}Zn_x)_2Mo_3O_8$ の電気磁気特性	赤星　大介	東邦大学	理学部	Magnetoelectric properties of $(Fe_{1-x}Zn_x)_2Mo_3O_8$ under high pressures	Daisuke Akahoshi	Toho University
121	構造相転移を持つ $BaCo_{1-x}Ni_xS_{2-y}$ 系化合物の圧力下磁化率測定	伊藤　昌和	鹿児島大学	総合科学域総合教育学系	Magnetic susceptibility on $BaCo_{1-x}Ni_xS_{2-y}$ with the structural transition under pressure	Masakazu Ito	Kagoshima University
122	〃	今村　有助	鹿児島大学	大学院理工学研究科	〃	Yusuke Imamura	Kagoshima University
123	〃	鹿島　頌太	鹿児島大学	大学院理工学研究科	〃	Shota Kashima	Kagoshima University
124	更なる超高圧印加による有機反強磁性絶縁体 λ-$(ET)_2GaCl_4$ の超伝導探索	小林　拓矢	埼玉大学	大学院理工学研究科	Search for superconductivity in organic antiferromagnetic insulator λ-$(ET)_2GaCl_4$　by further application of ultra-high pressures	Takuya Kobayashi	Saitama University
125	〃	綱川　仁志	埼玉大学	大学院理工学研究科	〃	Hotoshi Tsunakawa	Saitama University
126	〃	生沼　浩介	埼玉大学	大学院理工学研究科	〃	Kohsuke Oinuma	Saitama University
127	〃	小澤　宏彬	埼玉大学	大学院理工学研究科	〃	Hiroaki Ozawa	Saitama University
128	〃	伊藤 有咲	埼玉大学	大学院理工学研究科	〃	Arisa Ito	Saitama University
129	$HfTe_3$ の高圧力印加による CDW の消失と新規超伝導相の発現	加瀬　直樹	東京理科大学	理学部	Suppression of CDW and the emergence of new superconducting phase of $HfTe_3$	Naoki Kase	Tokyo University of Science
130	URhSn の圧力下物性研究	モーリヤ　アルビン	東北大学	金属材料研究所	High pressure studies on URhSn	Maurya Arvind	Tohoku University
131	Ni_2MnZ (Z= In, Sn, Sb) 強磁性ホイスラー合金の磁化の圧力効果	安達　義也	山形大学	大学院理工学研究科	Pressure effect of the magnetization for the ferromagnetic Heusler alloys Ni_2MnZ (Z= In, Sn, Sb)	Yoshiya Adachi	Yamagata University

No.	課題名	氏名	所属		Title	Name	Organization
132	〃	吉田　圭吾	山形大学	大学院理工学研究科	〃	Keigo Yoshida	Yamagata University
133	反強磁性ホイスラー合金 Ru_2MnZ (Z= Ge, Sn, Sb) のネール温度の圧力効果	安達　義也	山形大学	大学院理工学研究科	Pressure effect of the Nel temperature for the antiferromagnetic Heusler alloys Ru_2MnZ (Z= Ge, Sn, Sb)	Yoshiya Adachi	Yamagata University
134	〃	渡辺　健	山形大学	大学院理工学研究科	〃	Ken Watanabe	Yamagata University
135	RE_3TiBi_5 の圧力下電気抵抗測定	本山　岳	島根大学	大学院自然科学研究科	Electrical resistivity measurements of RE_3TiBi_5 (RE=rare earth) under pressure	Gaku Motoyama	Shimane University
136	〃	坪内　将紘	島根大学	大学院自然科学研究科	〃	Masahiro Tsubouchi	Shimane University
137	強磁性ウラン化合物 URh_6Si_4 の高圧物性	芳賀　芳範	日本原子力研究開発機構	先端基礎研究センター	High-pressure physical properties of ferromagnetic uranium compound URh_6Si_4	Yoshinori Haga	Japan Atomic Energy Agency
138	$PrPt_2Cd_{20}$ の高圧力下電気抵抗測定	広瀬　雄介	新潟大学	理学部	Electrical resistivity measurement under pressure of $PrPt_2Cd_{20}$	Yusuke Hirose	Niigata University
139	〃	高山　昂己	新潟大学	大学院自然科学研究科	〃	Koki Takayama	Niigata University
140	遷移金属カルコゲナイドの圧力下 dHvA 効果の研究	摂待　力生	新潟大学	理学部	de Haas-van Alphen effect under pressure in transition metal chalcogenide	Rikio Settai	Niigata University
141	〃	武藤　研太	新潟大学	大学院自然科学研究科	〃	Kenta Muto	Niigata University
142	重い電子系希土類化合物の dHvA 効果	摂待　力生	新潟大学	理学部	de Haas-van Alphen effect in heavy fermion cerium compounds	Rikio Settai	Niigata University
143	〃	佐野　純佳	新潟大学	大学院自然科学研究科	〃	Sumika Sano	Niigata University
144	キュービックアンビルセルを用いた NMR 測定開発	藤原　直樹	京都大学	大学院人間・環境学研究科	Development of NMR meansurements under pressure using a cubic-anvil cell	Naoki Fujiwara	Kyoto University
145	〃	中川　悟志	京都大学	大学院人間・環境学研究科	〃	Satoshi Nakagawa	Kyoto University
146	新しい Eu 化合物の圧力効果	光田　暁弘	九州大学	大学院理学研究院	Pressure effect on new Eu-based compounds	Akihiro Mitsuda	Kyushu University
147	〃	大山　耕平	九州大学	大学院理学府	〃	Oyama Kohei	Kyushu University
148	六方晶 $Hf_{1-x}Ta_xFe_{2+x}$ の磁気熱量効果	松本　圭介	愛媛大学	大学院理工学研究科	Magnetocaloric effect in $Hf_{1-x}Ta_xFe_{2+x}$	Keisuke Matsumoto	Ehime University

No.	課題名	氏名	所属		Title	Name	Organization
149	〃	高畦　恋	愛媛大学	大学院理工学研究科	〃	Ren Takaaze	Ehime University
150	直方晶 $GdNiX_{1-x}$(X=Si,Ge) の比熱	松本　圭介	愛媛大学	大学院理工学研究科	Specific heat study of $GdNiX_{1-x}$(X=Si,Ge)	Keisuke Matsumoto	Ehime University
151	〃	小林　将己	愛媛大学	大学院理工学研究科	〃	Masaki Kobayashi	Ehime University
152	キュービックアンビルセルを用いた NMR 測定開発	桑山　昴典	京都大学	大学院人間・環境学研究科	Development of NMR meansurements under pressure using a cubic-anvil cell	Takanori Kuwayama	Kyoto University
153	スピン三重項超伝導体 UTe_2 の磁性と超伝導の圧力効果	本多　史憲	東北大学	金属材料研究所	Effect of Pressure on the magnetism and superconductivity of a spin triplet superconductor UTe_2	Fuminori Honda	Tohoku University
担当所員：尾崎　泰助							
154	実験と計算の協奏による二次元材料の構造・電子状態解析及び制御	アントワーヌ　フロランス	北陸先端科学技術大学院大学	マテリアルサイエンス系	Analysis and control of crystal and electronic structures of 2D materials through concerted collaboration of experiment and theory	Antoine Fleurence	JAIST
155	〃	新田　寛和	北陸先端科学技術大学院大学	先端科学技術研究科	〃	Hirokazu Nitta	JAIST
担当所員：益田　隆嗣							
156	透過型ラウエ法による鉄マンガン基恒弾性合金の単結晶試料の評価	池田　陽一	東北大学	金属材料研究所	Transmission Laue diffraction measurements for characterization of single crystalline FeMn-based elinvar alloys	Yoichi Ikeda	Tohoku University
157	サイト選択アニオンドーピングによる $Ce(Te_{1-x}Se_x)_3$ の磁気抵抗測定	植田　大地	沖縄科学技術大学院大学	量子物質科学ユニット	Magnetoresistance measurement of site selective anion doping $Ce(Te_{1-x}Se_x)_3$	Daichi Ueta	Okinawa Institute of Science and Technology Graduate University
158	〃	大熊　隆太郎	沖縄科学技術大学院大学	岡田ユニット	〃	Ryutaro Okuma	Okinawa Institute of Science and Technology Graduate University
159	$Ce(Te_{1-x}Se_x)_3$ 単結晶試料の高エネルギー X 線ラウエ装置による結晶方位同定	小林　理気	琉球大学	理学部	Alignment of $Ce(Te_{1-x}Se_x)_3$ single crystals by high-energy X-ray Laue diffraction	Riki Kobayashi	University of the Ryukyus
160	〃	岡部　孝俊	琉球大学	大学院理工学研究科	〃	Takatoshi Okabe	University of the Ryukyus
161	$(Ce_{1-x}La_x)_5Ga_2Ge$ 単結晶試料の極低温比熱測定	小林　理気	琉球大学	理学部	Specific heat measurement at very low temperature on $(Ce_{1-x}La_x)_5Ga_2Ge$ systems	Riki Kobayashi	University of the Ryukyus
162	〃	岡部　孝俊	琉球大学	大学院理工学研究科	〃	Takatoshi Okabe	University of the Ryukyus
担当所員：金道　浩一							

No.	課題名	氏名	所属		Title	Name	Organization
163	幾何学的フラストレート磁性体の強磁場磁化測定	菊池　彦光	福井大学	学術研究院工学系部門	Magnetization measurements of the frustrated magnets	Hikomitsu Kikuchi	University of Fukui
164	重い電子系化合物が示す非従来型超伝導と磁性の相関	横山　淳	茨城大学	大学院理工学研究科	Interplay between unconventional superconductivity and magnetism in heavy-fermion compounds	Makoto Yokoyama	Ibaraki University
165	〃	ラフマント	茨城大学	大学院理工学研究科	〃	Rahmanto	Ibaraki University
166	新しいイルメナイト型キタエフ物質における新奇磁場誘起相の探索	原口　祐哉	東京農工大学	大学院工学研究院	Search for novel magnetic field induced phase in new ilmenite-type Kitaev compounds	Yuya Haraguchi	Tokyo University of Agriculture and Technology
167	〃	吉田　悠澄	東京農工大学	大学院工学研究院	〃	Yuto Yoshida	Tokyo University of Agriculture and Technology
168	〃	小日置　隆	東京農工大学	大学院工学研究院	〃	Yutaka Kobiki	Tokyo University of Agriculture and Technology
169	積層化合物 M_xTX_2(M:3d 遷移金属，T:Nb, Ta, X:S, Se)，$Fe_{5-\delta-x}Ni_xGeTe_2$ の強磁場磁化測定	道岡　千城	京都大学	大学院理学研究科	High-field magnetization measurement of layered compounds M_xTX2(M:3d transition metal，T:Nb, Ta, X:S, Se) and $Fe_{5-\delta-x}Ni_xGeTe_2$	Chishiro Michioka	Kyoto University
170	〃	山中　俊介	京都大学	大学院理学研究科	〃	Shunsuke Yamanaka	Kyoto University
171	構造相転移を持つ $BaCo_{1-x}Ni_xS_2$-y 系化合物の高磁場磁歪測定	伊藤　昌和	鹿児島大学	総合科学域総合教育学系	Magnetic strain on $BaCo_{1-x}Ni_xS_2$-y system with the structural transition in high magnetic field	Masakazu Ito	Kagoshima University
172	〃	鹿島　頌太	鹿児島大学	大学院理工学研究科	〃	Shota Kashima	Kagoshima University
173	金属ナノ結晶集合体の磁化特性	稲田　貢	関西大学	システム理工学部	Magnetic properties of metal nanocrystal assemblies	Mitsuru Inada	Kansai University
174	〃	米澤　諒	関西大学	大学院理工学部	〃	Ryo Yonezawa	Kansai University
175	topological Kondo insulator SmB_6,YbB_{12} の磁化特性と比熱	伊賀　文俊	茨城大学	理学部	Magnetic and thermal properties of topological Kondo insulator SmB_6 and YbB_{12}	Fumitoshi Iga	Ibaraki University
176	〃	松浦　航	茨城大学	大学院理工学研究科	〃	Wataru Matsuura	Ibaraki University
177	高圧合成新規希土類 Ce_{12} ホウ化物の強磁場中の磁化と比熱	伊賀　文俊	茨城大学	理学部	Magnetic and thermal properties in high magnetic fields of rare earth hexa- and dodeca-borides produced by high pressure synthesis	Fumitoshi Iga	Ibaraki University
178	〃	中山　裕之	茨城大学	大学院理工学研究科	〃	Hiroyuki Nakayama	Ibaraki University
179	高圧合成による Zr ベース R 置換 B_{12} の強磁場中の磁性と比熱，伝導	伊賀　文俊	茨城大学	理学部	Magnetic, transport and thermal properties in high magnetic fields of $Zr_{1-x}R_xB_{12}$ produced by high pressure synthesis	Fumitoshi Iga	Ibaraki University

No.	課題名	氏名	所属		Title	Name	Organization
180	〃	山田　貴大	茨城大学	大学院理工学研究科	〃	Takahiro Yamada	Ibaraki University
181	異常に大きな BiS_2 型層状化合物超伝導体の上部臨界磁場	加瀬　直樹	東京理科大学	理学部	Upper critical field of the BiS_2-based superconductor	Naoki Kase	Tokyo University of Science
182	オーバードープ Bi-2223 単結晶の磁気輸送特性	渡辺　孝夫	弘前大学	大学院理工学研究科	Magnetotransport properties of overdoped Bi-2223 single crystals	Takao Watanabe	Hirosaki University
183	〃	山口　隼平	弘前大学	大学院理工学研究科	〃	Shunpei Yamaguchi	Hirosaki University
184	ウラン系重い電子系化合物におけるその強磁場物性測定とスピン三重項超伝導の探索	清水　悠晴	東北大学	金属材料研究所	High-field experiments and exploration of odd-parity superconductors in uranium heavy-fermion systems	Yusei Shimizu	Tohoku University
担当所員：徳永　将史							
185	磁気光学法を用いた超伝導体中の磁束量子ダイナミクス観測	黒川　穂高	東京大学	大学院総合文化研究科	Observation of the dynamics of vortices in a superconductor by magneto-optical microscopy	Hodaka Kurokawa	The University of Tokyo
186	Pd_2MnGa 合金におけるメタ磁性転移の結晶方位依存性	許　畠	東北大学	大学院工学研究科	The crystal orientation dependence of metamagnetic transitions in Pd_2MnGa alloys	Xiao Xu	Tohoku University
187	〃	伊東　達矢	東北大学	大学院 工学研究科	〃	Tatsuya Ito	Tohoku University
188	スピネル化合物の強磁場磁化過程	香取　浩子	東京農工大学	大学院工学研究院	High-field magnetization process of spinel materials	Hiroko Katori	Tokyo University of Agriculture and Technology
189	〃	徳永　柊介	東京農工大学	大学院工学府	〃	Shunsuke Tokunaga	Tokyo University of Agriculture and Technology
190	〃	羽鳥　滋	東京農工大学	大学院工学府	〃	Shigeru Hatori	Tokyo University of Agriculture and Technology
191	重い電子系における強磁場中の電子状態研究	海老原　孝雄	静岡大学	学術院理学領域	Electronic states at high magnetic fields in Heavy Fermion systems	Takao Ebihara	Shizuoka University
192	〃	丸山　博史	静岡大学	大学院総合科学技術研究科	〃	Hiroshi Maruyama	Shizuoka University
193	トーラス型フェルミ面を持つラシュバ型半導体の量子極限伝導特性の研究	村川　寛	大阪大学	大学院理学研究科	High field study for quantum limit transport properties of torus Fermi surface in Rashba semiconductor	Hiroshi Murakawa	Osaka University
194	キャリア濃度制御した多層ディラック電子系 $BaMnX_2$ (X=Sb, Bi) の量子伝導の研究	酒井　英明	大阪大学	大学院理学研究科	Study of quantum transport phenomena in $BaMnX_2$ (X=Sb, Bi) hosting controlled quasi-2D Dirac-like carriers	Hideaki Sakai	Osaka University
195	〃	近藤　雅起	大阪大学	大学院理学研究科	〃	Masaki Kondo	Osaka University

No.	課題名	氏名	所属		Title	Name	Organization
196	〃	中川　賢人	大阪大学	大学院理学研究科	〃	Kento Nakagawa	Osaka University
197	ランタノイド Kitaev 型量子スピン液体の探索のための強磁場磁化過程測定	北川　健太郎	東京大学	大学院理学系研究科	High-field magnetization measurement for Lanthanoid Kitaev-type quantum spin liquid	Kentaro Kitagawa	The University of Tokyo
198	新規超伝導体 UTe_2 の電子状態の圧力効果の研究	本多　史憲	東北大学	金属材料研究所	Study of exotic electronic properties of a new superconductor UTe_2 under high pressure	Fuminori Honda	Tohoku University
199	正四角台塔反強磁性体の強磁場電気磁気特性の測定	木村　健太	東京大学	大学院新領域創成科学研究科	High-field magnetoelectric properties in square-cupola-based antiferromagnets	Kenta Kimura	The University of Tokyo
200	遍歴強磁性体 UNi_4P_2 の強磁場磁化測定による基底状態の解明	モーリヤ　アルビン	東北大学	金属材料研究所	High filed magnetization in itinerant ferromagnet UNi_4P_2	Maurya Arvind	Tohoku University
201	強磁性ウラン化合物の強磁場物性	芳賀　芳範	日本原子力研究開発機構	先端基礎研究センター	High-field physical properties of ferromagnetic uranium compounds	Yoshinori Haga	Japan Atomic Energy Agency
202	超強磁場下測定による磁性半金属 EuP_3 のフェルミ面解析	メイヨー　アレックス　浩	東京大学	大学院工学系研究科	Fermi surface analysis of magnetic semimetal EuP_3 measured under high magnetic field	Alex Hiro Mayo	The University of Tokyo
203	〃	高橋　英史	大阪大学	大学院基礎工学研究科	〃	Hidefumi Takahashi	Osaka University
204	重い電子系における強磁場中の電子状態研究	ジュマエダ・ジャトミカ	静岡大学	大学院自然科学教育部	Electronic states at high magnetic fields in Heavy Fermion systems	Jumaeda Jatmika	Shizuoka University
担当所員：松田　康弘							
205	近藤半導体 $(Yb,R)B_{12}$、ほか新規高圧合成物質のワンターンコイル 120T 強磁場磁化と伝導	伊賀　文俊	茨城大学	理学部	Magnetization and transport properties by using one-turn coil in a 120 T pulse magnet of Kondo insulator $(Yb,R)B_{12}$ and novel rare-earth borides producted by high-pressure synthesis	Fumitoshi Iga	Ibaraki University
206	〃	竹森　氷馬	茨城大学	大学院理工学研究科	〃	Hyouma Takemori	Ibaraki University
担当所員：小濱　芳允							
207	ハーフホイスラー超伝導体における強磁場下量子振動測定	芝内　孝禎	東京大学	大学院新領域創成科学研究科	Quantum oscillation measurements of half-Heusler superconductors under high magnetic field	Takasada Shibauchi	The University of Tokyo
208	〃	橋本　顕一郎	東京大学	大学院新領域創成科学研究科	〃	Kenichiro Hashimoto	The University of Tokyo
209	〃	水上　雄太	東京大学	大学院新領域創成科学研究科	〃	Yuta Mizukami	The University of Tokyo
210	〃	石原　滉大	東京大学	大学院新領域創成科学研究科	〃	Kota Ishihara	The University of Tokyo

No.	課題名	氏名	所属		Title	Name	Organization
211	正四角台塔反強磁性体 $Pb(TiO)Cu_4(PO_4)_4$ における強磁場中での電気磁気光学効果の研究	木村　健太	東京大学	大学院新領域創成科学研究科	Optical magnetoelectric effect of the square-cupola-based antiferromagnet $Pb(TiO)Cu_4(PO_4)_4$ in a high magnetic field	Kenta Kimura	The University of Tokyo
212	パルス強磁場を用いた強磁場 NMR 測定による量子磁性体の磁場誘起相の研究	井原　慶彦	北海道大学	大学院理学研究院	Pulsed field NMR study for field induced magnetic state in quantum magnets	Yoshihiko Ihara	Hokkaido University
213	〃	荒島　洸樹	北海道大学	大学院理学院	〃	Koki Arashima	Hokkaido University
214	水素ドープ SmFeAsO エピタキシャル薄膜の超高磁場下における上部臨界磁場測定	平松　秀典	東京工業大学	科学技術創成研究院	Upper critical magnetic fields measurements under extremely high magnetic fields of hydrogen-doped SmFeAsO epitaxial films	Hidenori Hiramatsu	Tokyo Institute of Technology
215	超強磁場電気抵抗測定による多電子ドープ La１１１１-H の上部臨界磁場の研究	河智　史朗	東京工業大学	元素戦略研究センター	Study of upper critical field in high doped La1111-H with using magnetoresistance measurement under ultra-high magnetic fields	Shiro Kawachi	Tokyo Institute of Technology
担当所員：小林　洋平							
216	次世代レーザーとレーザー加工の基礎技術研究	吉富　大	産業技術総合研究所	電子光技術研究部門	Basic research on next generation laser systems and laser machining technology	Dai Yoshitomi	National Institute of Advanced Industrial Science and Technology
217	〃	鳥塚　健二	産業技術総合研究所	電子光技術研究部門	〃	Kenji Torizuka	National Institute of Advanced Industrial Science and Technology
218	〃	高田　英行	産業技術総合研究所	電子光技術研究部門	〃	Hideyuki Takada	National Institute of Advanced Industrial Science and Technology
219	〃	奈良崎　愛子	産業技術総合研究所	電子光技術研究部門	〃	Aiko Narazaki	National Institute of Advanced Industrial Science and Technology
220	〃	小川　博嗣	産業技術総合研究所	分析計測標準研究部門	〃	Hiroshi Ogawa	National Institute of Advanced Industrial Science and Technology
221	〃	佐藤　大輔	産業技術総合研究所	分析計測標準研究部門	〃	Daisuke Satoh	National Institute of Advanced Industrial Science and Technology
222	〃	澁谷　達則	産業技術総合研究所	分析計測標準研究部門	〃	Tatsunori Shibuya	National Institute of Advanced Industrial Science and Technology
223	〃	馬場　大輔	産業技術総合研究所	分析計測標準研究部門	〃	Daisuke Baba	National Institute of Advanced Industrial Science and Technology
224	〃	盛合　靖章	産業技術総合研究所	先端オペランド計測技術オープンイノベーションラボラトリ	〃	Yasuaki Moriai	National Institute of Advanced Industrial Science and Technology
225	〃	黒田　隆之助	産業技術総合研究所	先端オペランド計測技術オープンイノベーションラボラトリ	〃	Ryunosuke Kuroda	National Institute of Advanced Industrial Science and Technology
226	〃	寺澤　英知	産業技術総合研究所	先端オペランド計測技術オー プンイノベーションラボラトリ	〃	Eichi Terasawa	National Institute of Advanced Industrial Science and Technology

No.	課題名	氏名	所属		Title	Name	Organization
227	青色半導体レーザー用ファイバ型光コンバイナの開発	藤本　靖	千葉工業大学	工学部	Development on fiber power combiner for GaN semiconductor lasers	Yasushi Fujimoto	Chiba Institute of Technology
228	レーザー加工された金属表面の超高速発光による研究	末元　徹	豊田理化学研究所		Study on laser ablated metal surfaces by ultrafast luminescence spectroscopy	Tohru Suemoto	Toyota Physical and Chemical Research Institute
229	レーザー加工状態の分光測定に関する研究 II	富田　卓朗	徳島大学	大学院社会産業理工学研究部	Study on laser modification by using optical spectroscopic measurement II	Takuro Tomita	Tokushima University
230	〃	山口　誠	秋田大学	大学院理工学研究科	〃	Makoto Yamaguchi	Akira University
231	パルスレーザーを用いた分光測定のための光源開発	大間知　潤子	関西学院大学	理工学部	Light source development for spectroscopy using pulse laser	Junko Omachi	Kansai Gakuin University
232	和周波発生による新たな赤外分光に資するファイバーレーザーシステムの開発	田中　耕一郎	京都大学	大学院理学研究科	Development of fiber laser systems for up-conversation infrared spectroscopy	Koichiro Tanaka	Kyoto University
233	〃	内田　健人	京都大学	大学院理学研究科	〃	Kento Uchida	Kyoto University
234	〃	北条　真之	京都大学	大学院理学研究科	〃	Masayuki Hojo	Kyoto University
235	短波長パルスレーザーによる CFRP 加工	森山　匡洋	東京大学	大学院理学系研究科	CFRP processing with short wavelength pulsed laser	Masahiro Moriyama	The University of Tokyo
担当所員：板谷　治郎							
236	時間分解非線形分光法によるコヒーレントフォノン測定系における磁気光学ユニットの構築	牧野　哲征	福井大学	学術研究院工学系部門	Magnetooptical effect of coherent phonons of by time-resolved nonlinear spectroscopy	Takayuki Makino	University of Fukui
237	時間分解非線形分光法を用いた希土類酸化物のコヒーレントフォノンにおける外部磁場効果の観測	山出　拓史	福井大学	大学院工学研究科	Magnetooptical effect of coherent phonons of rare-earth oxides studied by time-resolved nonlinear spectroscopy	Takuji Yamade	University of Fukui
238	〃	浅井　郁帆	福井大学	大学院工学研究科	〃	Takaho Asai	University of Fukui
239	〃	竹内 智哉	福井大学	大学院工学研究科	〃	Tomoya Takeuchi	University of Fukui
担当所員：近藤　猛							
240	スピン分解角度分解光電子分光による層状 MAX 層化合物のスピン偏極状態の研究	伊藤　孝寛	名古屋大学	シンクロトロン光研究センター	Spin- and angle-resolved photoemission study of spin-polarized electronic structure of nanolamellar MAX phase compounds	Takahiro Ito	Nagoya University
241	〃	林　直輝	名古屋大学	大学院工学研究科	〃	Naoki Hayashi	Nagoya University

No.	課題名	氏名	所属		Title	Name	Organization
242	〃	鍋平　直輝	名古屋大学大学院	大学院工学研究科	〃	Naoki Nabehira	Nagoya University
243	〃	古田　貫志	名古屋大学	大学院工学研究科	〃	Kanji Furuta	Nagoya University
244	〃	細谷　知輝	名古屋大学	大学院工学研究科	〃	Tomoki Hosoya	Nagoya University
245	トポロジカル絶縁体 $Bi_{1-x}Sb_x$ と垂直磁化膜 MnGa 界面におけるディラックコーンの観測	小林　正起	東京大学	大学院工学系研究科	Observation of Dirac cone state at the interface between topological insulator $Bi_{1-x}Sb_x$ and perpendicular magnet MnGa layers	Masaki Kobayashi	The University of Tokyo
246	ファンデルワールス結合を有する金属間化合物 $Ce(Te,Se)_3$ の光電子分光法による電子状態の観測	植田　大地	沖縄科学技術大学院大学	量子物質科学ユニット	Observation of electric state in a van der Waals compound $Ce(Te,Se)_3$ by ARPES	Daichi Ueta	Okinawa Institute of Science and Technology Graduate University
247	ファンデルワールス結合を有する金属間化合物 $Ce(Te,Se)_3$ の光電子分光法による電子状態の観測	大熊　隆太郎	沖縄科学技術大学院大学	岡田ユニット	Observation of electric state in a van der Waals compound $Ce(Te,Se)_3$ by ARPES	Ryutaro Okuma	OIST
担当所員：岡崎　浩三							
248	T’ 構造をもつ銅酸化物高温超伝導体の角度分解光電子分光による研究	チャン　ウェイル	上智大学	機能創造理工学科	Photoemission spectroscopy of electron-doped T'-cuprate superconductors	Zhang Weilu	Sophia University
249	励起子絶縁体と関連物質の時間分解光電子分光	溝川　貴司	早稲田大学	理工学術院　先進理工学部	Time-resolved photoemission study of excitonic insulators and related materials	Takashi Mizokawa	Waseda University
250	〃	密岡　拓心	早稲田大学	理工学術院	〃	Takumi Mitsuoka	Waseda University
251	励起子絶縁体 Ta_2NiSe_5 及びモット絶縁体 Ca_2RuO_4 における光誘起絶縁体 - 金属転移の研究	久保田　雄也	高輝度光科学研究センター	XFEL 利用研究推進室	Investigation of the photo-induced insulator-to-metal transition in an exitonic insulator Ta_2NiSe_5 and a Mott insulator Ca_2RuO_4	Yuya Kubota	JASRI
252	高分解能レーザー励起光電子顕微鏡を用いた鉄系超伝導体の電子ネマティック状態の実空間観察	橋本　顕一郎	東京大学	大学院新領域創成科学研究科	Real-space observation of electronic nematicity in iron-based superconductors by using a high-resolution laser photoemission electron microscope	Kenichiro Hashimoto	The University of Tokyo
253	〃	水上　雄太	東京大学	大学院新領域創成科学研究科	〃	Yuta Mizukami	The University of Tokyo
254	〃	石田　浩祐	東京大学	大学院新領域創成科学研究科	〃	Kousuke Ishida	The University of Tokyo
255	〃	辻井　優哉	東京大学	大学院新領域創成科学研究科	〃	Masaya Tsujii	The University of Tokyo
256	時間分解 ARPES を用いたノーダルライン半金属単層銅シリサイドの電子緩和過程の観測	高山　あかり	早稲田大学	先進理工学部	Observation of electronic relaxation process of nodal-line semimetal monolayer-Cu_2Si by time-resolved ARPES	Akari Takayama	Waseda University
257	〃	坂本　実可子	早稲田大学	先進理工学研究科	〃	Mikako Sakamoto	Waseda University

No.	課題名	氏名	所属		Title	Name	Organization
258	レーザー励起光電子顕微鏡を用いた抵抗変化メモリ材料のナノ物性計測	木下　健太郎	東京理科大学	理学部	Nano physical property measurement of resistance change memory material using laser excited photo-emission microscope	Kentaro Kinoshita	Tokyo University of Science
259	〃	奥田　裕司	東京理科大学	理学部	〃	Yuji Okuda	Tokyo University of Science
260	〃	福本　紳智	東京理科大学	理学部	〃	Shinji Fukumoto	Tokyo University of Science

一般研究員・大阪大学 先端強磁場科学研究センター / General Researcher・Center for Advanced High Magnetic Field Science Osaka University

No.	課題名	氏名	所属		Title	Name	Organization
担当所員：萩原　政幸（大阪大学）							
1	Fe-Ni-Cr 合金におけるマルテンサイト変態の時間依存性	福田　隆	大阪大学	大学院工学研究科	Time dependence of martensitic transformation in Fe-Ni-Cr alloys	Takashi Fukuda	Osaka University
2	パルス強磁場を用いた強相関電子系物質の強磁場物性の研究	竹内　徹也	大阪大学	低温センター	Magnetic properties of strongly correlated electron systems under pulsed high magnetic fields	Tetsuya Takeuchi	Osaka University
3	〃	大貫　惇睦	琉球大学	理学部	〃	Yoshichika Onuki	University of the Ryukyus
4	Ni_2MnX(X = In, Al, Sn, Sb) 系及び Pd_2MnSn 系の新規ホイスラー合金の超磁歪の高速磁場応答性の研究	左近　拓男	龍谷大学	理工学部	Research on time dependences of magnetstriction of Ni_2MnX(X = In, Al, Sn, Sb) type and Pd_2MnSn type Heusler alloys	Takuo Sakon	Ryukoku University
5	水平磁場印加によるタンパク質結晶の磁場効果の研究（前期の研究の継続）	牧　祥	大阪大谷大学	薬学部	Effect of protein crystallization by the application of horizontal magnetic force.(Continuation of the research)	Syou Maki	Osaka Ohtani University
6	HFESR を用いた配位子場分裂した f 電子副準位構造の決定	福田　貴光	大阪大学	大学院理学研究科	Determination of f-electronic sublevels arising from ligand field splittings by means of HFESR	Takamitsu Fukuda	Osaka University
7	〃	原田　篤大	大阪大学	大学院理学研究科	〃	Atsuhiro Harada	Osaka University
8	一次元交替ボンド反強磁性体の単結晶磁化過程	浅野　貴行	福井大学	学術研究院工学系部門	Magnetization process of one-dimensional bond-alternating antiferromagnet	Takayuki Asano	University of Fukui
9	〃	西首　時夫	福井大学	大学院工学研究科	〃	Tokio Nishikubi	University of Fukui
10	パルス強磁場用極低温実験装置の開発	野口　悟	大阪府立大学	大学院理学系研究科	Development of the cryostat for pulsed high magnetic field	Satoru Noguchi	Osaka Prefecture University
11	〃	中川　豪	大阪府立大学	大学院理学系研究科	〃	Takeshi Nakagawa	Osaka Prefecture University

No.	課題名	氏名	所属		Title	Name	Organization
12	1 次元構造を有するカルボン酸架橋錯体の構造と磁性に関する研究	本多　善太郎	埼玉大学	大学院理工学研究科	Structure and magnetic properties of carboxylate-bridged one-dimensional metal complexes	Zentaro Honda	Saitama University
13	高温超伝導体のパルス強磁場下電流電圧特性	掛谷　一弘	京都大学	大学院工学研究科	Current-voltage characteristics in high-Tc superconductors under pulsed high magnetic elds	Itsuhiro Kakeya	Kyoto Univeristy
14	三角格子反強磁性体の強磁場磁化過程	南部　雄亮	東北大学	金属材料研究所	High field magnetization on a triangular lattice	Yusuke Nambu	Tohoku University
15	新規量子スピン系の強磁場磁性	山口　博則	大阪府立大学	大学院理学系研究科	High-field magnetic properties of new quantum spin systems	Hironori Yamaguchi	Osaka Prefecture University
16	〃	岩崎　義己	大阪府立大学	大学院理学系研究科	〃	Yoshiki Iwasaki	Osaka Prefecture University
17	新しいパルス強磁場高圧下 ESR 装置の開発と応用	櫻井　敬博	神戸大学	研究基盤センター	Development and application of new pulsed high magnetic field high pressure ESR system	Takahiro Sakurai	Kobe University
18	三角格子反強磁性体 $CsCuCl_3$ のパルス強磁場下における圧力下磁化測定	櫻井　敬博	神戸大学	研究基盤センター	High pressure magnetization measurement of triangular antiferromagnet $CsCuCl_3$ under pulsed high magnetic field	Takahiro Sakurai	Kobe University
19	ワイル半金属のランダウ準位の磁場方位依存性の研究	村川　寛	大阪大学	大学院理学研究科	Angular dependent Landau level in Weyl semimetal	Hiroshi Murakawa	Osaka university
20	〃	駒田　盛是	大阪大学	大学院理学研究科	〃	Komada Moriyoshi	Osaka University
21	第二種ワイル半金属の強磁場中量子輸送特性の研究	村川　寛	大阪大学	大学院理学研究科	High magnetic fied study on transport properties of type II Weyl semimetals	Hiroshi Murakawa	Osaka university
22	〃	中岡　優大	大阪大学	大学院理学研究科	〃	Yudai Nakaoka	osaka university
23	強いスピン - 軌道相互作用を活かした酸化物スピントロニクス	松野　丈夫	大阪大学	大学院理学研究科	Oxide spintronics utilizing strong spin-orbit coupling	Matsuno Jobu	Osaka University
24	層状反強磁性体 $EuMnBi_2$ における Eu サイトの元素置換効果の解明	酒井　英明	大阪大学	大学院理学研究科	Study of the variation in antiferromagnetic order induced by chemical substations in $EuMnBi_2$	Hideaki Sakai	Osaka University
25	〃	中川　賢人	大阪大学	大学院理学研究科	〃	Nakagawa Kento	Osaka University
26	〃	近藤　雅起	大阪大学	大学院理学研究科	〃	Masaki Kondo	Graduate School of Science Osaka University
27	$SmB_6/SrB_6/CaB_6$ 人工超格子の強磁場中輸送係数測定	宍戸　寛明	大阪府立大学	大学院工学研究科	Transport measurements for $SmB_6/SrB_6/CaB_6$ superlattices under high magnetic field	Hiroaki Shishido	Osaka Prefecture University
28	$CaBa(Co_{1-x}Fe_x)_4O_7$(x=0,1/4,1/2,3/4,1) 単結晶試料の強磁場下での磁化・電気分極・ESR 測定	桑原　英樹	上智大学	理工学部	Magnetization, electric polarization, and ESR measurements for $CaBa(Co_{1-x}Fe_x)_4O_7$ (x=0,1/4,1/2,3/4,1) single crystals in pulsed high magnetic fields	Hideki Kuwahara	Sophia University

No.	課題名	氏名	所属		Title	Name	Organization
29	〃	遠藤　颯	上智大学	大学院理工学研究科	〃	Hayate Endo	Sophia University
30	正四角台塔反強磁性体の強磁場中 ESR	木村　健太	東京大学	大学院新領域創成科学研究科	High-field ESR measurements of square-cupola-based antiferromagnets	Kenta Kimura	The University of Tokyo
31	秩序型アニオン構造を持った酸水素化物 $EuVO_2H$ の強磁場磁化測定	高津　浩	京都大学	大学院工学研究科	High-field magnetization study of $EuVO_2H$ with an anion ordered structure	Hiroshi Takatsu	Kyoto Univeristy
32	ナノ構造を導入した希土類系高温超伝導薄膜における強磁場中臨界電流密度に関する研究	土屋　雄司	名古屋大学	工学部	Study on the critical current density in high-magnetic field in RE-based cuprate superconductors with nano-structure	Yuji Tsuchiya	Nagoya University
33	2 次元三角格子反強磁性体 $Mn(OH)_2$ の強磁場 ESR の異方性	佐藤　博彦	中央大学	理工学部	Anisotropic measurement of high-field ESR of two-dimensional triangular-lattice antiferromagnet $Mn(OH)_2$	Hirohiko Sato	Chuo University
34	〃	大寺　翔也	中央大学	大学院理工学研究科	〃	Ohtera Shoya	Chuo University
35	$REFe_2O_4$ の磁化測定（RE=Tm,Lu）	掛谷　一弘	京都大学	大学院工学研究科	Magnetization measurement in $REFe_2O_4$(RE=Tm,Lu)	Itsuhiro Kakeya	Kyoto University
36	〃	田中　勝久	京都大学	大学院工学研究科	〃	Katsuhisa Tanaka	Kyoto University
37	〃	キム　ユジン	京都大学	大学院工学研究科	〃	YouJin Kim	Kyoto University

物質合成・評価設備 G クラス / Materials Synthesis and Characterization G Class Researcher

No.	課題名	氏名	所属		Title	Name	Organization
1	フラストレートした 1 次元鎖三角格子系イリジウム酸化物の新奇磁性の研究	松平　和之	九州工業大学	大学院工学研究院	Study on novel magnetic property in frustrated iridates with 1D chains structure on the triangular lattice	Kazuyuki Matsuhira	Kyushu Institute of Technology
2	〃	花手　洋樹	九州工業大学	大学院工学研究院	〃	Hiroki Hanate	Kyushu Institute of Technology
3	空間反転対称性の破れた $CeTSi_3$(T = Rh, Ir, Pd, Pt) の多結晶試料の作成	植田 大地	沖縄科学技術大学院大学	量子物質科学ユニット	Sample growth of a non-centrosymmetric heavy-electron $CeTSi_3$ (T = Rh, Ir, Pd, Pt)	Daichi Ueta	Okinawa Institute of Science and Technology Graduate University
4	貫入型遍歴電子遷移金属炭化物・窒化物の磁気体積効果	和氣　剛	京都大学	大学院工学研究科材料工学専攻	Magneto-volume effect on itinerant electron interstitial transition metal carbides and nitrides	Takeshi Waki	Kyoto University
5	超臨界メタノール条件下でのエステル交換反応に固体触媒が与える影響	秋月　信	東京大学	大学院新領域創成科学研究科	The effect of solid catalysts on the ester exchange reaction in supercritical methanol	Makoto Akizuki	The University of Tokyo
6	〃	張　瑞子	東京大学	大学院新領域創成科学研究科	〃	Zhang　Ruizi	The University of Tokyo

No.	課題名	氏名	所属		Title	Name	Organization
7	高温高圧条件下の水 - メタノール溶媒が固体触媒反応に及ぼす影響の検討	秋月　信	東京大学	大学院新領域創成科学研究科	Investigation of the effect of hot compressed methanol-water mixed solvent on solid catalyzed reactions	Makoto Akizuki	The University of Tokyo
8	〃	島田　綾子	東京大学	大学院新領域創成科学研究科	〃	Shimada Ayako	The University of Tokyo
9	単結晶 $CaMn_{1-x}Sb_xO_3$ の誘電特性および磁気特性の研究	谷口　晴香	岩手大学	理工学部	Study of dielectric and magnetic properties of single crystalline $CaMn_{1-x}Sb_xO_3$	Haruka Taniguchi	Iwate University
10	数値計算を用いた泥岩中の化学的浸透現象に伴う歪についての検討	廣田　翔伍	東京大学	大学院新領域創成科学研究科	Numerical investigation of rock deformation caused by chemical osmosis in mudstones	Shogo Hirota	The University of Tokyo
11	ナノ構造制御材料を用いたクリーンエネルギーデバイス開発	細野　英司	産業技術総合研究所	省エネルギー研究部門	Development of devices for clean energy by using nanostructure controlled materials	Michihiro Ohta	National Institute of Advanced Industrial Science and Technology
12	〃	太田　道広	産業技術総合研究所	省エネルギー研究部門	〃	Eiji Hosono	National Institute of Advanced Industrial Science and Technology
13	〃	ジュド　プリヤンカ	産業技術総合研究所	省エネルギー研究部門	〃	Priyanka Jood	National Institute of Advanced Industrial Science and Technology
14	プラズマ風洞による宇宙往還機熱防護システムの動的酸化に関する研究	桃沢　愛	東京都市大学	工学部医用工学科	Investigation on dynamic oxidation of thermal protection system using plasma wind tunnel	Ai Momozawa	Tokyo City University
15	〃	田中　聖也	東京大学	大学院工学系研究科	〃	Seiya Tanaka	The University of Tokyo
16	〃	山田　慎	東京大学	大学院工学系研究科	〃	Shin Yamada	The University of Tokyo
17	新しい希土類磁石の探求	齋藤　哲治	千葉工業大学	工学部	Research of new rare-earth magnets	Tetsuji Saito	National Institute of Advanced Industrial Science and Technology
18	マイクロミキサを用いた機能性無機ナノ粒子の連続合成	陶　究	産業技術総合研究所	化学プロセス研究部門	Continuous synthesis of functional inorganic nanoparticles using a micromxer	Kiwamu Sue	National Institute of Advanced Industrial Science and Technology
19	天然鉱物の微細組織と化学組成変化の関係	永嶌　真理子	山口大学	大学院創成科学研究科	Effect of chemical variety on micro-texture in natural minerals	Mariko Nagashima	Yamaguchi University
20	超臨界二酸化炭素、塩水、岩石間の相互作用が起きる場の基礎的理解	秋月　信	東京大学	大学院新領域創成科学研究科	Research on fundamentals of interaction between supercritical carbon dioxide, brine and rock	Makoto Akizuki	The University of Tokyo
21	〃	外野　圭太	東京大学	大学院新領域創成科学研究科	〃	Hokano Keita	The University of Tokyo
22	静電浮遊法を用いた過冷却液体急冷法によるボロン系準結晶の探索	木村　薫	東京大学	大学院新領域創成科学研究科	Search for quasicrystalline boron using rapid quenching from super-cooled liquid by levitation technique	Kaoru Kimura	The University of Tokyo
23	〃	高橋　昂宏	東京大学	大学院新領域創成科学研究科	〃	Takahiro Takahashi	The University of Tokyo

No.	課題名	氏名	所属		Title	Name	Organization
24	カーボンナノチューブおよびグラフェンの媒分散処理方法探索及び、分散液を使用した高機能材料の作製	熊代　嗣生	東京大学	大学院工学系研究科	Search for establishing the method to disperse carbon nanotubes and graphene, and making the hybrid materials with the dispersion	Tsuguo Kumashiro	The University of Tokyo
25	$Sm_{1-x}Sr_xFeO_3$ ($0.1 \leqq x \leqq 0.9$) の高温における磁性と熱電特性に関する研究	中津川　博	横浜国立大学	大学院工学研究院	Magnetism and thermoelectric properties at high temperature in $Sm_{1-x}Sr_xFeO_3$($0.1 \leqq x \leqq 0.9$)	Hiroshi Nakatsugawa	Yokohama National University
26	準結晶・近似結晶の磁性に関する研究 III	鈴木　慎太郎	東京理科大学	基礎工学部	Magnetism of quasicrystal and approximants III	Shintaro Suzuki	Tokyo University of Science
27	多形物質 M_2GeO_5(M=V,Cr,Fe,Al,Ga) の磁化測定	香取　浩子	東京農工大学	大学院工学研究院	Magnetization measurements of polymorphism M_2GeO_5(M=V,Cr,Fe,Al,Ga)	Hiroko Katori	Tokyo University of Agriculture and Technology
28	〃	柿本　和勇	東京農工大学	工学府	〃	Kazuo Kakimoto	Tokyo University of Agriculture and Technology
29	〃	大木　祐明	東京農工大学	大学院工学研究院	〃	Yoshiaki Ohki	Tokyo University of Agriculture and Technology
30	新規イルメナイト型ハニカム格子磁性体の物性解明	原口　祐哉	東京農工大学	大学院工学研究院	Physical properties of novel ilmenite-type honeycomb lattice magnets	Yuya Haraguchi	Tokyo University of Agriculture and Technology
31	〃	有海　大樹	東京農工大学	工学府	〃	Hiroki Arikai	Tokyo University of Agriculture and Technology
32	層状ロジウム酸化物 K_xRhO_2 の磁気相図	岡崎　竜二	東京理科大学	理工学部	Magnetic phase diagram of the layered rhodium oxides K_xRhO_2	Ryuji Okazaki	Tokyo University of Science
33	〃	栗田　寛士	東京理科大学	大学院理工学研究科	〃	Kanji Kurita	Tokyo university of science
34	〃	坂林　北斗	東京理科大学	大学院理工学研究科	〃	Hokuto Sakabayashi	Tokyo University of Science
35	〃	石井　まゆ	東京理科大学	大学院理工学研究科	〃	Ishii Mayu	Tokyo University Of Science
36	ハーフメタルホイスラー合金の遍歴電子強磁性体のスピンゆらぎ理論による解析に関する研究	重田　出	鹿児島大学	大学院理工学研究科	Study on analysis of half-metallic Heusler alloys by the spin fluctuation theory of itinerant electron ferromagnets	Iduru Shigeta	Kagoshima University
37	ホイスラー化合物での反強磁性の研究	廣井　政彦	鹿児島大学	大学院理工学研究科	Study on antiferromagnetism in Heusler compounds	Masahiko Hiroi	Kagoshima University
38	〃	野々山　智仁	鹿児島大学	大学院理工学研究科	〃	Tomohito Nonoyama	Kagoshima University
39	レアメタルフリー磁性材料 L10-FeCo の磁気特性の解析	小嗣　真人	東京理科大学	基礎工学部材料工学科	Analysis of magnetic properties of rare-metal-free super magnet “L10-FeCo”	Masato Kotsugi	Tokyo University of Science
40	〃	高橋　優樹	東京理科大学	基礎工学部材料工学科	〃	Takahashi Yuuki	Tokyo University of Science

No.	課題名	氏名	所属		Title	Name	Organization
41	宇宙線望遠鏡の焦点面ライトガイドの反射率測定	吉田　龍生	茨城大学	理学部	Reflectance measurement of focal plane light concentrators for cosmic-ray telescopes	Tatsuo Yoshida	Ibaraki University
42	高温高圧下における下部マントル鉱物への窒素の取り込みに関する研究	福山　鴻	東京大学	大学院理学系研究科	The study on nitrogen incorporation into the lower-mantle minerals under high pressure and high temperature	Ko Fukuyama	The University of Tokyo
43	層状マンガン酸水素化物における圧力効果	山本　隆文	東京工業大学	フロンティア材料研究所	Pressure Effect on Layered Manganese Oxyhydride	Takafumi Yamamoto	Tokyo Institute of Technology
44	高圧中性子実験における発生可能な温度圧力拡大を目指した高圧セル開発	柿澤　翔	東京大学	地殻化学実験施設	Technical development of high pressure cell for high pressure neutron diffraction experiment	Sho Kakizawa	The University of Tokyo
45	新規遷移金属スクッテルダイト化合物の高圧合成と物性	丹羽　健	名古屋大学	大学院工学研究科	High-pressure synthesis and physical properties of novel transition metal skutterudite compounds	Ken Niwa	Nagoya University
46	〃	市川　将成	名古屋大学	大学院工学研究科	〃	Masanari Ichikawa	Nagoya University
47	塩化アンモニウムを用いた遷移金属窒化物の高圧合成	丹羽　健	名古屋大学	大学院工学研究科	High-pressure synthesis of transition metal nitrides using ammonium chloride as nitrogen source	Ken Niwa	Nagoya University
48	〃	生駒　鷹秀	名古屋大学	大学院工学研究科	〃	Takahide Ikoma	Nagoya University
49	高温高圧下における新規酸窒化物蛍光体の合成と発光特性評価	佐々木　拓也	名古屋大学	大学院工学研究科	Synthesis and characterization of oxynitride phosphors under high pressure and high temperature	Takuya Sasaki	Nagoya University
50	〃	近藤　信介	名古屋大学	大学院工学研究科	〃	Shinsuke Kondo	Nagoya University
51	超高圧力合成法を用いた３元系遷移金属 - メタロイド金属間化合物の創成	佐々木　拓也	名古屋大学	大学院工学研究科	High-pressure synthesis and crystal structure of novel ternary transition metal–metalloid intermetallic compounds	Takuya Sasaki	Nagoya University
52	〃	高野　航一	名古屋大学	大学院工学研究科	〃	Koichi Takano	Nagoya University
53	遷移金属ハライドの高圧合成	今井　良宗	東北大学	大学院理学研究科	High pressure synthesis of transition metal halides	Yoshinori Imai	Tohoku University
54	〃	今野　克哉	東北大学	大学院理学研究科	〃	Katsuya Konno	Tohoku University
55	ピストンシリンダー実験による高温高圧下での有機化合物の化学反応の解明	篠崎　彩子	北海道大学	大学院理学研究院	High-pressure and high-temperature experiments on chemical reaction of organic compounds.	Ayako Shiozaki	Hokkaido University
56	フラストレート系層状希土類化合物の高圧合成と磁気的性質	関根　ちひろ	室蘭工業大学	大学院工学研究科	High-pressure synthesis and magnetic properties of frustrated layered rare-earth compounds	Chihiro Sekine	Muroran Institute of Technology
57	〃	佐藤　雄也	室蘭工業大学	大学院工学研究科	〃	Yuya Sato	Muroran Institute of Technology

No.	課題名	氏名	所属		Title	Name	Organization
58	廃プラスチックの炭化による二酸化炭素回収および貯留	布浦　鉄兵	東京大学	環境安全研究センター	Carbon capture through carbonization of plastic waste	Teppei Nunoura	The University of Tokyo
59	〃	ジェニファー　チャー　ウィー　ファン	東京大学	大学院新領域創成科学研究科	〃	Jennifer Chia Wee Fern	The University of Tokyo
60	オレイン酸の超臨界水ガス化工程におけるニッケル触媒の不活性化メカニズムの解明	布浦　鉄兵	東京大学	環境安全研究センター	Nickel catalyst deactivation in supercritical water gasification of oleic acid	Teppei Nunoura	The University of Tokyo
61	〃	ダイアング　バタンガ	東京大学	大学院新領域創成科学研究科	〃	Diane Gubatanga	The University of Tokyo
62	エネルギー貯蔵型空気電池の電極活物質の開発	大友　順一郎	東京大学	大学院新領域創成科学研究科	Development of electrode materials of energy storage type - fuel cells	Junichiro Otomo	The University of Tokyo
63	〃	中西　泰介	東京大学	大学院新領域創成科学研究科	〃	Nakanishi Taisuke	The University of Tokyo
64	炭酸塩ルーピングにおける二酸化炭素利用法の開発	大友　順一郎	東京大学	大学院新領域創成科学研究科	Development of CO_2 utilization in carbonate looping	Junichiro Otomo	The University of Tokyo
65	〃	七瀬　浩希	東京大学	大学院新領域創成科学研究科	〃	Koki Nanase	The University of Tokyo
66	化学ループ法を用いた合成ガス製造システムの設計およびキャリア開発	大友　順一郎	東京大学	大学院新領域創成科学研究科	Development of carrier materials and system design for chemical looping syngas production systems	Junichiro Otomo	The University of Tokyo
67	〃	引間　脩	東京大学	大学院新領域創成科学研究科	〃	Shu Hikima	The University of Tokyo
68	プロトン伝導型固体酸化物燃料電池の電解質積層セルの開発及び界面挙動の研究	大友　順一郎	東京大学	大学院新領域創成科学研究科	Development of solid oxide fuel cells with bi-layer proton-conducting electrolyte thin films	Junichiro Otomo	The University of Tokyo
69	〃	阪田　一真	東京大学	大学院新領域創成科学研究科	〃	Kazuma Sakata	The University of Tokyo
70	燃料電池材料界面の局所測定手法の開発	大友　順一郎	東京大学	大学院新領域創成科学研究科	Development of microscale-measurement of hetero interface of SOFCs	Junichiro Otomo	The University of Tokyo
71	〃	那須　雄太	東京大学	大学院新領域創成科学研究科	〃	Yuta Nasu	The University of Tokyo
72	高温高圧水中でのバイオマス変換に使用するマイクロポーラス材料の安定性向上	大島　義人	東京大学	大学院新領域創成科学研究科	Improving stability of microporous material for biomass upgrading in sub- and supercritical water	Yoshito Oshima	The University of Tokyo
73	〃	アピバンボリラク　チャンウィット	東京大学	大学院新領域創成科学研究科	〃	Apibanboriak Chanwit	The University of Tokyo
74	カルシウムループ法によるメタン生成プロセスの開発	大友　順一郎	東京大学	大学院新領域創成科学研究科	Development of Ca looping process for production of methane	Junichiro Otomo	The University of Tokyo

No.	課題名	氏名	所属		Title	Name	Organization
75	〃	李　智漢	東京大学	大学院新領域創成科学研究科	〃	Jihan Lee	The University of Tokyo
76	プロトン伝導性固体電解質薄膜を用いた低温作動燃料電池・電解合成セルの開発	大友　順一郎	東京大学	大学院新領域創成科学研究科	Development of low-temperature solid oxide fuel cells and electrolysis cells using proton-conducting solid electrolyte thin films	Junichiro Otomo	The University of Tokyo
77	〃	松尾　拓紀	東京大学	大学院新領域創成科学研究科	〃	Hiroki Matsuo	The University of Tokyo
78	ケミカルループ燃焼法における酸素キャリアの反応モデリング	大友　順一郎	東京大学	大学院新領域創成科学研究科	Reaction modeling in chemical looping systems with new oxygen carrier materials	Junichiro Otomo	The University of Tokyo
79	〃	山村　泰平	東京大学	大学院新領域創成科学研究科	〃	Taihei Yamamura	The University of Tokyo
80	中温域でのアンモニア電解合成における新規電極触媒開発及び反応機構解明 (1)	大友　順一郎	東京大学	大学院新領域創成科学研究科	Development of new electrochemical catalyst for ammonia electrolysis and evaluation of reaction mechanism at intermediate temperature	Junichiro Otomo	The University of Tokyo
81	〃	今田　佳那	東京大学	大学院新領域創成科学研究科	〃	Kana Imata	The University of Tokyo
82	イオン及び電子伝導特性の制御による SOFC 性能の改善	大友　順一郎	東京大学	大学院新領域創成科学研究科	Improvement of solid-oxide electrolysis cells performance by controlling ionic and electronic transport properties.	Junichiro Otomo	The University of Tokyo
83	〃	オルティスコラレスフリアンアンドレス	東京大学	大学院新領域創成科学研究科	〃	Ortiz Corrales Julian Andres	The University of Tokyo
84	イオン一電子混合伝導体の異相界面の作製と輸送現象の解明	大友　順一郎	東京大学	大学院新領域創成科学研究科	Formation of heterojunction of mixed ionic electronic conductors and clarification of its transport phenomena	Junichiro Otomo	The University of Tokyo
85	〃	甚野　幸一	東京大学	大学院新領域創成科学研究科	〃	Koichi Jinno	The University of Tokyo
86	アンモニア電解合成の反応器設計	大友　順一郎	東京大学	大学院新領域創成科学研究科	Reactor design for ammonia electrosynthesis	Junichiro Otomo	The University of Tokyo
87	〃	福田　一峻	東京大学	大学院新領域創成科学研究科	〃	Kazutaka Fukuda	The University of Tokyo
88	スピンコート法による高 La/W 比のタングステン酸ランタン薄膜の低温合成およびセル性能評価	大友　順一郎	東京大学	大学院新領域創成科学研究科	Low temperature synthesis of high La/W ratio lanthanum tungstate thin film by spin coating and cell performance evaluation	Junichiro Otomo	The University of Tokyo
89	〃	戸田　亮輔	東京大学	大学院新領域創成科学研究科	〃	Ryousuke Toda	The University of Tokyo
90	中温域でのアンモニア電解合成における新規電極触媒開発及び反応機構解明 (2)	大友　順一郎	東京大学	大学院新領域創成科学研究科	Development of new electrochemical catalyst for ammonia electrolysis and evaluation of reaction mechanism at intermediate temperature	Junichiro Otomo	The University of Tokyo
91	〃	秋山　大樹	東京大学	大学院新領域創成科学研究科	〃	Daki Akiyama	The University of Tokyo

No.	課題名	氏名	所属		Title	Name	Organization
92	積層型燃料電池の輸送特性制御と電解合成への応用	大友　順一郎	東京大学	大学院新領域創成科学研究科	Control of transport properties of stacked fuel cells and its application to electrochemical synthesis	Junichiro Otomo	The University of Tokyo
93	〃	田島　星也	東京大学	大学院新領域創成科学研究科	〃	Seiya Tajima	The University of Tokyo
94	プロトン伝導固体酸化物を用いた鉄のアンモニア電解合成機構の解明	大友　順一郎	東京大学	大学院新領域創成科学研究科	Mechanism of Ammonia Electrosynthesis using Fe-based Catalysts with Proton-Conducting Solid Electrolyte	Junichiro Otomo	The University of Tokyo
95	〃	李　建毅	東京大学	大学院新領域創成科学研究科	〃	Chen-I Li	The University of Tokyo
96	アンモニア電解合成における選択性向上の検討	大友　順一郎	東京大学	大学院新領域創成科学研究科	Study on promotion of selectivity in ammonia electrosynthesis	Junichiro Otomo	The University of Tokyo
97	〃	山本　和範	東京大学	大学院新領域創成科学研究科	〃	Kazunori Yamamoto	The University of Tokyo
98	高温高圧水―アルコール混合溶媒が金属酸化物ナノ粒子の合成に与える影響の解明	大島　義人	東京大学	大学院新領域創成科学研究科	Research on the effect of water-alcohol mixture on metal oxide nanoparticle synthesis	Yoshito Oshima	The University of Tokyo
99	〃	劉　源	東京大学	大学院新領域創成科学研究科	〃	Yuan Liu	The University of Tokyo
100	メソポーラスマテリアル・グラフェンオキサイドに担持した金属触媒のキャラクタリゼーション	佐々木　岳彦	東京大学	大学院新領域創成科学研究科	Characterization of metal catalysts supported on mesoporous materials and graphene oxide	Takehiko Sasaki	The University of Tokyo
101	〃	木下　拓哉	東京大学	大学院新領域創成科学研究科	〃	Takuya Kinoshita	The University of Tokyo
102	超臨界水中での $NiFe_2O_4$/ 還元型酸化グラフェン粒子合成に関する研究	布浦　鉄兵	東京大学	環境安全研究センター	Study on supercritical water synthesis of $NiFe_2O_4$/reduced graphene oxide composite	Teppei Nunoura	The University of Tokyo
103	〃	周　暁雲	東京大学	大学院新領域創成科学研究科	〃	Xiaoyun Zhou	The University of Tokyo
104	超臨界水を利用した金属酸化物ナノ粒子の合成とその形態制御	大島　義人	東京大学	大学院新領域創成科学研究科	Synthesis and morphology control of metal oxide nanoparticles using supercritical water	Yoshito Oshima	The University of Tokyo
105	〃	織田　耕彦	東京大学	大学院新領域創成科学研究科	〃	Yasuhiko Orita	The University of Tokyo
106	チタン置換六方晶フェライトの化学組成と磁気異方性	植田　浩明	京都大学	大学院理学研究科	chemical composition and magnetic anisotropy of Ti-substituted hexaferrites	Hiroaki Ueda	Kyoto university
107	〃	奥津　陽太	京都大学	大学院理学研究科	〃	Yota Okutsu	Kyoto University
108	キャリアドープされたノーダルリング半金属における超伝導体探索	岡本　佳比古	名古屋大学	大学院工学研究科	Superconductivity in carrier-doped nodal-ring semimetal	Yoshihiko Okamoto	Nagoya University

No.	課題名	氏名	所属		Title	Name	Organization
109	高温高圧下で多軽元素が鉄ー含水ケイ酸塩系に及ぼす影響の解明	飯塚　理子	東京大学	大学院理学系研究科	Behavior of light elements in iron-silicate-water system under high pressure and high temperature	Riko Iizuka-Oku	The University of Tokyo
110	高圧下での $MoSi_2$ 型構造の $FeAl_2$ 結晶の作製	木村　薫	東京大学	大学院新領域創成科学研究科	High pressure synthesis of $MoSi_2$ type iron aluminide, $FeAl_2$ crystal	Kaoru Kimura	The University of Tokyo
111	〃	飛田　一樹	東京大学	大学院新領域創成科学研究科	〃	Kazuki Tobita	The University of Tokyo
112	希土類オルソフェライト単結晶成長とテラヘルツスピン制御	中嶋　誠	大阪大学	レーザー科学研究所	Single crystal growth for rare-earth orthoferrite and ultrafast terahertz spin control	Makoto Nakajima	Osaka University
113	〃	木本　翔大	大阪大学	レーザー科学研究所	〃	Shodai Kimoto	Osaka University
114	〃	小池　遥平	大阪大学	レーザー科学研究所	〃	Yohei Koike	Osaka University
115	マルチフェロイック関連物質における新規電子・構造物性の探求に関する研究	木村　剛	東京大学	大学院新領域創成科学研究科	Exploration of nontrivial electronic and structural properties in multiferroic-related materials	Tsuyoshi Kimura	The University of Tokyo
116	〃	木村　健太	東京大学	大学院新領域創成科学研究科	〃	Kenta Kimura	The University of Tokyo
117	〃	勝吉　司	東京大学	大学院新領域創成科学研究科	〃	Tsukasa Kazuyoshi	The University of Tokyo
118	〃	三澤　龍介	東京大学	大学院新領域創成科学研究科	〃	Ryusuke Misawa	The University of Tokyo
119	〃	林田　健志	東京大学	大学院新領域創成科学研究科	〃	Takeshi Hayashida	The University of Tokyo
120	〃	八木　直輝	東京大学	大学院新領域創成科学研究科	〃	Naoki Yagi	The University of Tokyo
121	強相関物質における回転対称性の破れとトポロジカル超伝導状態に関する研究	水上　雄太	東京大学	大学院新領域創成科学研究科	Studies on rotational symmetry breaking and topological superconductivity in strongly correlated electron systems	Yuta Mizukami	The University of Tokyo
122	〃	石田　浩祐	東京大学	大学院新領域創成科学研究科	〃	Kousuke Ishida	The University of Tokyo
123	〃	田中　桜平	東京大学	大学院新領域創成科学研究科	〃	Ohei Tanaka	The University of Tokyo
124	〃	石原　滉大	東京大学	大学院新領域創成科学研究科	〃	Kota Ishihara	The University of Tokyo
125	〃	辻井　優哉	東京大学	大学院新領域創成科学研究科	〃	Masaya Tsujii	The University of Tokyo

No.	課題名	氏名	所属		Title	Name	Organization
126	〃	斎藤　三樹彦	東京大学	大学院新領域創成科学研究科	〃	Mikihiko Saito	The University of Tokyo
127	外場制御可能な磁気超構造を有する物質の開発	有馬　孝尚	東京大学	大学院新領域創成科学研究科	Exploration of materials hosting controllable magnetic superstructure	Taka-hisa Arima	The University of Tokyo
128	〃	徳永　祐介	東京大学	大学院新領域創成科学研究科	〃	Yusuke Tokunaga	The University of Tokyo
129	〃	阿部　伸行	東京大学	大学院新領域創成科学研究科	〃	Nobuyuki Abe	The University of Tokyo
130	〃	藤間　友理	東京大学	大学院新領域創成科学研究科	〃	Yuri Fujima	The University of Tokyo
131	〃	近江　毅志	東京大学	大学院新領域創成科学研究科	〃	Tsuyoshi Omi	The University of Tokyo
132	〃	荒木 勇介	東京大学	大学院新領域創成科学研究科	〃	Araki Yusuke	The University of Tokyo
133	〃	佐藤　樹	東京大学	大学院新領域創成科学研究科	〃	Tatsuki Sato	The University of Tokyo
134	〃	山本　圭祐	東京大学	大学院新領域創成科学研究科	〃	Keisuke Yamamoto	The University of Tokyo
135	〃	渡辺　義人	東京大学	大学院新領域創成科学研究科	〃	Yoshito Watanabe	The University of Tokyo
136	〃	西　健太	東京大学	大学院新領域創成科学研究	〃	Kenta Nishi	The University of Tokyo
137	〃	柳内　晃	東京大学	大学院新領域創成科学研究科	〃	Hikaru Yagiuchi	The University of Tokyo
138	〃	尾亦　恭輔	東京大学	大学院新領域創成科学研究科	〃	Kyosuke Omata	The University of Tokyo
139	〃	磯貝　レオナ	東京大学	大学院新領域創成科学研究科	〃	Leona Isogai	The University of Tokyo
140	〃	吉田　健斗	東京大学	大学院新領域創成科学研究科	〃	Kento Yoshida	The University of Tokyo
141	バナジウムカルコゲナイドにおける動的短距離秩序状態の研究	片山　尚幸	名古屋大学	大学院工学研究科	Study of dynamic Short-Range ordering state in vanadium chalcogenides	Naoyuki Katayama	Nagoya University
142	〃	前田　秦	名古屋大学	大学院工学研究科	〃	Shin Maeda	Nagoya University

No.	課題名	氏名	所属		Title	Name	Organization
143	バナジウム硫化物・セレン化物におけるスピン軌道複合秩序状態	片山　尚幸	名古屋大学	大学院工学研究科	Spin-Orbital entangled ordered state in vanadium chalcogenides	Naoyuki Katayama	Nagoya University
144	〃	小島　慶太	名古屋大学	大学院応用物理学専攻	〃	Keita Kojima	Nagoya University
145	高温高圧下で多軽元素が鉄ー含水ケイ酸塩系に及ぼす影響の解明	フー　シュウジン	東京大学	大学院理学系研究科	Behavior of light elements in iron-silicate-water system under high pressure and high temperature	He Xuejing	The University of Tokyo
146	〃	市東　力	東京大学	大学院理学系研究科	〃	Chikara Shito	The University of Tokyo
147	強相関物質における回転対称性の破れと超伝導に関する研究	竹中　崇了	東京大学	大学院新領域創成科学研究科	Studies on rotational symmetry breaking and superconductivity in strongly correlated electron system	Takaaki Tanaka	The University of Tokyo

物質合成・評価設備 U クラス / Materials Synthesis and Characterization U Class Researcher

No.	課題名	氏名	所属		Title	Name	Organization
1	ペロブスカイト関連化合物の高圧合成	稲熊　宜之	学習院大学	理学部	High-pressure synthesis of perovskite-related compounds	Yoshiyuki Inaguma	Gakushuin University
2	〃	植田　紘一郎	学習院大学	理学部	〃	Koichiro Ueda	Gakushuin University
3	〃	森　紘夢	学習院大学	大学院自然科学研究科	〃	Hiromu Mori	Gakushuin University
4	〃	和泉　一成	学習院大学	大学院自然科学研究科	〃	Kazunari Izumi	Gakushuin University
5	誘起モット系における絶縁相､金属相（超伝導相）の磁化測定	宮川　和也	東京大学	大学院工学系研究科	Magnetism of Insulating Phase and Metallic(Superconductor) Phase in Organic Mott systems.	Kazuya Miyagawa	The University of Tokyo
6	燃料電池の電解質・電極の異相界面の解析と燃料電池の性能向上	大友　順一郎	東京大学	大学院新領域創成科学研究科	Analysis if heterogeneous inteface of electrolyte and electrode, and improvement of SOFC	Junichiro Otomo	The University of Tokyo
7	〃	黄　睿	東京大学	大学院新領域創成科学研究科	〃	Rui Huang	The University of Tokyo
8	高圧プレスによるカルサイト標準物質の合成	宮嶋　佑典	東京大学	大学院理学系研究科	Synthesis of calcite referance materials by a high-pressure press	Yusuke Miyajima	The University of Tokyo

長期留学研究員 / Long Term Young Researcher

No.	課題名	氏名	所属		Title	Name	Organization
1	有機半導体の分子吸着に伴って生じるトポロジカル表面状態の変化	北澤辰也	東京理科大学	大学院理工学研究科	Modification of Topological surface states upon adsorption of organic semiconductors	Tatsuya Kitazawa	Tokyo University of Science
2	PdPc の表面吸着によって生じる Cu(111) ショックレー状態の変化	下澤皐介	東京理科大学	理工学部	Modification of Cu(111)Shockley stateupon adsorption of PdPc	Kosuke Shimozawa	Tokyo University of Science

短期期留学研究員 / Short Term Young Researcher

No.	課題名	氏名	所属		Title	Name	Organization
1	単結晶表面上のメタンの解離吸着に関する表面科学研究	黄育杰	大阪大学	大学院工学研究科	Surface science study on methane dissociation over single crystal surfaces	Wong Yee Jie	Osaka University

令和元年度 中性子科学研究施設 共同利用課題一覧 / Joint Research List of Neutron Scattering Researcher 2019

No.	課題名	氏名	所属		Title	Name	Organization
・申請装置 4G: GPTAS							
1	GPTAS（汎用 3 軸中性子分光器）IRT 課題	佐藤　卓	東北大学	多元物質科学研究所	IRT project of GPTAS	Taku J Sato	Tohoku University
2	磁性準結晶中の隠れた磁気秩序の探索	佐藤　卓	東北大学	多元物質科学研究所	Hidden magnetic order in magnetic quasicrystals	Taku J Sato	Tohoku University
3	素励起に対する反転対称性の破れの影響	佐藤　卓	東北大学	多元物質科学研究所	Effect of non-centrosymmetricity to dispersions of elementary excitations	Taku J Sato	Tohoku University
4	歪んだ籠目格子遍歴磁性体 $Yb_3Ru_4Al_{12}$ の磁気構造	佐藤　卓	東北大学	多元物質科学研究所	Magnetic order in the 2D itinerant breathing kagome compound $Yb_3Ru_4Al_{12}$	Taku J Sato	Tohoku University
5	六方晶フェライト $Ba_2Zn_2Fe_{12}O_{22}$ および $BaFe_{12}O_{19}$ の超交換相互作用	内海　重宜	公立諏訪東京理科大学	工学部機械電気工学科	Superexchange interaction of hexagonal ferrites $Ba_2Zn_2Fe_{12}O_{22}$ and $BaFe_{12}O_{19}$	Shigenori Utsumi	Suwa University of Science
6	Sr_2RuO_4 の非弾性散乱	古川　はづき	お茶の水女子大学	基幹研究院 自然科学系	Inelastic neutron scattering experiments on Sr_2RuO_4	Hazuki Furukawa	Ochanomizu University
7	強磁性超伝導体における磁性と超伝導の研究	古川　はづき	お茶の水女子大学	基幹研究院 自然科学系	A study of magnetic state in ferromagnetic superconductors	Hazuki Furukawa	Ochanomizu University
8	空間反転対称性の破れた超伝導体の非弾性散乱	古川　はづき	お茶の水女子大学	基幹研究院 自然科学系	Inelastic neutron scattering experiments on non-centrosymmetric superconductors	Hazuki Furukawa	Ochanomizu University
9	トポロジカル超伝導体の非弾性散乱	古川　はづき	お茶の水女子大学	基幹研究院 自然科学系	Inelastic neutron scattering experiments on topological superconductors	Hazuki Furukawa	Ochanomizu University
10	二次元重い電子系化合物 $Ce(Te_{1-x}Se_x)_3$ の研究	小林　理気	琉球大学	理学部	Study of Two-Dimensional Heavy Fermion Compound $Ce(Te_{1-x}Se_x)_3$	Riki Kobayashi	University of the Ryukyus
11	パイロクロア反強磁性体 $Na_3T(CO_3)_2Cl$ の磁気励起	那波　和宏	東北大学	多元物質科学研究所	Spin excitations on the pyrochlore antiferromagnet $Na_3T(CO_3)_2Cl$	Kazuhiro Nawa	Tohoku University
12	量子スピン鎖におけるスピノンラシュバ分裂	那波　和宏	東北大学	多元物質科学研究所	Spinon Rashba splitting on the quantum spin chain	Kazuhiro Nawa	Tohoku University
13	反強磁性体 $CeNiC_2$ の Pt 置換効果	郷地　順	東京大学	物性研究所	Effect of Pt-substitution on the Antiferromagnetic Compound $CeNiC_2$	Jun Gouchi	The University of Tokyo
14	強誘電体の相転移機構（変位型及び秩序–無秩序型）に関する統一的理解の確立	重松　宏武	山口大学	教育学部	Establishment of the unified explanation about the phase transition mechanism (displacive and orderdisorder type) in Ferroelectrics	Hirotake Shigematsu	Yamaguchi University
15	スピンアイスにおけるトポロジカル相転移	門脇　広明	首都大学東京	理工学研究科物理学専攻	Topological phase transition in spin ice	Hiroaki Kadowaki	Tokyo Metoropolitan University

No.	課題名	氏名	所属		Title	Name	Organization
16	電気磁気交差相関現象を示す重い電子系反強磁性体 Ce_3TiBi_5 の磁気構造	阿曽　尚文	琉球大学	理学部物質地球科学科	Magnetic structure in a heavy fermion antiferromagnet Ce_3TiBi_5 exhibiting electromagnetic cross-correlation phenomenon	Naofumi Aso	University of the Ryukyus
17	熱電材料 Mg_3Sb_2 のフォノンダイナミクス	李　哲虎	産業技術総合研究所	省エネルギー研究部門	Phonon dynamics on thermoelectric material of Mg_3Sb_2	Chul-Ho Lee	National Institute of Advanced Industrial Science and Technology
・申請装置 5G: PONTA							
18	PONTA（高性能偏極中性子散乱装置）IRT 課題	益田　隆嗣	東京大学	物性研究所	IRT project of PONTA	Takatsugu Masuda	The university of tokyo
19	マグネトプランバイト型コバルト酸化物 $SrCo_{12}O_{19}$ の磁場誘起磁気秩序	浅井　晋一郎	東京大学	物性研究所	Field-induced magnetic order for magnetoplumbite-type cobalt oxide $SrCo_{12}O_{19}$	Shinichiro Asai	The University of Tokyo
20	メイプルリーフ格子物質 $MgMn_3O_7・3D_2O$ の粉末中性子回折実験	浅井　晋一郎	東京大学	物性研究所	Neutron Diffraction study of Maple Leaf Compound $MgMn_3O_7・3D_2O$	Shinichiro Asai	The University of Tokyo
21	メイプルリーフ格子物質 $MgMn_3O_7・3D_2O$ の中性子非弾性散乱	浅井　晋一郎	東京大学	物性研究所	Inelastic Neutron Scattering of Maple Leaf Compound $MgMn_3O_7・3D_2O$	Shinichiro Asai	The University of Tokyo
22	$Cu_2(4\text{-F-bza})_4(2\text{-mpyz})$ に吸着された酸素分子の磁気励起	浅井　晋一郎	東京大学	物性研究所	Magnetic Excitation in Oxygen Molecule Adsorbed in Nanoporous Metal Complex $Cu_2(4\text{-F-bza})_4(2\text{-mpyz})$	Shinichiro Asai	The University of Tokyo
23	スピン状態クロスオーバーが起こるダブルペロブスカイト型コバルト酸化物 Sr_2CoNbO_6 の中性子非弾性散乱研究	浅井　晋一郎	東京大学	物性研究所	Inelastic neutron scattering study for double perovskite cobalt oxide Sr_2CoNbO_6	Shinichiro Asai	The University of Tokyo
24	三角スピンチューブ $CsCrF_4$ の圧力下中性子回折	益田　隆嗣	東京大学	物性研究所	Neutron diffraction experiment on triangular spin tube $CsCrF_4$	Takatsugu Masuda	The University of Tokyo
25	鉄系超伝導体のスピン揺動	李　哲虎	産業技術総合研究所	省エネルギー研究部門	Spin fluctuations of iron-based superconductors	Chul-Ho Lee	National Institute of Advanced Industrial Science and Technology
26	磁場中の中性子回折を利用した $Ni_2V_2O_7$ のスピン系の決定	長谷　正司	物質・材料研究機構	中性子散乱グループ	Determination of the spin system in $Ni_2V_2O_7$ using neutron diffraction in magnetic fields	Masashi Hase	National Institute for Materials Science
・申請装置 6G: TOPAN							
27	TOPAN（東北大理：３軸型偏極中性子分光器）IRT 課題	藤田　全基	東北大学	金属材料研究所	IRT project of TOPAN	Masaki Fujita	Tohoku University
28	近藤半金属におけるワイルフェルミオンの磁気状態	岩佐　和晃	茨城大学	フロンティア応用原子科学研究センター	Magnetic states of Weyl fermion in Kondo semimetals	Kazuaki Iwasa	Ibaraki University
29	T' 構造銅酸化物 $Pr_{2-x}Ca_xCuO_4$ における磁気相関と超伝導の研究	藤田　全基	東北大学	金属材料研究所	Study of spin correlations and superconductivity in T'-structured cuprate oxide $Pr_{2-x}Ca_xCuO_4$	Masaki Fujita	Tohoku University
30	PLCCO の格子振動にみられる超伝導対称性の観測	池内　和彦	総合科学研究機構	中性子科学センター	Phonons and superconducting gap in PLCCO	Kazuhiko Ikeuchi	Comprehensive Research Organization for Science and Society

No.	課題名	氏名	所属		Title	Name	Organization
・申請装置 C1-1: HER							
31	HER (高エネルギー分解能 3 軸型中性子分光器) IRT 課題	益田　隆嗣	東京大学	物性研究所	IRT project of HER	Takatsugu Masuda	The university of tokyo
32	a-$Cu_2V_2O_7$ のマグノン電場効果	佐藤　卓	東北大学	多元物質科学研究所	Inelastic neutron scattering measurements on the a-$Cu_2V_2O_7$ under electric field	Taku J Sato	Tohoku University
33	量子スカーミオン励起の探索	佐藤　卓	東北大学	多元物質科学研究所	Quantum magnetic-skyrmion excitation	Taku J Sato	Tohoku University
34	素励起に対する反転対称性の破れの影響	佐藤　卓	東北大学	多元物質科学研究所	Effect of non-centrosymmetricity to dispersions of elementary excitations	Taku J Sato	Tohoku University
35	歪んだ籠目格子遍歴磁性体 $Yb_3Ru_4Al_{12}$ の磁気構造	佐藤　卓	東北大学	多元物質科学研究所	Magnetic order in the 2D itinerant breathing kagome compound $Yb_3Ru_4Al_{12}$	Taku J Sato	Tohoku University
36	近藤半金属におけるワイルフェルミオンの磁気状態	岩佐　和晃	茨城大学	フロンティア応用原子科学研究センター	Magnetic states of Weyl fermion in Kondo semimetals	Kazuaki Iwasa	Ibaraki University
37	T' 構造銅酸化物 $Pr_{2-x}Ca_xCuO_4$ における磁気相関と超伝導の研究	藤田　全基	東北大学	金属材料研究所	Study of spin correlations and superconductivity in T'-structured cuprate oxide $Pr_{2-x}Ca_xCuO_4$	Masaki Fujita	Tohoku University
38	量子スピン液体の研究	門脇　広明	首都大学東京	理工学研究科物理学専攻	Quantum spin liquid	Hiroaki Kadowaki	Tokyo Metoropolitan University
39	希土類元素を含むフラストレート系金属間化合物の中性子非弾性散乱実験による研究	植田　大地	沖縄科学技術大学院大学	量子物質科学ユニット	Study of dimer structure in frustrated Kondo compounds Ce_5Si_3 and Ce_5Ga_2Ge	Daichi Ueta	Okinawa Institute of Science and Technology Graduate University
40	YIG におけるマグノンポーラロン誘起反交差ギャップ	南部　雄亮	東北大学	金属材料研究所	Magnon polaron induced anticrossing gap in YIG	Yusuke Nambu	Tohoku University
・申請装置 C1-2: SANS-U							
41	SANS-U（二次元位置測定小角散乱装置）IRT 課題	柴山　充弘	東京大学	物性研究所	IRT project of SANS-U	Mitsuhiro Shibayama	The university of tokyo
42	極めて均一な高分子ゲルの一軸伸張時の網目構造の評価	Li　Xiang	東京大学	物性研究所中性子科学研究施設	Investigation of network structure of extremely homogeneous gel under uniaxial elongation	Xiang Li	The University of Tokyo
43	一軸伸長下における重水素化ラベリングを用いた ゲル内の高分子鎖の挙動	Li　Xiang	東京大学	物性研究所中性子科学研究施設	Deuterated polymer chain behavior in gel under uniaxial deformation	Xiang Li	The University of Tokyo
44	小角中性子散乱とセグメント重水素化によるマルチドメインタンパク質のドメイン運動の可視化	井上　倫太郎	京都大学	複合原子力科学研究所	Visualization of domain motion of multi-domain protein through segment deuteration and small-angle neutron scattering	Rintaro Inoue	Kyoto University
45	磁性準結晶中の隠れた磁気秩序の探索	佐藤　卓	東北大学	多元物質科学研究所	Hidden magnetic order in magnetic quasicrystals	Taku J Sato	Tohoku University

No.	課題名	氏名	所属		Title	Name	Organization
46	中性子小角散乱実験による Sr_2RuO_4 の異常金属状態の研究	古川　はづき	お茶の水女子大学	基幹研究院 自然科学系	Anomalous vortex state in Sr_2RuO_4 studied by SANS experiments	Hazuki Furukawa	Ochanomizu University
47	空間反転対称性の破れた超伝導体のヘリカル磁束格子の観測	古川　はづき	お茶の水女子大学	基幹研究院 自然科学系	Herical vortex phase on non-centrosymmetric superconductors	Hazuki Furukawa	Ochanomizu University
48	強磁性超伝導体における自発的磁束格子構造の研究	古川　はづき	お茶の水女子大学	基幹研究院 自然科学系	Spontaneous vortex phase in ferromagnetic superconductors	Hazuki Furukawa	Ochanomizu University
49	トポロジカル超伝導体の磁束格子	古川　はづき	お茶の水女子大学	基幹研究院 自然科学系	Vortex phase in topological superconductors	Hazuki Furukawa	Ochanomizu University
50	生体適合性ポリオリゴエチレングリコールメタクリレートゲルの微細構造変化の調査	呉羽　拓真	東京大学	物性研究所	Investigation of Changes in the Microscopic Structure of Poly(oligo ethylene glycol methacrylate)-based Hydrogels.	Takuma Kureha	The University of Tokyo
51	Phase diagram of the moving magnetic skyrmion lattice with plastic deformation in MnSi under high electric current	奥山　大輔	東北大学	多元物質科学研究所	Phase diagram of the moving magnetic skyrmion lattice with plastic deformation in MnSi under high electric current	Daisuke Okuyama	Tohoku University
52	完全に単分散な逆ミセルの構造可視化	藤井　翔太	北九州市立大学	環境技術研究所	Structural analysis of perfectly monodisperse reverse micelles	Shota Fujii	The University of Kitakyushu
53	SANS 測定による分子透過性ベシクルの poly(propylene oxide) 層中の水和量の決定	西村　智貴	京都大学	工学研究科　高分子化学専攻	Elucidating the degree of hydration of the poly (propylene oxide) block in carbohydrate-b-poly(propylene oxide) block-copolymer vesicle membranes by SANS measurements	Tomoki Nishimura	Kyoto University
54	界面不活性の働きをする界面活性剤	貞包　浩一朗	同志社大学	生命医科学部医情報学科	Surfactant molecules behaving as a surface-inactive agent	Koichiro Sadakane	Doshisha University
55	高圧条件下における２成分混合溶液の新奇な臨界挙動	貞包　浩一朗	同志社大学	生命医科学部医情報学科	Novel critical behavior in a mixture of water / organic solvent under high-pressure condition	Koichiro Sadakane	Doshisha University
56	イミダゾリウム系イオン液体中におけるエタノールクラスターの形成	高椋　利幸	佐賀大学	理工学部	Formation of Ethanol Clusters in Imidazolium-based Ionic Liquids	Toshiyuki Takamuku	Saga University
57	中性子小角散乱によるマルチドメイン蛋白質の溶液構造解析	中川　洋	日本原子力研究開発機構	階層構造研究グループ	Analysisi of solution structure of multi-domain protein by SANS	Hiroshi Nakagawa	Japan Atomic Energy Agency
・申請装置 C2-3-1: iNSE							
58	iNSE（中性子スピンエコー分光器)IRT 課題	Li　Xiang	東京大学	物性研究所中性子科学研究施設	IRT project of iNSE	Xiang Li	The University of Tokyo
59	相互作用面の配向に連動したトリユビキチンダイナミクスの研究	杉山　正明	京都大学	複合原子力科学研究所	Investigation on tri-ubiquitin dynamics associated with configurations of interaction interfaces	Masaaki Sugiyama	Kyoto University
60	界面不活性の働きをする界面活性剤	貞包　浩一朗	同志社大学	生命医科学部医情報学科	Surfactant molecules behaving as a surface-inactive agent	Koichiro Sadakane	Doshisha University
61	マルチドメイン蛋白質の動的構造と機能発現との関係性の解析	中川　洋	日本原子力研究開発機構	階層構造研究グループ	Analysis of relationship between structural dynamics and function of multi-domain protein	Hiroshi Nakagawa	Japan Atomic Energy Agency

No.	課題名	氏名	所属		Title	Name	Organization
62	$Mn_{1-x}Fe_xSi$ におけるスキルミオンのダイナミクス	左右田　稔	理化学研究所	創発物性科学研究センター	dynamics of skyrmion of $Mn_{1-x}Fe_xSi$	Minoru Soda	RIKEN
63	リン脂質膜の粘弾性に対するモデルスクランブラーゼペプチドの影響	中尾　裕之	富山大学	大学院医学薬学研究部	Effect of a model scramblase peptide on viscoelastic properties of phspholipid bilayers	Hiroyuki Nakao	University of Toyama
・申請装置 C3-1-1: AGNES							
64	AGNES（高分解能パルス冷中性子分光器）IRT 課題	山室　修	東京大学	物性研究所	IRT project of AGNES	Osamu Yamamuro	The University of Tokyo
65	PdPt 合金ナノ粒子中の水素の速いダイナミクス	山室　修	東京大学	物性研究所	Fast dynamics of hydrogen atoms in PdPt alloy nanoparticles	Osamu Yamamuro	The University of Tokyo
66	PdPt 合金ナノ粒子中の水素の遅いダイナミクス	山室　修	東京大学	物性研究所	Slow dynamics of hydrogen atoms in PdPt alloy nanoparticles	Osamu Yamamuro	The University of Tokyo
67	高水素密度・高 Li 伝導物質 Li_5MoH_{11} 中の水素の速いダイナミクス	山室　修	東京大学	物性研究所	Fast dynamics of Li_5MoH_{11} with high hydrogen-density and high lithium conductivity	Osamu Yamamuro	The University of Tokyo
68	高水素密度・高 Li 伝導物質 Li_5MoH_{11} 中の水素の遅いダイナミクス	山室　修	東京大学	物性研究所	Slow dynamics of Li_5MoH_{11} with high hydrogen-density and high lithium conductivity	Osamu Yamamuro	The University of Tokyo
69	超高エントロピー液体・アルキル化パーフルオロベンゼンの遅いダイナミクス	山室　修	東京大学	物性研究所	Slow dynamics of super-high entropy liquids alkylated perfluorobenzenes	Osamu Yamamuro	The University of Tokyo
・申請装置 C3-1-2: MINE1							
70	MINE1（京大複合研：多層膜中性子干渉計・反射率計）IRT 課題	日野　正裕	京都大学	複合原子力科学研究所	MINE1 (Multilayer neutron interferometer and reflectmeter)	Masahiro Hino	Kyoto University
71	MINE2（京大複合研：多層膜中性子干渉計・反射率計）IRT 課題	日野　正裕	京都大学	複合原子力科学研究所	MINE2 (Multilayer neutron interferometer and reflectmeter)	Masahiro Hino	Kyoto University
72	高分子 / 水界面における生体分子の吸着状態の解析	松野　寿生	九州大学	大学院工学研究院　応用化学部門（機能）	Analyses of adsorbed biomolecules at the polymer/water interface	Hisao Matsuno	Kyushu University
73	混合液体中における高分子薄膜の膨潤挙動	田中　敬二	九州大学	大学院工学研究院　応用化学部門	Swelling Behavior of Polymer Thin Films in Mixed Non-solvents	Keiji Tanaka	Kyushu University
・申請装置 T1-1: HQR							
74	HQR(高分解能中性子散乱装置)IRT 課題	大山　研司	茨城大学	理工学研究科	IRT project of HQR	Kenji Ohoyama	Ibaraki University
75	Rb_2MoO_4 における多形転移とソフトフォノン	重松　宏武	山口大学	教育学部	Polymorph Transition and Soft Phonon in Rb_2MoO_4	Hirotake Shigematsu	Yamaguchi University

No.	課題名	氏名	所属		Title	Name	Organization
76	強誘電体の相転移機構（変位型及び秩序−無秩序型）に関する統一的理解の確立	重松　宏武	山口大学	教育学部	Establishment of the unified explanation about the phase transition mechanism (displacive and orderdisorder type) in Ferroelectrics	Hirotake Shigematsu	Yamaguchi University
77	2 等辺三角格子 Ising 磁性体 $CoNb_2O_6$ のワニエ点における磁気相関	満田　節生	東京理科大学	理学部　物理	Magnetic correlation at Wannier point in isosceles-triangular lattice Ising magnet $CoNb_2O_6$	Setsuo Mitsuda	Tokyo University of Science
・申請装置 T1-2: AKANE							
78	AKANE（東北大金研：三軸型中性子分光器 ）IRT 課題	藤田　全基	東北大学	金属材料研究所	IRT project of AKANE	Masaki Fujita	Tohoku University
79	T' 構造銅酸化物 $Pr_{2-x}Ca_xCuO_4$ における磁気相関と超伝導の研究	藤田　全基	東北大学	金属材料研究所	Study of spin correlations and superconductivity in T'-structured cuprate oxide $Pr_{2-x}Ca_xCuO_4$	Masaki Fujita	Tohoku University
80	鉄系超伝導体のスピン揺動	李　哲虎	産業技術総合研究所	省エネルギー研究部門	Spin fluctuations of iron-based superconductors	Chul-Ho Lee	National Institute of Advanced Industrial Science and Technology
・申請装置 T1-3 HERMES							
81	HERMES（東北大金研：中性子粉末回折装置）IRT 課題	南部　雄亮	東北大学	金属材料研究所	IRT project of HERMES	Yusuke Nambu	Tohoku University
82	歪んだ籠目格子遍歴磁性体 $Yb_3Ru_4Al_{12}$ の磁気構造	佐藤　卓	東北大学	多元物質科学研究所	Magnetic order in the 2D itinerant breathing kagome compound $Yb_3Ru_4Al_{12}$	Taku J Sato	Tohoku University
83	Ga-Pd-Tb 2/1 近似結晶の磁気構造	佐藤　卓	東北大学	多元物質科学研究所	Neutron-diffraction study on antiferromagnetic structure in the Ga-Pd-Tb 2/1 quasicrystalline appoximant	Taku J Sato	Tohoku University
84	反転対称性の破れた 1 次元反強磁性体 $Cu_2(MoO_4)(SeO_3)$ の磁気構造	佐藤　卓	東北大学	多元物質科学研究所	Magnetic structure of noncentrosymmetric 1D antiferromagnet $Cu_2(MoO_4)(SeO_3)$	Taku J Sato	Tohoku University
85	Majumdar-Ghosh 物質の中性子粉末回折	南部　雄亮	東北大学	金属材料研究所	Neutron powder diffraction study on a Majumdar-Ghosh system	Yusuke Nambu	Tohoku University
86	PdRuRh ナノ粒子の構造と触媒活性	山室　修	東京大学	物性研究所	Structure and catalytic activity of PdRuRh alloy nanoparticles	Osamu Yamamuro	University of Tokyo
87	二重 K_2NiF_4 型 $(La_{1/2}Sr_{1/2})_4MnCoO_8$ と $(La_{1/2}Sr_{1/2})_4MnNiO_8$ における強磁性とカチオンオーダー	山本　孟	東北大学	多元物質科学研究所	Ferromagnetism and cation-ordering in double-K_2NiF_4-type $(La_{1/2}Sr_{1/2})_4MnCoO_8$ and $(La_{1/2}Sr_{1/2})_4MnNiO_8$	Hajime Yamamoto	Tohoku University
88	正方晶 Mn 化合物における過剰 Mn の結晶構造特性と磁気特性	岡田　宏成	東北学院大学	工学部	Structural and Magnetic properties of excess Mn in Tetragonal Mn Compound	Hironari Okada	Tohoku Gakuin University
89	近藤半金属におけるワイルフェルミオンの磁気状態	岩佐　和晃	茨城大学	フロンティア応用原子科学研究センター	Magnetic states of Weyl fermion in Kondo semimetals	Kazuaki Iwasa	Ibaraki University
90	$EuTGe_3$ (T=Rh, Ir) の磁気構造	松村　武	広島大学	大学院先端物質科学研究科	Magnetic Structure of $EuTGe_3$ (T=Rh, Ir)	Takeshi Matsumura	Hiroshima University

No.	課題名	氏名	所属		Title	Name	Organization
91	新規酸化物イオン伝導体の結晶構造解析とイオン伝導経路の解明	藤井　孝太郎	東京工業大学	理学院化学系	Crystal Structure Analysis and Investigation of Ion Diffusion Path of Novel Oxide-Ion Conductors	Kotaro Fujii	Tokyo Institute of Technology
92	T' 構造銅酸化物の超伝導発現と結晶構造の関係	藤田　全基	東北大学	金属材料研究所	Relation between superconducting mechanism and crystal structure in T' cuprate oxide	Masaki Fujita	Tohoku University
93	量子臨界点近傍にある $YbCo_2Zn_{20}$ の置換系試料の結晶構造と磁気構造	阿曽　尚文	琉球大学	理学部物質地球科学科	Crystal and magnetic structures in doped systems of $YbCo_2Zn_{20}$ in vicinity of a quantum critical point	Naofumi Aso	University of the Ryukyus
94	電気磁気交差相関現象を示す重い電子系反強磁性体 Ce_3TiBi_5 の磁気構造	阿曽　尚文	琉球大学	理学部物質地球科学科	Magnetic structure in a heavy fermion antiferromagnet Ce_3TiBi_5 exhibiting electromagnetic cross-correlation phenomenon	Naofumi Aso	University of the Ryukyus
95	擬一次元梯子格子鉄系化合物の磁気構造解析	青山　拓也	東北大学	理学研究科物理学専攻	Magnetic structure analysis of quasi one-dimensional ladder lattice iron compound	Takuya Aoyama	Tohoku University
96	新しい層状コバルト酸化物の磁気構造	山田　幾也	大阪府立大学	大学院工学研究科	Magnetic structures of novel layered cobalt oxides	Ikuya Yamada	Osaka Prefecture University
・申請装置 T2-2: FONDER							
97	FONDER(中性子 4 軸回折装置)IRT 課題	木村　宏之	東北大学	多元物質科学研究所	IRT proposal for FONDER (Neutron 4-circle diffractometer)	Hiroyuki Kimura	Tohoku University
98	量子スピンの三量体構造をもつ $Na_2Cu_3Ge_4O_{12}$ の単結晶による磁気構造解析	安井　幸夫	明治大学	理工学部	Magnetic Structure analysis of S=1/2 linear trimer system $Na_2Cu_3Ge_4O_{12}$ single-crystal	Yukio Yasui	Meiji University
99	塑性歪みを加えた Pt_3Fe 反強磁性体における強磁性の発現機構	小林　悟	岩手大学	理工学部	Mechanism of ferromagnetism in plastically deformed Pt_3Fe antiferromagnet	Satoru Kobayashi	Iwate University
100	マルチフェロイック $Tb_{0.5}Gd_{0.5}Mn_2O_5$ における磁気構造と強誘電性の研究	木村　宏之	東北大学	多元物質科学研究所	Magnetic structure and its relevance to the ferroelectricity in multiferroic $Tb_{0.5}Gd_{0.5}Mn_2O_5$	Hiroyuki Kimura	Tohoku University
101	T'-type Pr_2CuO_4 における結晶構造の還元効果	木村　宏之	東北大学	多元物質科学研究所	$O_x$ygen reduction effect on the crystal structure in the T' -structure of Pr_2CuO_{4+y}	Hiroyuki Kimura	Tohoku University
102	typeIII 型反強磁性体 Pt-Mn における整合ー非整合磁気相転移	高橋　美和子	筑波大学	数理物資系	Commensurate-Incommensurate Magnetic Phase Transition in Type-III Anti-ferromagnet Pt-Mn	Miwako Takahashi	Tsukuba University
・申請装置 Accessory							
103	アクセサリー IRT 課題	上床　美也	東京大学	物性研究所	IRT project of Accessory	Yoshiya Uwatoko	The University of Tokyo

令和元年度 軌道放射物性研究施設 共同利用課題一覧 / Joint Research List of Syncrotron Radiation Researcher 2019

播磨分室　BL07LSU / Harima Branch BL07LSU

No.	課題名	氏名	所属		Title	Name	Organization
1	高エネルギー密度二次電池正極材料のオペランド軟 X 線発光分光	朝倉　大輔	(国) 産業技術総合研究所	省エネルギー研究部門	Operando soft x-ray emission spectroscopy of rechargeable-battery cathode materials with high energy density	Daisuke Asakura	National Institute of Advanced Industrial Science and Technology
2	全固体リチウムイオン電池を用いたオペランド軟 X 線発光分光測定の開発	朝倉　大輔	(国) 産業技術総合研究所	省エネルギー研究部門	Development of operando soft X-ray emission spectroscopy by use of all-solid-state Li-ion battery	Daisuke Asakura	National Institute of Advanced Industrial Science and Technology
3	銅酸化物超伝導体 $Pr_{1.4-x}La_{0.6}Ce_xCuO_4$ における２キャリア状態の検証	石井　賢司	量子科学技術研究開発機構	放射光科学研究センター	Verification of two-carrier state in the cuprate superconductors $Pr_{1.4-x}La_{0.6}Ce_xCuO_4$	Kenji Ishii	National Institute for Quantum and Radiological Science and Technology
4	磁場中共鳴非弾性軟 X 線散乱（SX-RIXS）による Co_2FeSi および Mn_2VAl ホイスラー合金単結晶のスピン偏極電子状態の研究	梅津　理恵	東北大学	金属材料研究所	Spin-polarized electronic state of single crystal Co_2FeSi and Mn_2VAl Heusler alloys probed by resonant inelastic soft X-ray scattering (SX-RIXS) in magnetic field	Rie Umetsu	Tohoku University
5	高分解能軟 X 線発光分光によるスピネル型正極材料の酸素レドックス反応の解明	大久保　將史	東京大学	工学系研究科	Clarification of the oxygen redox reaction in spinel-type cathode materials by high-energy-resolution soft x-ray emission spectroscopy	Masashi Okubo	The University of Tokyo
6	アルカリイオン脱挿入による遷移金属酸化物の機能制御と電子状態との関連性の解明	大久保　將史	東京大学	工学系研究科	Investigation of relationship between the electronic structure and functionality in transition-metal oxides controlled by alkali-ion insertion/extraction	Masashi Okubo	The University of Tokyo
7	水素結合状態解析が導くレドックスフロー電池の溶媒和・脱溶媒和エネルギーの解明	大平　昭博	(国) 産業技術総合研究所	省エネルギー研究部門	Study on the local hydrogen bond of water to resolve the free energy of solvation and desolvation in redox flow batteries	Akihiro Oohira	National Institute of Advanced Industrial Science and Technology
8	PbS 量子ドット太陽電池における光励起キャリアの動的挙動に及ぼすサイズ効果と保護層の検証	小澤　健一	東京工業大学	大学院理工学研究科	Effect of size and capping layers of PbS quantum dots on photoexcited carrier dynamics in PbS quantum dot photovoltaic cell	Kenichi Ozawa	Tokyo Institute of Technology
9	硫化サマリウム SmS の光誘起価数転移の観測	木村　真一	大阪大学	大学院生命機能研究科	Direct observation of photo-induced valence transition of samarium monosulfide SmS	Shinichi Kimura	Osaka University
10	イットリウムドープ硫化サマリウムの温度・光誘起価数転移の観測	木村　真一	大阪大学	大学院生命機能研究科	Direct observation of thermal- and photo-induced valence transition of yttrium-doped samarium monosulfide $Sm_{1-x}Y_xS$	Shinichi Kimura	Osaka University
11	表面修飾パラジウムモデル触媒を用いた低温メタン酸化カップリング反応のオペランド雰囲気光電子分光測定	小板谷　貴典	分子科学研究所	物質分子科学研究領域	Low-temperature methane oxidative coupling on modified Pd model catalysts studied by operando AP-XPS	Takanori Koitaya	Institute for Molecular Science
12	n 型鉄系強磁性半導体におけるスピン偏極電荷移動の検証	小林　正起	東京大学	大学院工学系研究科	Configulation interaction in iron-based ferromagnetic semiconductors	Masaki Kobayashi	The University of Tokyo
13	X 線スペクトルイメージングによる p^+-WSe_2/n-MoS_2 ヘテロ接合 TFET デバイス構造における接合界面の電子状態解明	永村　直佳	(国) 物質・材料研究機構	高エネルギー光解析グループ	Investigation of local interface states in p^+-WSe_2/n-MoS_2 hetero junctions in TFET device structure	Naoka Nagamura	National Institute for Materials Science
14	生体親和性高分子中の中間水の性質解明に向けた軟 X 線吸収・発光分光解析	西村　慎之介	九州大学	先導物質化学研究所	Soft X-ray absorption and emission spectroscopy of the intermediate water in biocompatible polymers	Shinnosuke Nishimura	Kyushu University
15	サイト選択・時分割光電子ホログラフィーの確立とシリセン形成過程の観測	林　好一	名古屋工業大学	物理工学科	Development of site-selective and time-resolved photoelectron holography and its application to the structural observation of silicene formation	Kouichi Hayashi	Nagoya Institute of Technology

No.	課題名	氏名	所属		Title	Name	Organization
16	サイト選択及び時間分解光電子ホログラフィーによるシリセンの形成・相転移過程の原子レベル構造観察	林　好一	名古屋工業大学	物理工学科	Atomic level structural observation of formation and phase transition of silicence using site-selective and time-resolved photoelectron holography	Kouichi Hayashi	Nagoya Institute of Technology
17	原子レベルで制御されたモデル生体適合性有機分子表面上の界面水の電子状態観測	林　智広	東京工業大学	物理工学院	Analysis of the electronic structure of interfacial water formed on model biocompatible organic surfaces	Tomohiro Hayashi	Tokyo Institute of Technology
18	高速偏光スイッチングを利用した金属 Fe の磁気光学定数の膜厚依存性の測定	平田　靖透	東京大学	物性研究所	Measurement of the thickness dependence of the magnet-optical constants of metal Fe using fast polarization switching	Yasuyuki Hirata	The University of Tokyo
19	高速偏光スイッチングを利用した磁気光学測定による金属 Co の複素誘電率の決定	平田　靖透	東京大学	物性研究所	Determination of the complex permittivity of Co metal by magneto-optical measurement using fast polarization switching	Yasuyuki Hirata	The University of Tokyo
20	多次元オペランド X 線光電子分光の創出 (I)　産官学連携モデル試料の選定	吹留　博一	東北大学	電気通信研究所	Creation of multi-dimensional operando photoelectron spectroscopy (I) Selection of industry-government-academia collaborative model sample	Hirokazu Fukidome	Tohoku University
21	顕微共鳴光電子分光による全個体 Li イオン電池正極材料のオペランド測定	細野　英司	(国) 産業技術総合研究所	省エネルギー研究部門	Operando measurement of cathode materials for all-solid-state-lithium ion batteries by resonant X-ray photoemission microspectroscopy	Eiji Hosono	National Institute of Advanced Industrial Science and Technology
22	硫化物固体電解質を用いた単結晶 $LiNi_xCo_yAl_zO_2$ の顕微光電子マッピング測定	細野　英司	(国) 産業技術総合研究所	省エネルギー研究部門	Micro-XPS mapping measurement of single crystalline $LiNi_xCo_yAl_zO_2$/sulfide-based solid-state electrolyte	Eiji Hosono	National Institute of Advanced Industrial Science and Technology
23	軟 X 線非弾性散乱、非弾性回折を用いた生体高分子や多糖、電解液における水の役割と水和水の電子状態の研究	宮脇　淳	東京大学	物性研究所	Soft X-ray inelastic scattering and diffraction techniques applied for the study on the role of water and hydration in biopolymers, polysaccharides and electrolytes	Jun Miyawaki	The University of Tokyo
24	マグノニクス物質の SX-RIXS と散乱 X 線の偏光解析	宮脇　淳	東京大学	物性研究所	SX-RIXS and Polarization Analysis of Scattered X-ray of Magnonic Materials	Jun Miyawaki	The University of Tokyo
25	SX-RIXS と X 線偏光歳差分光によるマグノンのオペランド観測	宮脇　淳	東京大学	物性研究所	Operando observation of magnon by SX-RIXS and X-ray polarization precession spectroscopy	Jun Miyawaki	The University of Tokyo
26	時分割コヒーレント軟 X 線回折イメージングによる超高速磁気ダイナミクス研究	山崎　裕一	(国) 物質・材料研究機構	統合型材料開発・情報基盤部門	Ultra-fast magnetic dynamics revealed by time-resolved coherent soft x-ray diffraction imaging	Yuichi Yamasaki	National Institute for Materials Science
27	軟 X 線発光分光による高容量正極材料のアニオンレドックスの解明	藪内　直明	横浜国立大学	大学院理工学府	Investigation of the anion redox chemistry in high-capacity cathode materials by soft X-ray emission spectroscopy	Naoaki Yabuuchi	Yokohama National University
28	生体親和性ポリマー中の中間水および Li 過剰系正極の酸素レドックスにおける酸素の電子状態解析	山添　康介	東京大学	物性研究所	Electronic State analysis of oxygen in intermediate water in biocompatible polymers and positive electrode including excess lithium in Li ion battery by XAS and RIXS	Kosuke Yamazoe	The University of Tokyo
29	プラズモン増強サバティエ反応の時間分解オペランド軟 X 線分光観測	山本　達	東京大学	物性研究所	Plasmon-enhanced Sabatier reaction studied by time-resolved Operando soft X-ray spectroscopy	Susumu Yamamoto	The University of Tokyo
30	新規時間分解 X 線吸収分光法による光触媒材料における非占有状態キャリアダイナミクスの解明	山本　達	東京大学	物性研究所	Unoccupied states carrier dynamics in photocatalytic materials revealed by a novel time-resolved X-ray absorption spectroscopy	Susumu Yamamoto	The University of Tokyo
31	ルテニウム酸化物の電場印加下軟 X 線吸収・発光分光	吉田　鉄平	京都大学	大学院人間・環境学研究科	Soft x-ray absorption and emission studies of Ruthenium oxides under electric field	Teppei Yoshida	Kyoto University
32	オペランド XPS による単原子合金 Pd-Cu モデル触媒における CO_2 水素化反応の研究	吉信　淳	東京大学	大学院新領域創成科学研究科	Operando XPS study of CO_2 hydrogenation on a single-atom alloy Pd-Cu model catalyst	Jun Yoshinobu	The University of Tokyo

No.	課題名	氏名	所属		Title	Name	Organization
33	雰囲気 XPS によるナノ合金粒子および金属ヒドリド錯体の電子状態の研究	吉信　淳	東京大学	大学院新領域創成科学研究科	AP-XPS study of Electronic states of metal nano particles and metal hydride complex	Jun Yoshinobu	The University of Tokyo
34	Time resolved XAS study on the charge carrier dynamics on photoelectrodes in nanoseconds regions	Frank de Groot	Utrecht University		Time resolved XAS study on the charge carrier dynamics on photoelectrodes in nanoseconds regions	Frank de Groot	Utrecht University
35	Investigation of the Iron Doping Role in Cobalt Oxide Water Oxidation Catalysts using Co 2p3d RIXS	Olaf Ruediger	Max Plank Institute for Chemical Energy Conversion		Investigation of the Iron Doping Role in Cobalt Oxide Water Oxidation Catalysts using Co 2p3d RIXS	Olaf Ruediger	Max Plank Institute for Chemical Energy Conversion
36	Investigation of Cobalt Oxide Electrodeposited Self-Repair Thin Films for Water OxidationCatalysts using Co 2p3d RIXS	Olaf Ruediger	Max Plank Institute for Chemical Energy Conversion		Investigation of Cobalt Oxide Electrodeposited Self-Repair Thin Films for Water OxidationCatalysts using Co 2p3d RIXS	Olaf Ruediger	Max Plank Institute for Chemical Energy Conversion

柏キャンパス E 棟 / Laser and Synchrotron Research Laboratory in Kashiwa

No.	課題名	氏名	所属		Title	Name	Organization
1	スピン分解角度分解光電子分光による V_2AlC のスピン偏極状態の研究	伊藤　孝寛	名古屋大学	シンクロトロン光科学研究センター	Spin- and angle-resolved photoemission study of spin-polarized electronic structure of V_2AlC	Takahiro Ito	Nagoya University
2	スピン分解角度分解光電子分光による層状 MAX 層化合物のスピン偏極状態の研究	伊藤　孝寛	名古屋大学	シンクロトロン光科学研究センター	Spin- and angle-resolved photoemission study of spin-polarized electronic structure of nanolamellar MAX phase compounds	Takahiro Ito	Nagoya University
3	半導体基板上の金属的擬一次元表面状態におけるフェルミ準位近傍のスピン偏極構造	大坪　嘉之	大阪大学	生命機能研究科	Spin texture of the metallic quasi-1D surface states around Fermi level fabricated on semiconductor substrates	Yoshiyuki Ohtsubo	Osaka University
4	有機半導体の分子吸着に伴って生じるトポロジカル表面状態の変化	金井　要	東京理科大学	大学院理工学研究科	Modification of Topological surface states upon adsorption of organic semiconductors	Kaname Kanai	Tokyo University of Science
5	トポロジカル絶縁体を用いたスピン軌道トルク磁気メモリの表面状態解明	小林　正起	東京大学	大学院工学系研究科	Unveiling the surface state of spin-orbital torque magnetic memory using topological insulator	Masaki Kobayashi	The University of Tokyo
6	トポロジカル絶縁体 $Bi_{1-x}Sb_x$ と垂直磁化膜 MnGa 界面におけるディラックコーンの観測	小林　正起	東京大学	大学院工学系研究科	Obsevation of Dirac cone state at the interface between topological insulator $Bi_{1-x}Sb_x$ and perpendicular magnet MnGa layers	Masaki Kobayashi	The University of Tokyo
7	Investigation of topological properties in superconducting $TaSe_3$	近藤　猛	東京大学	物性研究所	Investigation of topological properties in superconducting $TaSe_3$	Takeshi Kondo	The University of Tokyo
8	第二種 Weyl 半金属 WTe_2 の角度とスピン分解光電子分光による研究	近藤　猛	東京大学	物性研究所	The angle- and spin-resolved photoemission spectroscopy research on type-II Weyl semimetal WTe_2	Takeshi Kondo	The University of Tokyo
9	2 次元ファンデルワールス強磁性体のスピン・角度分解電子分光による研究	黒田　健太	東京大学	物性研究所	Spin- and angle-resolved photoemission spectroscopy study of two dimensional van der Waals ferromagnets	Kenta Kuroda	The University of Tokyo
10	時間・スピン・角度分解光電子分光装置の開発	黒田　健太	東京大学	物性研究所	Development of time-, spin- and angle-resolved photoemission spectroscopy machine	Kenta Kuroda	The University of Tokyo
11	トポロジカル超伝導体の探索	坂野　昌人	東京大学	大学院工学系研究科	Search for topological insulators	Masato Sakano	The University of Tokyo

No.	課題名	氏名	所属		Title	Name	Organization
12	Study of the effect of excess Fe in Fe(Te,Se)	Peng Zhang	東京大学	物性研究所	Study of the effect of excess Fe in Fe(Te,Se)	Peng Zhang	The University of Tokyo
13	Study of topological states in $ZrTe_5$	Peng Zhang	東京大学	物性研究所	Study of topological states in $ZrTe_5$	Peng Zhang	The University of Tokyo
14	鉛単原子層のスピン偏極電子状態のスピン分解光電子分光	矢治　光一郎	東京大学	物性研究所	SARPES study of spin-polarized electronic states of a Pb atomic laye	Koichiro Yaji	The University of Tokyo
15	High-resolution spin-resolved electronic structure of 2D electron gas in $SrTiO_3$	Andres Santander	Paris-Sud University		High-resolution spin-resolved electronic structure of 2D electron gas in $SrTiO_3$	Andres Santander	Paris-Sud University
16	ドメイン制御された合金原子層のスピン構造研究	Shu-Jung Tang	Tsing Hua Univ.		Study of spin structure in domain-regulated alloy of atomic layer	Shu-Jung Tang	Tsing Hua University
17	SARPES study of band structure at the interfaces between bismuth and transition metal dichalcogenides	Rolalnd Stania	Institute for Basic Science		SARPES study of band structure at the interfaces between bismuth and transition metal dichalcogenides	Rolalnd Stania	Institute for Basic Science
18	ドープされた磁性トポロジカル絶縁体における高分解能スピン・角度分解光電子分光	福谷　圭祐	Institute for Basic Science		High-resolution spin- and angle-resolved photoemission spectroscopy of doped magnetic topological insulators	Keisuke Fukutani	Institute for Basic Science

令和元年度 スーパーコンピュータ共同利用課題一覧 / Joint Research List of Supercomputer System 2019

No.	課題名	氏名	所属	Title	Name	Organization
1. 第一原理計算 / First-Principles Calculation of Materials Properties						
1	量子論による半導体界面形成機構と電子物性の解明	押山　淳	名古屋大学未来材料・システム研究所	Mechanisms of Semiconducotr Interface Formation and its Electronic Properties based on Quantum Theory	Atsushi Oshiyama	Nagoya University
2	量子論による半導体界面形成機構と電子物性の解明	押山　淳	名古屋大学未来材料・システム研究所	Mechanisms of Semiconducotr Interface Formation and its Electronic Properties based on Quntum Theory	Atsushi Oshiyama	Nagoya University
3	高機能スピントロニクス磁性材料の電子構造解析および磁気的性質解析	小田　竜樹	金沢大学理工研究域数物科学系	Analyses on electronic structure and magnetic property in high-performance spintronics and magnetic materials	Tatsuki Oda	Kanazawa University
4	電極界面の物理	杉野　修	東京大学物性研究所	Physics of electrode interfaces	Osamu Sugino	The University of Tokyo
5	最強希土類永久磁石化合物 (Nd, R)2(Fe,Co)14B (R= 希土類) の第一原理磁気物性最適化	松本　宗久	高エネルギー加速器研究機構 物質構造科学研究所	Ab initio optimization of the champion rare earth magnet compound (Nd,R)2(Fe,Co)14B (R=rare earth)	Munehisa Matsumoto	KEK
6	高機能スピントロニクス磁性材料の電子構造解析および磁気的性質解析	小田　竜樹	金沢大学理工研究域数物科学系	Analyses on electronic structure and magnetic property in high-performance spintronics and magnetic materials	Tatsuki Oda	Kanazawa University
7	先端的第一原理シミュレーションによる物質開拓	常行　真司	東京大学大学院理学系研究科	Material exploration by advanced first-principles simulation	Shinji Tsuneyuki	The University of Tokyo
8	$BaZrO_3$ 系イオン伝導体のドーピングスキーム設計	笠松　秀輔	山形大学学術研究院	Designing doping schemes for $BaZrO_3$-based ion conductors	Shusuke Kasamatsu	Yamagata University
9	次世代二次電池界面・電解液に関する第一原理サンプリング研究	館山　佳尚	物質・材料研究機構　GREEN	DFT-MD sampling analysis of interfaces and electrolytes in novel batteries	Yoshitaka Tateyama	National Institute for Materials Science
10	超並列量子物質計算とデータ駆動科学の融合	星　健夫	鳥取大学大学院工学研究科	Unification of massively parallel quantum material simulation and data-driven science	Takeo Hoshi	Tottori University
11	パワー半導体における界面欠陥構造の特定とその低減法の提案 : 第一原理計 算からのアプローチ	松下　雄一郎	東京工業大学	Identification of interface-state defects in power semiconductors: Approach from ab-initio calculations	Yu-Ichiro Matsushita	Tokyo Institute of Technology
12	有限温度フォノン計算に基づく構造相転移の理解と予測	只野　央将	物質・材料研究機構	Predicting and understanding structural phase transition of solids from finite-temperature phonon calculations	Terumasa Tadano	National Institute for Materials Science
13	ファンデルワールス密度汎関数を用いた分子吸着金属表面の研究	濱田　幾太郎	大阪大学工学研究科	van der Waals density functional study of molecules adsorbed on metal surfaces	Ikutaro Hamada	Osaka University
14	密度汎関数法と溶液理論を用いた電気化学反応の解析	春山　潤	東京大学物性研究所	Electrochemical reaction analysis using density functional calculation + implicit solvation model	Jun Haruyama	The University of Tokyo
15	表面、界面、欠陥における原子構造と原子ダイナミクスの解析	渡邉　聡	東京大学大学院工学系研究科	Analyses of atomic structures and atom dynamics at surfaces, interfaces and defects	Satoshi Watanabe	The University of Tokyo

No.	課題名	氏名	所属	Title	Name	Organization
16	パワー半導体における欠陥構造とその電子物性の相関関係：第一原理計算からのアプローチ	松下　雄一郎	東京工業大学	Relation between defect structures and electronic properties in power semiconductors: Approach from ab-initio calculations	Yu-Ichiro Matsushita	Tokyo Institute of Technology
17	量子転移の第一原理計算	レービガー ハンネス	横浜国立大学大学院工学研究院	First principles calculation of quantum phase transitions	Hannes Raebiger	Yokohama National University
18	次世代二次電池界面・電解液に関する第一原理サンプリング研究	館山　佳尚	物質・材料研究機構　GREEN	DFT sampling analysis of interfaces and electrolytes in novel batteries	Yoshitaka Tateyama	National Institute for Materials Science
19	表面、界面、欠陥における原子構造と原子ダイナミクスの解析	渡邉　聡	東京大学大学院工学系研究科	Analyses of atomic structures and atom dynamics at surfaces, interfaces and defects	Satoshi Watanabe	The University of Tokyo
20	第一原理計算による金属過水素化物の金属化および超伝導機構の研究	明石　遼介	東京大学大学院理学系研究科	Ab initio study on the metallization and superconductivity in metallic superhydrides	Ryosuke Akashi	The University of Tokyo
21	金属／半導体界面のギャップ状態制御の物理：第一原理計算による研究	中山　隆史	千葉大学理学部物理学科	First-principles study on physics of gap-state control at metal/semiconductor interfaces	Takashi Nakayama	Chiba University
22	第一原理計算による二次電池用正極材料の解析	山田　淳夫	東京大学工学系研究科	First-principles analyses on the cathode materials for rechargeable batteries	Atsuo Yamada	The University of Tokyo
23	第一原理シミュレーションによる不均一触媒反応過程の研究	森川　良忠	大阪大学大学院工学研究科	First-principles Theoretical Study of Chemical Reactions in Heterogeneous Catalysts	Yoshitada Morikawa	Nagoya University
24	第一原理電子状態・輸送特性計算コード RSPACE の開発とデバイスシミュレーション	小野　倫也	神戸大学大学院工学研究科	Development of first-principles electronic-structure and transport calculation code RSPACE and simulations for device	Tomoya Ono	Kobe University
25	GaN 系パワーデバイス用ゲート絶縁膜の理論的設計	白石　賢二	名古屋大学未来材料・システム研究所	Theoretical Design of Gate Dielectrics of Future GaN Power Devices	Kenji Shiraishi	Nagoya University
26	高ドープイオン伝導体の第一原理配置サンプリング解析	笠松　秀輔	山形大学学術研究院	First-principles configurational sampling of highly-doped ionic conductors	Shusuke Kasamatsu	Yamagata University
27	第一原理計算を用いたクラスレート化合物の熱電特性解析	大西　正人	東京大学機械工学専攻	Analysis of Thermoelectric Properties of Clathrate Compounds with Ab Initio Calculations	Masato Ohnishi	The University of Tokyo
28	マルチフェロイク界面の第一原理計算	合田　義弘	東京工業大学物質理工学院材料系	First-principles calculations of multiferroic interfaces	Yoshihiro Gohda	Tokyo Institute of Technology
29	遷移金属磁性酸化物の第一原理電子状態計算	山内　邦彦	大阪大学産業科学研究所	First-principles density functional calculations of transition-metal magnetic oxides	Kunihiko Yamauchi	Osaka University
30	高圧力下における共有結合性液体・ガラスの構造と電子状態の第一原理計算	下條　冬樹	熊本大学大学院自然科学研究科	First-Principles Molecular-Dynamics Study of Structural and Electronic Properties of Covalent Liquids and Glasses under Pressure	Fuyuki Shimojo	Kumamoto University
31	有機溶媒中のイオン種の拡散プロセスの解明	赤木　和人	東北大学材料科学高等研究所	Elucidation of diffusion process of ionic species in organic solvent	Kazuto Akagi	Tohoku University
32	マルチスケール MD シミュレーションによる生体触媒反応メカニズムの解析	舘野　賢	兵庫県立大学大学院生命理学研究科	Multi-scale Hybrid Molecular Dynamics Simulations of Biological Catalysis	Masaru Tateno	University of Hyogo

No.	課題名	氏名	所属	Title	Name	Organization
33	電子ドープグラフェン / 水界面の第一原理分子動力学シミュレーション	大戸　達彦	大阪大学大学院基礎工学研究科	First-principles molecular dynamics simulation of electron-doped graphene/water interfaces	Tatsuhiko Ohto	Osaka University
34	有機 - 無機ハイブリッド熱電材料のエネルギー輸送	鞠　生宏	東京大学工学部機械工学科	Energy Transport in Hybrid Organic-Inorganic Thermoelectric Materials	Shenghong Ju	The University of Tokyo
35	永久磁石界面の第一原理的研究	立津　慶幸	名桜大学	First-principles study on grain boundaries of permanent magnets	Yasutomi Tatetsu	Meio University
36	新規リチウムイオン二次電池材料の電極特性解析：第一原理計算	籾田　浩義	大阪大学産業科学研究所	Electrode properties of novel lithium-ion secondary battery materials: First-principles calculations	Hiroyoshi Momida	Osaka University
37	原子層エッチングプロセスにおける表面反応解析	浜口　智志	大阪大学工学研究科	Analyses of Surface Reactions in Atomic Layer Etching Processes	Satoshi Hamaguchi	Osaka University
38	ナノ構造の量子伝導の第一原理計算	小林　伸彦	筑波大学 数理物質系物理工学域	First-principles study of quantum transport in nanostructures	Nobuhiko Kobayashi	University of Tsukuba
39	ナノ構造の励起電子・陽電子・原子動力学と光・熱電物性の第一原理計算	渡辺　一之	東京理科大学理学部	First-Principles Study of Excited Electron, Positron and Atom Dynamics and Optical and Thermoelectric Properties of Nanostructures	Kazuyuki Watanabe	Tokyo University of Science
40	ハイブリッド汎関数を用いた水 / 空気界面の第一原理分子動力学シミュレーション	大戸　達彦	大阪大学大学院基礎工学研究科	First-principles molecular dynamics simulation of the water/air interface using hybrid functionals	Tatsuhiko Ohto	Osaka University
41	磁性絶縁体における電界効果の第一原理的研究	石井　史之	金沢大学ナノマテリアル研究所	First-principles study of electric-field effect on magnetic insulator	Fumiyuki Ishii	Kanazawa University
42	ギ酸分解触媒及び酸素吸蔵材料の省貴金属化	國貞　雄治	北海道大学大学院工学研究院　附属エネルギー・マテリアル融合領域研究センター	Reduction of Rare Metals in Formic Acid Decomposition Catalysts and Oxygen Storage Materials	Yuji Kunisada	Hokkaido University
43	第一原理計算による有機強誘電体・圧電体の物性予測	石橋　章司	産業技術総合研究所	Prediction of properties of organic ferroelectrics and piezoelectrics by first-principles calculation	Shoji Ishibashi	National Institute of Advanced Industrial Science and Technology
44	燃料電池電極触媒及び水素透過膜の省貴金属化	坂口　紀史	北海道大学大学院工学研究院　附属エネルギー・マテリアル融合領域研究センター	Reduction of Rare Metals in Fuel Cell Catalysts and Hydrogen Permeable Membrane	Norihito Sakaguchi	Hokkaido University
45	電子フォノン相互作用の精密第一原理解析	南谷　英美	分子科学研究所	Ab-initio analysis of electron-phonon interaction	Emi Minamitani	Institute for Molecular Science
46	第一原理計算によるナノ物質の構造・機能の解明と予測	武次　徹也	北海道大学大学院理学研究院化学部門	Ab initio study on the structure and functions of nanomaterials	Tetsuya Taketsugu	Hokkaido University
47	GPP モデルを使用しない GW 法の開発	野口　良史	静岡大学工学部	GW method without GPP model	Yoshifumi Noguchi	Shizuoka University
48	ナノ構造の励起電子・陽電子・原子動力学と光・熱電物性の第一原理計算	渡辺　一之	東京理科大学理学部	First-Principles Study of Excited Electron, Positron and Atom Dynamics and Optical and Thermoelectric Properties of Nanostructures	Kazuyuki Watanabe	Tokyo University of Science
49	絶縁体非線形光吸収の第一原理計算	篠原　康	東京大学工学系研究科附属光量子科学研究センター	First-principles calculations for nonlinear light absorption of insulators	Yasushi Shinohara	The University of Tokyo

No.	課題名	氏名	所属	Title	Name	Organization
50	スピン偏極陽電子実験の可能性を広げるための第一原理的研究	斎藤　峯雄	金沢大学理工研究域数物科学系	First-principles study for widening the potential of spin-polarized positron experiments	Mineo Saito	Kanazawa University
51	第一原理計算による磁性熱電物質の結晶構造予測	石井　史之	金沢大学ナノマテリアル研究所	First-Principles Crystal Structure Prediction of Magnetic Thermoelectric Materials	Fumiyuki Ishii	Kanazawa University
52	イリジウム酸化物 $Ca_5Ir_3O_{12}$ の第一原理フォノン分散計算	中村　和磨	九州工業大学	Ab initio phonon calculation for $Ca_5Ir_3O_{12}$	Kazuma Nakamura	Kyushu Institute of Technology
53	アモルファス磁性体および永久磁石内アモルファス相界面に対する第一原理計算および磁気結合定数と局所構造の関係の解析	寺澤　麻子	東京工業大学	First principles calculations and analysis on relationship between exchange coupling constants and local structures for magnetic alloys and amorphous grain boundary phases in permanent magnets	Asako Terasawa	Tokyo Institute of Technology
54	スピン偏極陽電子実験の可能性を広げるための第一原理的研究	斎藤　峯雄	金沢大学理工研究域数物科学系	First-principles study for widening the potential of spin-polarized positron experiments	Mineo Saito	Kanazawa University
55	粒界原子ダイナミクスの解析に向けた機械学習駆動型分子シミュレーション	横井　達矢	名古屋大学大学院工学研究科	Machine-learning-driven molecular simulations for grain-boundary atomic dynamics	Tatsuya Yokoi	Nagoya University
56	ギ酸分解触媒及び酸素吸蔵材料の省貴金属化	國貞　雄治	北海道大学大学院工学研究院　附属エネルギー・マテリアル融合領域研究センター	Reduction of Rare Metals in Formic Acid Decomposition Catalysts and Oxygen Storage Materials	Yuji Kunisada	Hokkaido University
57	第一原理電子状態・輸送特性計算コード RSPACE の開発とデバイスシ ミュレーション	小野　倫也	神戸大学大学院工学研究科	Development of first-principles electronic-structure and transport calculation code RSPACE and simulations for device	Tomoya Ono	Kobe University
58	第一原理計算による高温水中の多価アルコールの反応過程の研究	佐々木　岳彦	東京大学大学院新領域創成科学研究科	Reaction processes of polyalcohols in high temperature water by First Principles Calculations	Takehiko Sasaki	The University of Tokyo
59	多成分系に対する分子動力学計算に用いるためのニューラルネットワーク力場の構築	島村　孝平	熊本大学大学院先端科学研究部	Construction of neural network force field for molecular dynamics simulation in multicomponent system	Kohei Shimamura	Kumamoto University
60	2 次元ヘテロ接合材料の面外熱伝導率の操作	胡　世謙	東京大学機械工学塩見研究室	manipulation of the cross-plane thermal conductivity on the 2D hetero-junction materials	Shiqian Hu	The University of Tokyo
61	結晶構造探索アルゴリズムの開発	山下　智樹	長岡技術科学大学	Development of algorithms in crystal structure prediction	Tomoki Yamashita	Nagaoka University of Technology
62	高性能フッ素ポリマーエレクトレットの開発	鈴木　雄二	東京大学大学院工学系研究科機械工学専攻	Development of High-performance Polymer Electret	Yuji Suzuki	The University of Tokyo
63	太陽光エネルギー変換における基礎過程の研究と材料設計指針獲得のための大規模第一原理計算	山下　晃一	京都大学	Large scale ab initio calculations on the fundamental processes of solar energy convergence devices and on designing principles for new materials	Koichi Yamashita	Kyoto University
64	人工光合成触媒と燃料電池触媒への計算物理化学からのアプローチ	西館　数芽	岩手大学理工学部	Computational physics and chemistry approach to develop the artificial photosynthesis and fuel cell catalysts	Kazume Nishidate	IWATE University
65	第一原理による機能性酸化物の原子構造および電子状態の解明	幾原　雄一	東京大学大学院工学系研究科総合研究機構	Ab initio calculations of atomic and electronic structures for functional oxide materials	Yuichi Ikuhara	The University of Tokyo
66	熱力学状態図の第一原理計算	中村　和磨	九州工業大学	Ab initio calculation for thermodynamic phase diagram	Kazuma Nakamura	Kyushu Institute of Technology

No.	課題名	氏名	所属	Title	Name	Organization
67	量子化学計算を用いた高性能フッ素ポリマーエレクトレットの開発	鈴木　雄二	東京大学大学院工学系研究科機械工学専攻	Development of High-performance Polymer Electret Using Quantum Chemical Analysis	Yuji Suzuki	The University of Tokyo
68	電子フォノン相互作用の第一原理精密解析	南谷　英美	分子科学研究所	Ab-initio analysis of electron-phonon interaction	Emi Minamitani	Institute for Molecular Science
69	第一原理計算によるモデルリアル触媒上の表面反応の探求 II	水上　渉	大阪大学 先導的学際研究機構	Exploration of surface reactions on model real catalyst II	Wataru Mizukami	Osaka University
70	熱電材料のマルチスケール計算設計	邵　成	東京大学機械工学塩見研究室	Multiscale computational design of thermoelectric materials	Cheng Shao	The University of Tokyo
71	第一原理計算による CARE 加工におけるプロセスと触媒材料の設計	稲垣　耕司	大阪大学大学院工学研究科	Analysis and Design of reaction process and catalyst material for CARE machining	Kouji Inagaki	Osaka University
72	DFT 計算による非接触原子間力顕微鏡のエネルギー散逸チャンネルで捉えた原子変位機構の解明	新井　豊子	金沢大学	DFT calculation of atomic displacement captured by energy dissipation channel of noncontact atomic force microscope	Toyoko Arai	Kanazawa University
73	第一原理分子動力学法に基づく人口網膜分子の安定性に関する研究	大村　訓史	広島工業大学工学部	Ab initio molecular dynamics study of stability of artificial retina molecule	Satoshi Ohmura	Hiroshima Institute of Technology
74	ナノ・分子構造の動的特性設計のための第一原理 / 機械学習連成計算	鶴田　健二	岡山大学大学院自然科学研究科	Hybrid Ab-Initio/Machine-Learning Computation for Designing Dynamical Properties of Nano/Molecular Structures	Kenji Tsuruta	Okayama University
75	燃料電池電極触媒及び水素透過膜の省貴金属化	坂口　紀史	北海道大学大学院工学研究院　附属エネルギー・マテリアル融合領域研究センター	Reduction of Rare Metals in Fuel Cell Catalysts and Hydrogen Permeable Membrane	Norihito Sakaguchi	Hokkaido University
76	有機半導体結晶の有限温度下の電子状態に向けたフォノン解析の実装	柳澤　将	琉球大学理学部物質地球科学科物理系	Implementation of the phonon analysis for organic semiconductor crystals	Susumu Yanagisawa	University of the Ryukyus
77	有機分子膜での構造歪み・欠陥の電子構造への影響に関する理論的研究	柳澤　将	琉球大学理学部物質地球科学科物理系	Structural distortion or defect in organic molecular thin film: theoretical study	Susumu Yanagisawa	University of the Ryukyus
78	ナノグラフェンの輸送と反応のシミュレーション	草部　浩一	大阪大学大学院基礎工学研究科	Transport and reaction properties of nanographene	Koichi Kusakabe	Osaka University
79	2 次元物質における電子状態および電子輸送特性制御に関する第一原理研究	江上　喜幸	北海道大学大学院工学研究院	First-principles study on controlling of electronic structures and electron-transport properties of 2-D materials	Yoshiyuki Egami	Hokkaido University
80	van der Waals 密度汎関数法による有機 - 金属界面の鏡像状態の理論的研究	濱本　雄治	大阪大学 大学院工学研究科 精密科学・応用物理学専攻	van der Waals density functional study of image potential states at organic-metal interfaces	Yuji Hamamoto	Osaka University
81	シリサイド薄膜系の原子構造と電子状態	服部　賢	奈良先端科学技術大学院大学物質創成科学研究科	Atomic structure and electronic states for silicide films	Ken Hattori	Nara Institute ofScience and Technology
82	カーボンナノチューブ・グラフェンの電子物性の解明：第一原理計算	藤本　義隆	東京工業大学大学院理工学研究科物性物理学専攻	First-principles investigation of electronic properties of carbon nanotubes and graphene	Yoshitaka Fujimoto	Tokyo Institute of Technology
83	イリジウム酸化物に対する第一原理有効模型導出および高精度解析	中村　和磨	九州工業大学	Ab initio calculations for Sr2IrO4 and Ca5Ir3O12	Kazuma Nakamura	Kyushu Institute of Technology

No.	課題名	氏名	所属	Title	Name	Organization
84	不純物半導体の転位に生じるリーク電流の第一原理的研究	原嶋　庸介	名古屋大学未来材料・システム研究所	First principles study on leaking current at a dislocation in doped semiconductors	Yosuke Harashima	Nagoya University
85	第一原理分子動力学法によるヘテロ界面原子構造および電子状態の解明	幾原　雄一	東京大学大学院工学系研究科総合研究機構	Study of atomic and electronic structure of hetero interface by first-principles molecular dynamics simulations	Yuichi Ikuhara	The University of Tokyo
86	プロトン伝導性固体電解質中のイオン電導機構解析とプロトン伝導体を用いた触媒表面反応への応用	大友　順一郎	東京大学大学院新領域創成科学研究科環境システム学専攻	Analysis of ion conduction in materials of proton-conducting solid electrolyte and application to catalytic surface reaction with proton conductors	Junichiro Otomo	The University of Tokyo
87	第一原理計算における電界を印加された Pt 薄膜における強磁性発現に関する研究	佐藤　徹哉	慶應義塾大学理工学部	Study of appearance of ferromagnetism by electric field application to Pt thin film	Tetsuya Sato	Keio University
88	有機 - 無機ハイブリッド熱電材料のエネルギー輸送	鞠　生宏	東京大学工学部機械工学科	Energy Transport in Hybrid Organic-Inorganic Thermoelectric Materials	Shenghong Ju	The University of Tokyo
89	合金触媒の原子構造と電子構造に関する理論的研究	野澤　和生	鹿児島大学理学部物理科学科	Atomic and electronic structures of intermetallic compound catalysts	Kazuki Nozawa	Kagoshima University
90	原子層状物質における電子状態および電子輸送特性制御に関する第一原理研究	江上　喜幸	北海道大学大学院工学研究院	First-principles study on controlling of electronic structures and electron-transport properties of atomic layered materials	Yoshiyuki Egami	Hokkaido University
91	希土類混晶磁石材料の磁気特性データ構築	赤井　久純	東京大学物性研究所	Data accumulation of magnetic properties of rare earth mixed crystal magnetic materials	Hisazumi Akai	The University of Tokyo
92	第一原理分子動力学法に基づくガラスの静的構造に関する研究	高良　明英	熊本大学学生支援部	First principles study on static structure of glass materials	Akihide Koura	Kumamoto University
93	照射損傷と格子間原子との相互作用の研究	大澤　一人	九州大学応用力学研究所	Study of interaction between radiation damage and interstitial atom	Kazuhito Ohsawa	Kyushu University
94	プロトン伝導性固体電解質中のイオン電導機構解析とプロトン伝導体を用いた触媒表面反応への応用	大友　順一郎	東京大学大学院新領域創成科学研究科環境システム学専攻	Analysis of ion conduction in materials of proton-conducting solid electrolyte and application to catalytic surface reaction with proton conductors	Junichiro Otomo	The University of Tokyo
95	遷移金属の吸着に伴う量子井戸バンドの変調を用いた Pd(100) 超薄膜の磁性制御	櫻木　俊輔	東京大学物性研究所	Controlling of magnetism in Pd(100) ultrathin films by modification of quantum-well states via adsorption of transition metals	Shunsuke Sakuragi	The University of Tokyo
96	磁性分子複合体・結晶・界面系の原子・磁気構造の解析と外部電場・磁場効果の調査	小幡　正雄	金沢大学理工研究域	Analysis on atomic and magnetic structure in magnetic molecular complex, crystal and interface and investigation of external electric and magnetic field effect	Masao Obata	Kanazawa University
97	対称および非対称磁気抵抗接合に基づく二次元物質	ハシュミ　アルカム	筑波大学計算科学研究センター	2D materials based symmetric and non-symmetric magnetoresistive junctions	Arqum Hashmi	University of Tsukuba
98	Sb 系テラヘルツトランジスタのための歪バンド構造設計	藤代　博記	東京理科大学	Strained Band-Structure Engineering for Antimonide-Based Terahertz Transistors	Hiroki Fujishiro	Tokyo University of Science
99	エタノール水溶液中の水，エタノールの電子状態	高橋　修	広島大学大学院理学研究科	Electronic state of water and ethanol in aqueous solution	Osamu Takahashi	Hiroshima University
100	第一原理分子動力学計算による van der Waals 相互作用の検証と振動スペクトル計算	平塚　将起	工学院大学機械工学科	Effect of van der Waals interaction on vibrational spectra from ab initio molecular dynamics simulation	Masaki Hiratsuka	Kogakuin University

No.	課題名	氏名	所属	Title	Name	Organization
101	ハーフメタル材料の有限温度特性に関する第一原理計算	三浦　良雄	物質・材料研究機構	A first-principles calculation on finite temperature effects of half-metallic ferromagnets	Yoshio Miura	National Institute for Materials Science
102	磁性分子複合体・結晶・界面系の原子・磁気構造の解析と外部電場・磁場効果の調査	小幡　正雄	金沢大学理工研究域	Analysis on atomic and magnetic structure in magnetic molecular complex, crystal and interface and investigation of external electric and magnetic field effect	Masao Obata	Kanazawa University
103	物質表面における場の量子論に基づく局所物理量解析	福田　将大	東京大学物性研究所	Local physical quantities analysis based on the quantum field theory in material surface	Masahiro Fukuda	The University of Tokyo
104	溶媒和を考慮した超臨界場における反応の理論計算	横　哲	東北大学材料科学高等研究所	Theoretical calculation of solvation and reaction in supercritical fluids	Akira Yoko	Tohoku University
105	希土類混晶磁石材料の磁気特性データ構築	赤井　久純	東京大学物性研究所	Data accumulation of magnetic properties of rare earth mixed crystal	Hisazumi Akai	The University of Tokyo
106	表面における電子 - 陽電子散乱の実時間発展シミュレーション	萩原　聡	国立研究開発法人量子科学技術研究開発機構	Real-time propagated simulation for electron-positron scattering at the surface	Satoshi Hagiwara	The National Institutes for Quantum and Radiological Science and Technology
107	第一原理バンド計算に基づく低エネルギーモデルの構築方法の開発	榊原　寛史	鳥取大学大学院工学研究科	Developments of a derivation method of a low-energy models in first-principles	Hirofumi Sakakibara	Tottori University
108	有機分子の超高圧処理による新規固体生成過程の第一原理計算	島田　敏宏	北海道大学　大学院工学研究院	First principle simulation on ultrahigh pressure synthesis of new material from organic molecules	Toshihiro Shimada	Hokkaido University
109	高次フォノン - フォノン散乱強度の第一原理計算	出倉　春彦	愛媛大学地球深部ダイナミクス研究センター	First-principles calculation of the higher-order phonon-phonon scattering strength	Haruhiko Dekura	Ehime University
110	化学還元により形成したグラフェンシートのSTM 像シミュレーション	有馬　健太	大阪大学 大学院 工学研究科	Simulation of STM images of graphene sheet after chemical reduction	Kenta Arima	Osaka University
111	凝集誘起発光についての理論的研究	山本　典史	千葉工業大学	Theoretical Study on the Aggregation-Induced Emission	Norifumi Yamamoto	Chiba Institute of Technology
112	超伝導密度汎関数理論の精度検証	河村　光晶	東京大学物性研究所	Benchmark of density functional theory for superconductors	Mitsuaki Kawamura	The University of Tokyo
113	様々な環境下における水の電子状態	高橋　修	広島大学大学院理学研究科	Electronic state of water under various environments	Osamu Takahashi	Hiroshima University
114	対称性に基づくデータ駆動的トポロジカル物質探索	押川　正毅	東京大学物性研究所	A data-driven investigation of topological materials based on symmetry	Masaki Oshikawa	The University of Tokyo
115	Ni 表面上２次元シリサイドの第一原理計算	福田　常男	大阪市立大学大学院工学研究科電子情報系専攻	First Principles Calculation of 2-Dimensional Silicides Formed on Nickel Surfaces	Tuneo Fukuda	Osaka City University
116	分子動力学シミュレーションと第一原理計算を用いた固体・液体界面における分子科学	城塚　達也	茨城大学	Molecular Science at Solid/Liquid Interfaces using Molecular Dynamics Simulation and Ab Initio Calculation	Tatsuya Joutsuka	Ibaraki University
117	第一原理計算に基づくマグネシウム合金の欠陥場の解析	松中　大介	信州大学工学部機械システム工学科	First-principles Study of Defects of Magnesium Alloys	Matsunaka Daisuke	Shinshu University

No.	課題名	氏名	所属	Title	Name	Organization
118	高圧下における液体 Fe-Si-O 混合系の構造と不混和性に関する第一原理分子動力学シミュレーション	大村　訓史	広島工業大学　工学部	Ab initio molecular dynamics study of structural properties and immiscibility in liquid Fe-Si-O mixtures under high pressure	Satoshi Ohmura	Hiroshima Institute of Technology
119	固体表面・界面、微粒子の新規電子物性の探索と実現	稲岡　毅	琉球大学理学部	Search and realization of novel electronic properties of solid surfaces and interfaces and of small particles	Takeshi Inaoka	University of the Ryukyus
120	磁気トンネル接合における磁気抵抗比、磁気異方性の第一原理解析	増田　啓介	物質・材料研究機構	First-principles study of magnetoresistance ratios and magnetic anisotropy in magnetic tunnel junctions	Keisuke Masuda	National Institute for Materials Science
121	水溶液中ケージド化合物の吸収スペクトルについての解析	樋山　みやび	群馬大学	Analysis of absorption spectra for caged compounds in aqueous solution	Miyabi Hiyama	Gunma University
122	機械学習を用いた半導体デバイス中の電流経路設計に関する研究	村口　正和	北海道科学大学	Study on carrier dynamics in nano scale semiconductor devices with machine learning	Masakazu Muraguchi	Hokkaido University of Science
123	有機修飾金属酸化物ナノ粒子の構造および物性に関する理論研究	横　哲	東北大学材料科学高等研究所	Theoretical study for structure and property of organic modified metal oxide nanoparticles	Akira Yoko	Tohoku University
124	定常電場印加下での強相関酸化物の電子構造計算	牧野　哲征	福井大学学術研究院工学系部門	Electronic structure calculation in strongly-correlated electron oxides under presence of static electric field	Takayuki Makino	University of Fukui
125	触媒インフォマティクスに向けた複合酸化物の表面物性計算	日沼　洋陽	千葉大学先進科学センター	Calculation of multication oxide surface properties for catalyst informatics	Yoyo Hinuma	Chiba University
126	ヨウ化銅を用いた低圧化学気相成長法によるルテニウム基板上銅膜の高速成長の第一原理計算	城塚　達也	茨城大学	Ab Initio Calculation of High-Rate Deposition of Copper Film by Low-Pressure Chemical Vapor Deposition with CuI on Ru Substrate	Tatsuya Joutsuka	Ibaraki University
127	磁気トンネル接合および巨大磁気抵抗素子における熱電性能の第一原理計算	山本　薫	物質・材料研究機構	First-principles calculation of thermoelectric properties for magnetic tunneling junctions and giant magneto-resistance devices	Kaoru Yamamoto	National Institute for Materials Science
128	銅酸化物におけるフォノン状態密度分布の第一原理計算	牧野　哲征	福井大学学術研究院工学系部門	Ab-initio calculation of phonon density-of-states spectra in cuprous oxides	Takayuki Makino	University of Fukui
129	PbS ナノ構造電子状態の不純物効果	首藤　健一	横浜国立大学・工学部	Impurity effects on electronic states of PbS nano-particles	Ken-Ichi Shudo	Yokohama National University
130	固体表面・界面、微粒子の新規電子物性の探索と実現 II	稲岡　毅	琉球大学理学部	Search and realization of novel electronic properties of solid surfaces and interfaces and of small particles II	Takeshi Inaoka	University of the Ryukyus
131	半導体表面界面における構造的素励起の研究	影島　博之	島根大学大学院自然科学研究科	Study on structural elementary excitations at semiconductor surfaces and interfaces	Hiroyuki Kageshima	Shimane University
132	Sb 系テラヘルツトランジスタのための歪バンド構造設計	藤代　博記	東京理科大学	Strained Band-Structure Engineering for Antimonide-Based Terahertz Transistors	Hiroki Fujishiro	Tokyo University of Science
133	デラフォサイト銅酸化物における電子格子相互作用の計算	牧野　哲征	福井大学学術研究院工学系部門	Calculation of electron-phonon interaction in delafossite-type cuprates	Takayuki Makino	University of Fukui
134	新たなナノスケール表面界面の電子物性の理論的研究	小林　功佳	お茶の水女子大学理学部物理学科	Theoretical study on electronic properties of new nanoscale surfaces and interfaces	Katsuyoshi Kobayashi	Ochanomizu University

No.	課題名	氏名	所属	Title	Name	Organization
135	線形応答理論の枠組みにおけるゼーベック係数の第一原理計算手法の開発	高　成柱	東京工業大学物質理工学院	Development of First-principles calculations method of Seebeck coefficient in the framework of linear response theory	Sonju Kou	Tokyo Institute of Technology
136	第一原理的計算手法の発展と適用	池田　浩章	立命館大学理工学部物理科学科	Development and application of the first-principles approach	Hiroaki Ikeda	Ritsumeikan University
137	超高圧下におけるケイ酸塩物質の構造と電子状態に関する第一原理的研究	三澤　賢明	岡山大学大学院自然科学研究科	First-principles study on the structures and electronic properties of silicates under high pressure	Masaaki Misawa	Okayama University
138	超伝導基板への吸着を応用したランタノイド 4f スピン検出に関する理論的研究	塚原　規志	群馬工業高等専門学校	Theoretical study of spin detection in lanthanoid atoms and molecules by adsorption on superconducting substrate	Noriyuki Tsukahara	Gunma College
139	クロムおよびマンガン合金の磁気特性の解析	小田　洋平	福島工業高等専門学校	Analysis of magnetic properties in Cr and Mn alloys	Yohei Kota	Fukushima College
140	金属クロムの磁性に対するひずみ効果の解析	小田　洋平	福島工業高等専門学校	Analysis of strain effect on magnetism in chromium metals	Yohei Kota	Fukushima College
141	様々な環境下における水の電子状態	高橋　修	広島大学大学院理学研究科	Electronic state of water under various environments	Osamu Takahashi	Hiroshima University
142	強磁性薄膜のバンド計算	秋山　了太	東京大学理学系研究科物理学専攻	Band calculation of ferromagnetic thin films	Ryota Akiyama	The University of Tokyo
143	第一原理計算によるエピタキシャル成長薄膜合成基板のスクリーニング	北川　健太郎	東京大学理学系研究科物理学専攻	Screening test for substrates on epitaxial growth of thin film	Kentaro Kitagawa	The University of Tokyo
144	トリディマイト多形の NMR スペクトル第一原理計算	神崎　正美	岡山大学惑星物質研究所	NMR spectrum calculations of tridymite polytypes by first-principles calculation	Masami Kanzaki	Okayama University
145	π電子系有機分子／金属界面の電子状態と分子間相互作用	有賀　哲也	京都大学理学研究科化学専攻	Electronic structure and interaction at the interface of pi-electron organic molecules and metals	Aruga Tetsuya	Kyoto University
2. 強相関 / Strongly Correlated Quantum Systems						
146	トポロジカル物質の量子輸送現象の数値解析	三澤　貴宏	東京大学物性研究所	Numerical analysis of quantum transport phenomena in topological materials	Takahiro Misawa	The University of Tokyo
147	電子状態理論と時間分解実験データの統合による強相関系での非平衡高温超伝導の解析手法創出	今田　正俊	早稲田大学理工学術院	Development of methodology for analysis of nonequilibrium superconductivity in strongly correlated systems via integration of electronic state theory and time-resolved experimental data	Masatoshi Imada	Waseda University
148	変分モンテカルロ法による励起スペクトルと非平衡ダイナミックス計算による量子スピン液体と高温超伝導の機構解明への貢献	今田　正俊	早稲田大学理工学術院	Mechanism of quantum spin liquid and high-Tc superconductivity studied by excitation spectra and nonequilibrium dynamics calculation by variational Monte Carlo methods	Masatoshi Imada	Waseda University
149	フラストレートした量子スピン系におけるエネルギー流相関の数値的研究	山地　洋平	東京大学大学院工学系研究科	Numerical studies on energy current correlations in frustrated quantum spin systems	Youhei Yamaji	The University of Tokyo
150	2 次元ウィグナー結晶の格子整合性に関する変分モンテカルロ計算	加藤　岳生	東京大学物性研究所	Variational Monte Carlo calculation of two-dimensional Wigner crystal under lattice commensurability	Takeo Kato	The University of Tokyo

No.	課題名	氏名	所属	Title	Name	Organization
151	異種アニオンから構成される梯子型電子状態における超伝導の可能性に関する研究	黒木　和彦	大阪大学	Study on the possibility of superconductivity in ladder-type electronic structures constructed from multiple anions	Kazuhiko Kuroki	Osaka University
152	スピン軌道結合と電子相関による量子物性の理論的研究	求　幸年	東京大学大学院工学系研究科	Theoretical study of quantum properties induced by spin-orbit coupling and electron correlation	Yukitoshi Motome	The University of Tokyo
153	強いスピン軌道結合がもたらす新奇量子物性の理論的研究	求　幸年	東京大学大学院工学系研究科	Theoretical study of novel quantum properties induced by strong spin-orbit coupling	Yukitoshi Motome	The University of Tokyo
154	強相関系の磁性・トポロジーと輸送現象	川上　則雄	京都大学大学院理学研究科	Study of magnetism, topology and transport phenomena in strongly correlated quantum systems	Norio Kawakami	Kyoto University
155	第一原理計算と量子多体計算による多バンド系の電子状態と超伝導	大野　義章	新潟大学	First-principles and quantum many-body calculations for electronic states and superconductivity in the multi-band systems	Yoshiaki Ono	Niigata University
156	点群対称性に基づいた新規スキルミオン結晶の探索	速水　賢	北海道大学理学部物理学科	Search for new types of skyrmion crystals based on point group symmetry	Satoru Hayami	Hokkaido University
157	軌道自由度をもつ相関電子系における非平衡ダイナミクスの数値解析	古賀　昌久	東京工業大学	Numerical analysis for nonequilibrium dynamics in correlated electron systems with orbital degrees of freedom	Akihisa Koga	Tokyo Institute of Technology
158	多極子と異方的超伝導の第一原理的研究	石塚　淳	京都大学	Multipole and anisotropic superconductivity from first principles	Jun Ishizuka	Kyoto University
159	熱力学極限で定式化された連続虚時間量子モンテカルロ法の開発と応用	大越　孝洋	東京大学大学院工学系研究科	Development and applications of continuous-time quantum Monte Carlo method in the thermodynamic limit	Takahiro Ohgoe	The University of Tokyo
160	強相関ダイナミクスが誘起する新奇トポロジカル現象	吉田　恒也	筑波大学　数理物質系	Novel topological phenomena induced by strongly correlated dynamics	Tsuneya Yoshida	University of Tsukuba
161	強相関系の磁性と超伝導：非平衡系の手法を含むアプローチによる解析	川上　則雄	京都大学大学院理学研究科	Study of magnetism and superconductivity in strongly correlated quantum systems using approaches including non-equilibrium methods	Norio Kawakami	Kyoto University
162	準周期構造をもつ二重交換系の磁性と伝導性	古賀　昌久	東京工業大学	Magnetic and transport properties in double-exchange systems with quasiperiodicity	Akihisa Koga	Tokyo Institute of Technology
163	ニッケル酸化物における金属絶縁体転移の機構解明	野村　悠祐	理化学研究所創発物性科学研究センター	Study on metal-insulator transition in nickel oxides	Yusuke Nomura	RIKEN
164	複合アニオン化合物における電子相関と超伝導の可能性に関する研究	黒木　和彦	大阪大学	Study on electron correlation and possible superconductivity in mixed-anion systems	Kazuhiko Kuroki	Osaka University
165	超ウラン系における２チャンネル近藤効果の研究	堀田　貴嗣	首都大学東京理学研究科	Research of Two-Channel Kondo Effect in Transuranium Systems	Takashi Hotta	Tokyo Metropolitan University
166	Γ_7 および Γ_8 伝導バンドと混成する多軌道アンダーソンモデルにおける２チャンネル近藤効果	堀田　貴嗣	首都大学東京理学研究科	Two-Channel Kondo Effect Emerging in a Multiorbital Anderson Model Hybridized with Γ_7 and Γ_8 Conduction Bands	Takashi Hotta	Tokyo Metropolitan University
167	時間変動する磁場下でのキタエフスピン液体の磁気状態	那須　譲治	横浜国立大学	Magnetic state of Kitaev spin liquid under time-dependent field	Joji Nasu	Yokohama National University

No.	課題名	氏名	所属	Title	Name	Organization
168	強相関系で発現する非エルミートトポロジカル物性	吉田　恒也	筑波大学数理物質系	Non-Hermitian topological phenomena in strongly correlated systems	Tsuneya Yoshida	University of Tsukuba
169	キタエフ量子スピン液体に対する磁場クエンチによる時間発展	那須　譲治	横浜国立大学	Time evolution by magnetic-field quench in Kitaev spin liquid	Joji Nasu	Yokohama National University
170	有機ディラック電子系α-(BEDT-TTF)$_2$I$_3$の電荷秩序相におけるスピン電荷分離	小林　晃人	名古屋大学大学院理学研究科	Spin-Charge Separation in Charge Order Phase of Organic Dirac Electron System α-(BEDT-TTF)$_2$I$_3$	Akito Kobayashi	Nagoya University
171	動的平均場理論＋量子モンテカルロ法による多軌道強相関電子系の研究	星野　晋太郎	埼玉大学	Dynamical mean-field theory + quantum Monte Carlo approach to strongly correlated electron systems with multi-orbitals	Shintaro Hoshino	Saitama University
172	磁性体の光誘起ダイナミクスと高次高調波	石原　純夫	東北大学大学院理学研究科	Photoinduced dynamics and high harmonic generation in magnetism	Sumio Ishihara	Tohoku University
173	温度グリーン関数の低ランクテンソル表現の探索	品岡　寛	埼玉大学理学部物理学科	Exploring low-rank tensor representation of Matsubara Green's functions	Hiroshi Shinaoka	Saitama University
174	有機ディラック電子系α-(BEDT-TTF)$_2$I$_3$の電荷秩序相におけるスピン電荷分離	小林　晃人	名古屋大学大学院理学研究科	Spin-Charge Separation in Charge Order Phase of Organic Dirac Electron System α-(BEDT-TTF)$_2$I$_3$	Akito Kobayashi	Nagoya University
175	ハバードモデルにおける超伝導及び磁性状態の研究	山田　篤志	千葉大学理学研究科	Superconductivity and magnetic properties of the Hubbard model	Atsushi Yamada	Chiba University
176	最大エントロピー法やスパースモデリングを用いた状態密度の推定	松田　康弘	東京大学物性研究所	Estimation of the density of states using Maximum entropy method and Sparse modeling	Yasuhiro Matsuda	The University of Tokyo
177	変分モンテカルロ法による強相関電子系の基底状態・励起状態の計算	渡部　洋	理化学研究所	Calculation for ground and excited states in strongly-correlated electron systems by variational Monte Carlo method	Hiroshi Watanabe	RIKEN
178	最適化モンテカルロ法および第一原理計算による強相関電子系の研究	柳沢　孝	産業技術総合研究所	Study of strongly correlated electron systems based on optimization Monte Carlo method and first-principles calculations	Takashi Yanagisawa	National Institute of Advanced Industrial Science andTechnology
179	最適化モンテカルロ法および第一原理計算による強相関電子系の研究	柳沢　孝	産業技術総合研究所	Study of strongly correlated electron systems based on optimization Monte Carlo method and first-principles calculations	Takashi Yanagisawa	National Institute of Advanced Industrial Science andTechnology
180	希土類金属化合物における置換可能非磁性元素のスクリーニング	小林　理気	琉球大学	Screening of substitutable non-magnetic element in rare-earth inter-metallic compounds	Riki Kobayashi	University of the Ryukyus
181	電荷秩序相における電子エネルギーのキャリア密度依存性	酒井　正俊	千葉大学大学院工学研究院電気電子	Excess Carrier Density Dependence of Electronic Energy in Charge Order Phase	Masatoshi Sakai	Chiba University
3. 巨視系の協同現象 / Cooperative Phenomena in Complex, Macroscopic Systems						
182	全原子・粗視化分子動力学シミュレーションによるソフトマターの分子論的解析	篠田　渉	名古屋大学大学院工学研究科	Molecular basis analysis of Soft Materials using All-Atom and Coarse-Grained Molecular Dynamics Simulations	Wataru Shinoda	Nagoya University
183	テンソルネットワーク表現に基づくキタエフ関連モデルの変分計算	川島　直輝	東京大学物性研究所	Variational calculation of Kitaev and related models with tensor-network representation	Naoki Kawashima	The University of Tokyo

No.	課題名	氏名	所属	Title	Name	Organization
184	高次特異値分解を応用したテンソルのリング分解とその応用	川島　直輝	東京大学物性研究所	Tensor-Ring Decomposition Based on HOSVD and Its Appication	Naoki Kawashima	The University of Tokyo
185	複雑流体中のキャビテーション流れの分子動力学シミュレーション	浅野　優太	東京大学物性研究所	Molecular Dynamics Simulation of Cavitating Flow in a Complex Fluid	Yuta Asano	The University of Tokyo
186	複雑流体中のカルマン渦キャビテーション	浅野　優太	東京大学物性研究所	Karman-Vortex Cavitation in a Complex Fluid	Yuta Asano	The University of Tokyo
187	パイロクロア格子上フラストレート模型におけるスピンと格子ひずみの同時ガラス転移	吉野　元	大阪大学サイバーメディアセンター	Simultaneous spin and Jahn-Teller glass transitions in a model frustrated system on pyrochlore lattice	Hajime Yoshino	Osaka University
188	量子多体系におけるエンタングルメント・量子相転移・量子ダイナミクス	藤堂　眞治	東京大学大学院理学系研究科	Entanglement, Quantum Phase Transition, and Quantum Dynamics in Quantum Many-body Systems	Synge Todo	The University of Tokyo
189	分子動力学シミュレーションによる全長アミロイドベータペプチドの凝集過程の研究	奥村　久士	自然科学研究機構生命創成探究センター	Aggregation process of full-length amyloid-beta peptides studied by molecular dynamics simulations	Hisashi Okumura	Institute for Molecular Science
190	フラストレート磁性体における新奇秩序	川村　光	大阪大学理学研究科	Novel order in frustrated magnets	Hikaru Kawamura	Osaka University
191	低次元系のスピンネマティック相の数値対角化による研究	坂井　徹	兵庫県立大学大学院物質理学研究科	Numerical Diagonalization Study on Spin Nematic Phase of Low-Dimensional Systems	Toru Sakai	University of Hyogo
192	生体膜の構造形成	野口　博司	東京大学物性研究所	structure formation of biomembrane	Hiroshi Noguchi	The University of Tokyo
193	機械学習の技術を用いたフラストレート磁性体の研究	野村　悠祐	理化学研究所　創発物性科学研究センター	Study on frustrated magnetism using machine learning	Yusuke Nomura	RIKEN
194	生体膜の構造形成	野口　博司	東京大学物性研究所	structure formation of biomembranes	Hiroshi Noguchi	The University of Tokyo
195	フラストレート磁性体の新規秩序とダイナミクスの研究	大久保　毅	東京大学大学院理学系研究科	Novel phases and dynamics in frustrated spin systems	Tsuyoshi Okubo	The University of Tokyo
196	大規模粗視化分子動力学法を用いた持続応力による結晶性高分子の破壊	樋口　祐次	東京大学物性研究所	Creep fracture process of crystalline polymers by large-scale molecular dynamics simulation	Yuji Higuchi	The University of Tokyo
197	高分子流体・固体のマルチスケール解析	村島　隆浩	東北大学大学院理学研究科	Multiscale analysis of polymeric fluids and solids	Takahiro Murashima	Tohoku University
198	Kitaev スピン液体の磁化過程に関する数値的研究	井戸　康太	東京大学物性研究所	Numerical studies on magnetization process of the Kitaev spin liquid	Kota Ido	The University of Tokyo
199	スレーター・モットクロスオーバー物質のダイナミクス	諏訪　秀麿	東京大学大学院理学系研究科	Dynamics of Slater-Mott crossover materials	Hidemaro Suwa	The University of Tokyo
200	ミニマル模型によるリラクサー誘電体の研究	富田　裕介	芝浦工業大学	Study of relaxor ferroelectrics by using a minimal model	Yusuke Tomita	Shibaura Institute of Technology

No.	課題名	氏名	所属	Title	Name	Organization
201	乱れた電子系における波動関数の解析	大槻　東巳	上智大学理工学部	Wave function analyses in disordered electron systems	Tomi Ohtsuki	Sophia University
202	大規模粗視化分子動力学法による結晶性高分子の壊れやすい構造の解明	樋口　祐次	東京大学物性研究所	Brittle structure of crystalline polymers by large-scale coarse-grained molecular dynamics simulation	Yuji Higuchi	The University of Tokyo
203	マテリアルズ・インフォマティクスによる熱機能材料の探索	塩見　淳一郎	東京大学工学系研究科	Screening for Thermal Functional Materials using Materials Informatics	Junichiro Shiomi	The University of Tokyo
204	蛋白質物性に強く関与するソフトモードの効率的サンプリングシミュレーション	北尾　彰朗	東京工業大学生命理工学院	Efficient sampling simulation of the soft modes significantly contribute to protein properties	Akio Kitao	The University of Tokyo
205	スピン液体相の汎関数くりこみ群による研究	加藤　雄介	東京大学総合文化研究科	Functional Renormalization Group Study of Quantum Spin Liquids	Yusuke Kato	The University of Tokyo
206	数値的手法によるバルクエッジ対応の普遍性の研究	初貝　安弘	筑波大学大学院数理物質科学研究科	Universality of bulk-edge correspondence by numerical methods	Yasuhiro Hatsugai	University of Tsukuba
207	高分子流体・固体のマルチスケール解析	村島　隆浩	東北大学大学院理学研究科	Multiscale analysis of polymeric fluids and solids	Takahiro Murashima	Tohoku University
208	蜂の巣格子上拡張キタエフ模型のスピン液体	鈴木　隆史	兵庫県立大学　大学院工学研究科	Quantum spin liquids in extended Kitaev models on a honeycomb lattice	Takafumi Suzuki	University of Hyogo
209	異方性のある量子スピン反強磁性鎖のトポロジカル磁化プラトー	坂井　徹	兵庫県立大学大学院物質理学研究科	Topological Magnetization Plateau of Quantum Antiferromagnetic Spin Chain with Anisotropies	Toru Sakai	University of Hyogo
210	分子動力学シミュレーションによる全長アミロイドベータペプチドの凝集過程の研究	奥村　久士	自然科学研究機構生命創成探究センター	Aggregation process of full-length amyloid-beta peptides studied by molecular dynamics simulations	Hisashi Okumura	Institute for Molecular Science
211	産業や医療に有用な新規タンパク質の合理的設計	新井　宗仁	東京大学大学院総合文化研究科	Computational rational design of novel proteins for industrial and pharmaceutical applications	Munehito Arai	The University of Tokyo
212	フラストレート磁性体における新奇秩序	川村　光	大阪大学理学研究科	Novel order in frustrated magnets	Hikaru Kawamura	Osaka University
213	希土類永久磁石における第一原理有限温度計算と実験測定のデータ同化	松本　宗久	高エネルギー加速器研究機構 物質構造科学研究所	Multiscale data assimilation between ab initio theory at finite temperatures and experiments for rare-earth permanent magnets	Munehisa Matsumoto	KEK
214	抗アレルギー薬の開発に向けたタンパク質デザイン	新井　宗仁	東京大学大学院総合文化研究科	Protein design toward the development of anti-allergy drugs	Munehito Arai	The University of Tokyo
215	非平衡定常系に拡張された熱力学関数による構造形成の研究	中川　尚子	茨城大学理学部	Macroscopic properties characterized by an extended thermodynamic functions to nonequilibrium	Naoko Nakagawa	Ibaraki University
216	動的スケーリング解析を利用したトポロジカル相転移の臨界普遍性の研究	尾関　之康	電気通信大学情報理工学研究科	Dynamical scaling analysis applied to studies on ciritical universality for topological phase transitions	Yukiyasu Ozeki	The University of Electro-Communications
217	$LaFe_2As_2$ における超伝導安定性	Jeschke Harald	岡山大学異分野基礎科学研究所	Stability of the superconductor $LaFe_2As_2$	Harald Jeschke	Okayama University

No.	課題名	氏名	所属	Title	Name	Organization
218	動的スケーリング解析を利用したトポロジカル相転移の臨界普遍性の研究 II	尾関　之康	電気通信大学情報理工学研究科	Dynamical scaling analysis applied to studies on ciritical universality for topological phase transitions II	Yukiyasu Ozeki	The University of Electro-Communications
219	スピン軌道絶縁体の動的スピン構造因子	諏訪　秀麿	東京大学大学院理学系研究科	Dynamical spin structure factor of spin-orbit insulator	Hidemaro Suwa	The University of Tokyo
220	フラストレートした量子磁性体に対する熱ゆらぎの効果	下川　統久朗	沖縄科学技術大学院大学	Thermal effect on the quantum frustrated magnetism	Tokuro Shimokawa	Okinawa Institute of Science and Technology Graduate University
221	量子スピン系の低エネルギー状態に関する数値的研究	中野　博生	兵庫県立大学大学院物質理学研究科	Numerical study on low-energy states of quantum spin systems	Hiroki Nakano	University of Hyogo
222	低次元フラストレート量子スピン系の強磁場相の研究	松田　康弘	東京大学物性研究所	Study on the high-field-induced phases of low dimensional frustrated quantum spin system	Yasuhiro Matsuda	The University of Tokyo
223	データ駆動科学の物質科学への展開	福島　孝治	東京大学大学院総合文化研究科	Development of data-driven science to materials science	Koji Hukushima	The University of Tokyo
224	磁性材料における順問題としての電子状態データの粗視化と逆問題としての実験データ解析の自己無撞着解析	松本　宗久	高エネルギー加速器研究機構 物質構造科学研究所	Self-consistent analysis between miroscopic electronic structure calculations and macroscopic data analysis for experimental measurements	Munehisa Matsumoto	KEK
225	カゴメ格子 Kitaev-Heisenberg 模型の有限温度の性質とスピンダイナミクス	遠山　貴己	東京理科大学理学部応用物理学科	Finite-Temperature Properties and Spin Dynamics in Kagome Kitaev-Heisenberg Model	Takami Tohyama	Tokyo University of Science
226	近赤外光を有効利用する色素の分子設計のための電子状態データベースの作成	小松　勇	国立天文台	Constructing the electronic structure database for the molecular design of pigments utilizing near infrared light	Yu Komatsu	National Astronomical Observatory of Japan
227	相転移キネティクスとポリアモルフィズム	渕崎　員弘	愛媛大学理工学研究科	Kinetics of phase transition and polyamorphism	Kazuhiro Fuchizaki	Ehime University
228	有機分子をインターカレートした FeSe における電子構造および超伝導のドープ量依存性	Jeschke Harald	岡山大学異分野基礎科学研究所	Doping dependence of electronic structure and superconductivity in FeSe intercalated by organic molecules	Harald Jeschke	Okayama University
229	物性における数値繰り込み群法の応用	原田　健自	京都大学大学院情報学研究科	Application of numerical renormalization group method in condensed-matter physics	Kenji Harada	Kyoto University
230	剛体球コロイド系における結晶核生成頻度の精密な測定	田中　肇	東京大学生産技術研究所	Precise measurement of crystal nucleation rate in a hard-sphere colloidal system	Hajime Tanaka	The University of Tokyo
231	非平衡初期緩和の温度スケーリングの一般化	野々村　禎彦	物質・材料研究機構	Generalization of temperature scaling in early-time nonequilibrium relaxation	Yoshihiko Nonomura	National Institute for Materials Science
232	フラストレート磁性体のスピン多極子ダイナミクスとスピン伝導	大西　弘明	日本原子力研究開発機構 先端基礎研究センター	Spin multipole dynamics and spin transport in frustrated magnets	Hiroaki Onishi	Japan Atomic Energy Agency
233	相転移キネティクスとポリアモルフィズム	渕崎　員弘	愛媛大学理工学研究科	Kinetics of phase transition and polyamorphism	Kazuhiro Fuchizaki	Ehime University
234	動的ヤンテラー効果を持つパイロクロア格子反強磁性ハイゼンベルグ模型における相転移	吉野　元	大阪大学サイバーメディアセンター	Phase transitions of an antiferromagnetic Heisenberg spin model with a dynamical Jahn-Teller effect on a pyrochlore lattice	Hajime Yoshino	Osaka University

No.	課題名	氏名	所属	Title	Name	Organization
235	シェル・モデルを用いた強誘電体の分子動力学シミュレーション V	橋本　保	産業技術総合研究所	Molecular dynamics simulation of ferroelectrics using a shell model V	Tamotsu Hashimoto	AIST
236	フラストレートした量子磁性体に対する熱ゆらぎの効果	下川　統久朗	沖縄科学技術大学院大学	Thermal effect on the quantum frustrated magnetism	Tokuro Shimokawa	Okinawa Institute of Science and Technology Graduate University
237	摩擦の物理	松川　宏	青山学院大学理工学部	Physics of Friction	Hiroshi Matsukawa	Aoyama Gakuin University
238	電気二重層の形成により界面局在場を形成するイオン液体の構造化とダイナミクスの解析	福井　賢一	大阪大学大学院基礎工学研究科	Analysis on Structuring and Dynamics of Ionic Liquid Forming Electric Double Layer as a Local Interfacial Field	Ken-Ichi Fukui	Osaka University
239	非対角固有状態熱化仮説に関する数値的研究	伊與田　英輝	東京大学工学系研究科	Numerical analysis on the off-diagonal eigenstate thermalization hypothesis	Eiki Iyoda	The University of Tokyo
240	ハミルトニアン行列の低ランク行列近似を用いた全固有値計算と量子スピン系への応用	五十嵐　亮	東京大学情報基盤センター	Full diagonalization using low-rank approximation to Hamiltonian matrices and its application to quantum spin models	Ryo Igarashi	The University of Tokyo
241	空間構造をもつ一次元量子スピン系の数値的研究	利根川　孝	神戸大学大学院理学研究科	Numerical Study of the One-Dimensional Quantum Spin Systems with Spatial Studies	Takashi Tonegawa	Kobe University
242	量子スピン系の低エネルギー状態に関する数値的研究	中野　博生	兵庫県立大学大学院物質理学研究科	Numerical study on low-energy states of quantum spin systems	Hiroki Nakano	University of Hyogo
243	実験結果を入力とした有効モデル推定	田村　亮	国立研究開発法人 物質・材料研究機構	Effective model estimation using experimental results	Ryo Tamura	National Institute for Materials Science
244	スパース推定による広域 X 線吸収微細構造計測の解析手法の確立	熊添　博之	熊本大学パルスパワー科学研究所	Establishment of new analysis method for extend X-ray absorption fine structure with sparse modeling	Hiroyuki Kumazoe	Kumamoto University
245	自由エネルギーランドスケープを用いた過冷却液体とタンパク質のダイナミックスの研究	吉留　崇	東北大学大学院工学研究科	Investigation of dynamics of a supercooled liquid and proteins using the free-energy landscape	Takashi Yoshidome	Tohoku University
246	分子動力学法による超臨界点近傍流体の物性評価	渡辺　宙志	慶応義塾大学理工学部	Molecular dynamics study of the properties of near-critical fluids	Hiroshi Watanabe	Keio University
247	ナノ構造下の電子状態制御：モデル化とその応用	苅宿　俊風	物材機構	Manipulation of electronic states with nanostructures: model construction and its application	Toshikaze Kariyado	NIMS
248	磁性体模型における新規なトポロジカル励起	赤城　裕	東京大学 大学院理学系研究科	Novel Topological Excitation in Magnet	Yutaka Akagi	The University of Tokyo
249	遷移金属カルコゲナイド物質の CDW 相における格子ダイナミクスの研究	村井　直樹	日本原子力研究開発機構	Lattice dynamics investigation of a charge-density-wave phase in transition metal chalcogenides	Naoki Murai	JAEA
250	階層性構造を有する有機材料の熱輸送スペクトルの解明	志賀　拓麿	東京大学大学院工学系研究科	Clarification of thermal transport spectra in hierarchical structured organic bulk materials	Takuma Shiga	The University of Tokyo
251	反応力場を用いた炭素構造体中の水の分子動力学計算	水口　朋子	京都工芸繊維大学	Molecular dynamics simulations of water confined in carbon structures with the reactive force field	Tomoko Mizuguchi	Kyoto Institute of Technology

No.	課題名	氏名	所属	Title	Name	Organization
252	X線多波回折によるタンパク質結晶構造解析法の研究	沖津　康平	東京大学 大学院工学系研究科	Study on an X-ray n-beam method to solve protein crystal structure	Kouhei Okitsu	The University of Tokyo
253	d 波超伝導体における熱ホール角の増大に対する研究	北　孝文	北海道大学理学部物理学科	studying the enhancement of the thermal Hall angle in d-wave superconductors	Takafumi Kita	Hokkaido University
254	拡張アンサンブル法によるレナード・ジョーンズ粒子系の相転移の研究	岡本　祐幸	名古屋大学大学院理学研究科	Study on phase transitions of Lennard-Jones fluid systems by generalized-ensemble algorithms	Yuko Okamoto	Nagoya University
255	拡張アンサブル法による複雑系の研究	岡本　祐幸	名古屋大学大学院理学研究科	Study on complex systems by generalized-ensemble algorithms	Yuko Okamoto	Nagoya University
256	臨界点近傍のコロイドのダイナミクスに対する流体力学的相互作用の影響	田中　肇	東京大学生産技術研究所	Impact of hydrodynamic interactions on colloidal dynamics near a critical point	Hajime Tanaka	The University of Tokyo
257	高次テンソル繰り込み群法の改善とその応用	森田　悟史	東京大学物性研究所	Improvement of higher-order tensor renormalization group method and its applications	Satoshi Morita	The University of Tokyo
258	分岐ネットワークの統計的性質	湯川　諭	大阪大学大学院理学研究科	Statistical Properties in a Branching Network	Satoshi Yukawa	Osaka University
259	ブリージングパイロクロア反強磁性体における局所格子歪みと磁場効果	青山　和司	大阪大学大学院理学研究科	Effects of a magnetic field on spin-lattice-coupled orders in breathing pyrochlore antiferromagnets	Kazushi Aoyama	Osaka University
260	ソフトマテリアルの秩序構造とその光学的性質の計算	福田　順一	九州大学　大学院理学研究院	Calculation of ordered structures and their optical properties of soft materials	Jun-Ichi Fukuda	Kyushu University
261	コロイドのネットワーク状相分離の粗大化メカニズム	田中　肇	東京大学生産技術研究所	Coarsening mechanism of network-forming phase separation in colloidal suspensions	Hajime Tanaka	The University of Tokyo
262	ガラスの遅いダイナミクスの構造的起源に関する研究	田中　肇	東京大学生産技術研究所	Study on the structural origin of glassy slow dynamics	Hajime Tanaka	The University of Tokyo
263	金属のフェムト秒発光ダイナミクス	小野　頌太	岐阜大学	Femtosecond luminescence dynamics of metals	Shota Ono	Gifu University
264	1次元フラストレート量子スピン系の数値的研究	飛田　和男	埼玉大学大学院理工学研究科	Numerical Study of One Dimensional Frustrated Quantum Spin Systems	Kazuo Hida	Saitama University
265	多スピン交換相互作用を含む系の磁性	安田　千寿	琉球大学理学部	Magnetism in the system with the multiple-spin exchange interactions	Chitoshi Yasuda	University of the Ryukyus
266	タンパク質分子機械に駆動されるフィラメントの二体衝突のシミュレーション	佐々木　一夫	東北大学大学院工学研究科	Simulation analysis of collision of two filaments driven by protein molecular motors	Kazuo Sasaki	Tohoku University
267	粗視化 MD 法を用いた環動ゲルの動的力学物性の解明	眞弓　皓一	東京大学大学院新領域創成科学研究科	Study on Dynamic Mechanical Properties of Slide-Ring Gels using Coarse-Grained MD Simulations	Koichi Mayumi	The University of Tokyo
268	全原子 MD 法を用いたポリロタキサンの微視的ダイナミクスの解明	眞弓　皓一	東京大学大学院新領域創成科学研究科	Study on Microscopic Dynamics of Polyrotaxanes using Full-Atomistic MD Simulations	Koichi Mayumi	The University of Tokyo

No.	課題名	氏名	所属	Title	Name	Organization
269	モンテカルロ非平衡初期緩和の統一的理解	野々村　禎彦	物質・材料研究機構	Unified understanding of early-time nonequilibrium relaxation in Monte Carlo simulations	Yoshihiko Nonomura	National Institute for Materials Science
270	Patchy 粒子系に関する分子シミュレーション	寺尾　貴道	岐阜大学工学部	Molecular simulation of patchy particles	Takamichi Terao	Gifu University
271	２次元反強磁性 XXZ モデルにおける古典スピン系の輸送現象	青山　和司	大阪大学大学院理学研究科	Transport properties of the antiferromagnetic classical XXZ model in two dimensions	Kazushi Aoyama	Osaka University
272	統計力学手法による保磁力機構の解明	西野　正理	物質・材料研究機構	Elucidation of coercivity mechanism by statistical physical approaches	Masamichi Nishino	National Institute for Materials Science
273	ペーストのメモリー効果の転移現象	中原　明生	日本大学理工学部	Transition in the memory effect of paste	Akio Nakahara	Nihon University
274	分子動力学計算法と教師なし機械学習を使った非晶質前駆体からの結晶形成機構の新しい解析方法構築	灘　浩樹	産業技術総合研究所	Construction of A New Method for Analysis of Crystallization Mechanism from Amorphous Precursor Using Molecular Dynamics Simulation Method and Unsupervised Machine Learning	Hiroki Nada	National Institute for Advanced Industrial Science and Technology
275	球体カゴメ系の一様帯磁率に対する Dzyaloshinskii-Moriya 相互作用と歪みの影響	福元　好志	東京理科大学	Effects of Dzyaloshinskii--Moriya interactions and structural distortions on magnetic susceptibilities of spherical-kagome spin-systems	Fukumoto Yoshiyuki	Tokyo University of Science
276	シリカガラスの圧力誘起相転移過程で出現する不均質構造の解明	若林　大佑	高エネルギー加速器研究機構物質構造科学研究所	Inhomogeneous structure of silica glass during the structural transformations under high pressure	Daisuke Wakabayashi	KEK
277	二体自己無撞着法を用いた超構造強相関物質の超伝導の理論的研究	西口　和孝	神戸大学大学院科学技術イノベーション研究科	Theoretical study for superconductivity in superstructured strongly correlated materials with two- particle self-consistent approach	Kazutaka Nishiguchi	Kobe University
278	時間変調された外場の下での光双安定現象の量子ダイナミクス	白井　達彦	早稲田大学グリーン・コンピューティング・システム研究機構	The analysis of the dynamical response to the optical bistability	Tatsuhiko Shirai	Waseda University
279	ソフトマテリアルの秩序構造とその光学的性質の計算	福田　順一	九州大学大学院理学研究院	Calculation of ordered structures and their optical properties of soft materials	Jun-Ichi Fukuda	Kyushu University
280	相互作用のない電子格子系間に光によって生成される量子もつれ状態の性質	石田　邦夫	宇都宮大学大学院工学研究科	Entanglement in remote electron-phonon systems created by photoirradiation	Kunio Ishida	Utsunomiya University
281	磁性薄膜における双極子相互作用と短距離相互作用の競合	小松　尚登	物質・材料研究機構	Competiton between dipolar and short-range interactions on the magnetic thin films	Hisato Komatsu	National Institute for Materials Science
282	フェムト秒領域における電子・格子・光相互作用系の非断熱ダイナミクス	石田　邦夫	宇都宮大学大学院工学研究科	Ultrafast nonadiabatic dynamics of electron-phonon-photon system	Kunio Ishida	Utsunomiya University
283	空間構造をもつ一次元量子スピン系の数値的研究	利根川　孝	神戸大学大学院理学研究科	Numerical Study of the One-Dimensional Quantum Spin Systems with Spatial Structures	Takashi Tonegawa	Kobe University
284	熱伝導と熱輻射の統一的理解	志賀　拓麿	東京大学大学院工学系研究科	Compherensive study on transition between heat conduction and radiative heat transfer	Takuma Shiga	The University of Tokyo
285	高密剛体球系における非平衡相転移と遅い緩和	礒部　雅晴	名古屋工業大学	Nonequilibrium phase transition and slow dynamics in the dense hard sphere systems	Masaharu Isobe	Nagoya Institute of Technology

No.	課題名	氏名	所属	Title	Name	Organization
286	フォノニック結晶の熱伝導解析	志賀　拓麿	東京大学大学院工学系研究科	Heat conduction analysis for phononic crystal	Takuma Shiga	The University of Tokyo
287	球体カゴメ系の磁場中低温比熱に対する Dzyaloshinskii-Moriya 相互作用 とランダムネスの効果	福元　好志	東京理科大学	Effects of Dzyaloshinskii-Moriya interactions and exchange randomness on low-temperature specific heats of spherical-kagome spin-systems	Fukumoto Yoshiyuki	Tokyo University of Science
288	横磁場イジングモデルにおける新規量子相の解析	堀田　知佐	東京大学総合文化研究科	Numerical studies on some new phases of the transverse Ising model	Chisa Hotta	The University of Tokyo
289	イジングマシンの性能向上を指向した統計力学研究	田中　宗	早稲田大学 グリーン・コンピューティング・システム研究機構	Study on Ising machines from a viewpoint of statistical mechanics	Shu Tanaka	Waseda University
290	フラストレート型遍歴磁性体における多重 Q 状態の磁気構造	内田　尚志	北海道科学大学	Magnetic structures of multiple-Q states in frustrated itinerant magnets	Takashi Uchida	Hokkaido University of Science
291	グラフェンのディラックコーン周りにおける不均一電子分布の超高速緩和	小野　頌太	岐阜大学	Ultrafast relaxation of inhomogeneous electron distribution around the Dirac cone in graphene	Shota Ono	Gifu University
292	Patchy 粒子系に関する分子シミュレーション	寺尾　貴道	岐阜大学工学部	Molecular simulation of patchy particles	Takamichi Terao	Gifu University
293	磁性薄膜における双極子相互作用と Dzyaloshinskii-Moriya 相互作用の競合	小松　尚登	物質・材料研究機構	Competiton between dipolar and Dzyaloshinskii-Moriya interactions on the magnetic thin films	Hisato Komatsu	National Institute for Materials Science
294	古典スピン系による磁化反転解析	檜原　太一	東京大学理学系研究科	Magnetization reversal process in classical spin systems	Taichi Hinokihara	The University of Tokyo
295	X 線多波回折理論による結晶構造解析法の研究	沖津　康平	東京大学 大学院工学系研究科	Study on crystal structure analysis using the X-ray multiple-beam diffraction theory	Kouhei Okitsu	The University of Tokyo
296	組織内での細胞誘導機構の数値的研究	松下　勝義	大阪大学理学研究科	Numerical Study of Cell Guiding Mechanism in Cellular Tissue	Katsuyoshi Matsushita	Osaka University
297	NISQ 量子コンピュータを用いた量子多体系の物性計算のシミュレーション	藤井　啓祐	大阪大学	Quantum simulation for quantum many body systems using noisy-intermediate-scale quantum computers	Keisuke Fujii	Osaka University
298	組織中の接着依存細胞ダイナミクス	松下　勝義	大阪大学理学研究科	Adhesion Inducing Cell Dynamics in Tissue	Katsuyoshi Matsushita	Osaka University
299	河川ネットワークの統計的性質	湯川　諭	大阪大学大学院理学研究科	Statistical Properties of a River Network	Satoshi Yukawa	Osaka University
300	ペーストの振動と剪断と磁場の記憶効果のシミュレーション	中原　明生	日本大学理工学部	Numerical simulation for memory of flow, vibration and magnetic field in paste	Akio Nakahara	Nihon University
301	量子ビットシステムの欠陥になどに対するロバスト性の検証	棚本　哲史	帝京大学	Simulation regarding robustness of qubit system again defects	Tetsufumi Tanamoto	Teikyo University
302	有向パーコレーション転移点近傍における界面の成長とゆらぎに関する数値的研究	深井　洋佑	理化学研究所 生命機能科学研究センター	Numerical simulation of interfacial growth and fluctuation near the directed percolation transition	Yohsuke Fukai	RIKEN

No.	課題名	氏名	所属	Title	Name	Organization
303	ゼオライト合成中における原子再配列の理論的、実験的検討	大久保　達也	東京大学大学院工学系研究科化学システム	Theoretical and experimental investigation on atomic configuration in zeolite syntheses	Tatsuya Okubo	The University of Tokyo
304	スピン・ボゾン模型の非マルコフ・ダイナミクスの数値計算	羽田野　直道	東京大学生産技術研究所	Numerical Calculations of Non-Markovian Dynamics of Spin-Boson Models	Naomichi Hatano	The University of Tokyo
305	正方格子反強磁性体 La_2MO_4(M = Cu, Ni) における非弾性光散乱	乗木　優作	北海道大学大学院理学研究院	Inelastic light scattering in the square-lattice antiferromagnets $La_2MO_4$$ (M = Cu, Ni)	Yusaku Noriki	Hokkaido University
306	相互作用粒子系の数値解析	舟木　直久	早稲田大学理工学術院	Numerical Analysis on Particle Interaction System	Tadahisa Funaki	Waseda University
307	曲がった初期条件のもとでの Kardar-Parisi-Zhang 普遍ゆらぎと変分公式	深井　洋佑	理化学研究所 生命機能科学研究センター	Kardar-Parisi-Zhang universal fluctuation with curved initial conditions and variational formula	Yohsuke Fukai	RIKEN
308	厳密対角化による量子パイロクロア磁性体の研究	門脇　広明	首都大学東京 理工学研究科	Exact diagonalization of quantum pyrochlore model	Hiroaki Kadowaki	Tokyo Metropolitan University
309	時間反転対称性の破れた超伝導体接合の数値解析法の研究	田沼　慶忠	秋田大学大学院理工学研究科	Study on numerical analysis method of superconducting junctions with broken time reversal symmetry states	Yasunari Tanuma	Akita University

令和元年度 スーパーコンピュータ計算物質科学スパコン共用事業課題一覧
/ Supercomputing Consortium for Computational Materials Science Project List of Supercomputer System 2019

前期 / The first half term

No.	課題名	氏名	所属		Title	Name	Organization
1	高機能半導体	押山　淳	名古屋大学	未来材料・システム研究所	Exploration of new-functionality and high-performance semiconductor devices	Atsushi Oshiyama	Nagoya University
2	スピン軌道相互作用の大きな物質での量子スピン液体相の追求	今田　正俊	早稲田大学		Studies on Quantum Spin Liquids in Materials with Strong Spin-Orbit Interaction	Masatoshi Imada	Waseda University
3	第一原理フェーズ・フィールド・マッピング	香山　正憲	産業技術総合研究所		First-Principles Phase Field Mapping	Masanori Kohyama	National Institute of Advanced Industrial Science and Technology
4	重点課題５「エネルギー変換 (化学エネルギー)	杉野　修	東京大学	物性研究所	Priority project 5--- energy conversion (chemical energy)	Osamu Sugino	The University of Tokyo
5	電解質液体とガラスに潜む長距離ゆらぎと輸送特性の分子動力学計算	芝　隼人	東北大学	金属材料研究所	Molecular dynamics study of long-ranged fluctuation and transport properties of　electrolyte and glassy liquids	Hayato Shiba	Tohoku University
6	交差検証を用いた解析接続結果に関する精度検証手法の開発	吉見　一慶	東京大学	物性研究所	Development of accuracy verification method on analytic continuation results using cross validation	Kazuyoshi Yoshimi	The University of Tokyo
7	第一原理計算を用いた有機伝導体における量子スピン液体の研究	三澤　貴宏	東京大学	物性研究所	Numerical Study of Quantum Spin Liquid in Organic Conductors using Ab initio Calculation	Takahiro Misawa	The University of Tokyo
8	光・電子融合デバイス	矢花　一浩	筑波大学	計算科学研究センター	Unified Photonic-Electronic Devices	Kazuhiro Yabana	University of Tsukuba
9	テンソルネットワーク法の物性物理学への応用	川島　直輝	東京大学	物性研究所	Application of Tensor Network Method to Condensed Matter Physics	Naoki Kawashima	The University of Tokyo
10	ポスト京課題７　サブ課題 G ④大型実験施設との連携	遠山　貴巳	東京理科大学	理学部第一部	Cooperation Research with Big Experimental Facilities	Takami Tohyama	Tokyo University of Science
11	エネルギーの変換・貯蔵 — 電気エネルギー：全電池シミュレータの基盤技術の開発研究	岡崎　進	名古屋大学	大学院工学研究科	Conversion and storage of energy - Fuel cells and secondary batteries: Research and development of fundamental technologies of battery simulators	Susumu Okazaki	Nagoya University
12	フラグメント分割型 GW/BSE 法の開発と有機光電子材料への応用	藤田　貴敏	分子科学研究所		Development of Fragment-Based GW/BSE Method and Application to Organic Optoelectronic Materials	Takatoshi Fujita	Institute for Molecular Science
13	データ駆動型マテリアルデザインによる新機能高エントロピー合金の探索	福島　鉄也	大阪大学	ナノサイエンスデザイン教育研究センター	Data-driven materials design for new functional high entropy alloys	Tetsuya Fukushima	Osaka University
14	二次電池材料の電子論	小口　多美夫	大阪大学	産業科学研究所	Electron Theory on Secondary-Battery Materials	Tamio Oguchi	Osaka University

No.	課題名	氏名	所属		Title	Name	Organization
15	貴金属フリーの汎用元素ナノ触媒に向けた第一原理計算	武次　徹也	北海道大学	大学院理学研究院	Ab initio study toward abundant element nanocatalysts with less precious metals	Tetsuya Taketsugu	Hokkaido University
16	高性能永久磁石・磁性材料	三宅　隆	産業技術総合研究所		High performance permanent magnets and magnetic materials	Takashi Miyake	National Institute of Advanced Industrial Science and Technology
17	ナトリウム系濃厚電解液の動的挙動解析	山田　淳夫	東京大学	大学院工学系研究科	Dynamical analyses on electrolytes for Na-ion batteries	Atsuo Yamada	The University of Tokyo
18	B、C、Nを用いた電子デバイス新物質の設計研究	斎藤　晋	東京工業大学	理学院	Materials design using B, C, and N for next-generation device	Susumu Saito	Tokyo Institute of Technology
19	磁性材料界面の第一原理計算	合田　義弘	東京工業大学	物質理工学院	First-principles study of magnetic-material interfaces	Yoshihiro Gohda	Tokyo Institute of Technology
20	複雑混相流動のマルチスケールシミュレーション	川勝　年洋	東北大学	大学院理学研究科	Multiscale simulations on complex multiphase flows	Toshihiro Kawakatsu	Tohoku University
21	複雑流体の分子動力学計算	野口　博司	東京大学	物性研究所	Molecular Dynamics Simulation of Complex Fluids	Hiroshi Noguchi	The University of Tokyo
22	次世代計算機を対象とした超並列電子状態計算とデータ駆動科学の融合	星　健夫	鳥取大学大学院	工学研究科	Massively parallel electronic structure calculation and data-driven science for next-generation supercomputers	Takeo Hoshi	Tottori University

後期 / The second half term

No.	課題名	氏名	所属		Title	Name	Organization
23	高機能半導体	押山　淳	名古屋大学	未来材料・システム研究所	Exploration of new-functionality and high-performance semiconductor devices	Atsushi Oshiyama	Nagoya University
24	第一原理ハミルトニアンに基づく分子性導体の量子スピン液体の研究	今田　正俊	早稲田大学		Studies on quantum spin liquids in molecular conductors based on first-principles Hamiltonian	Masatoshi Imada	Waseda University
25	第一原理フェーズ・フィールド・マッピング	香山　正憲	産業技術総合研究所		First-Principles Phase Field Mapping	Masanori Kohyama	National Institute of Advanced Industrial Science and Technology
26	電解質液体に対する電圧引加シミュレーション	芝　隼人	東北大学	金属材料研究所	Simulation of electrolyte liquids under constant potential bias	Hayato Shiba	Tohoku University
27	交差検証を用いた解析接続結果に関する精度検証手法の開発	吉見　一慶	東京大学	物性研究所	Development of accuracy verification method on analytic continuation results using cross validation	Kazuyoshi Yoshimi	The University of Tokyo
28	多変数変分モンテカルロ法を用いた動的構造因子の計算	三澤　貴宏	東京大学	物性研究所	Development of numerical method for calculating dynamical structure factors based on many-variable variational Monte Carlo method	Takahiro Misawa	The University of Tokyo
29	テンソルネットワーク法の物性物理学への応用	川島　直輝	東京大学	物性研究所	Application of Tensor Network Method to Condensed Matter Physics	Naoki Kawashima	The University of Tokyo

No.	課題名	氏名	所属		Title	Name	Organization
30	大規模 GW+BSE 法による有機光材料系の励起状態計算	藤田　貴敏	分子科学研究所		Large-scale GW+BSE excited-state calculations for organic optoelectronic materials	Takatoshi Fujita	Institute for Molecular Science
31	複雑混相流動のマルチスケールシミュレーション	川勝　年洋	東北大学	大学院理学研究科	Multiscale simulations on complex multiphase flows	Toshihiro Kawakatsu	Tohoku University
32	複雑流体の分子動力学計算	野口　博司	東京大学	物性研究所	Molecular Dynamics Simulation of Complex Fluids	Hiroshi Noguchi	The University of Tokyo
33	Mg_2SiO_4 の超高圧相における秩序無秩序転移	飯高　敏晃	理化学研究所		Order-disorder transition in the superhigh-pressure phase of Mg_2SiO_4	Toshiaki Iitaka	RIKEN
34	次世代計算機を対象とした超並列電子状態計算とデータ駆動科学の融合	星　健夫	鳥取大学大学院	工学研究科	Massively parallel electronic structure calculation and data-driven science for next-generation supercomputers	Takeo Hoshi	Tottori University
35	分子動力学シミュレーションを用いた長鎖高分子化学ポテンシャルの効率的な計算手法の開発	松林　伸幸	大阪大学大学院	基礎工学研究科	Development of calculation method of chemical potential for long-chain polymer melt using all-atom molecular dynamics simulation	Nobuyuki Matubayasi	Osaka University
36	オーダー N 第一原理電子状態計算による三元系金属ナノクラスターの熱力学的構造安定性と NOx 触媒機構の研究	尾崎　泰助	東京大学	物性研究所	Study on thermodynamic properties and NOx redox reactions of ternary alloy nanoclusters by O(N) density functional calculations	Taisuke Ozaki	The University of Tokyo

Publications

Division of Condensed Matter Science

Takigawa group

We have been performing nuclear magnetic resonance experiments on various quantum spin systems and strongly correlated electron systems to explore novel quantum phases with exotic ordering and fluctuation phenomena. The major achievements in the year 2019 include: (1) discovery of a novel tetragonal-orthorhombic-tetragonal sequence of continuous phase transition as a function of temperature in the spin-orbit coupled metallic pyrochlore compound $Cd_2Re_2O_7$ by ^{111}Cd-NMR measurements, (2) observation of dipolar and octupolar orders in the 5d double-perovskite oxide Ba_2MgReO_6, in which strong spin-orbit coupling combined with the cubic crystal field generates a quartet ground state with J_{eff}=3/2, providing ideal platform to explore multipolar order of t_{2g} electron systems.

1. *Field-Induced Switching of Ferro-Quadrupole Order Parameter in $PrTi_2Al_{20}$: T. Taniguchi, K. Hattori, M. Yoshida, H. Takeda, S. Nakamura, T. Sakakibara, M. Tsujimoto, A. Sakai, Y. Matsumoto, S. Nakatsuji and M. Takigawa, J. Phys. Soc. Jpn. **88** (2019) 084707(1-20).

2. ^{51}V-NMR study on the S= 1/2 square lattice antiferromagnet $K_2V_3O_8$: H. Takeda, H. Yasuoka, M. Yoshida, M. Takigawa, N. J. Ghimire, D. Mandrus and B. C. Sales, Phys. Rev. B **100** (2019) 054406.

3. Field-Orientation Effect on Ferro-Quadrupole Order in $PrTi_2Al_{20}$: S. Kittaka, T. Taniguchi, K. Hattori, S. Nakamura, T. Sakakibara, M. Takigawa, M. Tsujimoto, A. Sakai, Y. Matsumoto and S. Nakatsuji, J. Phys. Soc. Jpn. **89** (2020) 043701(1-5).

4. Regular-triangle trimer and charge order preserving the Anderson condition in the pyrochlore structure of CsW_2O_6: Y. Okamoto, H. Amano, N. Katayama, H. Sawa, K. Niki, R. Mitoka, H. Harima, T. Hasegawa, N. Ogita, Y. Tanaka, M. Takigawa, Y. Yokoyama, K. Takehana, Y. Imanaka, Y. Nakamura, H. Kishida and K. Takenaka, Nat Commun **11** (2020) 3144(1-8).

5. $PrTi_2Al_{20}$ における強四極子秩序変数の磁場によるスイッチング - 磁場に依存する四極子間相互作用について -: 谷口 貴紀 , 服部 一匡 , 橘高 俊一郎 , 瀧川 仁 , 固体物理 **55** (2020) 245-264.

Sakakibara group

We study magnetism and superconductivity of materials having low characteristic temperatures. These include heavy-electron systems, quantum spin systems and frustrated spin systems. The followings are some selected achievements in the fiscal year 2019. (1) We examined the helimagnetic transition of the cubic chiral magnet EuPtSi by means of high-precision magnetization measurements. At low fields, the temperature derivative of the magnetization dM/dT exhibits a sharp peak at $T_N(H)$, indicative of a first-order transition. By increasing H, the shape of dM/dT drastically changes above a certain field to an asymmetric step-like function. The results provide strong evidence for a tricritical point. The first-order transition in this system is driven by strong fluctuations of the order parameter whose component is large in number. (2) Ferroquadrupolar (FQ) transition in $PrTi_2Al_{20}$ has been studied by means of angle-resolved specific heat and rotational magnetocaloric measurements. The FQ transition occurring at 2 K is robust when H is applied along the [111]direction. By contrast, the FQ transition rapidly changes to a crossover when H>1 T is applied off the [111] direction. The results can be reproduced by using a phenomenological model in which an anisotropic field-dependent interaction between the quadrupole moments.

1. *Field-Induced Switching of Ferro-Quadrupole Order Parameter in $PrTi_2Al_{20}$: T. Taniguchi, K. Hattori, M. Yoshida, H. Takeda, S. Nakamura, T. Sakakibara, M. Tsujimoto, A. Sakai, Y. Matsumoto, S. Nakatsuji and M. Takigawa, J. Phys. Soc. Jpn. **88** (2019) 084707(1-20).

2. Fluctuation-Induced First-Order Transition and Tricritical Point in EuPtSi: T. Sakakibara, S. Nakamura, S. Kittaka, M. Kakihana, M. Hedo, T. Nakama and Y. Onuki, J. Phys. Soc. Jpn. **88** (2019) 093701(1-5).

3. †Superconductivity in PtSbS with a Noncentrosymmetric Cubic Crystal Structure: R. Mizutani, Y. Okamoto, H. Nagaso, Y. Yamakawa, H. Takatsu, H. Kageyama, S. Kittaka, Y. Kono, T. Sakakibara and K. Takenaka, J. Phys. Soc. Jpn. **88** (2019) 093709(1-4).

---

* Joint research among groups within ISSP.

4. †*Superconductivity of Electron-Doped $NdOBiS_2$ by Substitution of Mixed-Valence Ce Ions: N. Kase, M. Matsumoto, K. Kondo, J. Gouchi, Y. Uwatoko, T. Sakakibara and N. Miyakawa, J. Phys. Soc. Jpn. **88** (2019) 103703(1-5).

5. †Anisotropic magnetic-field response of quantum critical fluctuations in Ni-doped $CeCoIn_5$: M. Yokoyama, K. Suzuki, K. Tenya, S. Nakamura, Y. Kono, S. Kittaka and T. Sakakibara, Phys. Rev. B **99** (2019) 054506(1-6).

6. †Emergent critical phenomenon in spin-1/2 ferromagnetic-leg ladders: Quasi-one-dimensional Bose-Einstein condensate: Y. Kono, S. Kittaka, H. Yamaguchi, Y. Hosokoshi and T. Sakakibara, Phys. Rev. B **100** (2019) 054442(1-8).

7. †*S=1/2 ferromagnetic Heisenberg chain in a verdazyl-based complex: N. Uemoto, Y. Kono, S. Kittaka, T. Sakakibara, T. Yajima, Y. Iwasaki, S. Miyamoto, Y. Hosokoshi and H. Yamaguchi, Phys. Rev. B **99** (2019) 094418(1-6).

8. *Giant Anisotropic Magnetoresistance due to Purely Orbital Rearrangement in the Quadrupolar Heavy Fermion Superconductor PrV_2Al_{20}: Y. Shimura, Q. Zhang, B. Zeng, D. Rhodes, R. Schönemann, M. Tsujimoto, Y. Matsumoto, A. Sakai, T. Sakakibara, K. Araki, W. Zheng, Q. Zhou, L. Balicas and S. Nakatsuji, Phys. Rev. Lett. **122** (2019) 256601(1-6).

9. †Quasiparticle Evidence for the Nematic State above T_c in $Sr_xBi_2Se_3$: Y. Sun, S. Kittaka, T. Sakakibara, K. Machida, J. Wang, J. Wen, X. Xing, Z. Shi and T. Tamegai, Phys. Rev. Lett. **123** (2019) 027002(1-6).

10. *Unconventional field-induced spin gap in an S = 1/2 chiral staggered chain: J. Liu, S. Kittaka, R. D. Johnson, T. Lancaster, J. Singleton, T. Sakakibara, Y. Kohama, J. van Tol, A. Ardavan, B. H. Williams, S. J. Blundell, Z. E. Manson, J. L. Manson and P. A. Goddard, Phys Rev Lett **122** (2019) 057207(1-6).

11. *^{105}Pd NMR and NQR study of the cubic heavy fermion system $Ce_3Pd_{20}Si_6$: I. Jakovac, M. Horvatic, E. F. Schwier, A. Prokofiev, S. Paschen, H. Mitamura, T. Sakakibara and M. S. Grbic, J. Phys.: Condens. Matter **32** (2020) 245601(1-7).

12. *Field-Orientation Effect on Ferro-Quadrupole Order in $PrTi_2Al_{20}$: S. Kittaka, T. Taniguchi, K. Hattori, S. Nakamura, T. Sakakibara, M. Takigawa, M. Tsujimoto, A. Sakai, Y. Matsumoto and S. Nakatsuji, J. Phys. Soc. Jpn. **89** (2020) 043701(1-4).

13. †*Heavy Fermion State of $YbNi_2Si_3$ without Local Inversion Symmetry: S. Nakamura, K. Hyodo, Y. Matsumoto, Y. Haga, H. Sato, S. Ueda, K. Mimura, K. Saiki, K. Iso, M. Yamashita, S. Kittaka, T. Sakakibara and S. Ohara, J. Phys. Soc. Jpn. **89** (2020) 024705(1-5).

14. †Magnetic properties of a spin-1/2 honeycomb lattice antiferromagnet: Y. Kono, T. Okabe, N. Uemoto, Y. Iwasaki, Y. Hosokoshi, S. Kittaka, T. Sakakibara and H. Yamaguchi, Phys. Rev. B **101** (2020) 014437(1-6).

15. †Synthesis and Magnetic Properties of $M^{2+}Ti^{4+}$ Substituted $Ba_{12}Fe_{28}Ti_{15}O_{84}$: N. Yasuda, S. Kittaka, Y. Kono, T. Sakakibara, K. Kakizaki and K. Kamishima, J. Magn. Soc. Jpn. **44** (2020) 2005R004(1-5).

16. *Magnetization and Thermal Expansion Properties of Quantum Spin Ice Candidate $Pr_2Zr_2O_7$: N. Tang, A. Sakai, K. Kimura, S. Nakamura, M. Fu, Y. Matsumoto, T. Sakakibara and S. Nakatsuji, JPS Conf. Proc. **30** (2020) 011090(1-6).

17. *Single Crystal Growth and Unique Electronic States of Cubic Chiral EuPtSi and Related Compounds: Y. Ônuki, M. Kakihana, W. Iha, K. Nakaima, D. Aoki, A. Nakamura, F. Honda, M. Nakashima, Y. Amako, J. Gouchi, Y. Uwatoko, S. Nakamura, T. Sakakibara, T. Takeuchi, Y. Haga, H. Ikeda, H. Harima, M. Hedo and T. Nakama, JPS Conf. Proc. **29** (2020) 012001(1-9).

18. *Unique Skyrmion Phases and Conduction Electrons in Cubic Chiral Antiferromagnet EuPtSi and Related Compounds: Y. Ônuki, M. Kakihana, W. Iha, K. Nakaima, D. Aoki, A. Nakamura, F. Honda, M. Nakashima, Y. Amako, J. Gouchi, Y. Uwatoko, S. Nakamura, T. Sakakibara, T. Takeuchi, Y. Haga, H. Ikeda, H. Harima, M. Hedo and T. Nakama, JPS Conf. Proc. **30** (2020) 011008(1-11).

Mori group

We have successfully developed and unveiled unprecedented functional properties of the molecular materials. The major achievements in 2019 are summarized as follows: (1) We unveiled the mechanism of anhydrous organic proton conduction with dicarboxylic acids and imidazoles as an electrolyte of a fuel cell for medium temperatures. (2) We successfully fabricated and characterized the transistor properties of di- and tetramethoxy benzothienobenzothiophenes with and without hydrogen-bonding. (3) We constructed three- dimensional anionic molecular frameworks based on hydrogen-bonded metal dithiolene complexes and reveal the solvent effect.

1. †Charge Order and Poor Glass-forming Ability of an Anisotropic Triangular-lattice System, θ-$(BEDT\text{-}TTF)_2TlCo(SCN)_4$, Investigated by NMR: K. Miyagawa, T. Sato, H. Hashimoto, M. Kodama, K. Ohnoh, A. Ueda, H. Mori and K. Kanoda, J. Phys. Soc. Jpn. **88** (2019) 034705.

† Joint research with outside partners.

2. Hysteretic Current–Voltage Characteristics in the Deuterium-Dynamics-Triggered Charge-Ordered Phase of κ-D_3(Cat-EDT-TTF)$_2$: A. Ueda, K. Kishimoto, Y. Sunairi, J. Yoshida, H. Yamakawa, T. Miyamoto, T. Terashige, H. Okamoto and H. Mori, J. Phys. Soc. Jpn. **88** (2019) 034710.

3. †Dynamics of Water Molecules in a 3-Fold Interpenetrated Hydrogen-Bonded Organic Framework Based on Tetrakis (4-pyridyl)methane: D. Inokuchi, Y. Hirao, K. Takahashi, K. Matsumoto, H. Mori and T. Kubo, J. Phys. Chem. C **123** (2019) 6599.

4. New π-extended catecholato complexes of Pt(II) and Pd(II) containing a benzothienobenzothiophene (BTBT) moiety: synthesis, electrochemical behavior and charge transfer properties: K. Tahara, Y. Ashihara, T. Higashino, Y. Ozawa, T. Kadoya, K. Sugimoto, A. Ueda, H. Mori and M. Abe, Dalton Trans. **48** (2019) 7367.

5. †High-Temperature Cooperative Spin Crossover Transitions and Single-Crystal Reflection Spectra of [Fe^{III}(qsal)$_2$] (CH_3OSO_3) and Related Compounds: K. Takahashi, K. Yamamoto, T. Yamamoto, Y. Einaga, Y. Shiota, K. Yoshizawa and H. Mori, Crystals **9** (2019) 81.

6. Construction of three-dimensional anionic molecular frameworks based on hydrogen-bonded metal dithiolene complexes and the crystal solvent effect: S. Yokomori, A. Ueda, T. Higashino, R. Kumai, Y. Murakami and H. Mori, CrystEngComm **21** (2019) 2940-2948.

7. Di- and tetramethoxy benzothienobenzothiophenes: substitution position effects on the intermolecular interactions, crystal packing and transistor properties: T. Higashino, A. Ueda and H. Mori, New J. Chem. **43** (2019) 884.

8. †Strange metal from a frustration-driven charge order instability: T. Sato, K. Kitai, K. Miyagawa, M. Tamura, A. Ueda, H. Mori and K. Kanoda, Nature Mater **18** (2019) 229.

9. *Direct Evidence of Interfacial Hydrogen Bonding in Proton-Electron Concerted 2D Organic Bilayer on Au Substrate: S. Yamamoto, H. S. Kato, A. Ueda, S. Yoshimoto, Y. Hirata, J. Miyawaki, K. Yamamoto, Y. Harada, H. Wadati, H. Mori, J. Yoshinobu and I. Matsuda, e-J. Surf. Sci. Nanotechnol. **17** (2019) 49-55.

10. †Anhydrous Purely Organic Solid-State Proton Conductors: Effects of Molecular Dynamics on the Proton Conductivity of Imidazolium Hydrogen Dicarboxylates: Y. Sunairi, S. Dekura, A. Ueda, T. Ida, M. Mizuno and H. Mori, J. Phys. Soc. Jpn. **89** (2020) 051008.

11. *A computational examination of the electric-field-induced proton transfer along the interface hydrogen bond between proton donating and accepting self-assembled monolayers: Y. Kanematsu, H. S. Kato, S. Yoshimoto, A. Ueda, S. Yamamoto, H. Mori, J. Yoshinobu, I. Matsuda and M. Tachikawa, Chem. Phys. Lett. **741** (2020) 137091.

12. 有機結晶を舞台としたπ電子 - プロトンカップリング物性の新展開 : 森 初果 , 日本物理学会誌 74、No2 (2019) 82-92.

Osada group

Although the topological phases are difficult to be realized in organic molecular crystals, we demonstrate here that they can emerge in the *τ*-type organic layered conductors, *τ*-(EDO-S,S-DMEDT-TTF)$_2X_{1+y}$ and *τ*-(P-S,S-DMEDT-TTF)$_2X_{1+y}$ (X=$AuBr_2$, I_3, IBr_2). The conducting layers of these conductors have a highly symmetric checkerboard structure, which can be regarded as a modified Mielke lattice. Because their electronic structure inherits that of the Mielke lattice, their conduction and valence bands exhibits the quadratic band touching. The contact point splits into a pair of Dirac cones under uniaxial strain which breaks C_4-symmetry. In *τ*-type conductors, we can expect rather large spin-orbit coupling (SOC) as organic conductors. We show that the SOC in this case opens a topologically nontrivial gap at the band contact point, and the helical edge states exist in the gap. The actual *τ*-type conductors could be regarded as heavily-doped topological insulators, which could exhibit finite spin Hall effect.

1. Topological Properties of τ-Type Organic Conductors with a Checkerboard Lattice: T. Osada, J. Phys. Soc. Jpn. **88** (2019) 114707(1-7).

2. Anisotropy of Dirac cones and Van Hove singularity in an organic Dirac fermion system: A. Mori, M. Sato, T. Yajima, T. Konoike, K. Uchida and T. Osada, Phys. Rev. B **99** (2019) 035106(1-5).

3. †Highly anisotropic interlayer magnetoresitance in ZrSiS nodal-line Dirac semimetal: M. Novak S. N. Zhang, F. Orbanic, N. Biliskov, G. Eguchi, S. Paschen, A. Kimura, X. X. Wang, T. Osada, K. Uchida, M. Sato, Q. S. Wu, O. V. Yazyev and I. Kokanovi, Phys. Rev. B **100** (2019) 085137(1-7).

4. Quantum Hall Effect and Spin-Orbit Interaction: T. Osada, in: *Physics and Chemistry of Graphene: Graphene to Nanographene (Second Edition)*, Ch 7.1, edited by Toshiaki Enoki and Tsuneya Ando, (Jenny Stanford Publishing Pte. Ltd., Singapore, 2019), 501-526.

---

* Joint research among groups within ISSP.

5. 黒リン超薄膜の電子構造と物性 : 長田 俊人 ,「グラフェンから広がる二次元物質の新技術と応用」, 第 6 章 10 節 , 吾郷浩樹・齋藤理一郎 , (エヌ・ティー・エス , 東京 , 2020), 437-443.

Yamashita group

We have been studying (1) quantum criticality in heavy-fermion materials by ultra-low temperature cryostat, (2) thermal-Hall conductivity of exotic excitations in frustrated magnets and (3) a new technique for the study of strongly-correlated electron systems. In this year, we have performed (1) additional measurements of dHvA and Co NMR of $CeCoIn_5$ at ultralow temperatures, (2) thermal Hall measurements of another kagome compound, Cd kapellasite, (3) transport measurements of a chiral material Te, and (4) thermal transport studies of a chiral magnet $CsCuCl_3$.

1. *Thermal-transport studies of kagomé antiferromagnets: M. Y. M. Akazawa, M. Shimozawa, T. Shibauchi, Y. Matsuda, H. Ishikawa, T. Yajima, Z. Hiroi, M. Oda, H. Yoshida, H.-Y. Lee, J. H. Han and N. Kawashima, J. Phys.: Condens. Matter **32** (2019) 074001(11pp).

2. Boundary-limited and Glassy-like Phonon Thermal Conduction in $EtMe_3Sb[Pd(dmit)_2]_2$: M. Yamashita, J. Phys. Soc. Jpn. **88** (2019) 083702.

3. Thermal-transport studies of kagomé antiferromagnets: M. Yamashita, M. Akazawa, M. Shimozawa, T. Shibauchi, Y. Matsuda, H. Ishikawa, T. Yajima, Z. Hiroi, M. Oda, H. Yoshida, H.-Y. Lee, J. H. Han and N. Kawashima, J. Phys.: Condens. Matter **32** (2020) 074001.

4. †*Heavy Fermion State of $YbNi_2Si_3$ without Local Inversion Symmetry: S. Nakamura, K. Hyodo, Y. Matsumoto, Y. Haga, H. Sato, S. Ueda, K. Mimura, K. Saiki, K. Iso, M. Yamashita, S. Kittaka, T. Sakakibara and S. Ohara, J. Phys. Soc. Jpn. **89** (2020) 024705(1-5).

5. π 電子とプロトンの連動による新しい量子液体状態―絶対零度まで揺らぎ続ける電気・磁気双極子―（解説記事）: 下澤雅明・上田顕・橋本顕一郎・中惇 , 固体物理 **54** (2019) 43.

Division of Condensed Matter Theory

Tsunetsugu group

We have studied the dynamics of charge density wave order in organic compounds 1T-$TaSe_2$ upon laser pulse irradiation. Calculating the time evolution of electronic states and lattice distortions, we have shown the melting of charge density wave order and difference in time scale between electron and lattice degrees of freedom. Lattice distortions continue to proceed even after the laser irradiation ends. We continued the study of spin current under ac electric field. The effects of lattice disorders in high harmonic generation have also been investigated.

1. High-harmonic generation by electric polarization, spin current, and magnetization: T. N. Ikeda and M. Sato, Phys. Rev. B **100** (2019) 214424.

2. Photoinduced Dynamics of Commensurate Charge Density Wave in 1T-TaS2 Based on Three-Orbital Hubbard Model: T. N. Ikeda, H. Tsunetsugu and K. Yonemitsu, Appl. Sci. **9** (2019) 70.

3. Generation of DC, AC, and Second-Harmonic Spin Currents by Electromagnetic Fields in an Inversion-Asymmetric Antiferromagnet: T. N. Ikeda, Condens. Matter **4** (2019) 92.

4. Generalized hydrodynamic approach to charge and energy currents in the one-dimensional Hubbard model: Y. Nozawa and H. Tsunetsugu, Phys. Rev. B **101** (2020) 035121.

5. *Efficient Terahertz Harmonic Generation with Coherent Acceleration of Electrons in the Dirac Semimetal Cd_3As_2: B. Cheng, N. Kanda, T. N. Ikeda, T. Matsuda, P. Xia, T. Schumann, S. Stemmer, J. Itatani, N. P. Armitage and R. Matsunaga, Phys. Rev. Lett. **124** (2020) 117402.

6. Multivalley Free Energy Landscape and the Origin of Stripe and Quasi-Stripe CDW Structures in Monolayer MX2 Compounds: K. Nakatsugawa, S. Tanda and T. N. Ikeda, Sci. Rep. **10** (2020) 1239.

7. General description for nonequilibrium steady states in periodically driven dissipative quantum systems: T. N. Ikeda and M. Sato, Science Advances **6** (2020) eabb4019.

8. Disorder effects on the origin of high-order harmonic generation in solids: K. Chinzei and T. N. Ikeda, Phys. Rev. Research **2** (2020) 013033.

† Joint research with outside partners.

Kato group

The main research subject of Kato Lab. is transport properties in mesoscopic devices. We have studied (1) spin-current and its noise at the interface between a ferromagnetic insulator and a metal (or a superconductor), (2) microwave scattering in the subohmic spin-boson system, (3) subband picture of high-harmonic generation, and (4) Bell-state correlation in a Kondo quantum dot.

1. Surface plasmon polaritons in thin-film Weyl semimetals: T. Tamaya, T. Kato, K. Tsuchikawa, S. Konabe and S. Kawabata, J. Phys.: Condens. Matter **31** (2019) 305001(1-10).
2. Microwave Scattering in the Subohmic Spin-Boson Systems of Superconducting Circuits: T. Yamamoto and T. Kato, J. Phys. Soc. Jpn. **88** (2019) 094601(1-8).
3. Adiabatic almost-topological pumping of fractional charges in noninteracting quantum dots: M. Hasegawa, &. Jussiau and R. S. Whitney, Phys. Rev. B **100** (2019) 125420.
4. Bell-state correlations of quasiparticle pairs in the nonlinear current of a local Fermi liquid: R. Sakano, A. Oguri, Y. Nishikawa and E. Abe, Phys. Rev. B **99** (2019) 155106(1-7).
5. Microscopic theory of spin transport at the interface between a superconductor and a ferromagnetic insulator: T. Kato, Y. Ohnuma, M. Matsuo, J. Rech, T. Jonckheere and T. Martin, Phys. Rev. B **99** (2019) 144411(1-8).
6. Signature of the transition to a bound state in thermoelectric quantum transport: &. Jussiau, M. Hasegawa and R. S. Whitney, Phys. Rev. B **100** (2019) 115411(1-13).
7. Subband picture of high-harmonic generation in solids: T. Tamaya and T. Kato, Phys. Rev. B **100** (2019) 081203(R) (1-6).
8. Quantum Noise in Carbon Nanotubes as a Probe of Correlations in the Kondo Regime: M. Ferrier, R. Delagrange, J. Basset, H. Bouchiat, T. Arakawa, T. Hata, R. Fujiwara, Y. Teratani, R. Sakano, A. Oguri, K. Kobayashi and R. Deblock, J. Low Temp. Phys. **-** (2019) 1-34.
9. [*]mVMC—Open-source software for many-variable variational Monte Carlo method: T. Misawa, S. Morita, K. Yoshimi, M. Kawamura, Y. Motoyama, K. Ido, T. Ohgoe, M. Imada and T. Kato, Computer Physics Communications **235** (2019) 447.
10. Geometrical Optimization of Pumping Power under Adiabatic Parameter Driving: M. Hasegawa and T. Kato, J. Phys. Soc. Jpn. **89** (2020) 064706.
11. Effects of Tunnel-coupling Asymmetries on Fermi-liquid Transport through an Anderson Impurity: K. Tsutsumi, Y. Teratani, A. Oguri and R. Sakano, JPS conf. ser. **30** (2020) 011174(1-6).
12. 電流によって誘起される超伝導ドメイン：加藤 岳生 , 固体物理 **54** (2019) 451-457.
13. 非平衡状態にある近藤効果（その 2）近藤効果入門 1: 阪野 塁 , 小栗 章 , 固体物理 **55** (2020) 47-54.

Division of Nanoscale Science

Katsumoto group

By using spin-polarized quantum Hall edge channels, we proposed and experimentally confirmed a simple way to manipulate spins of electrons propagating over the channels by voltages applied on micro-fabricated gates. In the transport of double quantum well structures with (n-i-p-i-n)-type modulation doping, we found strong radio-frequency oscillation of current in the negative resistance regions. Whether this is an intrinsic effect coming from meta-stable charge states or an extrinsic circuit oscillation, is the next issue in this study.

1. Evidence for Spin-Triplet Electron Pairing in the Proximity-Induced Superconducting State of an Fe-Doped InAs Semiconductor: T. Nakamura, L. D. Anh, Y. Hashimoto, S. Ohya, M. Tanaka and S. Katsumoto, Phys. Rev. Lett. **122** (2019) 107001.
2. [†]Laser-Beam-Patterned Topological Insulating States on Thin Semiconducting MoS_2: H. Mine, A. Kobayashi, T. Nakamura, T. Inoue, S. Pakdel, D. Marian, E. Gonzalez-Marin, S. Maruyama, S. Katsumoto, A. Fortunelli, J. J. Palacios and J. Haruyama, Phys. Rev. Lett. **123** (2019) 146803.

[*] Joint research among groups within ISSP.

3. †Edge-derived magnetisms in very thin non-doped Bi_2Te_3 nanomesh: T. Kobayashi, H. Mine, T. Tokuda, Y. Hashimoto, S. Katsumoto and J. Haruyama, Appl. Phys. Lett. **115** (2019) 093101.

4. Spin Filtering Magnetoresistance in Double-Well Resonant Structures: T. Nakamura, Y. Hashimoto, T. Ke and S. Katsumoto, Phys. Status Solidi B **256** (2019) 1800560.

5. *Strain-induced spontaneous Hall effect in an epitaxial thin film of a Luttinger semimetal: T. Ohtsuki, Z. Tian, A. Endo, M. Halim, S. Katsumoto, Y. Kohama, K. Kindo, M. Lippmaa and S. Nakatsuji, Proc. Natl. Acad. Sci. USA **116** (2019) 8803-8808.

6. Spatial distribution of thermoelectric voltages in a Hall-bar shaped two-dimensional electron system under a magnetic field: A. Endo, K. Fujita, S. Katsumoto and Y. Iye, J. Phys. Commun. **3** (2019) 055005(1-19).

7. *Extracting the Chiral Contribution to the Negative Longitudinal Magnetoresistance in Epitaxial $Pr_2Ir_2O_7$ Thin Films: T. Ohtsuki, Z. Tian, A. Endo, M. Halim, S. Katsumoto, Y. Kohama, K. Kindo, M. Lippmaa and S. Nakatsuji, JPS Conf. Proc. **30** (2020) 011181(1-6).

8. † 微量微粒子修飾がもたらすグラフェンのトポロジカル絶縁体転移：春山 純志，勝本 信吾，中村 壮智，日本物理学会誌 **74** (2019) 839-844.

9. 薄膜材料の電気特性：勝本 信吾，「2020 年版薄膜作製応用ハンドブック」，第 2 章，權田俊一，(NTS 出版，東京，2020), 39-79.

Otani group

We have studied the following topics this year; spin conversion behaviors in bulk, the interfaces and the surfaces, electric field controlled spin-wave dynamics in ultrathin ferromagnetic films, and photoinduced Rashba spin to charge conversion. In the first topic, we have discovered a novel magnetic spin Hall effect and its inverse in a Weyl antiferromagnet Mn_3Sn, which shows a unique property of spin Hall effect with broken time-reversal symmetry. This finding is a remarkable achievement in antiferromagnetic spintronics achieved via collaboration with the Nakatsuji group at ISSP. We have performed spin absorption measurements so that we obtained the spin diffusion length of about 1 nm for Mn_3Sn polycrystals. From the continued study on the inverse Edelstein effect of a copper surface decorated with a lead phthalocyanine molecule, we found that the Cu surface decoration with a lead phthalocyanine monolayer gives rise to a maximum inverse Edelstein effect. Furthermore, we have discovered significant photoinduced spin-to-charge conversion via Rashba spin splitting in an unoccupied state above the Fermi level at the Cu/Bi_2O_3 interface. In terms of magnetization dynamics, we had an opportunity to write a review article highlighting recent progress in the development of electric-field-controlled magnonic devices, including present challenges, future perspectives, and the scope for further improvement.

1. Electric field control of spin waves in ultrathin CoFeB films: B. Rana, S. Choudhury, K. Miura, H. Takahashi, A. Barman and Y. Otani, Phys. Rev. B **100** (2019) 224412(1-9).

2. *Evaluation of spin diffusion length and spin Hall angle of the antiferromagnetic Weyl semimetal Mn_3Sn: P. K. Muduli, T. Higo, T. Nishikawa, D. Qu, H. Isshiki, K. Kondou, D. Nishio-Hamane, S. Nakatsuji and Y. Otani, Phys. Rev. B **99** (2019) 184425.

3. Relation between spin Hall effect and anomalous Hall effect in 3d ferromagnetic metals: Y. Omori, E. Sagasta, Y. Niimi, M. Gradhand, L. E. Hueso, F. Casanova and Y. Otani, Phys. Rev. B **99** (2019) 014403.

4. Two-dimensional electron gas in a metal/amorphous oxide interface with spin-orbit interaction: J. M. Flores-Camacho, J. Puebla, F. Auvray, A. Lastras-Martínez, Y. Otani and R. E. Balderas-Navarro, Phys. Rev. B **100** (2019) 235449(1-11).

5. Enhanced spin-to-charge current conversion at metal/oxide interfaces by lowering the temperature: H. Tsai, K. Kondou and Y. Otani, Jpn. J. Appl. Phys. **58** (2019) 110907(1-4).

6. Photoinduced Rashba Spin-to-Charge Conversion via an Interfacial Unoccupied State: J. Puebla, F. Auvray, N. Yamaguchi, M. Xu, S. Z. Bisri, Y. Iwasa, F. Ishii and Y. Otani, Phys. Rev. Lett. **122** (2019) 256401.

7. *Magnetic and magnetic inverse spin Hall effects in a non-collinear antiferromagnet: M. Kimata, H. Chen, K. Kondou, S. Sugimoto, P. K. Muduli, M. Ikhlas, Y. Omori, T. Tomita, A. H. MacDonald, S. Nakatsuji and Y. Otani, Nature **565** (2019) 627.

8. *Realization of Spin-dependent Functionality by Covering a Metal Surface with a Single Layer of Molecules: H. Isshiki, K. Kondou, S. Takizawa, K. Shimose, T. Kawabe, E. Minamitani, N. Yamaguchi, F. Ishii, A. Shiotari, Y. Sugimoto, S. Miwa and Y. Otani, Nano Lett. **19** (2019) 7119-7123.

9. Towards magnonic devices based on voltage-controlled magnetic anisotropy: B. Rana and Y. Otani, Commun Phys **2**

† Joint research with outside partners.

(2019) 90(1-12).

10. *Effect of sample size on anomalous Nernst effect in chiral antiferromagnetic Mn_3Sn devices: H. Narita, T. Higo, M. Ikhlas, S. Nakatsuji and Y. Otani, Appl. Phys. Lett. **116** (2020) 072404.

11. *Magneto-optical Kerr effect in a non-collinear antiferromagnet Mn_3Ge: M. Wu, H. Isshiki, T. Chen, T. Higo, S. Nakatsuji and Y. Otani, Appl. Phys. Lett. **116** (2020) 132408.

12. *Electrical manipulation of a topological antiferromagnetic state: H. Tsai, T. Higo, K. Kondou, T. Nomoto, A. Sakai, A. Kobayashi, T. Nakano, K. Yakushiji, R. Arita, S. Miwa, Y. Otani and S. Nakatsuji, Nature **580** (2020) 608-613.

13. *Structural and magnetic properties of Mn_3Ge films with Pt and Ru seed layers: A. Kobayashi, T. Higo, S. Nakatsuji and Y. Otani, AIP Advances **10** (2020) 015225(1-6).

14. Phase boundary exchange coupling in the mixed magnetic phase regime of a Pd-doped FeRh epilayer: J. R. Massey, K. Matsumoto, M. Strungaru, R. C. Temple, T. Higo, K. Kondou, R. F. L. Evans, G. Burnell, R. W. Chantrell, Y. Otani and C. H. Marrows, Phys. Rev. Materials **4** (2020) 024403(1-11).

15. Propagation dynamics of spin excitations along skyrmion strings: S. Seki, M. Garst, J. Waizner, R. Takagi, N. D. Khanh, Y. Okamura, K. Kondou, F. Kagawa, Y. Otani and Y. Tokura, Nat Commun **11** (2020) 256.

Komori group

Kondo effect of a Co adatom on the lattice-compressed clean Cu(001) surface is investigated using scanning tunneling microscopy/spectroscopy (STM/STS) on partially nitrogen-adsorbed surface. The Kondo temperature T_K observed in the tunneling spectrum decreases when the lattice is laterally compressed by the surrounding N-adsorbed areas. According to the results of our density functional calculations, the Co adatom position shifts toward the vacuum owing to the lateral lattice compression. Thus, the decrease of T_K is attributed to that of the hybridization strength between the adatom and substrate Cu atoms. Electronic states of the Sn atomic layer intercalated between graphene and the substrate SiC(0001) are studied by spin- and angle-resolved photoelectron spectroscopy. Two types of spin-polarized band splits, Rushba and Zeeman types, are found at the K point. This is due to the difference in the symmetry of the charge density. Growth and ferromagnetic properties of Fe_2N monatomic layers grown on Cu(111) are studied by STM/STS and soft X-ray magnetic circular dichroism. The magnetic moment and the coercive force are smaller than the Fe_2N monolayer on Cu(001) because of the strong hybridization with the Cu substrate.

1. Electronic and magnetic properties of the Fe_2N monolayer film tuned by substrate symmetry: T. Hattori, T. Miyamachi, T. Yokoyama and F. Komori, J. Phys.: Condens. Matter **31** (2019) 255001.

2. †*Coexistence of Two Types of Spin Splitting Originating from Different Symmetries: K. Yaji, A. Visikovskiy, T. Iimori, K. Kuroda, S. Hayashi, T. Kajiwara, S. Tanaka, F. Komori and S. Shin, Phys. Rev. Lett. **122** (2019) 126403.

3. †Fabrication of $L1_0$-FeNi by pulsed-laser deposition: M. Saito, H. Ito, Y. Suzuki, M. Mizuguchi, T. Koganezawa, T. Miyamachi, F. Komori, K. Takanashi and M. Kotsugi, Appl. Phys. Lett. **114** (2019) 072404.

4. *Ultrafast Unbalanced Electron Distributions in Quasicrystalline 30° Twisted Bilayer Graphene: T. Suzuki, T. Iimori, S. J. Ahn, Y. Zhao, M. Watanabe, J. Xu, M. Fujisawa, T. Kanai, N. Ishii, J. Itatani, K. Suwa, H. Fukidome, S. Tanaka, J. R. Ahn, K. Okazaki, S. Shin, F. Komori and I. Matsuda, ACS Nano **13** (2019) 11981.

5. Dynamic Interface Formation in Magnetic Thin Film Heterostructures: S. Nakashima, T. Miyamachi, Y. Tatetsu, Y. Takahashi, Y. Takagi, Y. Gohda, T. Yokoyama and F. Komori, Adv. Funct. Mater. **29** (2019) 1804594.

6. †Fabrication of $L1_0$-type FeCo ordered structure using a periodic Ni buffer layer: H. Ito, M. Saito, T. Miyamachi, F. Komori, T. Koganezawa, M. Mizuguchi and M. Kotsugi, AIP Advances **9** (2019) 045307.

7. †*Giant Rashba system on a semiconductor substrate with tunable Fermi level: Bi/GaSb(110)-(2×1): T. Nakamura, Y. Ohtsubo, N. Tokumasu, P. L. Fèvre, F. Bertran, S.-I. Ideta, K. Tanaka, K. Kuroda, K. Yaji, A. Harasawa, S. Shin, F. Komori and S.-I. Kimura, Phys. Rev. Materials **3** (2019) 126001(1-7).

8. Sensing surface lattice strain with Kondo resonance of single Co adatom: K. Iwata, T. Miyamachi, E. Minamitani and F. Komori, Appl. Phys. Lett. **116** (2020) 051604(1-4).

9. †Twisted bilayer graphene fabricated by direct bonding in a high vacuum: H. Imamura, A. Visikovskiy, R. Uotani, T. Kajiwara, H. Ando, T. Iimori, K. Iwata, T. Miyamachi, K. Nakatsuji, K. Mase, T. Shirasawa, F. Komori and S. Tanaka, Appl. Phys. Express **13** (2020) 075004(1-5).

10. *Edge-state correlation accelerates metal-insulator transition in topological semimetal nanofilms: S. Ito, M. Arita,

* Joint research among groups within ISSP.

J. Haruyama, B. Feng, W. -C. Chen, H. Namatame, M. Taniguchi, C. -M. Cheng, G. Bian, S. -J. Tang, T. -C. Chiang, O. Sugino, F. Komori and I. Matsuda, Science Advances **6** (2020) eaaz5015 (7 pages).

11. Realizing large out-of-plane magnetic anisotropy in $L1_0$ FeNi films grown by nitrogen-surfactant epitaxy on Cu(001): K. Kawaguchi, T. Miyamachi, T. Iimori, Y. Takahashi, T. Hattori, T. Yokoyama, M. Kotsugi and F. Komori, Phys. Rev. Materials **4** (2020) 054403(1-7).

12. *Fully spin-polarized bulk states in ferroelectric GeTe: J. Krempaský, M. Fanciulli, L. Nicolaï, J. Minár, H. Volfová, O. Caha, V. V. Volobuev, J. Sánchez-Barriga, M. Gmitra, K. Yaji, K. Kuroda, S. Shin, F. Komori, G. Springholz and J. Hugo Dil, Phys. Rev. Research **2** (2020) 013107(1-7).

13. Hexagonal iron nitride monolayer on Cu(001): Zigzag-line-in-trough alignment: M. Yamada, K. Ienaga, Y. Takahashi, T. Miyamachi and F. Komori, Surface Science **700** (2020) 121679.

Hasegawa group

We have on-going three projects using scanning tunneling microscopy (STM); the first one is on surface superconductivity using low temperature STM, the second is on nano-scale spin detection using spin-polarized STM, and the last is on local transport properties using scanning tunneling potentiometry (STP). Concerning surface superconductivity, we recently found that the out-of-plane critical magnetic field is strongly enhanced when the surface area is confined with surface steps less than the coherence length. We systematically investigated the width dependence of the critical field and found that the dependence is explained well with Ginzburg-Landau theory. Then in order to extend the enhancement to macroscopic scale we used a vicinal substrate and found the enhancement of the whole area on the surface superconductivity formed on it. Since the ultimately thin superconductors are already tolerant against in-plane magnetic field, our approach opens up a new way to make superconductors strong against magnetic fields in all directions. We are now developing a new local method to probe spin dynamics of nano-size structures including single atoms/molecules by detecting electron/ferromagnetic resonances based on spin-polarized STM. This year, we introduced radio-frequency (RF) cables into the STM head and successfully detected response of the RF irradiation in spin-polarized tunneling current. We are now adjusting the system and hopefully detect the resonance signals soon. Last year, we implemented a function of scanning tunneling potentiometry (STP) into a ultrahigh vacuum (UHV) STM setup, obtained electrochemical potential mappings on a clean silicon surface, and successfully measured electrical resistivity of single height steps on it. In order to improve the versatility, this year, we implemented the function into a low-temperature STM setup and found it works well. We plan to reveal quantum transport phenomena including spin's using the low-temperature STP in the next year.

1. Role of one-dimensional defects in the electrical transport through Si(111)−7×7 surface states: M. Hamada and Y. Hasegawa, Phys. Rev. B **99** (2019) 125402(1-5).

2. Bulk ferromagnetic tips for spin-polarized scanning tunneling microscopy: M. Haze, H.-H. Yang, K. Asakawa, N. Watanabe, R. Yamamoto, Y. Yoshida and Y. Hasegawa, Rev. Sci. Instrum. **90** (2019) 013704(1-5).

3. Defect-induced electronic structures on SnSe surfaces: K. Asakawa, F. Oguro, Y. Yoshida, H. Sakai, N. Hanasaki and Y. Hasegawa, Jpn. J. Appl. Phys. **58** (2019) SIIA06(1-3).

4. 走査トンネル顕微鏡による起動秩序の直接観察：物質表面に現れる新たな秩序： 吉田 靖雄 , H. Kim, C.-C. Lee, 長谷川 幸雄 , 固体物理 **54** (2019) 19-28.

5. *Scanning tunneling microscopy on cleaved Mn_3Sn(0001) surface: H.-H. Yang, C.-C. Lee, Y. Yoshida, M. Ikhlas, T. Tomita, A. Nugroho, T. Ozaki, S. Nakatsuji and Y. Hasegawa, Sci. Rep. **9** (2019) 9677(1-7).

Lippmaa group

A common feature of our research topics this year is the design of oxide crystal surfaces and surface layers. In collaboration with partners in Norway we studied the formation of interface layers on (111)-oriented polar perovskite surfaces. We determined the surface structure of water-etched $LaAlO_3$ crystals by ion scattering spectroscopy in collaboration with Korean colleagues. We studied the electronic properties of oxide surface quantum wells, and depth-graded electron-doped $SrTiO_3$, demonstrating that nanoscale carrier profile changes can be useful for efficient photogenerated charge extraction from an oxide semiconductor. We have also contributed to the design of new oxide film growth techniques, such as rapid beam-deflection PLD. Our long-term project on the study of pyrochlore iridate films also came to fruition this year.

1. *Imaging the Formation of Ferromagnetic Domains at the $LaAlO_3/SrTiO_3$ Interface: Y. Motoyui, T. Taniuchi, P. Scheiderer, J. N. Lee, J. Gabel, F. Pfaff, M. Sing, M. Lippmaa, R. Claessen and S. Shin, J. Phys. Soc. Jpn. **88** (2019) 034717(1-5).

2. Pulsed laser deposition with rapid beam deflection by a galvanometer mirror scanner: S. Maruyama, N. Sannodo,

† Joint research with outside partners.

R. Harada, Y. Anada, R. Takahashi, M. Lippmaa and Y. Matsumoto, Rev. Sci. Instrum. **90** (2019) 093901(1-9).

3. Gradient Carrier Doping as a Method for Maximizing the Photon-to-Current Efficiency of a $SrTiO_3$ Water-Splitting Photoanode: S. Kawasaki, R. Takahashi and M. Lippmaa, J. Phys. Chem. C **123** (2019) 15551-15556.

4. Experimental realization of atomically flat and AlO_2-terminated $LaAlO_3$(001) substrate surfaces: J. R. Kim, J. N. Lee, J. Mun, Y. Kim, Y. J. Shin, B. Kim, S. Das, L. Wang, M. Kim, M. Lippmaa, T. H. Kim and T. W. Noh, Phys. Rev. Mater. **3** (2019) 023801(1-8).

5. Synthesis and characterization of (111)-oriented $BaTiO_3$ thin films: T. Bolstad, K. Kjærnes, K. Raa, R. Takahashi, M. Lippmaa and T. Tybell, Mater. Res. Express **6** (2019) 056409(1-8).

6. [*]Strain-induced spontaneous Hall effect in an epitaxial thin film of a Luttinger semimetal: T. Ohtsuki, Z. Tian, A. Endo, M. Halim, S. Katsumoto, Y. Kohama, K. Kindo, M. Lippmaa and S. Nakatsuji, Proc. Natl. Acad. Sci. USA **116** (2019) 8803-8808.

7. [*]Growth of $Pr_2Ir_2O_7$ thin films using solid phase epitaxy: T. Ohtsuki, Z. Tian, M. Halim, S. Nakatsuji and M. Lippmaa, J. Appl. Phys. **127** (2020) 035303(1-9).

8. Noble metal clustering and nanopillar formation in an oxide matrix: M. Lippmaa, S. Kawasaki, R. Takahashi and T. Yamamoto, Jpn. J. Appl. Phys. **59** (2020) 010501(1-9).

9. Tuning the carrier density in $SrTiO_3/LaTiO_3/SrTiO_3$ quantum wells: J. N. Lee, X. Hou, R. Takahashi and M. Lippmaa, Appl. Phys. Lett. **116** (2020) 171601(1-5).

10. [*]Extracting the Chiral Contribution to the Negative Longitudinal Magnetoresistance in Epitaxial $Pr_2Ir_2O_7$ Thin Films: T. Ohtsuki, Z. Tian, A. Endo, M. Halim, S. Katsumoto, Y. Kohama, K. Kindo, M. Lippmaa and S. Nakatsuji, JPS Conf. Proc. **30** (2020) 011181(1-6).

11. Sacrificial Water-Soluble BaO Layer for Fabricating Free-Standing Piezoelectric Membranes: R. Takahashi and M. Lippmaa, ACS Appl. Mater. Interfaces (2020), accepted for publication.

Functional Materials Group

Yoshinobu group

We conducted several research projects in the fiscal year 2019: (1) The surface chemistry of hydrogen and formic acid on Pd-Cu single atom alloy model catalysts studied by SR-PES, IRAS, and TPD. (2) The adsorption and activation of CO_2 on Pt(997) studied by TPD. (3) The adsorption and activation of CH_4 on Pt(997) studied by IRAS, TPD and XPS. (4) LT-STM study of formic acid on Cu(997). (5) In-situ observation of CVD processes of graphene formation on a Cu surface. (6) AP-XPS study of organometallic complex. (7) XPS study of Pd deposited MoS_2.

1. [†]Intra-dimer row and inter-dimer row coupling of the vibrational modes of chemisorbed CO on Si(001)-c(4×2) observed by angle-dependent transmission infrared spectroscopy: S. Ohno, S. Shimizu, K. Tanaka, S. Yoshimoto and J. Yoshinobu, J. Chem. Phys. **151** (2019) 074702.

2. [*]Hydrogen adsorption and absorption on a Pd-Ag alloy surface studied using in-situ X-ray photoelectron spectroscopy under ultrahigh vacuum and ambient pressure: J. Tang, S. Yamamoto, T. Koitaya, Y. Yoshikura, K. Mukai, S. Yoshimoto, I. Matsuda and J. Yoshinobu, Appl. Surf. Sci. **463** (2019) 1161-1167.

3. [†*]Reversible low-temperature redox activity and selective oxidation catalysis derived from the concerted activation of multiple metal species on Cr and Rh-incorporated ceria catalysts: S. Ikemoto, X. Huang, S. Muratsugu, S. Nagase, T. Koitaya, H. Matsui, G.-I. Yokota, T. Sudoh, A. Hashimoto, Y. Tan, S. Yamamoto, J. Tang, I. Matsuda, J. Yoshinobu, T. Yokoyama, S. Kusaka, R. Matsuda and M. Tada, Phys. Chem. Chem. Phys. **21** (2019) 20868.

4. [*]Mass transport in the PdCu phase structures during hydrogen adsorption and absorption studied by XPS under hydrogen atmosphere: J. Tang, S. Yamamoto, T. Koitaya, A. Yoshigoe, T. Tokunaga, K. Mukai, I. Matsuda and J. Yoshinobu, Applied Surface Science **480** (2019) 419-426.

5. [*]CO_2 Activation and Reaction on Zn-Deposited Cu Surfaces Studied by Ambient-Pressure X-ray Photoelectron Spectroscopy: T. Koitaya, S. Yamamoto, Y. Shiozawa, Y. Yoshikura, M. Hasegawa, J. Tang, K. Takeuchi, K. Mukai, S. Yoshimoto, I. Matsuda and J. Yoshinobu, ACS Catal. **9** (2019) 4539-4550.

6. [*]Direct Evidence of Interfacial Hydrogen Bonding in Proton-Electron Concerted 2D Organic Bilayer on Au Substrate:

[*] Joint research among groups within ISSP.

S. Yamamoto, H. S. Kato, A. Ueda, S. Yoshimoto, Y. Hirata, J. Miyawaki, K. Yamamoto, Y. Harada, H. Wadati, H. Mori, J. Yoshinobu and I. Matsuda, e-J. Surf. Sci. Nanotechnol. **17** (2019) 49-55.

7. The roles of step-site and zinc in surface chemistry of formic acid on clean and Zn-modified Cu(111) and Cu(997) surfaces studied by HR-XPS, TPD, and IRAS: Y. Shiozawa, T. Koitaya, K. Mukai, S. Yoshimoto and J. Yoshinobu, J. Chem. Phys. **152** (2020) 044703.

8. *A computational examination of the electric-field-induced proton transfer along the interface hydrogen bond between proton donating and accepting self-assembled monolayers: Y. Kanematsu, H. S. Kato, S. Yoshimoto, A. Ueda, S. Yamamoto, H. Mori, J. Yoshinobu, I. Matsuda and M. Tachikawa, Chem. Phys. Lett. **741** (2020) 137091.

9. †*Surface Chemistry of Carbon Dioxide on Copper Model Catalysts Studied by Ambient-Pressure X-ray Photoelectron Spectroscopy: T. Koitaya, S. Yamamoto, I. Matsuda and J. Yoshinobu, e-J. Surf. Sci. Nanotechnol. **17** (2019) 169.

10. 2020年版薄膜作製応用ハンドブック（權田俊一監修）第３編第２章第７節「薄膜の表面・界面制御と信頼性」(p.883-p.888): 吉信 淳 , (NTS, Tokyo, Japan, 2020).

Akiyama group

In 2019, we made intensive study on development (fab-less production) of gain-sitched 1030-1060nm InGaAs laser diodes (LDs) for short seed-pulse generation below 10 ps (NEDO laser project). We also made haracterizations of material quality, basic LD performance, and advanced high-speed operations on intermediate and final evices. We studied novel solar cells, such as heat-recovery solar cells, Perovskite solar cells, and qunatum-dot solar cells for single- and multi-junction solar cells, partly supported by NEDO solar-cell project. We made bio- and chemi-physics studies on oxyluciferins and caged-luciferins, and colaborations on quantum-chemistry and molecular-dynamics calculations of these systems.

1. Light-Driven Electron-Hole Bardeen-Cooper-Schrieffer-Like State in Bulk GaAs: Y. Murotani, C. Kim, H. Akiyama, L. Pfeiffer, K. West and R. Shimano, Phys. Rev. Lett. **123** (2019) 197401.

2. Diagnosis of Perovskite Solar Cells Through Absolute Electroluminescence-Efficiency Measurements: J. Xue, X. Hu, Y. Guo, G. Weng, J. Jiang, S. Chen, Z. Zhu, J. Chu and H. Akiyama, Front. Phys. **7** (2019) 166.

3. *Photoabsorption Spectra of Aqueous Oxyluciferin Anions Elucidated by Explicit Quantum Solvent: Y. Noguchi, M. Hiyama, M. Shiga, H. Akiyama and O. Sugino, J. Chem. Theory Comput. **15** (2019) 5474.

4. Quantum-dot single-photon source on a CMOS silicon photonic chip integrated using transfer printing: R. Katsumi, Y. Ota, A. Osada, T. Yamaguchi, T. Tajiri, M. Kakuda, S. Iwamoto1, H. Akiyama and Y. Arakawa, APL Photonics **4** (2019) 036105.

5. Heat recovery solar cell: K. Kamide, T. Mochizuki, H. Akiyama and H. Takato, Physical Review Applied **12** (2019) 064001.

6. Multiwavelength GaN-Based Surface-Emitting Lasers and Their Design Principles: G. Weng, S. Chen, Y. Mei, Y. Liu, H. Akiyama, X. Hu, J. Liu, B. Zhang and J. Chu, ANNALEN DER PHYSIK **532** (2019) 1900308.

7. *In situ* wavelength tuning of quantum-dot single-photon sources integrated on a CMOS-processed silicon waveguide: R. Katsumi, Y. Ota, A. Osada, T. Tajiri, T. Yamaguchi, M. Kakuda, S. Iwamoto, H. Akiyama and Y. Arakawa, Appl. Phys. Lett. **116** (2020) 041103.

8. Lasing operation in the CsPbBr3 perovskite micron hemisphere cavity grown by chemical vapor deposition: H. Zhang, C. Zhao, S. Chen, J. Tian, J. Yan, G. Weng, X. Hu, J. Tao, Y. Pan, S. Chen, H. Akiyama and J. Chu, Chemical Engineering Journal **389** (2020) 124395.

9. Absolute electroluminescence imaging with distributed circuit modeling: Excellent for solar-cell defect diagnosis: J. Hong, Y. Wang, Y. Chen, X. Hu, G. Weng, S. Chen, H. Akiyama, Y. Zhang, B. Zhang and J. Chu, Prog Photovolt Res Appl **28** (2020) 295.

10. Modeling and design for low-cost multijunction solar cell via light-trapping rear texture technique: Applied in InGaP/GaAs/InGaAs triple junction: L. Zhu, Y. Hazama, A. Reddy, K. Watanabe, Y. Nakano, M. Sugiyama and H. Akiyama, Prog Photovolt Res Appl **28** (2020) 251.

11. Practical target values of Shockley–Read–Hall recombination rates in state-of-the-art triple-junction solar cells for realizing conversion efficiencies within 1% of the internal radiative limit: T. Nakamura, M. Imaizumi, H. Akiyama and Y. Okada, Prog Photovolt Res Appl **28** (2020) 417.

12. Theoretical Study of the Wavelength Selection for the Photocleavage of Coumarin-caged D-luciferin: J. Usukura,

† Joint research with outside partners.

M. Hiyama, M. Kurata, Y. Hazama, X. Qiu, F. M. Winnik, H. Akiyama and N. Koga, Photochem Photobiol (2020) php.13212, in print.

13. Quantitative immunohistochemistry using an antibody-fused bioluminescent protein: K.-Y. Wang, C. Wu, S. Shimajiri, H. Kubota, H. Akiyama and Y. Ohmiya, BioTechnique (2020), in print.

Sugino group

In this fiscal year, we have studied hydrogen on Pt(111) and in Si using first-principles simulation method to show the role of the nuclear quantum effect and non-adiabatic effect on the dynamics. These studies were done in the hydrogenomics project. We have also studied the oxygen reduction reaction on transition metals oxides using a high throughput method and predicted the a noble metal impurity and co-dopant can enhance the activity considerably. This result was obtained in collaboration with experimentalists under the NEDO project. We also studied the density functional theory to improve the reliability of the theoretical prediction of the electronic structures.

1. Direct coupling of first-principles calculations with replica exchange Monte Carlo sampling of ion disorder in solids: S. Kasamatsu and O. Sugino, J. Phys.: Condens. Matter **31** (2019) 085901.

2. Scaling Relation of Oxygen Reduction Reaction Intermediates at Defective TiO_2 Surfaces: Y. Yamamoto, S. Kasamatsu and O. Sugino, J. Phys. Chem. C **123** (2019) 19486.

3. [*]Photoabsorption Spectra of Aqueous Oxyluciferin Anions Elucidated by Explicit Quantum Solvent: Y. Noguchi, M. Hiyama, M. Shiga, H. Akiyama and O. Sugino, J. Chem. Theory Comput. **15** (2019) 5474.

4. Hydrogen at Electrochemical Interfaces: O. Sugino, J. Phys. Soc. Jpn. **89** (2020) 051013.

5. [*]Edge-state correlation accelerates metal-insulator transition in topological semimetal nanofilms: S. Ito, M. Arita, J. Haruyama, B. Feng, W. -C. Chen, H. Namatame, M. Taniguchi, C. -M. Cheng, G. Bian, S. -J. Tang, T. -C. Chiang, O. Sugino, F. Komori and I. Matsuda, Science Advances **6** (2020) eaaz5015 (7 pages).

Oka group

The Oka group have joined ISSP on 2020 January. We have studied the topological properties of Floquet states and proposed a classification scheme using the Wilson loop method. We have studied the spin-charge intertwined responses in 2D delafossites in collaboration with experimentalists in St. Andrews and MPI-CPfS.

Inoue group

In 2019, we reported the structural study of heliorhodopsin (HeR). It revealed that the retinal binding mechanism of HeR using fenestration in the transmembrane region. Also, the bioinformatic analysis and the study on the ultrafast photoisomerization process of HeR were reported. A new red-shifting mutation of sodium pump rhodopsin without impairing its ion transport activity was found by structure-based amino acid mutation. A new type of rhodopsin showing unique isomerization process and microbial rhodopsin without retinal binding lysine were identified. The atomic structure of *Gloeobacter* rhodopsin was revealed by x-ray crystallographic analysis.

1. Ultrafast Dynamics of Heliorhodopsins: S. Tahara, M. Singh, H. Kuramochi, W. Shihoya, K. Inoue, O. Nureki, O. Béjà, Y. Mizutani, H. Kandori and T. Tahara, J. Phys. Chem. B **123** (2019) 2507-2512.

2. Crystal Structure of Heliorhodopsin: W. Shihoya, K. Inoue, M. Singh, M. Konno, S. Hososhima, K. Yamashita, K. Ikeda, A. Higuchi, T. Izume, S. Okazaki, M. Hashimoto, R. Mizutori, S. Tomida, Y. Yamauchi, R. Abe-Yoshizumi, K. Katayama, S. P. Tsunoda, M. Shibata, Y. Furutani, A. Pushkarev, O. Béjà, T. Uchihashi, H. Kandori and O. Nureki, Nature **574** (2019) 132-136.

3. Engineered Functional Recovery of Microbial Rhodopsin without Retinal-Binding Lysine: Y. Yamauchi, M. Konno, D. Yamada, K. Yura, K. Inoue, O. Béjà and H. Kandori, Photochem. Photobiol. **95** (2019) 1116-1121.

4. Unique Photochemistry Observed in a New Microbial Rhodopsin: C. Kataoka, K. Inoue, K. Katayama, O. Béjà and H. Kandori, J. Phys. Chem. Lett. **10** (2019) 5117-5121.

5. X-ray Crystallographic Structure and Oligomerization of Gloeobacter Rhodopsin: T. Morizumi, W. -L. Ou, N. V. Eps, K. Inoue, H. Kandori, L. S. Brown and O. P. Ernst, Sci. Rep. **9** (2019) 11283.

6. Heliorhodopsins are Absent in Diderm (Gram-negative) Bacteria: Some Thoughts and Possible Implications for Activity: J. Flores-Uribe, G. Hevroni, R. Ghai, A. Pushkarev, K. Inoue, H. Kandori and O. Béjà, Environ. Microbiol.

[*] Joint research among groups within ISSP.

Rep. **11** (2019) 419-424.

7. Casting Light on Asgardarchaeota Metabolism in a Sunlit Microoxic Niche: P. -A. Bulzu, A. -S. Andrei, M. M. Salcher, M. Mehrshad, K. Inoue, H. Kandori, O. Béjà and R. Ghai, Nature Microbiol. **4** (2019) 1129-1137.

8. Red-shifting Mutation of Light-driven Sodium Pump Rhodopsin: K. Inoue, M. d. C. Marín, S. Tomida, R. Nakamura, Y. Nakajima, M. Olivucci and H. Kandori, Nature Commun. **10** (2019) 1993.

9. Optogenetic analysis of respiratory neuronal networks in the ventral medulla of neonatal rats producing channelrhodopsin in Phox2b-positive cells: K. Ikeda, H. Igarashi, H. Yawo, K. Kobayashi, S. Arata, K. Kawakami, M. Izumizaki and H. Onimaru, Pflugers Arch - Eur J Physiol **471** (2019) 1419.

10. Allosteric Communication to the Retinal Chromophore upon Ion Binding in a Light-driven Sodium Ion Pumping Rhodopsin: A. Otomo, M. Mizuno, K. Inoue, H. Kandori and Y. Mizutani, Biochemistry **59** (2020) 520-529.

11. Schizorhodopsins: A Novel Family of Rhodopsins from Asgard archaea that Function as Light-Driven Inward H+ Pumps: K. Inoue, S. P. Tsunoda, M. Singh, S. Tomida, S. Hososhima, M. Konno, R. Nakamura, H. Watanabe, P. -A. Bulzu, H. L. Banciu, A. -S. Andrei, T. Uchihashi, R. Ghai, O. Béjà and H. Kandori, Sci. Adv. **6** (2020) eaaz2441.

12. Infrared spectroscopic analysis on structural changes around the protonated Schiff base upon retinal isomerization in light-driven sodium pump KR2: S. Tomida, S. Ito, T. Mato, Y. Furutani, K. Inoue and H. Kandori, Biochimica et Biophysica Acta (BBA) - Bioenergetics **1861** (2020) 148190.

13. Physical disuse contributes to widespread chronic mechanical hyperalgesia, tactile allodynia, and cold allodynia through neurogenic inflammation and spino-parabrachio-amygdaloid pathway activation: Y. Ohmichi, M. Ohmichi, R. Tashima, K. Osuka, K. Fukushige, D. Kanikowska, Y. Fukazawa, H. Yawo, M. Tsuda, M. Naito and T. Nakano, PAIN (2020) 1, in print.

14. Gate-keeper of ion transport – a highly conserved helix-3 tryptophan in a channelrhodopsin chimera, C1C2/ChRWR: Y. Nagasaka, S. Hososhima, N. Kubo, T. Nagata, H. Kandori, K. Inoue and H. Yawo, Biophys. Physicobiol. / BPPB (2020), accepted for publication.

15. オプトジェネティクス触覚モデルによる異種感覚間可塑性の定量的解析： 阿部 健太，八尾 寛，生物物理 **59** (2019) 317-319.

16. 第3のロドプシン：ヘリオロドプシンの発見： 井上 圭一，神取 秀樹，B&I バイオサイエンスとインダストリー **77** (2019) 42-43.

17. 微生物型ロドプシンのもたらす新たな生物と光の関係とその応用：井上 圭一，生物工学会誌 **97** (2019) 616.

18. ハエトリグモにおける視覚機能とオプシンの吸収波長特性の関係： 永田 崇，寺北 明久，比較生理生化学 **36** (2019) 175-181.

19. 光で細胞を制御する―多様な微生物型ロドプシンとオプトジェネティクス―: 井上 圭一，光学 **49** (2020) 2-7.

20. ラットを用いたオプトジェネティクス（光遺伝学）：八尾 寛，深澤 有吾，冨田 浩史，五十嵐 敬幸，日本実験動物協会情報誌 LABIO 21 **80** (2020) 5-8.

Quantum Materials Group

Oshikawa group

We studied translation-invariant spin chains with a global SU(N) symmetry. The two symmetries (global SU(N) and the lattice translation) give rise to the PSU(N) × Z symmetry in the continuum limit, which have a mixed anomaly. By matching the mixed anomaly with the spin chain model, we identify a topological index for spin model evaluated as the total number of Young-tableaux boxes of spins per unit cell modulo N, which characterizes the "ingappability" of the system. A nontrivial index implies either a ground-state degeneracy in a gapped phase, which can be regarded as a field-theory version of the Lieb-Schultz-Mattis theorem. Furthermore, this index gives a restriction of the possible universality classes in a critical phase — the symmetry-protected critical phase, e.g. only a class of SU(N) Wess-Zumino-Witten theories can be realized in the low-energy limit of the given lattice model in the presence of the symmetries. Our method also leads to nontrivial constraints also apply when a higher global symmetry emerges in the model with a lower symmetry. Our prediction agrees with several examples known in previous studies of SU(N) models.

1. †Crossover of correlation functions near a quantum impurity in a Tomonaga-Luttinger liquid: C.-Y. Lo, Y. Fukusumi,

† Joint research with outside partners.

M. Oshikawa, Y.-J. Kao and P. Chen, Phys. Rev. B **99** (2019) 121103.

2. †Difficulties in operator-based formulation of the bulk quadrupole moment: S. Ono, L. Trifunovic and H. Watanabe, Phys. Rev. B **100** (2019) 245133.
3. †Extraction of topological information in Tomonaga-Luttinger liquids: M. Nakamura and S. C. Furuya, Phys. Rev. B **99** (2019) 075128.
4. †Geometric orbital magnetization in adiabatic processes: L. Trifunovic, S. Ono and H. Watanabe, Phys. Rev. B **100** (2019) 054408.
5. †Lieb-Schultz-Mattis type theorem with higher-form symmetry and the quantum dimer models: R. Kobayashi, K. Shiozaki, Y. Kikuchi and S. Ryu, Phys. Rev. B **99** (2019) 014402.
6. Polarization amplitude near quantum critical points: S. C. Furuya and M. Nakamura, Phys. Rev. B **99** (2019) 144426.
7. †Anomaly Matching and Symmetry-Protected Critical Phases in SU(N) Spin Systems in 1+1 Dimensions: Y. Yao, C.-T. Hsieh and M. Oshikawa, Phys. Rev. Lett. **123** (2019) 180201.
8. †Anomaly of the Electromagnetic Duality of Maxwell Theory: C.-T. Hsieh, Y. Tachikawa and K. Yonekura, Phys. Rev. Lett. **123** (2019) 161601.
9. Quantum phase transition and criticality in quasi-one-dimensional spinless Dirac fermions: Y. Tada, Physical Review B **100** (2019) 125145.
10. †Symmetry indicators for topological superconductors: S. Ono, Y. Yanase and H. Watanabe, Phys. Rev. Research **1** (2019) 013012.
11. Accessing electromagnetic properties of matter with cylindrical vector beams: H. Fujita, Y. Tada and M. Sato, New Journal of Physics **21** (2019) 073010.
12. †On gapped boundaries for SPT phases beyond group cohomology: R. Kobayashi, K. Ohmori and Y. Tachikawa, J. High Energ. Phys. **2019** (2019) 131.
13. Pin TQFT and Grassmann integral: R. Kobayashi, J. High Energ. Phys. **2019** (2019) 14.
14. †Stable Flatbands, Topology, and Superconductivity of Magic Honeycomb Networks: J. M. Lee, C. Geng, J. W. Park, M. Oshikawa, S.-S. Lee, H. W. Yeom and G. Y. Cho, Phys. Rev. Lett. **124** (2020) 137002.
15. †Refined symmetry indicators for topological superconductors in all space groups: S. Ono, H. C. Po and H. Watanabe, Sci. Adv. **6** (2020) eaaz8367 (1-14).
16. †Filling-enforced constraint on the quantized Hall conductivity on a periodic lattice: Y.-M. Lu, Y. Ran and M. Oshikawa, Annals of Physics **413** (2020) 168060.
17. †Proof of the Absence of Long-Range Temporal Orders in Gibbs States: H. Watanabe, M. Oshikawa and T. Koma, J Stat Phys **178** (2020) 926.
18. Non-local order parameters and quantum entanglement for fermionic topological field theories: K. Inamura, R. Kobayashi and S. Ryu, Journal of High Energy Physics **01** (2020) 121(1-30).
19. Cyclotron resonance in Kondo insulator: Y. Tada, Physical Review Research **2** (2020) 023194.
20. A generalized boundary condition applied to Lieb-Schultz-Mattis type ingappabilities and many-body Chern numbers: Y. Yao and M. Oshikawa, Phys. Rev. X (2020), accepted for publication.
21. カイラル超流動体の軌道角運動量は何によって決まるか？：多田 靖啓 , 日本物理学会誌 第 74 巻、第 2 号 (2019) 93.

Nakatsuji group

Our group focuses on designing new materials with fascinating emergent quantum phenomena, exploring the physics of such states under extreme conditions, and developing their spintronic and thermoelectric functionalities. Our primary research activities in 2019 are summarized as follow: (1) We discovered the dramatically enhanced transverse thermoelectric effect in iron-based binary ferromagnets Fe3*X* (*X* = Ga, Al), owing to novel topological features in their electronic band structure. We succeeded in fabricating thin films of these materials, which yield exceptional potential for a new generation of low-cost, flexible thermoelectric generators. (2) We achieved electrical switching of a topological antiferromagnetic state and its detection via the room-temperature anomalous Hall effect (AHE) using bilayer devices of Mn_3Sn and nonmagnetic metals. This

* Joint research among groups within ISSP.

work opens up a new exciting pathway of integrating topological antiferromagnetic states in spintronic technologies. (3) Our low-temperature transport measurements on the multipolar Kondo material PrV_2Al_{20} reveal a substantial AMR effect, signifying a Fermi surface reconstruction on entering the high-field quadrupolar ordered phase. Moreover, we observed a universal scaling behavior expected for the quadrupolar Kondo lattice in resistivity and magnetic susceptibility, which establishes the quadrupolar Kondo effect being the driving mechanism behind the non-Fermi-liquid phase of PrV_2Al_{20}. (4) We explored the full temperature-magnetic field phase diagram of the quantum spin ice candidates $Pr_2Zr_2O_7$ using a comprehensive set of magnetic and elastic probes, which unveil the crucial role of magnetoelastic coupling in generating the quantum dynamics in the system.

1. Crystal Structure in Quadrupolar Kondo Candidate $PrTr_2Al_{20}$(*Tr* = Ti and V): D. Okuyama, M. Tsujimoto, H. Sagayama, Y. Shimura, A. Sakai, A. Magata, S. Nakatsuji and T. J. Sato, J. Phys. Soc. Jpn. **88** (2019) 015001.

2. *Field-Induced Switching of Ferro-Quadrupole Order Parameter in $PrTi_2Al_{20}$: T. Taniguchi, K. Hattori, M. Yoshida, H. Takeda, S. Nakamura, T. Sakakibara, M. Tsujimoto, A. Sakai, Y. Matsumoto, S. Nakatsuji and M. Takigawa, J. Phys. Soc. Jpn. **88** (2019) 084707(1-20).

3. *Evaluation of spin diffusion length and spin Hall angle of the antiferromagnetic Weyl semimetal Mn_3Sn: P. K. Muduli, T. Higo, T. Nishikawa, D. Qu, H. Isshiki, K. Kondou, D. Nishio-Hamane, S. Nakatsuji and Y. Otani, Phys. Rev. B **99** (2019) 184425.

4. Homogeneous reduced moment in a gapful scalar chiral kagome antiferromagnet: A. Scheie, S. Dasgupta, M. Sanders, A. Sakai, Y. Matsumoto, T. R. Prisk, S. Nakatsuji, R. J. Cava and C. Broholm, Phys. Rev. B **100** (2019) 024414.

5. Effect of Anisotropic Hybridization in $YbAlB_4$ Probed by Linear Dichroism in Core-Level Hard X-Ray Photoemission Spectroscopy: K. Kuga, Y. Kanai, H. Fujiwara, K. Yamagami, S. Hamamoto, Y. Aoyama, A. Sekiyama, A. Higashiya, T. Kadono, S. Imada, A. Yamasaki, A. Tanaka, K. Tamasaku, M. Yabashi, T. Ishikawa, S. Nakatsuji and T. Kiss, Phys. Rev. Lett. **123** (2019) 036404.

6. *Giant Anisotropic Magnetoresistance due to Purely Orbital Rearrangement in the Quadrupolar Heavy Fermion Superconductor PrV_2Al_{20}: Y. Shimura, Q. Zhang, B. Zeng, D. Rhodes, R. Schönemann, M. Tsujimoto, Y. Matsumoto, A. Sakai, T. Sakakibara, K. Araki, W. Zheng, Q. Zhou, L. Balicas and S. Nakatsuji, Phys. Rev. Lett. **122** (2019) 256601(1-6).

7. 反強磁性体において実現した室温での巨大異常ネルンスト効果 - 磁気ワイルフェルミオンが織りなすトポロジカル現象： 冨田 崇弘 , 肥後 友也 , 中辻 知 , 固体物理 **54** (2019) 85-99.

8. Terahertz conductivity of the magnetic Weyl semimetal Mn_3Sn films: B. Cheng, Y. Wang, D. Barbalas, T. Higo, S. Nakatsuji and N. P. Armitage, Appl. Phys. Lett. **115** (2019) 012405.

9. *Magnetic and magnetic inverse spin Hall effects in a non-collinear antiferromagnet: M. Kimata, H. Chen, K. Kondou, S. Sugimoto, P. K. Muduli, M. Ikhlas, Y. Omori, T. Tomita, A. H. MacDonald, S. Nakatsuji and Y. Otani, Nature **565** (2019) 627.

10. *Scanning tunneling microscopy on cleaved Mn_3Sn(0001) surface: H.-H. Yang, C.-C. Lee, Y. Yoshida, M. Ikhlas, T. Tomita, A. Nugroho, T. Ozaki, S. Nakatsuji and Y. Hasegawa, Sci. Rep. **9** (2019) 9677 (1-7).

11. Linear polarization-dependent core-level photoemission spectroscopy in Yb-based valence fluctuating system: K. Kuga, Y. Kanai, H. Fujiwara, K. Yamagami, S. Hamamoto, Y. Aoyama, A. Sekiyama, A. Higashiya, T. Kadono, S. Imada, A. Yamasaki, K. Tamasaku, M. Yabashi, T. Ishikawa, S. Nakatsuji and T. Kiss, Journal of Electron Spectroscopy and Related Phenomena **/** (2019) **/**.

12. Unveiling hidden multipolar orders with magnetostriction: A. S. Patri, A. Sakai, S. Lee, A. Paramekanti, S. Nakatsuji and Y. B. Kim, Nat Commun **10** (2019) 4092.

13. Energy harvesting materials based on the anomalous Nernst effect: M. Mizuguchi and S. Nakatsuji, Sci. Technol. Adv. Mater. **20** (2019) 262-275.

14. *Strain-induced spontaneous Hall effect in an epitaxial thin film of a Luttinger semimetal: T. Ohtsuki, Z. Tian, A. Endo, M. Halim, S. Katsumoto, Y. Kohama, K. Kindo, M. Lippmaa and S. Nakatsuji, Proc. Natl. Acad. Sci. USA **116** (2019) 8803-8808.

15. 量子効果で 10 倍以上の磁気熱電効果を室温で実現：酒井 明人 , 中辻 知 , クリーンエネルギー **28** (2019) 34-38.

16. ワイル反強磁性体 Mn_3Sn における巨大な磁気光学カー効果と拡張磁気八極子ドメインの直接観測： 肥後 友也 , J-Physics **#7** (2019) 94.

17. ワイル磁性体 Co2MnGa における室温巨大異常ネルンスト効果：酒井 明人 , J-Physics **07** (2019) 47-49.

† Joint research with outside partners.

18. *Field-Orientation Effect on Ferro-Quadrupole Order in $PrTi_2Al_{20}$: S. Kittaka, T. Taniguchi, K. Hattori, S. Nakamura, T. Sakakibara, M. Takigawa, M. Tsujimoto, A. Sakai, Y. Matsumoto and S. Nakatsuji, J. Phys. Soc. Jpn. **89** (2020) 043701(1-4).

19. Unveiling Quadrupolar Kondo Effect in the Heavy Fermion Superconductor PrV_2Al_{20}: M. Fu, A. Sakai, N. Sogabe, M. Tsujimoto, Y. Matsumoto and S. Nakatsuji, J. Phys. Soc. Jpn. **89** (2020) 013704.

20. *Growth of $Pr_2Ir_2O_7$ thin films using solid phase epitaxy: T. Ohtsuki, Z. Tian, M. Halim, S. Nakatsuji and M. Lippmaa, J. Appl. Phys. **127** (2020) 035303 (1-9).

21. Anomalous transverse response of Co_2MnGa and university of the room-temperature α_ij^A/σ_ij^A ratio across topological magnets: L. Xu, X. Li, L. Ding, T. Chen, A. Sakai, B. Fauqué, S. Nakatsuji, Z. Zhu and K. Behnia, Phys. Rev. B **101** (2020) 180404.

22. *Effect of sample size on anomalous Nernst effect in chiral antiferromagnetic Mn_3Sn devices: H. Narita, T. Higo, M. Ikhlas, S. Nakatsuji and Y. Otani, Appl. Phys. Lett. **116** (2020) 072404.

23. *Magneto-optical Kerr effect in a non-collinear antiferromagnet Mn_3Ge: M. Wu, H. Isshiki, T. Chen, T. Higo, S. Nakatsuji and Y. Otani, Appl. Phys. Lett. **116** (2020) 132408.

24. *Electrical manipulation of a topological antiferromagnetic state: H. Tsai, T. Higo, K. Kondou, T. Nomoto, A. Sakai, A. Kobayashi, T. Nakano, K. Yakushiji, R. Arita, S. Miwa, Y. Otani and S. Nakatsuji, Nature **580** (2020) 608-613.

25. *Iron-based binary ferromagnets for transverse thermoelectric conversion: A. Sakai, S. Minami, T. Koretsune, T. Chen, T. Higo, Y. Wang, T. Nomoto, M. Hirayama, S. Miwa, D. Nishio-Hamane, F. Ishii, R. Arita and S. Nakatsuji, Nature **581** (2020) 53-57.

26. 硬 X 線光電子分光と基礎物性測定により明らかにした価数の量子臨界現象：久我 健太郎，松本 洋介，大川 万里生，中辻 知，放射光 **33** (2020) 1-8.

27. *Structural and magnetic properties of Mn_3Ge films with Pt and Ru seed layers: A. Kobayashi, T. Higo, S. Nakatsuji and Y. Otani, AIP Advances **10** (2020) 015225(1-6).

28. *Extracting the Chiral Contribution to the Negative Longitudinal Magnetoresistance in Epitaxial $Pr_2Ir_2O_7$ Thin Films: T. Ohtsuki, Z. Tian, A. Endo, M. Halim, S. Katsumoto, Y. Kohama, K. Kindo, M. Lippmaa and S. Nakatsuji, JPS Conf. Proc. **30** (2020) 011181(1-6).

29. *Magnetization and Thermal Expansion Properties of Quantum Spin Ice Candidate $Pr_2Zr_2O_7$: N. Tang, A. Sakai, K. Kimura, S. Nakamura, M. Fu, Y. Matsumoto, T. Sakakibara and S. Nakatsuji, JPS Conf. Proc. **30** (2020) 011090(1-6).

30. Large Nernst Effect and Thermodynamics Properties in Weyl Antiferromagnet: T. Tomita, M. Ikhlas and S. Nakatsuji, JPS Conf. Proc **30** (2020) 011009/1-7.

31. *Room-temperature terahertz anomalous Hall effect in Weyl antiferromagnet Mn3Sn thin films: T. Matsuda, N. Kanda, T. Higo, N. P. Armitage, S. Nakatsuji and R. Matsunaga, Nat Commun **11** (2020) 909.

32. Sample Quality Dependence of the Magnetic Properties in Non-Collinear Antiferromagnet Mn_3Sn: M. Ikhlas, T. Tomita and S. Nakatsuji, JPS. Conf. Proc **30** (2020) 011177.

33. Crystal structure and magnetic properties of the ferromagnet CoMnSb: H. Nakamura, M. Y. P. Akbar, T. Tomita, A. A. Nugroho and S. Nakatsuji, JPS Conference Proceedings **29** (2020) 013004(1-5).

Miwa group

We have studied following topics in this year: (1) Spectroscopy research for voltage-controlled magnetic anisotropy effect, (2) Giant spin-torque utilizing heat at the nanoscale, and (3) Physical reservoir computing. In the topic (1), we have performed x-ray magnetic circular dichroism spectroscopy to reveal giant perpendicular magnetic anisotropy and voltage effect on FeIr/MgO system (Phys. Rev. B 99, 184421). We published two review papers about comprehensive studies of voltage-controlled magnetic anisotropy effect (J. Phys. D: Appl. Phys. 52, 063001 etc). In the topic (2), we find that it is feasible to obtain giant spin-torque using heat-induced magnetic anisotropy change (Nat. Nanotechnol. 14, 40). In the topic (3), we performed physical reservoir computing using spin-torque oscillator (Appl. Phys. Lett. 114, 164401 etc.).

1. Microscopic origin of large perpendicular magnetic anisotropy in an FeIr/MgO system: S. Miwa, T. Nozaki, M. Tsujikawa, M. Suzuki, T. Tsukahara, T. Kawabe, Y. Kotani, K. Toyoki, M. Goto, T. Nakamura, M. Shirai, S. Yuasa and Y. Suzuki, Phys. Rev. B **99** (2019) 184421(1-7).

2. Quantitative and systematic analysis of bias dependence of spin accumulation voltage in a nondegenerate Si-based spin

* Joint research among groups within ISSP.

valve: S. Lee, F. Rortais, R. Ohshima, Y. Ando, S. Miwa, Y. Suzuki, H. Koike and M. Shiraishi, Phys. Rev. B **99** (2019) 064408(1-6).

3. Reservoir computing with dipole-coupled nanomagnets: H. Nomura, T. Furuta, K. Tsujimoto, Y. Kuwabiraki, F. Peper, E. Tamura, S. Miwa, M. Goto, R. Nakatani and Y. Suzuki, Jpn. J. Appl. Phys. **58** (2019) 070901(1-5).

4. Voltage-controlled magnetic anisotropy and Dzyaloshinskii–Moriya interactions in CoNi/MgO and CoNi/Pd/MgO: J. Suwardy, M. Goto, Y. Suzuki and S. Miwa, Jpn. J. Appl. Phys. **58** (2019) 060917(1-4).

5. Interface resonance in Fe/Pt/MgO multilayer structure with large voltage controlled magnetic anisotropy change: Y. Jibiki, M. Goto, M. Tsujikawa, P. Risius, S. Hasebe, X. Xu, K. Nawaoka, T. Ohkubo, K. Hono, M. Shirai, S. Miwa and Y. Suzuki, Appl. Phys. Lett. **114** (2019) 082405(1-5).

6. Physical reservoir computing based on spin torque oscillator with forced synchronization: S. Tsunegi, T. Taniguchi, K. Nakajima, S. Miwa, K. Yakushiji, A. Fukushima, S. Yuasa and H. Kubota, Appl. Phys. Lett. **114** (2019) 164101(1-5).

7. Magnetic anisotropy of ferromagnetic metals in low-symmetry systems: Y. Suzuki and S. Miwa, Physics Letters A **383** (2019) 1203-1206.

8. *Realization of Spin-dependent Functionality by Covering a Metal Surface with a Single Layer of Molecules: H. Isshiki, K. Kondou, S. Takizawa, K. Shimose, T. Kawabe, E. Minamitani, N. Yamaguchi, F. Ishii, A. Shiotari, Y. Sugimoto, S. Miwa and Y. Otani, Nano Lett. **19** (2019) 7119-7123.

9. Stability of spin XOR gate operation in silicon based lateral spin device with large variations in spin transport parameters: R. Ishihara, S. Lee, Y. Ando, R. Ohshima, M. Goto, S. Miwa, Y. Suzuki, H. Koike and M. Shiraishi, AIP Advances **9** (2019) 125326(1-6).

10. Microwave amplification in a magnetic tunnel junction induced by heat-to-spin conversion at the nanoscale: M. Goto, Y. Wakatake, U. K. Oji, S. Miwa, N. Strelkov, B. Dieny, H. Kubota, K. Yakushiji, A. Fukushima, S. Yuasa and Y. Suzuki, Nature Nanotech **14** (2019) 40-43.

11. Investigation of gating effect in Si spin MOSFET: S. Lee, F. Rortais, R. Ohshima, Y. Ando, M. Goto, S. Miwa, Y. Suzuki, H. Koike and M. Shiraishi, Appl. Phys. Lett. **116** (2020) 022403(1-5).

12. *Electrical manipulation of a topological antiferromagnetic state: H. Tsai, T. Higo, K. Kondou, T. Nomoto, A. Sakai, A. Kobayashi, T. Nakano, K. Yakushiji, R. Arita, S. Miwa, Y. Otani and S. Nakatsuji, Nature **580** (2020) 608-613.

13. *Iron-based binary ferromagnets for transverse thermoelectric conversion: A. Sakai, S. Minami, T. Koretsune, T. Chen, T. Higo, Y. Wang, T. Nomoto, M. Hirayama, S. Miwa, D. Nishio-Hamane, F. Ishii, R. Arita and S. Nakatsuji, Nature **581** (2020) 53-57.

14. Detection of Spin Transfer from Metal to Molecule by Magnetoresistance Measurement: H. Gamou, K. Shimose, R. Enoki, E. Minamitani, A. Shiotari, Y. Kotani, K. Toyoki, T. Nakamura, Y. Sugimoto, M. Kohda, J. Nitta and S. Miwa, Nano Lett. **20** (2020) 75-80.

15. Gate-Tunable Spin XOR Operation in a Silicon-Based Device at Room Temperature: R. Ishihara, Y. Ando, S. Lee, R. Ohshima, M. Goto, S. Miwa, Y. Suzuki, H. Koike and M. Shiraishi, Phys. Rev. Applied **13** (2020) 044010(1-9).

16. 電界効果で界面の磁性を制御する：三輪 真嗣 , 鈴木 基寛 , 辻川 雅人 , 野崎 隆行 , 日本物理学会誌 **74** (2019) 714-719.

17. Perpendicular magnetic anisotropy and its electric-field-induced change at metal-dielectric interfaces: S. Miwa, M. Suzuki, M. Tsujikawa, T. Nozaki, T. Nakamura, M. Shirai, S. Yuasa and Y. Suzuki, J. Phys. D: Appl. Phys. **52** (2019) 063001(1-22).

18. X 線磁気円二色性分光を用いた金属磁性体の電界効果素子研究：三輪 真嗣 , 鈴木 基寛 , 辻川 雅人 , 野崎 隆行 , まぐね **14** (2019) 146-152.

19. スピントルク発振器を用いた物理リザバー計算：常木 澄人 , 谷口 知大 , 三輪 真嗣 , 中嶋 浩平 , 久保田 均 , まぐね **14** (2019) 335-340.

20. Recent Progress in the Voltage-Controlled Magnetic Anisotropy Effect and the Challenges Faced in Developing Voltage-Torque MRAM: T. Nozaki, T. Yamamoto, S. Miwa, M. Tsujikawa, M. Shirai, S. Yuasa and Y. Suzuki, Micromachines **10** (2019) 327(1-31).

21. ナノ磁性体中の熱を利用したマイクロ波技術：後藤 穣 , 若竹 陽介 , U. K. Oji, 三輪 真嗣 , 鈴木 義茂 , 久保田 均 , 薬師寺 啓 , 福島 章雄 , 湯浅 新治 , N. Strelkov and B. Dieny, 自動車技術 **73** (2019) 96-97.

22. 量子スピントロニクス現象を示す新物質について：三輪 真嗣 , 電気学会誌 **139** (2019) 601-606.

† Joint research with outside partners.

23. 電圧トルク MRAM に向けた新材料探索と磁化反転制御技術開発：野崎 隆行 , 山本 竜也 , 三輪 真嗣 , 鈴木 義茂 , 湯浅 新治 , まぐね **15** (2020) 15-23.

Division of Data-Integrated Materials Science

Fukushima group

Recently, the constructions of materials databases using first-principles calculations have been actively carried out. Combining such materials databases and data-mining technique, one can not only analyze the mechanisms of physical phenomena, but also design new functional materials. Actually, there are several large materials databases, such as Materials Project, Open Quantum Materials Database (OQMD), and Novel Materials Discovery (NOMAD), which researchers can freely access. However, these inorganic materials databases are only for compounds with stoichiometric compositions and do not contain information about configurational disordered systems. In this year, in order to construct the materials databases for configurational disordered systems, we have developed an automatic high-throughput calculation method on the basis of the Korringa-Kohn-Rostoker (KKR) Green's function method. There are several merits in the KKR Green's function method, compared to other first-principles approaches. The most important advantage is the ability to perform the calculations of alloys and impurity doped systems, combining with the coherent potential approximation (CPA). Additionally, since the Green's function is directory calculated in this method, physical quantities, e.g., magnetic exchange interactions and transport properties, can be efficiently calculated by the linear response theory. Automatic high-throughput calculations by first-principles approaches are not easy tasks, because we need to appropriately control many numerical parameters and self-consistent procedures. For example, in the KKR Green's function method, the energy integration of the Green's function is performed in the complex energy plane to obtain the electron density. This complex energy contour must cover the valence bands and depends on systems. Our python interface for the high-throughput calculations enable to determine the numerical parameters and to manage the self-consistent procedures completely automatically. For the electronic structure calculations, the AkaiKKR program package is employed. The automatic high-throughput calculations have been demonstrated for quaternary high entropy alloys with BCC and FCC solid solution phases, where 4 principal elements have the same atomic concentration and are randomly distributed in the crystals. The number of the target elements are 38 as follows: Al, Si, Sc, Ti, V, Cr, Mn, Fe, Co, Ni, Cu, Zn, Ga, Ge, Y, Zr, Nb, Mo, Tc, Ru, Rh, Pd, Ag, Cd, In, Sn, Hf, Ta, W, Re, Os, Ir, Pt, Au, Hg, Tl, Pb and Bi. We randomly choose the 4 elements from the above target elements and construct a quaternary high entropy alloy. Since both the BCC and FCC cases are considered, the total number of the systems is 147,630. All calculations are done by the ISSP supercomputer, system B. We succeeded in automatically converging 99.97% of the systems, i.e., 147598/147630. The constructed database is quite useful for the design of new functional materials. For example, in the cases of high-performance soft magnets, the high magnet moments and Curie temperatures are needed. Using the database, we can screen the candidate systems immediately. Here, it is concluded that FeCoXY, FeCoNiY, and MnFeCoY systems are good candidates for the high-performance soft magnets.

1. Experimental verification of the origin of positive linear magnetoresistance in CoFe(V1−xMnx)Si Heusler alloys: S. Yamada, S. Kobayashi, A. Masago, L. S. R. Kumara, H. Tajiri, T. Fukushima, S. Abo, Y. Sakuraba, K. Hono, T. Oguchi and K. Hamaya, Phys. Rev. B **100** (2019) 195137(1-6).

2. Theoretical prediction of maximum Curie temperatures of Fe-based dilute magnetic semiconductors by first-principles calculations: T. Fukushima, H. Shinya, A. Masago, K. Sato and H. Katayama-Yoshida, Appl. Phys. Express **12** (2019) 063006(1-5).

3. Valence states and the magnetism of Eu ions in Eu-doped GaN: T. Nunokawa, Y. Fujiwara, Y. Miyata, N. Fujimura, T. Sakurai, H. Ohta, A. Masago, H. Shinya, T. Fukushima, K. Sato and H. Katayama-Yoshida, J. Appl. Phys **127** (2020) 083901(1-7).

4. High Curie temperature in Eu-doped GaN caused by volume-compensated Ga-vacancy: A. Masago, H. Shinya, T. Fukushima, K. Sato and H. Katayama-Yoshida, AIP Adv. **10** (2020) 025216(1-4).

5. Spin injection through energy-band symmetry matching with high spin polarization in atomically controlled ferromagnet/ferromagnet/ semiconductor structures: M. Yamada, F. Kuroda, M. Tsukahara, S. Yamada, T. Fukushima, K. Sawano, T. Oguchi1 and K. Hamaya, NPG Asia Mater. (2020), accepted for publication.

6. First-principles study of magnetism and phase stabilities of V2 based antiferromagnetic Heusler alloys: F. Kuroda, T. Fukushima and T. Oguch, J. Appl. Phys (2020), accepted for publication.

---

* Joint research among groups within ISSP.

Materials Design and Characterization Laboratory

Hiroi group

The superconducting pyrochlore oxide $Cd_2Re_2O_7$ has been investigated as a candidate spin–orbit-coupled metal (SOCM), in which specific Fermi liquid instability is expected to lead to an odd-parity order with spontaneous inversion-symmetry breaking and parity-mixing superconductivity. A domain control at low temperature has been carried out by means of biaxial and uniaxial pressures to study the intrinsic anisotropy in the transport properties. A novel Li-in conduction mechanism was proposed for the super-ionic conductor LGPS.

1. One-dimensionalization by Geometrical Frustration in the Anisotropic Triangular Lattice of the 5d Quantum Antiferromagnet $Ca_3ReO_5Cl_2$: D. Hirai, K. Nawa, M. Kawamura, T. Misawa and Z. Hiroi, J. Phys. Soc. Jpn. **88** (2019) 044708.

2. Crystal structure and magnetic properties of the 5dtransition metal oxides $AOsO_4$ (A = K, Rb, Cs): J.-I. Yamaura and Z. Hiroi, Phys. Rev. B **99** (2019) 155113.

3. *Evaluation of spin diffusion length and spin Hall angle of the antiferromagnetic Weyl semimetal Mn_3Sn: P. K. Muduli, T. Higo, T. Nishikawa, D. Qu, H. Isshiki, K. Kondou, D. Nishio-Hamane, S. Nakatsuji and Y. Otani, Phys. Rev. B **99** (2019) 184425.

4. †*Magnetoelastic couplings in the deformed kagome quantum spin lattice of volborthite: A. Ikeda, S. Furukawa, O. Janson, Y. H. Matsuda, S. Takeyama, T. Yajima, Z. Hiroi and H. Ishikawa, Phys. Rev. B **99** (2019) 140412(R)(1-5).

5. †*Contrasting Pressure-Induced Metallization Processes in Layered Perovskites, α-Sr_2MO_4(M=V,Cr): T. Yamauchi, T. Shimazu, D. Nishio-Hamane and H. Sakurai, Phys. Rev. Lett. **123** (2019) 156601.

6. * カゴメ銅鉱物ボルボサイトにおける軌道転移とフラストレート磁性：広井 善二，石川 孟，小濱 芳允，固体物理 **54** (2019) 117-130.

7. †*Topochemical synthesis of phase-pure Mo_2AlB_2 through staging mechanism: K. Kim, C. Chen, D. Nishio-Hamane, M. Okubo and A. Yamada, Chem. Commun. **55** (2019) 9295.

8. Weak Anisotropic Lithium-Ion Conductivity in Single Crystals of $Li_{10}GeP_2S_{12}$: R. Iwasaki, S. Hori, R. Kanno, T. Yajima, D. Hirai, Y. Kato and Z. Hiroi, Chem. Mater. **31** (2019) 3694.

9. *Minakawaite and platinum–group minerals in the placer from the clinopyroxenite area in serpentinite mélange of Kurosegawa belt, Kumamoto Prefecture, Japan: D. Nisio–Hamane, T. Tanaka and T. Shinmachi, Journal of Mineralogical and Petrological Sciences **114** (2019) 252.

10. †*Magnetic Properties of $SmFe_3$-Type Sm–Zr–Fe–Co–Ti Melt-Spun Ribbons: T. Saito, T. Horita and D. Nishio-Hamane, Mater. Trans. **60** (2019) 1384.

11. *Engelhauptite: A variant of S=1/2 kagome antiferromagnet: H. Ishikawa, D. Nishio-Hamane, A. Miyake, M. Tokunaga, A. Matsuo, K. Kindo and Z. Hiroi, Phys. Rev. Materials **3** (2019) 064414(1-5).

12. †*Magnetic properties of $SmFe_{12}$-based magnets produced by spark plasma sintering method: T. Saito, F. Watanabe and D. Nishio-Hamane, Journal of Alloys and Compounds **773** (2019) 1018.

13. *The effects of high pressure and superheating on the planar growth of Al_3Ni phase in hypo-peritectic Al-30wt%Ni alloy: X. H. Wang, H. W. Wang, C. M. Zou, Z. J. Wei, Y. Uwatoko, J. Gouchi, D. Nishio-Hamane and H. Gotou, Journal of Alloys and Compounds **772** (2019) 1052-1060.

14. †*Contrasted Sn substitution effects on Dirac line node semimetals $SrIrO_3$ and CaIrO: M. Negishi, N. Hiraoka, D. Nishio-Hamane and H. Takagi, APL Materials **7** (2019) 121101.

15. *A series of magnon crystals appearing under ultrahigh magnetic fields in a kagomé antiferromagnet: R. Okuma, D. Nakamura, T. Okubo, A. Miyake, A. Matsuo, K. Kindo, M. Tokunaga, N. Kawashima, S. Takeyama and Z. Hiroi, Nature Communications **10** (2019) 1229(7).

16. *Possible observation of quantum spin-nematic phase in a frustrated magnet: Y. Kohama, H. Ishikawa, A. Matsuo, K. Kindo, N. Shannon and Z. Hiroi, Proc. Nat. Acad. Sci. U.S.A. **116** (2019) 10686-10690.

17. †*Phase stability and thermoelectric properties of semiconductor-like tetragonal $FeAl_2$: K. Tobita, K. Kitahara, Y. Katsura, N. Sato, D. Nishio-Hamane, H. Gotou and K. Kimura, Science and Technology of Advanced Materials **20** (2019) 937.

18. †*Synthesis of $Sm(Co,Fe)_4B$ compounds by rapid quenching and subsequent heat treatment: T. Saito and D. Nishio-

† Joint research with outside partners.

Hamane, Intermetallics **107** (2019) 6.

19. †*Synthesis and crystal chemistry of mukhinite, V-analogue of clinozoisite on the join $Ca_2Al_3Si_3O_{12}(OH)$–$Ca_2Al_2VSi_3O_{12}(OH)$: M. Nagashima, D. Nishio-Hamane, N. Nakano and T. Kawasaki, Phys Chem Minerals **46** (2019) 63.

20. Variation in Superconducting Symmetry Against Pressure on Noncentrosymmetric Superconductor $Cd_2Re_2O_7$ Revealed by $^{185/187}$Re Nuclear Quadrupole Resonance: S. Kitagawa, K. Ishida, T. C. Kobayashi, Y. Matsubayashi, D. Hirai and Z. Hiroi, J. Phys. Soc. Jpn. **89** (2020) 053701.

21. Titanium Hydride Complex $BaCa_2Ti_2H_{14}$ with 9-Fold Coordination: T. Yajima, H. Nakajima, T. Honda, K. Ikeda, T. Otomo, H. Takeda and Z. Hiroi, Inorg. Chem. **59** (2020) 4228.

Kawashima group

We developed highly efficient methods, algorithms, and parallelized programs based on the tensor network (TN) method and applied them to relevant physical problems, which include the following: (1) development of decomposition method of a high-ranked tensor into a ring of smaller low-ranked tensors, (2) development of TN method for boundary phenomena, (3) application of TN method to dynamical phase transition, (4) study of Kitaev spin liquid by TN variational functions, (5) study of quantum spin liquid realized in α-$RuCl_3$ in a magnetic field, (6) reduction of computational cost of HOTRG in high spatial dimensions, and (7) exact-diagonalization study of dynamics of spin-phonon coupled systems.

1. *Thermal-transport studies of kagomé antiferromagnets: M. Y. M. Akazawa, M. Shimozawa, T. Shibauchi, Y. Matsuda, H. Ishikawa, T. Yajima, Z. Hiroi, M. Oda, H. Yoshida, H.-Y. Lee, J. H. Han and N. Kawashima, J. Phys.: Condens. Matter **32** (2019) 074001(11pp).

2. Detecting Signals of Weakly First-order Phase Transitions in Two-dimensional Potts Models: S. Iino, S. Morita, N. Kawashima and A. W. Sandvik, J. Phys. Soc. Jpn. **88** (2019) 034006.

3. Fast Algorithm for Generating Random Bit Strings and Multispin Coding for Directed Percolation: H. Watanabe, S. Morita, S. Todo and N. Kawashima, J. Phys. Soc. Jpn. **88** (2019) 024004(8pages).

4. *Finite-Size Effects on Kármán Vortex in Molecular Dynamics Simulation: Y. Asano, H. Watanabe and H. Noguchi, J. Phys. Soc. Jpn. **88** (2019) 075003.

5. Boundary tensor renormalization group: S. Iino, S. Morita and N. Kawashima, Phys. Rev. B **100** (2019) 035449.

6. Entropy Governed by the Absorbing State of Directed Percolation: K. Harada and N. Kawashima, Phys. Rev. Lett. **123** (2019) 090601.

7. Gapless Kitaev Spin Liquid to Classical String Gas through Tensor Networks: H.-Y. Lee, R. Kaneko, T. Okubo and N. Kawashima, Phys. Rev. Lett. **123** (2019) 087203.

8. Calculation of higher-order moments by higher-order tensor renormalization group: S. Morita and N. Kawashima, Computer Physics Communications **236** (2019) 65-71.

9. *mVMC—Open-source software for many-variable variational Monte Carlo method: T. Misawa, S. Morita, K. Yoshimi, M. Kawamura, Y. Motoyama, K. Ido, T. Ohgoe, M. Imada and T. Kato, Computer Physics Communications **235** (2019) 447.

10. *SIMD vectorization for the Lennard-Jones potential with AVX2 and AVX-512 instructions: H. Watanabe and K. M. Nakagawa, Computer Physics Communications **237** (2019) 1-7.

11. *A series of magnon crystals appearing under ultrahigh magnetic fields in a kagomé antiferromagnet: R. Okuma, D. Nakamura, T. Okubo, A. Miyake, A. Matsuo, K. Kindo, M. Tokunaga, N. Kawashima, S. Takeyama and Z. Hiroi, Nature Communications **10** (2019) 1229(7).

12. Abelian and non-Abelian chiral spin liquids in a compact tensor network: H.-Y. Lee, R. Kaneko, T. Okubo and N. Kawashima, Phys. Rev. B **101** (2020) 035140.

13. Boundary conformal spectrum and surface critical behavior of classical spin systems:A tensor network renormalization study: S. Iino, S. Morita and N. Kawashima, Phys. Rev. B **101** (2020) 155418.

14. Magnetic field induced quantum phases in a tensor network study of Kitaev magnets: H.-Y. Lee, R. Kaneko, L. E. Chern, T. Okubo, Y. Yamaji and N. K. &. Y. B. Kim, Nature Communications **11** (2020) 1639.

15. Magnetic field induced competing phases in spin-orbital entangled Kitaev magnets: L. E. Chern, R. Kaneko, H.-Y. Lee

* Joint research among groups within ISSP.

and Y. B. Kim, Phys. Rev. Research **2** (2020) 013014.

16. * 分子動力学計算による複雑流体中のカルマン渦の解析：浅野 優太 , 渡辺 宙志 , 野口 博司 , 分子シミュレーション学会誌 " アンサンブル " **22** (2020) 157-162.

Uwatoko group

Recently, a clamp-type cubic anvil high pressure cell that can generate pressure over 7 GPa at 3 K was developed for low-temperature high-pressure neutron diffraction measurements. The characteristics of the clamp-type cubic anvil high pressure cell have been presented and its performances are demonstrated by measuring magnetic neutron scattering under pressure on MnP single crystal samples. New pressure induced unconventional superconductivity has been discovered on $CeNiC_2$ at near 11 GPa. The transition temperature T_c is 3.5 K, the highest in all Ce heavy-fermion superconductors, implying quite strong electron pairings with a high-energy scale. The n-type $HgCr_2Se_4$ show a very unique single-valent FM metallic system which involves strong coupling between lattice, electronic, and magnetic degrees of freedom. High pressure suppresses the FM order by enhancing the AFM exchange couplings, and gradually stabilizes the spiral magnetic and insulating ground state. On the other hand, the magnetic field can easily modify the magnetic interactions to switch the ground state back to the FM metallic state. In the $Cr_{0.0005}NbSe_2$ superconductor, hydrostatic pressure has been shown a very effective means to significantly enhance T_c, J_c, , H_{irr}, and flux pinning. The pressure introduces more point defects in sample, and it is responsible for enhancement J_c. The hydrostatic pressure stabilizes a strong δl pinning mechanism. In addition, the point pinning is more dominant than surface pinning under high pressure. The pressure enhanced the H_{c1}, H_{c2}, H_{irr}, and reduces both coherence length and penetration depth which are responsible for the pinning mechanism. A two-stage 6-8 multi-anvil apparatus for accurate high-pressure and low-temperature measurements has been developed. By using tungsten carbide second-stage cubes with truncated corners of 3 mm and castable octahedral gasket with an edge length of 6 mm, we can generate pressures over 20 GPa at a relatively low loading force of 100 ton.

1. Development of cubic anvil type high pressure apparatus for neutron diffraction: S. E. Dissanayake, M. Matsuda, K. Munakata, H. Kagi, J. Gouchi and Y. Uwatoko, J. Phys.: Condens. Matter **31** (2019) 384001(1-5).

2. Effect of pressure on the self-hole-doped superconductor $RbGd_2Fe_4As_4O_2$: J. P. Sun, Z.-C. Wang, Z. Y. Liu, S. X. Xu, T. Eto, Y. Sui, B. S. Wang, Y. Uwatoko, G.-H. Cao and J.-G. Cheng, J. Phys.: Condens. Matter **31** (2019) 044001(1-7).

3. ^{77}Se-NMR Study under Pressure on 12%-S Doped FeSe: T. Kuwayama, K. Matsuura, Y. Mizukami, S. Kasahara, Y. Matsuda, T. Shibauchi, Y. Uwatoko and N. Fujiwara, J. Phys. Soc. Jpn. **88** (2019) 033703.

4. †*Superconductivity of Electron-Doped $NdOBiS_2$ by Substitution of Mixed-Valence Ce Ions: N. Kase, M. Matsumoto, K. Kondo, J. Gouchi, Y. Uwatoko, T. Sakakibara and N. Miyakawa, J. Phys. Soc. Jpn. **88** (2019) 103703(1-5).

5. Temperature–Pressure Phase Diagram of Antiferromagnet CeAl: R. Tsunoda, Y. Hirose, T. Koitabashi, Y. Sase, R. Kulkarni, A. Thamizhavel, S. K. Dhar, J. Gouchi, Y. Uwatoko and R. Settai, J. Phys. Soc. Jpn. **88** (2019) 034707(1-5).

6. Coexistence of localized and heavy itinerant states in antiferromagnetic $CePtGe_2$: T. Nakano, S. Onuma, N. Takeda, K. Uhlirova, J. Prokleska, V. Sechovsky, J. Gouchi and Y. Uwatoko, Phys. Rev. B **100** (2019) 035107(1-6).

7. Enhanced orbital fluctuations in Mg-doped MnV_2O_4 single crystals: Q.-Y. Liu, Z.-Y. Liu, X.-B. Zhou, T. Yajima, Y. Uwatoko, J.-G. Cheng, L. Tao, Z.-G. Liu, M.-X. Huo, X.-J. Wang and Y. Sui, Phys. Rev. B **100** (2019) 224418(1-6).

8. Exotic superconductivity in noncentrosymmetric and magnetic $CeNiC_2$ revealed under high pressure: S. Katano, M. Ito, K. Shibata, J. Gouchi, Y. Uwatoko, K. Matsubayashi, H. Soeda and H. Takahashi, Phys. Rev. B **99** (2019) 100501(1-5).

9. Pressure-induced enhancement of superconductivity and quantum criticality in the 12442-type hybrid-structure superconductor $KCa_2F_4As_4F_2$: B. Wang, Z.-C. Wang, K. Ishigaki, K. Matsubayashi, T. Eto, J. Sun, J.-G. Cheng, G.-H. Cao and Y. Uwatoko, Phys. Rev. B **99** (2019) 014501(1-6).

10. †*Large Enhancement of Thermoelectric Efficiency Due to a Pressure-Induced Lifshitz Transition in SnSe: T. Nishimura, H. Sakai, H. Mori, K. Akiba, H. Usui, M. Ochi, K. Kuroki, A. Miyake, M. Tokunaga, Y. Uwatoko, K. Katayama, H. Murakawa and N. Hanasaki, Phys. Rev. Lett. **122** (2019) 226601(1-6).

11. Magnetic-Competition-Induced Colossal Magnetoresistance in n-Type $HgCr_2Se_4$ under High Pressure: J.-P. Sun, Y.-Y. Jiao, C.-J. Yi, S.-E. Dissanayake, M. Matsuda, Y. Uwatoko, Y.-G. Shi, Y.-Q. Li, Z. Fang and J.-G. Cheng, Phys. Rev. Lett. **123** (2019) 047201(1-6).

12. In-Field Heat Treatment Effect on Nitridation of Sm_2Fe_{17}: M. Onoue, R. Kobayashi, Y. Mitsui, R. Y. Umetsu, Y. Uwatoko and K. Koyama, Mater. Trans. **60** (2019) 2179.

13. Pressure-induced hydrogen localization coupled to a semiconductor–insulator transition in a hydrogen-bonded molecular conductor: A. Ueda, K. Kishimoto, T. Isono, S. Yamada, H. Kamo, K. Kobayashi, R. Kumai, Y. Murakami,

† Joint research with outside partners.

J. Gouchi, Y. Uwatoko, Y. Nishio and H. Mori, RSC Adv. **9** (2019) 18353-18358.

14. *Novel excitations near quantum criticality in geometrically frustrated antiferromagnet $CsFeCl_3$: S. Hayashida, M. Matsumoto, M. Hagihala, N. Kurita, H. Tanaka, S. Itoh, T. Hong, M. Soda, Y. Uwatoko and T. Masuda, Sci. Adv. **5** (2019) eaaw5639(1-5).

15. High-pressure phase of $CrSb_2$: A new quasi-one-dimensional itinerant magnet with competing interactions: Y. Y. Jiao, Z. Y. Liu, M. A. McGuire, S. Calder, J. -Q. Yan, B. C. Sales, J. P. Sun, Q. Cui, N. N. Wang, Y. Sui, Y. Uwatoko, B. S. Wang, X. L. Dong and J. -G. Cheng, Phys. Rev. Materials **3** (2019) 074404(1-10).

16. Suppression of the antiferromagnetic metallic state in the pressurized $MnBi_2Te_4$: K. Y. Chen, B. S. Wang, J. -Q. Yan, D. S. Parker, J. -S. Zhou, Y. Uwatoko and J. -G. Cheng, Phys. Rev. Materials **3** (2019) 094201(1-9).

17. †Magnetic anisotropy of single-crystal ferromagnetic Ce_3RuSn_6: K. Wakiya, T. Tomaki, M. Kimura, M. Uehara, J. Gouchi, Y. Uwatoko and I. Umehara, Journal of Magnetism and Magnetic Materials **471** (2019) 274-277.

18. Weak itinerant-electron ferromagnetism of CrAlGe modified by 3d transition metal: H. Masumitsu, S. Yoshinaga, Y. Mitsui, R. Y. Umetsu, M. Hiroi, Y. Uwatoko and K. Koyama, Journal of Magnetism and Magnetic Materials **492** (2019) 165677(1-5).

19. †Anomalous ferromagnetic ordering in EuCuP: W. Iha, M. Kakihana, S. Matsuda, F. Honda, Y. Haga, T. Takeuchi, M. Nakashima, Y. Amako, J. Gouchi, Y. Uwatoko, M. Hedo, T. Nakama and Y. Ônuki, Journal of Alloys and Compounds **788** (2019) 361-366.

20. Intermediate valence state of Ce in the novel quaternary compound $CeRu_2Sn_2Zn_{18}$: K. Wakiya, Y. Sugiyama, T. Komagata, M. Uehara, H. Sato, J. Gouchi, Y. Uwatoko and I. Umehara, Journal of Alloys and Compounds **797** (2019) 309-313.

21. *The effects of high pressure and superheating on the planar growth of Al_3Ni phase in hypo-peritectic Al-30wt%Ni alloy: X. H. Wang, H. W. Wang, C. M. Zou, Z. J. Wei, Y. Uwatoko, J. Gouchi, D. Nishio-Hamane and H. Gotou, Journal of Alloys and Compounds **772** (2019) 1052-1060.

22. Enhancement of superconducting properties and flux pinning mechanism on $Cr_{0.0005}NbSe_2$ single crystal under Hydrostatic pressure: S. Arumugam, M. Krishnan, K. Ishigaki, J. Gouchi, R. Pervin, G. Kalai Selvan, P. M. Shirage and Y. Uwatoko, Sci Rep **9** (2019) 347(1-12).

23. Robust two-gap strong coupling superconductivity associated with low-lying phonon modes in pressurized Nb_5Ir_3O superconductors: B. Wang, Y. Zhang, S. Xu, K. Ishigaki, K. Matsubayashi, J.-G. Cheng, H. Hosono and Y. Uwatoko, Chinese Phys. B **28** (2019) 107401(1-7).

24. Correction for Li et al., Pressure-induced phase transitions and superconductivity in a black phosphorus single crystal: X. Li, J. Sun, P. Shahi, M. Gao, A. H. MacDonald, Y. Uwatoko, T. Xiang, J. B. Goodenough, J. Cheng and J. Zhou, Proc Natl Acad Sci USA **116** (2019) 1065.

25. Nuanced superconductivity in endohedral gallide Mo_8Ga_{41}: P. Neha1, P. Sivaprakash, K. Ishigaki, G. Kalaiselvan, K. Manikandan, R. S. Dhaka and Y. Uwatoko, Materials Research Express **6** (2019) 016002.

26. Development of High-Field and High-Pressure ESR System and Application to Triangular Antiferromagnet $CsCuCl_3$: R. Okuto, E. Ohki, T. Sakurai, K. Hijii, H. Takahashi, E. Ohmichi, S. Okubo, H. Ohta, Y. Uwatoko and H. Tanaka, Appl Magn Reson **50** (2019) 1059(1059-1065).

27. Development of two-stage multi-anvil apparatus for low-temperature measurements: K. Ishigaki, J. Gouchi, S. Nagasaki, J. G. Cheng and Y. Uwatoko, Pap. Phys. **11** (2019) 110006(1-6).

28. Pressure-induced Lifshitz transition in $FeSe_{0.88}S_{0.12}$ probed via ^{77}Se-NMR: T. Kuwayama, K. Matsuura, Y. Mizukami, S. Kasahara, Y. Matsuda, T. Shibauchi, Y. Uwatoko and N. Fujiwara, Pap. Phys. **11** (2019) 110003(1-4).

29. Pressure effect on the magnetoresistivity of topological semimetal RhSn: S. Xu, S. Xu, J. Sun, B. Wang, Y. Uwatoko, T. Xia and J. Cheng, J. Phys.: Condens. Matter **32** (2020) 355601(1-6).

30. Magnetoelectric Effect in the Antiferromagnetic Ordered State of Ce_3TiBi_5 with Ce Zig-Zag Chains: M. Shinozaki, G. Motoyama, M. Tsubouchi, M. Sezaki, J. Gouchi, S. Nishigori, T. Mutou, A. Yamaguchi, K. Fujiwara, K. Miyoshi and Y. Uwatoko, J. Phys. Soc. Jpn. **89** (2020) 033703(1-5).

31. Quantum Criticality of Valence Transition for the Unique Electronic State of Antiferromagnetic Compound $EuCu_2Ge_2$: J. Gouchi, K. Miyake, W. Iha, M. Hedo, T. Nakama, Y. Ônuki and Y. Uwatoko, J. Phys. Soc. Jpn. **89** (2020) 053703 (1-5).

---

* Joint research among groups within ISSP.

32. High pressure investigation of an organic three-dimensional Dirac semimetal candidate having a diamond lattice: A. Kiswandhi, M. Maesato, S. Tomeno, Y. Yoshida, Y. Shimizu, P. Shahi, J. Gouchi, Y. Uwatoko, G. Saito and H. Kitagawa, Phys. Rev. B **101** (2020) 245124(1-7).

33. *Magnetotransport properties of tellurium under extreme conditions: K. Akiba, K. Kobayashi, T. C. Kobayashi, R. Koezuka, A. Miyake, J. Gouchi, Y. Uwatoko and M. Tokunaga, Phys. Rev. B **101** (2020) 245111(1-6).

34. Physical properties and pressure-induced superconductivity in the single-crystalline band insulator SnO: S. Xu, Y. Zou, J. Sun, Z. Liu, X. Yu, J. Gouchi, Y. Uwatoko, Z. G. Cheng, B. Wang and J. Cheng, Phys. Rev. B **101** (2020) 104501 (1-8).

35. Pressure-Driven Eu^{2+}-Doped $BaLi_2Al_2Si_2N_6$: A New Color Tunable Narrow-Band Emission Phosphor for Spectroscopy and Pressure Sensor Applications: Y. Wang, T. Seto, K. Ishigaki, Y. Uwatoko, G. Xiao, B. Zou, G. Li, Z. Tang, Z. Li and Y. Wang, Adv. Funct. Mater. **1** (2020) 2001384(1-10).

36. *Single Crystal Growth and Unique Electronic States of Cubic Chiral EuPtSi and Related Compounds: Y. Ônuki, M. Kakihana, W. Iha, K. Nakaima, D. Aoki, A. Nakamura, F. Honda, M. Nakashima, Y. Amako, J. Gouchi, Y. Uwatoko, S. Nakamura, T. Sakakibara, T. Takeuchi, Y. Haga, H. Ikeda, H. Harima, M. Hedo and T. Nakama, JPS Conf. Proc. **29** (2020) 012001(1-9).

37. *Unique Skyrmion Phases and Conduction Electrons in Cubic Chiral Antiferromagnet EuPtSi and Related Compounds: Y. Ônuki, M. Kakihana, W. Iha, K. Nakaima, D. Aoki, A. Nakamura, F. Honda, M. Nakashima, Y. Amako, J. Gouchi, Y. Uwatoko, S. Nakamura, T. Sakakibara, T. Takeuchi, Y. Haga, H. Ikeda, H. Harima, M. Hedo and T. Nakama, JPS Conf. Proc. **30** (2020) 011008(1-11).

38. Pressure effect on the anomalous Hall effect of ferromagnetic Weyl semimetal $Co_3Sn_2S_2$: Z. Y. Liu, T. Zhang, S. X. Xu, P. T. Yang, Q. Wang, H. C. Lei, Y. Sui, Y. Uwatoko, B. S. Wang, H. M. Weng, J. P. Sun and J. -G. Cheng, Phys. Rev. Materials **4** (2020) 044203(1-9).

39. Heat treatment effect on the magnetic properties and martensitic transformations of MnCoGe: K. Noguchi, R. Kobayashi, Y. Mitsui, R. Y. Umetsu, J. Gouchi, Y. Uwatoko and K. Koyama, Journal of Magnetism and Magnetic Materials **499** (2020) 166199(1-5).

40. Magnetic field-induced nitridation of Sm_2Fe_{17}: M. Onoue, R. Kobayashi, Y. Mitsui, R. Y. Umetsu, Y. Uwatoko and K. Koyama, Journal of Alloys and Compounds **835** (2020) 155193(1-7).

41. Quasi-one-dimensional magnetic interactions and conduction electrons in $EuCu_5$ and $EuAu_5$ with the characteristic hexagonal structure: S. Matsuda, J. Ota, K. Nakaima, W. Iha, J. Gouchi, Y. Uwatoko, M. Nakashima, Y. Amako, F. Honda, D. Aoki, A. Nakamura, T. Takeuchi, Y. Haga, H. Harima, M. Hedo, T. Nakama and Y. Ônuki, Philosophical Magazine **JAN 2020** (2020) 1-14.

42. Redetermination of the crystal structure of R_5Si_4(R= Pr, Nd) from single-crystal X-ray diffraction data: K. Yokota, R. Watanuki, M. Nakashima, M. Uehara, J. Gouchi, Y. Uwatoko and I. Umehara, Acta Crystallogr E Cryst Commun **76** (2020) 510.

43. Pressure-Induced Metallization and Structural Phase Transition in the Quasi-One-Dimensional $TlFeSe_2$: Z.-Y. Liu, Q.-X. Dong, P.-F. Shan, Y.-Y. Wang, J.-H. Dai, R. Jana, K.-Y. Chen, J.-P. Sun, B.-S. Wang, X.-H. Yu, G.-T. Liu, Y. Uwatoko, Y. Sui, H.-X. Yang, G.-F. Chen and J.-G. Cheng, Chinese Phys. Lett. **37** (2020) 047102.

Ozaki group

The interplay of hopping parameters that can give rise to flat bands in consequence of quantum interference in electronic, photonic, and other interesting materials has become an extensively studied topic. Most of the recognized structures having flat bands are lattices that can be understood by the mathematical theory of line graphs, such as the Lieb, kagome, and checkerboard lattices. We theoretically explored possible novel lattices having flat bands rather than widely known lattices such as Kagome, Lieb, checker board lattices, and demonstrated that the structures that can realize the same kinds of flat bands given by those well-known lattices hosting exotic quantum phases are more flexible. The flat bands belonging to the recognized structures can be ideally embedded into new structures that cannot be considered as the original ones in terms of a unitary transformation. The uncovered mechanism enriches the understanding of physics behind the localized quantum states and broadens the choice of materials that can be used for designing electronic and photonic devices from the zero band dispersion. With the theoretical prediction, we have been collaborating with experimental groups who have been trying to experimentally realize one of the predicted structures. Our collaboration between theoretical and experimental groups seems to have a possitive evidence.

1. Efficient Algorithm Based on Liechtenstein Method for Computing Exchange Coupling Constants Using Localized Basis Set: A. Terasawa, M. Matsumoto, T. Ozaki and Y. Gohda, J. Phys. Soc. Jpn. **88** (2019) 114706.

† Joint research with outside partners.

2. Hidden mechanism for embedding the flat bands of Lieb, kagome, and checkerboard lattices in other structures: C.-C. Lee, A. Fleurence, Y. Yamada-Takamura and T. Ozaki, Phys. Rev. B **100** (2019) 045150.

3. Transport properties of rocksalt-type cluster sulfides V4GeS8 and Mn substitution effect: M. Miyata, T. Ozaki and M. Koyano, Jpn. J. Appl. Phys. **58** (2019) 061008.

4. [*]Scanning tunneling microscopy on cleaved Mn_3Sn(0001) surface: H.-H. Yang, C.-C. Lee, Y. Yoshida, M. Ikhlas, T. Tomita, A. Nugroho, T. Ozaki, S. Nakatsuji and Y. Hasegawa, Sci. Rep. **9** (2019) 9677(1-7).

5. Formation of hBN monolayers through nitridation of epitaxial silicene on diboride thin films: K. Aoyagi, F. B. Wiggers, R. Friedlein, F. Gimbert, A. Fleurence, T. Ozaki and Y. Yamada-Takamura, Journal of Applied Physics **126** (2019) 135305.

6. Parametrization of LSDA+U for noncollinear magnetic configurations: Multipolar magnetism in UO2: S. L. Dudarev, P. Liu, D. A. Andersson, C. R. Stanek, T. Ozaki and C. Franchini, Phys. Rev. Materials **3** (2019) 083802.

7. OpenMX Viewer: A web-based crystalline and molecular graphical user interface program: Y.-T. Lee and T. Ozaki, Journal of Molecular Graphics and Modelling **89** (2019) 192.

8. Benchmark of density functional theory for superconductors in elemental materials: M. Kawamura, Y. Hizume and T. Ozaki, Phys. Rev. B **101** (2020) 134511.

9. Structural investigation of ternary PdRuM (M = Pt, Rh, or Ir) nanoparticles using first-principles calculations: H. Akiba, O. Yamamuroa and T. Ozaki, RSC Advances **10** (2020) 16527.

10. Neural network atomic potential to investigate the dislocation dynamics in bcc iron: H. Mori and T. Ozaki, Phys. Rev. Materials **4** (2020) 040601(R).

Noguchi group

We have studied the membrane shape transformations by proteins. (1) effects of chirality, (2) F-BAR protein adhesion, (3) detachment from a flat substrate, and (4) electrostatic interactions. We also studeid (5) fracture of polymer material, (6) the finite-size effects on Karman vortex, and (7) treatment of angular-momentum conservation in the Navier-Stokes equation.

1. [*]Finite-Size Effects on Kármán Vortex in Molecular Dynamics Simulation: Y. Asano, H. Watanabe and H. Noguchi, J. Phys. Soc. Jpn. **88** (2019) 075003.

2. Cup-to-vesicle transition of a fluid membrane with spontaneous curvature: H. Noguchi, J. Chem. Phys. **151** (2019) 094903.

3. Angular-momentum conservation in discretization of the Navier-Stokes equation for viscous fluids: H. Noguchi, Phys. Rev. E **99** (2019) 023307.

4. Coarse-grained molecular dynamics simulation for uptake of nanoparticles into a charged lipid vesicle dominated by electrostatic interactions: N. Shimokawa, H. Ito and Y. Higuchi, Phys. Rev. E **100** (2019) 012407.

5. Stress Transmitters at the Molecular Level in the Deformation and Fracture Processes of the Lamellar Structure of Polyethylene via Coarse-Grained Molecular Dynamics Simulations: Y. Higuchi, Macromolecules **52** (2019) 6201.

6. Detachment of a fluid membrane from a substrate and vesiculation: H. Noguchi, Soft Matter **15** (2019) 8741.

7. Limiting shapes of confined lipid vesicles: B. Kavcic, A. Sakashita, H. Noguchi and P. Ziherl, Soft Matter **15** (2019) 602-614.

8. [*]SIMD vectorization for the Lennard-Jones potential with AVX2 and AVX-512 instructions: H. Watanabe and K. M. Nakagawa, Computer Physics Communications **237** (2019) 1-7.

9. Curvature induction and sensing of the F-BAR protein Pacsin1 on lipid membranes via molecular dynamics simulations: Md. Iqbal Mahmood, H. Noguchi and K.-I. Okazaki, Sci Rep **9** (2019) 14557.

10. Shape transition from elliptical to cylindrical membrane tubes induced by chiral crescent-shaped protein rods: H. Noguchi, Sci Rep **9** (2019) 11721.

11. [†]Effects of cavitation on Kármán vortex behind circular-cylinder arrays: A molecular dynamics study: Y. Asano, H. Watanabe and H. Noguchi, J. Chem. Phys. **152** (2020) 034501.

12. [*] 分子動力学計算による複雑流体中のカルマン渦の解析：浅野 優太 , 渡辺 宙志 , 野口 博司 , 分子シミュレーション学会誌

[*] Joint research among groups within ISSP.

" アンサンブル " **22** (2020) 157-162.

13. †Rational Design Principles of Attenuated Cationic Lytic Peptides for Intracellular Delivery of Biomacromolecules: N. Tamemoto, M. Akishiba, K. Sakamoto, K. Kawano, H. Noguchi and S. Futaki, Mol. Pharmaceutics **17** (2020) 2175-2185.

Materials Synthesis and Characterization group

1. Effects of Y substitution on the electronic structure and charge dynamics of SmS: Y. Yokoyama, H. Hasegawa, Y. Mizuno, D. Asai, Y. Okamoto, H. S. Suzuki, K. Takehana, Y. Imanaka and K. Takenaka, Phys. Rev. B **100** (2019) 245143.

2. *Evaluation of spin diffusion length and spin Hall angle of the antiferromagnetic Weyl semimetal Mn_3Sn: P. K. Muduli, T. Higo, T. Nishikawa, D. Qu, H. Isshiki, K. Kondou, D. Nishio-Hamane, S. Nakatsuji and Y. Otani, Phys. Rev. B **99** (2019) 184425.

3. †*S=1/2 ferromagnetic Heisenberg chain in a verdazyl-based complex: N. Uemoto, Y. Kono, S. Kittaka, T. Sakakibara, T. Yajima, Y. Iwasaki, S. Miyamoto, Y. Hosokoshi and H. Yamaguchi, Phys. Rev. B **99** (2019) 094418(1-6).

4. †*Contrasting Pressure-Induced Metallization Processes in Layered Perovskites, α-Sr2MO4(M=V,Cr): T. Yamauchi, T. Shimazu, D. Nishio-Hamane and H. Sakurai, Phys. Rev. Lett. **123** (2019) 156601.

5. †*Topochemical synthesis of phase-pure Mo2AlB2 through staging mechanism: K. Kim, C. Chen, D. Nishio-Hamane, M. Okubo and A. Yamada, Chem. Commun. **55** (2019) 9295.

6. *Minakawaite and platinum–group minerals in the placer from the clinopyroxenite area in serpentinite mélange of Kurosegawa belt, Kumamoto Prefecture, Japan: D. NISHIO–HAMANE, T. TANAKA and T. SHINMACHI, Journal of Mineralogical and Petrological Sciences **114** (2019) 252.

7. †*Magnetic Properties of SmFe3-Type Sm–Zr–Fe–Co–Ti Melt-Spun Ribbons: T. Saito, T. Horita and D. Nishio-Hamane, Mater. Trans. **60** (2019) 1384.

8. Ultrafast electronic relaxation dynamics in a valence fluctuation material $Sm_{0.83}Y_{0.17}S$: R. Ikeda, H. Watanabe, Y. Negoro, Y. Takeno, K. Imura, H. S. Suzuki, N. K. Sato and S. Kimura, J. Phys.: Conf. Ser. **1220** (2019) 012005.

9. †*Magnetic properties of SmFe12-based magnets produced by spark plasma sintering method: T. Saito, F. Watanabe and D. Nishio-Hamane, Journal of Alloys and Compounds **773** (2019) 1018.

10. *The effects of high pressure and superheating on the planar growth of Al_3Ni phase in hypo-peritectic Al-30wt%Ni alloy: X. H. Wang, H. W. Wang, C. M. Zou, Z. J. Wei, Y. Uwatoko, J. Gouchi, D. Nishio-Hamane and H. Gotou, Journal of Alloys and Compounds **772** (2019) 1052-1060.

11. Giant isotropic negative thermal expansion in Y-doped samarium monosulfides by intra-atomic charge transfer: K. Takenaka, D. Asai, R. Kaizu, Y. Mizuno, Y. Yokoyama, Y. Okamoto, N. Katayama, H. S. Suzuki and Y. Imanaka, Sci Rep **9** (2019) 122.

12. †*Contrasted Sn substitution effects on Dirac line node semimetals SrIrO3 and CaIrO3 : M. Negishi, N. Hiraoka, D. Nishio-Hamane and H. Takagi, APL Materials **7** (2019) 121101.

13. †*Phase stability and thermoelectric properties of semiconductor-like tetragonal $FeAl_2$: K. Tobita, K. Kitahara, Y. Katsura, N. Sato, D. Nishio-Hamane, H. Gotou and K. Kimura, Science and Technology of Advanced Materials **20** (2019) 937.

14. †*Synthesis of Sm(Co,Fe)4B compounds by rapid quenching and subsequent heat treatment: T. Saito and D. Nishio-Hamane, Intermetallics **107** (2019) 6.

15. †*Synthesis and crystal chemistry of mukhinite, V-analogue of clinozoisite on the join Ca2Al3Si3O12(OH)–Ca2Al2VSi3O12(OH): M. Nagashima, D. Nishio-Hamane, N. Nakano and T. Kawasaki, Phys Chem Minerals **46** (2019) 63.

16. Kondo-Induced Giant Isotropic Negative Thermal Expansion: D. G. Mazzone, M. Dzero, AM. M. Abeykoon, H. Yamaoka, H. Ishii, N. Hiraoka, J. -P. Rueff, J. M. Ablett, K. Imura, H. S. Suzuki, J. N. Hancock and I. Jarrige, Phys. Rev. Lett. **124** (2020) 125701.

† Joint research with outside partners.

Neutron Science Laboratory

Shibayama group

Shibayama group has been exploring the structure and dynamics of soft matter, especially polymer gels, micelles, thermo-responsive polymers, and thermosets, utilizing a combination of small-angle neutron scattering (SANS), small-angle X-ray scattering (SAXS), and dynamic light scattering (DLS). The objectives are to elucidate the relationship between the structure and variety of novel properties/functions of polymer gels/resins. The highlights of 2019 include investigations of (1) Rheo-SANS study on micellar structures, (2) Formation of clusters in whiskies during maturation process, (3) In situ residual stress analysis in a phenolic resin and copper composite, (4) Dynamics of critical clusters, (5) Dynamics for microgel suspension, (6) Polymer gel with a highly ordered three-dimensional network, and so on.

1. Viscoelastic change of block copolymer ion gels in a photo-switchable azobenzene ionic liquid triggered by light: C. Wang, K. Hashimoto, R. Tamate, H. Kokubo, K. Morishima, X. Li, M. Shibayama, F. Lu, T. Nakanishi and M. Watanabe, Chem. Commun. **55** (2019) 1710-1713.

2. †Dynamics of Critical Clusters Synthesized by End-Coupling of Four-Armed Poly(ethylene glycol)s: X. Li, T. Noritomi, T. Sakai, E. P. Gilbert and M. Shibayama, Macromolecules **52** (2019) 5086-5094.

3. †Transport and Mechanical Properties of ABA-type Triblock Copolymer Ion Gels Correlated with Their Microstructures: K. Hashimoto, M. Hirasawa, H. Kokubo, R. Tamate, X. Li, M. Shibayama and M. Watanabe, Macromolecules **52** (2019) 8430-8439.

4. Network structure evolution of a hexamethylenetetramine-cured phenolic resin: A. Izumi, Y. Shudo and M. Shibayama, Polym J **51** (2019) 155-160.

5. Chiral crystal-like droplets displaying unidirectional rotational sliding: T. Kajitani, K. Motokawa, A. Kosaka, Y. Shoji, R. Haruki, D. Hashizume, T. Hikima, M. Takata, K. Yazawa, K. Morishima, M. Shibayama and T. Fukushima, Nature Mater. **18** (2019) 266-272.

6. Polymer gel with a flexible and highly ordered three-dimensional network synthesized via bond percolation: X. Li, S. Nakagawa, Y. Tsuji, N. Watanabe and M. Shibayama, Sci. Adv. **5** (2019) eaax8647(1 - 7).

7. Precision polymer network science with tetra-PEG gels—a decade history and future: M. Shibayama, X. Li and T. Sakai, Colloid Polym Sci **297** (2019) 1-12.

8. Rheo-SANS study on relationship between micellar structures and rheological behavior of cationic gemini surfactants in solution: H. Iwase, R. Kawai, K. Morishima, S.-I. Takata, T. Yoshimura and M. Shibayama, Journal of Colloid and Interface Science **538** (2019) 357-366.

9. Formation of Clusters in Whiskies During the Maturation Process: K. Morishima, N. Nakamura, K. Matsui, Y. Tanaka, H. Masunaga, S. Mori, T. Iwashita, X. li and M. Shibayama, Journal of Food Science **84** (2019) 59-64.

10. 光から観たゲル微粒子 : 呉羽 拓真 , 柴山 充弘 , 高分子 **68** (2019) 497-498.

11. 高強度イオンゲル膜を用いた CO2 分離 : 橋本 慧 , 藤井 健太 , 柴山 充弘 , ケミカルエンジニヤリング **64** (2019) 32-38.

12. †JRR-3 における中性子散乱全国共同利用 : 柴山 充弘 , 放射線 **45** (2019) 89-95.

13. ゲルの構造解析 : 柴山 充弘 ,「ゲルの科学」, 第 7 章 , 長田義仁 , (講談社 , 東京 , 2020), 439-505.

14. 膨潤と収縮の速度論 : 柴山 充弘 ,「ゲルの科学」, 第 5 章 , 長田義仁 , (講談社 , 東京 , 2020), 345-378.

Yamamuro group

Our laboratory is studying chemical physics of complex condensed matters by using neutron scattering, X-ray diffraction, calorimetric, dielectric, and viscoelastic techniques. Our target materials are glasses, liquids, and various disordered systems. In this year, the heat capacity, synchrotron-radiation X-ray diffraction and quasielastic neutron scattering (QENS) experiments were performed for super-high entropy liquid, alkylated perfluorobenzene (PFB), C_nC_{n+4}-PFB (n = 4, 6, 8). These experiments revealed that the alkyl-chains are highly disordered and moving very rapidly, stabilizing a liquid state by entropy effect. The QENS experiment of a novel hydrogen-cluster material Li_6NbH_{11} was carried out to demonstrate that the NbH_9 cluster is rotating rapidly with a low energy barrier probably reflecting the unusual shape of the cluster. Another QENS work on $Pd_{0.8}Pt_{0.2}H_{0.36}$ nanoparticles showed that H atoms possibly give rise to tunneling diffusion at low temperature. We have conducted an in-situ neutron diffraction experiment of the PdRu alloy nanoparticles supported on CZ (CeO_2-ZrO_2) under flow condition of model car-exhaust gases. This experiment provided important information for the actual catalytic reaction to remove CO and NOx gases. Other than the above neutron scattering experiments, synchrotron-radiation X-ray diffraction exper-

* Joint research among groups within ISSP.

iments were conducted for vapor-deposited benzene-based molecules and a novel metal-organic framework (MOF) material which absorbs water and is vitrified by dehydration at high temperature.

1. Neutron scattering studies of static and dynamic correlation lengths in alkali metal borate glasses: S. Kojima, V. N. Novikov, M. Kofu and O. Yamamuro, Journal of Non-Crystalline Solids **518** (2019) 18-23.

2. Structural and Thermodynamic Studies of Hydrogen Absorption/Desorption Processes on PdPt Nanoparticles: H. Akiba, H. Kobayashi, H. Kitagawa, K. Ikeda, T. Otomo, T. Yamamoto, S. Matsumura and O. Yamamuro, J. Phys. Chem. C **123** (2019) 9471.

3. Soft chromophore featured liquid porphyrins and their utilization toward liquid electret applications: A. Ghosh, M. Yoshida, K. Suemori, H. Isago, N. Kobayashi, Y. Mizutani, Y. Kurashige, I. Kawamura, M. Nirei, O. Yamamuro, T. Takaya, K. Iwata, A. Saeki, K. Nagura, S. Ishihara and T. Nakanishi, Nature Commun. **10** (2019) 4210.

4. Universality and Structural Implications of the Boson Peak in Proteins: H. Nakagawa, Y. Joti, A. Kitao, O. Yamamuro and M. Kataoka, Biophysical Journal **117** (2019) 229.

5. Dynamics of Atomic Hydrogen in Palladium Probed by Neutron Spectroscopy: M. Kofu and O. Yamamuro, J. Phys. Soc. Jpn. **89** (2020) 051002.

6. Rational Synthesis for a Noble Metal Carbide: T. Wakisaka, K. Kusada, D. Wu, T. Yamamoto, T. Toriyama, S. Matsumura, H. Akiba, O. Yamamuro, K. Ikeda, T. Otomo, N. Palina, Y. Chen, L. S. R. Kumara, C. Song, O. Sakata, W. Xie, M. Koyama, Y. Kubota, S. Kawaguchi, R. L. Arevalo, S. M. Aspera, E. F. Arguelles, H. Nakanishi and H. Kitagawa, J. Am. Chem. Soc. **142** (2020) 1247.

7. New Insights on the Formation Process and Thermodynamics of the α-Phase $PdH(D)_x$ through Direct Enthalpy Measurement of H(D) Dissolution: S. Dekura, H. Akiba, O. Yamamuro, H. Kobayashi, M. Maesato and H. Kitagawa, J. Phys. Chem. C **124** (2020) 8663-8668.

Masuda group

The goal of our research is to discover a new quantum phenomenon and to reveal the mechanism of it. In this fiscal year we studied the following topics; neutron scattering study of the quasi-one-dimensional antiferromagnet $Ba_2CoSi_2O_7$, magnon pairs and spin-nematic correlation in the spin seebeck effect, novel excitations near quantum criticality in geometrically frustrated antiferromagnet $CsFeCl_3$, and magnetic states of coupled spin tubes with frustrated geometry in $CsCrF_4$.

1. A Possible Magnetic Structure of the Cluster-Based Haldane Compound Fedotovite $K_2Cu_3O(SO_4)_3$: M. Hase, K. C. Rule, J. R. Hester, J. A. Fernandez-Baca, T. Masuda and Y. Matsuo, J. Phys. Soc. Jpn. **88** (2019) 094708(1-5).

2. Substitution Effects on Magnetic Ground States with Geometrical Spin Frustration in Triangular Spin Tubes Formed in $CsCrF_4$ and α-$KCrF_4$: H. Manaka, H. Morita, T. Akasaka, Y. Miura, M. Hagihala, S. Hayashida, M. Soda and T. Masuda, J. Phys. Soc. Jpn. **88** (2019) 114703(1-13).

3. Neutron scattering study of the quasi-one-dimensional antiferromagnet $Ba_2CoSi_2O_7$: M. Soda, T. Hong, M. Avdeev, H. Yoshizawa, T. Masuda and H. Kawano-Furukawa, Phys. Rev. B **100** (2019) 144410(1-6).

4. Magnon Pairs and Spin-Nematic Correlation in the Spin Seebeck Effect: D. Hirobe, M. Sato, M. Hagihala, Y. Shiomi, T. Masuda and E. Saitoh, Phys. Rev. Lett. **123** (2019) 117202(1-7).

5. Development of Compact High Field Pulsed Magnet System for New Sample Environment Equipment at MLF in J-PARC: M. Watanabe, H. Nojiri, S. Itoh, S. Ohira-Kawamura, T. Kihara, T. Masuda, T. Sahara, M. Soda and R. Takahashi, JPS Conf. Proc. **25** (2019) 011024(1-5).

6. Progress in High Resolution Chopper Spectrometer HRC by improving collimator and Fermi chopper: S. Itoh, T. Yokoo, T. Masuda, S. Asai, H. Saito, D. Kawana, R. Sugiura, T. Asami and Y. Ihata, Physica B: Condensed Matter **568** (2019) 76-80.

7. [*]Novel excitations near quantum criticality in geometrically frustrated antiferromagnet $CsFeCl_3$: S. Hayashida, M. Matsumoto, M. Hagihala, N. Kurita, H. Tanaka, S. Itoh, T. Hong, M. Soda, Y. Uwatoko and T. Masuda, Sci. Adv. **5** (2019) eaaw5639(1-5).

8. Magnetic states of coupled spin tubes with frustrated geometry in CsCrF4: M. Hagihala, S. Hayashida, M. Avdeev, H. Manaka, H. Kikuchi and T. Masuda, npj Quantum Mater. **4** (2019) 14(1-9).

9. Horizontal Line Nodes in Sr2RuO4 Proved by Spin Resonance: K. Iida, M. Kofu, K. Suzuki, N. Murai, S. Ohira-Kawamura, R. Kajimoto, Y. Inamura, M. Ishikado, S. Hasegawa, T. Masuda, Y. Yoshida, K. Kakurai, K. Machida and

[†] Joint research with outside partners.

S. Lee, J. Phys. Soc. Jpn. **89** (2020) 053702(1-5).

10. Emergent spin-1 Haldane gap and ferroelectricity in a frustrated spin- 1/2 ladder: H. Ueda, S. Onoda, Y. Yamaguchi, T. Kimura, D. Yoshizawa, T. Morioka, M. Hagiwara, M. Hagihala, M. Soda, T. Masuda, T. Sakakibara, K. Tomiyasu, S. Ohira-Kawamura, K. Nakajima, R. Kajimoto, M. Nakamura, Y. Inamura, N. Reynolds, M. Frontzek, J. S. White, M. Hase and Y. Yasui, Phys. Rev. B **101** (2020) 140408(1-16).

11. Helical and collinear spin density wave order in the S = 1/2 one-dimensional frustrated chain compound NaCuMoO4(OH) investigated by neutron scattering: S. Asai, T. Oyama, K. Nawa, A. Nakao, K. Munakata, K. Kuwahara, M. Hagihala, S. Itoh, Z. Hiroi and T. Masuda, Phys. Rev. B **101** (2020) 144437(1-8).

12. Zero-energy excitation in the classical kagome antiferromagnet NaBa2Mn3F11: S. Hayashida, H. Ishikawa, Y. Okamoto, T. Okubo, Z. Hiroi, G. J. Nilsen, H. Mutka and T. Masuda, Phys. Rev. B **101** (2020) 214409.

13. The f-electron State of the Heavy Fermion Superconductor NpPd5Al2 and the Isostructural Family: N. Metoki, A. A. Aczel, D. Aoki, S. Chi, J. A. Fernandez-Baca, J.-C. Griveau, M. Hagihala, T. Hong, Y. Haga, K. Ikeuchi, Y. Inamura, K. Kamazawa, R. Kajimoto, H. Kitazawa, T. Masuda, M. Matsuda, M. Nakamura, J. Ohtsuki, D. Pajerowski, H. S. Suzuki, E. Yamamoto and H. Yamauchi, JPS Conf. Proc. **30** (2020) 011123(1-6).

14. Establishing the carrier scattering phase diagram for ZrNiSn-based half-Heusler thermoelectric materials: Q. Ren, C. Fu, Q. Qiu, S. Dai, Z. Liu, T. Masuda, S. Asai, M. Hagihala, S. Lee, S. Torri, T. Kamiyama, L. He, X. Tong, C. Felser, D. J. Singh, T. Zhu, J. Yang and J. Ma, Nat Commun **11** (2020) 3142(1-9).

Nakajima group

Nakajima group started from October 2019, and has been studying magnetic materials showing cross-correlated phenomena originating from symmetry of the magnetic structures. One example is multiferroics, in which spontaneous electric polarization is induced by symmetry breaking in magnetic order. Y-type hexaferrite $Ba_{2-y}Sr_yCo_2Fe_{12-x}Al_xO_{22}$ (BSCoFAO) is known to exhibit the spin-driven ferroelectricity near room temperature. Our collaborators in RIKEN systematically grew high-quality of single crystals of BSCoFAO with varying Ba/Sr ratio. We performed neutron scattering experiments on these crystals, revealing that the multiferroic phase has a double-fan-type magnetic structure. Another example is the magnetic skyrmion lattice, which is an array of vortex-like spin objects. We have studied an intermetallic compound $Gd_3Ru_4Al_{12}$ with a breathing Kagome lattice by means of neutron and resonant X-ray scattering, revealing that this system exhibits successive field-induced magnetic phase transitions, in which the skyrmion lattice phase appears as a first-field-induced phase at an intermediate temperature. Most of the research activities mentioned above were published with Nakajima's previous affiliation (Quantum Phase Electronics Center and RIKEN Center for Emergent Matter Science). A full publication list is shown in Nakajima group's website.

1. Nanometric square skyrmion lattice in a centrosymmetric tetragonal magnet: N. D. Khanh, T. Nakajima, X. Yu, S. Gao, K. Shibata, M. Hirschberger, Y. Yamasaki, H. Sagayama, H. Nakao, L. Peng, K. Nakajima, R. Takagi, T.-H. Arima, Y. Tokura and S. Seki, Nat. Nanotechnol. **15** (2020) 444.

International MegaGauss Science Laboratory

Kindo group

We have developed some new magnets. One magnet has a bore of 22 mm diameter, which is larger than the standard magnet. This magnet can produce the field up to 60 Tesla with a duration of about 40 msec. Another magnet is a Long-Pulse magnet. This magnet was developed to generate the field with a duration of about 100 msec. by using a capacitor bank of 10 MJ. This magnet is used for the High-Field Collaboratory Project at the High Filed Laboratory of Osaka University.

1. †High-field Magnetism of the Honeycomb-lattice Antiferromagnet $Cu_2(pymca)_3(ClO_4)$: A. Okutani, T. Kida, Y. Narumi, T. Shimokawa, Z. Honda, K. Kindo, T. Nakano, Y. Nozue and M. Hagiwara, J. Phys. Soc. Jpn. **88** (2019) 013703(4pages).

2. †Magnetic Properties of S = 1/2 Antiferromagnetic Alternating Chain in a New Salt (o -MePy-V)(TCNQ): Y. Iwasaki, Y. Sasaki, Y. Hosokoshi, A. Matsuo, K. Kindo and H. Yamaguchi, J. Phys. Soc. Jpn. **88** (2019) 044709(1-5).

3. †Reduction of the Ordered Magnetic Moment by Quantum Fluctuation in the Antiferromagnetic Spin-5/2 Dimer Compound $FeVMoO_7$: M. Hase, J. R. Hester, K. C. Rule, V. Yu. Pomjakushin, A. Matsuo and K. Kindo, J. Phys. Soc. Jpn. **88** (2019) 034711(6pages).

4. †Successive Phase Transition at Ambient Pressure in CeCoSi: Single Crystal Studies: H. Tanida, K. Mitsumoto, Y. Muro,

---

* Joint research among groups within ISSP.

T. Fukuhara, Y. Kawamura, A. Kondo, K. Kindo, Y. Matsumoto, T. Namiki, T. Kuwai and T. Matsumura, J. Phys. Soc. Jpn. **88** (2019) 054716(1-10).

5. *Thermodynamic Investigation of Metamagnetism in Pulsed High Magnetic Fields on Heavy Fermion Superconductor UTe_2: S. Imajo, Y. Kohama, A. Miyake, C. Dong, M. Tokunaga, J. Flouquet, K. Kindo and D. Aoki, J. Phys. Soc. Jpn. **88** (2019) 083705(1-5).

6. †*Difference in magnetic and ferroelectric properties between rhombohedral and hexagonal polytypes of AgFeO2: A single-crystal study: N. Terada, Y. Ikedo, H. Sato, D. D. Khalyavin, P. Manuel, F. Orlandi, Y. Tsujimoto, Y. Matsushita, A. Miyake, A. Matsuo, M. Tokunaga and K. Kindo, Phys. Rev. B **99** (2019) 064402(1-11).

7. †*Enhancement of the effective mass at high magnetic fields in $CeRhIn_5$: L. Jiao, M. Smidman, Y. Kohama, Z. S. Wang, D. Graf, Z. F. Weng, Y. J. Zhang, A. Matsuo, E. D. Bauer, H. Lee, S. Kirchner, J. Singleton, K. Kindo, J. Wosnitza, F. Steglich, J. D. Thompson and H. Q. Yuan, Phys. Rev. B **99** (2019) 045127(6).

8. †Evidence of low-energy singlet excited states in the spin-1/2 polyhedral clusters {Mo72V30} and {W72V30} with strongly frustrated kagome networks: T. Kihara, H. Nojiri, Y. Narumi, Y. Oshima, K. Kindo, C. Heesing, J. Schnack and A. Müller, Phys. Rev. B **99** (2019) 064430(8).

9. †Magnetic structure and high-field magnetization of the distorted kagome lattice antiferromagnet $Cs_2Cu_3SnF_{12}$: K. Matan, T. Ono, G. Gitgeatpong, K. de Roos, P. Miao, S. Torii, T. Kamiyama, A. Miyata, A. Matsuo, K. Kindo, S. Takeyama, Y. Nambu, P. Piyawongwatthana, T. J. Sato and H. Tanaka, Phys. Rev. B **99** (2019) 224404(1-12).

10. †*Magnetoelectric behavior from cluster multipoles in square cupolas: Study of Sr(TiO)Cu4(PO4)4 in comparison with Ba and Pb isostructurals: Y. Kato, K. Kimura, A. Miyake, M. Tokunaga, A. Matsuo, K. Kindo, M. Akaki, M. Hagiwara, S. Kimura, T. Kimura and Y. Motome, Phys. Rev. B **99** (2019) 024415(1-12).

11. †Observation of a metamagnetic transition in the 5f heavy-fermion compound UNi_2Al_3 : Magnetization studies up to 90 T for single-crystalline $U(Pd_{1-x}Ni_x)_2Al_3$: K. Mochidzuki, Y. Shimizu, A. Kondo, A. Matsuo, D. Li, D. Aoki, Y. Homma, F. Honda, J. Flouquet, D. Nakamura, S. Takeyama and K. Kindo, Phys. Rev. B **100** (2019) 165137(1-8).

12. *Successive electric-polarization switches in the S=1/2 skew chain Co2V2O7 induced by a high magnetic field: R. Chen, J. F. Wang, Z. W. Ouyang, M. Tokunaga, A. Y. Luo, L. Lin, J. M. Liu, Y. Xiao, A. Miyake, Y. Kohama, C. L. Lu, M. Yang, Z. C. Xia, K. Kindo and L. Li, Phys. Rev. B **100** (2019) 140403(1-5).

13. †Successive phase transitions and magnetization plateau in the spin-1 triangular-lattice antiferromagnet $Ba_2La_2NiTe_2O_{12}$ with small easy-axis anisotropy: M. Saito, M. Watanabe, N. Kurita, A. Matsuo, K. Kindo, M. Avdeev, H. O. Jeschke and H. Tanaka, Phys. Rev. B **100** (2019) 064417(1-12).

14. †Two magnetization plateaus in the kagome fluoride $Cs_2LiTi_3F_{12}$: R. Shirakami, H. Ueda, H. O. Jeschke, H. Nakano, S. Kobayashi, A. Matsuo, T. Sakai, N. Katayama, H. Sawa, K. Kindo, C. Michioka and K. Yoshimura, Phys. Rev. B **100** (2019) 174401(1-7).

15. *Quantum Critical Dynamics of Heisenberg-Ising Chain in a Longitudinal Field: Many-Body Strings versus Fractional Excitations: Z. Wang, M. Schmidt, A. Loidl, J. Wu, H. Zou, W. Yang, C. Dong, Y. Kohama, K. Kindo, D. I. Gorbunov, S. Niesen, O. Breuning, J. Engelmayer and T. Lorenz, Phys. Rev. Lett. **123** (2019) 067202.

16. †*Topological transitions among skyrmion- and hedgehog-lattice states in cubic chiral magnets: Y. Fujishiro, N. Kanazawa, T. Nakajima, X. Z. Yu, K. Ohishi, Y. Kawamura, K. Kakurai, T. Arima, H. Mitamura, A. Miyake, K. Akiba, M. Tokunaga, A. Matsuo, K. Kindo, T. Koretsune, R. Arita and Y. Tokura, Nat. Commun. **10** (2019) 1059(1-8).

17. *Engelhauptite: A variant of S=1/2 kagome antiferromagnet: H. Ishikawa, D. Nishio-Hamane, A. Miyake, M. Tokunaga, A. Matsuo, K. Kindo and Z. Hiroi, Phys. Rev. Materials **3** (2019) 064414(1-5).

18. †Frustrated magnetism in the J_1–J_2 honeycomb lattice compounds $MgMnO_3$ and $ZnMnO_3$ synthesized via a metathesis reaction: Y. Haraguchi, K. Nawa, C. Michioka, H. Ueda, A. Matsuo, K. Kindo, M. Avdeev, T. J. Sato and K. Yoshimura, Phys. Rev. Materials **3** (2019) 124406(1-9).

19. *Thermodynamic evidence of magnetic-field-induced complete valley polarization in bismuth: A. Iwasa, A. Kondo, S. Kawachi, K. Akiba, Y. Nakanishi, M. Yoshizawa, M. Tokunaga and K. Kindo, Sci Rep **9** (2019) 1672(1-8).

20. *Multiple topological states in iron-based superconductors: P. Zhang, Z. Wang, X. Wu, K. Yaji, Y. Ishida, Y. Kohama, G. Dai, Y. Sun, C. Bareille, K. Kuroda, T. Kondo, K. Okazaki, K. Kindo, X. Wang, C. Jin, J. Hu, R. Thomale, K. Sumida, S. Wu, K. Miyamoto, T. Okuda, H. Ding, G. D. Gu, T. Tamegai, T. Kawakami, M. Sato and S. Shin, Nature Phys **15** (2019) 41-48.

21. *Strain-induced spontaneous Hall effect in an epitaxial thin film of a Luttinger semimetal: T. Ohtsuki, Z. Tian, A. Endo,

† Joint research with outside partners.

M. Halim, S. Katsumoto, Y. Kohama, K. Kindo, M. Lippmaa and S. Nakatsuji, Proc. Natl. Acad. Sci. USA **116** (2019) 8803-8808.

22. *A series of magnon crystals appearing under ultrahigh magnetic fields in a kagomé antiferromagnet: R. Okuma, D. Nakamura, T. Okubo, A. Miyake, A. Matsuo, K. Kindo, M. Tokunaga, N. Kawashima, S. Takeyama and Z. Hiroi, Nature Communications **10** (2019) 1229(7).

23. *Possible observation of quantum spin-nematic phase in a frustrated magnet: Y. Kohama, H. Ishikawa, A. Matsuo, K. Kindo, N. Shannon and Z. Hiroi, Proc. Nat. Acad. Sci. U.S.A. **116** (2019) 10686-10690.

24. †Multi-Step Magnetic Transitions in $EuNiIn_4$: S. Ikeda, K. Kaneko, Y. Tanaka, T. Kawasaki, T. Hanashima, K. Munakata, A. Nakao, R. Kiyanagi, T. Ohhara, K. Mochizuki, A. Kondo, K. Kindo, Y. Homma, M. D. Frontzek and H. Kobayashi, J. Phys. Soc. Jpn. **89** (2020) 014707(1-7).

25. †Angle-dependent nontrivial phase in the Weyl semimetal NbAs with anisotropic Fermi surface: M. Komada, H. Murakawa, M. S. Bahramy, T. Kida, K. Yokoi, Y. Narumi, K. Kindo, M. Hagiwara, H. Sakai and N. Hanasaki, Phys. Rev. B **101** (2020) 045135(1-6).

26. *Observation of in-plane magnetic field induced phase transitions in FeSe: J. M. Ok, C. I. Kwon, Y. Kohama, J. S. You, S. K. Park, J.-H. Kim, Y. J. Jo, E. S. Choi, K. Kindo, W. Kang, K.-S. Kim, E. G. Moon, A. Gurevich and J. S. Kim, Phys. Rev. B **101** (2020) 224509.

27. *Extracting the Chiral Contribution to the Negative Longitudinal Magnetoresistance in Epitaxial $Pr_2Ir_2O_7$ Thin Films: T. Ohtsuki, Z. Tian, A. Endo, M. Halim, S. Katsumoto, Y. Kohama, K. Kindo, M. Lippmaa and S. Nakatsuji, JPS Conf. Proc. **30** (2020) 011181(1-6).

Tokunaga group

The metamagnetic transition has been observed in UTe_2, which is expected to realize the spin-triplet superconducting state. The increase of the electron specific heat coefficient with the metamagnetic transition is estimated through the thermodynamic consideration of the high field magnetization measurements taken at various temperatures. In this material, field-induced superconductivity has also been reported in this metamagnetic phase. We have provided valuable information on the electronic state behind magnetic field-induced superconductivity in the early stages of the rapidly advancing physical properties research for this material.

1. Metamagnetic Transition in Heavy Fermion Superconductor UTe_2: A. Miyake, Y. Shimizu, Y. J. Sato, D. Li, A. Nakamura, Y. Homma, F. Honda, J. Flouquet, M. Tokunaga and D. Aoki, J. Phys. Soc. Jpn. **88** (2019) 063706(1-5).

2. *Thermodynamic Investigation of Metamagnetism in Pulsed High Magnetic Fields on Heavy Fermion Superconductor UTe_2: S. Imajo, Y. Kohama, A. Miyake, C. Dong, M. Tokunaga, J. Flouquet, K. Kindo and D. Aoki, J. Phys. Soc. Jpn. **88** (2019) 083705(1-5).

3. *Bidirectional surface photovoltage on a topological insulator: T. Yoshikawa, K. Sumida, Y. Ishida, J. Chen, M. Nurmamat, K. Akiba, A. Miyake, M. Tokunaga, K. A. Kokh, O. E. Tereshchenko, S. Shin and A. Kimura, Phys. Rev. B **100** (2019) 165311(1-6).

4. †*Difference in magnetic and ferroelectric properties between rhombohedral and hexagonal polytypes of $AgFeO_2$: A single-crystal study: N. Terada, Y. Ikedo, H. Sato, D. D. Khalyavin, P. Manuel, F. Orlandi, Y. Tsujimoto, Y. Matsushita, A. Miyake, A. Matsuo, M. Tokunaga and K. Kindo, Phys. Rev. B **99** (2019) 064402(1-11).

5. †Direct coupling of ferromagnetic moment and ferroelectric polarization in $BiFeO_3$: S. Kawachi, S. Miyahara, T. Ito, A. Miyake, N. Furukawa, J.-I. Yamaura and M. Tokunaga, Phys. Rev. B **100** (2019) 140412(1-5).

6. †Magnetic and electrical properties of the ternary compound $U_2Ir_2Si_5$ with one-dimensional uranium zigzag chains: D. X. Li, F. Honda, A. Miyake, Y. Homma, Y. Haga, A. Nakamura, Y. Shimizu, A. Maurya, Y. J. Sato, M. Tokunaga and D. Aoki, Phys. Rev. B **99** (2019) 054408(1-9).

7. †*Magnetoelectric behavior from cluster multipoles in square cupolas: Study of $Sr(TiO)Cu_4(PO_4)_4$ in comparison with Ba and Pb isostructurals: Y. Kato, K. Kimura, A. Miyake, M. Tokunaga, A. Matsuo, K. Kindo, M. Akaki, M. Hagiwara, S. Kimura, T. Kimura and Y. Motome, Phys. Rev. B **99** (2019) 024415(1-12).

8. *Successive electric-polarization switches in the S=1/2 skew chain $Co_2V_2O_7$ induced by a high magnetic field: R. Chen, J. F. Wang, Z. W. Ouyang, M. Tokunaga, A. Y. Luo, L. Lin, J. M. Liu, Y. Xiao, A. Miyake, Y. Kohama, C. L. Lu, M. Yang, Z. C. Xia, K. Kindo and L. Li, Phys. Rev. B **100** (2019) 140403(1-5).

9. †*Large Enhancement of Thermoelectric Efficiency Due to a Pressure-Induced Lifshitz Transition in SnSe:

* Joint research among groups within ISSP.

T. Nishimura, H. Sakai, H. Mori, K. Akiba, H. Usui, M. Ochi, K. Kuroki, A. Miyake, M. Tokunaga, Y. Uwatoko, K. Katayama, H. Murakawa and N. Hanasaki, Phys. Rev. Lett. **122** (2019) 226601(1-6).

10. †*Topological transitions among skyrmion- and hedgehog-lattice states in cubic chiral magnets: Y. Fujishiro, N. Kanazawa, T. Nakajima, X. Z. Yu, K. Ohishi, Y. Kawamura, K. Kakurai, T. Arima, H. Mitamura, A. Miyake, K. Akiba, M. Tokunaga, A. Matsuo, K. Kindo, T. Koretsune, R. Arita and Y. Tokura, Nat. Commun. **10** (2019) 1059(1-8).

11. *Engelhauptite: A variant of S=1/2 kagome antiferromagnet: H. Ishikawa, D. Nishio-Hamane, A. Miyake, M. Tokunaga, A. Matsuo, K. Kindo and Z. Hiroi, Phys. Rev. Materials **3** (2019) 064414(1-5).

12. Quantized surface transport in topological Dirac semimetal films: S. Nishihaya, M. Uchida, Y. Nakazawa, R. Kurihara, K. Akiba, M. Kriener, A. Miyake, Y. Taguchi, M. Tokunaga and M. Kawasaki, Nat Commun **10** (2019) 2564(1-7).

13. *Thermodynamic evidence of magnetic-field-induced complete valley polarization in bismuth: A. Iwasa, A. Kondo, S. Kawachi, K. Akiba, Y. Nakanishi, M. Yoshizawa, M. Tokunaga and K. Kindo, Sci Rep **9** (2019) 1672(1-8).

14. *A series of magnon crystals appearing under ultrahigh magnetic fields in a kagomé antiferromagnet: R. Okuma, D. Nakamura, T. Okubo, A. Miyake, A. Matsuo, K. Kindo, M. Tokunaga, N. Kawashima, S. Takeyama and Z. Hiroi, Nature Communications **10** (2019) 1229(7).

15. *^{105}Pd NMR and NQR study of the cubic heavy fermion system $Ce_3Pd_{20}Si_6$: I. Jakovac, M. Horvatic, E. F. Schwier, A. Prokofiev, S. Paschen, H. Mitamura, T. Sakakibara and M. S. Grbic, J. Phys.: Condens. Matter **32** (2020) 245601(1-7).

16. †*Bulk quantum Hall effect of spin-valley coupled Dirac fermions in the polar antiferromagnet BaMnSb2: H. Sakai, H. Fujimura, S. Sakuragi, M. Ochi, R. Kurihara, A. Miyake, M. Tokunaga, T. Kojima, D. Hashizume, T. Muro, K. Kuroda, T. Kondo, T. Kida, M. Hagiwara, K. Kuroki, M. Kondo, K. Tsuruda, H. Murakawa and N. Hanasaki, Phys. Rev. B **101** (2020) 081104(1-7).

17. High-field ultrasonic study of quadrupole ordering and crystal symmetry breaking in $CeRhIn_5$: R. Kurihara, A. Miyake, M. Tokunaga, Y. Hirose and R. Settai, Phys. Rev. B **101** (2020) 155125(1-8).

18. Magnetic phase diagram enriched by chemical substitution in a noncentrosymmetric helimagnet: T. Sato, Y. Araki, A. Miyake, A. Nakao, N. Abe, M. Tokunaga, S. Kimura, Y. Tokunaga and T.-H. Arima, Phys. Rev. B **101** (2020) 054414(1-6).

19. †Magnetic structures and quadratic magnetoelectric effect in $LiNiPO_4$ beyond 30 T: E. Fogh, T. Kihara, R. Toft-Petersen, M. Bartkowiak, Y. Narumi, O. Prokhnenko, A. Miyake, M. Tokunaga, K. Oikawa, M. K. Sørensen, J. C. Dyrnum, H. Grimmer, H. Nojiri and N. B. Christensen, Phys. Rev. B **101** (2020) 024403(1-12).

20. *Magnetotransport properties of tellurium under extreme conditions: K. Akiba, K. Kobayashi, T. C. Kobayashi, R. Koezuka, A. Miyake, J. Gouchi, Y. Uwatoko and M. Tokunaga, Phys. Rev. B **101** (2020) 245111(1-6).

21. †High-Mobility 2D Hole Gas at a $SrTiO_3$ Interface: L. D. Anh, S. Kaneta, M. Tokunaga, M. Seki, H. Tabata, M. Tanaka and S. Ohya, Adv. Mater. **32** (2020) 1906003(1-7).

22. Magnetic field induced antiferromagnetic cone structure in multiferroic $BiFeO_3$: M. Matsuda, S. E. Dissanayake, T. Hong, Y. Ozaki, T. Ito, M. Tokunaga, X. Z. Liu, M. Bartkowiak and O. Prokhnenko, Phys. Rev. Materials **4** (2020) 034412(1-6).

Y. Matsuda group

The high-magnetic-field x-ray diffraction study on the solid oxygen was performed with synchrotron x-rays at BL22XU of the SPring-8. A giant magnetostriction due to the strong spin-lattice coupling had been reported in alpha oxygen. It has been found by our study that the change in the lattice constant is smaller than 10^{-4} even at high magnetic fields of up to 25 T, which is two orders of magnitude smaller than that expected from the results of the previous report. Considering the energy balance between the elastic energy and the magnetic energy, it seems to be reasonable having the absence of the giant magnetostriction. The first-order alpha-theta magnetic-field-induced phase transition in oxygen around 120 T thus is expected to happen with a distinct sharp change in the crystal lattice without gradual expansion at smaller magnetic fields. The magnetostriction in the deformed Kagome spin system volborthite has been investigated in pulsed magnetic fields and a significant 1/3 plateau has been observed in the field variation of the striction. A comparison between the magnetic field dependences of the striction and magnetization allows us to discuss the correlation function of spins. Non-polar magnetic compound Pb_2MnO_4 and a high-T_c cuprate $LaSrCuO_4$ have also been investigated in pulsed magnetic fields of up to 60 T and 100 T, respecively.

1. High magnetic field x-ray diffraction study of the α phase of solid oxygen: Absence of giant magnetostriction: Y. H. Matsuda, A. Shimizu, A. Ikeda, T. Nomura, T. Yajima, T. Inami, K. Takahashi and T. C. Kobayashi, Phys. Rev. B **100** (2019) 214105(1-7).

† Joint research with outside partners.

2. †*Magnetoelastic couplings in the deformed kagome quantum spin lattice of volborthite: A. Ikeda, S. Furukawa, O. Janson, Y. H. Matsuda, S. Takeyama, T. Yajima, Z. Hiroi and H. Ishikawa, Phys. Rev. B **99** (2019) 140412(R)(1-5).

3. †Metamagnetic transitions and magnetoelectric coupling in acentric and nonpolar Pb_2MnO_4: D. Chandrasekhar Kakarla, H. C. Wu, D. J. Hsieh, P. J. Sun, G. J. Dai, J. -Y. Lin, J. L. Her, Y. H. Matsuda, L. Z. Deng, M. Gooch, C. W. Chu and H. D. Yang, Phys. Rev. B **99** (2019) 195129(1-9).

4. ファイバーブラッググレーティングを用いた高速 100MHz ひずみ測定装置の構築と超強磁場中スピン格子物性の開拓： 池田 暁彦 , 松田 康弘 , 固体物理 **54** (2019) 147- 157.

5. †*Pauli-limit upper critical field of high-temperature superconductor La1.84Sr0.16CuO4: D. Nakamura, T. Adachi, K. Omori, Y. Koike and S. Takeyama, Sci Rep **9** (2019) 16949(1-8).

6. †The Temperature Dependence of the Magnetization Process of the Kondo Insulator YbB_{12}: Y. H. Matsuda, Y. Kakita and F. Iga, Crystals **10** (2020) 26(1-7).

7. †*Direct measurement of resistivity in destructive pulsed magnetic fields: Y. Kohama, F. Nabeshima, A. Maeda, A. Ikeda and Y. H. Matsuda, Review of Scientific Instruments **91** (2020) 033901(1-5).

Kohama group

We have investigated high-field properties in many different systems, such as $CeRhIn_5$, $AgVOAsO_4$, $Co_2V_2O_7$, volborthite, $BaCo_2V_2O_8$, V_5Se_8, $LiCuVO_4$, $Pr_2Ir_2O_7$, and UIrGe. With newly developed measurement techniques, specific heat and magnetooptics, we could reveal the field-induced phenomena such as QCP, spin nematic state, and electronic nematic state. We also have constructed a new type of capacitor bank for the generation of pulsed magnetic fields with the second order timescale.

1. *Thermodynamic Investigation of Metamagnetism in Pulsed High Magnetic Fields on Heavy Fermion Superconductor UTe_2: S. Imajo, Y. Kohama, A. Miyake, C. Dong, M. Tokunaga, J. Flouquet, K. Kindo and D. Aoki, J. Phys. Soc. Jpn. **88** (2019) 083705(1-5).

2. †*Enhancement of the effective mass at high magnetic fields in $CeRhIn_5$: L. Jiao, M. Smidman, Y. Kohama, Z. S. Wang, D. Graf, Z. F. Weng, Y. J. Zhang, A. Matsuo, E. D. Bauer, H. Lee, S. Kirchner, J. Singleton, K. Kindo, J. Wosnitza, F. Steglich, J. D. Thompson and H. Q. Yuan, Phys. Rev. B **99** (2019) 045127(6).

3. Field-induced double dome and Bose-Einstein condensation in the crossing quantum spin chain system $AgVOAsO_4$: F. Weickert, A. A. Aczel, M. B. Stone, V. Ovidiu Garlea, C. Dong, Y. Kohama, R. Movshovich, A. Demuer, N. Harison, M. B. G. A. Steppke, M. Brando, H. Rosner and A. A. Tsirlin, Phys. Rev. B **100** (2019) 104422.

4. *Successive electric-polarization switches in the S=1/2 skew chain $Co_2V_2O_7$ induced by a high magnetic field: R. Chen, J. F. Wang, Z. W. Ouyang, M. Tokunaga, A. Y. Luo, L. Lin, J. M. Liu, Y. Xiao, A. Miyake, Y. Kohama, C. L. Lu, M. Yang, Z. C. Xia, K. Kindo and L. Li, Phys. Rev. B **100** (2019) 140403(1-5).

5. Viscosity measurements in pulsed magnetic fields by using a quartz-crystal microbalance: T. Nomura, S. Zherlitsyn, Y. Kohama and J. Wosnitza, Rev. Sci. Instrum. **90** (2019) 065101.

6. *Quantum Critical Dynamics of Heisenberg-Ising Chain in a Longitudinal Field: Many-Body Strings versus Fractional Excitations: Z. Wang, M. Schmidt, A. Loidl, J. Wu, H. Zou, W. Yang, C. Dong, Y. Kohama, K. Kindo, D. I. Gorbunov, S. Niesen, O. Breuning, J. Engelmayer and T. Lorenz, Phys. Rev. Lett. **123** (2019) 067202.

7. * カゴメ銅鉱物ボルボサイトにおける軌道転移とフラストレート磁性： 広井 善二 , 石川 孟 , 小濱 芳允 , 固体物理 **54** (2019) 117-130.

8. *Unconventional field-induced spin gap in an S = 1/2 chiral staggered chain: J. Liu, S. Kittaka, R. D. Johnson, T. Lancaster, J. Singleton, T. Sakakibara, Y. Kohama, J. van Tol, A. Ardavan, B. H. Williams, S. J. Blundell, Z. E. Manson, J. L. Manson and P. A. Goddard, Phys Rev Lett **122** (2019) 057207(1-6).

9. *Multiple topological states in iron-based superconductors: P. Zhang, Z. Wang, X. Wu, K. Yaji, Y. Ishida, Y. Kohama, G. Dai, Y. Sun, C. Bareille, K. Kuroda, T. Kondo, K. Okazaki, K. Kindo, X. Wang, C. Jin, J. Hu, R. Thomale, K. Sumida, S. Wu, K. Miyamoto, T. Okuda, H. Ding, G. D. Gu, T. Tamegai, T. Kawakami, M. Sato and S. Shin, Nature Phys **15** (2019) 41-48.

10. Shubnikov–de Haas oscillations in the three-dimensional Dirac fermion system Ca_3PbO: Y. Obata, Y. Kohama, S. Matsuishi and H. Hosono, Phys Rev B **99** (2019) 115133.

11. *Strain-induced spontaneous Hall effect in an epitaxial thin film of a Luttinger semimetal: T. Ohtsuki, Z. Tian, A. Endo, M. Halim, S. Katsumoto, Y. Kohama, K. Kindo, M. Lippmaa and S. Nakatsuji, Proc. Natl. Acad. Sci. USA **116** (2019)

* Joint research among groups within ISSP.

8803-8808.

12. *Possible observation of quantum spin-nematic phase in a frustrated magnet: Y. Kohama, H. Ishikawa, A. Matsuo, K. Kindo, N. Shannon and Z. Hiroi, Proc. Nat. Acad. Sci. U.S.A. **116** (2019) 10686-10690.

13. Magnetocaloric effect and spin-strain coupling in the spin-nematic state of $LiCuVO_4$: M. Gen, T. Nomura, D. I. Gorbunov, S. Yasin, P. T. Cong, C. Dong, Y. Kohama, E. L. Green, J. M. Law, M. S. Henriques, J. Wosnitza, A. A. Zvyagin, V. O. Cheranovskii, R. K. Kremer and S. Zherlisyn, Phys. Rev. Research **1** (2019) 033065(1-8).

14. *Intrinsic 2D Ferromagnetism in V5Se8 Epitaxial thin films: M. Nakano, Y. Wang, S. Yoshida, H. Matsuoka, Y. Majima, K. Ikeda, Y. Hirata, Y. Takeda, H. Wadati, Y. Kohama, Y. Ohigashi, M. Sakano, K. Ishizaka and Y. Iwasa, Nano Letter **19** (2019) 8806-8810.

15. Electronic band structure of (111) $SrRuO_3$ thin films: An angle-resolved photoemission spectroscopy study: H. Ryu, Y. Ishida, B. Kim, J. R. Kim, W. J. Kim, Y. Kohama, S. Imajo, Z. Yang, W. Kyung, S. Hahn, B. Sohn, I. Song, M. Kim, S. Huh, J. Jung, D. Kim, T. W. Noh, S. Das and C. Kim, Phys. Rev. B **102** (2020) 041102.

16. Magnetization process of the breathing pyrochlore magnet $CuInCr_4S_8$ in ultrahigh magnetic fields up to 150 T: M. Gen, Y. Okamato, M. Mori, K. Takenaka and Y. Kohama, Phys. Rev. B **101** (2020) 054434.

17. *Observation of in-plane magnetic field induced phase transitions in FeSe: J. M. Ok, C. I. Kwon, Y. Kohama, J. S. You, S. K. Park, J.-H. Kim, Y. J. Jo, E. S. Choi, K. Kindo, W. Kang, K.-S. Kim, E. G. Moon, A. Gurevich and J. S. Kim, Phys. Rev. B **101** (2020) 224509.

18. *Extracting the Chiral Contribution to the Negative Longitudinal Magnetoresistance in Epitaxial $Pr_2Ir_2O_7$ Thin Films: T. Ohtsuki, Z. Tian, A. Endo, M. Halim, S. Katsumoto, Y. Kohama, K. Kindo, M. Lippmaa and S. Nakatsuji, JPS Conf. Proc. **30** (2020) 011181(1-6).

19. †*Direct measurement of resistivity in destructive pulsed magnetic fields: Y. Kohama, F. Nabeshima, A. Maeda, A. Ikeda and Y. H. Matsuda, Review of Scientific Instruments **91** (2020) 033901(1-5).

20. Angle dependence of H_{c2} with a crossover between the orbital and paramagnetic limits: H. Matsuoka, M. Nakano, T. Shitaokoshi, Y. Wang, Y. Kashiwabara, S. Yoshida, Y. Kohama, T. Ouchi, K. Ishizaka, M. Kawasaki, T. Nojima and Y. Iwasa, Phys. Rev. Research **2** (2020) 012064(R).

21. Van der Waals $SnSe_{2(1-x)}S_{2x}$ Alloys: Composition-Dependent Bowing Coefficient and Electron–Phonon Interaction: Z. R. Kudrynskyi, X. Wang, J. Sutcliffe, M. A. Bhuiyan, Y. Fu, Z. Yang, O. Makarovsky, L. Eaves, A. Solomon, V. T. Maslyuk, Z. D. Kovalyuk, L. Zhang and A. Patanè, Advanced Functional Materials **30** (2020) 1908092.

Laser and Synchrotron Research Center

Kobayashi group

We are developing ultra-short pulse laser and its applications. In 2019, we have developed >20 GHz repetition rate mode-locked oscillator, which would be useful for industrial and scientific applications.

1. Kerr-lens mode locking above a 20 GHz repetition rate: S. Kimura, S. Tani and Y. Kobayashi, Optica **6** (2019) 532-533.

2. Raman-assisted broadband mode-locked laser: S. Kimura, S. Tani and Y. Kobayashi, Sci Rep **9** (2019) 3738(1-6).

3. Direct generation of femtosecond vortex beam from a Yb:KYW oscillator featuring a defect-spot mirror: S. Wang, Z. Zhao, I. Ito and Y. Kobayashi, OSA Continuum **2** (2019) 523-530.

4. Monolithic LiF or MgF_2 lens-window-prism device for coherent 10.7 eV beam source with 1 MHz repetition rate: Z. Zhao, K. Kuroda, A. Harasawa, T. Kondo, S. Shin and Y. Kobayashi, Chin. Opt. Lett. **17** (2019) 051406.

5. †Study on nonthermal–thermal processing boundary in drilling of ceramics using ultrashort pulse laser system with variable parameters over a wide range: A. Narazaki, H. Takada, D. Yoshitomi, K. Torizuka and Y. Kobayashi, Appl. Phys. A **126** (2020) 252.

6. Subgigahertz-resolution table-top spectrograph calibrated with a 4-GHz optical frequency comb: M. Endo, T. Sukegawa, A. Silva and Y. Kobayashi, J. Astron. Telesc. Instrum. Syst. **6** (2020) 1.

7. カーレンズモード同期レーザーを用いた高繰り返し光周波数コムの開発：木村 祥太，谷 峻太郎，小林 洋平，光技術コンタ

† Joint research with outside partners.

クト **57** (2019) 3-9.

8. *Gerard A. Mourou 博士とチャープパルス増幅法：渡部 俊太郎，鍋川 康夫，板谷 治郎，小林 洋平，科学 82 巻 2 号 (2019) 131-137.

Harada group

We have encouraged users the use of operando photoemission and soft X-ray emission measurements for battery materials and catalysts. One of the outstanding works in 2019 is the elucidation of structure-activity correlations in a nickel manganese oxide, which is an oxygen evolution reaction catalyst and was applied the operando soft X-ray emission analysis for the first time. In 2019 we have performed 14 collaborative works at BL07LSU HORNET end-station. Among them, six proposals were related to the battery electrode, while four are solid-state physics. With a strong collaboration with a group at Stockholm University in Sweden, we continue RIXS works on bulk liquid water and proved the existence of micro-inhomogeneity in liquid water by a detailed analysis of excitation energy dependence. Using beamtimes for beamline tuning we continued feasibility studies including test experiments with companies. Some of them are combined with the Grant-in-Aid for Scientific Research on Innovative Area project named "Aquatic Functional Materials" starting from July.

1. †Half-metallicity of Mn2VAl ferrimagnet revealed by resonant inelastic soft x-ray scattering in a magnetic field: R. Y. Umetsu, H. Fujiwara, K. Nagai, Y. Nakatani, M. Kawada, A. Sekiyama, F. Kuroda, H. Fujii, T. Oguchi, Y. Harada, J. Miyawaki and S. Suga, Phys. Rev. B **99** (2019) 134414(1-10).

2. †Measurements of ultrafast dissociation in resonant inelastic x-ray scattering of water: K. Yamazoe, J. Miyawaki, H. Niwa, A. Nilsson and Y. Harada, J. Chem. Phys. **150** (2019) 204201(1-7).

3. †*Operando* soft X-ray emission spectroscopy of the Fe_2O_3 anode to observe the conversion reaction: D. Asakura, Y. Nanba, M. Okubo, H. Niwa, H. Kiuchi, J. Miyawaki, M. Oshima, E. Hosono and Y. Harada, Phys. Chem. Chem. Phys. **21** (2019) 26351-26357.

4. †Mn 2p resonant X-ray emission clarifies the redox reaction and charge-transfer effects in $LiMn_2O_4$: D. Asakura, Y. Nanba, E. Hosono, M. Okubo, H. Niwa, H. Kiuchi, J. Miyawaki and Y. Harada, Phys. Chem. Chem. Phys. **21** (2019) 18363-18369.

5. †Elucidation of Structure–Activity Correlations in a Nickel Manganese Oxide Oxygen Evolution Reaction Catalyst by Operando Ni L-Edge X-ray Absorption Spectroscopy and 2p3d Resonant Inelastic X-ray Scattering: M. A. Samarai, A. W. Hahn, A. B. Askari, Y.-T. Cui, K. Yamazoe, J. Miyawaki, Y. Harada, O. Rüdiger and S. DeBeer, ACS Appl. Mater. Interfaces **11** (2019) 38595-38605.

6. †Operando measurement of single crystalline $Li_4Ti_5O_{12}$ with octahedral-like morphology by microscopic X-ray photoelectron spectroscopy: K. Akada, T. Sudayama, D. Asakura, H. Kitaura, N. Nagamura, K. Horiba, M. Oshima, E. Hosono and Y. Harada, Journal of Electron Spectroscopy and Related Phenomena **233** (2019) 64-68.

7. †Microscopic photoelectron analysis of single crystalline $LiCoO_2$ particles during the charge-discharge in an all solid-state lithium ion battery: K. Akada, T. Sudayama, D. Asakura, H. Kitaura, N. Nagamura, K. Horiba, M. Oshima, E. Hosono and Y. Harada, Sci Rep **9** (2019) 12452(1-7).

8. †Do X-ray spectroscopies provide evidence for continuous distribution models of water at ambient conditions?: L. G. M. Pettersson, Y. Harada and A. Nilsson, Proc Natl Acad Sci USA **116** (2019) 17156-17157.

9. *Direct Evidence of Interfacial Hydrogen Bonding in Proton-Electron Concerted 2D Organic Bilayer on Au Substrate: S. Yamamoto, H. S. Kato, A. Ueda, S. Yoshimoto, Y. Hirata, J. Miyawaki, K. Yamamoto, Y. Harada, H. Wadati, H. Mori, J. Yoshinobu and I. Matsuda, e-J. Surf. Sci. Nanotechnol. **17** (2019) 49-55.

I. Matsuda group

In 2019, varieties of surface chemistry were revealed by joint-researches of near-ambient pressure XPS at SPring-8 BL07LSU. The laboratory has worked on developing advanced experimental techniques for the next-generation synchrotron radiation facility. Especially, a new light source of the segmented undulator for extensive polarization controls is designed. In material science, carrier dynamics of the atomic layer system, such as quasi-crystalline bilayer graphene, are revealed by time-resolved photoemission spectroscopy.

1. †*Photoinduced valence dynamics in $EuNi_2(Si_{0.21}Ge_{0.79})_2$ studied via time-resolved x-ray absorption spectroscopy: Y. Yokoyama, K. Kawakami, Y. Hirata, K. Takubo, K. Yamamoto, K. Abe, A. Mitsuda, H. Wada, T. Uozumi, S. Yamamoto, I. Matsuda, S. Kimura, K. Mimura and H. Wadati, Phys. Rev. B **100** (2019) 115123(1-6).

2. *Symmetry-breaking and spin-blockage effects on carrier dynamics in single-layer tungsten diselenide: R.-Y. Liu,

* Joint research among groups within ISSP.

M.-K. Lin, P. Chen, T. Suzuki, P. C. J. Clark, N. K. Lewis, C. Cacho, E. Springate, C.-S. Chang, K. Okazaki, W. Flavell, I. Matsuda and T.-C. Chiang, Phys. Rev. B **100** (2019) 214309.

3. Superstructure-Induced Splitting of Dirac Cones in Silicene: B. Feng, H. Zhou, Y. Feng, H. Liu, S. He, I. Matsuda, L. Chen, E. F. Schwier, K. Shimada, S. Meng and K. Wu, Phys. Rev. Lett. **122** (2019) 196801(1-6).

4. 時間分解軟 X 線光電子分光による電子状態の動的観察：松田 巌 , 応用物理 **88** (2019) 716-719.

5. 偏光変調型軟 X 線を用いた複素誘電率の直接測定：久保田 雄也 , 赤井 久純 , 平田 靖透 , 松田 巌 , 日本物理学会誌 **74** (2019) 646.

6. *Hydrogen adsorption and absorption on a Pd-Ag alloy surface studied using in-situ X-ray photoelectron spectroscopy under ultrahigh vacuum and ambient pressure: J. Tang, S. Yamamoto, T. Koitaya, Y. Yoshikura, K. Mukai, S. Yoshimoto, I. Matsuda and J. Yoshinobu, Appl. Surf. Sci. **463** (2019) 1161-1167.

7. SACLA による軟 X 線非線形光学現象の開拓：山本 真吾 , 松田 巌 , 放射光 **32** (2019) 307 (7 pages).

8. †Enhanced Photoresponsivity of Fullerene in the Presence of Phthalocyanine: A Time-Resolved X-ray Photoelectron Spectroscopy Study of Phthalocyanine/C_{60}/TiO_2 (110): K. Ozawa, S. Yamamoto, M. D'angelo, Y. Natsui, N. Terashima, K. Mase and I. Matsuda, J. Phys. Chem. C **123** (2019) 4388-4395.

9. †*Reversible low-temperature redox activity and selective oxidation catalysis derived from the concerted activation of multiple metal species on Cr and Rh-incorporated ceria catalysts: S. Ikemoto, X. Huang, S. Muratsugu, S. Nagase, T. Koitaya, H. Matsui, G.-I. Yokota, T. Sudoh, A. Hashimoto, Y. Tan, S. Yamamoto, J. Tang, I. Matsuda, J. Yoshinobu, T. Yokoyama, S. Kusaka, R. Matsuda and M. Tada, Phys. Chem. Chem. Phys. **21** (2019) 20868.

10. *Ultrafast Unbalanced Electron Distributions in Quasicrystalline 30° Twisted Bilayer Graphene: T. Suzuki, T. Iimori, S. J. Ahn, Y. Zhao, M. Watanabe, J. Xu, M. Fujisawa, T. Kanai, N. Ishii, J. Itatani, K. Suwa, H. Fukidome, S. Tanaka, J. R. Ahn, K. Okazaki, S. Shin, F. Komori and I. Matsuda, ACS Nano **13** (2019) 11981.

11. Electronic structure of a monoatomic Cu_2Si layer on a Si(111) substrate: M. Cameau, R. Yukawa, C. -H. Chen, A. Huang, S. Ito, R. Ishibiki, K. Horiba, Y. Obata, T. Kondo, H. Kumigashira, H. -T. Jeng, M. D'angelo and I. Matsuda, Phys. Rev. Materials **3** (2019) 044004-1.-5.

12. Semimetallicity of free-standing hydrogenated monolayer boron from MgB_2: I. Tateishi, N. T. Cuong, C. A. S. Moura, M. Cameau, R. Ishibiki, A. Fujino, S. Okada, A. Yamamoto, M. Araki, S. Ito, S. Yamamoto, M. Niibe, T. Tokushima, D. E. Weibel, T. Kondo, M. Ogata and I. Matsuda, Phys. Rev. Materials **3** (2019) 024004(1-8).

13. *Mass transport in the PdCu phase structures during hydrogen adsorption and absorption studied by XPS under hydrogen atmosphere: J. Tang, S. Yamamoto, T. Koitaya, A. Yoshigoe, T. Tokunaga, K. Mukai, I. Matsuda and J. Yoshinobu, Applied Surface Science **480** (2019) 419-426.

14. *CO_2 Activation and Reaction on Zn-Deposited Cu Surfaces Studied by Ambient-Pressure X-ray Photoelectron Spectroscopy: T. Koitaya, S. Yamamoto, Y. Shiozawa, Y. Yoshikura, M. Hasegawa, J. Tang, K. Takeuchi, K. Mukai, S. Yoshimoto, I. Matsuda and J. Yoshinobu, ACS Catal. **9** (2019) 4539-4550.

15. *Direct Evidence of Interfacial Hydrogen Bonding in Proton-Electron Concerted 2D Organic Bilayer on Au Substrate: S. Yamamoto, H. S. Kato, A. Ueda, S. Yoshimoto, Y. Hirata, J. Miyawaki, K. Yamamoto, Y. Harada, H. Wadati, H. Mori, J. Yoshinobu and I. Matsuda, e-J. Surf. Sci. Nanotechnol. **17** (2019) 49-55.

16. Segmented Undulator for Extensive Polarization Controls in ≤1 nm-rad Emittance Rings: I. Matsuda, S. Yamamoto, J. Miyawaki, T. Abukawa and T. Tanaka, e-J. Surf. Sci. Nanotechnol. **17** (2019) 41-48.

17. Photoinduced hydrogen release from hydrogen boride sheets: R. Kawamura, N. T. Cuong, T. Fujita, R. Ishibiki, T. Hirabayashi, A. Yamaguchi, I. Matsuda, S. Okada, T. Kondo and M. Miyauchi, Nature Commun. **10** (2019) 4880 (10 pages).

18. †A Surface Science Approach to Unveiling TiO2 Photocatalytic Mechanism: Correlation between Photocatalytic Activity and Carrier Lifetime: K. Ozawa, S. Yamamoto, K. Mase and I. Matsuda, e-J. Surf. Science. Nanotechnol. **17** (2019) 130-147.

19. Two-dimensional conducting layer on SrTiO3 surface induced by hydrogenation: Y. Takeuchi, R. Hobara, R. Akiyama, A. Takayama, S. Ichinokura, R. Yukawa, I. Matsuda and S. Hasegawa, Phys. Rev. B **101** (2020) 085422(1-6).

20. *Element-selectively tracking ultrafast demagnetization process in Co/Pt multilayer thin films by the resonant magneto-optical Kerr effect: K. Yamamoto, S. E. Moussaoui, Y. Hirata, S. Yamamoto, Y. Kubota, S. Owada, M. Yabashi, T. Seki, K. Takanashi, I. Matsuda and H. Wadati, Appl. Phys. Lett. **116** (2020) 172406(1-5).

† Joint research with outside partners.

21. *A computational examination of the electric-field-induced proton transfer along the interface hydrogen bond between proton donating and accepting self-assembled monolayers: Y. Kanematsu, H. S. Kato, S. Yoshimoto, A. Ueda, S. Yamamoto, H. Mori, J. Yoshinobu, I. Matsuda and M. Tachikawa, Chem. Phys. Lett. **741** (2020) 137091.

22. *Edge-state correlation accelerates metal-insulator transition in topological semimetal nanofilms: S. Ito, M. Arita, J. Haruyama, B. Feng, W. -C. Chen, H. Namatame, M. Taniguchi, C. -M. Cheng, G. Bian, S. -J. Tang, T. -C. Chiang, O. Sugino, F. Komori and I. Matsuda, Science Advances **6** (2020) eaaz5015 (7 pages).

23. Geometrical Frustration of B-H Bonds in Layered Hydrogen Borides Accessible by Soft Chemistry: S. Tominaka, R. Ishibiki, A. Fujino, K. Kawakami, K. Ohara, I. Matsuda, H. Hosono and T. Kondo, Chem **6** (2020) 406-418.

24. †*Surface Chemistry of Carbon Dioxide on Copper Model Catalysts Studied by Ambient-Pressure X-ray Photoelectron Spectroscopy: T. Koitaya, S. Yamamoto, I. Matsuda and J. Yoshinobu, e-J. Surf. Sci. Nanotechnol. **17** (2019) 169.

25. Monatomic Two-Dimensional Layers: Modern Experimental Approaches for Structure, Properties, and Industrial Use: I. M. ed., (Elsevier, Amsterdam, Netherland, 2019).

Itatani group

We carried out transient soft-x-ray spectroscopy using isolated attosecond pulses in the water window (photon energy spans from 280 to 540 eV). Broadband isolated attosecond pulses are now routinely generated with an accurate control of carrier-envelope phases of the driver laser as well as a precise feedback of the pump and probe path length, which resulted in ~50 attosecond pump-probe precision. We measured absorption spectra for NO molecules that were irradiated by intense IR fields at the nitrogen *K* edge around 400 eV. We time-resolved the generation process of NO^+ ions via field ionization, molecular vibration of NO^+ ions, and molecular orientation of NO molecules, all of these dynamics occurred in the hierarchal manner on the time scales from attoseconds to subpicoseconds. Indeed this experiment is the one at the highest photon energy in attosecond soft-X-ray spectroscopy. We also developed intense MIR sources at 3.5 μm, and applied these sources to several experiments on solid samples. In the case of gold-coated grating, we discovered highly directional resonant-like photoemission, which arose from the generation of propagating surface plasmon that enhanced the localized near fields at the tip of the grating structure. High harmonic generation in a hybrid organic-inorganic perovskite thin film was firstly observed. Sub-cycle spectroscopy for MIR field-induced dynamics for proton-mediated ferroelectricity was carried out, and we demonstrated that the ferroelectricity was controlled by direct phonon excitation. The collaboration with time-resolved ARPES groups continued, and we observed intriguing photo-induced phenomena in twisted bilayer graphene and FeSe.

1. †Ultrafast Control of Ferroelectricity with Dynamical Repositioning of Protons in a Supramolecular Cocrystal Studied by Femtosecond Nonlinear Spectroscopy: T. Umanodan, K. Kaneshima, K. Takeuchi, N. Ishii, J. Itatani, H. Hirori, Y. Sanari, K. Tanaka, Y. Kanemitsu, T. Ishikawa, S.-Y. Koshihara, S. Horiuchi and Y. Okimoto, J. Phys. Soc. Jpn. **88** (2019) 013705.

2. 位相安定な中赤外光源とサブサイクル分光： 金島 圭佑，石井 順久，竹内 健悟，板谷 治郎，固体物理 **54** (2019) 165-172.

3. Optical parametric amplification of carrier-envelope phase-stabilized mid-infrared pulses generated by intra-pulse difference frequency generation: N. Ishii, P. Xia, T. Kanai and J. Itatani, Opt. Express **27** (2019) 11447.

4. *Ultrafast Unbalanced Electron Distributions in Quasicrystalline 30° Twisted Bilayer Graphene: T. Suzuki, T. Iimori, S. J. Ahn, Y. Zhao, M. Watanabe, J. Xu, M. Fujisawa, T. Kanai, N. Ishii, J. Itatani, K. Suwa, H. Fukidome, S. Tanaka, J. R. Ahn, K. Okazaki, S. Shin, F. Komori and I. Matsuda, ACS Nano **13** (2019) 11981.

5. Real-time observation of electronic, vibrational, and rotational dynamics in nitric oxide with attosecond soft x-ray pulses at 400 eV: N. Saito, H. Sannohe, N. Ishii, T. Kanai, N. Kosugi, Y. Wu, A. Chew, S. Han, Z. Chang and J. Itatani, Optica **6** (2019) 1542.

6. †High-order harmonic generation from hybrid organic–inorganic perovskite thin films: H. Hirori, P. Xia, Y. Shinohara, T. Otobe, Y. Sanari, H. Tahara, N. Ishii, J. Itatani, K. L. Ishikawa, T. Aharen, M. Ozaki, A. Wakamiya and Y. Kanemitsu, APL Materials **7** (2019) 041107.

7. *Photoinduced possible superconducting state with long-lived disproportionate band filling in FeSe: T. Suzuki, T. Someya, T. Hashimoto, S. Michimae, M. Watanabe, M. Fujisawa, T. Kanai, N. Ishii, J. Itatani, S. Kasahara, Y. Matsuda, T. Shibauchi, K. Okazaki and S. Shin, Commun. Phys. **2** (2019) 115.

8. Resonant-Like Field Enhancement by Nanoscale Grating-Coupled Propagating Surface Plasmonics and Localized Surface Plasmons in the Mid-Infrared Range: Implications for Ultrafast Plasmonic Electron Sources: T. Mizuno, K. Takeuchi, K. Kaneshima, N. Ishii, T. Kanai and J. Itatani, Applied Nano Materials **2** (2019) 7067-7073.

9. *Efficient Terahertz Harmonic Generation with Coherent Acceleration of Electrons in the Dirac Semimetal Cd_3As_2:

* Joint research among groups within ISSP.

B. Cheng, N. Kanda, T. N. Ikeda, T. Matsuda, P. Xia, T. Schumann, S. Stemmer, J. Itatani, N. P. Armitage and R. Matsunaga, Phys. Rev. Lett. **124** (2020) 117402.

10. 中赤外光パルスを用いた固体高次高調波発生とその偏光特性：石井 順久，金島 圭佑，夏 沛宇，斎藤 成之，金井 輝人，板谷 治郎，レーザー研究 **49** (2020) 168-173.

11. *Gerard A. Mourou 博士とチャープパルス増幅法： 渡部 俊太郎，鍋川 康夫，板谷 治郎，小林 洋平，科学 82 巻 2 号 (2019) 131-137.

Kondo group

We use angle-resolved photoemission spectroscopy (ARPES) with ultrahigh energy resolution. The main findings in 2019 was a weak topological insulator state in β-Bi_4I_4.

1. *A weak topological insulator state in quasi-one-dimensional bismuth iodide: R. Noguchi, T. Takahashi, K. Kuroda, M. Ochi, T. Shirasawa, M. Sakano, C. Bareille, M. Nakayama, M. D. Watson, K. Yaji, A. Harasawa, H. Iwasawa, P. Dudin, T. K. Kim, M. Hoesch, V. Kandyba, A. Giampietri, A. Barinov, S. Shin, R. Arita, T. Sasagawa and T. Kondo, Nature **566** (2019) 518.

2. *Low-energy electron-mode couplings in the surface bands of Sr_2RuO_4 revealed by laser-based angle-resolved photoemission spectroscopy: S. Akebi, T. Kondo, M. Nakayama, K. Kuroda, S. Kunisada, H. Taniguchi, Y. Maeno and S. Shin, Physical Review B **99** (2019) 081108(R).

3. Strongly anisotropic high-temperature Fermi surface of the Kondo semimetal CeNiSn revealed by angle-resolved photoemission spectroscopy: C. Bareille, T. -S. Nam, T. Takabatake, K. Kuroda, T. Yajima, M. Nakayama, S. Kunisada, S. Akebi, M. Sakano, S. Sakuragi, R. Noguchi, B. I. Min, S. Shin and T. Kondo, Physical Review B **100** (2019) 045133.

4. *Multiple topological states in iron-based superconductors: P. Zhang, Z. Wang, X. Wu, K. Yaji, Y. Ishida, Y. Kohama, G. Dai, Y. Sun, C. Bareille, K. Kuroda, T. Kondo, K. Okazaki, K. Kindo, X. Wang, C. Jin, J. Hu, R. Thomale, K. Sumida, S. Wu, K. Miyamoto, T. Okuda, H. Ding, G. D. Gu, T. Tamegai, T. Kawakami, M. Sato and S. Shin, Nature Phys **15** (2019) 41-48.

5. Density Wave Probes Cuprate Quantum Phase Transition: T. A. Webb, M. C. Boyer, Y. Yin, D. Chowdhury, Y. He, T. Kondo, T. Takeuchi, H. Ikuta, E. W. Hudson, J. E. Hoffman and M. H. Hamidian, Physical Review X **9** (2019) 021021.

6. Dirac Surface States in Intrinsic Magnetic Topological Insulators $EuSn_2As_2$ and $MnBi_2nTe_{3n+1}$: H. Li, S.-Y. Gao, S.-F. Duan, Y.-F. Xu, K.-J. Zhu, S.-J. Tian, J.-C. Gao, W.-H. Fan, Z.-C. Rao, J.-R. Huang, J.-J. Li, D.-Y. Yan, Z.-T. Liu, W.-L. Liu, Y.-B. Huang, Y.-L. Li, Y. Liu, G.-B. Zhang, P. Zhang, T. Kondo, S. Shin, H.-C. Lei, Y.-G. Shi, W.-T. Zhang, H.-M. Weng, T. Qian and H. Ding, Physical Review X **9** (2019) 041039.

7. Band structure of overdoped cuprate superconductors: Density functional theory matching experiments: K. P. Kramer, M. Horio, S. S. Tsirkin, Y. Sassa, K. Hauser, C. E. Matt, D. Sutter, A. Chikina, N. B. M. Schröter, J. A. Krieger, T. Schmitt, V. N. Strocov, N. C. Plumb, M. Shi, S. Pyon, T. Takayama, H. Takagi, T. Adachi, T. Ohgi, T. Kawamata, Y. Koike, T. Kondo, O. J. Lipscombe, S. M. Hayden, M. Ishikado, H. Eisaki, T. Neupert and J. Chang, Physical Review B 99 **9** (2019) 224509.

8. †*Bulk quantum Hall effect of spin-valley coupled Dirac fermions in the polar antiferromagnet $BaMnSb_2$: H. Sakai, H. Fujimura, S. Sakuragi, M. Ochi, R. Kurihara, A. Miyake, M. Tokunaga, T. Kojima, D. Hashizume, T. Muro, K. Kuroda, T. Kondo, T. Kida, M. Hagiwara, K. Kuroki, M. Kondo, K. Tsuruda, H. Murakawa and N. Hanasaki, Phys. Rev. B **101** (2020) 081104(1-7).

9. Three-dimensional electronic structure in ferromagnetic Fe_3Sn_2 with breathing kagome bilayers: H. Tanaka, Y. Fujisawa, K. Kuroda, R. Noguchi, S. Sakuragi, C. Bareille, B. Smith, C. Cacho, S. W. Jung, T. Muro, Y. Okada and T. Kondo, Phys. Rev. B **101** (2020) 161114.

10. *Radial Spin Texture in Elemental Tellurium with Chiral Crystal Structure: M. Sakano, M. Hirayama, T. Takahashi, S. Akebi, M. Nakayama, K. Kuroda, K. Taguchi, T. Yoshikawa, K. Miyamoto, T. Okuda, K. Ono, H. Kumigashira, T. Ideue, Y. Iwasa, N. Mitsuishi, K. Ishizaka, S. Shin, T. Miyake, S. Murakami, T. Sasagawa and T. Kondo, Phys. Rev. Lett. **124** (2020) 136404.

Matsunaga group

We have investigated light-matter interactions and light-induced nonequilibrium phenomena in solids by utilizing terahertz (THz) pulse. With developing polarization-resolved THz time-domain spectroscopy system, we observed a large anomalous

† Joint research with outside partners.

Hall effect in a Weyl antiferromagnet Mn_3Sn film at room temperature, realizing the noncontact ultrafast readout of the antiferromagnetic order in the picosecond timescale. In addition, with developing intense THz pulse generation technique, we discovered extremely-efficient THz high-harmonic generation in a Dirac semimetal Cd_3As_2 thin film at room temperature. By time-resolved THz spectroscopy, we also demonstrated that the mechanism of THz harmonic generation is the coherent acceleration of Dirac electrons in momentum space for the first time as theoretically anticipated over the decade.

1. Light-induced nonequilibrium response of the superconducting cuprate $La_{2-x}Sr_xCuO_4$: H. Niwa, N. Yoshikawa, K. Tomari, R. Matsunaga, D. Song, H. Eisaki and R. Shimano, Phys. Rev. B **100** (2019) 104507.

2. Infrared Activation of the Higgs Mode by Supercurrent Injection in Superconducting NbN: S. Nakamura, Y. Iida, Y. Murotani, R. Matsunaga, H. Terai and R. Shimano, Phys. Rev. Lett. **122** (2019) 257001.

3. [*]Efficient Terahertz Harmonic Generation with Coherent Acceleration of Electrons in the Dirac Semimetal Cd_3As_2: B. Cheng, N. Kanda, T. N. Ikeda, T. Matsuda, P. Xia, T. Schumann, S. Stemmer, J. Itatani, N. P. Armitage and R. Matsunaga, Phys. Rev. Lett. **124** (2020) 117402.

4. [*]Room-temperature terahertz anomalous Hall effect in Weyl antiferromagnet Mn_3Sn thin films: T. Matsuda, N. Kanda, T. Higo, N. P. Armitage, S. Nakatsuji and R. Matsunaga, Nat Commun **11** (2020) 909.

Okazaki group

We have investigated superconducting-gap structures of unconventional superconductors by a low-temperature and high-resolution laser ARPES apparatus and transient electronic structures in photo-excited non-equilibrium states by a time-resolved ARPES apparatus using EUV and SX lasers. In the academic year 2019, we have revealed the detailed superconducting gap structures of $SrFe_2(As_{0.65}P_{0.35})_2$ and $Pr_{1.3-x}La_{0.7}Ce_xCuO_4$ by high-resolution laser ARPES. In addition, we have investigated the non-equilibrium electronic states of FeSe by HHG laser time-resolved ARPES, and found the possible superconducting state is realized in this material.

1. [†*]*d*-wave superconducting gap observed in the protect-annealed electron-doped cuprate superconductors $Pr_{1.3-x}La_{0.7}Ce_xCuO_4$: M. Horio, K. Koshiishi, S. Nakata, K. Hagiwara, Y. Ota, K. Okazaki, S. Shin, S. Ideta, K. Tanaka, A. Takahashi, T. Ohgi, T. Adachi, Y. Koike and A. Fujimori, Phys. Rev. B **100** (2019) 054517.

2. [*]Symmetry-breaking and spin-blockage effects on carrier dynamics in single-layer tungsten diselenide: R.-Y. Liu, M.-K. Lin, P. Chen, T. Suzuki, P. C. J. Clark, N. K. Lewis, C. Cacho, E. Springate, C.-S. Chang, K. Okazaki, W. Flavell, I. Matsuda and T.-C. Chiang, Phys. Rev. B **100** (2019) 214309.

3. [*]Ultrafast Unbalanced Electron Distributions in Quasicrystalline 30° Twisted Bilayer Graphene: T. Suzuki, T. Iimori, S. J. Ahn, Y. Zhao, M. Watanabe, J. Xu, M. Fujisawa, T. Kanai, N. Ishii, J. Itatani, K. Suwa, H. Fukidome, S. Tanaka, J. R. Ahn, K. Okazaki, S. Shin, F. Komori and I. Matsuda, ACS Nano **13** (2019) 11981.

4. [†*]Band-dependent superconducting gap in $SrFe_2(As_{0.65}P_{0.35})_2$ studied by angle-resolved photoemission spectroscopy: H. Suzuki, T. Kobayashi, S. Miyasaka, K. Okazaki, T. Yoshida, M. Horio, L. C. C. Ambolode, Y. Ota, H. Yamamoto, S. Shin, M. Hashimoto, D. H. Lu, Z. -X. Shen, S. Tajima and A. Fujimori, Sci Rep **9** (2019) 16418.

5. [*]Multiple topological states in iron-based superconductors: P. Zhang, Z. Wang, X. Wu, K. Yaji, Y. Ishida, Y. Kohama, G. Dai, Y. Sun, C. Bareille, K. Kuroda, T. Kondo, K. Okazaki, K. Kindo, X. Wang, C. Jin, J. Hu, R. Thomale, K. Sumida, S. Wu, K. Miyamoto, T. Okuda, H. Ding, G. D. Gu, T. Tamegai, T. Kawakami, M. Sato and S. Shin, Nature Phys **15** (2019) 41-48.

6. [*]Photoinduced possible superconducting state with long-lived disproportionate band filling in FeSe: T. Suzuki, T. Someya, T. Hashimoto, S. Michimae, M. Watanabe, M. Fujisawa, T. Kanai, N. Ishii, J. Itatani, S. Kasahara, Y. Matsuda, T. Shibauchi, K. Okazaki and S. Shin, Commun. Phys. **2** (2019) 115.

[*] Joint research among groups within ISSP.

The Institute for Solid State Physics (ISSP), The University of Tokyo

Address	5-1-5 Kashiwanoha, Kashiwa, Chiba, 277-8581, Japan
Phone	+81-4-7136-3207
Home Page	https://www.issp.u-tokyo.ac.jp